Horizontal Shear Design of Concrete Interfaces in Beam and Slab Structures

Von der Fakultät für Bauingenieurwesen der Rheinisch-Westfälischen Technischen Hochschule Aachen zur Erlangung des akademischen Grades einer Doktorin der Ingenieurwissenschaften genehmigte Dissertation

vorgelegt von

Katrin Marie Wieneke

Berichter: Univ.-Prof. Dr.-Ing. Josef Hegger
Prof. Dr. Linh Cao Hoang

Tag der mündlichen Prüfung: 04.07.2019

Abstract

In composite beam and slab structures, horizontal concrete interfaces occur between concrete cast at different times, e.g. due to section wise concrete casting or in precast construction. To achieve a quasi-monolithic load bearing behaviour, the horizontal shear transfer across the interface must be verified. In present design codes, interface shear resistance is calculated with semi-empirical design equations accounting for load resistance terms of adhesion, friction induced by normal stress, and friction induced by clamping of interface reinforcement. The design equations are mainly built upon similar theoretical backgrounds but experimental data from different small size test series. Small size tests localise interface shear to small interface areas with concentrated load application, in contrast to composite beam and slab structures, where horizontal interface shear develops due to composite action. The transfer of results from small size tests to structural members, however, requires further investigation. Additionally, interface shear resistance values differ significantly among codes, which bares potential improvements in terms of efficiency and level of reliability of the design equations.

The objective of this thesis was to improve the formulation of interface shear resistance in terms of efficiency and level of reliability, for monotonic and cyclic loading conditions. Therefore, consistent and critically reviewed databases were developed using test results from experimental investigations in literature and own tests. The databases specifically distinguish between small size tests and structural members to investigate the effects of test setup on interface shear resistance. Further classifications were made regarding the load resistance terms by distinguishing between interfaces with and without interface reinforcement and normal stress. By means of systematic evaluation of the databases with the interface shear equations according to Eurocode 2, including the National Annex of Germany, the draft for the next Eurocode 2, Model Code 2010, ACI 318-14 and AASHTO LFRD, the different design equations were compared and assessed regarding efficiency and level of safety.

Based on the results of the database evaluations, a modified interface shear equation was derived following the design concept for the next generation of Eurocode 2. For an efficient and safe estimation of interface resistance, the coefficients of adhesion and friction were determined independently using isolated databases. To account for a sufficient level of reliability, partial safety factors for adhesion and friction were derived by probabilistic evaluation methods according to Eurocode 0. For fatigue, the verification of stress range in the interface reinforcement was revised and improved based on own experimental investigations with semi-precast slabs with lattice girders under cyclic loading. For structural members, the database evaluation shows an inverse relationship between interface width and interface shear resistance. This effect was captured with an additional coefficient of interface width in the adhesive term of the modified interface shear equation. The validation of the modified interface shear equation with test results of structural members shows an improved and reliable estimation of interface shear resistance.

Kurzfassung

Bei der Herstellung von Balken und Plattentragwerken entstehen häufig Fugen zwischen Betonen unterschiedlichen Alters, z.B. als Arbeitsfugen zwischen Betonierabschnitten oder im Fertigteilbau zwischen Fertigteil und Ortbeton. Zur Sicherstellung eines quasi-monolithischen Tragverhaltens ist die Übertragung von Schubspannungen in Fugenebene von entscheidender Bedeutung. In aktuellen Bemessungsnormen wird die Tragfähigkeit von Verbundfugen mit einem semi-empirischen Bemessungsansatz unter Berücksichtigung der Traganteile aus Adhäsion, Reibung durch Normalspannung sowie Reibung durch Klemmwirkung der Bewehrung beschrieben. Die Bemessungsgleichungen basieren auf ähnlichen Modellvorstellungen, wurden jedoch vorwiegend auf Grundlage von Kleinkörperversuchen verschiedener Versuchsserien hergeleitet. In Kleinkörperversuchen werden i.d.R. kleine Fugenflächen durch konzentrierte Krafteinleitung beansprucht, wohingegen in Balken und Plattentragwerken die Schubspannungen in Fugenebene durch Druckkraftänderungen infolge Biegung entstehen. Die Übertragung der Versuchsergebnisse von Kleinkörpern auf Bauteile erscheint daher fraglich. Zudem weichen die Fugentragfähigkeiten verschiedener Bemessungsnormen teils erheblich voneinander ab, wodurch ein Verbesserungspotential besonders hinsichtlich der Wirtschaftlichkeit und des Sicherheitsniveaus aufzeigt wird.

Das Ziel dieser Arbeit war die Überprüfung und Verbesserung der Schubfugenbemessung für ruhende und nicht ruhende Belastung unter den Aspekten der Wirtschaftlichkeit und des Sicherheitsniveaus. Basierend auf umfangreichen Literaturrecherchen und eigenen experimentellen Untersuchungen wurden konsistente Datenbanken erstellt und kritisch überprüft. Zur Untersuchung der Einflüsse aus dem Versuchsaufbau sowie der einzelnen Traganteile der Schubfugenbemessung unterscheiden die Datenbanken zum einen zwischen Kleinkörper- und Bauteilversuchen, zum anderen zwischen Versuchen mit und ohne Normalspannung sowie mit und ohne Fugenbewehrung. Durch systematische Datenbankauswertungen mit den Bemessungsansätzen nach Eurocode 2, einschließlich Nationalem Anhang für Deutschland, dem Entwurf für den neuen Eurocode 2, Model Code 2010, ACI 318-14 und AASHTO LFRD wurden die verschiedenen Bemessungsgleichungen hinsichtlich der beiden Kriterien Wirtschaftlichkeit und Sicherheitsniveau verglichen und bewertet.

Aufbauend auf den Datenbankauswertungen wurde ein modifizierter Bemessungsansatz auf Grundlage des Neuvorschlags von Eurocode 2 für statische und zyklische Belastungen abgeleitet. Hierzu wurden Rauigkeitsbeiwerte für Adhäsion und Reibung durch isolierte Datenbankbetrachtungen bestimmt, um anschließend mittels probabilistischer Verfahren nach Eurocode 0 Teilsicherheitsbeiwerte für Adhäsion und Reibung herzuleiten. Basierend auf eigenen Untersuchungen an Elementdecken mit Gitterträgern unter Ermüdungsbeanspruchung wurde der Nachweis der Spannungsschwingbreite in der Fugenbewehrung für nicht ruhende Belastungen überarbeitet und verbessert. Zudem konnte im Rahmen der Datenbankauswertung eine Abnahme der Fugentragfähigkeit mit zunehmender Fugenbreite festgestellt werden. Zur Berücksichtigung dieses Einflusses wurde ein zusätzlicher Parameter für den Adhäsionstraganteil in der Bemessungsgleichung hergeleitet. Die Validierung der vorgeschlagenen Bemessungsgleichung mit Versuchen an Balken- und Plattenbauteilen zeigt eine verbesserte und sichere Abschätzung der Fugentragfähigkeit.

Table of contents

Notations

In the following, the most important units, abbreviations and symbols are listed. Unlisted symbols are explained in the text where they appear.

Units

Strain:	%, ‰
Force:	N, kN, MN
Stress:	N/mm², MN/m², MPa
Distance:	mm, cm, m
Angle	degree (°)

Abbreviations

COV	coefficient of variation
S-N	fatigue strength

Capital Latin Letters

A_c	cross-sectional area of concrete
A_{int}, A_{cv}	cross-sectional area of interface
A_s	cross-sectional area of reinforcing steel
A_{si}, A_{vf}	cross-sectional area of reinforcement across the interface
$A_{v,min}$	cross-sectional area of minimum reinforcement
C_1, C_2	factor considering concrete strength
D_{dow}	shear resistance due to dowel action
E	young's modulus, effects of action
E_d	design effects of action
E_k	characteristic effects of action
F	force
F_c	compressive force
F_{cdi}	normal design force in in-situ concrete
F_{cd}	resulting design compression force of the section
F_{fric}	frictional resistance
F_s	tensile force in reinforcement
G	limit state function
K_1	fraction of concrete strength to resist interface shear
K_2	factor for limiting interface shear resistance
$K_{p,E}$	quantile factor of effects of action
$K_{p,R}$	quantile factor of resistance
M	moment
N	number of load cycles
N^*	reference number of load cycles
V	shear force, volume
V_{Edi}	applied design shear force

V_u, V_{ui}	ultimate shear force, acting shear force
V_n, V_{ri}	factored shear resistance
V_{nh}, V_{ni}	horizontal interface shear resistance
$V_{n,max}$	maximum factored shear resistance
V_{test}	shear force determined by test
P	external clamping force
P_c	permanent net compressive force normal to the interface
R	resistance
R_d	design resistance
R_k	characteristic resistance
R_t	roughness depth
R_p	maximum profile peak
T	tensile force
V_x	coefficient of variation
X_d	design value
X_k	characteristic value
$X_{k,5\%}$	characteristic 5% quantile value
X_m	mean value

Lowercase Latin Letters

$a_{s,min}$	area of minimum reinforcement per unit length
a	distance between load application and support
b	width
b_w	width of the web
b_i, b_{int}	width of interface
c	coefficient of adhesion
c_{fat}	coefficient of adhesion for fatigue
c_k	characteristic coefficient of adhesion
c_m	mean coefficient of adhesion
c_{stat}	coefficient of adhesion for monotonic loading
d_b	diameter of dowel
d_g	aggregate size
dx	length of infinitesimal element
d_s	diameter of reinforcement
d	diameter; effective depth
f_c	concrete strength
f_c’	specified cylinder concrete compressive strength after 28 days
$f_{c,cyl}$	cylinder concrete compressive strength
$f_{cm,cube}$	mean cube concrete compressive strength
$f_{cm,cyl}$	mean cylinder concrete compressive strength
$f_{c,prism}$	concrete compressive strength of prism
f_{c1}	uni-axial concrete compressive strength

f_{cd}	design concrete compressive strength
f_{ck}	characteristic concrete compressive strength
f_{cm}	mean concrete compressive strength
f_{ct}	concrete tensile strength
f_{ct1}	uni-axial concrete tensile strength
$f_{ct,sp}$	splitting concrete tensile strength
f_{ctm}	mean concrete tensile strength
f_{ctk}	characteristic concrete tensile strength
f_{ctd}	design concrete tensile strength
$f_{ct,flex}$	flexural concrete tensile strength
f_t'	uniaxial tensile strength
f_y	yield strength of reinforcement
f_{yd}	design yield strength
f_{yk}	characteristic yield strength of reinforcement
h	height
h_{insitu}	height of insitu concrete layer
h_{pre}	height of precast element
h_{total}	height of total cross section
k	constant
k_1, k_2	inclination of S-N curve
k_n	quantile factor
$k_{d,n}$	quantile factor for design
k_t	coefficient of the tensile forces in reinforcement
k_f	coefficient for the flexural resistance of reinforcement
l	length
n	number of load cycles, number of tests
m_x, m_y	mean value
p_f	failure probability
s	spacing of interface reinforcement, slip
s_{bar}	bar spacing
s_x, s_y	standard deviation
t	time
v	vertical displacement
v_{Edi}	applied design shear stress of interface
v_{max}	maximum shear stress
v_{Rdi}	design interface shear resistance
$v_{Rdi,max,fat}$	maximum design interface shear resistance for fatigue
v_u, v_{ui}	ultimate shear stress
w	deflection, vertical displacement
x_i	test data
z	lever arm of internal forces

Greek Letters and Symbols

α	inclination of interface reinforcement, coefficient of flexural resistance of the reinforcement
α_1, α_2, α_3	parameters determined by regression analysis
α_E	weighting factor for effects of actions
α_R	weighting factor for resistance
β	ratio of transferable normal force across the interface, reliability index
γ_{adh}	partial safety factor of adhesion
γ_c	partial safety factor of concrete
γ_E	partial safety factor for effects of action
γ_{fric}	partial safety factor of friction
γ_m	partial safety factor for material
γ_R, γ_M	partial safety factor for resistance
γ_{Rd}	partial safety factor for model equation
γ_s	partial safety factor of reinforcement
$\gamma_{s,fat}$	partial safety factor of reinforcement for fatigue
δ	deviation; error term, displacement
Δ	deviation, change of distance, range
ε	strain
θ	angle of compression strut, angle between interface reinforcement
κ_1	coefficient of the tensile forces in the reinforcement
κ_2	coefficient of flexural resistance of reinforcement
λ	wave length, coefficient of concrete density
λ_b	coefficient of interface width
μ	coefficient of friction; mean value
μ_E	mean value of effects of action
μ_G	mean value of limit state function
μ_m	mean coefficient of friction
μ_k	characteristic coefficient of friction
μ_R	mean value of resistance
ν	strength reduction factor
ρ	reinforcement ratio
ρ_{int}	interface reinforcement ratio
ρ_l	longitudinal reinforcement ratio
ρ_{min}	minimum reinforcement ratio
σ	stress
σ_a	stress amplitude
σ_c	standard deviation of concrete strength
σ_i	standard deviation
σ_m	medium stress
σ_{max}	maximum stress
σ_{min}	minimum stress

σ_n	normal stress
σ_E	standard deviation of effects of action
σ_G	standard deviation of limit state function
σ_R	standard deviation of resistance
$\Delta\sigma$	stress range
$\Delta\sigma_m$	mean value of stress range
$\Delta\sigma_p$	p-quantile of stress range
$\Delta\sigma_{Rsk}$	approved characteristic stress range
$\Delta\sigma_s$	stress range in reinforcement
τ	shear stress
τ_{adh}	adhesive shear strength
τ_{fric}	frictional shear strength
τ_{Rdi}	design shear resistance of interface
τ_{Rki}	characteristic shear resistance of interface
$\Delta\tau_{Rdi}$	design shear stress range resistance of interface
$\Delta\nu_{Rdi,fat,LG}$	design shear stress range resistance of interfaces with lattice girders
τ_{test}	tested shear stress
τ_{reinf}	shear strength of reinforcement
Ø	diameter
ϕ	internal angle of internal friction, partial safety factor for shear

Indices

adh	adhesion
c	concrete, compression
ct	concrete tensile
calc	determined by calculation
d	design
E	applied action
fat	fatigue
fric	friction
int	interface
k	characteristic
LG	lattice girders
m	mean
n	normal
R	resistance
reinf	reinforcement
s	steel
stat	static
t	tensile
test	determined by tests
y	yield

1 Introduction

1.1 Backgrounds

In beam and slab structures, horizontal interfaces occur between concrete cast at different times e.g. due to section wise concrete casting, in precast construction between precast element and insitu concrete, or in context of strengthening of existing structures between the existing structure and the strengthening concrete layer. Whereas in common building practice composite beam and slab structures are generally subjected to monotonic loading, cyclic loading conditions occur in industrial construction or due to traffic loads on bridges. To guarantee a sufficient load bearing resistance of the composite structure for monotonic and cyclic loading conditions, a quasi-monolithic load bearing behaviour must prevail. Since the location of the concrete interface represents a significant weakness in the structure, sufficient bond between the concrete layers must be ensured to guarantee an adequate shear transfer across the interface and thus, a quasi-monolithic load bearing behaviour of the structure.

To quantify the interface shear resistance of composite structures, experimental investigations and theoretical analyses were conducted over the past decades. Current model concepts for interface shear are based on shear friction theory, which was developed in the 1960s and describes the interface shear resistance by frictional resistance due to clamping of interface reinforcement. Assumptions based on the *Mohr-Coulomb* analogy further enhanced the understanding of interface shear resistance and added two load resistance terms for adhesion and friction induced by external normal stress. A main influencing parameter of the interface resistance in model concepts is the roughness of the interface, which affects the adhesive as well as the frictional resistance due to normal stress and interface reinforcement.

1.2 Motivation

The design approaches according to present design codes are mainly built upon the theoretical backgrounds described above. Considering the design regulations of Eurocode 2, Eurocode 2 with the National Annex of Germany, the draft for the next Eurocode 2, Model Code 2010, ACI 318-14 and AASHTO LFRD, the interface shear resistance is described by the three load resistance terms of adhesion, friction induced by normal stress and friction induced by clamping of interface reinforcement. Whereas the European design expressions formulate the adhesive resistance by terms of concrete strength, the American Codes define constant adhesive strengths depending on interface roughness. Additionally, the expressions of Model Code 2010 and the new approach of Eurocode 2 for concrete toppings extend the resistance term of interface reinforcement by considering the effect of dowel action. To capture the influence of interface roughness, the design codes define roughness coefficients depending on interface roughness

classification. The roughness coefficients were mainly determined on the basis of experimental test data from different test series. Additionally, the experimental test data is predominantly based on small size tests. Small size tests localise interface shear to small interfaces with concentrated load application, in contrast to composite beam and slab structures, where the horizontal interface shear develops due to composite action. The transfer of results from small size tests to structural members, however, is not straightforward and requires further investigation. Additionally, the calculated interface shear resistances differ up to several orders of magnitude among codes, which bares potential for improvements in terms of efficiency and level of safety of the design equations. Furthermore, the design regulations according to the present codes provide different assumptions for the fatigue verification of concrete interfaces with and without interface reinforcement.

To verify the design equations and to achieve an efficient and safe design for composite beam and slab structures, no complete, consistent, and critically reviewed databases, which distinguish between small size tests and structural members as well as between monotonic and cyclic loading, exist yet. Database evaluations from literature concentrate either on small size tests or structural members, or comprise a limited number of test series. The current development of a revised interface shear design concept for Eurocode 2 as well as the ACI 445D Shear Friction Database development is an opportunity to develop consistent and critically reviewed databases, to assess the present design expressions for monotonic and cyclic loading conditions and to revise interface shear design in terms of efficiency and level of safety.

1.3 Objectives and outline

The objective of this thesis is to revise and assess the design of interface shear transfer in present design codes based on comprehensive and systematic evaluations of existing and new experimental data. Special care is put on distinguishing between test setups (small size tests and structural member tests), load resistance terms (interfaces without normal stress and interface reinforcement for adhesion, interfaces with externally applied normal stress for friction and interfaces with interface reinforcement) and loading conditions (monotonic and cyclic loading). Based on the evaluation results, this thesis aims to improve the horizontal interface shear design based on the design concept of the next Eurocode 2 in terms of efficiency and level of safety.

The presented thesis consists of eight chapters. The content of each chapter is briefly summarised in the following:

- Chapter 2 provides theoretical backgrounds on horizontal concrete interfaces subjected to shear. The models of load bearing behaviour of composite beam and slab structures regarding shear transfer across the interface as well as the load bearing mechanisms of interface shear resistance are presented. Due to the high

influence of interface roughness, the fundamentals of roughness classification are introduced. To capture the influence of cyclic loading conditions on the interface shear behaviour, Chapter 2 also holds a brief introduction on reinforced concrete and concrete interfaces subjected to fatigue.

- Chapter 3 gives an overview of the development of model concepts for interface shear, which form the basis of interface shear design regulations in present design codes. Additionally, interface shear regulations according to Eurocode 2, Eurocode 2 with the National Annex of Germany, the draft for the next Eurocode 2, Model Code 2010, ACI 318-14 and AASHTO LFRD are presented and compared.

- Chapter 4 presents existing experimental investigations on interface shear from literature, distinguishing between test setup, load resistance terms and loading conditions, focusing on test parameters, test results and influencing parameters. The presented tests render the outline for the development of the databases in Chapter 6.

- Chapter 5 documents the results of own experimental investigations on the fatigue behaviour of semi-precast slabs with lattice girders, conducted within a research project at the Institute of Structural Concrete, RWTH Aachen University. In this context, the fundamentals of semi-precast slabs with lattice girders, the results of small size tests with lattice girder diagonals and the derivation of fatigue-strength curves to verify the stress range in the lattice girders are presented. Additionally, a test programme of 14 semi-precast slab specimens with lattice girders and two sub-tests each is documented. The investigated parameters were slab thickness, interface reinforcement ratio, concrete strength and interface roughness. The chapter presents the test programme and test results as well as test evaluations and comparison to design regulations.

- Chapter 6 presents the development and evaluation of consistent and critically reviewed databases based on comprehensive literature research (Chapter 4) and own investigations (Chapter 5). The databases distinguish between small size and structural member tests, interfaces with and without normal stress and interface reinforcement as well as monotonic and cyclic loading conditions. To assess the interface shear design regulations presented in Chapter 3, the databases were systematically evaluated regarding efficiency and level of safety.

- Chapter 7 describes the derivation of a modified interface shear equation based on the design concept for the next Eurocode 2. By considering isolated databases with small size tests (Chapter 6) and probabilistic evaluation methods according to Eurocode 0, roughness parameters and partial safety factors were derived separately for adhesion and friction. To verify the modified approach with structural members, the influence of structural dimensions was captured by an additional

coefficient of interface width. Furthermore, the verification for fatigue was revised and improved based on the results of own experimental investigations (Chapter 5).

- Chapter 8 summarises and concludes the investigations and scientific findings of this thesis and points out potentials for future research.

2 Theoretical backgrounds

2.1 Introduction

In structural building practice, interfaces describe planes between different materials (e.g. steel and concrete or concrete cast at different times) or components. To guarantee sufficient load bearing behaviour of the structure, the interfaces must be designed and built to transfer shear, tensile or compressive stress. Interfaces between concrete cast at different times form joints in the structure which, depending on orientation and location, accomplish different purposes.

In composite beam and slab structures, shear stress develops across horizontal interfaces due to composite actions and sufficient shear transfer must be ensured to verify the bending resistance. In this context, Figure 2-1 shows two examples of typical cross sections with horizontal interfaces which are subjected to shear. The interfaces occur e.g. due to section wise concrete casting between web and flange or between beam and slab (Figure 2-1 (1)), in precast construction between precast element and insitu concrete (Figure 2-1 (2)) or in context of strengthening of existing structures between the existing structure and strengthening concrete layer (Figure 2-1 (3)).

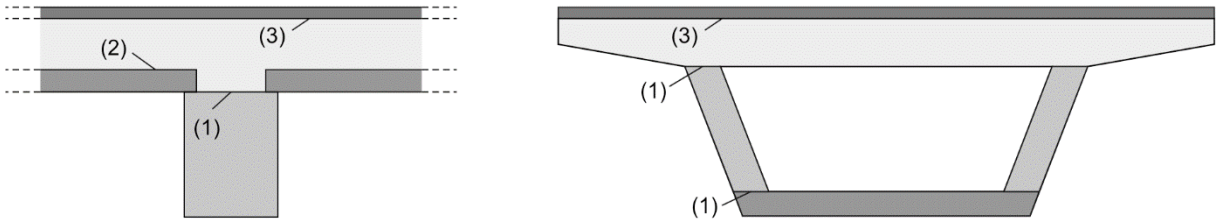

(1) interface between beam-slab connection/ web-flange connection
(2) interface between precast element and insitu concrete
(3) interface between existing structure and strengthening layer

Figure 2-1: Interfaces in concrete construction: (a) structural joints, (b) joints between structural element and layer of concrete strengthening

If the load transfer across the interface cannot be ensured by the interface itself, interface reinforcement can be applied to increase the interface resistance. In this context, Figure 2-2 summarises different examples of interface reinforcement systems commonly used in building practice. For interfaces between beam-slab connections, stirrups are generally used as interface reinforcement (Figure 2-2 (1)). Besides beam-slab connections, stirrups can also be applied as interface reinforcement between precast element and insitu concrete. A commonly used alternative to stirrups as interface reinforcement in semi-precast slabs is the prefabricated reinforcement system with lattice girders (Figure 2-2 (2)). Stud systems present another prefabricated reinforcement system which can also be applied as interface reinforcement for strengthening of existing concrete layers (Figure 2-2 (3)). Depending on design and geometry, the reinforcement systems can also be accounted as shear reinforcement.

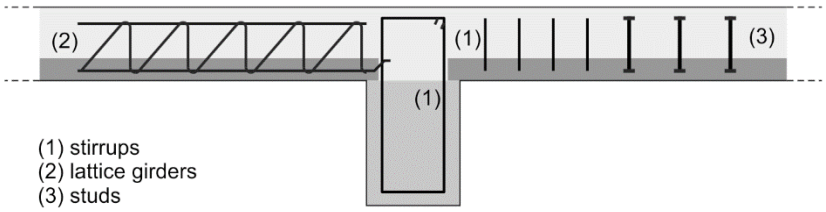

Figure 2-2: Common examples of interface reinforcement

The following chapter presents the theoretical background of the shear transfer across horizontal interfaces as well as of interface shear resistance. In order to qualify the roughness of the interface, different models and measuring methods are presented. Since interfaces in concrete structures may also be subjected to cyclic loading, the following chapter gives a short introduction and summary of fatigue behaviour of concrete interfaces as well as of fatigue design.

2.2 Horizontal shear transfer

2.2.1 Introduction

Even though interfaces between concrete cast at different times can be realised as vertical and horizonal interfaces and can be subjected to compression, tension or shear, the investigations in this thesis focus on beam and slab structures with horizontal interfaces parallel to the structure's longitudinal axis.

2.2.2 Load bearing behaviour of composite beam and slab structures

Generally, composite structures with concrete cast at different times must be designed to achieve a load bearing behaviour of monolithic structures. For the design at ultimate and serviceability limit state, the internal forces can be determined in accordance to monolithic sections. However, the particular elements of the composite section must also be verified for state of construction.

To guarantee a monolithic load bearing behaviour, interfaces subjected to shear must be firmly connected to achieve rigid bond, which eliminates relative slip of both sides of the interface. Under the condition of rigid bond (Figure 2-3 (a)), a linear strain distribution across the structure's cross section can be assumed and thus, a monolithic design can be accepted. If the applied shear stress exceeds the resistance of rigid bond, relative slip occurs at the interface and two individual strain distributions act in the two concrete layers (Figure 2-3 (b)).

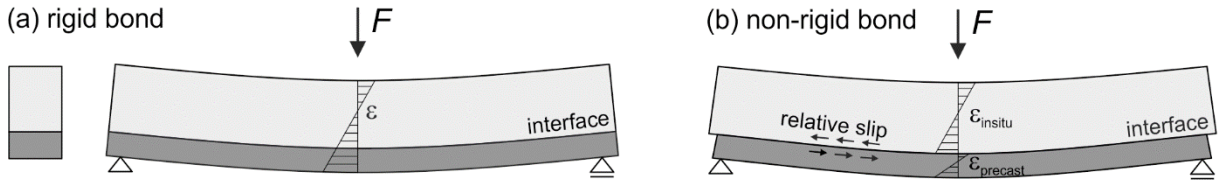

Figure 2-3: Qualitative depiction of rigid bond (a) and non-rigid bond (b) of a composite beam [Zil10]

Even though the requirements of rigid bond must be satisfied to achieve a monolithic load bearing behaviour, some regulations in design concepts allow non-rigid bond when interface reinforcement is applied. For these cases, the design regulations are defined conservatively with additional construction rules to ensure sufficient shear force transfer at ultimate limit state as well as effective quasi-monolithic load bearing behaviour at service load level [Zil10].

2.2.3 Model concept for horizontal interface shear

According to the general assumption of composite action in beam and slab structures, horizonal interface shear results from the change of the acting internal forces along the structure's axis. Figure 2-4 (a) shows a composite beam under uniform load q with the resulting moment M and shear force distribution V.

The acting moment can be expressed by the compressive force F_c and the tensile force F_s, acting with an internal lever arm z. Considering an infinitesimal element with the length dx (Figure 2-4 (b)), the change of moment can be expressed by the change of compression force dF_c and the change of tensile force dF_S, respectively. For composite sections, horizontal shear stress τ act at the interface between the concrete layers. Generally, the compressive force due to the acting moment can be described by $F_c = M/z$ and the change of moment along the element dx with the shear force V by $dM = V \cdot dx$. For interfaces in the tensile zone, the full compressive force must be transferred across the interface. Thus, extracting the composite section at the interface, the force equilibrium at the insitu concrete layer gives the relation in Eq. (2-1).

$$\tau \cdot dx \cdot b = dF_c \tag{2-1}$$

The shear stress acting at the interface can therefore be determined following Eq. (2-2).

$$\tau = dF_c/(dx \cdot b) = dM/(dx \cdot b \cdot z) = \mathrm{V} \cdot dx/(dx \cdot b \cdot z) = V/(b \cdot z) \tag{2-2}$$

For interfaces in the compression zone, only the change of compressive forces in the insitu concrete must be transferred across the interface (Figure 2-4 (c)). The shear stress at the interface can therefore be reduced by the ratio of the change of compressive force between top edge and interface dF_{c1} and the total change of compressive force in the cross section with $dF_c = dF_{c1} + dF_{c2}$ as shown in Eq. (2-3).

$$\tau = (F_{c1}/F_c) \cdot V/(b \cdot z) \tag{2-3}$$

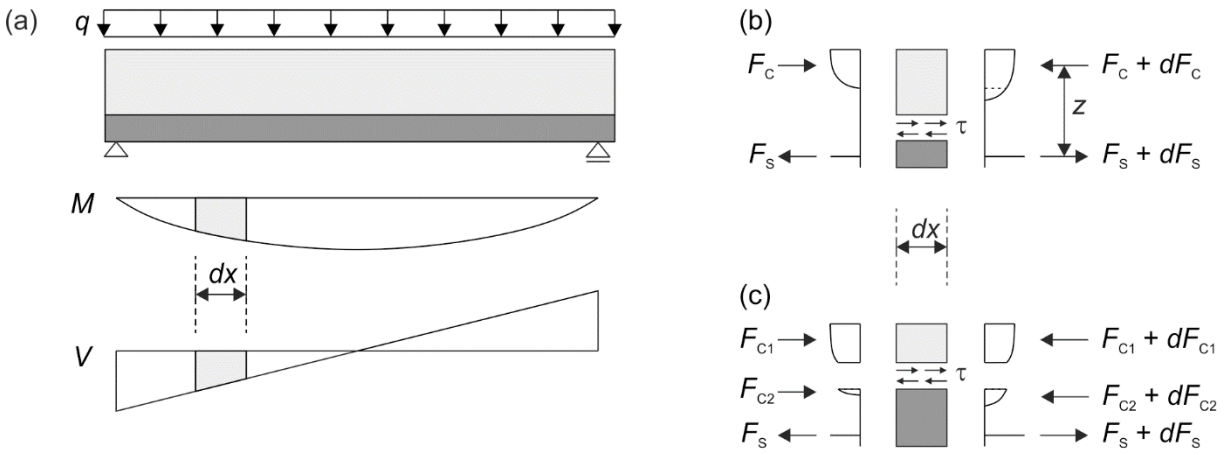

Figure 2-4: Internal forces of a simply supported beam under uniform load: (a) Moment and shear forces distribution, (b) internal forces acting at infinitesimal element with interface in tensile zone, (c) internal forces acting at infinitesimal element with interface in compression zone

However, the aforementioned concept to determine the horizontal shear stress at an interface gives an idealised model for interface design. According to the general mechanical understanding of shear stresses in a structure, the shear stress is defined as a variable which helps to calculate the principle stress state in the structure [Mör27]. Among other variables, the principle compressive and tensile stress can be determined for state I (uncracked) and for state II (cracked) [Leo84]. If the principle concrete tensile stress increase, cracks occur perpendicular to the trajectories for tension and grow along the trajectories for compression. Thus, shear failure may actually be caused by exceeding the tensile strength of the concrete. In this context, Figure 2-5 shows the stress trajectories of an uncracked simply supported beam with two point loads and an interface at the bottom of the section (a) as well as with an interface at the top of the section (b).

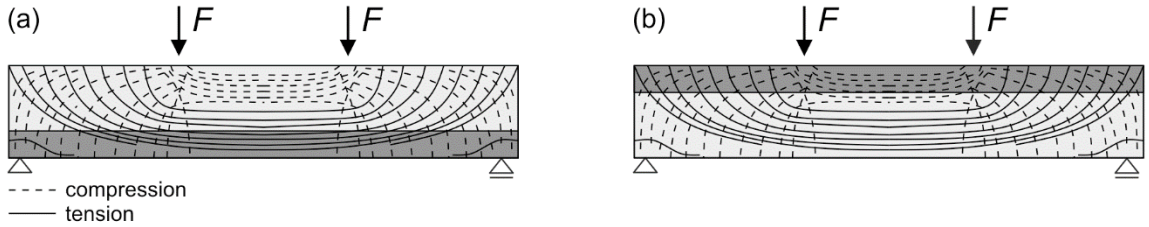

Figure 2-5: Stress trajectories of a simply supported beam according to [Leo84] with an interface in the tensile zone (a) and in the compressive zone (b) [Len12]

The principle tensile stress at the bottom proceed parallel to the member's axis and thus, flexural cracks may occur perpendicular to the interface. For interfaces at the top of the section, the principle tensile stress act perpendicular to the member's axis, which may lead to tensile stress in the interface. This can be confirmed by comparative analysis in [Len12], where tensile stress only occur along interfaces at the top of the member. However, the magnitude of these principle tensile stress was determined to be very small and

would hardly lead to interface failure. Thus, for simply supported beams, interface failure only occurred at interfaces at the bottom of the cross section, where flexural cracks proceed along the interface.

In this context, the effect of concrete interfaces at the bottom and the top of a composite cross section regarding the crack development of continuous beam and slab structures is qualitatively shown in Figure 2-6. For composite slabs, the interface is generally located at the bottom of the cross section (Figure 2-6 (a)). In the range of positive moments with tensile stress at the bottom of the cross section, interface failure can occur after flexural cracks proceed along the interface. Following this qualitive crack development, the flexural cracks at the top of the cross section in the range of mid-support proceed to shear cracks, which reach the interface at the bottom of the cross section at comparable higher load levels. In contrast to composite slabs, interfaces in composite T-beams with beam-slab connections are generally located at the top of the cross section. As shown in Figure 2-6 (b), the flexural cracks at the mid-support of the beam meet the interface at comparable smaller load levels than the shear cracks in the range of the positive moment, where the crack must develop along the entire cross section to meet the interface. However, to the knowledge of the author no experimental test programmes exist with systematic test series on interface locations and continuous beams to confirm this assumption.

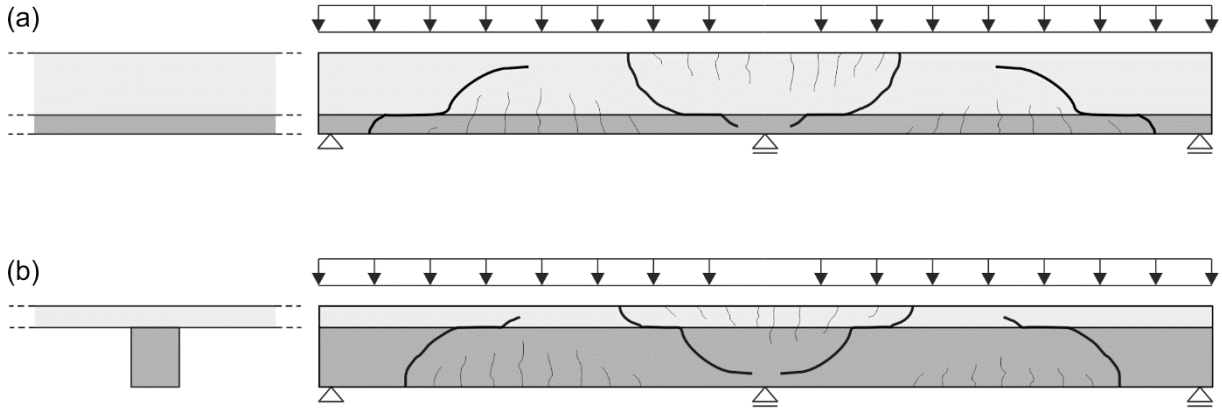

Figure 2-6: Crack development across interfaces in continuous composite slabs (a) and T-beams with beam-slab connections (b)

A comprehensive explanation of the load transfer across interfaces can be found e.g. in [Zil10] and [Len12].

2.3 Shear resistance of concrete interfaces

2.3.1 Introduction

The overall load bearing behaviour of composite beam and slab structures is generally comparable to monolithic structures. Thus, influences like concrete strength, shear slenderness, geometry, longitudinal and shear reinforcement, effective depth, prestressing

and loading conditions apply. However, interfaces cause additional weaknesses of the structure which may affect the load bearing behaviour. Due to the different properties of concrete cast at different times as well as the condition of the interface, the influencing factors on the load resistance increase significantly.

The common understanding of the interface shear resistance is based on theoretical considerations and experimental investigation of small size specimens and structural member tests. The main terms of interface resistance are generally formulated as adhesion, friction and interface reinforcement. Besides the influences of normal stress acting perpendicular to the interface and reinforcement bars crossing the interface, further influences may affect the bond behaviour. Examples of currently known influences are concrete properties (e.g. strength, aggregates and age), surface condition (e.g. roughness, humidity, cleanness) and load conditions (e.g. magnitude, distribution, monotonic or cyclic). Evaluations of experimental investigations from literature (e.g. [Heg99], [Heg03], [Rei04], [Beu05], [Zil06], [Len12]) show, that only partial aspects of interface shear transfer are investigated to date. Not considering all influencing parameters as well as the inability to separately investigate the main load bearing capacities complicates reliable investigations and evaluations. Due to effects of e.g. different shrinkage, unknown size effects and different stress states in the structure depending on test-setup und load conditions, the test results and findings achieved by small size specimens must not necessarily be contagious for beam and slab specimens [Zil06].

2.3.2 Theoretical considerations for interface shear resistance

The first approaches to describe the load bearing mechanism of a sudden failure across an interface without interface reinforcement were published in the 1960s by *Zelger and Rüsch* [Zel61], using analogies to the friction hypothesis according to *Mohr-Coulomb* [Zil06].

According to Mohr's failure criterion, the limiting shear stress in a plane τ is considered as a function of the normal stress σ and can be expressed according to Eq. (2-4).

$$|\tau| = f(\sigma) \tag{2-4}$$

The function of the shear stress can be assumed as a straight line and written as the *Coulomb* equation according to Eq.(2-5).

$$|\tau| = c - \sigma \cdot \tan\phi \tag{2-5}$$

With
c coefficient of cohesion
ϕ angle of internal friction

The coefficient of cohesion and the angle of internal friction are material constants which must be determined by experimental investigations [Che88][Nie11]. Regarding

the simple friction hypothesis according to *Coulomb*, the horizonal forces must be proportional to the normal forces. Thus, the expression tanϕ for limiting case can be expressed by a proportionality or friction factor $\tan\phi = \mu$.

A modification of the *Mohr-Coulomb* failure criterion is shown in Figure 2-7. Therefore, the formulation of the shear stress written in Eq. (2-5) is shown by the failure line enveloping the stress circle of the uniaxial tensile stress f_t' and the uniaxial compressive stress f_c'. The failure line is additionally extended by a limitation of the tensile area regarding $\sigma = f_t$'.

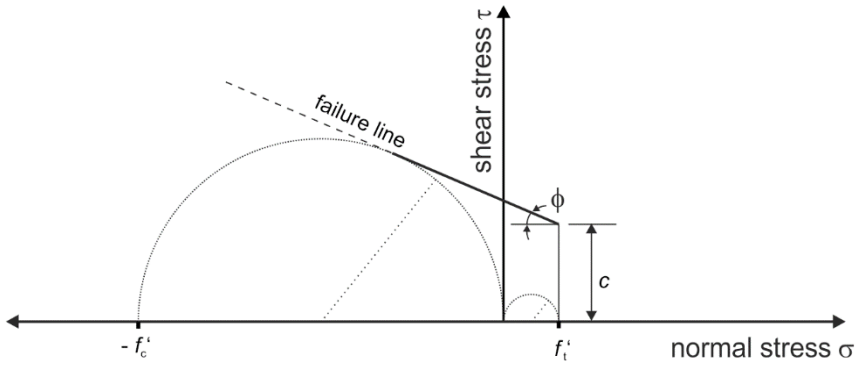

Figure 2-7: Modified *Mohr-Coulomb* failure criteria [Ran08]

According to [Zil06], the upper limit of the load resistance can be estimated by using this failure criterion combined with static and kinematic limit theorems [Che88]. A more detailed description of the interface shear transfer based on the theory of plasticity can be found e.g. in [Nie11].

Transferring the *Mohr-Coulomb* analogy to concrete with interfaces, the limit shear stress τ_{int} of an interface without reinforcement can be determined according to Eq. (2-6).

$$\left| \tau_{int} \right| = \tau_{adh} - \mu \cdot \sigma_n \tag{2-6}$$

With

τ_{adh}	shear resistance due to adhesion
μ	friction factor
σ_n	normal stress (positive for tension)

The aforementioned formulation regarding the shear stress at failure state does not consider the transferable shear stress after relative slip of an interface. After exceeding the adhesive strength of an interface, a crack occurs along the interface which leads to horizonal displacement *w* and - depending on the roughness of an interface - to a vertical displacement *v*.

To consider the shear stress transferred across an idealised interface with saw-tooth, where the frictional resistance is induced by clamping of the interface reinforcement, *Birkeland & Birkeland* [Bir66] and *Mast* [Mas68] developed the shear-friction theory

in the 1960s. This theory has been modified and extended by various researchers (s. Chapter 3.2) and is the basis for the design concepts in the common design regulations. Therefore, the applied and the reaction forces acting at a concrete interface along the plane *m-m* are shown in Figure 2-8 (a) [Bir66].

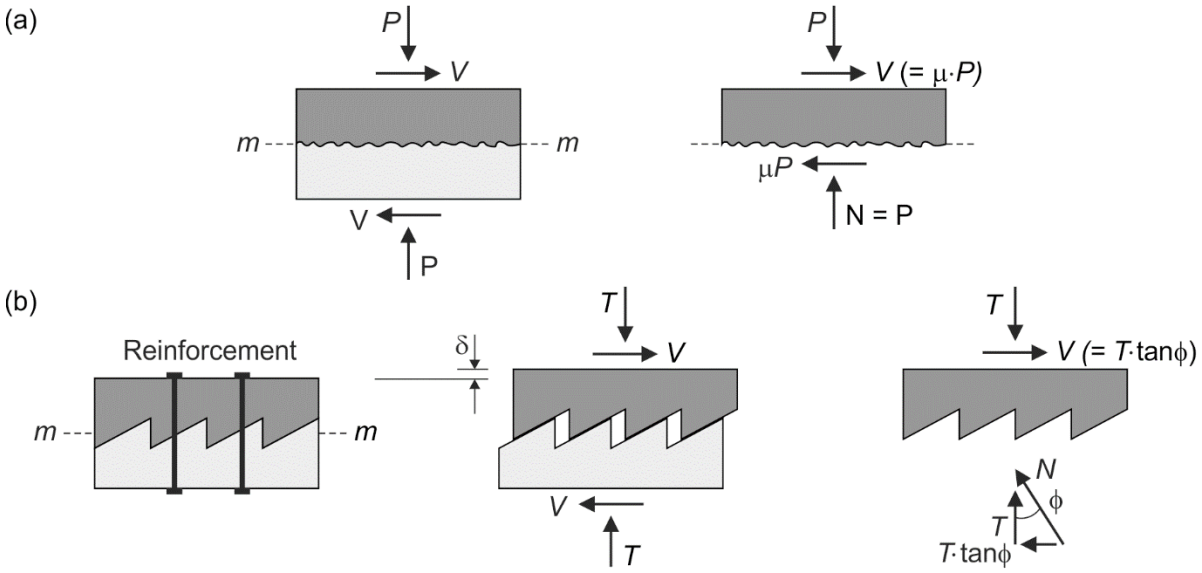

Figure 2-8: Applied forces and reaction forces at (a) a concrete interface and (b) a saw-tooth model of an interface according to the shear-friction theory [Bir66]

The external shear force V tends to produce slippage along the interface, which is resisted by the external clamping force P and the frictional force μP (Eq. (2-7)).

$$V = \mu \cdot P \tag{2-7}$$

For rough interfaces, the horizonal displacement also induces vertical displacement δ. If reinforcement crosses the interface, tension develops in the reinforcement bars. With the reinforcement sufficiently anchored at both sides of the interface, tensile stress in the reinforcement induce a clamping effect, which results in compression stress acting on the interface. The roughness is depicted by saw-teeth with an inclination of ϕ, which leads to the expression of shear force V in Eq. (2-8) (Figure 2-8(b)).

$$V = T \cdot \tan\phi \tag{2-8}$$

The ultimate shear capacity of the interface is reached when yielding of the reinforcement occurs ($T = A_s \cdot f_y$).

Considering the model concepts of *Mohr-Coulomb* and shear-friction theory for interface shear, Equation (2-6) can be rewritten with three main load bearing mechanisms [Ack92]. The interface shear resistance τ_{int} can then be expressed by Eq. (2-9). However, it must be mentioned that these three mechanisms are activated at different times of the loading process and occur at different stages of crack development.

$$\tau_{int} = \tau_{adh} + \tau_{fric} + \tau_{reinf} \tag{2-9}$$

With

τ_{adh} shear resistance due to adhesion

τ_{fric} shear resistance due to friction and aggregate interlock

τ_{reinf} shear resistance due to interface reinforcement

2.3.3 Load bearing mechanism

The main terms of interface shear resistance are adhesion, friction induced by normal stress (aggregate interlock) or by clamping of interface reinforcement. The mechanisms act at different displacement states and thus, exhibit a certain correlation. To investigate the load transfer across an interface, structural member tests can give a reflection of the real situation in the structure, including all effects of load bearing resistances. Nevertheless, to separately demonstrate the load bearing mechanisms, small size tests can give a more isolated understanding. In this context, Figure 2-9 shows a schematic depiction of the three load bearing mechanisms with corresponding qualitative shear stress-displacement curves determined by small size tests.

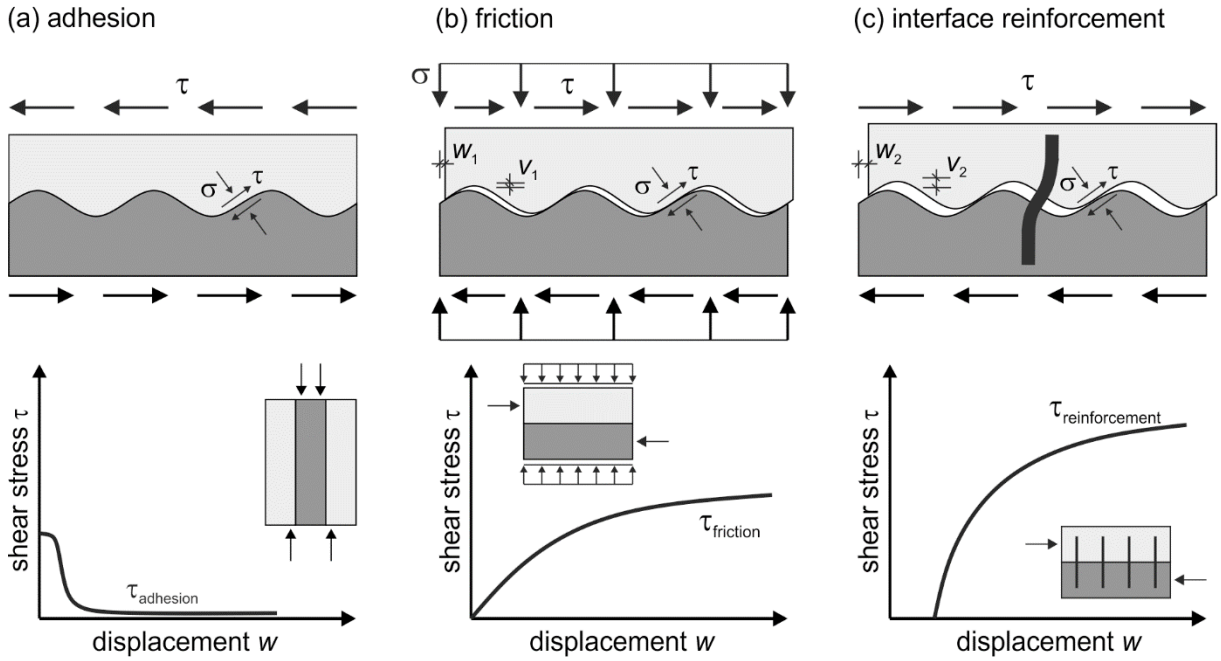

Figure 2-9: Schematic depiction of load bearing mechanisms for interface shear: (a) adhesion, (b) friction, (c) interface reinforcement

The interface roughness has a major effect on the terms of interface capacities. Therefore, Figure 2-10 shows shear stress-displacement curves determined by small size tests with different interface qualities according to [Ran08]. In the following, the mechanisms of adhesion, friction induced by normal stress and interface reinforcement are explained in detail.

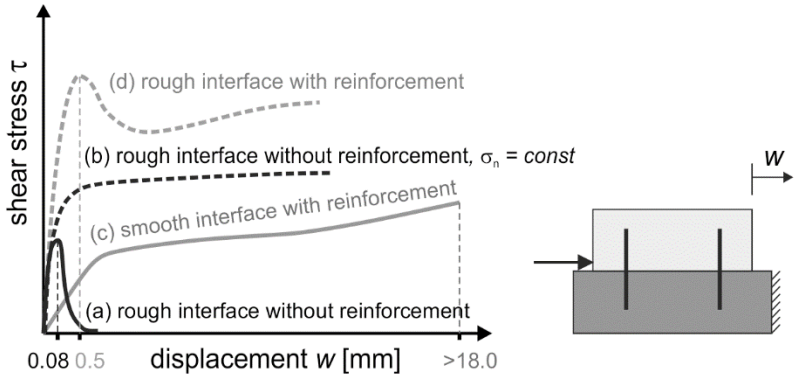

Figure 2-10: Test results of small size specimens with smooth and rough interfaces and with and without interface reinforcement conducted by [Ran08]

Adhesion

After casting the new concrete layer, adhesive bond occurs as a material property between old and new concrete. For adhesive bond, it can be distinguished between specific and mechanical adhesion [Zil10]. The specific adhesion is generally influenced by physical and chemical interaction on molecular level, as well as e.g. covalent and ionic bond. The mechanical adhesion occurs due to infiltration of the new concrete's liquid material in the pores of the old concretes by capillary forces, which develop a micro-mechanical interlock after concrete hardening.

High influences on strength of adhesive bond are concrete properties of both, old and new concrete, especially the concrete tensile strength, as well as size and roughness of the interface. Further influences are the absorbance of the old concrete, the flowability of the new concrete as well as the cleanness of the interface. In this context, [Len12] developed a design expression for uncracked interfaces, which also includes several additional influences, such as cement properties, structure of aggregates and humidity conditions. Extensive investigations on the behaviour of adhesive bond can be found e.g. in [Sch96a][Rei04][Mül09][Len12].

If shear stress act on the interface (Figure 2-9 (a)), the structural behaviour can be compared to monolithic structures until very small relative slip occurs and the adhesive strength is exceeded. According to [Ack92], the adhesive stress curves run constantly and then drops linearly after a relative slip of w = 0.02 mm. After a relative slip of w = 0.05 mm, no adhesive stress transfer can be assumed. The failure occurs abruptly and after unimpeded crack opening [Zil10]. In this context, Figure 2-10 (a) shows the shear stress-displacement curve of a small size specimen with a rough interface without interface reinforcement. In accordance to the schematic depiction in Figure 2-9 (a), the curve shows almost no relative slip of the interface until reaching the maximum adhesive bond stress. After adhesive failure, no shear stresses can be transfers and thus, relative slip increases.

Friction and aggregate interlock

An additional compressive stress acting perpendicular to the interface activates the load bearing mechanism of friction (Figure 2-9 (b)). After adhesive bond is exceeded and cracks develop along the interface, the compressive stress cause an interlocking effect of the aggregates and thus, further shear stress can be transferred. In this process, the crack opening increases with increasing relative slip. An important influence of the frictional resistance is the magnitude of the compressive stress and the roughness of the interface. With increasing roughness of the interface, larger interlocking effects lead to higher transferable shear stress. The shear stress-displacement curve in Figure 2-10 (b) shows for interfaces with constant compressive stress, a continuous transition between adhesive and frictional bond. According to [Zil10], the crack opening is controlled by the stress perpendicular to the interface and the micromechanical interlocking of the adhesive bond may still be partially present.

Among others, REINECKE [Rei04] investigated the influence of normal stress on the shear transfer across concrete interfaces. According to his investigations, the frictional resistance of sandblasted interfaces due to aggregate interlock fails after a relative slip of $w = 0.03 – 0.05$ mm and is independent of the applied normal stress. However, with increasing normal stress, higher shear stresses must be applied to achieve interface failure. For smooth interfaces, the maximum shear stress is reached after $w = 0.01$ mm, which may be caused by less interlocking possibilities of smooth surfaces compared to rough surfaces. According to [Rei04], the effect of concrete strength on aggregate interlock is subordinate.

Interface reinforcement

In cracked interfaces where adhesive bond is exceeded, the shear stress can only be transmitted by friction due to normal stress and the load bearing capacity of reinforcement crossing the interface. The stiffness of the structure with non-rigid bond depends mainly on the stiffness of the interface and thus, from the load bearing behaviour of aggregate interlock and interface reinforcement [Win13]. The load bearing behaviour of the interface reinforcement for non-rigid bond is influenced by the vertical and horizontal displacement of the interface (Figure 2-9 (c)) and can be described by a combination of dowel action (Figure 2-11 (a)) and clamping effect [Ack92][Ran97].

The activation of dowel action in the reinforcement bar occurs due to relative horizontal displacement of old and new concrete layer. For dowel action, it can be distinguished between the three mechanisms of bending, shear and a combined tension-shear (kinking), which occurs due to high displacements [Pau74] ((Figure 2-11 (b-d)). Requirements for a full activation of dowel action is a sufficient concrete cover and a sufficient embedding depth of the reinforcing bar [Ran97].

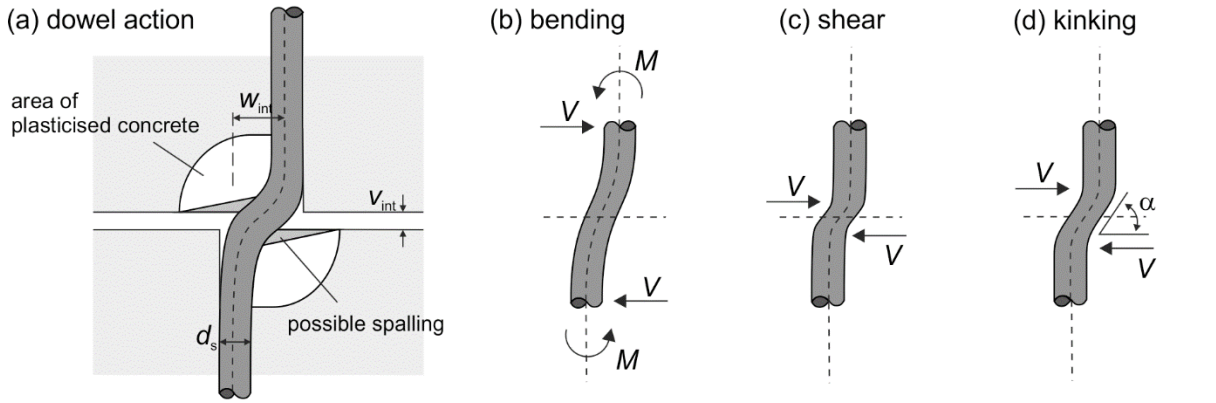

Figure 2-11: Schematic depiction of dowel action (a), and the load bearing mechanisms bending (b), shear (c) and kinking (d) [Pau74]

With sufficient concrete cover, a multi-axial stress state develops in the concrete surrounding the reinforcing bar at both sides of the cracked interface. After increasing interface displacement, the concrete plasticises in the curvature of the bent bar and the bar partially detaches from the concrete at the opposite side of displacement. Thus, for high displacements, no unimpaired bond between reinforcement and concrete can be assumed. With further increasing lever arm, the bending capacity of the bar becomes decisive for the load bearing resistance, which is achieved after a plastic hinge develops in the reinforcing bar. For bending failure, the bar should be embedded in the concrete with at least $6d_s$ at both sides. If no sufficient concrete cover is available, the bar may break the concrete cover and concrete failure occurs. According to [Zil10], the bending mechanism is decisive for dowel action. The mechanism of shear is subordinate and kinking only occurs after very large interface displacements and is therefore neglectable for common building practice.

Especially for rough interfaces, shear stresses lead to crack openings with vertical displacements v_{int} and longitudinal strain develop in the reinforcing bars. If the reinforcement bars are sufficiently anchored at both sides of the interface (a factor of 0.5 for σ_s/f_y is generally recommended [Ran13]), the steel stresses act in equilibrium with the compressive stress perpendicular to the interface plane and activate additional frictional forces (clamping effect). In this context, Figure 2-10 (c) and (d) show the shear stress-displacement curve of a smooth and a rough surface. For the smooth surface, the shear stress transition between adhesive bond the activation of reinforcement is smooth, whereas for the rough surfaces, the shear stress drops after an adhesive peak and can then be further increased due to the activated clamping effect. However, it must be mentioned that with high additional tensile stress in the reinforcing bar, the plastic bending moment decreases and thus, the achievable shear resistance reduces. If the bar is fully utilised for tension, it cannot contribute to the shear resistance due to dowel action [Zil10].

For reinforcing bars with an inclination towards the interface of $\alpha \neq 90°$, shear stress and horizontal slip induce longitudinal strains in the reinforcement which are independent

of the vertical displacement (crack opening) and thus, independent of the surface roughness. Therefore, the shear stress is partially carried by the reinforcement. However, it is assumed that only interface reinforcement perpendicular to the interface or inclined towards the direction of the relative slip can participate in the shear transfer mechanism [Zil10].

Superposition of load bearing mechanisms

For the general expression for interface shear, which includes the three load bearing mechanisms of adhesion, friction due to externally applied normal stress and reinforcement (Eq. (2-9)) [Ack92], the state of the horizontal displacement has a major effect on the activation of each load resistance term. The shear stress-displacement curves in Figure 2-10 show, that a superposition of the maximum terms would lead to an overestimation of interface resistance. Especially the necessary displacement to activate the term of reinforcement seems to be contrary to the activation of adhesion. However, due to the interaction of the three mechanisms, an isolated consideration is hardly possible. Thus, the interactional effects must be considered by evaluating experimental test data for the calibration of the coefficients for adhesion and friction [Zil10].

2.4 Classification of interface roughness

2.4.1 Introduction

The roughness of interfaces in concrete structures has an important influence on interface shear resistance. The general understanding of ‘roughness’ is the geometrical deviation of an ideal and smooth surface. For all structural cases, deviations appear on surfaces, but with varying dimensions. Regarding concrete surfaces, a fractal character appears with increasing resolution, showing fine topographies with similar fundamental structure [Zil04].

A general large-scale distinction of a surface profile can be made between global and local roughness (Figure 2-12 (a)). The global roughness, also called waviness, describes surface deviations with wavelength $\lambda > 10\,\text{cm}$ (Figure 2-12 (b) and (c)). The local or macro roughness characterises finer surface deviations due to e.g. surface roughening or exposure of aggregates. Micro roughness and microstructure describe small deviations caused by surface structure of aggregates or crystallisation (Figure 2-12 (c)). An overview of the scale of surface deviations according to [Rei04] is summarised in Table 2-1.

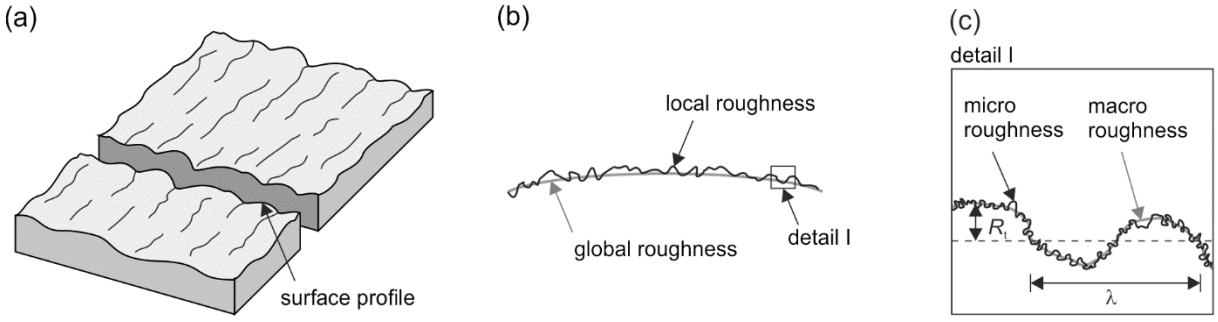

Figure 2-12: Surface profile of a concrete surface (a) [Vog17][D4287], example of global and local roughness (b) with detail (c) [Rei04]

Table 2-1: Scale of surface deviation according to [Rei04]

Roughness	Classification	Magnitude
global	large-scale deviation due to inaccurate concreting	$\lambda > 10$ cm $R_t < 3.5$ mm
local / macro	variable deviation due to intentional roughening of surface or exposure of aggregates	0.5 mm < R_t < 3.5 mm
micro	variable micro deviation due to surface structure of aggregates and deformations after e.g. sandblasting	10 µm < R_t < 0.5 mm
microstructure	deviation of crystallization	$R_t < 10$ µm

λ: wavelength of surface deviation; R_t: roughness depth as amplitude of surface deviation

In general, the understanding of roughness is not clearly determined and must be defined depending on the field of application. For example DIN EN ISO 13475-1 [D13473] and DIN EN ISO 4287 [D4287] define roughness parameters using a two-dimensional surface profile as a sectional plane through a concrete body (Figure 2-12 (a)). In common building practice, the roughness of a concrete surface is usually not defined by sectional profiles but by volumetric methods where the concrete surface is partially packed by a substrate. Knowing the volume and spreading behaviour of the certain substrate, the roughness of the surface can be implied.

To determine the roughness of an interface, it can be distinguished between comparative methods (e.g. photographic method), contracting methods (e.g. sand-patch-method or touching-method) and not contracting methods (e.g. laser-triangulation and photogrammetry). Whereas photographic methods only give subjective information about the surface roughness, touching methods and laser-triangulation can achieve an accurate detail of a surface profile with including a large number of surface parameters. A new development of surface projection is the photogrammetric method, which reflects a surface by a three-dimensional surface profile. The commonly used volumetric methods however, only determine one roughness parameter [Wie18][Zil04]. the following chapter presents commonly known methods for roughness classification as well as roughness parameters.

2.4.2 Methods for roughness classification

Photographic methods

The photographic documentation compares concrete surfaces only qualitatively. A comparison of a surface is only possible, if camera location and light-source are similar. Besides the angle of the camera, the distance of the light source has a significant influence on quality and interpretation of the documentation [Rei04]. A quantitative estimation of surface roughness by simple photographic methods is hardly possible. Further developments to achieve an accurate surface profiles and roughness parameter by photographic documentation are photogrammetric methods, introduced in the following.

Photogrammetric methods

Photogrammetric methods are not contracting methods which allows a three-dimensional measurement of a surfaces using image acquisition. Therefore, a database provides a number of images of the interface, depending on object size and accuracy. The images are taken regularly by the same camera from different perspectives. By using a multi-sectional evaluation procedure, a three-dimensional object can be reconstructed by two-dimensional images. Typical results of the measurement are spatial coordinates of single points, lattice models or textured 3D-photo models, which pattern a reconstruction of the surface. Using photogrammetric methods to determine the roughness parameters of concrete surfaces is still in the developing procedure. A detailed explanation of the basic approaches can be found in [Wie18].

Touching methods

With the touching method, surfaces are sensed mechanically by a fine tip. The tip is regularly moved line wise over the surface. By recording the horizontal and vertical displacement, surface profiles can be developed.

The touching method has its origin in mechanical engineering and was used in several research projects to determine the roughness of concrete surfaces (e.g. [Das86a], [Rei04], [Zil04]). The profile was recorded by inductive displacement sensors placed on a steel rail with measuring points in small distances. High resolutions comparable to optical measuring systems could not be achieved [Zil04].

Sand-patch method

An established and easy method to determine the roughness of a concrete surface is the sand-patch method according to KAUFMANN [Kau71]. For this volumetric method, a defined volume of sand with a certain grain size is applied on the concrete surface and circularly distributed with a plastic or wooden plate. If no further distribution is possible, the diameter of the sand circle is measured in at least two directions. With the parameter of the sand-volume V and the mean measured diameter d, the height of a fictive cylinder

can be determined (Figure 2-13). The height of the idealised cylinder corresponds to the mean roughness depth according to Eq. (2-10).

$$R_t = \frac{4 \cdot V}{\pi \cdot d^2} \tag{2-10}$$

According to [DA600], at least three measurements are necessary to determine the mean roughness depth of a concrete surface.

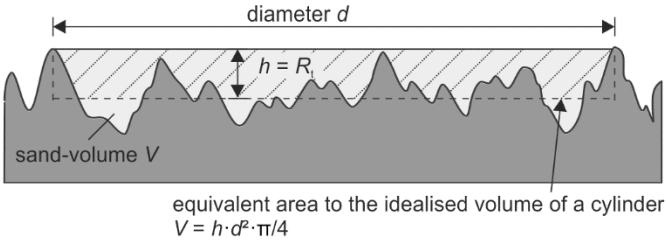

Figure 2-13: Definition of the roughness depth R_t determined by the sand-patch method according to KAUFMANN [Zil10]

In common building practice, the application of the sand-patch-method can follow different codes and guidelines. Even though the procedure is similar, the boundary conditions vary depending on the guideline and field of application. In this context, Table 2-2 summarised the common codes and guidelines for Germany.

Table 2-2: Codes and guidelines to determine the roughness with volumetric methods

Code	Substrate	Aggregate size [mm]	Quantity [cm³]	Tool
DAfStb Rili SIB	quartz-sand	0.1 – 0.3	25 – 50	wooden plate Ø 50 mm
DIN EN 1766	quartz-sand	0.05 – 0.1	5 – 25	plastic plate Ø 65 mm
DIN EN 13036-1	glass-sand	0.177 – 0.25	≥ 25	wooden plate Ø 50 mm
KAUFMANN	standard-sand (1)	0.063 – 0.2	~10 (14g)	wooden plate Ø 50 mm
ZTV-ING	quartz-sand	0.1 – 0.5	25 – 50	wooden plate Ø 50 mm

Source: DAfStb Rili SIB [DRi96]; DIN EN 1766 [D1766]; DIN EN 13036-1 [D13036], KAUFMANN [Kau71]; ZTV-ING [ZTV03]; (1): standard-sand I, fine grain (DIN 1164)

The applicability of the sand-patch method is limited to horizontal surfaces. Additionally, only one roughness parameter can be determined to describe the surface roughness. Furthermore, a reliable and reproduceable determination of the mean roughness depth is hardly possible since the accuracy of the results depend significantly from the experience and skill of the user [Vog17].

Laser-triangulation

A method to determine a two-dimensional surface profile is the laser-triangulation. This system comprises a point-laser-source, a sensitive detector and further optical components (Figure 2-14).

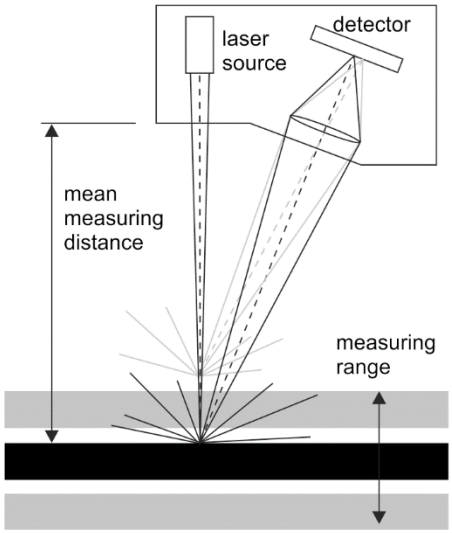

Figure 2-14: Illustration of a laser-triangulation system [Vog17][Wie18]

Laser source and detector are positioned in defined distance and angel to the surface. The emitted light of the laser source is diffusely reflected by the surface and partially sent back to the scanner. The scanner packs the light by an optic lens and impinges the detector. If the distance between laser source and surface varies, the point of the reflected light in the sensor changes likewise. Using simple geometrical relations, a distance can be calculated by the change of signal. These distances are recorded as coordinates, which develop a two-dimensional profile with different measuring points while reading a linear line with the laser beam. The simultaneous collection of measuring points leads to a short measuring time and high accuracy.

As stated in [Vog17] and [Wie18], it is not necessary to measure the whole concrete surface for calculating roughness parameters. Depending on the surface quality, about ten measurements with line profiles may be sufficient to guarantee a good statistic evaluation. Investigations by MELLMANN & OPPAT [Mell08] show a direct influence of the length of the measuring line regarding the correlation of the results measured by the sand-patch method and laser-based methods. The laser-triangulations systems presented in [Vog17] uses a measuring length of 50 mm with 640 measuring points. For comparison of other methods to determine the roughness of surfaces, [Mell08] introduces the two-dimensional parameter $R_{t,laser}$. By using additional mathematical adjustments, the results can be compared to the mean roughness depth determined by the sand-patch method. The required functions and factors were derived empirically by several comparisons between laser- and sand-patch method [Sch17]. A detailed description of the laser-triangulation method gives [Vog17].

2.4.3 Parameters to quantify the surface roughness

To quantify the roughness of an interface, several parameters were identified in literature. As an example, DIN EN ISO 4287 [D4287] defines parameters like the height of the maximum profile peak, the depth of the maximum profile valley, the maximum height difference of the profile and the mean height of the profile elements. A comprehensive introduction of the parameters and their correlation can be found in [San06], [San10] and [San13].

To identify the roughness of concrete interfaces, the most established parameters in literature and building practice are shown in Figure 2-15 [Sch96a]. The maximum profile height R_y describes the distance between the line touching the profile peaks (upper contact-line) and the line touching the profile valleys (lower contact-line). The maximum profile peak R_p defines the distance between the upper contact line and the centreline. In this context, the centreline intersects a profile section of a certain length with a minimum sum of quadratic profile deviations and thus, corresponds the results of a linear regression of measuring points along a profile surface.

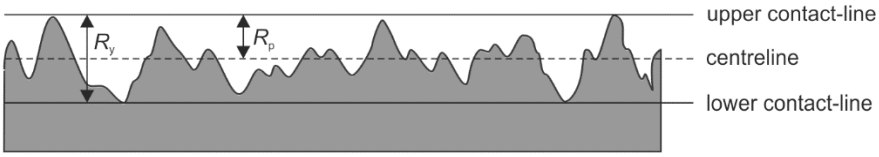

Figure 2-15: Examples of parameters to describe the roughness of an interface [Sch96a]

However, the aforementioned depiction of the determination of roughness methods and parameters shows that the roughness of an interface cannot be identified explicitly since the measurement and interpretation depend on a variety of influences such as roughness parameter, measuring method and range as well as data evaluation. For building practice, the measuring method must be convertible on site and reliable. Nevertheless, a high scatter and high dependency of the accomplishment must be expected for roughness measurement. Thus, the regulations need to consider these restrictions by constraints for a reliable estimation.

Additional information about parameters to quantify the surface roughness can be found in Annex C.1.

2.5 Fatigue of reinforced concrete and concrete interfaces

2.5.1 Introduction

Cyclic loading conditions in concrete structures may occur depending on field of application and use. For example in bridge structures, cyclic loading conditions occur due to traffic or rail loads. In industrial construction, cyclic loading may occur due to e.g. forklift traffic, oscillating machinery or crane runways as well as in wind power plants. For

construction materials, such as concrete and reinforcing steel, the recurrent loading may result in damage of the material's structure. Thus, the material resistance under cyclic loading is generally a lot smaller compared to the material strength under monotonic loading conditions. By further load repetition, the proceeding damage may lead to fatigue failure of the material.

The fatigue behaviour of reinforced concrete structures generally corresponds to the load bearing behaviour under static loading, but on smaller load levels. The failure modes depend on geometry, size, reinforcement type and degree of reinforcement as well as the type of loading (e.g. bending or shear). The common failure modes for static and fatigue failure are failure of longitudinal reinforcement or shear reinforcement, failure of concrete under compression or tension, failure of the compression strut or anchorage failure of longitudinal or shear reinforcement. However, the failure cause may be different for static and fatigue failure. For the shear capacity under cyclic loading conditions, a prediction of the decisive failure cause is hardly possible due to the crack formation and propagation as well as the resulting stress redistributions between concrete and reinforcement capacity [Tew14][Hil19].

Since structural members with horizontal concrete interfaces can be subjected to cyclic loading conditions, the interface shear resistance must also be verified for fatigue. Therefore, the fatigue behaviour of concrete and reinforcement must be considered. In this context, the fatigue behaviour of concrete interfaces as well as the structural fatigue design according to [EC2] and [EC2NAD] are presented in the following. The fundamentals of fatigue, as well as the fatigue behaviour of reinforcing steel and concrete can be found in Annex C.2.

2.5.2 Fatigue behaviour of concrete interfaces

The fatigue behaviour of concrete interfaces has only been roughly investigated to date. According to the common design concepts, rigid bond must be estimated under fatigue loading, which allows the assumptions of interface shear stress based on theory of elasticity. Due to fatigue loading however, the adhesive bond between the concrete layers can be reduced significantly [Zil10]. Thus, the basic failure mechanisms of concrete interfaces can be distinguished in adhesive failure and failure of interface reinforcement.

According to investigations by [Zil04] and [Chu76], adhesive failure can be excluded for fatigue loads with shear stress less than 50 % of the static interface shear resistance referred to $N \leq 1{,}000{,}000$ number of load-cycles. Due to the high scatter of fatigue resistance combined with the high scatter of interface shear resistance and the low number of systematic test series especially for large number of load-cycles, the value can only be described as an approximation. According to a number of interface fatigue test data evaluated by [Ran05], a ratio of fatigue to static interface strength of 40 % should be appropriate for $N = 2{,}000{,}000$ load cycles. Additionally, [Ran05] suggests interfaces

under high fatigue shear stresses (e.g. concrete toppings on bridges) to have at least a rough surface.

Assuming impaired adhesive bond under cyclic loading conditions, the clamping effect of the reinforcement leads to axial tension in the reinforcement bars crossing the interface and frictional bond is activated. Neglecting additional flexural influences in the bar due to horizontal displacement, the stress range in the interface reinforcement must be verified in accordance to the structural fatigue design presented in Chapter 2.5.3.

Test programmes investigating the fatigue behaviour of concrete interface will be presented in Chapter 4.2.5 and 4.3.4.

2.5.3 Structural fatigue design

The fatigue verification according to the provisions in Eurocode 2 [EC2] and Eurocode 2 with the National Annex of Germany [EC2NAD] distinguish between fatigue design of concrete and fatigue design of reinforcement. As shown in Figure 2-16, the verification of concrete generally limits the maximum and minimum compressive stress for compression and the maximum and minimum shear force for shear without shear reinforcement. The verification of reinforcement is structured in three stages with increasing calculating effort.

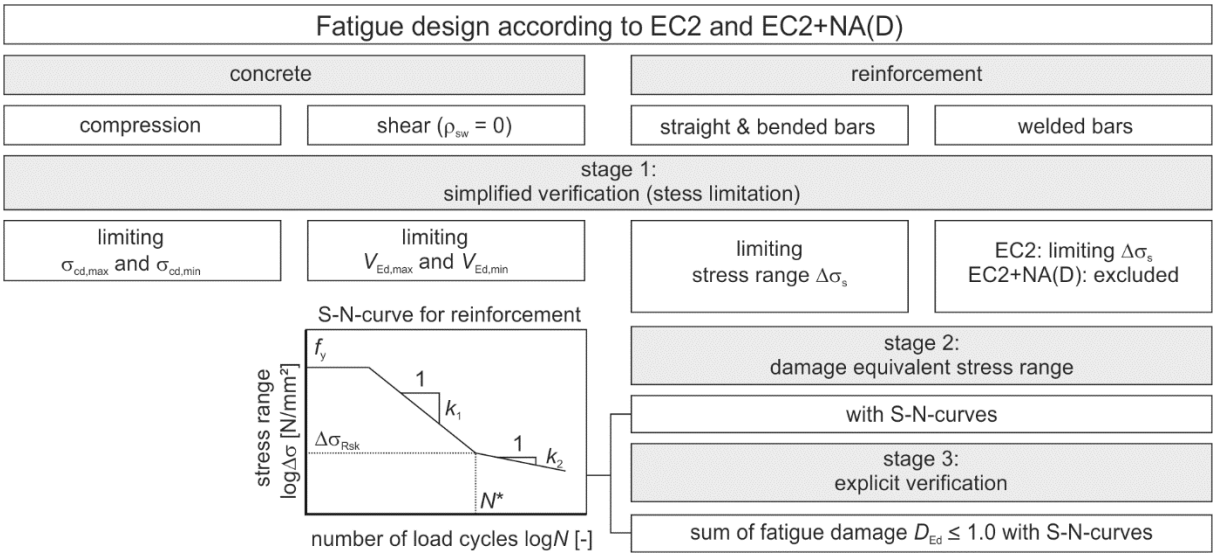

Figure 2-16: Stages of fatigue design for concrete and reinforcement according to EC2 [EC2] and EC2+NA(D) [EC2NAD]

The verification according to stage 1 for reinforcement bars under tension limits the acting stress range in the reinforcement under the frequent load combination $\Delta\sigma_{s,freq}$ to an evaluated approved stress range $\Delta\sigma_{s,app}$ for high number of load cycles of $N = 10$ million, $\Delta\sigma_{s,app}$ as shown in Eq. (2-11).

$$\Delta\sigma_{s,freq} \leq \Delta\sigma_{s,app} \tag{2-11}$$

Whereas [EC2] allows a stress limitation in stage 1 for both, straight and bent as well as welded bars, [EC2NAD] only allows the simplified verification for straight and bent bars. For welded bars and reinforcement steel mashes, the approved stress ranges are generally regulated in general technical approvals.

In stage 2, the verification limits a damage equivalent stress range $\Delta\sigma_{S,equ}$ in accordance to Eq. (2-12).

$$\gamma_{F,fat} \cdot \Delta\sigma_{S,equ} \leq \frac{\Delta\sigma_{Rsk}}{\gamma_{S,fat}} \tag{2-12}$$

The acting stress range is described by a stress range $\Delta\sigma_{S,equ}$ which causes an equivalent damage for N^* load cycles as operating loads acting in the specified life cycle. The fatigue resistance for straight and bent as well as welded bars $\Delta\sigma_{Rsk}$ can be calculated for N^* load cycles by S-N-curves given in the codes. The partial safety factor for applied fatigue loads is set to $\gamma_{F,fat} = 1.0$ and for the fatigue resistance of reinforcing steel to $\gamma_{S,fat} = 1.15$.

The explicit verification of stage 3 is the most economic and explicit verification for fatigue. For multiple stress cycles with different stress ranges, the damages are added according to the linear damage accumulation hypothesis of *Palmgren Miner* and must fulfil the sum of damages D_{Ed} caused by the decisive fatigue load as stated in Eq. (2-13).

$$D_{Ed} = \sum_{i=1}^{j} D_{Ed} = \sum_{i=1}^{j} \frac{n(\Delta\sigma_i)}{N(\Delta\sigma_i)} \leq 1.0 \tag{2-13}$$

For every applied stress range $\Delta\sigma_i$, the ratio of applied load cycle n and bearable load cycle N is added. The bearable load cycle N can be determined by the S-N-curves of the reinforcement depending on the approved stress range $\Delta\sigma_{Rsk}$ for N^* load cycles and the gradients k_1 and k_2 defining the scope for fatigue strength as well as endurance strength (Figure 2-16). The parameters describing the S-N-curve are defined in [EC2] and [EC2NAD] for straight and bent as well as for welded bars.

3 Models for horizontal interface shear transfer

3.1 Introduction

The development of models to describe the shear transfer across concrete planes and interfaces started in the 1960 with first formulations of the shear friction theory. For longitudinal shear, the shear friction theory is a generally excepted theory which was modified and extended by various researchers and is the bases for most current design expressions. The fundamental understanding of interface shear is based on investigations with shear transfer across interfaces between concrete cast at different times as well as the shear transfer across concrete cracks.

In the following, the development of different model concept to describe the interface shear transfer across concrete interfaces from literature are presented. Based on these model concepts, design expression and regulation were determined. In this context, this chapter introduces the design expression of Eurocode 2 [EC2], Eurocode 2 with the National Annex of Germany [EC2NAD], the draft for the new Eurocode 2 [prEC2:18], Model Code 2010 [MC10], as well as the two prevailing concrete design codes in the United States of America, ACI 318-14 [ACI318] and AASHTO LRFD Bridge Design Specifications [AA-L].

3.2 Development of models for horizontal interface shear

3.2.1 Introduction

The beginning of developing models to describe the shear transfer across a shear plane was made by ANDERSON [And60] in the 1960s. Based on this model, researchers modified the expression by considering the influence of static system and normal stress perpendicular to the shear plane. In the mid-1960s, BIRKELAND & BIRKELAND [Bir66] developed the shear friction theory, which is generally accepted by researchers until today. The formulation was extended and modified by several researches over the decades. Other milestones in the development of interface shear formulations can be named MATTOCK & HAWKINS [Mat72] who developed the modified shear friction theory considering the influence of cohesion, the model of LOOV [Loo78] who introduced the effect of concrete strength, WALRAVEN [Wal81] and [Wal87] who investigated the effect of aggregate interlock and TSOUKANTAS & TASSIOS [Tso89] introduced a slip based formulation with considering the effect of clamping stress and dowel action of the interface reinforcement, followed by ACKERMANN [Ack92] and RANDL [Ran97] who developed expressions considering the parts of adhesion, friction induced by external compressive stress as well as compressive stress due to clamping of reinforcement. RANDL [Ran97] additional introduces the term of dowel action to the design expression.

Besides concrete interfaces with prepared or unprepared surfaces between concrete cast at different times, as well as with and without interface reinforcement, the shear transfer across crack interfaces in precracked concrete specimens were investigated by many researchers. Even though this thesis only comprises interfaces between concrete cast at different times, investigations with precracked specimens have a high influence on the model development for interface shear transfer. The initiation of the development of models for horizontal interfaces as well as other models which are not presented in this chapter can be found in Annex C.3. Since some parameters in the presented design equations were derived in imperial units, for the sake of a consistency, all parameters were translated to metric units.

3.2.2 Model of BIRKELAND & BIRKELAND

The development of the shear friction theory started in 1966 by BIRKELAND & BIRKELAND [Bir68]. The shear friction theory idealises a concrete interface to a regular sawtooth model, where the shear stress is transferred across the interface by friction due to tensile stress in the reinforcement (s. Chapter 2.3.2). They proposed a linear expression to calculate the shear force resistance V according to Eq. (3-1).

$$V = A_s \cdot f_y \cdot \tan\phi = A_s \cdot f_y \cdot \mu \;\leftrightarrow\; v_u = \rho \cdot f_y \cdot \mu \tag{3-1}$$

With

A_s	cross-sectional area of reinforcement
f_y	yield strength of reinforcement
ϕ	internal angle of friction
μ	friction coefficient ($\tan\phi = \mu$)

At this state, the friction coefficient μ was determined empirically for monolithic structures, intentionally roughened concrete surfaces as well as smooth concrete interfaces and interfaces between concrete and steel. Furthermore, application limits were defined with a maximum reinforcement ratio of 1.5 %, a maximum shear stress of 5.52 N/mm^2 and a minimum concrete strength of 27.58 N/mm^2.

According to [San09] and [Pat92], BIRKELAND [Bir68] modified his initial expression of shear friction theory (Eq. (3-1)) to a nonlinear term by parabolic fitting, which reduces the effect of larger reinforcement degrees and yield strength to the influence on the ultimate shear stress v_u (Eq. (3-2)).

$$v_u = \mu \cdot \sqrt{\rho \cdot f_y} \tag{3-2}$$

3.2.3 Model of MATTOCK & HAWKINS

A modified shear friction theory was developed by MATTOCK & HAWKINS [Mat72] for shear transfer across a crack in monolithic concrete. They described the shear resistance

by a function including the capacities of cohesion, which was defined as a constant of 1.38 N/mm² as well as the capacities of externally applied normal stress σ_n and reinforcement (Eq. (3-3)).

$$v_u = 1.38\ (\text{N/mm}^2) + \mu \cdot (\rho \cdot f_y + \sigma_n) \tag{3-3}$$

With
μ friction coefficient ($\mu = 0.8$ for monolithic concrete)
f_y yield strength of reinforcement
σ_n normal stress of interface

The upper limit of shear transfer was defined to be dependent of the concrete strength or an experimentally derived constant (Eq. (3-4)).

$$v_{max} = \min \begin{Bmatrix} 0.3 \cdot f_c \\ 10.34\ \text{N/mm}^2 \end{Bmatrix} \tag{3-4}$$

Following the investigations in [Mat72], MATTOCK [Mat74] modified the expression of Eq. (3-3) using average values derived from further investigations. Therefore, he increased the capacity of cohesion to 2.76 N/mm². Additionally, he extended the expression to account the effect of inclined interface reinforcement (Eq. (3-5)).

$$v_u = 2.76 \cdot \sin^2\theta + \rho \cdot f_s \cdot (\mu \cdot \sin^2\theta - 0.5 \cdot \sin 2\theta) \tag{3-5}$$

With
θ angle between interface and reinforcement
μ friction coefficient ($\mu = 0.8$ for monolithic concrete)
f_s effective strength of reinforcement
with $f_s = 0$ for $0 \le \theta < 51.3°$
$f_s = -1.6 \cdot f_y \cdot \cos(\theta + 38.7°)$ for $51.3° \le \theta < 90°$
$f_s = f_y$ for $90° \le \theta \le 180°$

The limitations regarding the effective steel resistance were determined by experimental results. The investigations show that bars with an inclination parallel to the compressive strut were subjected to compression (Figure 3-1 (a)), whereas bars with higher inclinations until an angle of $\theta = 90°$ to the interface were partially subjected to compressive and partially to tensile strain (Figure 3-1 (b)). Bars with inclinations $\ge 90°$ were subjected to considerable tensile strains (Figure 3-1 (c)).

In [Mat75], MATTOCK ET AL. compared investigations of corbel type push-off tests to the calculated shear strength according to the nonlinear expression of the shear friction theory [Bir66] and to the modified shear friction theory [Mat72]. The comparison showed less conservative results for the evaluation with the formulation of the modified shear friction theory.

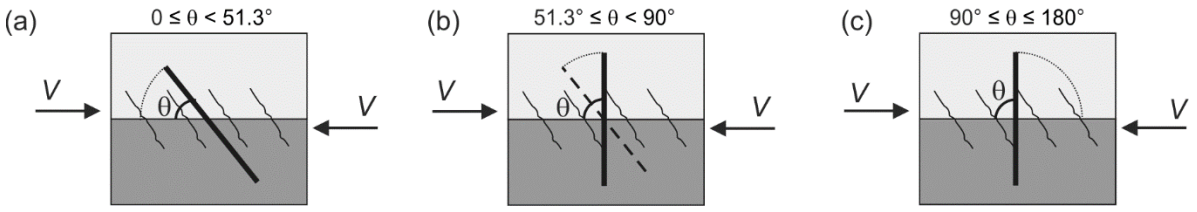

Figure 3-1: Limits of inclination of interface reinforcement regarding the effective strength of the reinforcement

Following the model of [Wal81] (s. Chapter 3.2.5), which considers the effect of concrete strength on shear friction resistance, MATTOCK [Mat88] introduces the effect of concrete strength on the term of cohesion, which results in the expression according to Eq. (3-6)).

$$v_u = 0.467 \cdot f_c^{0.545} + \mu \cdot (\rho \cdot f_y + \sigma_{pu}) \leq 0.3 \cdot f_c \tag{3-6}$$

MATTOCK [Mat81] (cited by [San09]) investigated the effect of cyclic loading on the shear transfer across concrete interfaces. Therefore, he adopted his design expressions for normal weight and lightweight concrete to test results under cyclic loading conditions. To calculate the fatigue shear resistance, he reduces the ultimate shear strength to 80 % for monolithic sections and rough interfaces, and to 60 % for cracked interfaces.

3.2.4 Model of LOOV

The first researcher who explicitly introduced the influence of concrete strength to the expression of the nonlinear shear friction theory was LOOV [Loo78], cited by [Pat92] and [San09]. The expression for the ultimate shear resistance follows Eq. (3-7).

$$\frac{v_u}{f_c} = k \cdot \sqrt{\frac{\rho \cdot f_y + \sigma_n}{f_c}} \tag{3-7}$$

With

f_c concrete compressive strength

k constant (0.5 for initially uncracked concrete)

Following the model of LOOV, the influence of concrete strength was considered in various expressions for interface shear, based on shear friction theory and the modified shear friction theory.

To extend the formulation in Eq. (3-7) to concrete composite beams with rough interfaces, LOOV & PATNAIK [Loo94] considered the effect of concrete density and introduced Eq. (3-8).

$$v_u = k \cdot \lambda \cdot \sqrt{(0.1 + \rho \cdot f_y) \cdot f_c} \tag{3-8}$$

With

k constant (0.5 for composite and 0.6 for monolithic sections)

λ coefficient for concrete density

3.2.5 Model of WALRAVEN

To describe the shear transfer across a concrete crack due to aggregate interlock, WALRAVEN [Wal81] developed a stochastic two-phase model. The model idealises the aggregates as spherical particles which are embedded in a cement matrix. Since the stiffness of the aggregates is generally stiffer than the stiffness of the cement matrix, the crack development surrounds the particles as shown in Figure 3-2 (a).

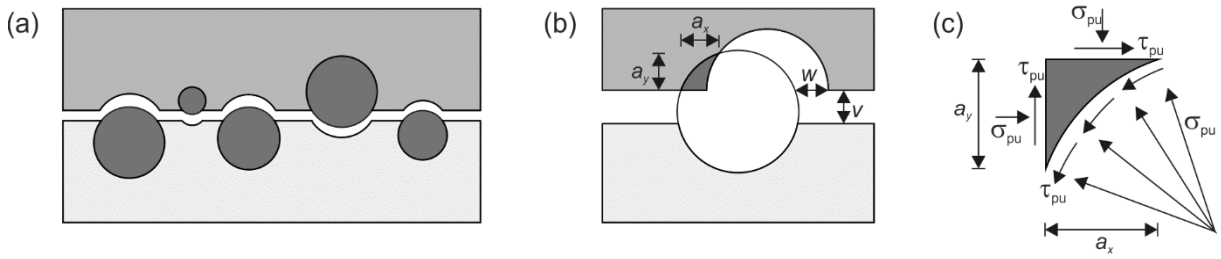

Figure 3-2: Structure of crack plane (a), contact area between cement matrix and aggregate (b), stress contribution at contact are due to shear displacement (c) [Wal81]

The particles across the concrete plane are randomly distributed and the particle rate is affected by the grading curve. Due to shear displacement, the particles intrude the cement matrix (Figure 3-2 (b)) and a stress distribution along the contact area occurs. The radial normal stress σ_{pu} and tangential shear stress τ_{pu} (Figure 3-2 (c)) are generally defined according to Eq. (3-9).

$$\tau_{pu} = \mu \cdot \sigma_{pu} \tag{3-9}$$

For friction across a concrete crack, [Wal81] introduces a friction factor of $\mu = 0.4$ which is independent of aggregate grading and concrete strength. To define the shear stress at a concrete crack, the stress at all contact areas are integrated considering crack width, shear displacement, maximum particle size and total aggregate volume per unit volume of concrete. According to [Ran97], the model gives a good estimation for shear transfer across a crack plane compared to experimental results.

By further investigations, WALRAVEN ET AL. [Wal87] considered the effect of concrete strength on the shear friction capacity. Based on the model describing aggregate interlock [Wal81], they developed the expression written in Eq. (3-10).

$$v_u = C_1 \cdot (\rho \cdot f_y)^{C_2} \tag{3-10}$$

With

C_1, C_2 factor considering the concrete strength

$C_1 = 0.822 \cdot f_{c,cube}^{0.406}$

$C_2 = 0.159 \cdot f_{c,cube}^{0.303}$

with

$f_{c,cyl} = 0.85 \cdot f_{c,cube}$ (150 mm)

3.2.6 Model of TSOUKANTAS & TASSIOS

The researchers TSOUKANTAS & TASSIOS [Tso89] published a research programme with interface shear specimens under monotonic and cyclic loading conditions. They determined a high influence on the load bearing resistance due to horizontal and vertical displacement of the interface as well as by the acting normal stress perpendicular to the interface.

The developed model describes the ultimate shear force at an interface V_u as a sum of the shear frictional resistance due to compressive force acting on the interface F_{fric} and the shear resistance due to dowel action D_{dow} (Eq. (3-11)), both depending on the horizontal shear displacement s. The frictional resistance was derived experimentally for smooth and rough interfaces.

$$V_u = F_{fric} + D_{dow} \tag{3-11}$$

In this context, Figure 3-3 (a) shows the qualitative curve of the ratio of frictional shear stress τ_{fr} and ultimate frictional shear stress $\tau_{fr,u}$ over the ratio of displacement s to ultimate displacement s_u for smooth and rough surfaces.

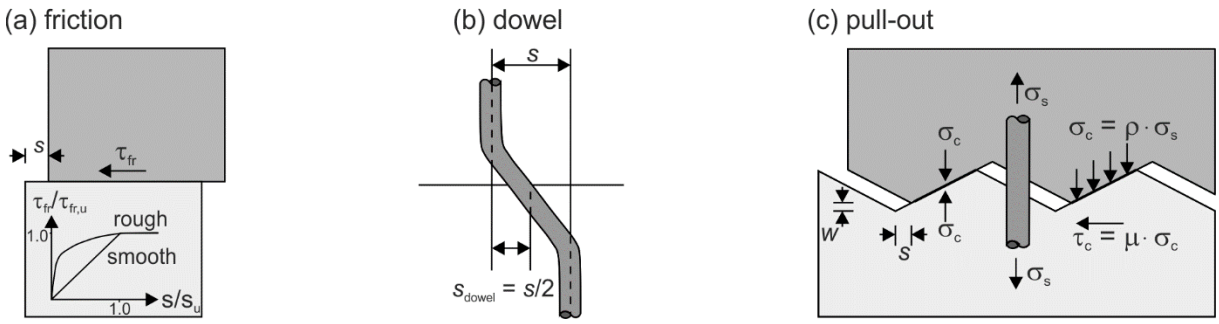

Figure 3-3: Effect of displacement on the mechanisms of friction (a), dowel action (b) and axial stress (c) according to [Tso89]

They developed a relation of the ultimate frictional force F_{fric} considering the normal stress at the interface due to internal and external loads σ_c over the area of the interface A_{int} for smooth and rough interfaces according to Eq. (3-12) and (3-13), where only the

frictional shear stress of a rough interface is dependent on the characteristic concrete compressive strength f_{ck}.

$$F_{fric,smooth} = 0.4 \cdot \sigma_c \cdot A_{int} \tag{3-12}$$

$$F_{fric,rough} = 0.5 \cdot \sqrt[3]{f_{ck}^2 \cdot \sigma_c} \cdot A_{int} \tag{3-13}$$

The effect of dowel action accounts for a displacement of $s_{dowel} = s/2$ (Figure 3-3 (b)). Besides the effect of dowel action, the formulation in Eq. (3-14) considers the effect of axial stress in the reinforcement (Figure 3-3 (c)), position of dowel, as well as the effect of concrete strength.

$$D_{dow} = 0.5 \cdot \delta \cdot d_b^2 \cdot \sqrt{f_{ck} \cdot f_y \cdot (1 - \xi^2)} \tag{3-14}$$

With

δ position of dowel regarding the concrete cover

d_b diameter of dowel

ξ effect of axial stresses acting simultaneously in the bar
$\xi = \sigma_s / f_y$

TSOUKANTAS & TASSIOS [Tso89] also investigated the effect of cyclic loading conditions on the interface shear transfer. Previous research conducted by e.g. CHUNG & CHUNG [Chu76], MATTOCK [Mat81] and WALRAVEN [Wal87] with test specimens under cyclic loading conditions limit the ultimate shear stress at the crack or interface by reducing the static strength to $\tau_{fat} = 0.55 \cdot \tau_{stat}$ [Chu76], $0.60 \cdot \tau_{stat}$ [Mat81] and $0.65 \cdot \tau_{stat}$ [Wal87]. By applying these limitations, a fatigue failure can be prevented.

Nevertheless systematic experimental data under cyclically imposed slip was missing, TSOUKANTAS & TASSIOS [Tso89] assumed a reduction of shear resistance for fully reserved displacement according to Figure 3-4.

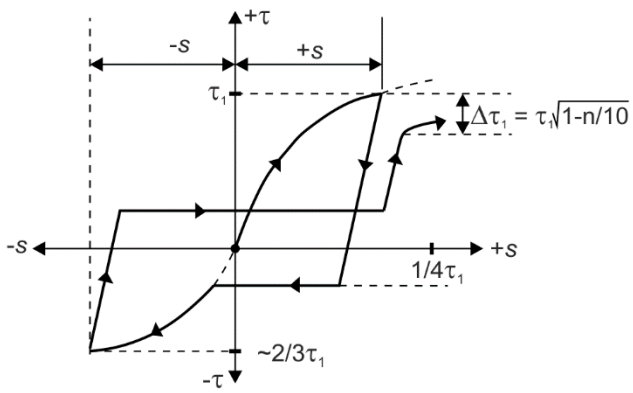

Figure 3-4: Assumed shear stress-displacement curve under reversed displacement [Tas87][Tso89]

By experimental investigations in [Tas87], an empirical expression of frictional degradation was derived to give an estimation of the ratio of the frictional resistance after n load cycles compared to the resistance of one cycle. The expression considers the slip after n load cycles s_n and the ultimate slip under monotonic loading s_u (Eq. (3-15) and (3-16)). Even though the expression generally accounts for cyclic loading, tests were conducted to only six load cycles.

$$\frac{\tau_{fric,n}}{\tau_{fric,1}} = 1 - \frac{1}{7} \cdot \sqrt{n-1} \text{ for } s_n > s_u \text{ (smooth)} \tag{3-15}$$

$$\frac{\tau_{fric,n}}{\tau_{fric,1}} = 1 - \left[0.002 \cdot (n-1) \cdot \left(\frac{\sigma_c}{f_c} \right)^{-1} \cdot \frac{s_n}{s_u} \right]^n \text{ (rough)} \tag{3-16}$$

Besides the estimation of the frictional shear resistance, the stress range in the reinforcement under cyclic loading conditions was limited to 33.3 % of the steel stress in the reinforcement depending on the slip of the bar.

Based on the investigations of TSOUKANTAS & TASSIOS [Tso89], ACKERMANN [Ack92] presents a formulation considering the interface shear displacement. Regarding the effect of reinforcement, he distinguishes between the load bearing resistance due to clamping effect and dowel action by the model of an elastically embedded bar. Considering the minimum amount of interface reinforcement, he suggested reinforcement which fully covers the adhesive capacity of the interface to achieve ductile structural behaviour. However, high minimum reinforcement degrees appear by this expression.

3.2.7 Model of RANDL

The model developed by RANDL [Ran97] follows the assumptions made by [Ack92], but considering the maximum load resistance for every limit state. In accordance to [Ack92], he describes the interface shear resistance by the sum of the three load bearing capacities adhesion, friction and reinforcement. For the reinforcement term, he distinguished between clamping effect (tensile forces in the reinforcement increase the frictional resistance) and dowel action (reinforcement subjected to bending and shear).

The effects of adhesive and frictional bond were considered based on theory of plasticity with *Coulombs* shear friction hypothesis and the effect of the clamping stress is based on the shear friction theory. For considering the effect of dowel action, he idealises the reinforcement bar as an elastically supported beam which is embedded at one side of the interface. After horizontal displacement and concrete plasticisation near the concrete surface, a plastic hinge develops in the bar due to maximum moment which leads to ultimate limit state. The maximum stress p_{max} in the plastic zone of the concrete h (Figure 3-5 (a)) is assumed to be rectangular, whereas the stress distribution σ_b underneath the plastic zone z_1 is simplified with ideal-elastic behaviour in accordance to the assumption of an elastically simply supported beam [Ran13].

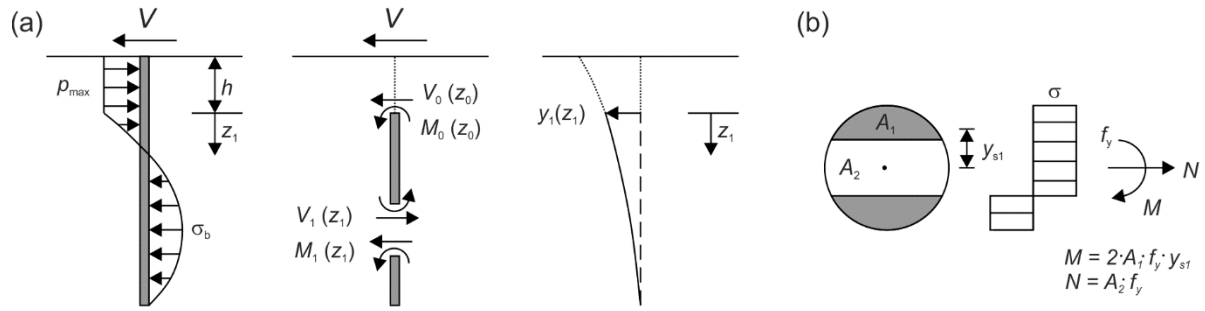

Figure 3-5: Model of an idealised embedded dowel under shear loading (a), M-N-interaction of a bar section for an interface shear connector (b) [Ran13]

According to the results of an experimental programme (s. Chapter 4.2.4), an increase of normal stress in the interface reinforcement subjected to horizontal displacement is nor possible until reaching the yield strength of the steel, which may be explained by the interaction of moment and normal forces in the reinforcement (Figure 3-5 (b)). He also found a direct correlation between interface roughness and the ratio of dowel action and clamping effect. For rough interfaces, higher vertical displacement could be determined after horizontal displacement compared to smooth interfaces which leads to the assumption of higher clamping action.

The proposed design expression is given in Eq. (3-17).

$$\tau_u = \tau_{uc} + \mu \cdot (\rho \cdot \kappa \cdot f_y + \sigma_n) + \alpha \cdot \rho \cdot \sqrt{f_y \cdot f_c} \tag{3-17}$$

With

τ_{uc}	shear resistance of adhesion
μ	coefficient of friction
ρ	interface reinforcement ratio
κ	coefficient of efficiency for tensile forces in the reinforcement
f_y	yield strength of reinforcement
σ_n	normal compressive stress
α	coefficient of flexural resistance of the reinforcement
f_c	concrete compressive strength

An extensive description of the model can be found in e.g. [Ran97] and [Ran13].

3.2.8 Discussion of models

As mentioned above, milestones of the development of model concepts for interface shear can be named shear friction theory by BIRKELAND & BIRKELAND [Bir66], modified shear friction theory by MATTOCK & HAWKINS [Mat72], consideration of concrete strength by LOOV [Loo78] and aggregate interlock by WALRAVEN [Wal87], as well as an expression considering three slip-independent load bearing mechanisms of adhesion,

friction and reinforcement by ACKERMANN [Ack92] and RANDL [Ran97]. For comparison, Figure 3-6 shows the calculate shear strength over the interface reinforcement ratio for a concrete with a compressive strength of f_c = 30 N/mm² and a smooth interface (a) as well as a rough interface (b). Since the presented model of TSOUKANTAS & TASSIOS [Tso89] describes the term of dowel action using parameters not considered in the compared equations, the model was not included in the comparison.

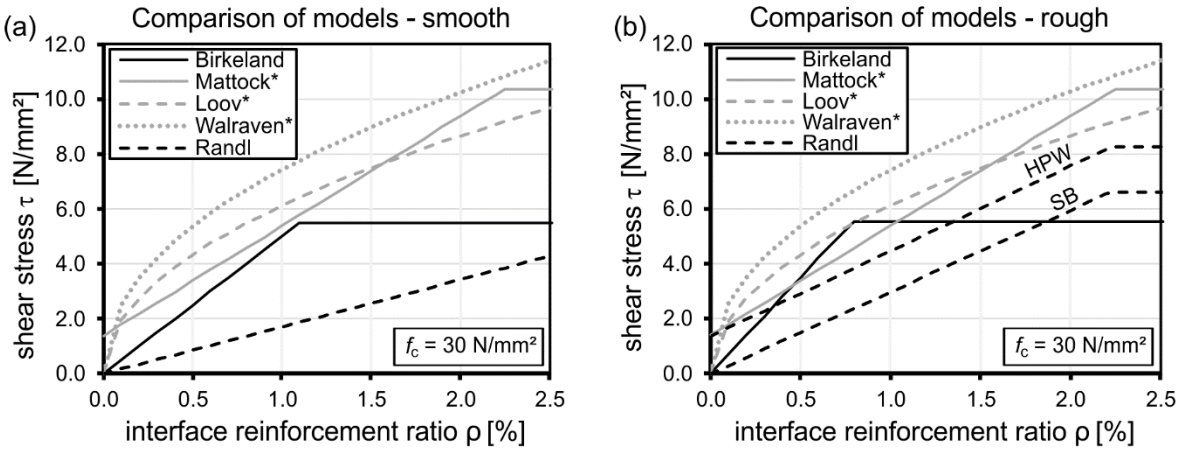

Figure 3-6: Comparison of milestones of interface shear models for smooth (a) and rough interfaces (b)

The basic expressions according to MATTOCK & HAWKINS, LOOV and WALRAVEN were initially derived to describe the shear transfer across a concrete crack and thus, are independent of the surface roughness (grey lines). The expression according to WALRAVEN shows a strong and nonlinear increase of calculated shear stress with increasing reinforcement ratio followed by the expression of LOOV. The curve according to MATTOCK & HAWKINS considers the adhesive resistance with 1.38 N/mm² and shows a linear increase until the upper limit for shear stress is reached.

The roughness dependent formulations of BIRKELAND & BIRKELAND and RANDL (black lines) show a linear curve limited by the maximum shear capacity. For shear friction theory, the effect of increasing roughness only results in a steeper inclination and thus, higher calculated shear stress for smaller reinforcement ratios. The formulation according to RANDL shows a slight increase of shear stress for smooth interfaces which does not reach the upper shear stress limit in the observed limits. For rough interfaces, sandblasted interfaces (SB) and interfaces subjected to high-pressure water (HPW) show a similar inclination of the curve. Even though both interface treatments result in rough interfaces, the expression does not allow a consideration of adhesive bond for sandblasted surfaces.

3.3 Interface shear models in current design concepts

3.3.1 Introduction

Based on the models presented in Chapter 3.2, design equations were derived to verify the interface shear resistance in composite beam or slab structures for different design codes. In the following, the formulations according to Eurocode 2 (EC 1992-1-1:2004) [EC2], Model Code 2010 [MC10], as well as the two prevailing concrete design codes in the United States of America, ACI 318-14 [ACI318] and AASHTO LRFD Bridge Design Specifications [AA-L] are presented. For Eurocode 2, the regulations differ for the European standardised version EC 1992-1-1:2004 [EC2], the national annex of Germany [EC2NAD] and the draft for the next Eurocode 2 prEN1992-1-1:2018 [prEC2:18]. Therefore, the expressions are presented separately.

Generally, the expressions formulated in all codes are based on the assumptions made by shear friction theory and modified shear friction theory and define of the load bearing capacities of adhesion, friction induced by normal stress and reinforcement. The applied shear stress must not exceed the interface shear resistance with satisfying a certain level of safety. None of the following design expressions includes the effect of constrains on the applied stress, e.g. by irregular shrinkage of the two concrete layers. Additional verifications regarding crack width or deflection must not be considered. The aim of the design expressions is to achieve a quasi-monolithic lead bearing behaviour of the structure.

Whereas the provisions according to [EC2], [EC2NAD], [prEC2:18] and [MC10] only account for interfaces with concrete cast at different times, the provisions according to [ACI318] and [AA-L] also allow the calculation of interface shear resistance across a shear plane in a concrete crack.

For the sake of consistency, the formulations in the American codes, which are originally formulated in imperial units, were translated to metric units.

3.3.2 Provision of EC2:2004

The interface shear provision adopted in [EC2] are based on the regulations published in Model Code 1978 [MC78] and Model Code 1990 [MC90]. For verification, the interface shear resistance v_{Rdi} must exceed the applied shear stress v_{Edi} (with index i for interface) according to Eq. (3-18).

$$v_{Edi} \leq v_{Rdi} \tag{3-18}$$

For horizontal shear due to composite action in beam and slab structures, the applied shear force can be determined by internal force balance (Chapter 2.2.3) and described by Eq. (3-19).

$$v_{Edi} = \beta \cdot V_{Ed} / (b_i \cdot z) \tag{3-19}$$

With

β ratio of the transferable normal force across the interface
interface in tension zone: $\beta = 1{,}0$
interface in compression zone: $\beta = F_{cdi} / F_{cd} \leq 1{,}0$ (Figure 3-7 (a))
with
F_{cdi} for the normal force in the insitu concrete layer
F_{cd} for the resulting compression force of the section

V_{Ed} acting shear force

b_i width of interface

z lever arm of internal forces in the composite section ($z = 0.9 \cdot d$)

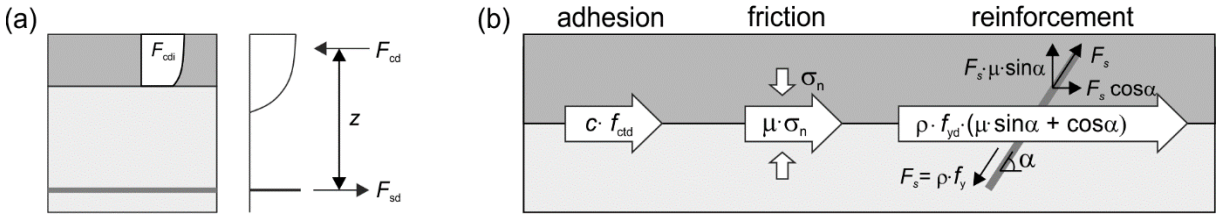

Figure 3-7: Transferable normal stress across an interface in the compression zone (a), design model of interface shear according to EC2 (b) [Fin16]

The interface resistance includes the load bearing terms of adhesion, friction and reinforcement (Figure 3-7 (b)) and can be summarised to Eq. (3-20) with additionally limiting the interface resistance to a maximum interface resistance depending on the concrete strength.

$$v_{Rdi} = c \cdot f_{ctd} + \mu \cdot \sigma_n + \rho \cdot f_{yd} \cdot (\mu \cdot \sin\alpha + \cos\alpha) \leq 0.5 \cdot \nu \cdot f_{cd} \tag{3-20}$$

With

c coefficient of adhesion

f_{ctd} design value of concrete tensile strength of the weaker concrete layer

μ coefficient of friction

σ_n external normal stress perpendicular to the interface acting simultaneously with the shear stress
compressive stress: $0 \leq \sigma_n \leq 0.6 \cdot f_{cd}$
tensile stress: $\sigma_n < 0$ with $c \cdot f_{ctd} = 0$

ρ interface reinforcement ratio $\rho = A_{si} / A_i$
with
A_{si} the area of reinforcement crossing the interface including shear reinforcement from shear design with sufficient anchorage at both sides of the interface
A_i the area of the interface

f_{yd} design yield strength of the interface reinforcement
α inclination of interface reinforcement $45° \leq \alpha \leq 90°$
ν strength reduction factor for concrete cracked in shear and variable in the national annexes but recommended as $\nu = 0.6 \cdot (1 - f_{ck} / 250)$
f_{cd} design concrete cylinder compressive strength

The coefficients of adhesion and friction depend of the condition and roughness of the interface surface and are generally defined as national parameters. However, the coefficients defined in [EC2] are listed in Table 3-1.

Table 3-1: Classification of the surface and coefficients of adhesion and friction according to [EC2]

Interface	Classification	c [-]	μ [-]
very smooth	surface cast against steel, plastic or special prepared wooden moulds	0.025 – 0.1	0.5
smooth	slip formed or extrudes surface, free surface without further treatment	0.2	0.6
rough	surface with at least 3mm roughness at about 40 mm spacing achieved by raking, exposing of aggregate or other methods	0.4	0.7
indented	surface with indentations according to Figure 3-8.	0.5	0.9

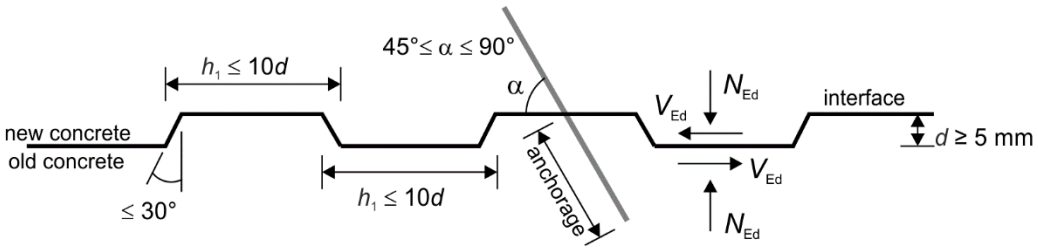

Figure 3-8: Required surface conditions for an indented surface according to [EC2]

For uneven shear distributions, the interface reinforcement may be distributed in accordance to Figure 3-9. A minimum reinforcement across the interface is not included in the design of [EC2].

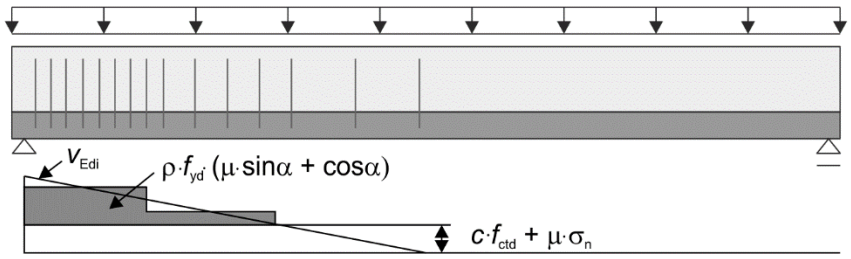

Figure 3-9: Required interface reinforcement along the structure's axis

For fatigue loading, the shear resistance for adhesion in Eq. (3-20) must be halved with $c_{fat} = 0.5 \cdot c_{stat}$.

3.3.3 Provisions of EC2+NA(D)

Since [EC2] works as an international regulation for European countries, the National Annexes may define certain alterations and modifications. Generally, the provisions of the National Annex of Germany [EC2NAD] describe the interface shear resistance in accordance to the [EC2] provisions. Thus, Eq. (3-19) applies for calculating the applied shear stress. The calculation of interface resistance follows Eq. (3-21).

$$v_{Rdi} = c \cdot f_{ctd} + \mu \cdot \sigma_n + \rho \cdot f_{yd} \cdot (1.2 \cdot \mu \cdot \sin\alpha + \cos\alpha) \leq 0.5 \cdot \nu \cdot f_{cd} \tag{3-21}$$

Compared to the [EC2] approach, certain changes were developed considering evaluations of test data [Zil06].

- The factors for calculating the term of adhesion and friction (c and μ) were slightly modified (Table 3-2) and the roughness quality of indented surfaces was extended including exposed aggregates with $d_g \geq 16$ mm and a roughness of at least 6 mm. To practically quantify the roughness of surfaces, reference values according to the sand-patch method of KAUFMANN [Kau71] (Chapter 2.4.2) were defined.
- The shear resistance of the clamping effect of reinforcement was increased. Thus, the term considering the vertical component of the reinforcement was increased by the factor 1.2. The factor is based on the verification of interface shear transfer according to the recent German design code DIN 1045-1 [D1045-1], which can be mechanically interpreted as an additional shear resistance due to dowel action [DA600].
- For limiting the interface shear resistance, the term of maximal shear resistance was decreased, since the data base, especially for very smooth and smooth surfaces, is very small. Therefore, the factor ν was defined depending on the interface roughness (Table 3-2). For very smooth interfaces however, a design would be excluded since $v = 0$ applies. Nevertheless, the shear resistance due to friction can be accounted for very smooth surfaces but must be limited to the maximum shear capacity of a smooth surface with $v = 0.2$, which leads to the limitation of $\mu \cdot \sigma_n \leq 0.1 \cdot f_{cd}$. For concrete classes $\geq$ C55/67, the strength reduction factors v in Table 3-2 must be multiplied by the term $1.1 - f_{ck}/500$.

In addition to the regulations of [EC2], more specific construction rules were introduced. Thus, interface reinforcement inclined in the direction of the compressive strut (declining towards the support) should not be considered for design ($90° < \alpha \leq 135°$). Construction rules defined for shear resistance generally apply for interface shear. Based on [Fur16], the maximum longitudinal spacing of interface reinforcement in slab structures without required shear reinforcement is defined as $2.5 \cdot h \leq 300$ mm and for transverse spacing $5 \cdot h \leq 700$ mm and 375 mm to the edges.

Contrary to [EC2], the adhesive interface shear capacity must be neglected for fatigue $c_{fat} = 0 \cdot c_{stat}$.

Table 3-2: Classification of the surface and coefficients of adhesion and friction according to [EC2NAD]

Interface	Classification	c [-]	μ [-]	ν [-]
very smooth	surface cast against steel, plastic or special prepared wooden moulds	0.0[1)]	0.5	0
smooth	slip formed or extrudes surface, free surface without further treatment	0.2	0.6	0.2
rough	surface with at least 3 mm roughness at about 40 mm spacing achieved by raking, exposing of aggregate or other methods (e.g. $R_t \geq 1.5$ mm)	0.4	0.7	0.5
indented	surfaces with exposed aggregates of $d_g \geq 16$ mm and a roughness of at least 6 mm (e.g. $R_t \geq 3.0$ mm)	0.5	0.9	0.7
	surface with indentations according to Figure 3-8.			

[1)] higher values must be proved by special verifications; R_t: mean roughness depth achieved by the sand-patch method according to KAUFMANN [Kau71]

3.3.4 New Proposal of prEC2:2018

In context of the revision process of [EC2], the regulations for shear at interfaces defined in the new proposal ppEC2:2018 [prEC2:18] are presented in the following. For the sake of consistency, the shear stress acting at an interface are named τ_{Edi} for the applied interface shear stress and τ_{Rdi} for the interface shear resistance, respectively.

For composite action, the applied shear stress due to horizontal shear is defined in accordance to [EC2] (Eq. (3-19)). For calculating the interface shear resistance, the regulations are extended by a term considering interfaces with interface reinforcement not sufficiently anchored (e.g. toppings on flexural composite members), which is based on the Model Code 2010 [MC10] provisions.

The design of interfaces without interface reinforcement and interfaces with interface reinforcement where yielding of the interface reinforcement can be provided due to sufficient anchorage, the interface shear resistance τ_{Rdi} may be calculated according to Eq. (3-22).

$$\tau_{Rdi} = c_{v1} \cdot \sqrt{f_{ck}}/\gamma_c + \mu_v \cdot \sigma_n + \rho \cdot f_{yd} \cdot \left(\mu_v \cdot \sin\alpha + \cos\alpha\right) \leq 0.5 \cdot \nu \cdot f_{cd} \tag{3-22}$$

Compared to the [EC2] provisions, the following changes may be named.

- For the sake of clarity, indexes are included for the coefficient of adhesion c_{v1} and friction μ_v. The classifications of the coefficients are summarised in Table 3-3.
- The term considering the adhesive capacity was rewritten by substituting the concrete tensile strength by considering the square root of the characteristic concrete compressive strength f_{ck}, reduced by the partial safety factor of concrete $\gamma_c = 1.5$.

- The permitted angle of the interface reinforcement was extended to a lower limit of $35° \leq \alpha \leq 90°$ based on experiences with lattice girders. For shear reinforcement however, the limits $45° \leq \alpha \leq 90°$ apply.
- The maximum interface shear capacity is defined to be 50 % of the strength reduction factor ν and design concrete cylinder compressive strength f_{cd} for 90° inclined shear reinforcement. Since no particular information regarding strength reduction for interface shear are provided, v may be taken as 0.5 in accordance to the shear design regulations when the limits of the permissible angle of compression strut $\cot\theta$ are satisfied ($1.0 \leq \cot\theta \leq 2.5$ for ordinary reinforced members without normal force).

For interfaces with interface reinforcement insufficiently anchored and thus, yielding of the reinforcement cannot be provided, the design follows Eq.(3-23). The expression is based on Model Code 2010 [MC10], which considers the effect of clamping and dowel action of the reinforcement. Nevertheless Eq.(3-23) accounts for insufficient anchorage, the interface reinforcement should be anchored for at least $0.5 \cdot f_{yd}$ with a minimum embedment length of $8 \cdot Ø$ (with Ø as bar diameter) if no other anchorage method are applied. The coefficients of adhesion, clamping effect and dowel action may be taken from Table 3-3.

$$\tau_{Rdi} = c_{v2} \cdot \sqrt{f_{ck}}/\gamma_c + \mu_v \cdot \sigma_n + k_t \cdot \rho \cdot f_{yd} \cdot \mu_v + k_f \cdot \rho \cdot \sqrt{f_{yd} \cdot f_{cd}} \tag{3-23}$$

With

c_{v2} coefficient of adhesion, $c_{v2} = 0$ for tensile stress perpendicular to the interface

k_t coefficient of the tensile forces in the reinforcement due to the clamping effect

k_f coefficient for the flexural resistance of the reinforcement due to dowel action. If the longitudinal distance of a bar to the structures edge is $\leq 10 \cdot Ø$, $k_f = 0$ applies

The classifications of surface quality were extended by distinguishing intermediate surfaces according to [EC2] between very rough and keyed surfaces. The classification of all surface conditions as well as reinforcement classifications are described in Table 3-3 and Figure 3-10. However, for very rough interfaces with minimum interface reinforcement sufficiently anchored and permissibly angled, the verification may be omitted.

Table 3-3: Classification of the surface and coefficients of adhesion and friction according to [prEC2:18]

Interface	Classification	c_{v1} [-]	μ_v [-]	c_{v2} [-]	k_t [-]	k_f [-]
very smooth	surface cast against steel, plastic or special prepared wooden moulds	0.0095	0.5	-	0	1.5
smooth	surface with less than 3 mm roughness, e.g. a free surface left without further treatment after compacting	0.075	0.6	-	0.5	1.1
rough	surface with at least 3 mm roughness (from peak to valley measured at maximum 40 mm spacing) achieved by raking, exposing of aggregate or other methods (Figure 3-10 (a))	0.15	0.7	0.035	0.5	0.9
very rough	surface with at least 6 mm roughness (from peak to valley measured at maximum 40 mm spacing) achieved by raking, exposing of aggregate or other methods (Figure 3-10 (a))	0.19	0.9	0.070	0.5	0.9
keyed[1)]	surface with shear keys according to Figure 3-10 (c)	0.37	0.9	-	-	-

[1)]: factors for keyed interfaces should be applied for the area of each key with $A_i = b_{i,eff} \cdot l_{i,eff}$ and $\tau_{Edi} = V_{Edi} \cdot A_i$

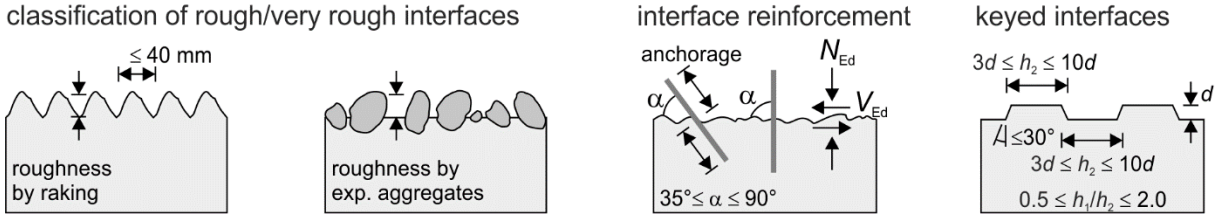

Figure 3-10: Classification of rough and very rough interfaces (a), classification of interface reinforcement (b), classification for keyed interfaces (c)

The detailing rules regarding spacing are adopted from the regulations in [EC2NAD]. Deviating from [EC2] and [EC2NAD], the expression in [prEC2:18] defines minimum reinforcement $a_{s,min}$ along edges of slabs, where delamination of the insitu concrete cannot be prevented by confinement due to permanent loads (e.g. walls) according to Eq. (3-24). Since the design of beam structures requires minimum shear reinforcement, no additional regulation regarding minimum interface shear reinforcement are formulated.

$$a_{s,min} = t_{min} \cdot f_{ctm} / f_{yk} \tag{3-24}$$

With

t_{min} minimum thickness of old and new concrete layer
f_{ctm} mean tensile strength of the respective concrete layer
f_{yk} characteristic yield strength of reinforcement

For fatigue, [prEC2:18] limits the verification to rough, very rough and keyed interfaces. The design distinguishes between interfaces without and interfaces with interface reinforcement. If no reinforcement crosses the interface, the maximum applied shear stress must be limited to 50 % of the static adhesive strength whereas the full resistance of normal stress can be considered (Eq. (3-25)).

$$\tau_{Rdi} = 0.5 \cdot c_{v1} \cdot \sqrt{f_{ck}}/\gamma_c + \mu_{v,fat} \cdot \sigma_n \leq \nu \cdot f_{cd} \tag{3-25}$$

If reinforcement crosses the interface, the approved stress range in the reinforcement bars must be verified. Therefore, the resistance term of adhesion is omitted and a reduced inclination of compression strut from 45° to 25° is assumed. The flatter inclination is considered by a reduction factor of $1/\cot\theta \approx 0.45$ with $\theta = 25°$ as shown in Eq. (3-26).

$$\Delta\tau_{Rdi} = \mu_{v,fat} \cdot \sigma_n + \rho \cdot \frac{1}{0.45} \cdot \frac{\Delta\sigma_{Rsk}}{\gamma_{s,fat}} \cdot \left(\mu_{v,fat} \cdot \sin\alpha + \cos\alpha\right) \leq \nu \cdot f_{cd} \tag{3-26}$$

With

$\Delta\sigma_{Rsk}$ approved characteristic stress range in the reinforcement derived by S-N curves depending on expected number of load cycles.

$\gamma_{s,fat}$ partial safety factor of reinforcement under fatigue $\gamma_{s,fat} = 1.15$

3.3.5 Provision of Model Code 2010

The interface shear design according to Model Code 2010 [MC10] is based on a shear friction model developed by RANDL [Ran97] (s. Chapter 3.2.7) which considers the capacity of interface reinforcement by distinguishing between the clamping effect and bending effect of dowel action.

For verification, the interface shear resistance τ_{Rdi} must exceed the applied shear stress τ_{Edi} considering the partial safety factors. For determining the applied shear stress, the assumptions according to [EC2] (Eq. (3-19)) apply.

To calculate the interface shear resistance, two scenarios are defined. The scenario of rigid bond for interfaces without interface reinforcement where good adhesive bond can be assumed and no tensile stress acts perpendicular to the interface, as well as the scenario of non-rigid bond, where interface slip is allowed and interface reinforcement is applied.

For rigid bond, brittle slip behaviour is assumed and usually no - or low degrees of interface reinforcement ($0 \leq \rho \leq 0.05$ %) are applied. Therefore, the interface shear resistance is only influenced by the load bearing capacities of adhesion and friction (Eq. (3-27)).

$$\tau_{Rdi} = c_a \cdot f_{ctd} + \mu \cdot \sigma_n \leq 0.5 \cdot \nu \cdot f_{cd} \tag{3-27}$$

With

c_a coefficient for adhesion

μ coefficient of friction

σ_n lowest compression stress acting on the interface

ν reduction factor accounting for the strength of the diagonal concrete strut
$\nu = 0.55 \cdot (30/f_{ck})^{1/3} \leq 0.55$

The aforementioned coefficients depend on the surface quality of the interface. In accordance to [EC2], the classification of very rough interfaces includes shear keys. The surface classification with corresponding coefficients of adhesion and friction are summarised in Table 3-4.

Table 3-4: Surface classifications and adhesive coefficients for rigid bond according to [MC10]

Interface	Classification	c_a [-]	μ [-]	
			$f_{ck} \geq 20$ N/mm²	$f_{ck} \geq 35$ N/mm²
very smooth	surface cast against steel, plastic or timber formwork	0.025	0.5	0.5
smooth	surface left as cast, slightly treated after casting against formwork, mean roughness depth of $R_t \leq 1.5$ mm achieved by the sand-patch method	0.2	0.6	0.6
rough	surface intensely roughened with $R_t \geq 1.5$ mm	0.4	0.7	0.7
very rough / shear keys	surface intensely roughened with $R_t \geq 3.0$ mm	0.5	0.8	1.0

R_t: mean roughness depth achieved by the sand-patch method according to KAUFMANN [Kau71]

If rigid bond cannot be guaranteed or the applied shear stress exceeds the adhesive resistance, non-rigid bond behaviour is assumed. For these cases, interface reinforcement must be applied across the interface. The shear resistance of the reinforcement distinguished between capacity due to axial stress (clamping effect) and bending of the reinforcement (dowel action). The design equation follows Eq. (3-28).

$$\tau_{Rd} = c_r \cdot f_{ck}^{1/3} + \mu \cdot (\sigma_n + \rho \cdot \kappa_1 \cdot f_{yd} \cdot \sin\alpha + \cos\alpha) + \kappa_2 \cdot \rho \cdot \sqrt{f_{yd} \cdot f_{cd}} \leq \beta_c \cdot \nu \cdot f_{cd} \tag{3-28}$$

With

c_r coefficient for adhesion

μ coefficient of friction

κ_1 coefficient of the tensile forces in the reinforcement due to the clamping effect

κ_2 coefficient for the flexural resistance of the reinforcement due to dowel action

β_c coefficient of angle of the diagonal concrete strut

The coefficients for non-rigid bond behaviour depend on the surface qualities as listed in Table 3-4 and are summarised in Table 3-5.

Table 3-5: Design coefficients for the non-rigid bond verification according to [MC10]

Interface	c_r [-]	κ_1 [-]	κ_2 [-]	μ [-]		β_c [-]
				$f_{ck} \geq 20$ N/mm²	$f_{ck} \geq 35$ N/mm²	
very smooth	0	0	1.5	0.5	0.5	0.3
smooth	0	0.5	1.1	0.6	0.6	0.4
rough	0.1	0.5	0.9	0.7	0.7	0.5
very rough / shear keys	0.2	0.5	0.9	0.8	1.0	0.5

In accordance to [EC2], a stepwise distribution of the interface reinforcement following the shear stress distribution may be used (Figure 3-9). For smooth surfaces however, the flexibility of surface even allows a redistribution of forces, which may lead to a uniform distribution of interface reinforcement. For cases where interface reinforcement is required, a minimum reinforcement should be applied covering the loss of adhesion and aggregate interlock in order to prevent brittle failure. The minimum reinforcement ratio ρ_{min} for beam members is calculated according to Eq. (3-29). By considering redistributional effects, which may be expected for slab members, the minimum reinforcement ratio may be reduced (Eq. (3-30)).

$$\rho_{min,beam} = 0.2 \cdot f_{ctm} / f_{yk} \geq 0.001 \tag{3-29}$$

$$\rho_{min,slab} = 0.12 \cdot f_{ctm} / f_{yk} \geq 0.0005 \tag{3-30}$$

To prevent delamination of the concrete overlay for cases were confinement cannot be guaranteed, the provision of [prEC2:18] (Eq. (3-24)) apply.

Under fatigue loading conditions, the adhesive coefficients for rigid bond must be reduced to $c_{a,fat} = 0.5 \cdot c_{a,stat}$, whereas for non-rigid bond the entire shear resistance must be reduced to $\tau_{Rdi,fat} = 0.4 \cdot \tau_{Rdi,stat}$. A detailed description of the interface shear design according to [MC10] can be found in [Ran13].

3.3.6 Provisions of ACI 318-14

The ‘Building Code Requirements for Structural Concrete’ by the American Concrete Institute (ACI) are reported by the ACI Committee 318 and formulated in the standard ACI 318-14 [ACI318]. The code formulates shear friction for all cases where shear

transfer across a given plane must be considered. Besides interface shear between concrete cast at different times, shear transfer across existing or potential cracks or across interfaces between dissimilar materials are considered.

For interface shear verification, [ACI318] compares the factored shear resistance V_n with the acting shear force V_u according to Eq. (3-31).

$$\phi \cdot V_n \geq V_u \tag{3-31}$$

With

ϕ partial safety factor for shear design $\phi = 0.75$

In contrast to the regulations in [EC2] and [MC10], the shear resistance distinguishes between vertical and horizontal shear due to composite action. To classify the interface surface quality, [ACI318] only distinguishes between surfaces intentionally roughened to a roughness amplitude of 0.25 inch (6.4 mm) and surfaces not intentionally roughened.

The interface resistance for vertical shear V_n is based on the basic shear friction theory and can be calculated depending on the properties of the shear plane as well as on the concrete type according to Eq. (3-32).

$$\phi \cdot V_n = \phi \cdot A_{vf} \cdot f_y \cdot (\mu \cdot \sin\alpha + \cos\alpha) \tag{3-32}$$

With

A_{vf} cross sectional area of interface reinforcement

f_y characteristic yield strength of interface reinforcement with a maximum of $f_{y,max}$ = 60,000 psi = 413,7 N/mm^2

μ coefficient of friction
$\mu = 1.0\lambda$ for intentionally roughened surfaces
$\mu = 0.6\lambda$ for surfaces not intentionally roughened
With
$\lambda = 1.0$ for normal weight concrete
$\lambda = 0.75$ for lightweight concrete

α angle between the interface reinforcement and the interface plane

If permanent net compression stress occurs across the interface, a load bearing capacity due to normal stress may be added to reduce the amount of interface reinforcement. However, if the inclination of the interface reinforcement leads to compressive stress in the reinforcement in the direction of shear, the shear friction equation does not apply ($V_n = 0$).

Since the formulation of the interface shear resistance may become unconservative for some cases (e.g. [Kah02][Mat01]), upper limits on the shear friction strength are necessary. For monolithic structures and intentionally roughened surfaces Eq. (3-33), and for not intentionally roughened surfaces Eq. (3-34) applies.

Intentionally roughened surfaces:

$$\phi \cdot V_{n,max} \leq \phi \cdot \max \begin{cases} 0.2 \cdot f_c' \cdot A_c \\ (3.31\ [N/mm^2] + 0.08 \cdot f_c') \cdot A_c \\ 11.03\ [N/mm^2] \cdot A_c \end{cases} \tag{3-33}$$

Not intentionally roughened surfaces:

$$\phi \cdot V_{n,max} \leq \phi \cdot \min \begin{cases} 0.2 \cdot f_c' \cdot A_c \\ 5.52\ [N/mm^2] \cdot A_c \end{cases} \tag{3-34}$$

With
f_c' specific cylinder concrete compressive strength after 28 days
A_c cross sectional area on concrete participating the load transfer

For horizontal interfaces in composite flexural members, [ACI318] gives special regulations and limitations for horizontal shear transfer which distinguish the design not only by the interface roughness, but also by the magnitude of the shear force and the amount of interface reinforcement.

Generally, the upper limit of longitudinal interface shear verification is defined as $V_u < \phi \cdot 3.45[N/mm^2] \cdot b_v \cdot d$, where b_v is the width of the surface of the interface and d is the effective depth, which is limited to $0.8h$. For interface shear due to composite action which exceeds the upper limit, the formulations described above with the shear resistance according to Eq. (3-32) applies.

For small shear forces with $V_u \leq \phi \cdot 3.45[N/mm^2] \cdot b_v \cdot d$, the shear resistance shall be calculated depending on the surface roughness and the interface reinforcement. Thus, a minimum interface reinforcement $A_{v,min}$ must be applied for all cases where interface reinforcement is required to resist horizontal shear (Eq. (3-35)).

$$A_{v,min} \geq \max \begin{cases} 0.75 \cdot \sqrt{f_c'} \cdot \dfrac{b_w \cdot s}{f_y} \\ 0.35\ [N/mm^2] \cdot \dfrac{b_w \cdot s}{f_y} \end{cases} \tag{3-35}$$

With

b_w width of the web or contact surface where the interface reinforcement is applied

s spacing of interface reinforcement

If the designed interface reinforcement exceeds the minimum reinforcement ($A_v \geq A_{v,min}$), the horizontal shear resistance V_{nh} for surfaces intentionally roughened to an amplitude of approximately 6.4 mm can be calculated according to Eq. (3-36).

$$\phi \cdot V_{nh} = \phi \cdot \min \begin{cases} \lambda \cdot \left(1.79\ [\mathrm{N/mm^2}] + 0.6 \cdot \frac{A_v \cdot f_{yt}}{b_v \cdot s} \right) \cdot b_v \cdot d \\ 3.45\ [\mathrm{N/mm^2}] \cdot b_v \cdot d \end{cases} \tag{3-36}$$

With

A_v cross sectional area of transverse reinforcement

f_{yt} specified yield strength of transverse reinforcement

b_v width of horizontal interface

d effective depth

For interfaces which are not intentionally roughened and with interface reinforcement exceeding the minimum reinforcement, as well as for all other case, the horizontal shear resistance is given by Eq. (3-37). This implies that interfaces without interface reinforcement must be intentionally roughened to an amplitude of approximately 6.4 mm and the interface resistance is limited to 0.56 N/mm^2 according to Eq. (3-37).

$$\phi \cdot V_{nh} = \phi \cdot 0.56\ [\mathrm{N/mm^2}] \cdot b_v \cdot d \tag{3-37}$$

The interface reinforcement may consist of single bars or wires, multiple bar stirrups or vertical legs of welded wire reinforcement and must be sufficiently anchored at both sides of the interface. The longitudinal spacing of the bars is limited to the maximum of 61 cm and four times the least dimension of the supported element.

For fatigue loading conditions, the provisions according to ACI 318-14 do not include any specific regulations regarding interface shear design.

3.3.7 Provisions of AASHTO LRFD Bridge Design Specifications

Besides the regulations in ACI 318-14, specifications for bridge structures are governed by the American Association of State Highway and Transportation Officials (AASHTO). The AASHTO currently provides two guidelines for the design of concrete bridges, the ‘Standard Specifications for Highway Bridges’ [AA-S] and the ‘Load Resistance Factor Design Bridge Design Specifications’ (LFRD). For interface shear, the provisions in the standard specification are similar to the regulations in [ACI318] whereas the regulations in the LFRD Bridge Design Specifications [AA-L] are more developed and specified and thus, presented in the following.

In accordance to the [ACI318] provisions, [AA-L] considers interface shear transfer across potential cracks, interfaces between dissimilar materials, between concrete cast at different times and between different elements of the cross section. As specifically stated in [AA-L], interface reinforcement must be applied across the interface.

For design, the interface shear resistance V_{ri} shall satisfy the condition in Eq. (3-38).

$$V_{ri} = \phi \cdot V_{ni} \geq V_{ui} \tag{3-38}$$

With

ϕ resistance factor for shear
$\phi = 0.9$ for normal weight concrete
$\phi = 0.8$ for lightweight concrete
$\phi = 1.0$ for extreme limit states

V_{ni} nominal interface shear resistance

V_{ui} factored interface shear force due to loading condition

For composite action, the factored interface shear stress along the interface can be determined according to Eq. (3-39).

$$v_{ui} = V_{u1} / (b_{vi} \cdot d_v) \tag{3-39}$$

With

V_{u1} shear force

b_{vi} interface width considered to be engaged in shear transfer

d_v distance between centroid of tension steel and the mid-thickness of the slab to compute a factored interface shear stress

The nominal interface shear resistance considers the load bearing capacities of adhesion, friction and reinforcement based on modifications of shear friction theory. In accordance to the regulations in [EC2] and [MC10], the term of adhesion is defined depending on the roughness of the interface but in the contrary, not depending on the concrete strength (Eq. (3-40)).

$$\phi \cdot V_{ni} = \phi \cdot (c \cdot A_{cv} + \mu \cdot (A_{vf} \cdot f_y + P_c)) \tag{3-40}$$

With

c cohesion factor [N/mm^2]

μ friction factor

A_{cv} area of concrete considered to be engaged in interface shear $A_{cv} = b_{vi} \cdot L_{vi}$ with
b_{vi} the interface width considers to be engaged in shear transfer
L_{vi} interface length considers to be engaged in shear transfer

A_{vf} area of interface reinforcement within the area A_{vc}

f_y design value of yield strength of interface reinforcement with $f_y \leq 414$ N/mm²

P_c permanent net compressive force normal to the interface, for tensile forces $P_c = 0$

If the normal force acting at the interface is tensile, additional reinforcement must be provided with a cross section A_{vpc} according to Eq. (3-41).

$$A_{vpc} = \frac{P_c}{\phi \cdot f_y} \tag{3-41}$$

The minimum reinforcement which must be applied across the interface follows Eq. (3-42).

$$A_{vf} = \frac{0.05 \cdot A_{cv}}{f_y} \tag{3-42}$$

The calculated interface shear resistance for longitudinal shear should not exceed the limit according to Eq. (3-43).

$$\phi \cdot V_{ni} = \phi \cdot \min \begin{cases} K_1 \cdot f_c' \cdot A_{cv} \\ K_2 \cdot A_{cv} \end{cases} \tag{3-43}$$

With

f_c' specified concrete compressive strength of the weaker concrete

K_1 fraction of concrete strength to resist interface shear

K_2 limiting interface shear resistance

The coefficients of cohesion, friction and maximum concrete strength of girder and slab bridges are summarised in dependence of concrete type and surface condition in Table 3-6. The values were determined by experimental data according to e.g. [Loo94] and [Kah02]. For vertical shear across a crack in e.g. brackets, corbels or ledges, the cohesion factor shall be taken as $c = 0$.

Table 3-6: Coefficients for calculating the interface shear resistance according to [AA-L]

	c [N/mm²]	μ [-]	K_1 [-]	K_2 [N/mm²]
concrete places against a clean concrete surface, free of laitance but not intentionally roughened	0.52	0.6	0.5	5.52
normal weight concrete placed against a clean concrete surface, free of laitance, with a surface intentionally roughened to an amplitude of 6.4 mm	1.65	1.0	0.25	10.34
lightweight concrete placed against a clean concrete surface, free of laitance, with a surface intentionally roughened to an amplitude of 6.4 mm	1.65	1.0	0.25	6.89

The reinforcement applied as interface reinforcement may consist of single bars, multiple leg stirrups or welded wire fabric. The reinforcement must be sufficiently anchored at both sides of the interface by embedment, hooks, mechanical methods like headed studs or welding on order to guarantee yielding of the reinforcement. The longitudinal centre to centre spacing of the interface shear connectors in beams or girders shall not exceed 122 cm or the depth of the member, whereas for cast-in-place box girders, the spacing is limited to 61 cm.

The provisions according to [AA-L] do not include any specific regulations regarding interface shear transfer for fatigue loading conditions.

3.3.8 Comparison of design provisions

The codes presented in the previous chapters are based on the model concepts of *Mohr-Coulomb* and shear friction theory, but with different modifications and considerations of the influence of the interface roughness. Comparing the safety concept of the codes, the regulations according to [EC2], [EC2NAD], [prEC2:18], and [MC10] use a semi-probabilistic safety concept with applying safety factors on the applied permanent and life loads, as well as material safety factors for the material resistances. [ACI318] and [AA-L] use global safety factors reducing the shear resistance.

To calculate the applied shear stress for composite action in beam and slab structures, all codes consider the acting shear force as the governing influence. Whereas [EC2], [EC2NAD], [prEC2:18], and [MC10] calculate the lever arm of the internal forces as $z = 0.9d$, [ACI318] assumes the inner lever arm with the full effective depth and [AA-L] defines the inner lever arm as the distance between the centroid of the tension steel and the mid-thickness of the slab.

A comparison of all presented codes, distinguishing between the load resistance terms, is presented in Table 3-7.

For calculating the interface shear resistance, all models define the load bearing resistances by terms of adhesions, friction induced by normal stress and reinforcement and limit the interface shear resistance to a maximum interface capacity. For the term of interface reinforcement, all codes but [MC10] agree on the shear friction formulation with friction induced by clamping of the interface reinforcement. In [MC10] however, an additional term of dowel action is introduced. In [prEC2:18], the additional term of dowel action is adopted for interfaces with reinforcement not sufficiently anchored. The definition of roughness differs between the European codes with generally classifying interfaces as very smooth, smooth, rough, very rough (indented) and keyed, and the American Codes only distinguish between surfaces intentionally roughened and not intentionally roughened. For considering the friction term, all codes agreed on normal shear stress and a friction coefficient. The term of adhesion however, is described by concrete strength and roughness coefficients in [EC2], [EC2NAD], [prEC2:18], and

[MC10], whereas [ACI318] and [AA-L] assume constant adhesive strength depending on the interface roughness. The maximum shear resistance is applied for all codes to be depended on the concrete compressive strength, but only the terms of [EC2] and [prEC2:18] being independent of the interface classification. For fatigue, the American Code do not provide specific regulations. For interfaces without interface reinforcement, [EC2],[prEC2:18] and [MC10] define a reduced adhesive strength of 50 %, whereas [EC2NAD] neglects the resistance term of adhesion. For the verification of stress range in the interface reinforcement, [prEC2:18] provides a design expression which omits the adhesive resistance and assumes a flatter inclination of the compression strut with the factor 1/0.45. The regulations in [MC10] limit the fatigue resistance to 40 % of the static resistance.

Table 3-7: Comparison of introduced codes regarding the formulation of load bearing capacities adhesion, friction, reinforcement and maximum shear resistance

	Adhesion	Friction	Reinforcement	Max. shear resistance
EC2	$c \cdot f_{ctd}$	$\mu \cdot \sigma_n$	$\rho \cdot f_{yd} \cdot (\mu \cdot \sin\alpha + \cos\alpha)$	$0.5 \cdot \nu \cdot f_{cd}$
EC2+NA(D)	$c \cdot f_{ctd}$	$\mu \cdot \sigma_n$	$\rho \cdot f_{yd} \cdot (1.2 \cdot \mu \cdot \sin\alpha + \cos\alpha)$	$0.5 \cdot \nu \cdot f_{cd}$
prEC2:2018	$c_{v1} \cdot \sqrt{f_{ck}}/\gamma_c$	$\mu_v \cdot \sigma_n$	$\rho \cdot f_{yd} \cdot (\mu_v \cdot \sin\alpha + \cos\alpha)$	$0.5 \cdot \nu \cdot f_{cd}$
(toppings)	$c_{v2} \cdot \sqrt{f_{ck}}/\gamma_c$	$\mu_v \cdot \sigma_n$	$k_t \cdot \rho \cdot \mu_v \cdot f_{yd} + k_f \cdot \rho \cdot \sqrt{f_{yd} \cdot f_{cd}}$	
MC2010				
rigid bond	$c_a \cdot f_{ctd}$	$\mu \cdot \sigma_n$	–	$0.5 \cdot \nu \cdot f_{cd}$
non-rigid bond	$c_r \cdot f_{ck}^{1/3}$	$\mu \cdot \sigma_n$	$\mu \cdot \rho \cdot \kappa_1 \cdot f_{yd}$ [(1)] $+ \kappa_2 \cdot \rho \cdot \sqrt{f_{yd} \cdot f_{cd}}$ [(2)]	$\beta_c \cdot \nu \cdot f_{cd}$
ACI 318				
<u>for shear stress ≤ $\phi \cdot 3.45$ [(3)]</u>				
intentionally roughened & without rfcmnt	$\phi \cdot 0.56$ [(3)]	– [(4)]	–	$\phi \cdot 3.45$ [(3)]
with rfcmnt	$\phi \cdot \lambda \cdot 1.76$ [(3)]	– [(4)]	$\phi \cdot \mu \cdot \rho \cdot f_y$	
<u>for shear stress ≥ $\phi \cdot 3.45$ [(3)]</u>				intentionally roughened: $\phi \cdot \max\begin{cases} 0.2 \cdot f_c' \\ 3.31^{(3)} + 0.08 \cdot f_c' \\ 11.03^{(3)} \end{cases}$
	–	– [(4)]	$\phi \cdot \rho \cdot f_y \cdot (\mu \cdot \sin\alpha + \cos\alpha)$	not intentionally roughened: $\phi \cdot \min\begin{cases} 0.2 \cdot f_c' \\ 5.52^{(3)} \end{cases}$
AASHTO LFRD	$\phi \cdot c$	$\phi \cdot \mu \cdot \sigma_n$	$\phi \cdot \mu \cdot \rho \cdot f_y$	$\min\begin{cases} K_1 \cdot f_c' \\ K_2 \end{cases}$

rfcmnt: reinforcement; [(1)]: clamping effect; [(2)]: dowel action;[(3)]: in [N/mm²]; [(4)]: not specifically defined but may be considered

Since not only the equations themselves, but the roughness definition with corresponding design coefficients differ among codes, a comparison of shear resistance equations is only possible qualitatively. However, Figure 3-11 shows the comparison of the design equations for interfaces without interface reinforcement and normal stress. Therefore, the calculated design shear stress τ_{Rdi} is plotted over the mean value of concrete tensile strength f_{ctd}. For comparison, the interface classifications according to [ACI318] and [AA-L] are defined as smooth surfaces for not intentionally roughened interfaces in Figure 3-11 (a) and very rough surfaces for intentionally roughened surfaces in Figure 3-11 (b).

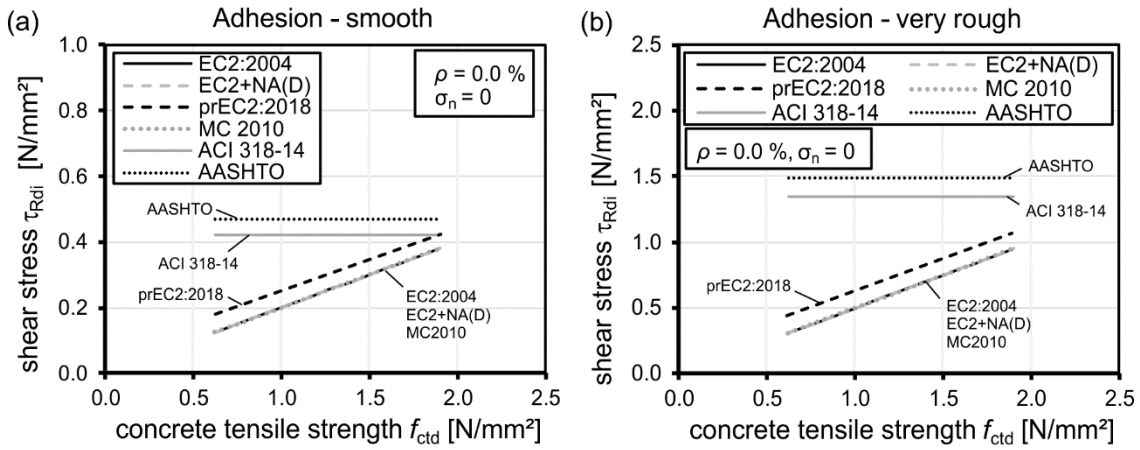

Figure 3-11: Comparison of codes regarding the term of adhesion for smooth (a) and very rough interfaces (b)

The comparison in Figure 3-11 shows, that the constant adhesive strength in the American standards give higher values compared to the European codes. Since the European equations define the interface resistance by terms of the concrete strength, the calculated adhesive resistance increases with increasing concrete strength. The expression of [prEC2:18] leads to slightly higher interface shear strengths than [EC2],[EC2NAD] and [MC10] give similar values.

To compare the influence of the amount of interface reinforcement, Figure 3-12 shows the curves of calculated shear strength over the interface reinforcement ratio ρ for a characteristic concrete compressive strength of f_{ck} = 25 N/mm² and without normal stress.

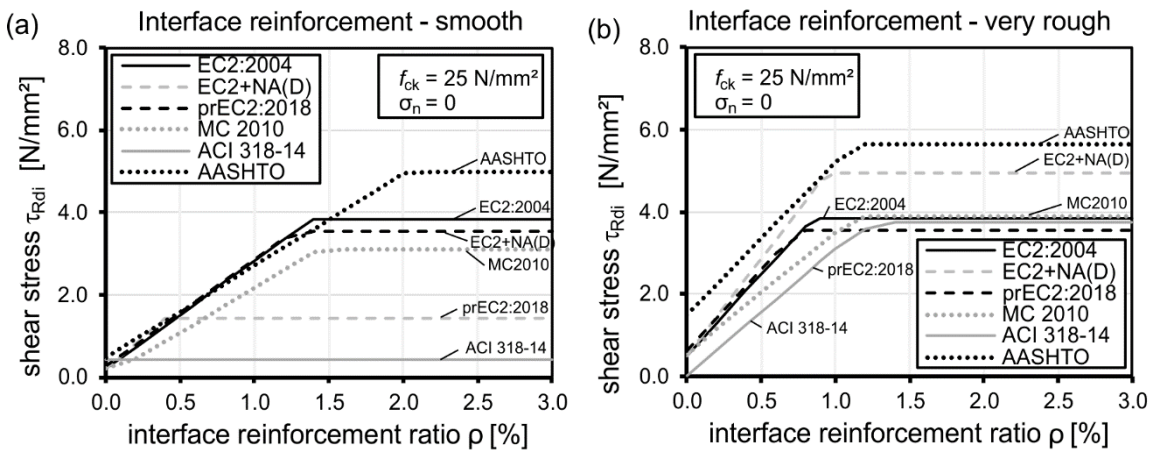

Figure 3-12 Comparison of codes regarding the term of interface reinforcement for smooth (a) and very rough interfaces (b)

Since [ACI318] does not consider the term of interface reinforcement for smooth surface (Figure 3-12 (a)), the calculated shear stress is described by a constant which forms the lower limit of the comparison. For all other equations, the design curves increase with an almost similar inclination with increasing reinforcement ratio, with [MC10] giving the lowest values. The main difference between the codes is the upper limit of the interface shear equations. Therefore, [AA-L] gives the highest values, and [EC2NAD] shows the lowest limit with additionally reducing the maximum shear resistance with a factor considering the interface roughness. For very rough interfaces (Figure 3-12 (b)) the adhesive terms ($\rho = 0$) differ significantly and the inclinations vary slightly. In accordance to smooth interfaces, the upper limits of interface resistance are defined differently, with [AA-L] giving the highest, and [ACI318] giving the lowest limit.

To examine the influence of maximum shear resistance, Figure 3-13 compares the formulations for smooth interfaces (a) and very rough interfaces (b) over the design concrete compressive strength f_{cd}. The equation according to [prEC2:18] is independent of the surface quality and thus, gives the highest values for smooth interfaces. The [EC2] expression is also independent of the concrete strength but with lower values for high concrete strengths. For smooth interfaces, the American codes do not include an influence of the concrete strength, whereas for very rough interfaces, an influence is defined for small concrete strengths. The highest influence of the interface roughness gives the [EC2NAD] approach and thus, shows the highest interface resistances for very rough interfaces and high concrete strength.

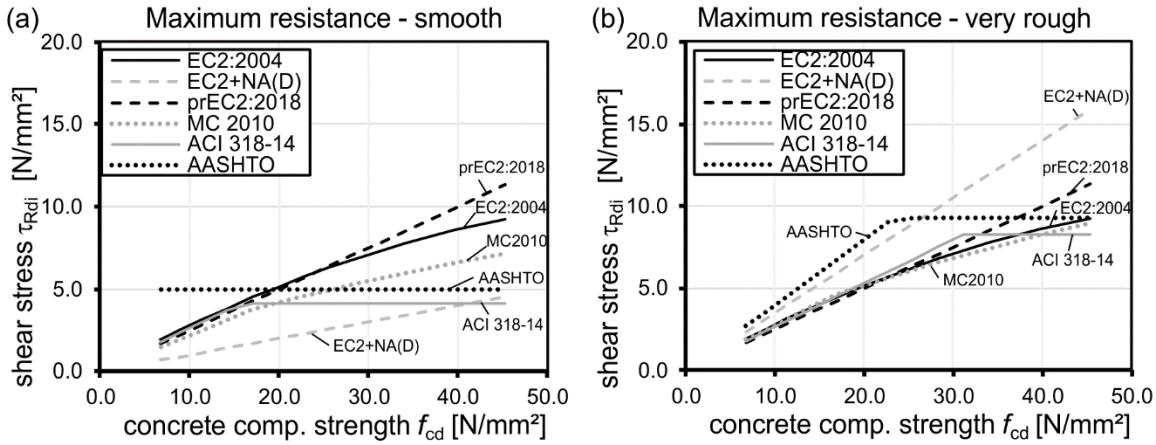

Figure 3-13: Comparison of codes regarding the term of maximum interface shear resistance for smooth (a) and very rough interfaces (b)

For all evaluated codes, the effect of friction induced by normal stress is expressed by the applied normal stress and a roughness coefficient. However, in common building practice, normal stress in composite beam and slab structures is generally induces by the self-weight of the insitu concrete and thus, is comparatively small.

4 Previous experimental investigations

4.1 Introduction

To investigate the load bearing mechanisms of concrete-to-concrete interfaces, several researchers conducted experimental investigations to achieve better understanding of particular influencing factors for different load bearing mechanisms and their collaboration in a structural element. For individual examinations of the load bearing mechanisms (adhesion, friction or aggregate interlock and interface reinforcement), small size specimens present a good and efficient method to consider the many varying influencing parameters for interface shear like interface roughness and condition, concrete strength, age and composition (e.g. aggregates or additives), interface reinforcement (e.g. shape, amount and anchorage) as well as the applied load (considering e.g. normal stress, bending and cyclic loading conditions). In beam and slab structures, the longitudinal shear transfer across an interface does not develop due to pure shear, but due to composite action. Thus, due to the interaction of the different load bearing mechanisms in the structures, the interface shear resistance as well as the crack development and stress states may differ from results achieved by small size tests. To investigate the effect of interface shear transfer on the structural behaviour, composite bending tests with beam and slab specimens were conducted and presented in literature.

In the following chapter, governing results from test series with small size tests as well as beam and slab tests are presented. Detailed overviews of the test series presented in this chapter, as well as further test series evaluated within the database evaluation in Chapter 6, including test setup, dimensions, material properties, test parameters and failure shear stresses can be found in Annex B.

4.2 Small size specimen

4.2.1 Introduction

An overview of the generally used test setups for small size tests in literature gives Figure 4-1. Investigations for the isolated adhesive strength of interfaces were commonly conducted by tensile tests (a) and splitting tensile tests (b). Since the adhesive bond directly correlates with the tensile strength of the interface, these investigations examine the influence of tensile stress on the interface bond. For adhesive shear strength, the commonly used test setups are push-off tests (c), push through tests (g) and sliding walls (h). In corbel tests (e) and eccentric sliding walls (i), the load resultant regularly acts in the interface, but with additional moments along the interface induced by the eccentricity of the applied forces. To investigate the influence of normal stress acting perpendicular to the interface, modified push-off tests (d) and modified corbels (f) with inclined interfaces give constant ratios of shear and normal stress at the interface. To control the magnitude of normal stress independent from shear stress, normal stress can

be applied externally to the specimens e.g. for push-off and push-though tests as well as for corbels and sliding walls. For investigating the effect of interface reinforcement, the small size tests presented in Figure 4-1 could also be conducted with interface reinforcement, such as stirrups, bars and dowels across the interface to investigate the general load bearing mechanism, shape, amount and efficient anchorage.

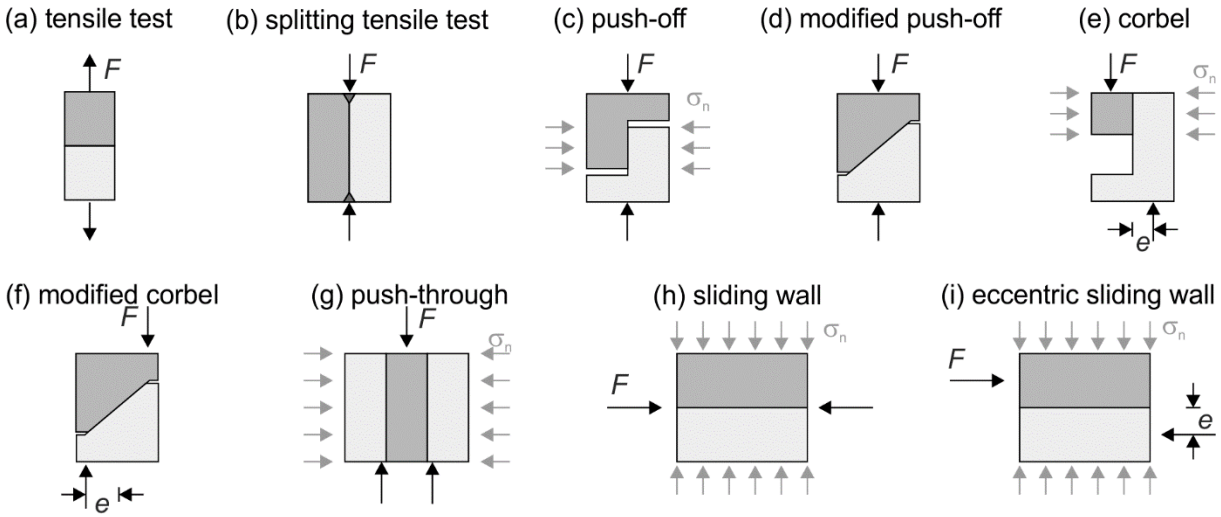

Figure 4-1: Small size tests for investigating the interface resistance of concrete cast at different times

In the following, results collected by selected test series from literature are presented considering investigations for adhesive bond, aggregate interlock due to normal stress as well as clamping of interface reinforcement and dowel action.

4.2.2 Investigations for adhesion

In composite concrete structures with concrete-to-concrete interfaces, complex stress states with a combination of normal and shear stress occur at the interface [Lin06_1]. Thus, investigations considering adhesive bond basically differentiate between tensile and shear tests determining the stress state parallel and orthogonal to the interface.

Investigations to determine the influence of interface roughness and carbonation of concrete on the adhesive tensile strength were reported e.g. in [Sch96b], [Blo89] (cited by [Rei04]) and [Blo98] using the tensile tests setup as shown in Figure 4-1 (a). Even though the results of the tensile strength showed high scatter, an increase of bond strength with increasing interface roughness could be determined. Thus, for high interface roughnesses, the concrete failure may not necessarily occur in the interface but in the weaker concrete layer.

In concrete composite members, interfaces are commonly stressed parallel to the interface due to shear stress. Commonly used tests setups for adhesive shear strength are push-through and push-off tests as shown in Figure 4-2, here exemplarily depicted by DASCHNER [Das86a], RANDL [Ran97] and REINECKE [Rei04].

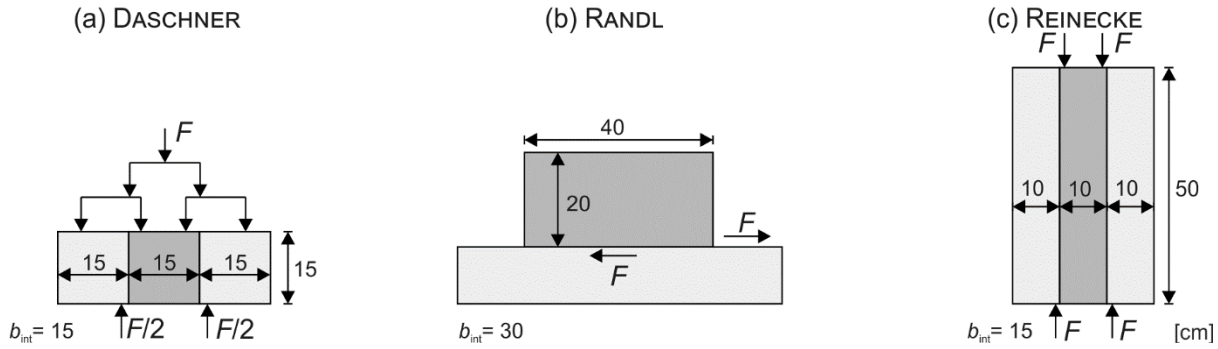

Figure 4-2: Test setups to investigate the adhesive shear strength conducted by DASCHNER [Das86a] (a), RANDL [Ran97] (b) and REINECKE [Rei04] (c)

For all test series, the adhesive shear failure occurred as brittle failure after the adhesive bond was exceeded. In accordance to the adhesive tensile tests, an increase of shear resistance with increasing interface roughness could be determined, but with very large scatter. The investigations by [Das86a] only showed small influence of concrete strength of both concrete layers, whereas the investigations by [Rei04] led to an significantly higher increase of interface shear resistance with increasing concrete strength of the new concrete compared to an increase of concrete strength of the old concrete. Considering the concrete properties, [Rei04] determined no influence of aggregate type but higher shear strengths for dry concrete surfaces compared to wet surfaces. [Ran97] stated an influence of the interface size on the adhesive shear resistance. With unimpaired bond, the shear stress is mostly transferred at the edge of the interface. The inner zone is mainly ineffective until the crack develops, and the edge region spread in the direction of shear. Especially for long interfaces, the elastic stress distribution concentrates in the edge region. Thus, the mean shear stress is influenced by the length of the interface.

4.2.3 Investigations for aggregate interlock and friction

After the applied shear stress exceeds the adhesive resistance of the interface, a crack opens along the interface. If normal stress act perpendicular to the interface, the horizontal displacement is prevented by frictional resistance or aggregate interlock. To determine the frictional resistance of concrete interfaces, experimental investigations were conducted by test specimens with interfaces between concrete cast at different times as well as monolithic precracked specimens to analyse the shear transfer across a concrete crack. Even though the surface of an interface between concrete cast at different times generally differs from a crack surface, the results from the investigations have partially been transferred.

To determine the shear resistance of a cracked surfaces, investigations with monolithic precracked specimens and applied normal stress have been conducted by e.g. [Hof69], [Wal81], [Nis62] and [Das86a] (cited by [Ran97]) as well as [Rei04] and [Tas87]. The test setups are shown in Figure 4-3.

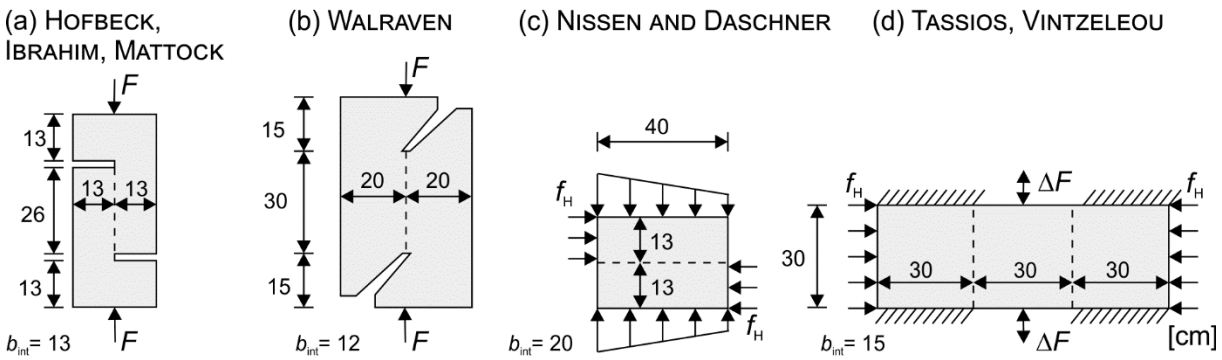

Figure 4-3: Test setups for inter-crack shear with monolithic specimens according to [Hof69] (a), [Wal81] (b), [Nis62] and [Das86a] cited by [Ran97] and [Rei04] (c), [Tas87] (d), [Rei04]

As expected, the precracked specimens reached higher displacements compared to monolithic specimens, with sudden appearance after loading where the initial displacement occurred after complete crack formation. According to [Hof69], the precracked specimens yielded 20 – 30 % less load compared to monolithic specimens. Whereas [Hof69] only determined an influence of the concrete strength for high interface reinforcement ratios, the investigations by [Wal81], [Nis62], [Das82] and [Tas87] showed an increase of shear resistance with increasing concrete strength and normal stress.

In contrast to precracked specimens, the condition of the interface between concrete cast at different times mainly depends on the surface treatment. To evaluate the transition between adhesive bond and shear resistance due to aggregate interlock, [Han60] compared load-displacement curves from sliding wall tests with T-cross sections and normal stress induced by clamping of the interface reinforcement as shown in Figure 4-4 (a).

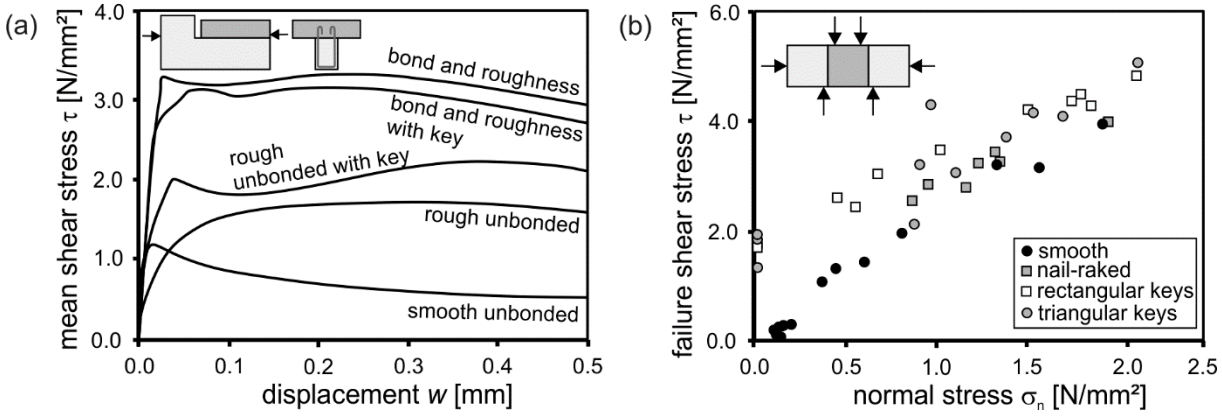

Figure 4-4: Test setup and shear stress-displacement curves by [Han60] (a) and relation of failure shear stress and normal stress for different roughnesses according to [Das86a] (b)

To exclude the effect of the amount of interface reinforcement, he subtracted the load-displacement curves by stirrups-only curves (specimens without interface bond). Whereas for smooth surfaces, no further shear stress could be applied after failure of the adhesive resistance, rough surfaces showed a further increase of shear resistance after an adhesive peak at between 0.02 and 0.03 mm displacement due to aggregate interlock.

The relation of externally applied normal stress and interface shear resistance was investigated in several test programmes, e.g. published in [Das86a], [Mai98] (cited by [Rei04]), [Rei04] and [Ran08], using push-off and push-through tests with controlled normal stress, as well as modified push-off tests with a constant ratio of shear- and normal stress due to inclined interfaces. As exemplarily shown by a test series reported in [Das86a] (Figure 4-4 (b)), a linear relation between applied normal stress and shear strength could be determined and with increasing interface roughness, higher shear stresses could be transferred. An increase of interface shear resistance with increasing normal stress and interface roughness could also be determined by modified push-off tests in [Mai98], [Rei04] and [Ran08], but with higher scatter of test data. Additionally, [Rei04] determined a minor influence of the concrete strength of the new concrete layer on the interface resistance due to aggregate interlock and normal stress.

4.2.4 Investigations for interface reinforcement

According to the general model concept for interface shear design, the predominant effect of interface reinforcement is the clamping effect, where tensile stress in the reinforcement prevent the interface opening, and the resulting compressive stress across the interface leads to frictional forces. If horizontal displacement of the interfaces occurs, the bending of the reinforcement bars leads to an additional load resistance term of dowel action (s. Chapter 2.3.3).

To investigate the effect of friction induced by clamping of the interface reinforcement, test series have been conducted in accordance to the test-setups presented in Chapter 4.2.3, e.g. by [Bir66], [Hof69], [Mat72] and [Mat74], using monolithic precracked specimens as well as specimens with concrete cast at different times. The results of the test series correspond to the results from the investigations with applied normal stress, where the interface shear resistance increased with increasing normal stress (in this case induced by increasing amount of interface reinforcement) and increasing interface roughness.

The interface shear resistance due to dowel action has been investigated by test series in e.g. [Hof69], [Pau74], [Tso89], [Mat72] and [Ran97]. To minimize the effects of adhesion and friction, bondbreaker was partially applied between the concrete layers. According to investigations in [Hof69], a load resistance due to dowel action can only be activated when relative displacement occurs between the concrete layers. With a test programme published in [Pau74], the effect of dowel action was examined by shear tests with smooth and waxed surfaces to prevent adhesive bond of the surfaces. The load-displacement curves for test specimens with different reinforcement ratios are shown in Figure 4-5 (a). As expected, the shear resistance increases with increasing reinforcement ratio. According to steel strain measurement, all bars were yielding after approximately 2.5 mm displacement. However, after the slip was further increased to 12.7 mm, the load could be further increased about 88 % for $\rho = 0.31$ %, about 43 % for the $\rho = 0.69$ %

and only about 9 % for ρ = 1.23 %. This indicates, that the smallest bar diameters account for the largest post-elastic stress gain due to kinking effect. However, even though the load increase due to dowel action was significant in the test series, [Pau74] stated that due to the large necessary displacements for the activation of this load bearing mechanism, dowel action should not be considered as a variable component for shear resistance along construction joints.

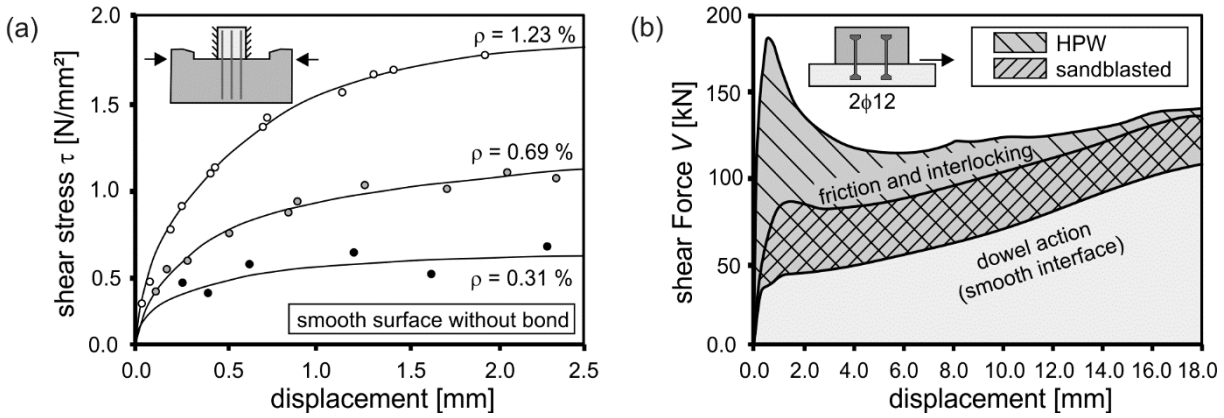

Figure 4-5: Test setup and load-displacement curves relationships for investigations for dowel action [Pau74] (a), load-displacement curves of sandblasted and HPW interfaces with shear dowels according to [Ran97][Ran08] (b)

A research programme to examine the interaction of clamping effect and dowel action was reported in [Ran97][Ran05]. The push-off tests with dowels as interface reinforcement were conducted with surfaces roughened by sandblasting and high-pressure water (HPW). The shear resistance of dowel action was determined by smooth unbonded interfaces. The load-displacement curves for a sandblasted and a HPW interface are shown in Figure 4-5 (b). Whereas the dowel resistance increases until failure, the load-displacement curves for the rough interfaces reach their maximum after about 0.5 – 1.5 mm when the resistances of adhesion and aggregate interlock were exceeded. [Ran05] describes the further increase of shear stress with increasing displacement by the kinking effect of the reinforcement. Additionally, strain measurement of the reinforcement showed yielding due to interaction of normal force and bending.

4.2.5 Investigations under cyclic loading

Experimental investigations determining the effect of cyclic loading on the interface shear resistance have been reported e.g. in [Tas87]. To examine the loss of bearable shear stress under repeated loading, they tested push-through tests with smooth and rough surfaces under low-cycle fatigue up to eight load cycles. For smooth interfaces, the shear stress-displacement curve in Figure 4-6 (a) depicts only small fret of shear resistance, whereas for rough surfaces, the displacement curve in Figure 4-6 (b) shows a large decrease of shear resistance with increasing number of load cycles and similar interface slip. [Tas87] explained this effect by fret of the rough surface profiles, which may reduce the frictional resistance of the interface.

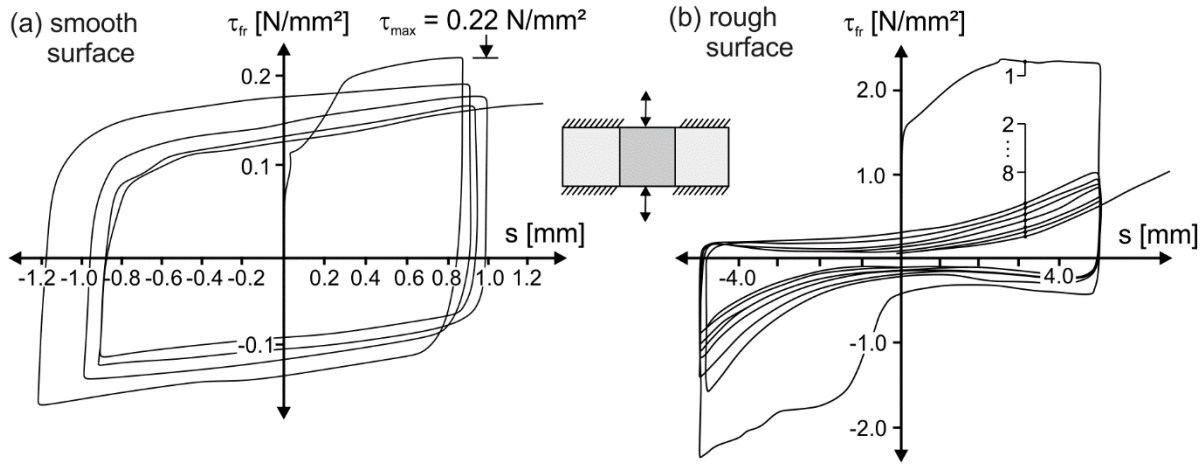

Figure 4-6: Typical shear stress – displacement curves under cyclic loading for smooth interfaces (a) and rough interfaces (b) according to [Tas87]

Cyclic tests to examine the fatigue resistance of adhesive bond have been published in [Zil04] with push-through tests varying the interface roughness and concrete strength. The specimens were tested with a upper shear stresses between 50 and 90 % of the ultimate shear strength of a static reference test and the lower shear stress was set to be about 30 – 40 % of the upper shear stress. After reaching the reference number of load cycles (N = 1.0 – 2.0 mil.) the specimens were tested monotonically until failure. Even though the test results showed large scatter, the displacement measurements after N = 1.0 mil. load cycles showed almost no fracture during testing for upper shear stress about 50 % of the static shear strength.

A decrease of interface shear resistance under cyclic loading conditions has also been reported in [Ran05] and [Ran13] with tests in accordance to Chapter 4.2.4, Figure 4-5 (b). The specimens were tested with upper shear stress between 41 – 60 % of the static ultimate shear strength up to N = 2.0 mil. load cycles. By statistically evaluating the test results including test series with precracked fatigue tests in [Pru88], a limit for the ratio of upper shear stress and ultimate static shear resistance of 42 % was derived for design, which was adapted for the fatigue verifications defined in Model Code 2010 [MC10] (s. Chapter 3.3.5).

4.3 Beam and slab specimen

4.3.1 Introduction

For composite beam and slab specimens, more complex stress states can be expected at the interface due to load redistributions and crack development caused by the interaction of flexure and shear. Comparing beam and slab specimens however, the main difference are the dimensions of the structure as well as the location of the interface in the cross section. For beam specimens, the concrete interface commonly occurs between flange or slab with a comparatively small width, whereas for slab specimens, the interface is

commonly located at the bottom of the cross section. Therefore, the interface generally covers the whole structure and thus, yields higher possibilities of stress distributions. On the contrary, the larger interface areas in slab structures provide higher possibilities of blemished in the bond structure, which might have a negative effect on the interface shear resistance. Additionally, due to common construction rules, a minimum amount of shear reinforcement must be applied in beam specimens, whereas the design of slabs does not necessarily require shear reinforcement.

4.3.2 Investigations with beam specimens

The experimental investigations in literature with composite beam specimens were conducted predominantly by T-beam cross sections, tested in three- or four point simply supported beam tests with and without interface reinforcement [Han60], [Sae64], [Das86a], [Loo94], [Kah04]. The failure of the composite beams without interface reinforcement indicated a different load bearing behaviour compared to monolithic beams with individual strain distributions acting in the cross sections. Generally, it was observed that with increasing load, shear cracks formed from flexural cracks and after reaching the interface, the cracks developed along the interface. For all test series, the crack development along the interface decreases with increasing interface roughness and thus, higher shear stresses could be transferred.

In a test programme conducted by [Han60] two individual strain distributions were observed in the two concrete layers after interface delamination. In the old concrete layer, the upper parts of the flexural cracks were closing, indicating compression in the upper part of the old concrete section. In the new concrete layer, tensile stresses above the interface led to flexural cracks at the bottom of the new concrete section. The failure was induced by shear cracks in the concrete topping. Investigations in [Sae64] examined the influence of interface roughness, as well as the influence of shear span, location of the interface in the cross section and the amount of interface reinforcement. For the beam tests, three types of failure could be observed. Beams with high shear span to depth ratios ($a/d = 7.29$) mostly failed in bending, but with little horizontal cracks along the interface between load and support but no horizontal cracks at the end of the beams. The specimens with smaller shear slendernesses ($a/d = 2.14$ and 3.43) failed either due to a combination of flexure and shear or predominantly due to shear cracks, which were forming from flexural cracks and developing along the interface until reaching the end of the beam. If interface reinforcement was applied, higher shear stresses could be transferred. Regarding the position of the interface, interfaces placed below the neutral axis somehow gained higher loads than interfaces placed above the neutral axis. However, increasing the concrete strength only showed little influence on the shear capacity of the interface. Similar results were achieved by a test programme conducted by [Das86a]. For T-beams without interface reinforcement, the interface failure mode was brittle, whereas for specimens with interface reinforcement, the tests showed a quasi-monolithic

load bearing behaviour and the shear cracks were crossing the interface without considerable displacement. The failure mechanism was mostly defined as concrete crushing in the web or yielding of the shear reinforcement. T-beam specimens in [Loo94] with interfaces left as cast and coarse aggregates showed no significant interface slip and stirrup stress until horizontal shear stress of $\tau = 1.5 - 2.0$ N/mm². The effectiveness of stirrups improved with increasing distance from midspan but being ineffective in the support area. An influence of the concrete strength of the flanges was observed by [Kah04]. For flanges with lower concrete strengths, the simply supported T-beams showed flexural failure, and flanges with high strength concrete failed by concrete crushing of the flanges between the load points.

To investigate the influence of different shrinkage and creep as well as stress redistribution due to strain differences between prestressed planks and the added concrete layers, [Abe72] published a test series with rectangular beams and prestressed planks without interface reinforcement. Generally, it could be observed that the interfaces roughened by wire brushing were sufficient to avoid horizontal shear failure, which only occurred after yielding of the flexural reinforcement. If the new concrete layer was cast after shrinkage and creep of the prestressed plank already took place, compressive stress occurred in the prestressed element increasing the effect of prestressing. However, tensile stress developed in the new concrete layer which had an additional weakening effect on the interface shear resistance.

4.3.3 Investigations with slab specimens

To determine the hypothesis that interface reinforcement in composite slabs may be neglected under certain conditions, [Reh80] conducted semi-precast slab specimens as shown in Figure 4-7. The specimens were tested in four-point bending tests with a shear span to depth ratio of $a/h = 4.0$. The crack patterns of all specimens, except those with smooth surfaces weakened by oil, showed horizontal cracks forming from flexural cracks close to the support, developing along the interface and inclining to a shear crack towards the load application. For the very smooth and oiled interface, a delamination of the new concrete occured along the whole structural axis (Figure 4-7 (b)).

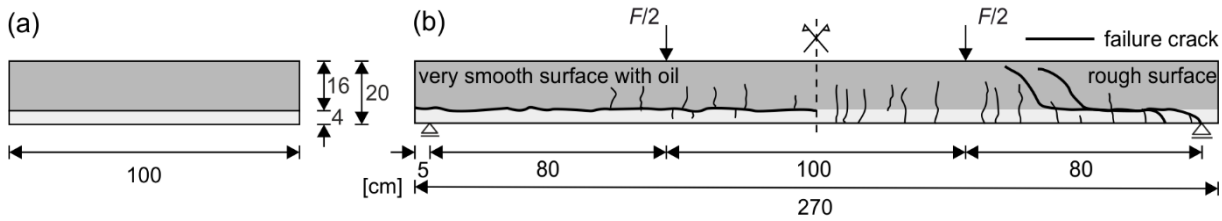

Figure 4-7: Slab specimens conducted by [Reh80]: Cross section (a), span with crack patterns for a very smooth and rough interface (b)

However, according to these investigations, interface reinforcement can be neglected if the acting shear stress is less than 50 % of the full shear strength according to the regulations in [D1045] and the interface is sufficiently roughened. Smooth interfaces as well

as surfaces left as cast shall not be not permitted for interfaces without interface reinforcement.

Investigation with prestressed semi-precast composite slabs without interface reinforcement published in [Heg03] were conducted with high strength concrete for the precast slabs and normal strength insitu concrete. The interfaces were left as cast or roughened by raking. For all specimens, a typical shear failure in accordance to failure of monolithic specimens occurred. A delamination of the interface could only be observed by very small horizontal cracks which did not participate is the failure crack pattern.

4.3.4 Investigations under cyclic loading

Following the investigations by [Sae64], [Bad67] examined the effect of cyclic loading on the interface shear strength of concrete composite T-beams. The test parameters for the four-point bending tests were interface roughness, interface reinforcement ratio and shear slenderness. The cyclic loading was applied by 250 cycles per minute with upper loads between 70 – 124 % of the reference tests by [Sae64] and lower loads about 20 % of the upper loads. If no failure occurred during cyclic testing until reaching $N = 2.0$ mil. load cycles, the specimens were tested until monotonic failure. The load bearing behaviour of the fatigue tests generally corresponded to monolithic tests with similar crack distributions but larger scatter in beard number of load cycles and for the load displacement curves. With increasing interface roughness, the interface shear resistance could be increased. The influence of interface reinforcement was increasing proportional to the amount of reinforcement crossing the interface and with increasing shear slenderness, the shear resistance decreased.

According to results from a test programme with 4-point bending T-beam tests under cyclic loading in [Chu76], where the test parameters were interface reinforcement ratio and magnitude of the applied load, a fatigue failure of the interface is not probable if the upper load is smaller than 55 % of the static reference load or if the interface shear stress is smaller than $\tau = 2.75$ N/mm². The interfaces were roughened by exposing the aggregates and the cyclic load was applied with 240 cycles per minute until reaching $N = 1.0$ mil. load cycles. The upper load was 70 % and the lower load was 10 % of the ultimate load of reference tests.

For semi-precast slabs with stirrups as interface reinforcement, as well as T-beams under high fatigue loads, a research programme was published in [Sch96a][Sch96c][Sch96d]. The test parameters were the interface roughness, interface reinforcement ratio and concrete strength of both, precast and insitu concrete. The four-point bending tests with $a/d = 3.0$ were subjected to 1.25 of the service loads and then, cyclically loaded between 0.5 and 1.0 of the service loads until reaching $N = 2.0$ mil. load-cycles. If no fatigue failure occurred, the tests were monotonically loaded until failure. The results of the tests showed, that for surfaces left as cast, as well as for rough surfaces, the load bearing behaviour and crack patterns were similar to monolithic structures, with cracks crossing

the interface without significant displacement. Thus, the interface reinforcement was mainly not stressed in the interface area.

To investigate the fatigue behaviour of semi-precast slabs with lattice girders, several fatigue tests were conducted in the 1980s. The test programmes and important test results are presented in Chapter 5.2.2.

An overview of the presented test series with test setup, dimensions, material properties, test parameters and failure shear stress can be found in Annex B.

5 Own experimental investigations

5.1 Introduction

For precast constructions, lattice girders are prefabricated reinforcement systems to be installed in semi-precast elements, e.g. in semi-precast slabs or element walls. On building site, the semi-precast elements are finished with insitu concrete. The prefabrication reduces construction time in the building process and minimises the risk of mistakes while assembling. On site, the precast element can be used as slab formwork and the lattice girders combined with insitu concrete ensure a quasi-monolithic bearing behaviour. Lattice girders can be used to secure transport and assembling for building state, and for final state, the lattice girders can be used as interface reinforcement. Depending on type and disposition, lattice girders can also account for shear reinforcement [Fur14][Fur16]. In buildings, semi-precast slabs are generally subjected to monotonic loading. However, in industrial constructions due to e.g. forklift trucks or oscillating machinery, as well as in bridge construction, the semi-precast slabs may be subjected to cyclic loading conditions due to traffic loads.

The design of semi precast slabs with lattice girders follows the general technical approvals for the lattice girders, which are based on the National Annex of Eurocode 2 [EC2NAD]. For fatigue, the fatigue-strength-curves (S-N-curves) defined in [EC2NAD] for profiled bars, which are either bent or welded, are not applicable for lattice girders. Due to the geometric condition with a combination of bent and point-welded bars with a smooth surface, the design in the technical approvals is limited to a simplified fatigue verification. The design regulations in the general technical approvals were derived based on fatigue tests in literature. To improve and expand the limits of application, theoretical and experimental investigations have been conducted at the Institute of Structural Concrete (IMB), RWTH Aachen University.

The following chapter starts with the background on lattice girders as interface reinforcement in semi-precast slabs for fatigue. Subsequently, two experimental programmes conducted at IMB are presented. Starting with small size tests to determine S-N-Curves for lattice girders and followed by a test programme to investigate the fatigue behaviour of semi-precast slabs with lattice girders. The test programmes were conducted during a research programme initiated by the Research Association of the German Concrete and Precast Industry e.V. and funded by the German Federation of Industrial Research Association (AiF, IGF number 18407 N/1). A detailed description can be found in [Heg17].

5.2 Lattice girders for fatigue

5.2.1 Introduction

Whereas a large number of lattice girder types exist for monotonic loading, only three types of lattice girders are approved for fatigue in semi-precast slabs and three for element walls. The lattice girders approved for fatigue are manufactured by the companies *Badische Drahtwerke GmbH* (B-Tec) and *Filigran Trägersysteme GmbH & Co.KG* (Filigran) and summarised with corresponding number of technical approvals in Table 5-1.

Table 5-1: Lattice girders with general technical approval for fatigue

	semi-precast slabs		element walls	
	B-Tec	*Filigran*	*B-Tec*	*Filigran*
	KTS Z-15.1-38	EQ Z-15.1-93	KTS Z-15.2-100	EQ Z-15.2-40
	KT100 Z-15.1-136	–	–	–
	–	–	KTW Z-15.2-9	–

Z-15.1-38 [DZ-38]; Z-15.1-93 [DZ-93], Z-15.2-100[DZ-40][DZ-136] [DZ-100], Z-15.2-40 [DZ-40]; Z-15.1-136 [DZ-136]; Z-15.2-9 [DZ-9]

Lattice girders *B-Tec KTS* [DZ-38] and *Filigran EQ* [DZ-93] are structurally identical, approved for semi-precast slabs as well as element walls and can also account as shear reinforcement. Due to the wide range of application as well as the small mandrel diamenter, which has an adverse effect on the fatigue strength, these lattice girder types have been chosen for the following theoretical and experimental investigations.

The geometries of lattice girders *B-Tec KTS* [DZ-38] and *Filigran EQ* [DZ-93] for a height of 10 – 16 cm and 17 – 30 cm are shown in Figure 5-1.

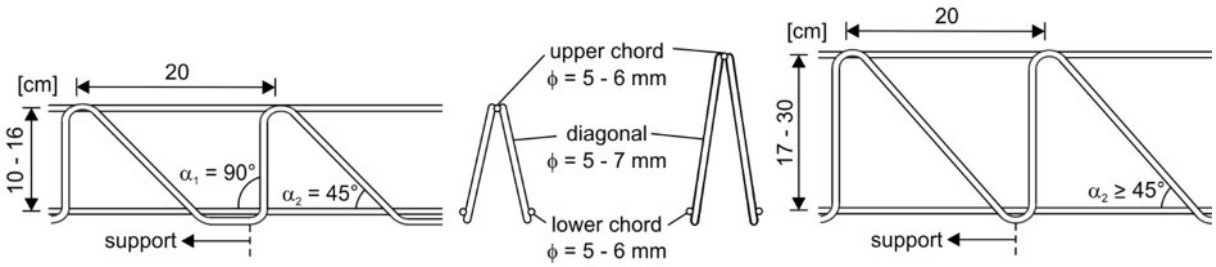

Figure 5-1: Geometries of lattice girder *KTS* [DZ-38] and *EQ* [DZ-93]

As mentioned in Chapter 2.3.3, reinforcement bars declining towards the support cannot be accounted for interface reinforcement. Due to the 90° inclination of every second diagonal and the other diagonals being inclined towards the support, all bars can be

included for interface shear design. If the height of the girder covers the structures height and follows the construction rules of shear reinforcement, the lattice girders can be accounted for shear design.

5.2.2 Fatigue tests from literature

The fatigue behaviour of semi-precast slabs with lattice girders has been investigated in order to derive design specifications in the technical approvals. In this context, 29 fatigue tests have been conducted and described in literature. For semi-precast slabs with lattice girders KTS [Sch85], EQ [Web89] and KT100 [Sch81][Sch82][Sch83], the specimens were tested with simply supported slabs with two point loads. For element walls with KTW [Web95], the specimens were tested as simply supported slabs with cantilevers. Table 5-2 dedicates lattice girder types, number of tests and test setups.

Table 5-2: Fatigue tests with lattice girders from literature

	Geometry	Lattice girder		Test setup
		B-Tec	*Filigran*	
slabs	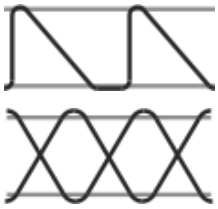	KTS *n* = 10	EQ *n* = 2	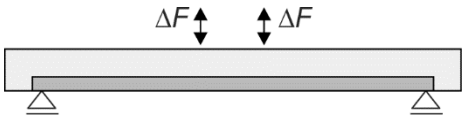
		KT100 *n* = 14		
walls	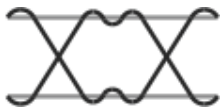	KTW *n* = 3		

n: no. of tests; test reports: KTS: [Sch85]; EQ: [Web89]; KT100: [Sch81][Sch82][Sch83]; KTW: [Web95]

All fatigue tests were cyclically loaded with a frequency of $f = 2.0 – 2.5$ Hz and a constant load range up to $N = 2.0$ million load cycles. The upper load limit for the cyclic loading was determined to generate a tensile stress in the diagonals of 70 % of the yield strength, which results in a load exceeding the approved operating load by 25 %. The applied stress range in the diagonals varied between $\Delta\sigma_{Dia} = 180 – 230$ N/mm². After reaching the $N = 2.0$ mil. load cycles, the specimens were loaded monotonically until failure. Comprehensively for all test series, the shear span to effective depth ratio was kept between $a/d = 3.4 – 3.8$, the concrete compressive strength varied between $f_{cm,cyl} = 16.1 – 39.3$ N/mm² for the precast slab and $f_{cm,cyl} = 13.9 – 32.5$ N/mm² for the insitu concrete. The lattice girders in the slab's cross section were placed in one, two or three rows in order to determine the effect of the amount of interface reinforcement. The interface quality was left as cast, left as cast with additional bond breaker or intentionally roughened by raking. Figure 5-2 shows an exemplary test specimen from the test series conducted for lattice girder KTS [Sch85].

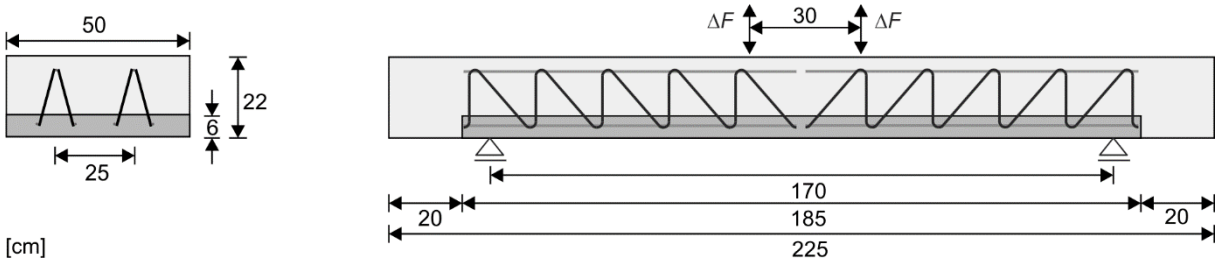

Figure 5-2: Test specimen and test setup for fatigue tests with lattice girders KTS according to [Sch85]

Most of the fatigue tests ended either by fatigue bending failure or after residual failure after reaching the reference number of load cycles. Interface shear failure only occurred for four specimens during cyclic loading and for two specimens after residual load. These specimens had a smooth surface including bond breaker. A pure shear failure did not occur during these investigations.

To specifically determine the fatigue resistance of the critical section of the lattice girders at the bent and welded node between diagonal and chord, additional small size tests have been conducted with lattice girders *B-Tec KTW* and *Filigran EQ* (s. Table 5-2) . Therefore, the diagonals were cast in concrete cubes with a concrete strength of B25 and with an interruption of bond by a cladding tube installed until the welded node (Figure 5-3 (a)). The cyclic loading was applied to the diagonal with a constant stress range and a frequency of $f = 100$ Hz.

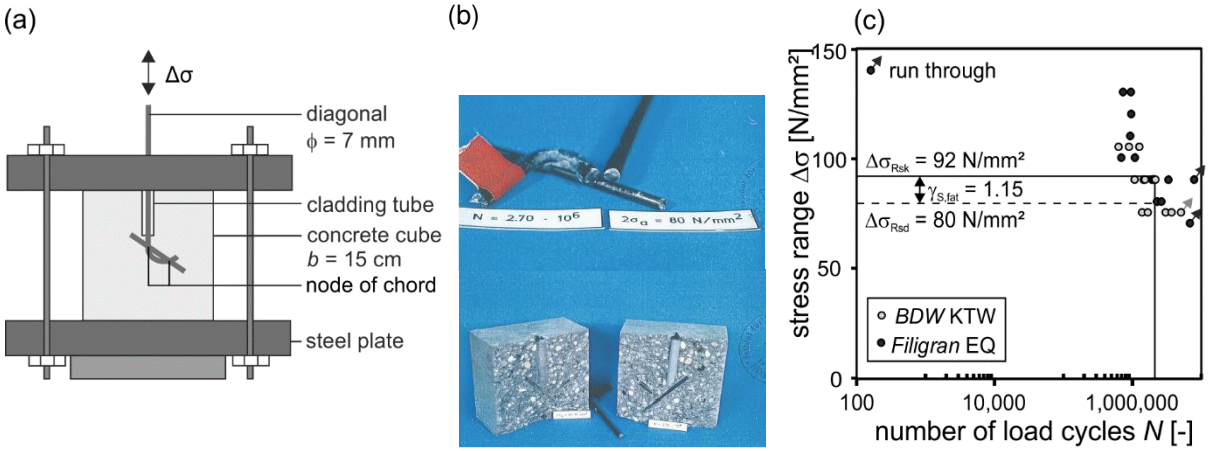

Figure 5-3: Investigations to determine the stress range resistance according to [Web89] [Web95]: test setup (a), fracture of node (b) and test results (c)

All small size tests failed in the welded node between diagonal and chord (Figure 5-3 (b)). In Figure 5-3 (c), the applied stress ranges are shown with the corresponding number of load cycles. With these test results, a characteristic approved stress range of $\Delta\sigma_{Rsk} = 92$ N/mm^2 could be determined for $N = 2.0$ mil. load cycles, which was adopted to the fatigue verification of lattice girders (s. Chapter 5.2.3).

5.2.3 Design of semi-precast slabs with lattice girders

The design of semi-precast slabs with lattice girders follows the general technical approval of the lattice girders, which are based on the regulations of [EC2NAD]. Generally, the design of lattice girders KTS [DZ-38] and EQ [DZ-93] is in accordance to the regulations in [EC2NAD]. For cyclic loading, the chords cannot be included in the determination of longitudinal reinforcement. For interface shear, the formulations and material coefficients apply in accordance to Chapter 3.3.3. However, the maximum shear resistance differs from the [EC2NAD] expression and is limited to the values in Table 5-3. The values were adopted from the limitations defined in [D1045] and reduced to 50 %.

Table 5-3: Maximum shear resistance of lattice girders KTS and EQ for normal weight concrete according to the general technical approvals [DZ-38][DZ-93]

	C20/25	C25/30	C30/37	C35/45	C40/50	C45/55	C50/60
$v_{Rd,max}$ [N/mm²]	2.4	2.8	3.3	3.6	3.8	4.0	4.1

For fatigue, the stress range in the diagonals of the lattice girders has to be verified. Due to absence of S-N-curves, a verification of stage 2 or stage 3 is excluded and thus, the verification is limited to a simplified verification with an approved characteristic stress range of $\Delta\sigma_{Rsk} = 92$ N/mm² for $N = 2.0$ mil. load cycles.

For interface shear design, the fatigue resistance of the lattice girders is derived by converting the interface shear equation of [EC2NAD] (Eq. (3-21)). For semi-precast slabs with lattice girders under cyclic loading, the interface must have at least a rough surface. Thus, the formulation is modified by considering the coefficients for rough interfaces ($\mu = 0.7$), neglecting the term of adhesion for fatigue ($c = 0$) and the term of friction ($\mu \cdot \sigma_n = 0$). Furthermore, the stress range is increased by the term 1/0.6. The factor 0.6 is based on regulations in DIN 1045:88 [D1045], which includes the conservative estimation of a shallow angle of compression strut by a reduction factor of 0.85 and a correction factor 0.7 for the enhanced fracture potential of the bent diagonals [Ber89]. Substituting the yield strength of the reinforcement by the approved stress range and the partial fatigue safety factor for steel, as well as implying the inclination of every second angle of the diagonals with $\alpha_1 = 90°$, the verification of stress range at an interface with lattice girders follows Eq. (5-1).

$$\Delta v_{Rdi,fat,LG} = \rho \cdot \frac{\Delta\sigma_{Rsk}}{\gamma_{s,fat}} \cdot (1.4 \cdot \sin\alpha_2 + 1.67 \cdot \cos\alpha_2) \tag{5-1}$$

With

ρ interface reinforcement ratio of lattice girders

$\Delta\sigma_{Rsk}$ approved characteristic stress range
$\Delta\sigma_{Rsk} = 92$ N/mm² for $N = 2.0$ mil. load cycles

$\gamma_{s,fat}$ partial safety factor of reinforcement under fatigue $\gamma_{s,fat} = 1.15$

α_2 inclination of inclined diagonal in accordance to Figure 5-1

The design value of the applied shear stress shall not exceed the limitation of Eq. (5-2) with the static maximum shear resistance according to Table 5-3.

$$v_{Rdi,max,fat} = 0.5 \cdot v_{Rdi,max,stat} \tag{5-2}$$

Additionally, certain detailing rules have to be satisfied for fatigue. The interface shall at least have a rough surface with a height of the precast slab with a minimum depth of $h_{pre} \geq 6$ cm. The lattice girders shall have a minimum height of $h_{LG} \geq 10$ cm with an inclination of the diagonals of $\alpha_2 \geq 45°$ and the lower chords cannot be accounted as longitudinal reinforcement. The diameter of the longitudinal reinforcement in the precast slab is limited to $Ø_{sl,max} = 16$ mm and shall be sufficiently anchored at the supports. Furthermore, a stepwise distribution of the longitudinal reinforcement is not permitted.

5.3 Small size fatigue tests to determine S-N-curves for lattice girders

5.3.1 Introduction

Due to absence of fatigue-strength curves (S-N-curves) for lattice girders, the fatigue design of semi-precast slabs with lattice girders is limited to a simplified verification by limiting the stress range in the diagonals to $\Delta\sigma_{Rsk} = 92$ N/mm² for $N = 2.0$ mil. load cycles. In order to extend the range of application by deriving S-N-curves for lattice girders, small size fatigue tests with lattice girder diagonals cast in concrete cubes have been conducted at the Institute of Structural Concrete, RWTH Aachen using the procedure of the *Interactive method*. This procedure had also been adapted to derive S-N-curves for other lattice girder systems, e.g. in [Fur19]. In the following, methods to determine S-N-curves are presented, followed by the experimental investigations and statistic evaluation conducted at IMB.

5.3.2 Methods to determine the fatigue strength of reinforcing steel

In literature, different procedures are provided to determine the endurance fatigue strength and S-N-curves for reinforcing steel. Most methods are based on several cyclic tests with a constant stress range each. In the following, the procedures of the *PROBIT method* (endurance fatigue strength) as well as the *Stair-step method* and the *Interactive*

method (S-N-curves) are presented. An overview of additional methods can be found in [Blo03].

PROBIT method

The *PROBIT method* [Bux86] generally serves the determination of the endurance fatigue strength of materials. Therefore, 50 specimens are tested at similar magnitudes in a range of the estimated endurance fatigue strength until a predefined number of load cycles. By considering the number of run-through specimens, the survival probability can be determined for every magnitude. By this relationship, the mean values and the measure of scatter of the endurance fatigue strength can be implied.

Stair-Step method

The *Stair-Step method* is a common procedure to determine S-N-curves and is described in [Bux86] and [Dub95]. For the tested material, the endurance fatigue strength its scattering range are estimated based on experience values. The estimated scattering range is then allocated in about four equally sized parts. The first specimen is tested on a medium load level and the load levels of the following specimens are stepwise increased for run through specimens and decreased for specimens with failure. Following this procedure, the mean value of the fatigue strength can be approached. By considering the standard variation, a function for the fatigue strength with arbitrary survival probabilities can be extrapolated. According to [Dub95], a number of 15 – 20 tests are required, whereas [Bux86] demands a number of 40 specimens.

Interactive method

To determine a complete and reliable S-N-curve, covering the whole range between low cycle fatigue strength and high cycle fatigue strength (Figure 5-4 (a)) with a comparable small number of test specimens, [Blo03], [Mau10a] and [Mau10b] presented the *Interactive method*. By applying this method, predefining the tested load levels shall be avoided and a statistically consistent approximation of the quantiles with self-defined level of reliability for all ranges of S-N-curves shall be assured. Additionally, by evaluation with the *Interactive method*, partial safety factors based on DIN EN 1990 [EC0] for covering scatter can be derived.

For the determination of S-N-curves, three to five monotonic and 20 – 25 cyclic tests with constant stress ranges are necessary with preferably similar test specimens. The load level of the first test is defined to be about the yield strength of the specimen. During the further process of the test programme, the stress curve of the S-N-curve is approached by adjusting the load level to incrementally approximate the high cycle fatigue strength. Therefore, the applied stress range is varied with defining either a constant minimum shear stress or maximum shear stress, respectively. The statistic evaluations follow the experimental programme, starting after the fourth fatigue test. In the first

instance, the mean function of the fatigue strength is developed incrementally, followed by generating a quantile function with arbitrary confidence level. An exemplarily description of the test procedure is shown in Figure 5-4 (b).

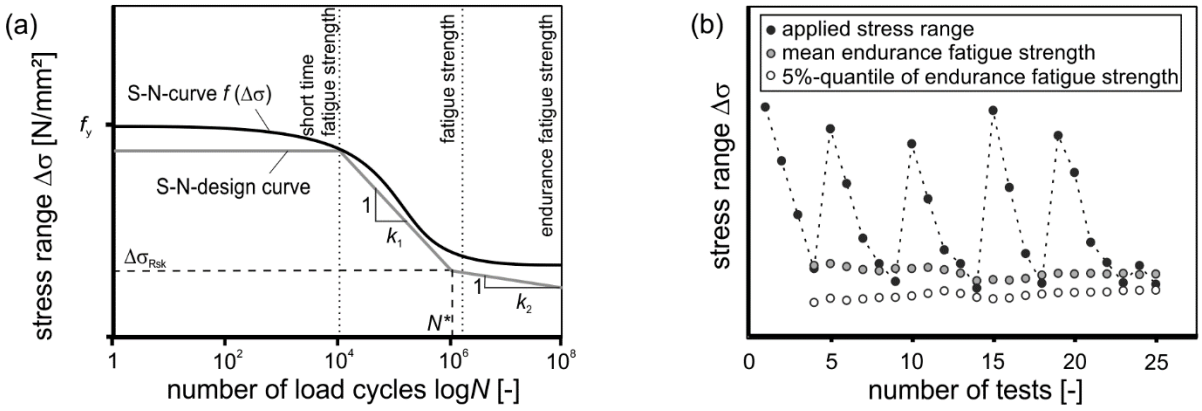

Figure 5-4: Function covering the S-N-curve (a) and process description of test procedure (b) according to the *Interactive method* [Mau10a]

The function of the S-N-curve $f(\Delta\sigma)$ to determine the fatigue strength depending on the number of load cycles N follows Eq. (5-3).

$$f(\Delta\sigma) = \alpha_1 + (f_u - \sigma_{min} - \alpha_1)\cdot\alpha_2^{\ln(N)^{\alpha_3}} \tag{5-3}$$

With

f_u	tensile strength of steel specimens
σ_{min}	minimum stress of cyclic loading in the specimen
$\alpha_1, \alpha_2, \alpha_3$	parameters determined by regression analysis

The regression parameter α_1 corresponds to the endurance resistance and the dimensionless parameters α_2 and α_3 describe the slope of the S-N-curve for the fatigue strength limited to the boundaries $0 < \alpha_2 < 1$ and $\alpha_3 > 0$.

To transfer the mean curve in a quantile function with arbitrary confidence level, quantile factors can be determined by calculating p-quantiles following Eq. (6-3).

$$\Delta\sigma_p = \Delta\sigma_m \pm k_n \cdot \Delta\bar{\sigma} \tag{5-4}$$

With

$\Delta\sigma_p$	p-quantile of $\Delta\sigma$ with significance level $\leq (1\text{-}W)$ with W as confidence level
$\Delta\sigma_m$	mean value of sample
k_n	quantile factor
$\Delta\bar{\sigma}$	standard deviation of sample

To develop a S-N-curve in accordance to the trilinear design curves defined in [EC2] and [EC2NAD] (Figure 5-4 (a)), the gradients k_1 and k_2 can be defined as upper limits

by $k_2 = 2 \cdot k_1 - 1$. An extensive description of determining S-N-curves with the *Interactive method* can be found in [Blo03], [Mau10a] and [Mau10b].

5.3.3 Description of test specimens and test setup

For determining S-N-Curves of a representative lattice girder, small size specimens have been conducted with lattice girder diagonals cast in concrete cubes. For the experimental investigations, lattice girder type *Filigran* EQ [DZ-93] with the maximum height of 30 cm has been chosen. This lattice girder is equivalent to *B-Tec* KTS [DZ-38] and presents an adverse geometry with the small mandrel diameter between diagonal and vertical bar and the point welded node between lower and upper chord. To minimise the scatter of test results, all girder diagonals in the experimental investigations came from one production batch.

To evaluate the fatigue strength of the welded nodes, the sections between diagonal and lower chord as well as between diagonal and upper chord have been investigated. Whereas two diagonals are welded to the upper chord, only one diagonal is welded to the lower chord. For the test specimens, the critical areas were cut out of the girder and casted in a formwork cube with dimension of b = 15 cm and a concrete class of C20/25 (Figure 5-5 (a) and (b)). In order to ensure a direct load application at the critical node, a cladding tube was built in the formwork to prevent bond between concrete and reinforcing bar. The lower and upper chord had a diameter of $Ø_{chord}$ = 5 mm and were cast up to the edges of the cube to prevent restraints at the ends of the chords. The diagonal had a length of 30 cm and a diameter of $Ø_{dia}$ = 7 mm, which satisfies the required test length of 140 mm or $14 \cdot Ø$ = 98 mm according to [D15630].

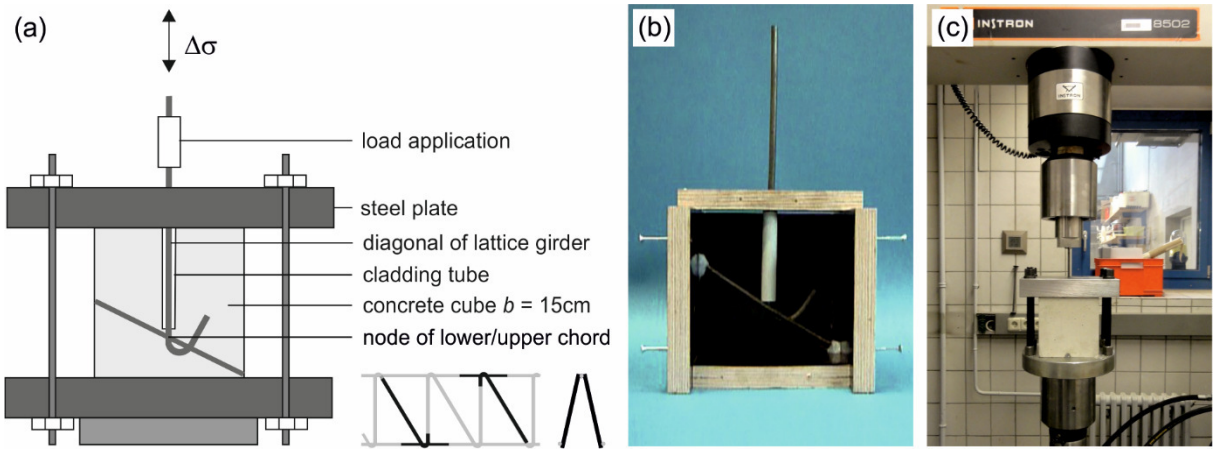

Figure 5-5: Schematic depiction of fatigue test setup (a), node of lattice girder in formwork (b) and test setup for fatigue tests (c)

5.3.4 Test procedure

According to the test procedure of the *Interactive Method* (s. Chapter 5.3.2), three to five monotonic tests as well as 20 – 25 fatigue tests are necessary to determine a S-N-curve of a material. For the monotonic tests, three concrete cubes for each, lower chord

and upper chord, have been conducted. The specimens have been tested upside down in a test rig by clamping the diagonal bar with wedges. The load was applied displacement controlled by a test cylinder until steel failure.

For the fatigue tests, the concrete cubes were clamped between two steel plates and the cyclic loading from the test cylinder was introduced by wedge anchorage to the diagonal (Figure 5-5 (c)). The load was applied with a frequency of f = 20 Hz up to N = 5.0 mil. load cycles.

The stress ranges were defined following the test procedure depicted in Figure 5-4 (b). In accordance to [Mau10b], the minimum stress was determined to σ_{min} = 125 N/mm² and the stress ranges were applied by adjusting the maximum load σ_{max}. Even though constant minimum stress contradicts the general determination of a constant maximum stress for establishing the fatigue resistance of reinforcement with of σ_{max} = 300 N/mm² [D488][D15630], the *Interactive method* recommends a constant minimum stress to cover stress ranges $\Delta\sigma \geq 300$ N/mm² and to ensure a more realistic evaluation with considering constant permanent loads of the structure. The fatigue tests started with a maximum stress in the range of the yield strength. For the following four tests, the stress range was decreased stepwise until reaching the estimated endurance fatigue strength. Due to the parallel statistic evaluation of the test results, the path of applied stress ranges could be subsequently adjusted. Test specimens exceeding the limit of load cycles were declared as run through specimens and were cyclically tested with a higher stress range. To achieve a reasonable path of S-N-curve after statistic evaluation, 33 tests with lower chords and 25 tests with upper chords were conducted.

5.3.5 Results of small size fatigue tests

The lattice girder diagonals subjected to monotonic tensile stress failed with the fracture being located between load application and welded node (Figure 5-6 (a)). Failure in the immediate area of load application and welded node with a distance $\leq 4 \cdot Ø_{dia}$ did not occur. The yield strength of the static test was determined to f_y = 564 – 573 N/mm² for the specimens with diagonals and lower chords and between f_y = 558 – 567 N/mm² for diagonals and upper chords.

For both, the lower and upper chord nodes, failure of the diagonal in the fatigue tests occurred at the welding. In this context, Figure 5-6 (b) shows the fractured diagonal of a lower chord node which was subjected to a stress range of $\Delta\sigma$ = 375 N/mm² and bore N = 162,177 load cycles and Figure 5-6 (c) gives a detailed view of the fatigue fracture.

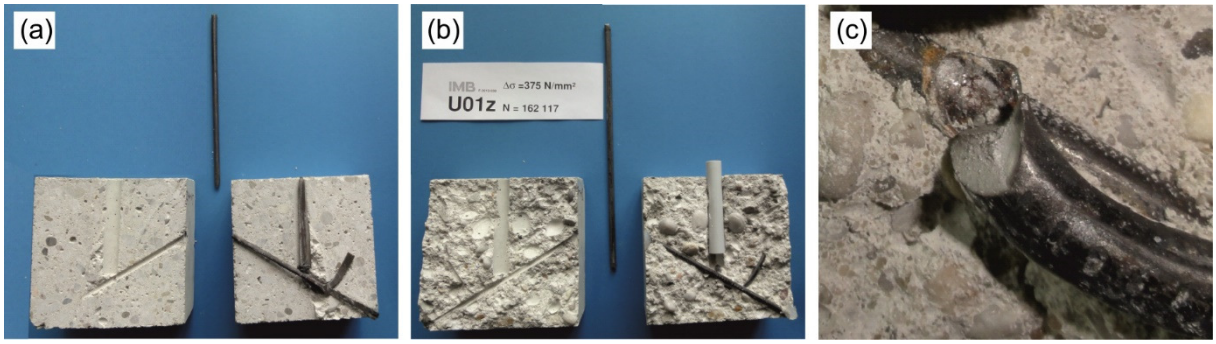

Figure 5-6: Fracture pattern of small size specimen under monotonic loading (a), cyclic loading (b) and fatigue fracture of welded node (c)

The test results of the static and fatigue tests of lower and upper chords are shown in Figure 5-7. For comparison, the test results from fatigue tests from literature [Web89] [Web95] (Chapter 5.2.2) were added to the diagram. The comparison of the applied stress range $\Delta\sigma$ and borne number of load cycles N for the lower chords (black points) and upper chords (grey points) shows a similar distribution of test results. For the majority of cases, the upper chord tests bore less load cycles for high stress ranges but with less scatter compared to the lower chords. The required stress range according to the technical approval of the lattice girders with $\Delta\sigma_{Rsk} = 92$ N/mm^2 for $N = 2.0$ mil. load cycles were satisfied for all tests.

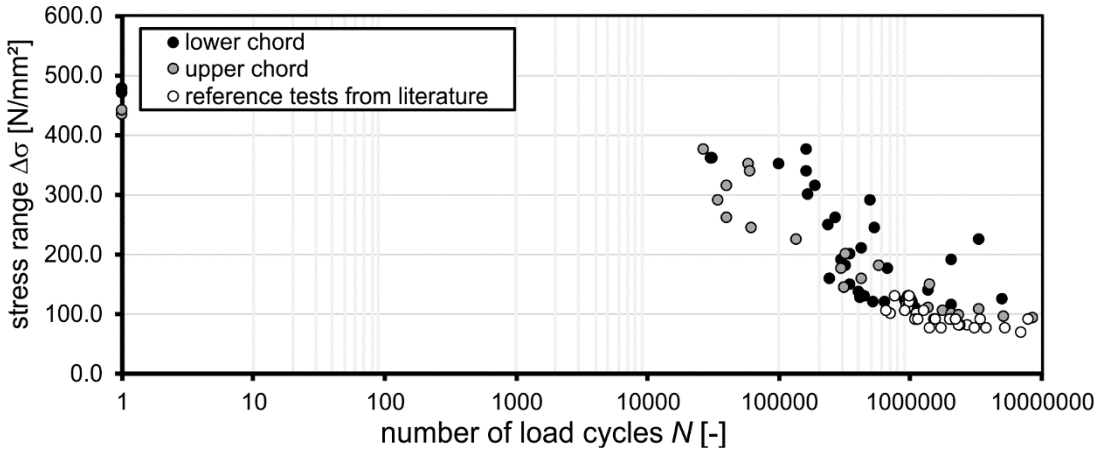

Figure 5-7: Test results of small size fatigue tests for lower and upper chords with reference tests from literature

The comparison of the tests results from literature shows the extended range of the fatigue-strength relation, especially for high stress ranges and low number of load cycles. In the range of small stress amplitudes, the own investigations bore a higher number of load cycles for the majority of cases.

5.3.6 Evaluation of S-N-curves for lattice girders

The small size fatigue tests were evaluated based on *Interactive method*, separately for lower and upper chords as well as for the overall test data. The analysis only included

the test data of the own investigations and excluded the test results from literature. The determination of the mean function of the test data follows Eq. (5-3) (Chapter 5.3.2) by regression analysis with the method of least error squares. The yield strength determined by the static test was considered by a number of load cycles $N = 1$. Figure 5-8 (a) shows the mean functions of the individual evaluations as well as the overall evaluation in double logarithmic illustration

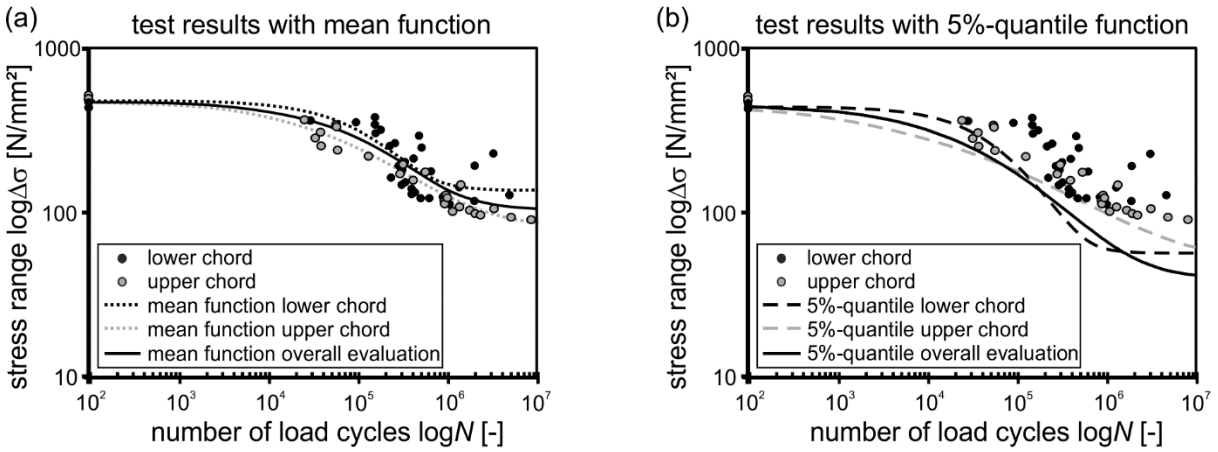

Figure 5-8: Fatigue test results of lower and upper chords with mean functions (a) and 5 %-quantile functions (b)

By considering standard deviation and quantile factors (Eq. (5-4), Chapter 5.3.2), the mean function could be transferred to quantile function with arbitrary confidence level. In this context, Figure 5-8 (b) depicts the 5 %-quantile functions for the individual and the overall evaluations. For a confidence level of 90 %, the quantile factors k_n result in 1.69 for the lower chord, 1.71 for the upper chord and 1.64 for the overall evaluation.

The analysis confirms, that tests with lower chords (black points and black dotted curve) bore more load cycles compared to tests with upper chords (grey points and grey dotted curve), but with higher scatter. This influences the 5 %-quantile function, especially in the range of fatigue strength. The 5 %-quantile curve of the overall evaluation (black curve) only exceeds the curves of the individual evaluation in the range of short time fatigue strength for the upper chords and in the range of fatigue strength for the lower chords. However, the borne stress ranges of all test data are located above the overall evaluation.

For applying the S-N-curves in structural building practice, the overall evaluation was used in order to derive consistent design S-N-curves based on the design format of [EC2] and [EC2NAD]. In this context, three strategies of analysis were followed. To satisfy the safety level defined in [EC0], the first strategy was a derivation based on the 5 %-quantile function. In analogy to the S-N-curves in [EC2] and [EC2NAD], the second point of the trilinear curve was adopted to $N^* = 1.0$ mil. load cycles with the corresponding stress range of $\Delta\sigma_{Rsk} = 67$ N/mm². The gradients of the S-N-curve in the range of

fatigue strength k_1 and the range of endurance fatigue strength k_2 were determined considering the requirement $k_2 = 2 \cdot k_1 - 1$ to $k_1 = 3.5$ and $k_2 = 6$ in order to approximate the 5 %-quantile function over the whole range of short time fatigue strength, fatigue strength and endurance fatigue strength. The scope of the S-N-curve is shown in Figure 5-9 (a) and the parameters are summarised in Table 5-4 (a).

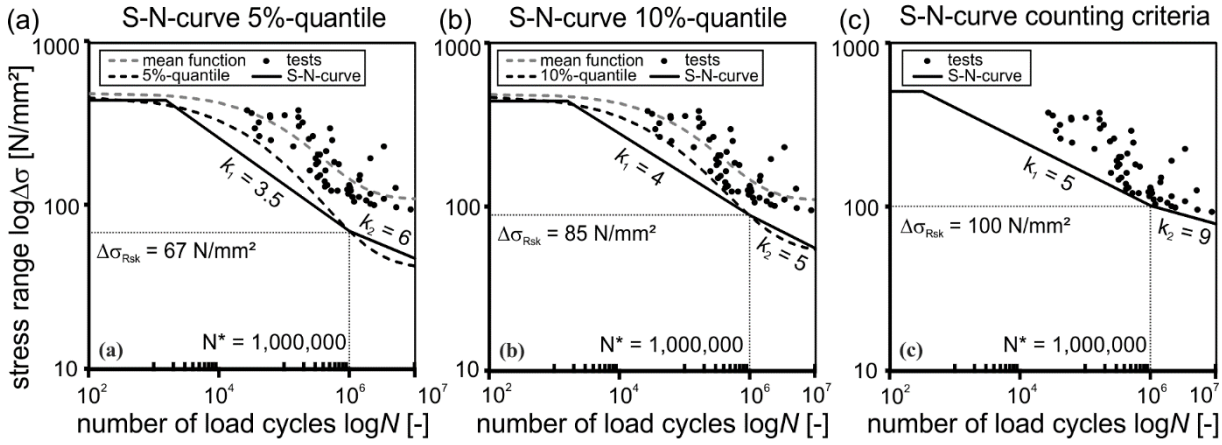

Figure 5-9: Proposals of S-N-curves for lattice girders using the confidence level of 5 %-quantiles (a), 10 %-quantiles (b) and the counting criteria (c)

Table 5-4: Overview of parameters for proposals of design S-N-curves for lattice girders

(a) S-N design curve 5 %-quantiles	(b) S-N design curve 10 %-quantiles	(c) S-N design curve counting criteria
N^* = 1,000,000	N^* = 1,000,000	N^* = 1,000,000
$\Delta\sigma_{Rsk}$ = 67 N/mm²	$\Delta\sigma_{Rsk}$ = 85 N/mm²	$\Delta\sigma_{Rsk}$ = 100 N/mm²
k_1 = 3.5	k_1 = 4	k_1 = 5
k_2 = 6	k_2 = 5	k_2 = 9

Due to the high scatter of test data, the S-N-curve according to the 5 %-quantile evaluation gives a too conservative estimation. Since the load in the small size specimens was directly applied to the weak point of the lattice girder (welded node) and failure of a structural member does not occur after fracture of a single bar, the test setups depict the most adverse case. In the structure however, failure of one bar does not introduce fatigue failure of the interface. The released stress in the interface after failure of one bar can be redistributed to other sections of the lattice girders and thus, several fatigue failures of lattice girders are necessary until structural failure occurs. In order to provide proposals for a more economic design, this effect was considered to transfer the results from small size tests to structural size. Thus, two additional strategies were followed. The first alternative strategy was to decrease the quantile factors in the statistic evaluation to 10 %-quantiles. The 10 %-quantile function as well as the approximated design S-N-curve is shown in Figure 5-9 (b). For N^* = 1.0 mil. load cycles the corresponding stress range

was set to $\Delta\sigma = 85$ N/mm². The gradient coefficients are adopted analogous to the coefficients in EC2+NA(D) for welded bars to $k_1 = 4$ and $k_2 = 5$ (Table 5-4 (b)).

With the second alternative strategy, the design S-N-curve was calibrated to deceed all stress ranges determined by the small size tests (counting criteria). The scope of the design curve was approximated to the test data to follow the design curve in [EC2NAD] for stirrups as shear reinforcement. Therefore, the approved stress range for stirrups of $\Delta\sigma = 175$ N/mm² for $N^* = 1.0$ mil. load cycles was reduced to $\Delta\sigma = 100$ N/mm² maintaining the coefficients $k_1 = 5$ and $k_2 = 9$ (Figure 5-9 (c) and Table 5-4 (c)). According to this evaluation, the curve corresponds to the approved stress range of lattice girders of $\Delta\sigma = 92$ N/mm² for $N^* = 2.0$ mil. load cycles.

5.4 Fatigue tests on semi-precast slabs with lattice girders

5.4.1 Introduction

The interface fatigue verification of semi-precast slabs with lattice girders in technical approvals [DZ-38][DZ-93] are based on investigations from literature (s. Chapter 5.2.2). To extend the limited data basis and to verify the investigations from literature, 14 test specimens with two sub-tests have been conducted with semi-precast slab sections under cyclic loading. The specimens were designed as single-span slabs and were tested in four-point bending tests (sub-test I) and three-point bending tests (sub-test II), respectively.

In three test series with lattice girders KTS [DZ-38] and EQ [DZ-93], the test parameters were varied in the range of the technical approvals. The parameters were slab thickness (16 – 36 cm), amount of lattice girders (2 rows for pure interface reinforcement, 3 rows for medium and 4 rows for high interface reinforcement ratios) and concrete strength (C25/30 – C50/60). Additionally, the influence of the interface roughness has been investigated. An overview of the test programme gives Figure 5-10.

The realisation of the required rough interfaces is difficult to implement in the prefabrication plants, especially for large interface reinforcement ratios. Thus, in order to investigate the effect of untreated interfaces, concrete surfaces were tested without mechanical post-treatment to be very smooth and oiled or left as cast with a roughness depth of $R_t = 0.4$ mm. Achieving the minimum roughness depth of a rough interface according the regulations in [EC2NAD] with $R_t \geq 1.5$ mm without mechanical post-treatment is difficult to implement. Therefore, a smaller limit of a rough surface in accordance to [D1045-1] with $R_t = 0.9$ mm (‘rough’) without mechanical post-treatment has been investigated. For comparison, also a rough interface with slightly roughening after concrete casting was provided.

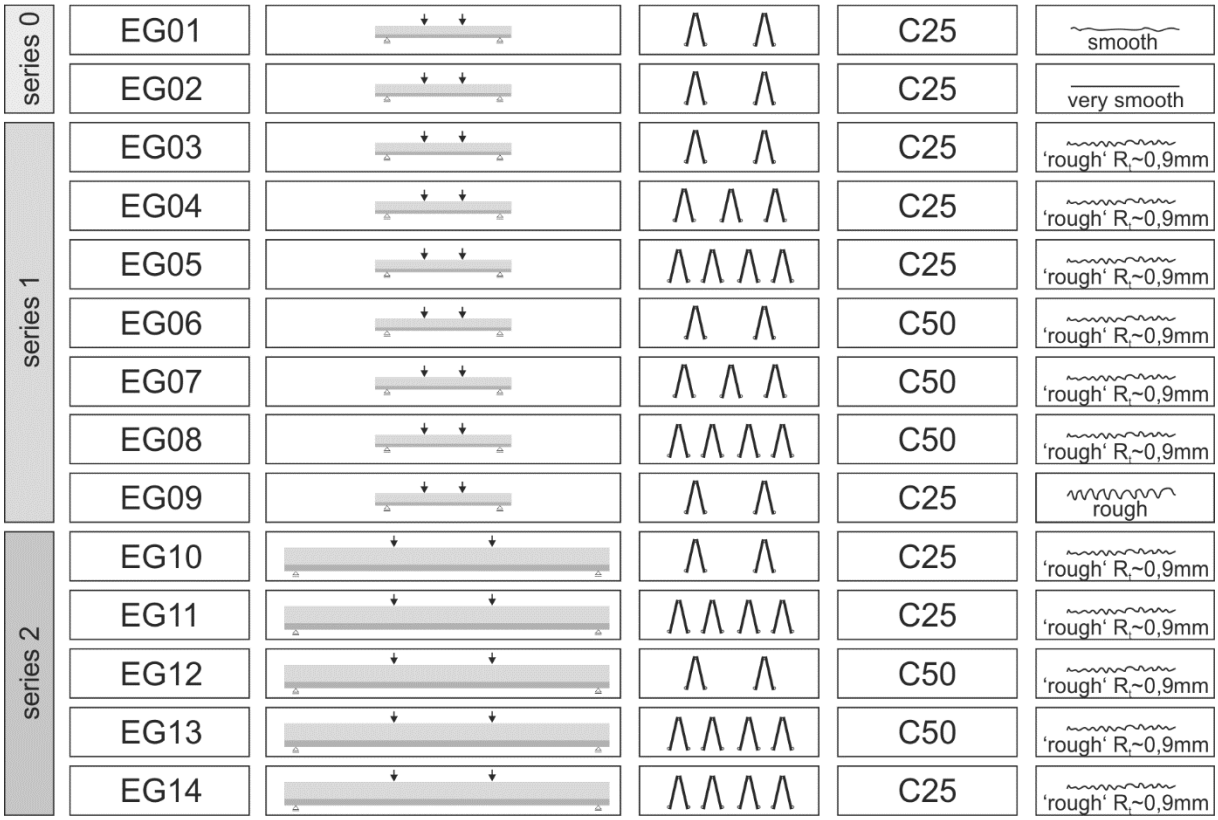

Figure 5-10: Overview of test specimens and test parameters

Since the applied lattice girders KTS and EQ may also be accounted as shear reinforcement, the shear capacity has been investigated during the research programme. The test results considering the shear resistance can be found in [Heg17][Wie17a][Wie17b].

5.4.2 Description of test specimens

For the test specimens, the precast slabs were manufactured with a slab thickness of h_{pre} = 7 cm and a width of b = 85 cm. To extend the application of the limited diameter of the longitudinal reinforcement in the technical approvals of $Ø_l \leq 16$ mm and to exclude flexural failure, longitudinal reinforcement bars with $Ø_l$ = 20 mm and a yield strength of f_y = 900 N/mm² with a longitudinal reinforcement ratio of ρ_l = 2.0 % were applied. The lower chords of the lattice girders have not been accounted as longitudinal reinforcement.

The applied lattice girders were the structurally identical shear lattice girders KTS (*B-tec*) and EQ (*Filigran*) with a girder height of 10 cm for the 16 cm slabs and 30 cm for the 36 cm slabs. For specimen EG14, the concrete cover in the compression zone was reduced and thus, the slab thickness was decreased to 33 cm. The span of the slabs for the four-point bending tests was defined to $3 \cdot a$, with a being the distance between load application and support, to achieve a shear slenderness of a/d = 4.0. The geometrical parameters of the test series are summarised in Table 5-5.

Table 5-5: Dimensions and geometrical parameters of test specimens

	series 0	series 1	series 2
dimensions (l/b/h) [cm]	190/85/16	180/85/16	420/85/36 (EG10-13) 390/85/33 (EG14)
height precast slab / insitu concrete [cm]	7/9	7/9	7/29 (EG10-13) 7/26 (EG14)
effective depth d [cm]	13	13	33 (EG10-13) / 30 (EG14)
distance load-support a [cm]	50	50	130
lattice girder type	KTS 100	KTS 100	EQ 30
shear slenderness a/d	4.0	4.0	4.0
long. reinforcement ρ_l [%]	2.0	2.0	2.0

l = total length; b = width; h = total height

5.4.3 Fabrication of test specimens

The precast slabs for the initial specimens of series 0 with two rows of lattice girders were manufactured in the prefabrication plant *ELSKES* in Kamp-Lintfort, Germany. The reinforcement in the precast slab was in accordance to Figure 5-11, but with a support overlay of 20 cm and additional stirrups along the slab's ends. The slabs were cast with a concrete C25/30 and a surface left as cast. After concrete hardening, the precast slabs were transported to the laboratory of IMB. Before applying the insitu concrete with an aspired concrete strength of C25/30, the interface of EG02 was additionally weakened by oil to prevent adhesive bond and to achieve a very smooth surface quality.

The specimens of the following test series 1 and 2 were manufactured at IMB in order to ensure an exact disposal of reinforcement and surface roughness and to prevent previous damage of the measurement devices in the slabs. The precast slabs of test series 1 generally followed series 0, but with a smaller support overlay of 15 cm and without edge stirrups in order to test a more adverse case for interface shear failure. The roughness of the interface was aspired to be R_t = 0.9 mm for specimens EG03 – EG08 without mechanical post-treatment. Specimen EG09 had a rough surface by slightly roughening after concrete casting. In test series 1, two, three and four rows of lattice girders were applied and the concrete strength for both, precast slab and insitu concrete varied between C25/30 and C50/60. For the specimens of test series 2 with a precast slab of 7 mm, the interface roughness was about R_t = 0.9 mm, in accordance to series 1. The insitu concrete layer for EG10 – EG13 was 29 cm. In order to determine the effect of the height of the concrete cover in the compression zone, the insitu concrete layer of specimen EG14 was reduced to 26 cm. The interface reinforcement varied between two and four rows of lattice girders and the concrete strength was C25/30 and C50/60. Figure 5-11 exemplarily shows dimensions and reinforcement detail of series 1 specimens with two rows of lattice girders (EG03, EG06 and EG09). The parameters and

material properties of the test specimens are summarised in Table 5-6. The reinforcement details of the other specimens as well as the material properties of concrete and reinforcement are illustrated in Annex A.

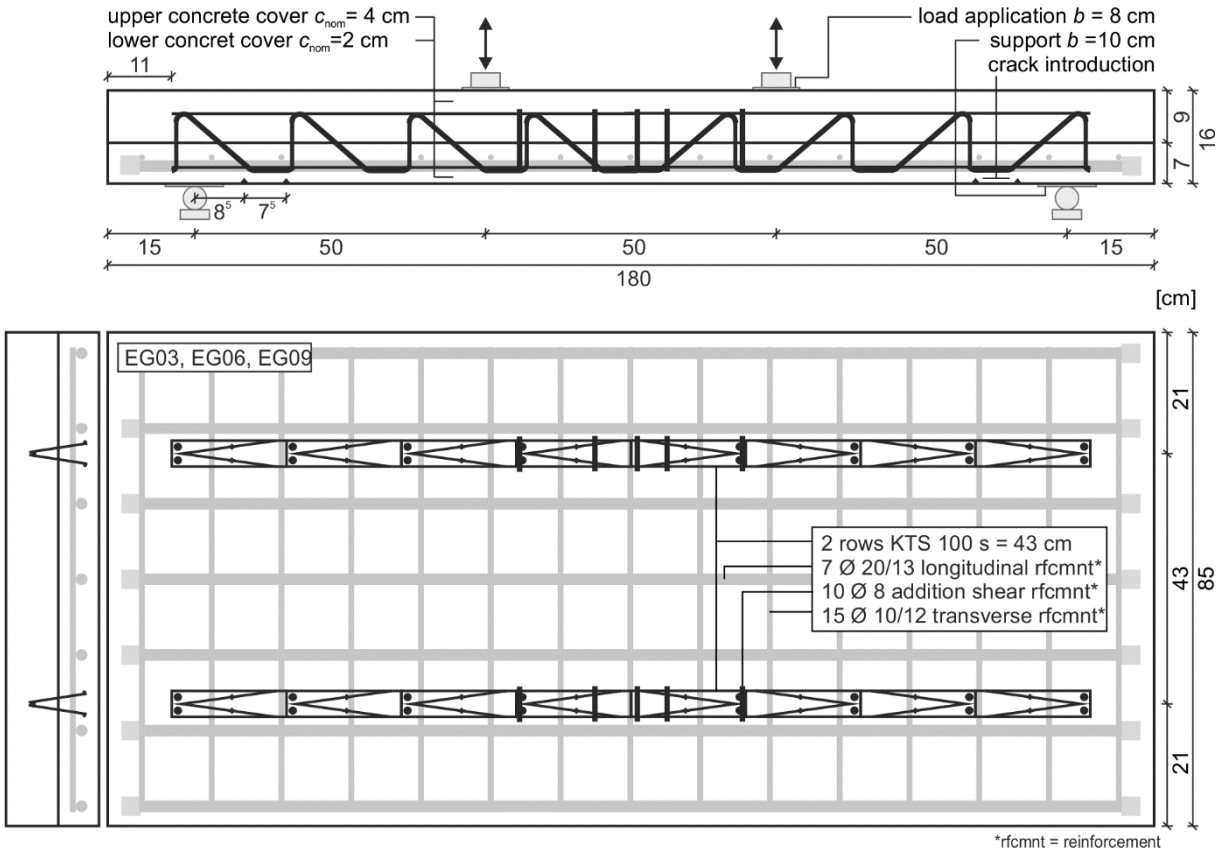

Figure 5-11: Reinforcement detail of specimens EG03, EG06 and EG09

The longitudinal reinforcement consisted of bars $Ø_l$ = 20 mm with a yield strength of f_y = 900 N/mm² to prevent flexural failure. According to the technical approvals of the lattice girders, the longitudinal reinforcement must be fully anchored at the support. Since extending the support overlay and applying additional stirrup arms along the edges would have a positive effect on the interface shear resistance, the anchorage of the longitudinal bars was enhanced by screw-nuts. The transverse reinforcement was determined to be 20 % of the longitudinal reinforcement with $Ø_t$ = 10 mm bars and yield strength of f_y = 500 N/mm². To ensure a crack formation of flexural cracks in the area of the welded sections of the lattice girders, triangular crack introducers were placed underneath the welded point where the initiation of developing shear cracks from flexural cracks was expected. To prevent shear failure of the slab at midspan between the load application point and support in the second sub-tests, additional stirrups were applied, since the diagonals of the lattice girders declining towards the support cannot fully participate in the shear resistance.

Table 5-6: Parameters and material properties of test specimens

Test	h_{ges}	a	n_{LG}	$f_{ym,LG}$	n_l	$f_{ym,l}$	$f_{cm,pre}$	$f_{cm,insitu}$	rough-ness	$R_{t,sand}$	$R_{t,laser}$
	[cm]	[cm]	[-]	[N/mm²]	[-]	[N/mm²]	[N/mm²]	[N/mm²]	[-]	[mm]	[mm]
EG01	16	50	2	546	7	954	25.3	35.6	smooth	0.24	0.42
EG02	16	50	2	546	7	954	25.6	33.9	very smooth[1]	0.26	0.43
EG03	16	50	2	546	7	939	27.7	33.2	'rough' (R_t≈0.9)	0.64	-
EG04	16	50	3	546	7	939	27.9	34.0	'rough' (R_t≈0.9)	0.93	-
EG05	16	50	4	546	7	939	28.2	35.2	'rough' (R_t≈0.9)	0.78	-
EG06	16	50	2	546	7	939	51.1	61.3	'rough' (R_t≈0.9)	0.97	1.33
EG07	16	50	3	546	7	939	51.1	61.3	'rough' (R_t≈0.9)	1.01	1.19
EG08	16	50	4	546	7	939	51.4	61.3	'rough' (R_t≈0.9)	1.07	1.04
EG09	16	50	2	546	7	939	32.9	34.4	rough (R_t>1.5)	2.02	-
EG10	36	130	2	554	18	939	36.0	32.0	'rough' (R_t≈0,9)	0.82	1.01
EG11	36	130	4	554	18	939	37.2	36.0	'rough' (R_t≈0,9)	0.78	0.85
EG12	36	130	2	554	18	939	48.6	55.6	'rough' (R_t≈0.9)	1.02	0.63
EG13	36	130	4	554	18	939	49.0	56.8	'rough' (R_t≈0.9)	1.19	1.67
EG14	33	120	4	554	17	939	31.5	34.8	'rough' (R_t≈0.9)	0.96	-

h_{ges}: overall slab height; a: distance between load application and support; n_{LG}: number of lattice girder rows; $f_{ym,LG}$: mean yield strength of the diagonals of the lattice girders; n_l: number of longitudinal reinforcement bars; $f_{ym,l}$: mean yield strength of longitudinal reinforcement; $f_{cm,pre}$: mean concrete compressive strength of precast slab; $f_{cm,in\text{-}situ}$: mean concrete compressive strength of insitu concrete; $R_{t,sand}$: mean roughness depth by sand patch method, $R_{t,laser}$: mean roughness depth by laser triangulation, [1]: additionally weakened by formwork oil

To verify the surface quality of the precast slabs, the roughness of the interface was measured by the sand-patch-method according to KAUFMANN [Kau71] and by laser-triangulation with a new laser system [Vog17] (s. Chapter 2.4.2). For the sand-patch method, a minimum of three measurements were performed by applying a defined amount of sand to the surface and measuring the diameter after circular spreading with a wooden plate (Figure 5-12 (a)). For the laser-triangulation, about 10 two-dimensional measure lines were recorded by the laser system (Figure 5-12 (b)). A comparison of the determined roughness depths by the two methods is depicted in Figure 5-12 (c). Since

the laser-triangulation system with the small measuring ranges and flexible handling, can also record the rougher edge areas of the slabs, the determined roughness depths are generally larger compared to the sand-patch method. The determined mean values of roughness depth according to both methods are listed in Table 5-6.

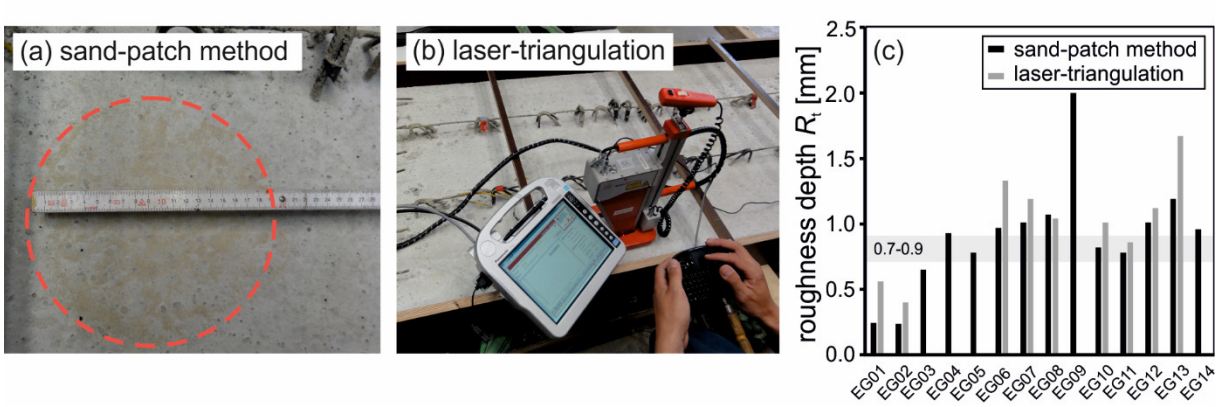

Figure 5-12: Measuring method for test specimens: sand-patch method (a) and laser triangulations (b), comparison of measures roughness depths (c)

For documentation of the tests, continuous measurements were made by electronical documentation. The disposal of the measurement devices is depicted exemplarily for specimen EG10 in Figure 5-13. To record the strain development in the reinforcement, strain gauges (*SG*) were applied to the diagonals, welded points and lower chords of the lattice girders in the range of the expected interface and shear cracks, as well as on the longitudinal reinforcement in the range of maximum moments (Figure 5-13 (a)). The measurement of the horizontal and vertical displacement of the interface, the crack opening of the shear crack and the deflection of the specimen was implemented by displacement transducers (*W*) (Figure 5-13 (b)).

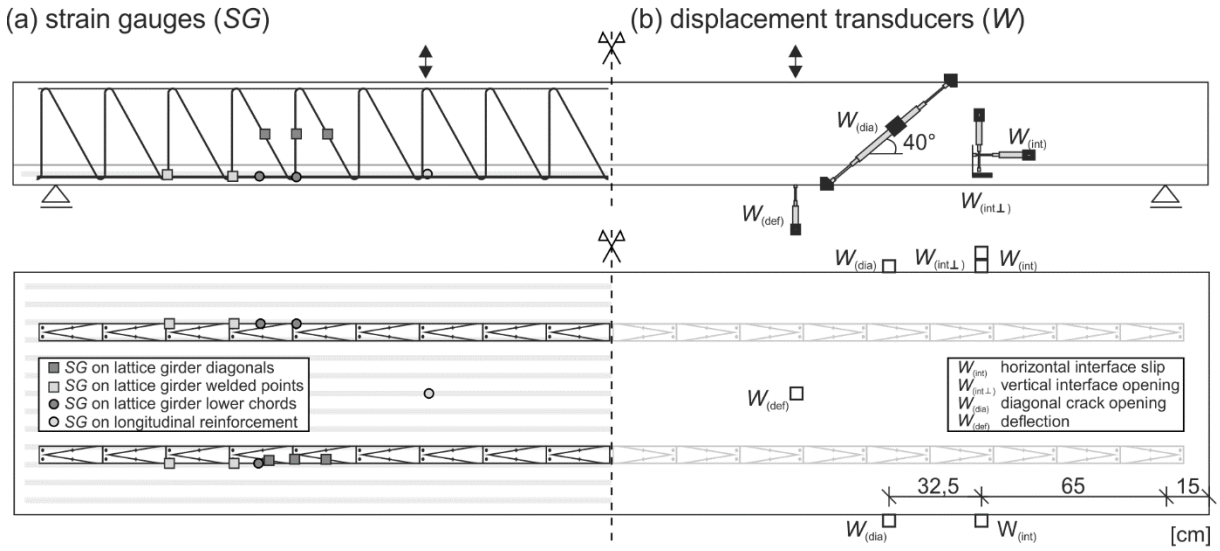

Figure 5-13: Measurement instrumentation for specimen EG10: strain gauges (*SG*) at reinforcement and displacement transducers (*W*)

5.4.4 Test setup and test conduction

For the first sub-tests, the single span slabs were supported on support blocks with steel rollers. The load from the test cylinders was transferred by a steel girder so that the shear spans were one third of the total span. A schematic depiction of the test setup gives Figure 5-14 (a), and Figure 5-15 (a) and (b) show the test setups in the laboratory at IMB. By the test setup of a four-point bending test, the shear force is constant at both ends of the slab between load application and support. The mid area between the load application points is free of shear with a constant, maximum moment.

After fatigue failure of the weaker end in the first sub-tests, the specimens were transferred to three-point bending tests by moving the support from the fractured side to the previous load application. The fractured ends of the specimens were wedged by steel profiles. Thus, the fatigue tests could be continued in the second sub-tests as a three-point bending tests by subjecting the unimpaired side to the same shear load until fatigue failure (Figure 5-14 (b) and Figure 5-15 (c) and (d)).

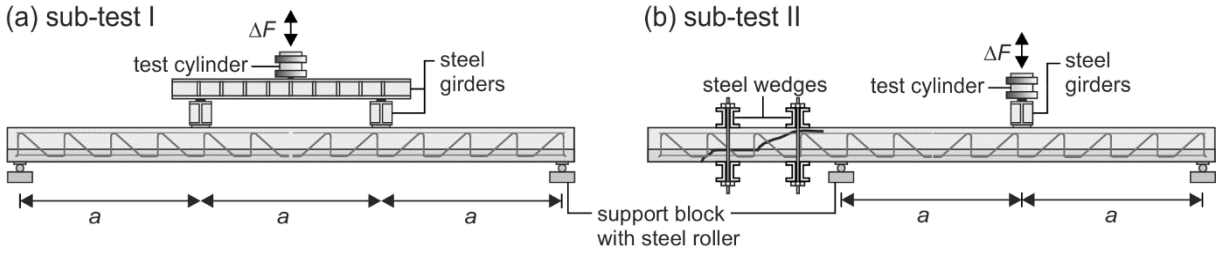

Figure 5-14: Schematic test setup of fatigue tests: sub-test I (a), sub-test II (b)

The fatigue tests in series 0 were started by deformation-controlled monotonic loading with 0.5 mm/min until flexural cracks reached the interface. This load level was defined as maximum load for the cyclic loading. For test series 1 and 2, the maximum loads were previously defined to be 60 % to 80 % of the calculated static interface resistance according to [EC2NAD]. For specimens with an interface roughness of $R_t \approx 0.9$ mm, the interface resistance of a rough interface was presumed. The reference values for specimens with high interface reinforcement ratios were the calculated static shear resistance.

After applying the initial maximum load, the load range was defined to be between 30 % to 75 % of the maximum load. Thereby, the calculated stress ranges in the lattice girders were aspired to be about $\Delta\sigma_s = 200$ *N*/mm². The fatigue load was applied force-controlled starting with a frequency of $f = 0.1$ Hz with continuous measurements of strain gauges and displacement transducers. After 100 load cycles, the frequency was increased to $f = 2.89$ or 5.78 Hz, depending on the deflection of the specimens. The displacement and strain measurements were monitored in periods after 1000 or 2000 load cycles. Depending on borne number of load cycles, crack distribution as well as displacement and strain measurements, the load range was increased in the first instance followed by increasing the maximum load.

After failure of one side of the specimen in the first sub-test, the unimpaired side was subjected to the ultimate load levels of the first sub-test. If the state of fracture did not allow proceeding the fatigue test, the second side was monotonically loaded until failure.

Figure 5-15: Test setup for fatigue tests: sub-test I for test series 0/1 (a), sub-test I for test series 2 (b), sub-test II for test series 0/1 (c), sub-test II for test series 2 (d)

The implemented maximum shear forces and shear force ranges of the initial fatigue loading and the fatigue loading when failure occurred are summarised in Table 5-8. Annex A.4 gives a comprehensive depiction of the applied load history for each specimen.

5.4.5 Test results

The maximum shear forces and shear force ranges at the beginning of the fatigue tests as well as when fatigue failure occurred, are listed in Table 5-7 (series 0 and 1) and Table 5-8 (series 2) for the first and second sub-tests. The fatigue loading caused progressing crack formation with increasing deformation, crack widths and steel strains in the reinforcement. As expected, the fatigue tests with several million load cycles showed a higher scatter compared to static tests. The scatter involves failure mode, interface displacement, stress of lattice girders and borne number of load cycle. The failure mode as well as borne number of load cycles are listed in Table 5-7 (series 0 and 1) and Table 5-8 (series 2).

Table 5-7: Overview of applied load, number of load cycles and stress ranges (series 0 and 1)

Test	$V_{max,1}$ [kN]	ΔV_1 [kN]	N_1 [-]	$V_{max,f}$ [kN]	ΔV_f [kN]	N_f [-]	N_{ges} [-]	$\Delta\sigma_{calc,1}$ [N/mm²]	$\Delta\sigma_{max,test}$ [N/mm²]	failure
EG01a	116	35	1,50E6	162	58	0,18E6	4,18E6	109	270	F / Q
EG01b	162	58	350				4,18E6			Q
EG02a	116	35	1,50E6	116	58	1,16E6	2,66E6	109	215*	F
EG02b	116	58	0,93E6				3,59E6			F / Q
EG03a	152	90	2,07E6				2,07E6	279	230*	F / Q
EG03b	152	90	1,17E6				3.25E6			Q
EG04a	165	83	3,00E6	165	112,5	1,36E6	4,36E6	171	215*	Q
EG04b	260[1]									Q
EG05a	226	133	2,70E4				2,70E4	176	125	V_{DZ}
EG05b	271[1]									Q
EG06a	172	105	2,25E6	197	120	0,35E6	2,60E6	326	195	F / Q
EG06b	197	120	1,12E4				2,62E6			F / Q
EG07a	172	88	2,00E6	197	120	3,32E4	4,03E6	121	55	Q
EG07b	197	120	2,25E6				6,28E6			Q
EG08a	215	110	2,0E6	215	152,5	1,95E6	3,95E6	171	115*	Q
EG08b	-[2]									
EG09a	155	93	8677				8677	187	175*	F / Q
EG09b	155	61	1,09E6				1,10E6			F / Q

a: sub-test I; b: sub-test II; V_{max1}: maximum shear force at start of test; ΔV_1: shear force range at start of test; N_1: number of load cycles after first loading ; $V_{max,f}$: maximum shear force at failure; ΔV_f: shear force range at failure; N_f: number of load cycles after last loading at failure; N_{ges}: overall number of load cycles; $\Delta\sigma_{calc,1}$: calculated stress range in lattice girders according to technical approval with ΔV_1; $\Delta\sigma_{max,test}$: measured maximum stress range in lattice girders by strain gauges; F: interface failure; Q: shear failure; V_{DZ}: anchorage failure of lattice girder in the compression zone; V_L: anchorage failure of longitudinal reinforcement; *: fracture of lattice girders; [1]: residual load capacity; [2]: no sub-test II

Table 5-8: Overview of applied load, number of load cycles and stress ranges (series 2)

Test	$V_{max,1}$ [kN]	ΔV_1 [kN]	N_1 [-]	$V_{max,f}$ [kN]	ΔV_f [kN]	N_f [-]	N_{ges} [-]	$\Delta\sigma_{calc,1}$ [N/mm²]	$\Delta\sigma_{max,test}$ [N/mm²]	failure
EG10a	282	150	2,00E6	372	225	1000	2,00E6	193	100*	F / Q
EG10b	-[2]									
EG11a	537	195	0,31E6				0,31E6	125	115	V_{DZ}/ V_L
EG11b	537	195	0,90E6				1,21E6			V_L
EG12a	359	135	2,00E6	420	233	0,74E6	4,12E6	173	255*	F / Q
EG12b	420	233	0,35E6				4,47E6			Q / V_L
EG13a	519	165	435				435	105	115	V_{DZ}/ V_L
EG13b	519	165	9129				9564			V_L
EG14a	487	178	1,63E6				1.63E6	125	175	V_{DZ}/ V_L
EG14b	487	178	2,87E4				1.66E6			Q / V_L

a: sub-test I; b: sub-test II; V_{max1}: maximum shear force at start of test; ΔV_1: shear force range at start of test; N_1: number of load cycles after first loading ; $V_{max,f}$: maximum shear force at failure; ΔV_f: shear force range at failure; N_f: number of load cycles after last loading at failure; N_{ges}: overall number of load cycles; $\Delta\sigma_{calc,1}$: calculated stress range in lattice girders according to technical approval with ΔV_1; $\Delta\sigma_{max,test}$: measured maximum stress range in lattice girders by strain gauges; F: interface failure; Q: shear failure; V_{DZ}: anchorage failure of lattice girder in the compression zone; V_L: anchorage failure of longitudinal reinforcement; *: fracture of lattice girders; [1]: residual load capacity; [2]: no sub-test II

Specimens with low interface reinforcement ratios realised by two rows of lattice girders (EG01 – EG03, EG06, EG09, EG10 and EG12) bore, except for specimen EG09, a minimum of $N = 2.0$ mil. load cycles. Independent of concrete strength and interface roughness, a combination of interface and shear failure occurred. Slabs with medium interface reinforcement ratios and three rows of lattice girders (EG04 and EG07) failed predominately by shear failure with only small crack development along the interface. For tests with high interface reinforcement ratios (EG05, EG08, EG11, EG13 and EG14), only EG08 showed a clear shear crack after $N > 2.0$ mil. load cycles. For the other highly reinforced and highly loaded specimens, failure occurred generally due to anchorage failure of the lattice girder in the compression zone of the slab or failure of the anchorage of the longitudinal reinforcement at the support. In the following, the influence of interface roughness, interface reinforcement ratio, slab thickness and steel strains are presented. An influence of the concrete strength could not be determined.

Influence of interface roughness

During the test programme, the interface roughness was varied by specimens in series 0 and 1 with concrete strength of C25 and two rows of lattice girder. Therefore, the following interface conditions were investigated:

- left as cast with bond breaker (very smooth, EG02)
- left as cast with a roughness depth of R_t = 0.24 mm determined by the sand-patch method (smooth, EG01)
- left as cast with an aspired roughness depth of $R_t \approx 0.9$ mm ('rough', EG03)
- left as cast with slightly roughening to $R_t \approx 2.0$ mm after casting (rough, EG09)

The crack patterns and borne number of load cycles of the four specimens are shown in Figure 5-16. For all investigated interface roughness, delamination of the interface could be determined. For specimen EG02 with a very smooth surface, delamination already occurred during initial static loading. The crack formation along the interface for EG01 with a smooth surface appeared during the cyclic loading (N > 1.5 mil load cycles). Both specimens failed due to shear of the interface. Since the specimens EG01 and EG02 were designed with a longer support overlay and additional stirrups along the ends of the slab, the unimpeded shear of the insitu concrete layer was additionally counteracted. For EG03 with an interface with a low roughness, the failure occurred due to delamination of the insitu concrete layer with considerable horizontal slip after a shear crack developed towards the support. Specimens EG09 with a rough interface failed in a combination of interface and shear but without complete delamination of the insitu concrete.

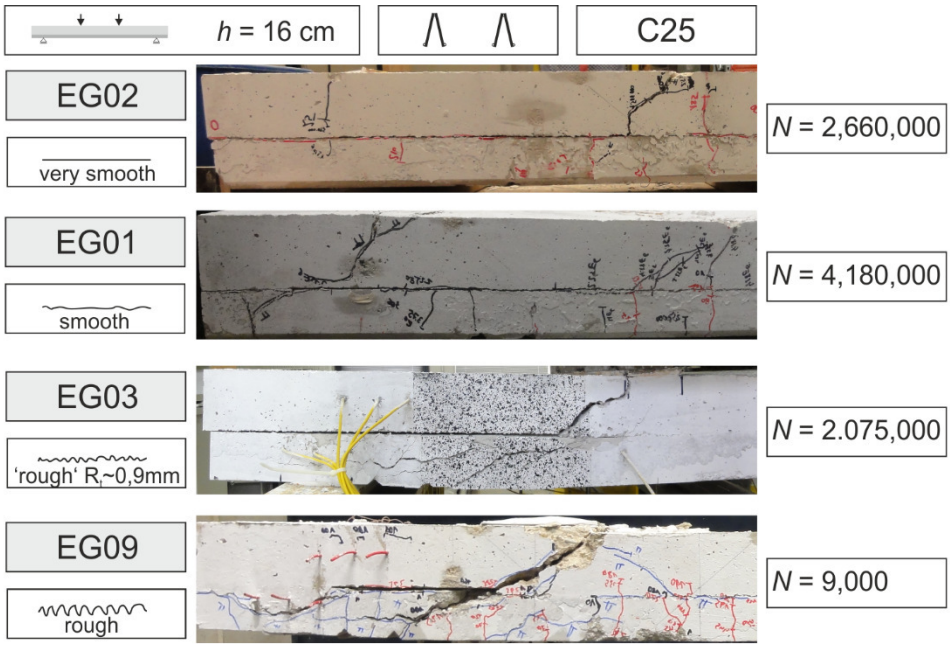

Figure 5-16: Influence of interface roughness: crack patterns of specimens EG01, EG02, EG03 and EG06

Except for specimen EG09 with a slightly roughened surface, all specimens exceeded $N > 2.0$ mil load cycles. Despite the applied fatigue load and the concrete properties of specimen EG09 were similar to EG03, fatigue failure occurred after $N = 9{,}000$ load cycles. After monotonic loading, no crack could be observed at the interface. The horizontal and vertical displacement of the interface occurred after $N = 2{,}000$ load cycles and gradually increased until failure. The early failure might be explained by insufficient bond between the concrete layers, e.g. due to unintended blemishes in the interface. Thus, the early failure of the rough interface can be evaluated as aberration and needs further investigations. After exposure, the lattice girders showed fractures of the welded nodes in the area of the failure crack. By the strain measurements of the lattice girders, stress ranges of $\Delta\sigma = 175$ N/mm² could be determined at the welded nodes. Since the strain gauges were not placed in the immediate area of the failure crack, the stress ranges in the fractured girder nodes might have been considerably higher.

To compare the flexural behaviour of the composite specimens, Figure 5-17 (a) shows the load deflection curves of specimen EG01 – EG03 for the static initial loading and the first load cycle. Despite similar concrete properties, specimen EG02 with a very smooth surface showed a lower stiffness with a deflection of 7 mm. Thus, separate load bearing behaviour of precast slab and insitu concrete layer can be assumed. With increasing interface roughness, the inclination of the load-deflection curves increases for specimens EG01 and EG03, which confirms an improvement of composite action.

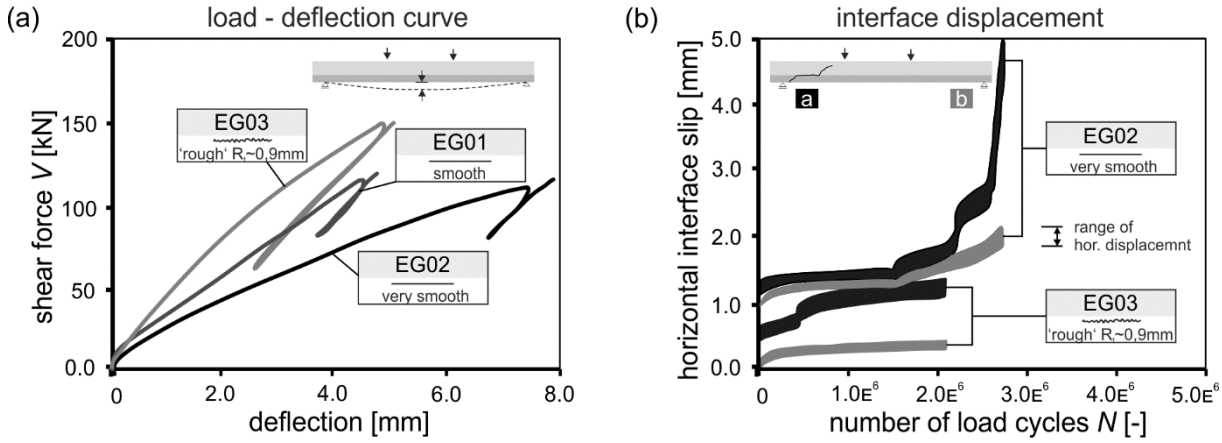

Figure 5-17: Influence of interface roughness: load-deflection curve of specimens EG01 – EG03 (a), development of horizontal slip for specimens EG02 and EG03

A comparison of the development of horizontal interface displacement of specimen EG02 and EG03 is shown in Figure 5-17 (b). The measured horizontal slip at the side of fatigue failure (black curve) shows interface slip after the static initial loading of 1.5 mm for EG02 and 0.7 mm for EG03. During the fatigue loading, the interface slip remained mainly constant for EG02 and increased gradually after increasing the load range. For EG03, a constant increase of interface slip could be determined during the fatigue test with an stepwise increase after about $N = 500.000$ load cycles. This might

be induced by failure of the lattice girder diagonal located in the area of the slip measurement. For this diagonal, stress ranges of $\Delta\sigma = 230$ N/mm² and fracture after exposure of the specimen could be determined. The horizontal slip of the unimpaired side only showed small displacements with slight increase during the first fatigue sub-test. A failure however, did not occur for another $N > 1.5$ mil. load cycles.

Influence of interface reinforcement ratio

Figure 5-18 shows the influence of the interface reinforcement ratio realised by two, three and four rows of lattice girders by crack patterns of the failure crack in the first sub-test. The compared specimens of series 1 had a concrete strength of C25 and an interface roughness of about $R_t = 0.9$ mm.

Test specimen EG03 with small interface reinforcement ratio shows a clear interface failure with considerable interface slip of 1.5 cm. Specimen EG04 with a medium interface reinforcement ratio failed by a shear crack without horizontal interface displacement and only small interface opening. For specimen EG05 with a high interface reinforcement ratio and high fatigue shear loading, the comparable small number of load cycles, with the unfractured lattice girders as well as the crack formation leads to the assumption of anchorage failure of the lattice girder in the compression zone. However, a delamination of the interface could also be identified.

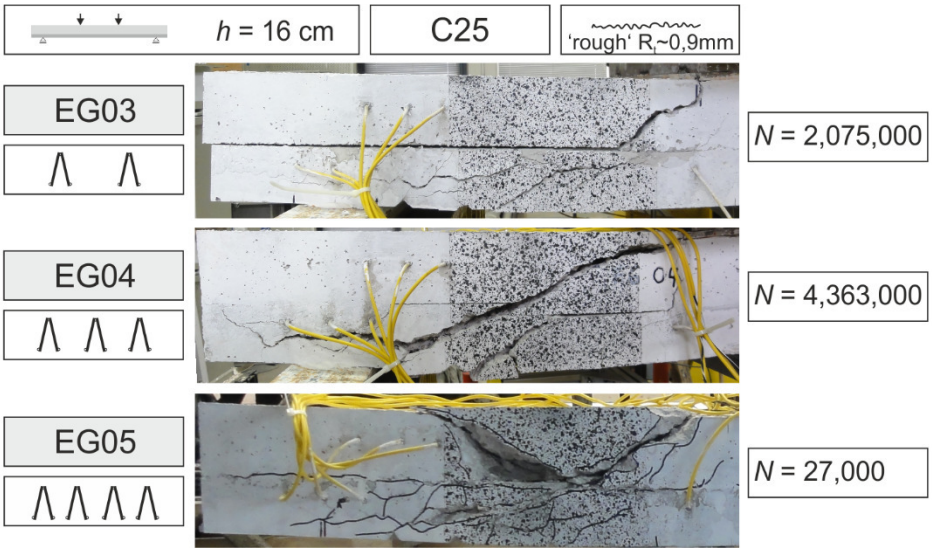

Figure 5-18: Comparison of interface reinforcement ratio: Crack patterns of specimens EG03, EG04 and EG05

Influence of slab thickness

With similar shear slenderness of $a/d = 4.0$, higher interface resistances could be determined for thinner slabs with shorter spans compared to thicker slabs with longer spans. Thus, a size effect for the interface resistance may be presumed for the interface capacity.

To compare the influence of the slab thickness for a thin specimen with $h = 16$ cm (EG06) and a thick specimen with $h = 36$ cm (EG12), Figure 5-19 shows the crack formation at ultimate fatigue load as well as the load history of the fatigue test and the measured crack width of the interface and the major shear crack. Both specimens had two rows of lattice girders, a concrete strength of C50 and an interface roughness about $R_t \approx 0.9$ mm. The crack formation shows a clear crack development along the interface for the large specimen (EG12) and a shear crack without interface displacement for the small specimen (EG06). For qualitative comparison of the load history, the applied shear force in the fatigue tests is related to the calculated static shear force according to [EC2NAD] V_{test}/V_{calc} and depicted over the number of load cycles N. With displacement transducers, the development of interface crack width w_{int} and shear crack width w_{dia} could be measured during the fatigue test. Despite the high related shear force, the crack widths of the small specimen EG06 were smaller than $w_{int/dia} < 0.2$ mm until reaching $N = 2.25$ mil. load cycles. Whereas the crack width of the interface remained mostly constant, the crack width of the shear crack increased after increasing the load level after $N > 2.25$ mil. load cycles until failure. The larger specimen EG12 with comparatively smaller loading showed large crack widths of $w_{dia} = 0.4$ mm already after initial loading. The crack width increased slightly after increasing the load range and gradually after increasing the maximum load until failure. The measurement of the interface opening only showed small crack widths after initial loading but increased gradually after increasing the load range.

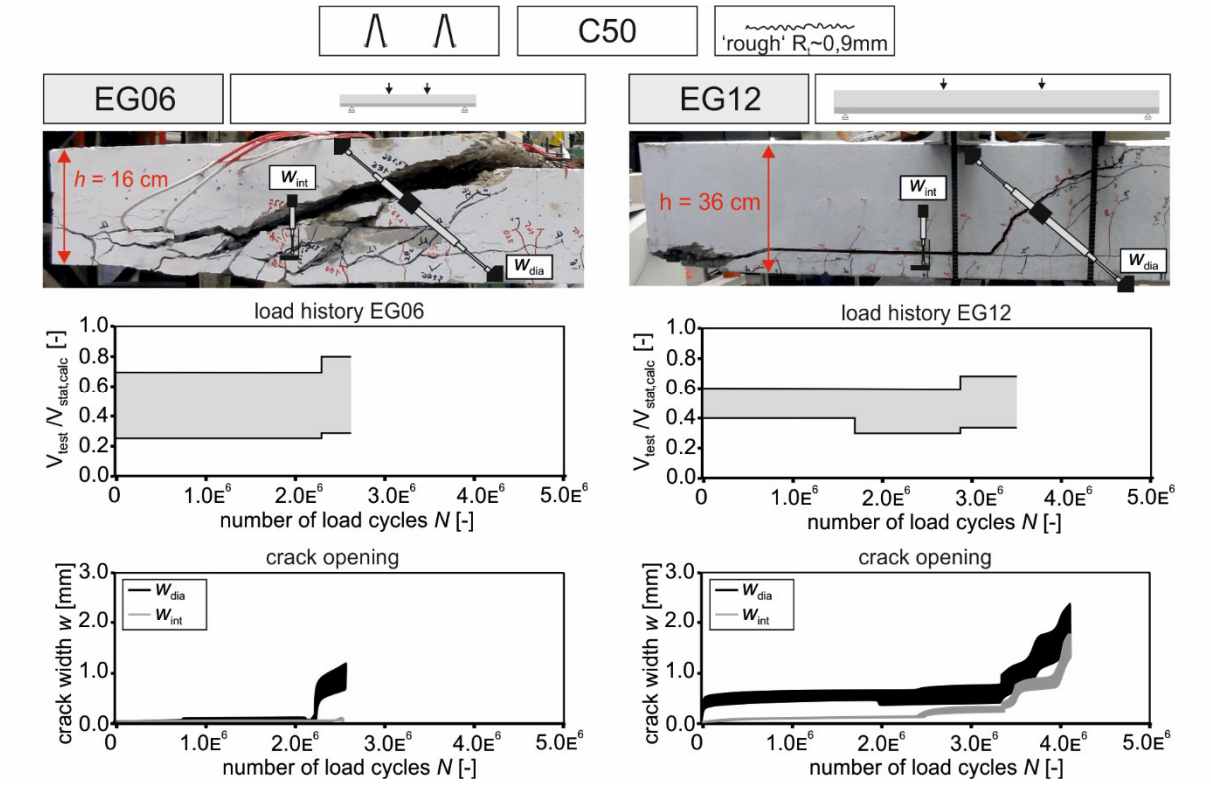

Figure 5-19: Comparison of slab thickness: Crack patterns, load history and measured crack width of interface and shear crack for specimens EG06 and EG12

Influence of steel strains

Figure 5-20 exemplarily shows the measured steel strains of the diagonals ε_{dia} and the welded node ε_{wel} of the lattice girders for specimens EG12, to evaluate the influence of the stress ranges in the lattice girders. The stress range in the diagonals of the lattice girders calculated from the measured steel strain range was about $\Delta\sigma$ = 167 N/mm² for a period of N > 2.0 mil. load cycles. This exceeds the approved stress range according to the technical approvals of the lattice girders of $\Delta\sigma_{Rsk}$ = 92 N/mm² by 76 %. The measured stress ranges of the welded nodes was determined to be only $\Delta\sigma$ = 42 N/mm² since the cracks did not develop along the welded nodes. After exposure of the lattice girders, fractures could only be determined in the diagonal and rectangular bars of the lattice girders (Figure 5-20). As mentioned in context of the influence of interface roughness, specimen EG03 showed a clear increase of horizontal slip after failure of lattice girder diagonal. However, failure of one diagonal did not induce structural failure.

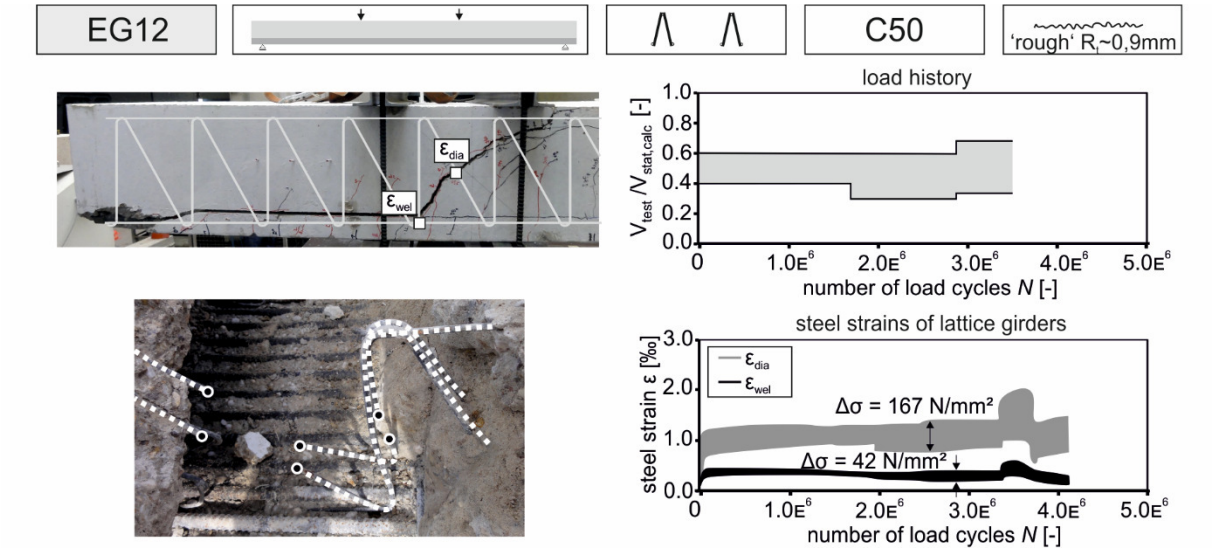

Figure 5-20: Influence of steel strains: load history, strain measurements of lattice girder and fractured lattice girder for specimen EG12

Table 5-7 and Table 5-8 compares the largest measured stress ranges in the lattice girders $\Delta\sigma_{max,test}$ to the calculated stress ranges $\Delta\sigma_{calc,1}$, determined by the initially applied shear force range ΔV_1 according to the interface fatigue regulations of the technical approvals [DZ-38][DZ-93]. The measured stress ranges in the diagonals of the lattice girders, as well as the calculated stress ranges were generally larger than the stress range of the technical approvals with $\Delta\sigma_{Rsk}$ = 92 N/mm². Structural failure of the slabs induced by fatigue failure of the lattice girders (in Table 5-8, tests with fractured lattice girders are labelled by * in the column of $\Delta\sigma_{max,test}$) could generally not be determined after the initially applied load level. Despite for specimen EG09, which can be assessed as aberration, structural failure with fractured lattice girders could only be determined for specimens with large numbers of load cycles and high stress ranges.

5.4.6 Test evaluation and comparison to design regulations

To assess the interface shear concepts of the general technical approval of the lattice girders [DZ-38][DZ-93], [EC2] and [EC2NAD] for fatigue, the conducted fatigue tests and the fatigue tests from literature (s. Chapter 5.2.2) were evaluated by the calculated stress ranges in the lattice girders. For the 47 fatigue tests, the calculated characteristic stress ranges $\Delta\sigma_{test,Rki}$ were related to the approved stress range according the technical approvals $\Delta\sigma_{Rsk}$ = 92 N/mm² and plotted over the borne number of load cycles (Figure 5-21). Even though the design is limited to N = 2.0 mil. load cycles, all tests were related to the approves stress range of $\Delta\sigma_{Rsk}$ = 92 N/mm². Specimens with divergent failure modes, e.g. anchorage failure of lattice girders or longitudinal reinforcement, were excluded. To determine the calculated stress range, the applied shear force ranges ΔV were calculated in accordance to Eq. (3-19), Chapter 3.3.2 to the applied shear stress range $\Delta v = \beta \cdot \Delta V / (b_i \cdot z)$ with β = 1.0. The applied shear stress range was then implemented in the interface shear design expression according to [EC2] (Eq. (3-20), Chapter 3.3.2), [EC2NAD] (Eq. (3-21), Chapter 3.3.3) and the technical approval (TA) of the lattice girders (Eq. (5-1), Chapter 5.2.3), without partial safety factors.

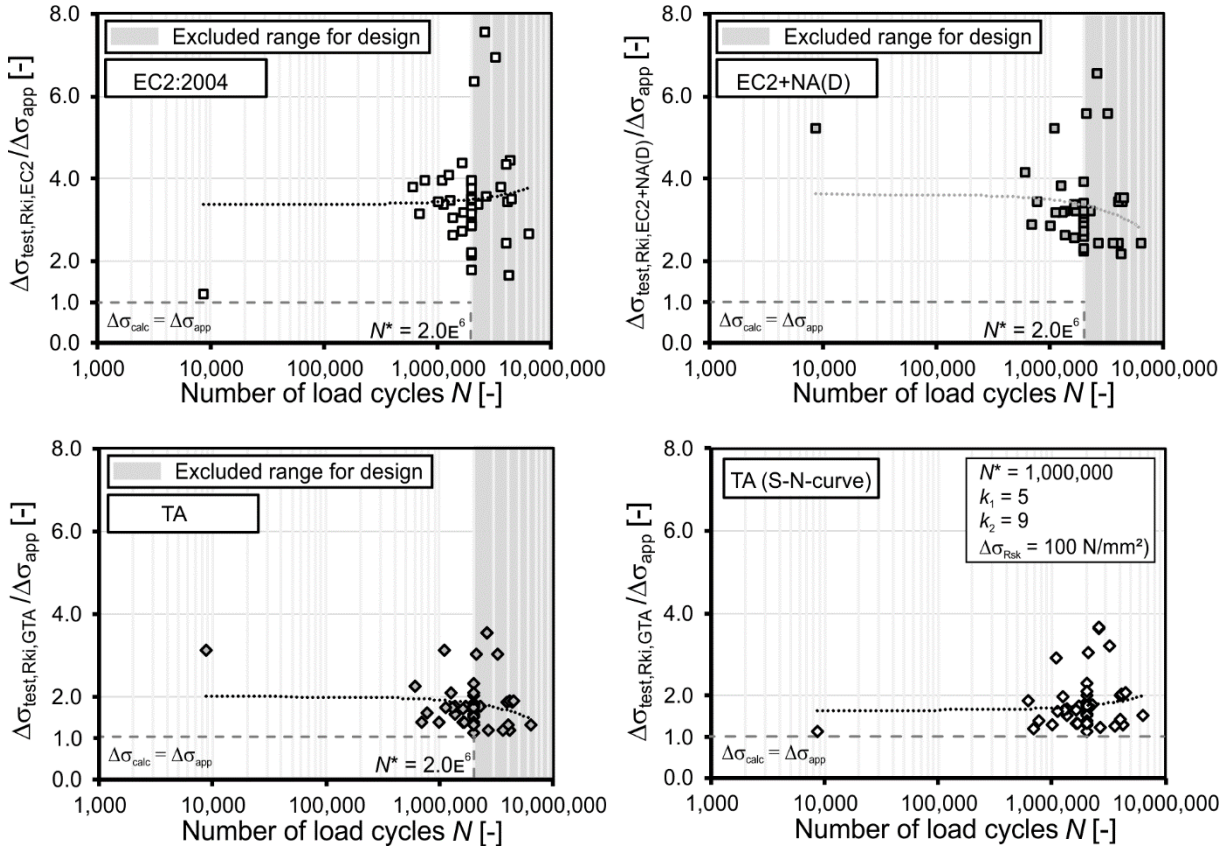

Figure 5-21: Evaluation of calculated stress ranges for the design of lattice girders as interface reinforcement

The best accordance to the test data gives the expression of the TA (Figure 5-21, bottom left). The expression according to [EC2] (Figure 5-21, top left), which allows a 50 % consideration of the adhesive term for fatigue, and the expression according to [EC2NAD] (Figure 5-21, top right) which neglects the term of adhesion for fatigue and increases the resistance of the interface reinforcement by the factor 1.2 show a similar trend level. The [EC2] approach however, gives a larger range of scatter, especially for large numbers of load cycles, whereas [EC2NAD] shows a decrease of scatter for large numbers of load cycles.

To verify the S-N-curves for lattice girders derived in Chapter 5.3, the test data was evaluated considering the S-N-curve derived by the counting criteria with the parameters listed in Figure 5-21, bottom right. Therefore, the approved characteristic stress ranges were calculated depending on the borne number of load cycles for each test. Figure 5-21, bottom right shows the calculated stress ranges in the lattice girders according to the regulations in the TA related to the approved stress ranges. Compared to the evaluation with an approved stress range of $\Delta\sigma_{Rsk}$ = 92 N/mm² (Figure 5-21, bottom left), the evaluation with the S-N-curves gives a better agreement, especially for especially for $N \leq 2.0$ mil. load cycles. For $N > 2.0$ mil. load cycles, the S-N-curve gives smaller allowable stress ranges, which lead to slightly higher related stress ranges in the lattice girders. However, with the S-N-curve, the range of application for fatigue design of lattice girders can be extended to a reliable verification allowing $N > 2.0$ mil. load cycles.

Besides the fatigue verification of the reinforcement, the fatigue resistance of the concrete must be verified in accordance to the design concepts in [EC2], [EC2NAD] and TA. Therefore, the concrete stress must be limited. By evaluating the own experimental investigations, the stress limits can be confirmed. Furthermore, the valid range for the simplified verification of concrete under shear for N = 1.0 mil. load cycles can be approved. Despite the adverse interface quality of the specimen, the maximum resistance of the interface can be complied. For the tests with low reinforcement ratios, the maximum interface resistance is generally not decisive since prior failure of the interface reinforcement occurs. The permissible range of the maximum fatigue resistance of the compression strut can also be satisfied by the test specimens with high interface reinforcement ratios. A detailed description of the evaluation for the maximum fatigue resistance can be found in [Heg17].

The construction rules for semi-precast slabs with lattice girders defined in the technical approvals can generally be confirmed. In order to extend the application of the diameter of the longitudinal reinforcement, $Ø_l$ = 20 mm bars were applied. Due to the high longitudinal reinforcement ratios, and the dense assembly, especially in the thick slabs, anchorage failure occurred for some specimens. Thus, sufficient anchorage and concrete cover must be provided. For high interface reinforcement ratios, a sufficient anchorage in the compression zone must be ensured, especially for high shear loads.

5.5 Summary

To investigate the fatigue behaviour of semi-precast slabs with lattice girders, S-N-curves were derived from small size tests with lattice girder diagonals cast in concrete cubes. Subsequently, the fatigue behaviour of slab specimens was investigated by 14 fatigue tests with two sub-tests. The test parameters were interface roughness, slab thickness, interface reinforcement ratio and concrete strength.

For the fatigue tests, higher scatter occurred compared to static tests. The scatter concerns failure mode, interface delamination, strain of lattice girders and borne number of load cycles. The failure of specimens with low degrees of interface reinforcement was generally induced by interface failure after high numbers of load cycles with $N > 2.0$ mil. Therefore, the bearable fatigue load level generally increased with increasing roughness. Only one specimen with a rough interface had premature failure, which might be explained by aberration and must be further investigated. Specimens with medium interface reinforcement ratios failed predominantly by shear with only small interface delamination. The failure of specimens with high interface reinforcement ratios was generally introduced by anchorage failure of the lattice girder in the compression zone or by anchorage failure of the longitudinal reinforcement. With similar shear slenderness of $a/d = 4.0$, higher interface resistances could be determined for thinner slabs with shorter spans compared to thicker slabs with longer spans, which may lead to the assumption of a size effect for interface capacity. The stress ranges in the lattice girders determined by test results were considerably higher compared to the approved stress range according to the technical approvals. A direct comparison between static and fatigue resistance is not possible due to absent missing tests.

The fatigue design regulations of lattice girders according to the technical approvals can generally be confirmed by this test programme, however, they are conservative. By applying the derived S-N-curves, the evaluation leads to a better agreement of design expression and test data for $N \leq 2.0$ mil. load cycles. Furthermore, the range of fatigue application for lattice girders could be extended to $N > 2.0$ mil. load cycles.

6 Development and evaluation of experimental databases

6.1 Introduction

To evaluate the interface shear design equations according to the codes presented in Chapter 3.3, consistent and critically reviewed databases with interface shear tests provide an essential foundation. By using systematically processed test data, predictability and level of reliability of design expressions can be determined and compared. Furthermore, the accuracy of the considered influencing parameters can be evaluated. The evaluated design codes are Eurocode 2 [EC2], Eurocode 2 with the National Annex of Germany [EC2NAD], the draft for the next Eurocode 2 [prEC2:18], Model Code 2010 [MC10], ACI 318-14 [ACI318] and AASHTO LFRD[AA-L].

The coefficients accounting for the influence of interface roughness were derived using different, mostly isolated test series. To verify the design equations, no complete, consistent and critically reviewed database evaluations existed, which distinguish between small size tests and structural members as well as between monotonic and cyclic loading. Database evaluations from literature concentrate either on small size tests or structural members or are not entirely comprehensible. For interface shear, database evaluations are published e.g. in [Heg99], [Zil06], [Krc16] and [Sol17]. To develop a consistent assembly of test data, existing databases shall be merged, harmonised and reviewed within the current Shear Friction Database development of *ACI 445D*.

In order to accomplish a complete overview of existing test data as well as to ensure a consistent and critically reviewed data base for evaluation of interface shear equations, test reports were collected, reviewed and evaluated within this thesis. To systematically evaluate the interface shear regulations by tests presented in literature (an extract of the evaluated test series can be found in Chapter 4), and by own investigations (s. Chapter 5.4), the collected test data was assigned in sub-databases to investigate the different effects of structural behaviour, load bearing mechanisms and loading conditions. Therefore, two major data bases were developed distinguishing between small size tests and structural members with beam and slab specimens. Considering the loading conditions, the major databases were divided in specimens with monotonic and cyclic loading conditions. To separately investigate the effect of externally applied normal stress and interface reinforcement, the databases were further separated in specimens without interface reinforcement (rfcmnt) and with interface reinforcement. Thus, eight sub-databases were the basis for the database evaluation presented in this chapter. The structure and classification of the databases is shown in Figure 6-1.

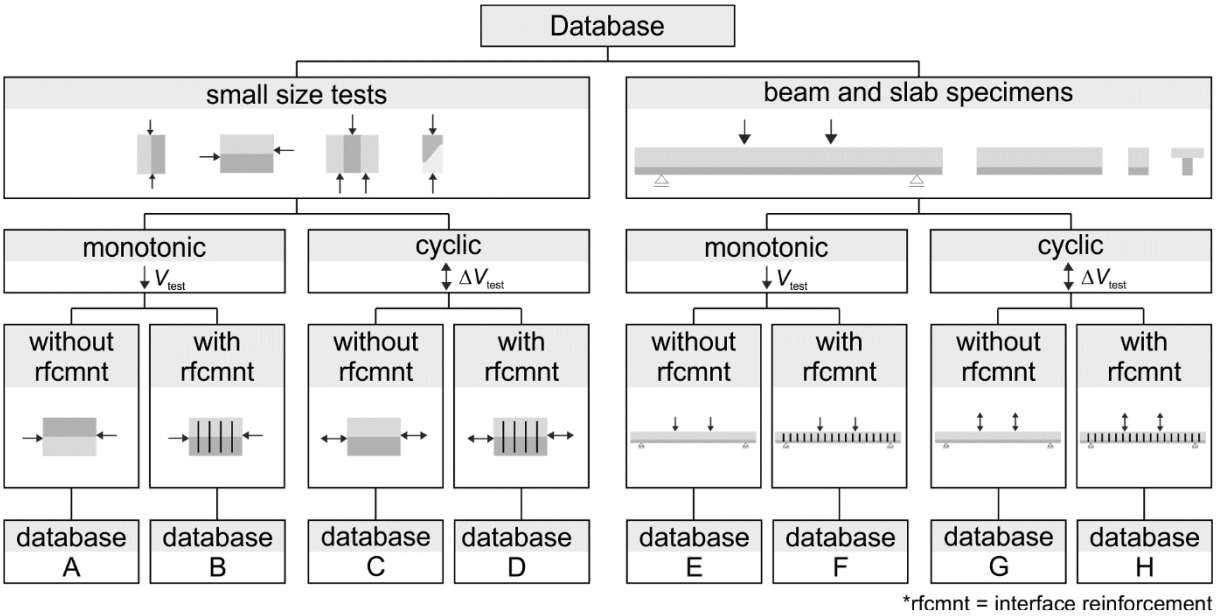

Figure 6-1: Overview of databases with small size test as well as beam and slab specimens

6.2 Database preparation and evaluation criteria

6.2.1 Introduction

To develop consistent and critically reviewed databases, test reports were compiled from literature. The test data was summarised and categorised in the corresponding sub-databases, considering the major selection criteria of specimen type, loading conditions and interface reinforcement as stated in Figure 6-1. For each test, the relevant test parameters of geometry, interface condition, material parameters of concrete and reinforcement as well as ultimate load and failure mode were assessed. Since the collected test reports presume different definitions of interface condition, determinations of concrete strength and units for stress and dimensions, the data was converted to achieve a consistent base for evaluation. Furthermore, selection criteria were defined to fulfil the application limits of the database evaluation for horizontal interfaces in beam and slab structures.

6.2.2 Selection criteria and harmonisation of test data

Database filter

The comprehensive collected data were filtered to only comprise specimens with complete test data (sufficient documentation of interface roughness, geometrical and material properties as well as ultimate load). The evaluation range was limited in terms of concrete to concrete interfaces commonly used in building practice. Therefore, specimens with keyed interfaces as well as grout injected interfaces were not considered. The limits of concrete strength were defined in accordance to the application limits of [EC2] to 12 N/mm² $\leq f_{ck} \leq$ 100 N/mm². Besides tests with lattice girders, no tests with smooth reinforcement surfaces were evaluated.

The databases with small size specimens only consider specimens subjected to pure shear, which excludes tensile and splitting tests. Precracked specimens, which were conducted to investigate the shear transfer across existing cracks, as well as specimens where the load application results in a load resultant along the interface but combined with considerable moment acting in the interfaces (e.g. modified corbels and sliding walls) were excluded. For both, small size tests as well as beam and slab specimens, tests with prior failure (e.g. interface delamination before testing) and different failure mode were not considered.

The database filter can be summarised to:

- undefined or incomplete test data
- keyed interfaces
- grout injected interfaces
- monolithic precracked specimens
- tensile and splitting test
- tests with considerable moment eccentricity acting in the interface
- limit of concrete strength 12 N/mm² $\leq f_{ck} \leq$ 100 N/mm².
- prior failure or different failure mode

For consistency, test parameters originally formulated in imperial and pound units were translated to metric and newton units. The ultimate load was defined and calculated to shear stress τ in N/mm².

Interface classification

The classification of the interface surface condition in the test reports does not follow consistent regulations. Therefore, the documented surface conditions were categorised in consistent interface classes for a comparable database evaluation as shown in Table 6-1.

The introduced surface classifications generally correspond to the classifications defined in [prEC2:18], which is similar to the regulations in [EC2], [EC2NAD] and [MC10]. Differing from the expression in [EC2NAD], the classifications in [EC2] do not distinguish between very rough and keyed surfaces, but only defines indented surfaces as keyed surfaces. For very rough surfaces in accordance to Table 6-1, no classification is included. Thus, for the [EC2] evaluation, interfaces with very rough surfaces were evaluated as rough surfaces. The surface classifications in [ACI318] and [AA-L] only distinguish between surfaces not intentionally roughened and intentionally roughened to an amplitude of at least 6.4 mm (s. Chapter 3.3). Thus, for the evaluation with the [ACI318] and [AA-L] provisions, intentionally roughened surfaces were defined as very rough surfaces and the remaining surface classes were defined as not intentionally roughened.

Table 6-1: Classification of the surface condition for the database evaluation

Interface	Classification
very smooth	- concrete cast against formwork, plastic, steel or similar material
smooth	- surfaces left as cast
	- surfaces additionally smoothed
	- surfaces cast against formwork and lightly sandblasted
	- surfaces with a mean roughness depth R_t < 1,5 mm determined by the sand-patch-method
	- surfaces with a maximum roughness of 3 mm (peak to valley)
rough	- surfaces additionally roughened by raking, brushing or similar methods to a roughness between 3 mm and 6 mm (peak to valley)
	- surfaces with exposed aggregates by e.g. sandblasting or other methods to a roughness between 3 mm and 6 mm (peak to valley)
	- surfaces with a mean roughness depth $R_t \geq$ 1,5 mm determined by the sand-patch-method
very rough	- surfaces additionally roughened by raking, brushing or similar methods to a minimum roughness of 6 mm (peak to valley)
	- surfaces with exposed aggregates by e.g. sandblasting or other methods to a minimum roughness of 6 mm (peak to valley)
	- surfaces with a mean roughness depth $R_t \geq$ 3,0 mm determined by the sand-patch-method

Conversion of concrete strength

According to the evaluated design concepts defined in the European codes, the adhesive term of the interface shear strength is defined by the concrete tensile strength or to be proportional to the square or cubic root of the characteristic concrete compressive strength. The concrete compressive strength in these concepts is defined to be determined by a cylinder (150/300 [mm]). The tensile strength is the maximum stress under centric tension and can be specified by spitting tests or flexural tests.

In case the evaluated test reports determine the concrete compression strength with specimens of different sizes or shape (e.g. cubes), the values were converted to the uniaxial concrete compressive strength f_{c1}, using the relations described in [Rei12]. Thus, the cylinder concrete compressive strength $f_{c,cyl}$ of a 150/300 [mm] cylinder can be recalculated with Eq. (6-1).

$$f_{1c} = 0.95 \cdot f_{c,cyl} \tag{6-1}$$

Table 6-2 summarises the conversion factors of different specimens to the uniaxial concrete compressive strength f_{1c} according to [Rei12].

Table 6-2: Conversion of different test specimens' dimensions into the uniaxial concrete compressive strength according to [Rei12]

specimen	dimension [mm]	uniaxial concrete compressive strength
cylinder	150 / 300	$f_{1c} = 0.95 \cdot f_{c,cyl,150/300}$
	100 / 300	$f_{1c} = 1.0 \cdot f_{c,cyl,100/300}$
	100 / 200	$f_{1c} = 0.92 \cdot f_{c,cyl,100/200}$
cube	100	$f_{1c} = 0.68 \cdot f_{c,cube,100}$
	150	$f_{1c} = 0.75 \cdot f_{c,cube,150}$
	200	$f_{1c} = 0.79 \cdot f_{c,cube,200}$
prism	120 / 120 / 360	$f_{1c} = 1.0 \cdot f_{c,prism}$

f_{1c}: uniaxial concrete compressive strength; $f_{c,cyl,150/300}$: cylinder concrete compressive strength of a cylinder with diameter/height of 150/300 mm; $f_{c,cube,100}$: concrete compressive strength of a cube with a side length of 100 mm; $f_{c,prism}$: concrete compressive strength of a prism

Since test reports usually report mean values of the concrete compressive strength, the mean cylinder concrete compressive strength $f_{cm,cyl}$ must be converted to the characteristic concrete compressive strength f_{ck} for evaluation. [EC2] and [MC10] determine the relation of mean and characteristic value according to Eq. (6-2).

$$f_{ck} = f_{cm,cyl} - \Delta f \tag{6-2}$$

For concrete cast on site, the codes formulate $\Delta f = 8$ N/mm^2. To evaluate databases with tests conducted under laboratory conditions, the transformation factor can be reduced to $\Delta f = 4$ N/mm^2 [Rei12].

The concrete tensile strength is commonly specified by splitting or bending tests. The uniaxial tensile strength f_{ct1} can be calculated by the splitting tensile strength $f_{ct,sp}$ determined by a 150/300 [mm] cylinder or prism using the relation defined in [EC2] (Eq. (6-3)).

$$f_{ct1} = 0.9 \cdot f_{ct,sp} \tag{6-3}$$

The flexural tensile strengths $f_{ct,flex}$ determined by bending tests can be converted into the uniaxial tensile strength according to the definition in [MC10] as a function of the depth of the test beam h_b (Eq. (6-4)).

$$f_{ct1} = \frac{0.6 \cdot h_b^{0.7}}{1 + 0.06 \cdot h_b^{0.9}} \cdot f_{ct,flex} \tag{6-4}$$

For test reports providing both, splitting and flexural tensile strength, the splitting tensile strength was the governing strength for further calculations. To evaluate the databases, the uniaxial concrete tensile strength was defined as the mean concrete tensile strength f_{ctm}. If the test reports do not provide the concrete tensile strength of the specimens, the

concrete compressive strength was converted by empiric relations as described in [Rei12]. The translation of concrete compressive to tensile strength according to [EC2] and [MC10] differs for lower concrete strength classes (≤ C50/60) and higher concrete strength classes (> C50/60) and can be calculated according to Eq.(6-5) and (6-6).

$$f_{ctm} = 0.3 \cdot f_{ck}^{2/3} \text{ for} \leq C50/60 \tag{6-5}$$

$$f_{ctm} = 2.12 \cdot \ln(1 + 0.1(f_{ck} + \Delta f)) \text{ for} > C50/60 \tag{6-6}$$

To transfer the mean concrete tensile strength to characteristic level, the relation in Eq. (6-7) according to [EC2] and [MC10] was used.

$$f_{ctk,0.05} = 0.7 \cdot f_{ctm} \text{ for 5 \% - fractile values} \tag{6-7}$$

6.2.3 Statistic evaluation of databases

To compare the test data to the interface shear design regulations defined in the selected codes, the experimental failure shear stress τ_{test} was related to the calculated shear stress τ_{calc}. The test parameters in the database collected from test reports are generally formulated as mean values. Thus, an evaluation with mean values would be appropriate to compare the design equations, not considering fractile values and safety factors for materials. However, the coefficients regarding the surface classification in the interface shear equations were derived using the characteristic values of test data. Furthermore, the expressions of the European design codes consider the terms of adhesive strength by terms of the design concrete tensile strength f_{ctd} ([EC2], [EC2NAD] and [MC10] for rigid bond), by the square root of the characteristic concrete compressive strength $f_{ck}^{1/2}/\gamma_c$ ([prEC2:18]) and the cubic root $f_{ck}^{1/3}$ ([MC10] for non-rigid bond). According to [EC2], the characteristic concrete compressive strength f_{ck} is defined by the mean concrete compressive strength f_{cm} with a constant standard deviation σ_c (Eq. (6-8)). Thus, for increasing concrete strength, the coefficient of variation COV decreases and the influence of scatter reduces.

$$f_{ck} = f_{cm} - 8 \text{ N/mm²} = f_{cm} - 1.645 \cdot \sigma_c \rightarrow \sigma_c = 4.9 \text{ N/mm²} \tag{6-8}$$

For design expressions, $f_{ck}^{1/2}$ and $f_{ck}^{1/3}$ were introduced to describe the concrete tensile strength, which corresponds to be proportional to the concrete tensile strength. For mean evaluation however, a calculation with e.g. $f_{cm}^{1/2} = (f_{ck} + 8)^{1/2}$ would lead to a general reduction of standard deviation. In this context, Figure 6-2 compares the expressions of concrete tensile strength expressed on mean and characteristic level by the ratios of mean values $f_{ctm}/f_{cm}^{1/2}$ and the characteristic values $f_{ctk}/f_{ck}^{1/2}$ over the mean concrete compressive strength. The concrete tensile strength was therefore calculated in accordance to Eqs. (6-5) to (6-7). The evaluation shows, that the ratio of mean strengths shows larger deviations Δ_m from the mean value of the mean concrete strengths $X_{m,m}$ compared to the mean value of characteristic strengths $X_{m,k}$ with the deviation Δ_k.

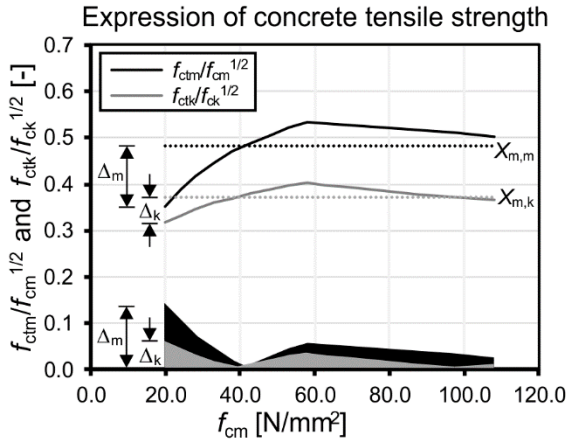

Figure 6-2: Comparison of expressions for mean and characteristic concrete tensile strength

Since the characteristic expressions of concrete tensile strength and square root of characteristic concrete compressive strength show smaller deviations over the practical range of concrete strength, the databases were evaluated on characteristic level. Regarding the American Codes, it has to be mentioned, that the design concepts of [ACI318] and [AA-L] do not define the adhesive resistance by terms of concrete strength but introduce constant adhesive strengths and use a global safety factors for design.

For the statistic evaluation of databases, a log-normal distribution of test data was assumed. This is in accordance to [JOI00], which recommends a log-normal distribution for shear. To determine mean values m_x, standard deviation s_x, coefficient of variation COV and characteristic 5 % quantiles $X_{k,5\%}$ of the test data x_i for a number of n tests, the test data must be logarithmised with $\ln(x_i)$. The mean value m_y and standard deviation s_y of the logarithmised test data are calculated in accordance to Eq. (6-9) and Eq. (6-10) [EC0].

$$m_y = \frac{1}{n}\sum \ln(x_i) \tag{6-9}$$

$$s_y = \sqrt{\frac{1}{n-1}\sum (\ln x_i - m_y)^2} \tag{6-10}$$

The mean value m_x and standard deviation s_x as well as the coefficient of variation COV for the test data after logarithmised determination of statistic values can be calculated according to Eqs. (6-11) to (6-13).

$$m_x = \exp\left(m_y + \frac{s_y^2}{2}\right) \tag{6-11}$$

$$s_x = \exp\left(m_y + \frac{s_y^2}{2}\right) \cdot \sqrt{\exp\left(s_y^2\right) - 1} \tag{6-12}$$

$$\mathrm{COV} = \frac{s_x}{m_x} = \sqrt{\exp\left(s_y^2\right) - 1} \tag{6-13}$$

The determination of the 5 % characteristic quantile ratio of the test evaluation follows Eq. (6-14).

$$X_{k,5\%} = \exp\left(m_y + k_n \cdot s_y\right) \tag{6-14}$$

The 5 % quantile values k_n were adopted from [EC0] with a confidence level of 75 % and considering the number of test specimens for an unknown coefficient of variation COV (Table 6-3).

Table 6-3: k_n values for the characteristic 5 % quantiles [EC0]

n	3	4	5	6	8	10	20	30	∞
COV known	1.89	1.83	1.8	1.77	1.74	1.72	1.68	1.67	1.64
COV unknown	3.37	2.63	2.33	2.18	2.00	1.92	1.76	1.73	1.64

6.3 Database evaluation with small size tests

6.3.1 Introduction

For the database with small size specimens, a total of 1161 tests could be collected from 30 research publications and test reports. After applying the database filter (s. Chapter 6.2.2), the complete database was reduced as shown in Figure 6-3. The filter criteria of tests with incomplete documentation and different failure mode also includes test specimens which failed before testing as well as aberration specimens. Specimens were only defined as aberration specimens if the tested shear resistance exceeded the shear resistance of comparable specimens by their multiple.

The selected database consists of 553 tests for evaluation. For separately evaluating the contributions of adhesion, friction by applied normal stress and by reinforcement, the data was separated in sub-databases. The database for adhesion (A-1) includes 83 specimens conducted as push-off or push-through tests without externally applied normal stress or reinforcement. Database A-2 holds 145 tests with specimens with externally applied normal stress. To determine the contribution of reinforcement, 266 tests can be evaluated in database B. Since the expressions in the design equations formulate the effect of normal stress and reinforcement by considering the effect of friction, the same friction factor μ is used. Thus, database AB includes 39 tests where both, interface reinforcement and normal stress was applied. Small size specimens under cyclic loading conditions without interface reinforcement could only be collected from one test report with a number of 20 tests. In literature, fatigue tests with small size specimens with interface reinforcement could not be found.

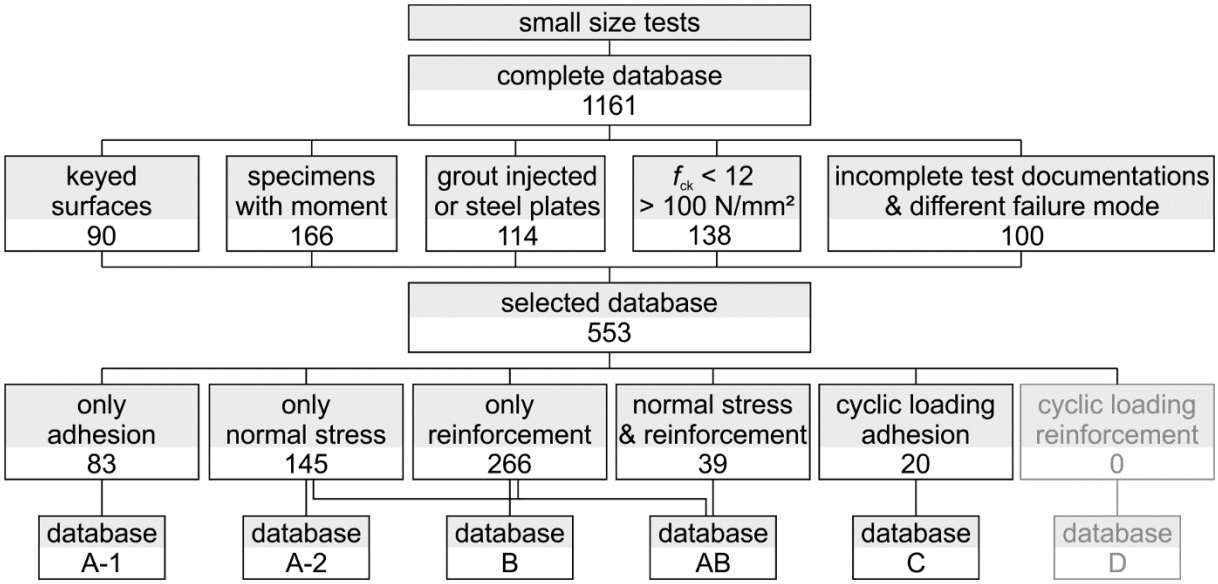

Figure 6-3: Overview of databases with small size tests

An overview of the researchers and test reports included in the database for the complete database as well as for the selected database can be found in Annex B.1. In the following chapters, the evaluations of the sub-databases are presented separately for the considered design codes. Annex B.1 holds the complete compilation of the evaluation diagrams.

6.3.2 Database A-1: Adhesion

For an isolated consideration of interface resistance due to adhesion, only tests were evaluated which did neither include interface reinforcement nor externally applied normal stress. The distributions of the 83 evaluated tests regarding interface classification, dimension of interface, concrete strength of precast and insitu concrete as well as the decisive smaller concrete strength for design are shown in Figure 6-4 and Figure 6-5.

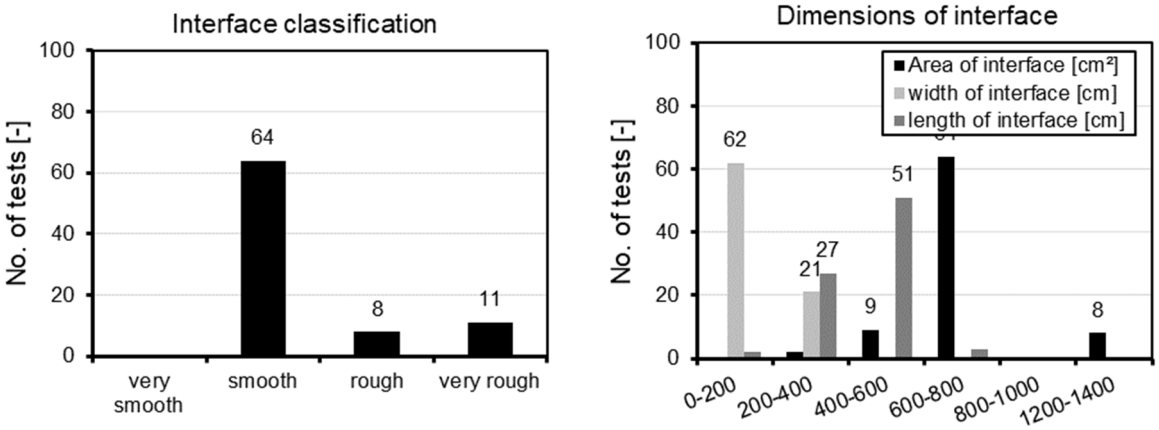

Figure 6-4: Distribution of 83 small size tests for isolated adhesive strength regarding interface classification and interface dimensions

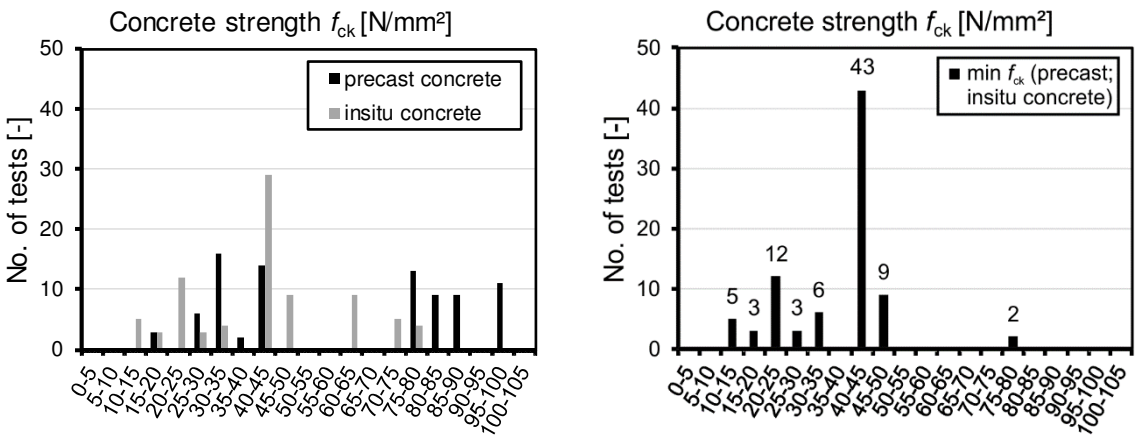

Figure 6-5: Distribution of 83 small size tests for isolated adhesive strength regarding concrete strengths

To assess the design equations of the considered design codes, the ultimate shear stress of the interface from tests τ_{test} was compared to the calculated characteristic adhesive strength with $\tau_{calc} = \tau_{Rk,i}$. If test reports only provide failure loads V_{test}, the failure interface shear stress was calculated by $\tau_{test} = V_{test} / A_{int}$, with A_{int} being the area of interface.

The evaluation of the test data according to the considered design equations with corresponding characteristic design expressions, number of evaluated tests, mean value X_m, coefficient of variation COV and characteristic 5 % quantile ratio $X_{5\%}$ are summarised in Table 6-4.

Table 6-4: Statistic evaluation of small size tests for adhesion in database A-1 with $\tau_{test}/\tau_{Rk,i}$

Code	$\tau_{Rk,i} = \tau_{adh}$	No. of tests	X_m	COV	$X_{5\%}$
EC2:2004	$c \cdot f_{ctk}$	83	3.18	0.41	1.53
EC2+NA(D)	$c \cdot f_{ctk}$	83	3.07	0.39	1.53
prEC2:2018	$c \cdot f_{ck}^{1/2}$	83	3.06	0.37	1.57
MC2010	$c \cdot f_{ctk}$	83	3.07	0.39	1.53
ACI 318	τ_{adh} = const.	11	5.42	0.14	4.09
AASHTO	τ_{adh} = const.	83	2.81	0.49	1.15

X_m: mean value τ_{Rki}/τ_{calc}, COV: coefficient of variation, $X_{5\%}$: characteristic 5 % quantile ratio

For calculating the adhesive strength, [EC2], [EC2NAD], [MC10] refer to the concrete tensile strength, whereas [prEC2:18] formulates the square root of the characteristic concrete compressive strength. The high coefficients of variation with COV = 0.37 – 0.41 for the European codes show the high scatter of test data. This was expected, since the interfaces form a weak plane in the monolithic material structure, which can only by partially controlled. The coefficient of variation of the [EC2] evaluation gives a higher value, since the interface classification only allows very rough interfaces to be considered as rough surfaces. The definition of the concrete tensile strength being proportional

to the square root of the characteristic concrete compressive strength according to [prEC2:18] gives the lowest, but still high coefficient of variation. Table 6-5 depicts a more detailed evaluation of codes by summarising the coefficients of adhesion as well as the statistic evaluation for each interface classification. As expected, the scatter of test data decreases with increasing interface roughness. Especially for smooth interfaces, high coefficients of variation are determined. This confirms, that the bond development for smooth interfaces depicts a critical range which can hardly be controlled and specified. Additionally, influencing parameters as e.g. concrete consistency, water saturation and cleanness of interface have an effect on the adhesive strength which cannot be assessed by the design expressions.

Table 6-5: Evaluation of database A-1 with τ_{test}/τ_{Rki} isolated for interface classification

Code	Interface classification	Coefficient of adhesion	No. of tests	X_m	COV	$X_{5\%}$
EC2:2004 [EC2]	very smooth	0.025	-	-	-	-
	smooth	0.20	64	3.03	0.42	1.42
	rough	0.40	19	3.69	0.30	2.08
	very rough	(1)	-	-	-	-
EC2+NA(D) [EC2NAD]	very smooth	0	-	-	-	-
	smooth	0.20	64	3.03	0.42	1.42
	rough	0.40	8	3.15	0.35	1.50
	very rough	0.50	11	3.26	0.20	2.21
prEC2:2018 [prEC2:18]	very smooth	0.0095	-	-	-	-
	smooth	0.075	64	3.07	0.40	1.47
	rough	0.15	8	3.17	0.34	1.30
	very rough	0.19	11	3.09	0.16	2.28
MC 2010 [MC10]	very smooth	0.025	-	-	-	-
	smooth	0.20	64	3.03	0.42	1.42
	rough	0.40	8	3.15	0.35	1.50
	very rough	0.50	11	3.26	0.20	2.21
ACI318 [ACI318]	not roughened	(2)	-	-	-	-
	roughened	0.56 N/mm²	11	5.42	0.14	4.09
AASHTO [AA-L]	not roughened	0.52 N/mm²	72	2.96	0.51	1.19
	roughened	1.66 N/mm²	11	1.83	0.14	1.38

X_m: mean value τ_{Rki}/τ_{calc}, COV: coefficient of variation, $X_{5\%}$: characteristic 5 % quantile ratio, (1): very rough surfaces are classified as rough surfaces; (2): No regulations for interfaces not intentionally roughened without interface reinforcement

The design regulations in [AA-L] specifically demand concrete interface to be reinforced. However, since the design equation also includes an adhesive resistance term,

specimens without interface reinforcement were evaluated by only applying the adhesive resistance. The design equations of the American codes [ACI318] and [AA-L] only distinguish between intentionally roughened and not intentionally roughened surfaces. Additionally, the regulations according to [ACI318] define different design expressions for vertical and horizontal interfaces. For small size tests, the regulations for vertical interfaces apply, which exclude interfaces without interface reinforcement. To provide an evaluation of the adhesive resistance, the adhesive strengths for horizontal interfaces were applied in these investigations. Nevertheless, only interfaces intentionally roughened are allowed without interface reinforcement. Therefore, only test data with very rough interfaces could be evaluated. Divergent from the European design expressions, the American codes define the adhesive resistance as a constant strength depending on the interface roughness. [ACI318] defined a low adhesive strength of $\tau_{adh} = 0.56$ N/mm² for intentionally roughened surfaces, which gives a lower coefficient of variation of COV = 0.14 with a high mean value $X_m = 5.42$. The adhesive strengths in [AA-L] result in a very high coefficient of variation for not intentionally roughened surfaces with COV = 0.51 and $X_m = 2.96$ and a lower coefficient of variation and mean value COV = 0.14 and $X_m = 1.83$ for intentionally roughened surfaces.

Due to the high coefficients of variation generally determined by interface shear tests, the coefficients of adhesion as well as the adhesive strengths were calibrated to achieve high mean values and thus, high characteristic 5 % quantile ratios. For all evaluated codes, the 5 % quantile ratios exceed the minimum value of $X_{5\%} \geq 1.0$ and thus, can be considered on the safe side.

For interfaces without interface reinforcement and without externally applied normal stress, the main influencing parameters are the concrete tensile strength and the interface roughness. Experimental and numerical investigations from literature show, that the inner zone of the interface is mainly ineffective until the crack develops, and with progressing crack distribution, the edge regions develop in the direction of shear. Especially for long interfaces, the elastic stress distribution concentrates in the edge regions and thus, the mean shear stress decreases with increasing length of the interface. For large interfaces however, higher possibilities of blemishes in the bond structure can be estimated. Another investigated influence was the test setup. Even though the test data was filtered to specimens with a theoretically pure shear stress state at the interface, complex stress states may occur at the interface due to deviation of load application, load dispersals or unintended eccentricities. In the following, the influences of tensile strength, interface roughness, interface dimensions and test setup are evaluated.

Influence of roughness

The determination of interface roughness is generally subjective, and no overall defined parameters exist to ensure a consistent classification of interface roughness. In database A-1 however, the interface roughness was measured by the sand-patch methods accord-

ing to KAUFMANN [Kau71] for 63 specimens and the mean roughness depth R_t was determined. Figure 6-6 shows the failure shear stress related to the characteristic concrete tensile strength over the determined roughness depth R_t.

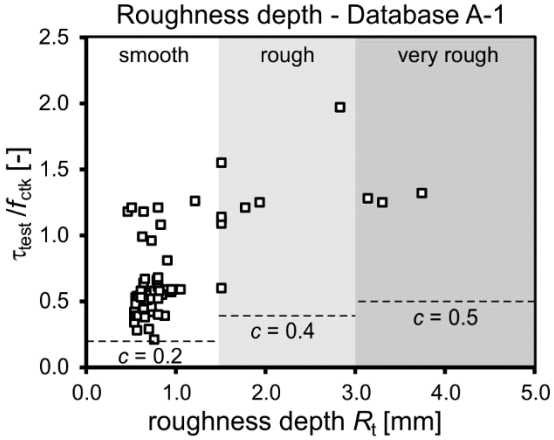

Figure 6-6: Influence of interface roughness determined by database A-1

For the evaluated test data, an increase of interface resistance can be determined. The coefficients of adhesion c as defined in [EC2], [EC2NAD] and [MC10] for an adhesive resistance with $\tau_{Rk,i} = c \cdot f_{ctk}$ describe the lower limit of test data. Especially test results for smooth interfaces show a wide range of scatter, covering the range between lower limit and resistances comparable to rough interfaces. For rough and very rough interfaces however, the interface shear resistances exceed the characteristic value of the tensile strength.

Influence of tensile strength

The adhesive resistance directly correlates with the concrete tensile strength. In this context, Figure 6-7 depicts the test data related to the calculated adhesive resistance according to [EC2NAD] with an characteristic adhesive resistance of $c \cdot f_{ctk}$ and according to [prEC2:18] with $c \cdot f_{ck}^{1/2}$. Figure 6-8 shows the evaluation of [AA-L] with a constant adhesive strength of $\tau_{Rk,I} = 0.52$ N/mm² for interfaces not intentionally roughened and $\tau_{Rk,i} = 1.66$ N/mm² for interfaces intentionally roughened.

The comparison with [EC2NAD] and [prEC2:18] gives a wide distribution of test results for all interface roughnesses. The formulation of the concrete tensile strength in [EC2NAD] shows a general decrease of tested interface resistance with increasing tensile strength whereas for the formulation of the square root of the characteristic concrete strength in [prEC2:18], the inclination of the trendline flattens and thus, gives a slightly better estimation of adhesive strength. The constant adhesive strengths according to [AA-L] give an almost constant estimation for intentionally roughened surfaces whereas for not intentionally roughened surface, the comparably small adhesive strength underestimates the test results with increasing concrete tensile strength.

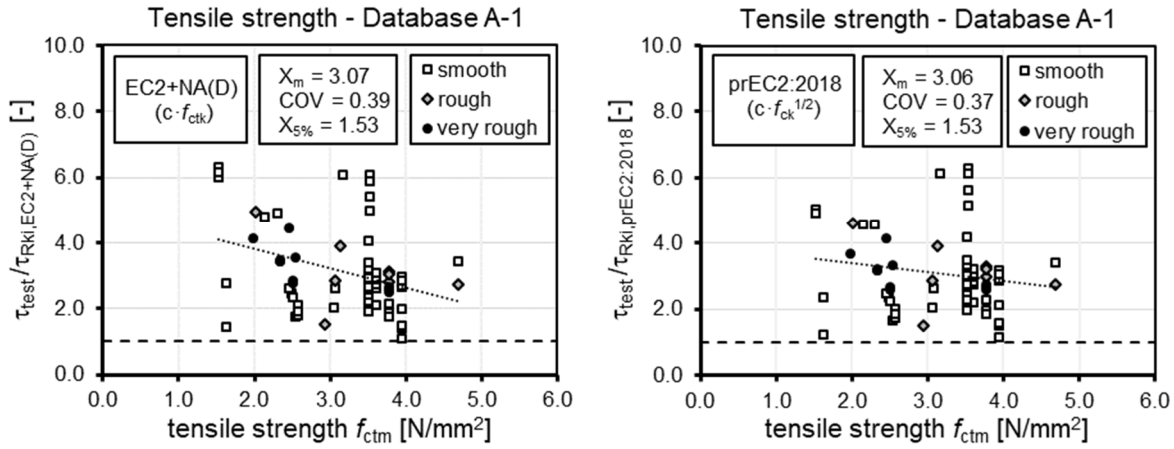

Figure 6-7: Influence of tensile strength on the related interface resistance according to [EC2NAD] and [prEC2:18]

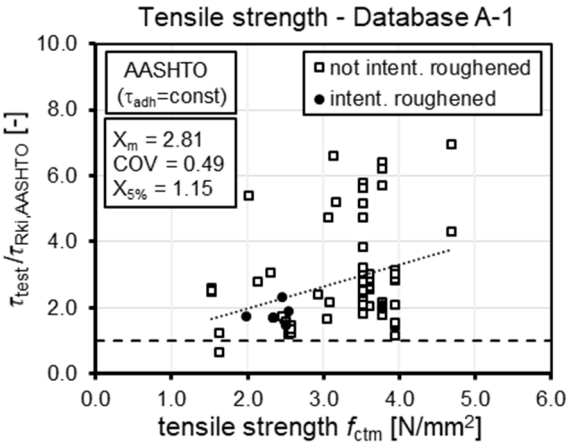

Figure 6-8: Influence of tensile strength on the related interface resistance according to [AA-L] for database A-1 (83 tests)

Influence of test-setup and interface dimensions

To examine the influence of test-setup, Figure 6-9 (top left) depicts the ratio of tested to calculated interface resistance according to [EC2NAD] over the concrete tensile strength, comparing the results of push-off and push-through specimens (s. Chapter 4.2) for smooth interfaces. The wide range of scatter for both test-setups show no clear difference in interface shear resistance.

Figure 6-9 (top right) depicts the influence of the dimension of the test specimens by the length of the interface as well as by the width of the interface. Even though an influence of the interface dimensions was expected, the test results show no clear influence. However, the evaluation of the interface area (Figure 6-9 (bottom)) shows an increase of related interface resistance with increasing interface area, which is mainly caused by the increasing range of scatter of tested interface resistances for larger interfaces. The predictability regarding test-setup and dimension considering tests with pure adhesive bond must be scrutinised, since the high scatter of test results and the absence of systematic

test series investigating the influence of test-setup and dimension do not allow a reliable statement.

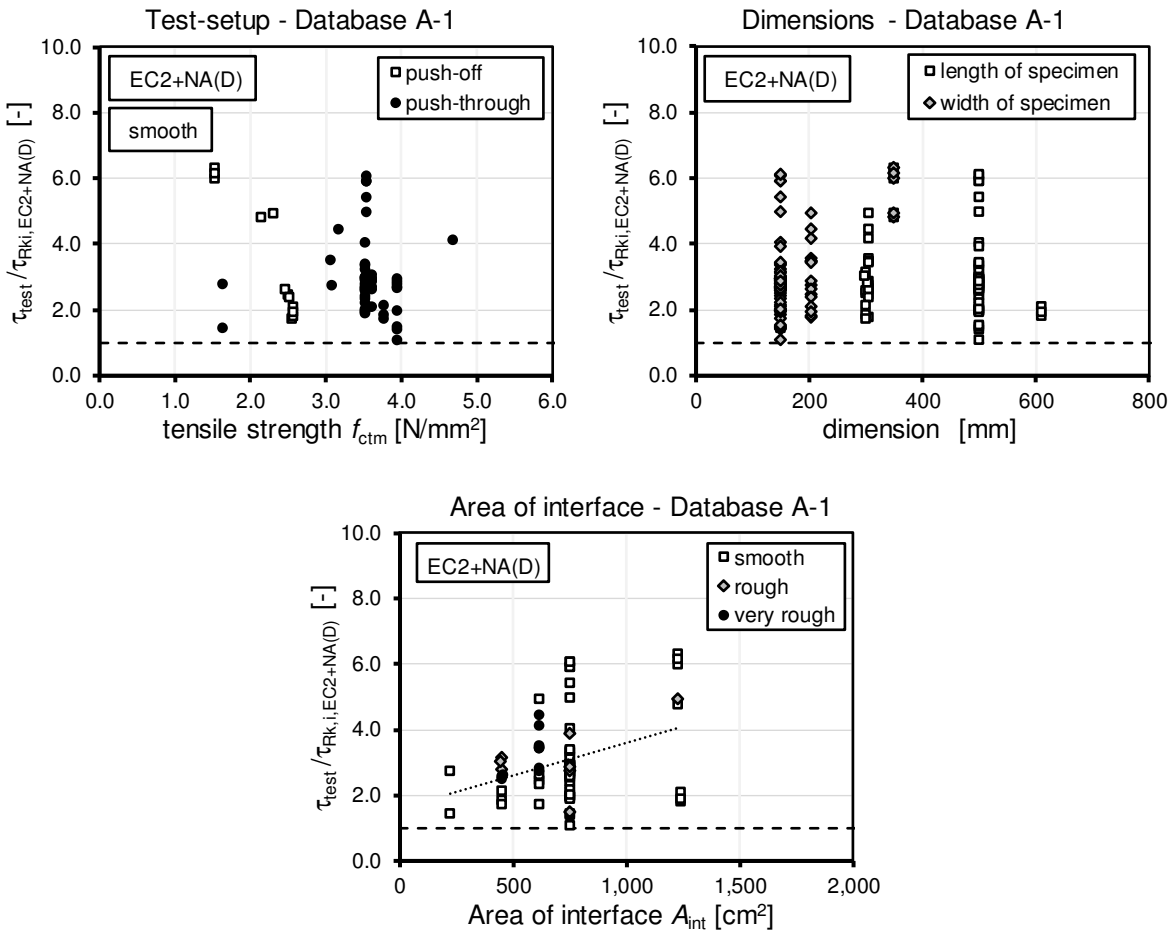

Figure 6-9: Influence of test-setup, interface dimensions and area of interface for an evaluation according to [EC2NAD]

6.3.3 Database A-2: Friction

According to the design expressions in the evaluated codes, the interface shear resistance can be increased by normal compressive stress perpendicular to the interface. For all evaluated codes, the effect of normal stress σ_n is considered by $\tau_{fric} = \mu \cdot \sigma_n$ with the coefficient of friction μ depending on the interface roughness. An isolated evaluation of friction term without considering the adhesive resistance is not possible. However, considering the adhesive term as defined in the evaluated codes, the effect of normal stress can be evaluated. Therefore, database A-2 holds 145 small size tests with externally applied normal stress and without interface reinforcement. Figure 6-10 depicts the distribution of the test data regarding the interface classification and maximum applied normal stress. For the consideration of the adhesive term, Figure 6-11 shows the distribution of precast and insitu concrete strength as well as the decisive minimum concrete strength for design.

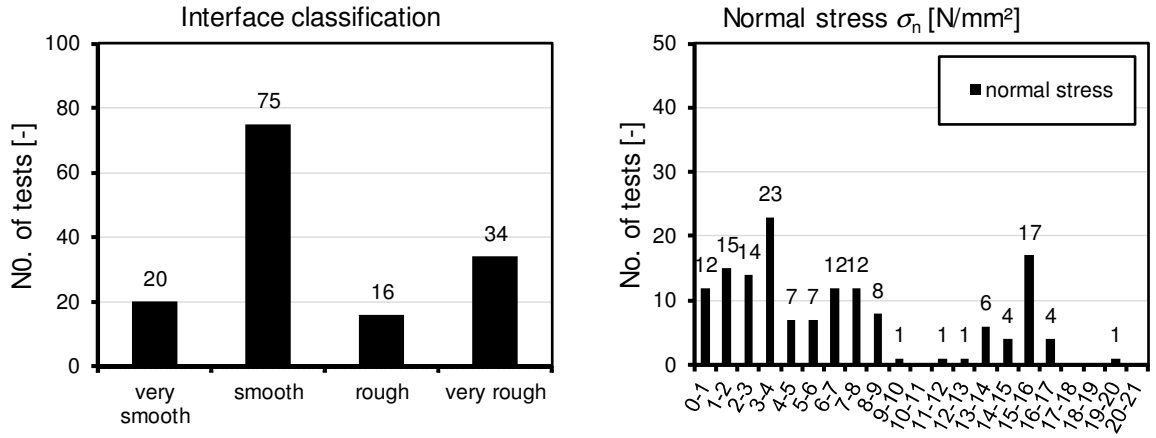

Figure 6-10: Distribution of 145 small size tests with normal stress regarding interface classification and normal stress

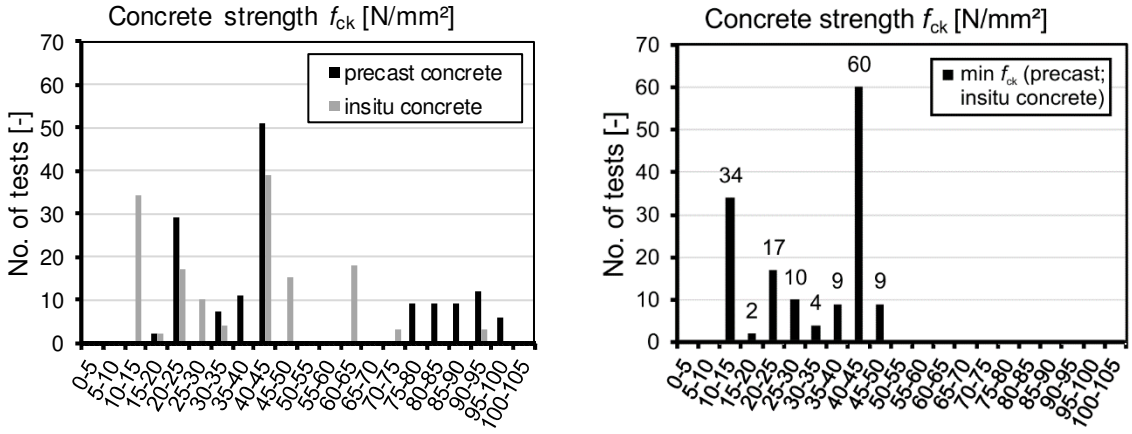

Figure 6-11: Distribution of 145 small size tests with normal stress regarding concrete strength

The evaluation of the design codes for the ratio of tested to calculated characteristic interface shear resistance τ_{test}/τ_{Rki} with corresponding number of tests, mean value X_m, coefficient of variation COV and characteristic 5 % quantile ratio $X_{5\%}$ is summarised in Table 6-6.

Table 6-6: Statistic evaluation of small size tests for friction in database A-2 with τ_{test}/τ_{Rki}

Code $\tau_{Rk,i}$ =	τ_{adh}	+	τ_{fric}	No. of tests	X_m	COV	$X_{5\%}$
EC2:2004	$c \cdot f_{ctk}$		$\mu \cdot \sigma_n$	145	2.46	0.28	1.51
EC2+NA(D)	$c \cdot f_{ctk}$		$\mu \cdot \sigma_n$	145	2.34	0.28	1.42
prEC2:2018	$c \cdot f_{ck}^{1/2}$		$\mu \cdot \sigma_n$	145	2.32	0.29	1.40
MC2010	$c \cdot f_{ctk}$		$\mu \cdot \sigma_n$	145	2.35	0.27	1.46
ACI 318	τ_{adh} = const.		$\mu \cdot \sigma_n$	34	2.11	0.29	1.25
AASHTO	τ_{adh} = const.		$\mu \cdot \sigma_n$	145	2.24	0.43	1.03

X_m: mean value τ_{Rki}/τ_{calc}, COV: coefficient of variation, $X_{5\%}$: characteristic 5 % quantile ratio

The regulations of [ACI318] do not give an explicit formulation for calculating frictional resistance due to normal stress but allow an additional consideration for positive influences due to normal forces. Thus, an expression for frictional resistance in accordance to the other evaluated codes was assumed with applying the friction coefficients defined in [ACI318] for the frictional resistance due to interface reinforcement. Since [ACI318] does not allow a verification of not intentionally roughened interfaces without interface reinforcement, the evaluation is limited to 35 specimens with very rough interfaces.

Table 6-7: Evaluation of database A-2 with τ_{test}/τ_{Rki} isolated for interface classification

Code	Interface classification	Coefficient of adhesion	Coefficient of friction μ	No. of tests	X_m	COV	$X_{5\%}$
EC2:2004 [EC2]	very smooth	0.025	0.5	20	2.28	0.27	1.38
	smooth	0.2	0.6	75	2.36	0.31	1.37
	rough	0.4	0.7	50	2.69	0.20	1.88
	very rough	(1)	-	-	-	-	-
EC2+NA(D) [EC2NAD]	very smooth	0	0.5	20	2.34	0.27	1.40
	smooth	0.2	0.6	75	2.36	0.31	1.37
	rough	0.4	0.7	16	2.88	0.19	2.02
	very rough	0.5	0.9	34	2.04	0.20	1.41
prEC2:2018 [prEC2:18]	very smooth	0.0095	0.5	20	2.27	0.27	1.38
	smooth	0.075	0.6	75	2.35	0.31	1.36
	rough	0.15	0.7	16	2.94	0.19	2.05
	very rough	0.19	0.9	34	2.02	0.20	1.40
MC 2010 [MC10]	very smooth	0.025	0.5	20	2.28	0.27	1.38
	smooth	0.20	0.6	75	2.36	0.31	1.37
	rough	0.40	0.7	16	2.88	0.19	2.02
	very rough	0.50	0.8(2) / 1.0(3)	34	2.15	0.16	1.63
ACI318 [ACI318]	not roughened	(4)	-	-	-	-	-
	roughened	0.56 N/mm²	1.0(5)	34	2.11	0.29	1.25
AASHTO [AA-L]	not roughened	0.52 N/mm²	0.6	111	2.44	0.45	1.09
	roughened	1.66 N/mm²	1	34	1.61	0.20	1.13

X_m: mean value τ_{Rki}/τ_{calc}, COV: coefficient of variation, $X_{5\%}$: characteristic 5 % quantile ratio, (1): very rough surfaces are classified as rough surfaces; (2): for $f_{ck} \geq 20$ N/mm²; (3): $f_{ck} \geq 35$ N/mm²; (4): No regulations for interfaces not intentionally roughened without interface reinforcement; (5): no particular regulations to consider normal stress defined – coefficient adapted from reinforcement term

Compared to the evaluation of specimens with pure adhesion, mean value and coefficient of variation decrease for the database with applied normal stress. However, the still high coefficients of variation between COV = 0.27 and 0.29 and mean values between $X_m = 2.32$ and 2.46 give characteristic 5 % quantile ratios of $X_{5\%} = 1.40 – 1.51$.

The American codes define higher coefficients of friction for both, intentionally roughened and not intentionally roughened surfaces which leads, combined with the constant terms of adhesion, to lower mean values and higher coefficients of variations. However, a characteristic 5 % quantile ratio of $X_{5\%} \geq 1.0$ can still be achieved. In accordance with database A-1, the isolated evaluations for each interface classification in Table 6-7 shows an increase of mean value and coefficient of variation with increasing interface roughness for all codes.

The influence of tensile strength on the adhesive term and normal stress on the frictional term according to the database evaluation with [prEC2:18] and [AA-L] is depicted in Figure 6-12.

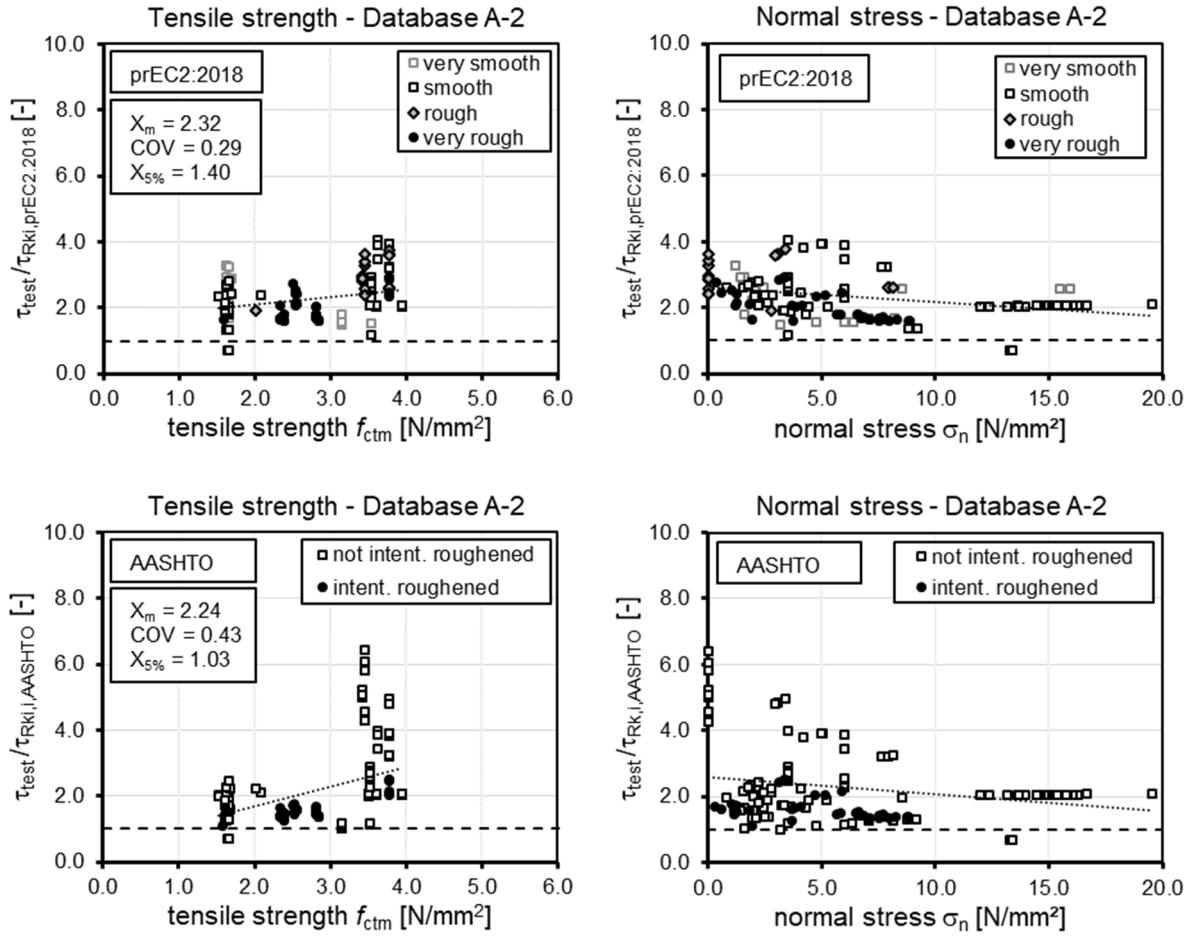

Figure 6-12: Influence of tensile strength and normal stress for an evaluation according to [EC2NAD] and [AA-L] for database A-2 (145 tests)

Due to the applied normal stress, no considerable influence of the tensile strength could be determined for the evaluated data with the [prEC2:18] expression. Confirming the statistic evaluation, the scatter decreases compared to tests without normal stress. The influence of normal stress shows a small decrease of interface resistance with increasing magnitude of normal stress. The evaluation according to [AA-L] in Figure 6-12 with constant adhesive terms shows higher scatter of test data. Especially for not intentionally

roughened surfaces and higher tensile strengths, the assumption of a constant adhesive strength seems inappropriate. The high scatter, especially for small normal stress, may as well be attributed to the constant adhesive strength. Regarding the influence of specimens' dimensions and test setup, no considerable influences could be determined by the evaluated test data.

To limit the magnitude of normal stress, the European codes introduce a limitation of applied external normal stress of $0.6 \cdot f_{cd}$ to exclude progress of fracture due to normal stress. In this context, Figure 6-13 shows the related resistance for the [EC2NAD] evaluation over the ratio of normal stress to characteristic concrete compressive strength σ_n/f_{ck}. For the excluded range $0.6 < \sigma_n/f_{ck}$, a decrease of related interface shear resistance can be determined. For normal stress larger 60 % of the characteristic concrete strength, the calculated interface resistances exceed the experimental strength. Thus, the limitation of normal stress to $0.6 \cdot f_{cd}$ seems reasonable.

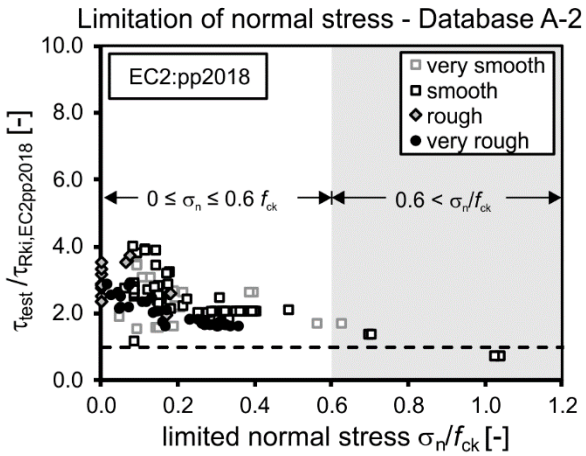

Figure 6-13: Limitation of normal stress according to [prEC2:18]

6.3.4 Database B: Interface reinforcement

For the database evaluation of small size tests with interface reinforcement, 266 tests without externally applied normal stress could be evaluated. Since the evaluated codes generally describe the effect of interface reinforcement by clamping effect, which - according to shear friction theory - results in additional frictional forces, $\tau_{int} = \tau_{adh} + \tau_{reinf}$ applies. The expression according to [prEC2:18] for concrete toppings where no sufficient anchorage of the reinforcement bars can be provided, as well as the [MC10] provisions, introduce an additional load bearing resistance due to dowel action. However, for the evaluation of test data, the resistance term of adhesion as well as for reinforcement is considered. Figure 6-14 and Figure 6-15 show the distribution of the test data regarding interface classification, reinforcement ratio, concrete strength of precast and insitu concrete as well as the decisive concrete strength for design.

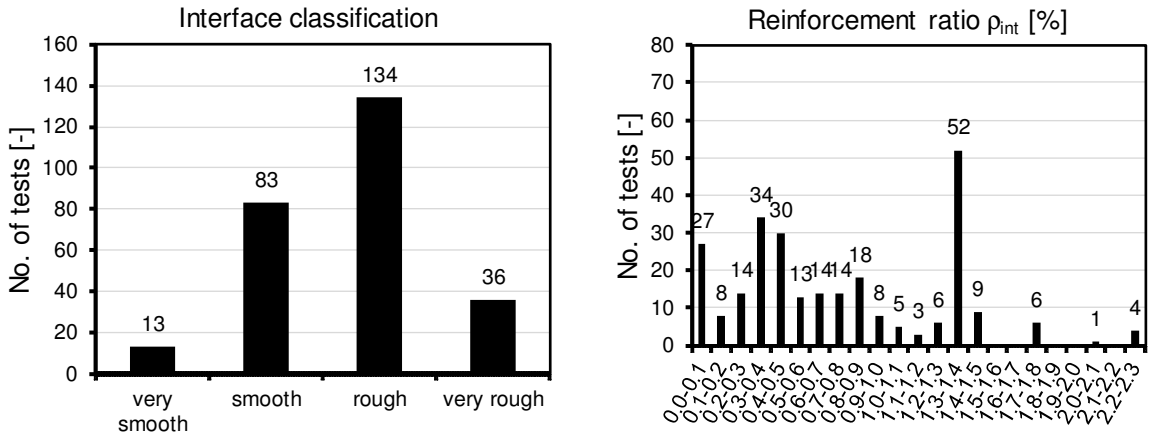

Figure 6-14: Distribution of 266 small size tests with interface reinforcement regarding interface classification and interface reinforcement ratio

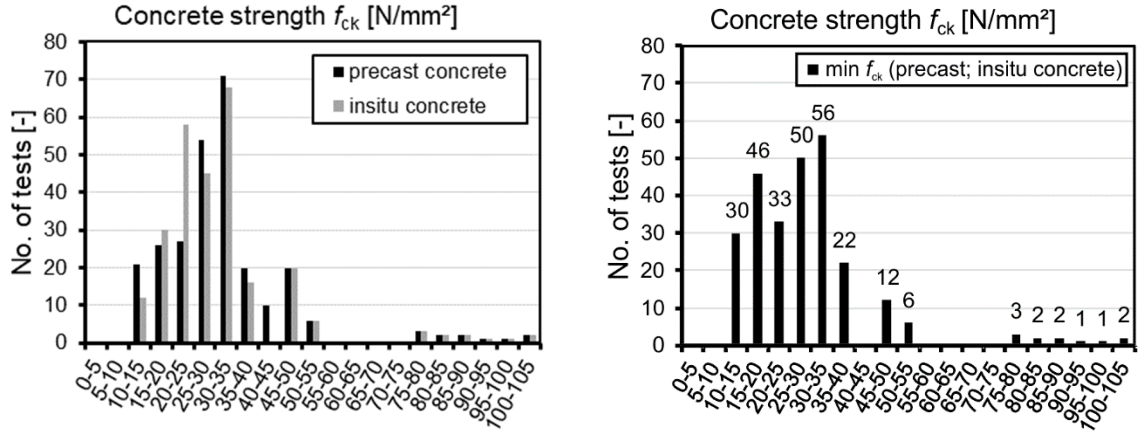

Figure 6-15: Distribution of 266 small size tests with interface reinforcement regarding concrete strength

The expression of adhesive strengths and terms of interface reinforcement of the evaluated codes are summarised in Table 6-8. For specimens with bondbreaker, the term of adhesion was generally neglected for evaluation. An exception was made for a number of twelve tests with rough interfaces and bondbreaker conducted by [Ran97], which shows a high underestimation of calculated resistance compared to the achieved experimental resistance by only considering the term of reinforcement. For these specimens, it was assumed that adhesive bond did develop despite bondbreaker.

Differing from the evaluation without interface reinforcement, [ACI318] allows an evaluation for not intentionally roughened interfaces with interface reinforcement. Thus, all 266 tests could be evaluated by all codes. Table 6-8 gives the statistic results of the evaluation for the experimental resistance compared to the calculated characteristic interface shear resistance.

Table 6-8: Statistic evaluation of small size tests with interface reinforcement in database B with τ_{test}/τ_{Rki}

Code $\tau_{Rk,i}$ =	τ_{adh}	+	τ_{reinf}	No. of tests	X_m	COV	$X_{5\%}$
EC2:2004	$c \cdot f_{ctk}$		$\rho \cdot f_{yk} \cdot (\mu \cdot \sin\alpha + \cos\alpha)$	266	1.63	0.30	0.96
EC2+NA(D)	$c \cdot f_{ctk}$		$\rho \cdot f_{yk} \cdot (1.2 \cdot \mu \cdot \sin\alpha + \cos\alpha)$	266	1.38	0.32	0.78
prEC2:2018	$c \cdot f_{ck}^{1/2}$		$\rho \cdot f_{yd} \cdot (\mu_v \cdot \sin\alpha + \cos\alpha)$	266	1.56	0.31	0.91
(toppings)	$c \cdot f_{ck}^{1/2}$		$k_t \cdot \rho \cdot \mu_v \cdot f_{yk} + k_f \cdot \rho \cdot \sqrt{f_{yk} \cdot f_{ck}}$	266	2.00	0.35	1.08
MC2010	$c \cdot f_{ck}^{1/3}$		$k_1 \cdot \rho \cdot \mu_v \cdot f_{yk} + k_2 \cdot \rho \cdot \sqrt{f_{yk} \cdot f_{ck}}$	266	2.14	0.37	1.12
ACI 318	-		$\rho \cdot f_{yk} \cdot (\mu \cdot \sin\alpha + \cos\alpha)$	266	2.67	0.60	0.92
AASHTO	τ_{adh} = const.		$\rho \cdot f_{yk} \cdot (\mu \cdot \sin\alpha + \cos\alpha)$	266	1.67	0.68	0.50

X_m: mean value τ_{Rki}/τ_{calc}, COV: coefficient of variation, $X_{5\%}$: characteristic 5 % quantile ratio

For comparison, the design expressions of the evaluated codes can be divided into three groups. The equations in [EC2], [EC2NAD] and [prEC2:18] include the term of adhesion considering the concrete tensile strength, and the term of reinforcement by considering the clamping effect as well as a horizontal component for inclined reinforcement. The evaluations lead to high coefficients of variations between COV = 0.3 and 0.32 and mean values between X_m = 1.38 and 1.63. [EC2NAD] increases the resistance of reinforcement by the factor 1.2, which results in a smaller mean value but a higher coefficient of variation. All three codes do not fulfil the claimed characteristic 5 % quantile ratio of $X_{5\%}$ = 1.0, with [EC2NAD] giving the smallest ratio of 0.78. Contrary to the evaluation of specimens without interface reinforcement, the isolated evaluation for each roughness class in Table 6-9 shows an increase of coefficient of variation with increasing interface roughness.

The second group includes the expressions of [prEC2:18] for concrete toppings and the [MC10] expression, which formulate the term of reinforcement by a combination of clamping effect and dowel action. The database evaluation yields to higher mean values (X_m = 2.0 and 2.14) and higher coefficients of variation (COV = 0.35 and 0.37) compared to the expressions only considering the clamping effect. However, due to the high mean values, the characteristic 5 % quantile ratio exceed the limit of $X_{5\%}$ = 1.0.

The expressions of [ACI318] for vertical interfaces with interface reinforcement does not include a term of adhesion, whereas [AA-L] defines constant adhesive strength depending on the interface roughness. Both equations consider the resistance of reinforcement by terms of clamping effect. However, not considering the adhesive resistance leads to a high mean value of X_m = 2.67 with a high coefficient of variation of COV = 0.60. The high coefficients of variation are mainly influenced by the high scatter of not intentionally roughened interfaces. Even though the mean value decreases to 1.67 for the expression of [AA-L], the coefficient of variation increased to COV = 0.68.

Table 6-9: Evaluation of database B with τ_{test}/τ_{Rki} isolated for interface classification

	Interface classification	Coefficient of adhesion	Coefficient of friction μ	No. of tests	X_m	COV	$X_{5\%}$
EC2:2004 [EC2]	very smooth	0.025	0.5	13	1.01	0.19	0.70
	smooth	0.2	0.6	83	1.44	0.28	0.87
	rough	0.4	0.7	170	1.77	0.26	1.13
	very rough	(1)					
EC2+NA(D) [EC2NAD]	very smooth	0	0.5	13	0.84	0.19	0.59
	smooth	0.2	0.6	83	1.22	0.28	0.74
	rough	0.4	0.7	134	1.59	0.26	1.01
	very rough	0.5	0.9	36	1.15	0.30	0.67
prEC2:2018 [prEC2:18]	very smooth	0.0095	0.5	13	1.01	0.19	0.70
	smooth	0.075	0.6	83	1.43	0.28	0.87
	rough	0.15	0.7	134	1.77	0.24	1.16
	very rough	0.19	0.9	36	1.27	0.29	0.75
prEC2:2018 (toppings)	very smooth	–	0.5 (k_f/k_t=0/1.5)	13	1.01	0.19	0.70
	smooth	–	0.6 (k_f/k_t=0.5/1.5)	83	1.59	0.29	0.95
	rough	0.035	0.7 (k_f/k_t=0.5/0.9)	134	2.41	0.27	1.50
	very rough	0.07	0.9 (k_f/k_t=0.5/0.9)	36	1.63	0.26	1.02
MC 2010 [MC10]	very smooth	0.025	0.5 (k_1/k_2=0/1.5)	13	1.51	0.12	1.19
	smooth	0.20	0.6 (k_1/k_2=0.5/1.1)	83	1.64	0.29	0.98
	rough	0.40	0.7 (k_1/k_2=0.5/0.9)	134	2.60	0.29	1.56
	very rough	0.50	0.8(2) / 1.0(3) (k_1/k_2=0.5/0.9)	36	1.79	0.28	1.07
ACI318 [ACI318]	not roughened	–	0.6	230	2.81	0.61	0.95
	roughened	–	1.0	32	1.80	0.38	0.89
AASHTO[AA-L]	not roughened	0.52 N/mm²	0.6	230	1.79	0.70	0.52
	roughened	1.66 N/mm²	1.0	36	0.93	0.28	0.55

X_m: mean value τ_{Rki}/τ_{calc}, COV: coefficient of variation, $X_{5\%}$: characteristic 5 % quantile ratio, (1): very rough surfaces correspond to rough surfaces (2): for $f_{ck} \geq 20$ N/mm²; (3): $f_{ck} \geq 35$ N/mm²; k_f and k_1: coefficient considering the clamping effect; k_t and k_2: coefficient considering the effect of dowel action

To assess the influence of reinforcement ratio, Figure 6-16 shows the ratio of experimental and calculated interface resistance for the regulations in [prEC2:18], [EC2NAD], [MC10] and [ACI318]. The formulations of [prEC2:18], [EC2] and [EC2NAD] give a good estimation of the reinforcement ratio. For tests with rough interfaces however, the calculated interface shear resistance generally gives larger underestimations of test results, whereas for very smooth interfaces, the calculated resistance generally overestimates the experimental results. The increase of reinforcement term by the factor 1.2 for

[EC2NAD] does not influence the trendline, but results in an increase of mean value. Describing the term of reinforcement by an interaction of clamping effect and dowel action according to [MC10] shows an increase of related interface resistance with increasing interface reinforcement ratio. Especially for rough interfaces with small reinforcement ratios, the calculated interface resistances exceed the experimental data. The expression of [ACI318] without adhesive term shows large scatter for all test data. Especially for not intentionally roughened interfaces with small interface reinforcement ratios, neglecting the adhesive resistance gives very small calculated resistances, where the experimental resistance exceeds the calculated resistance by up to 13 times. With increasing reinforcement ratio, the influence of the neglected adhesive resistance decreases, but - compared to the other evaluations - still underestimates the experimental data.

As determined for database A-1 and A-2, a considerable effect of test setup and interface dimension could not be assessed.

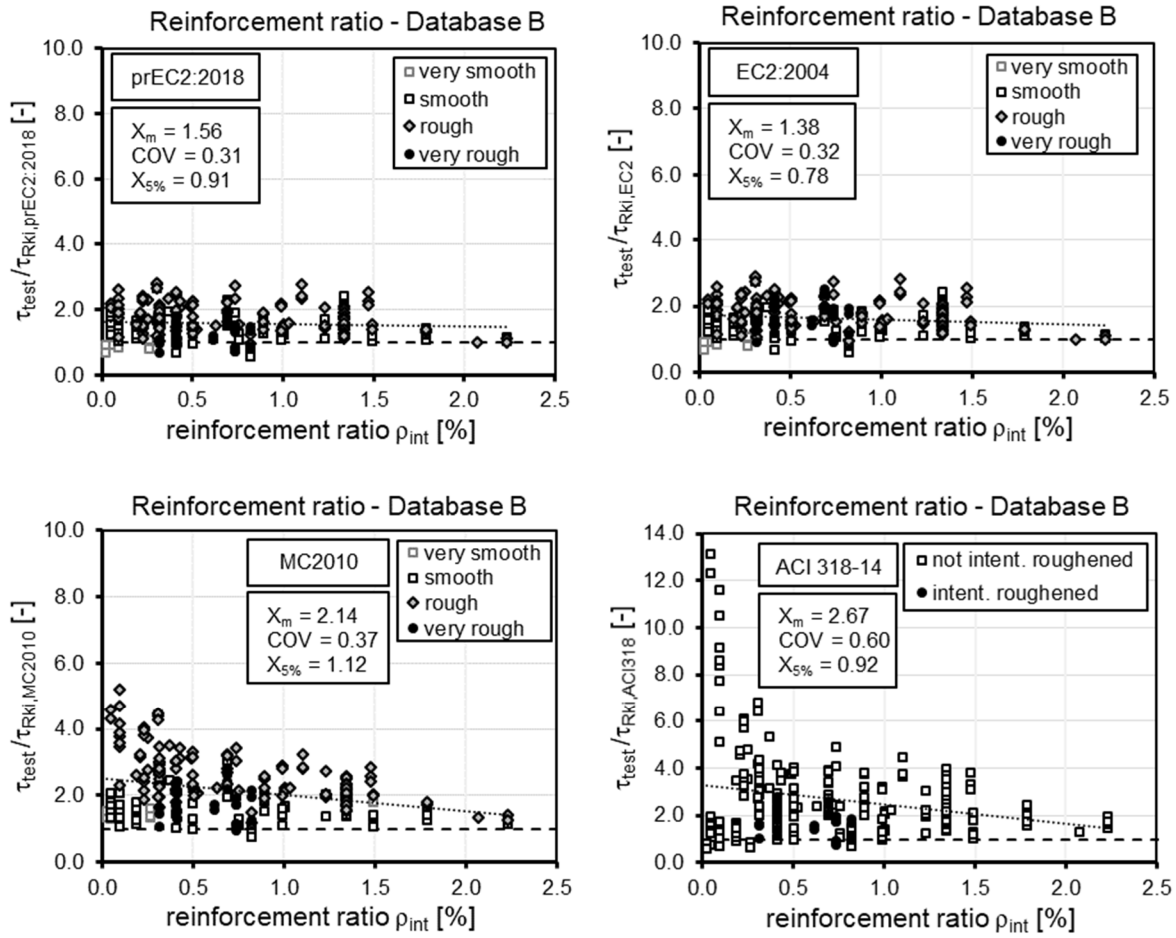

Figure 6-16: Influence reinforcement ratio for an evaluation according to [EC2], [EC2NAD], [MC10] and [ACI318] for database B (266 tests)

6.3.5 Database AB: Friction and interface reinforcement

According to the model concept for interface shear, the interface shear resistance can be determined by the three load bearing mechanisms of adhesion, friction due to normal stress and interface reinforcement. In the design expressions, the surface classification for the frictional effect of both, normal stress and reinforcement is considered by the coefficient of friction μ. The isolated evaluation for friction due to normal stress in database A-2 shows a decrease of coefficient of variation with increasing interface roughness, whereas the evaluation for interface reinforcement with database B yields to increased coefficient of variations with increasing interface roughness. The determined coefficients of variation were slightly higher with smaller mean values. To evaluate the interaction of both load bearing capacities, 39 specimens could be evaluated where external normal stress and interface reinforcement was applied. From the 39 tests, one specimen had a smooth surface and 38 specimens had a rough surface. The results of the evaluation with comparing experimental to calculated interface strength are summarised in Table 6-10. The statistic values of mean values, coefficient of variation and characteristic 5 % quantile ratios are generally comparable to the evaluation of specimens where only interface reinforcement was applied, but with higher mean values and thus, higher 5 % characteristic ratios. This is in accordance to the isolated evaluation of specimens with normal stress (database A-2) and specimens with interface reinforcement (database B).

Table 6-10: Statistic evaluation of small size tests with normal stress and interface reinforcement in database AB with τ_{test}/τ_{Rki}

Code τ_{Rki} =	τ_{adh}	+	τ_{fric}	+	τ_{reinf}	Σ	X_m	COV	$X_{5\%}$
EC2:2004	$c \cdot f_{ctk}$		$\mu \cdot \sigma_n$		$\rho \cdot f_{yk} \cdot (\mu \cdot \sin\alpha + \cos\alpha)$	39	1.71	0.31	0.98
EC2+NA(D)	$c \cdot f_{ctk}$		$\mu \cdot \sigma_n$		$\rho \cdot f_{yk} \cdot (1.2 \cdot \mu \cdot \sin\alpha + \cos\alpha)$	39	1.58	0.32	0.89
prEC2:2018	$c \cdot f_{ck}^{1/2}$		$\mu \cdot \sigma_n$		$\rho \cdot f_{yd} \cdot (\mu_v \cdot \sin\alpha + \cos\alpha)$	39	1.72	0.32	0.96
(toppings)	$c \cdot f_{ck}^{1/2}$		$\mu \cdot \sigma_n$		$k_t \cdot \rho \cdot \mu_v \cdot f_{yk} + k_f \cdot \rho \cdot \sqrt{f_{yk} \cdot f_{ck}}$	39	2.42	0.41	1.15
MC2010	$c \cdot f_{ck}^{1/3}$		$\mu \cdot \sigma_n$		$\mu \cdot \rho \cdot \kappa_1 \cdot f_{yk} + \kappa_2 \cdot \rho \cdot \sqrt{f_{yk} \cdot f_{ck}}$	39	2.66	0.48	1.10
ACI 318	–		$\mu \cdot \sigma_n$		$\rho \cdot f_{yk} \cdot (\mu \cdot \sin\alpha + \cos\alpha)$	39	3.12	1.05	0.50
AASHTO	τ_{adh} = const.		$\mu \cdot \sigma_n$		$\rho \cdot f_{yk} \cdot (\mu \cdot \sin\alpha + \cos\alpha)$	39	2.36	0.41	1.10

X_m: mean value τ_{Rki}/τ_{calc}, COV: coefficient of variation, $X_{5\%}$: characteristic 5 % quantile ratio

6.3.6 Database C: Fatigue without interface reinforcement

To investigate the fatigue behaviour of concrete interfaces without interface reinforcement, 20 tests could be evaluated in the database. The tests were conducted within one test series published in [Zil04] and are presented in Chapter 4.2.5. The fatigue tests were conducted using push-through tests with nine smooth and eleven rough interfaces. The original test report holds 24 test specimens, but three specimens failed prior testing and one test failed due to mismanagement of the load cylinder with sudden load increase

during cyclic load. The minimum characteristic concrete compressive strength was about f_{ck} = 79 N/mm² for six specimens and f_{ck} = 38 N/mm² for 14 specimens.

For the database evaluation, only the adhesive terms of the design equations could be considered. Since the regulations in [ACI318] and [AA-L] do not include considerations of cyclic loading for interface shear design, both codes could not be evaluated. The regulations in [EC2], [prEC2:18] and [MC10] reduce the coefficient of adhesion to 50 % with $c_{fat} = 0.5 \cdot c_{stat}$ for fatigue, whereas [EC2NAD] defines $c_{fat} = 0$ and thus, neglects a fatigue resistance of adhesion.

To evaluate the 20 fatigue tests, the tested maximum shear stress was compared to the static characteristic interface shear strength. According to [EC2] and [MC10], the interface resistance is calculated by $\tau_{Rki,calc} = c \cdot f_{ctk}$ and both expressions include similar coefficients of adhesion for smooth and rough interfaces. For [prEC2:18], the interface resistance is calculated by $\tau_{Rki,calc} = c \cdot f_{ck}^{1/2}$ using adjusted coefficients of adhesion. For the evaluated test data, the calculated static interface resistance according to [prEC2:18] only differ by 1% compared to resistances according to [EC2] and [MC10]. Thus, only results determined by [EC2] and [MC10] are presented in the following.

The fatigue behaviour of concrete has a strong dependence on the applied mean load level. Therefore, Figure 6-17 (left) shows the upper and lower applied shear stress related to the calculated static adhesive strength according to [EC2] and [MC10]. The fatigue tests were terminated after N = 1.0 or 2.0 mil. load cycles. Only three specimens with rough interfaces failed prior reaching the reference number of load cycles. The applied maximum load generally exceeded the calculated characteristic adhesive resistance between 140 and 370 %. Only three specimens with applied maximum loads did not reach the calculated static resistance.

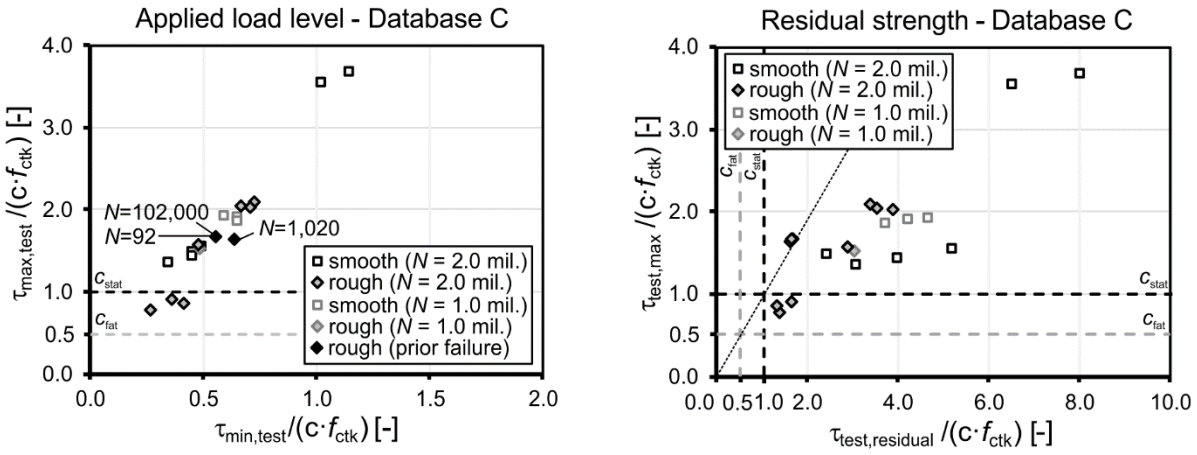

Figure 6-17: Applied load level related to calculated characteristic adhesive strength (left) and residual resistance related to calculated characteristic adhesive strength (right)

For specimens which reached the reference number of load cycles, the static residual strength was determined. As shown in Figure 6-17 (right), the residual resistances after

the fatigue test could be determined to be between 166 and 800 % of the calculated static resistance. However, most specimens achieved suitable number of load cycles with maximum stress exceeding the defined limit of 50 % of the calculated static resistance. Test measurements in [Zil04] also showed no fracture progress for fatigue loads of 50 % of the static resistance. Thus, a consideration of a reduction of 50 % for fatigue is conservative considering the test programme, but due to the high scatter of fatigue strength and adhesive resistance combined with the limited number of tests data, the estimation seems suitable.

6.4 Database evaluation with beam and slab specimens

6.4.1 Introduction

To investigate the interface shear resistance for beam and slab specimens, where horizontal interface shear occurs due to composite action, separate databases were collected. For the databases with beam and slab specimens, 300 tests could be found from 28 research publications and test reports. After applying the database filter (s. Chapter 6.2.2), the complete database was reduced as shown in Figure 6-18. Tests with different failure modes were filtered out, if previous bending or anchorage failure of longitudinal or interface reinforcement occurred or if no interface failure could be determined and shear failure or failure of compression zone was decisive at a load level exceeding a multiple of the interface shear resistance.

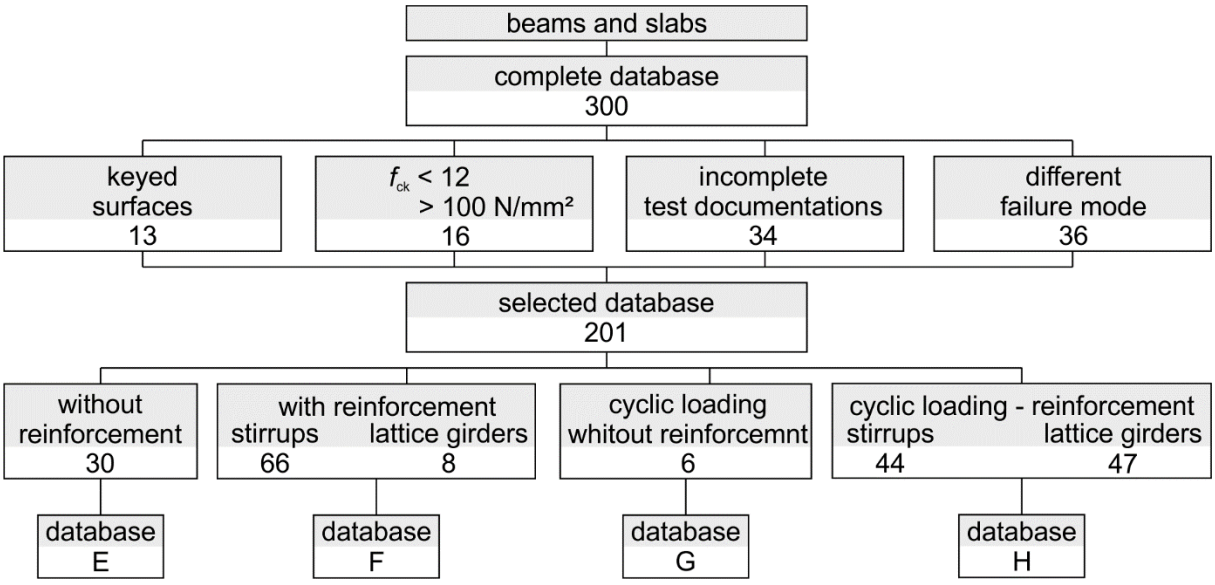

Figure 6-18: Overview of databases with beam and slab specimens

The selected database consists of a total of 201 tests which was allocated to four subdatabases. Database E and F include specimens under monotonic loading conditions, whereas database G and H account for cyclic loading. Database E holds beam and slab specimens without interface reinforcement, where the calculated interface resistance is mainly affected by the adhesive resistance. Since all tests were conducted with a single

point load, the capacity of normal stress could only be activated by the self-weight of the insitu concrete layer. Compared to the calculated adhesive and reinforcement resistance, the resistance of normal stress due to self-weight is insignificant. For database F, beam and slab tests with interface reinforcement were separated in specimens with stirrups as interface reinforcement and specimens with lattice girders under cyclic loading. Database G includes beams and slabs under cyclic loading conditions in order to assess the fatigue behaviour of adhesion in structural members. Following the allocation of database F, database H distinguishes between tests with stirrups and lattice girders. An overview of complete and selected database as well as the compilation of all evaluation diagrams according to the considered codes can be found in Annex B.2.

In the following chapter, the evaluation of the sub-databases are presented separately for the considered design codes.

6.4.2 Database E: Without interface reinforcement

To investigate the applicability of the adhesive terms in the design equations, 30 composite beam and slab specimens could be evaluated. The distribution of the tests in database E regarding interface classification, dimensions of interface, concrete strength of precast and insitu concrete as well as minimum concrete strength of precast and insitu concrete for design are summarised in Figure 6-19 and Figure 6-20. Since all evaluated tests were conducted in three- or four-point bending tests, the length of the interface was defined as shear length *a* being the distance between load application and support.

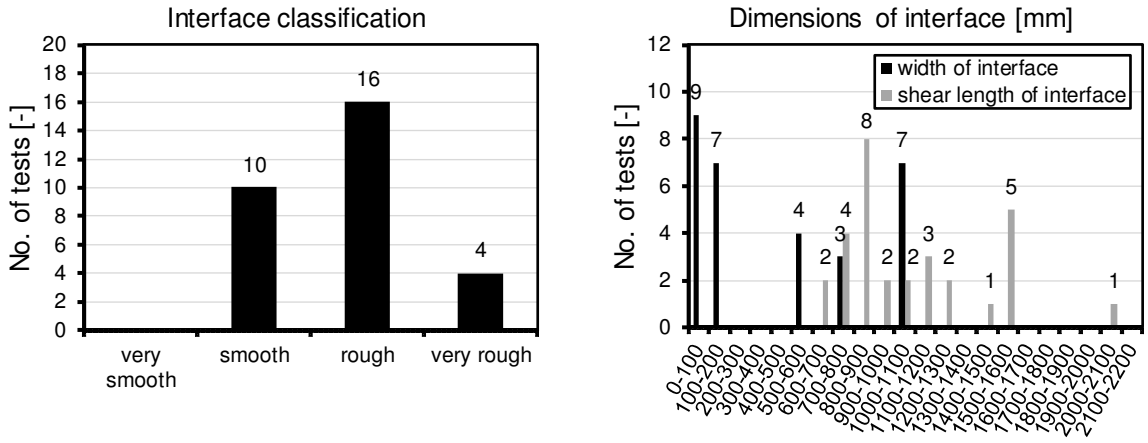

Figure 6-19: Distribution of interface classification and interface dimensions for 30 beam and slabs specimens without interface reinforcement

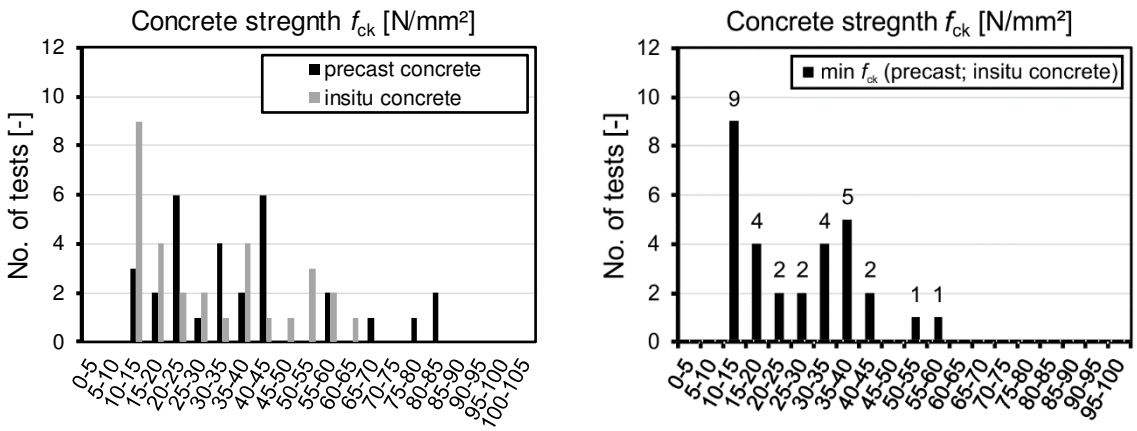

Figure 6-20: Distribution concrete strength of precast and insitu concrete as well as of the decisive smaller concrete strength for 30 beam and slabs specimens without interface reinforcement

To determine the applied interface shear stress τ_{test}, the applied test loads were calculated to acting shear force V_{test} divided by the area of interface b_{int} and the lever arm of internal forces with $z = 0.9 \cdot d$ and d being the effective depth of the specimen (Eq. (6-15)). For all specimens, the calculated compression zone was located in the insitu concrete layer and no reduction of transferable compressive force was necessary.

$$\tau_{test} = V_{Test} / (b_{int} \cdot z) \tag{6-15}$$

For shear design, effective depth and shear slenderness have a decisive effect on the shear resistance. The calculated interface shear resistance however, does not include an effect of these parameters. To investigate the influence of both parameters, the corresponding distributions are shown in Figure 6-21.

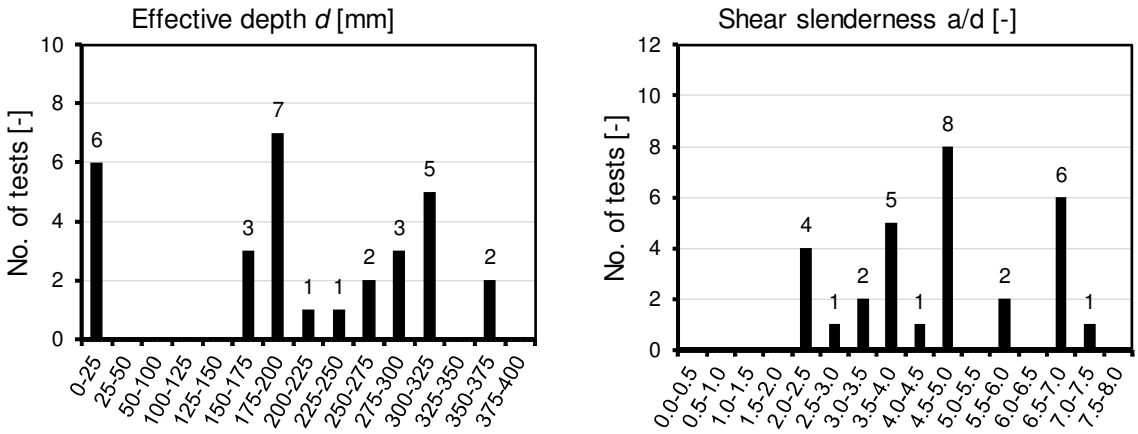

Figure 6-21: Distribution of effective depth and shear slenderness for 30 beam and slab specimens without interface reinforcement in database E

To assess the applicability of the evaluated design equations, the databases were evaluated by referring the experimental interface shear strength τ_{test} to the calculated charac-

teristic interface shear resistance τ_{Rki} with τ_{test}/τ_{Rki}. The evaluations of the test data according to the considered design equations with corresponding characteristic design expression, number of evaluated tests, mean value X_m, coefficient of variation COV and characteristic 5 % quantile ratio $X_{5\%}$ are summarised in Table 6-11. The European design equations as well as [AA-L] do not distinguish between vertical and horizontal interfaces. Thus, the evaluation criteria described in Chapter 6.3.2 apply. The evaluation according to [ACI318] formulates different expressions for horizontal and vertical interfaces. For horizontal interfaces, a design of interfaces not intentionally roughened is excluded. Thus, only four specimens could be evaluated.

Table 6-11: Statistic evaluation of beam and slab specimens in database E with τ_{test}/τ_{Rki}

Code	$\tau_{Rk,i} = \tau_{adh}$	No. of tests	X_m	COV	$X_{5\%}$
EC2:2004	$c \cdot f_{ctk}$	30	4.86	0.56	1.71
EC2+NA(D)	$c \cdot f_{ctk}$	30	4.68	0.54	1.70
prEC2:2018	$c \cdot f_{ck}^{1/2}$	30	4.35	0.51	1.70
MC2010	$c \cdot f_{ctk}$	30	4.68	0.54	1.70
ACI 318	τ_{adh} = const.	4	5.37	0.40	1.83
AASHTO	τ_{adh} = const.	30	4.54	0.64	1.40

X_m: mean value τ_{Rki}/τ_{calc}, COV: coefficient of variation, $X_{5\%}$: characteristic 5 % quantile ratio

Compared to the evaluation of the adhesive term with small size tests in Chapter 6.3.2, generally larger mean values between X_m = 4.35 and 4.86 with larger coefficients of variation between COV = 0.51 and 0.56 were achieved for the European codes. The smallest mean value and coefficient of variation shows the expression of [prEC2:18]. The highest coefficient of variation of COV = 0.64 yields the constant adhesive strength according to [AA-L] combined with a high mean value of X_m = 4.54. For small size tests without interface reinforcement and normal stress, a decreasing coefficient of variation could be determined with increasing interface roughness. The evaluation of beam and slab specimens does not show this effect (Table 6-12). The highest scatter was achieved by specimens with rough interfaces, which might be constituted by the highest number of evaluable tests. However, considering the small number of evaluated specimens, the coefficients of variations and high mean values still achieve characteristic 5 % quantile ratios of $X_{5\%} \geq 1.0$.

For concrete interfaces in composite members, the evaluations of design expressions lead to very high scatter. This was expected, since already the evaluation of small size tests with concentrated load application in Chapter 6.3.2 showed large scatter. Besides the influence of tensile strength and interface roughness, the interface shear resistance of composite members without interface reinforcement may be affected by additional parameters. Thus, load distributions may affect the actual stress state at the interface and additional scattering factors may occur, which generally influence the load bearing behaviour of beams and slabs. To investigate parameters which generally affect the load

bearing behaviour of beams and slabs, the influence of shear slenderness, prestressing of the precast concrete, location of the interface in the cross section, area of interface regarding shear span and width of the interface are presented in the following.

Table 6-12: Evaluation of database E with τ_{test}/τ_{Rki} isolated for interface classification

Code	Interface classification	Coefficient of adhesion	No. of tests	X_m	COV	$X_{5\%}$
EC2:2004 [EC2]	very smooth	0.025				
	smooth	0.20	10	5.60	0.40	2.50
	rough	0.40	20	4.47	0.61	1.40
	very rough	(1)				
EC2+NA(D) [EC2NAD]	very smooth	0				
	smooth	0.20	10	5.60	0.40	2.50
	rough	0.40	16	3.96	0.60	1.25
	very rough	0.50	4	5.19	0.38	1.85
prEC2:2018 [prEC2:18]	very smooth	0.0095				
	smooth	0.075	10	5.09	0.33	2.62
	rough	0.15	16	3.86	0.58	1.25
	very rough	0.19	4	4.39	0.38	1.55
MC 2010 [MC10]	very smooth	0.025				
	smooth	0.20	10	5.60	0.40	2.50
	rough	0.40	16	3.96	0.60	1.25
	very rough	0.50	4	5.20	0.38	1.85
ACI318 [ACI318]	not roughened	(2)				
	roughened	0.56 N/mm²	4	5.37	0.40	1.83
AASHTO[AA-L]	not roughened	0.52 N/mm²	26	4.93	0.54	1.81
	roughened	1.66 N/mm²	4	1.81	0.40	0.62

X_m: mean value τ_{Rki}/τ_{calc}, COV: coefficient of variation, $X_{5\%}$: characteristic 5 % quantile ratio, (1): very rough surfaces are classified as rough surfaces; (2): No regulations for interfaces not intentionally roughened without interface reinforcement

Influence of tensile strength

The influence of concrete tensile strength on the related characteristic interface resistance according to [EC2NAD], [prEC2:18] and [AA-L] is shown in Figure 6-22. In accordance with the small size tests, a decrease of relative experimental resistance with increasing tensile strength can be determined for both EC2 expressions, whereas the [prEC2:18] evaluation gives a slightly flatter trendline. Compared to rough interfaces, interfaces with smooth and very rough interfaces show larger scatter and higher underestimations of calculated characteristic resistances. The decrease of relative interface

resistance with increasing tensile strength may be caused by a loss of ductility for high concrete strengths.

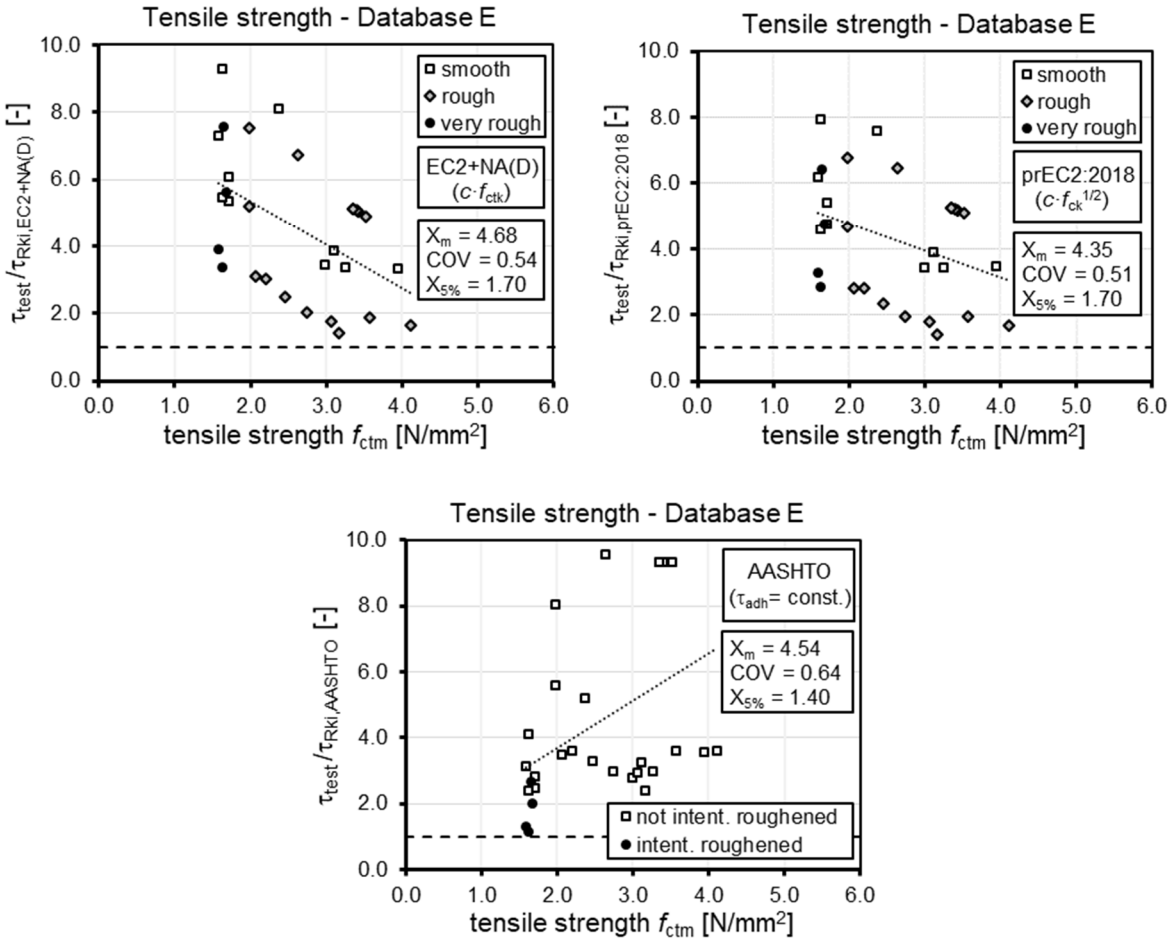

Figure 6-22: Influence of tensile strength on the related resistance according to [EC2NAD], [prEC2:18] and [AA-L] for database E (30 tests)

The assumption of constant adhesive strength according to [AA-L] shows a large range of scatter for not intentionally roughened surfaces.

Influence of shear slenderness

According to the general understanding of shear in simply supported beams and slabs, the shear resistance increases with decreasing shear slenderness. Additionally, by direct transfer of strut action to the support, higher shear resistances can develop. Despite the high range of scatter for the evaluation of shear slenderness with the [prEC2:18] approach (Figure 6-23, left), a small decrease of interface resistance with increasing shear slenderness can be identified. Thus, an interaction of shear and interface shear in the structure can be assumed. Additionally, the direct strut for small shear slendernesses may cause additional normal stress at the interface, which increases the local interface shear resistance.

Influence of prestressing

Prestressing of the precast elements induces compressive stress in the cross section. Assuming interface shear due to composite action, the constant compressive stress results in no additional change of compressive stress along the structure's axis. Depending on the time of casting the insitu concrete layer, creep and shrinkage may affect the bond behaviour between the two concrete layers. If the new concrete layer is cast after shrinkage and creep of the prestressed plank already had finished, the shrinkage of the new concrete layer induces compressive stress to the surface of the prestressed element which may have an additional positive effect on the load bearing resistance. Nevertheless, additional tensile stresses occur in the new concrete layer which may have an additional weakening effect on the bond behaviour. However, the comparison of prestressed and non-prestressed specimens with rough interfaces in Figure 6-23, (right) show no influence on the bond resistance, since the test results show large scattering of interface resistances.

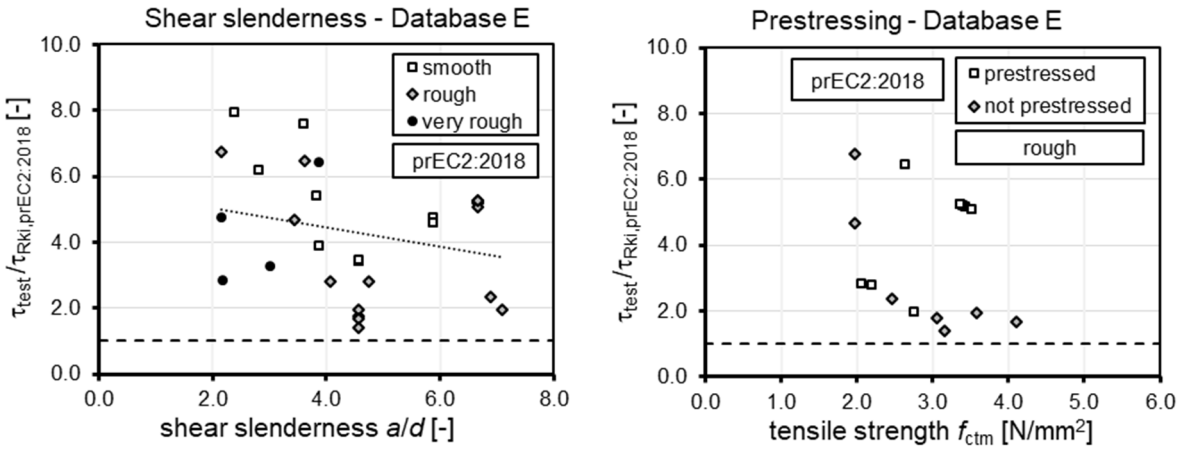

Figure 6-23: Influence of shear slenderness and prestressing according to [prEC2:18] for database E

Influence of interface location and dimension

To assess the location of the interface in the structure, the related interface resistance according to [prEC2:18] is depicted over the ratio of height of insitu concrete layer h_{insitu} and the total height of the cross section h_{total} (Figure 6-24, left). For small insitu concrete layers at the top of the cross section with small h_{insitu}/h_{total} ratios, higher interface shear resistance could be reached in the test programmes. For simply supported beam and slab specimens, the crack development starts from flexural cracks at the bottom of the cross section, progressing towards the interface. For interfaces at the top of the cross section, the shear cracks reach the interface at higher stress states and thus, higher interface resistances can be determined. As shown in Figure 6-24 (right), the interface resistance decreases with increasing interface width. For e.g. T-beams, small interfaces are generally positioned between beam and slab at the top of the cross section, whereas large interfaces in slabs generally occur at the bottom of the cross section. Additionally, the

potential of blemishes and low stress redistributions due to missing transverse reinforcement increases with increasing interface dimensions, which may lead to higher failure potential and thus, smaller interface resistances. For the shear span of the interface defined as the distance between load application and support with constant shear force distribution in the three- and four-point bending test, no considerable influence could be determined in the evaluation of Database E.

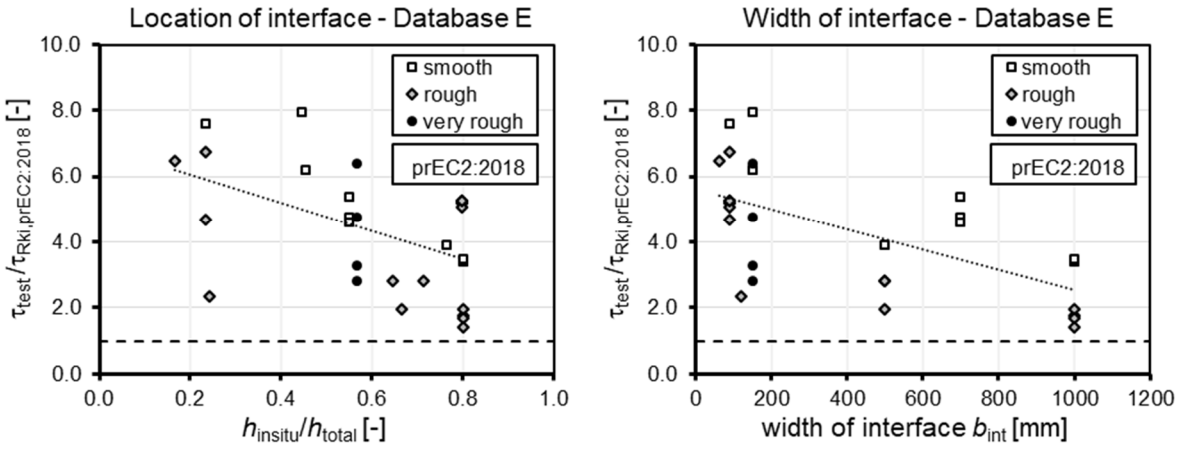

Figure 6-24: Comparison of experimental to calculated interface shear resistance according to [prEC2:18] regarding interface location and dimension

Due to the limited number of tests and the very large scatter of test results, the described influences can only be observed qualitatively. To allow a reliable estimation of further influencing factors on the interface shear strength due to composite action, systematic test series with minimum potential of scatter are necessary. For all tests in the database, the roughness has only been determined for four specimens. Thus, an evaluation regarding the effect of a roughness parameter would not be convincing.

6.4.3 Database F: With interface reinforcement

For the evaluation of beam and slab specimens with interface reinforcement, 66 tests with stirrups as interface reinforcement and eight tests with lattice girders could be evaluated.

Evaluation of Database F-1 with stirrups as interface reinforcement

The distributions of the 66 tests with stirrups regarding interface classification, interface reinforcement ratio, characteristic concrete compressive strength of precast and insitu concrete as well as the decisive minimum concrete strength for design are shown in Figure 6-25.

For the database evaluation, the terms of adhesion, friction due to normal stress and friction due to interface reinforcement can be considered. The expression of [prEC2:18] for concrete toppings where no sufficient anchorage of the reinforcement bars can be provided, as well as the [MC10] provisions introduce an addition load bearing resistance

of dowel action. Since constant normal stress in the test specimens were only induced by self-weight of the insitu concrete, the effect of the frictional term is insignificant. The expressions of adhesive strengths and interface reinforcement according to evaluated codes are summarised in Table 6-13.

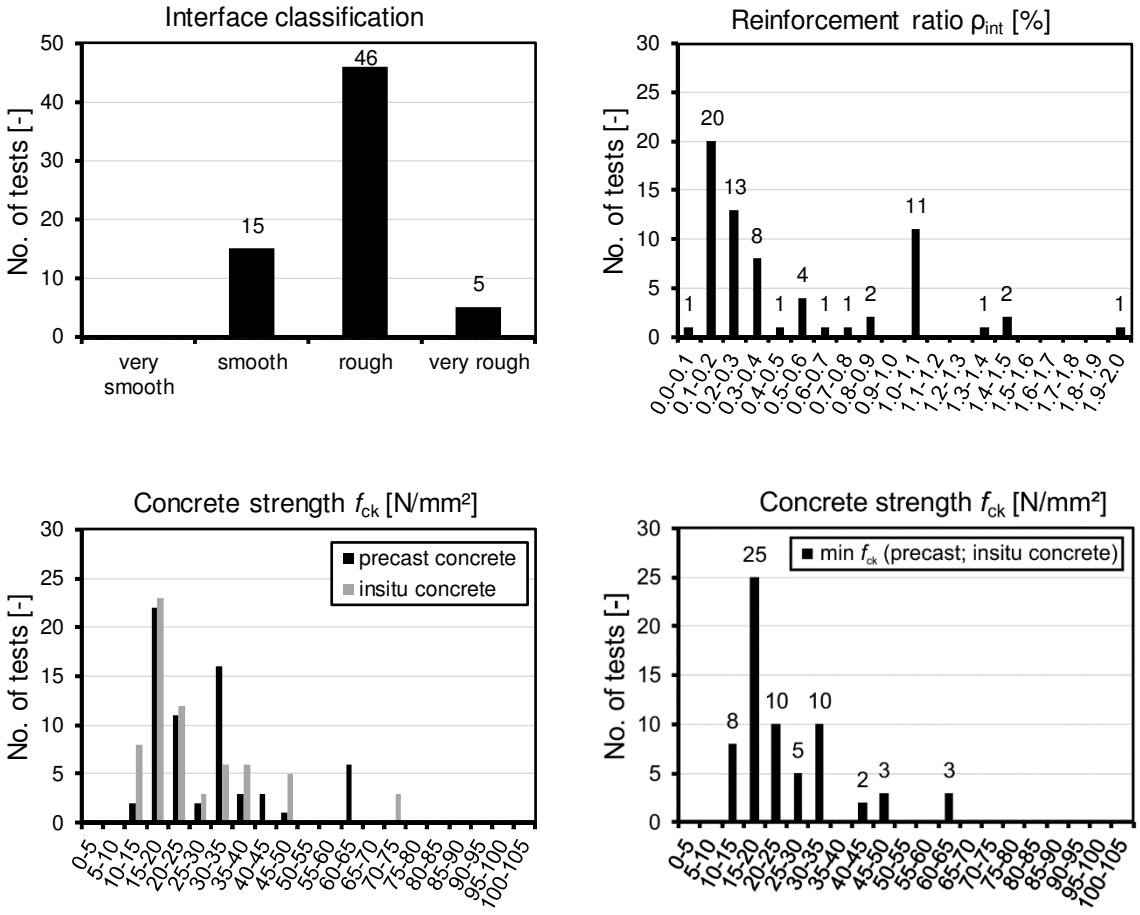

Figure 6-25: Distribution of 66 beam and slab specimens with interface reinforcement in database F-1

The provisions of [ACI318] limit the design of not intentionally roughened surfaces with interface reinforcement to constant interface shear resistances. For interfaces intentionally roughened, an adhesive strength of 1.76 N/mm² can be assessed. If the applied shear stress exceeds the limit of 3.45 N/mm², the calculation follows the regulations for vertical interface shear with only considering the term of reinforcement.

Compared to the evaluation of beam and slab specimens without interface reinforcement, smaller coefficients of variation and smaller mean values are achieved. The smallest coefficient of variation gives the expression of [prEC2:18] with COV = 0.38. The increase of the reinforcement term with the factor 1.2 according to [EC2NAD] yields to a smaller mean value compared to [EC2], but with a similar coefficient of variation. The constant adhesive term according to [AA-L] only gives slightly higher coefficients of

variation and mean values. Considering the effect of interface reinforcement as a combination of clamping effect and dowel action according to [prEC2:18] for concrete topping and [MC10] results in higher coefficients of variation and higher mean values. The regulations in [ACI318] give the highest coefficient of variation of COV = 0.50 and a very high mean value of $X_m = 5.65$. The separate evaluations for each roughness classification (Table 6-14) show high coefficients of variation for both, intentionally roughened and not intentionally roughened interfaces. The very high coefficient of variation of COV = 1.03 and mean value $X_m = 6.75$ for intentionally roughened surfaces are mainly caused by the high applied shear stress with corresponding limitation to vertical shear design. Neglecting this limitation, the evaluation for intentionally roughened surfaces results in $X_m = 2.01$, COV = 0.27 and $X_{5\%} = 1.04$. For a not intentionally roughened surface, the design would be limited to a constant interface strength, which underestimated the interface shear resistance and thus, lead to very high mean values and coefficients of variation ($X_m = 7.40$, COV = 0.46 and $X_{5\%} = 3.19$). However, despite the high scatter of test data, the high mean values for all design regulations lead to characteristic 5 % quantile ratios of $X_{5\%} > 1.0$.

Table 6-13: Statistic evaluation of beam and slab specimens with stirrups as interface reinforcement in database F with τ_{test}/τ_{Rki}

Code τ_{Rki} =	τ_{adh}	+	τ_{fric}	+	τ_{reinf}	Σ	X_m	COV	$X_{5\%}$
EC2:2004	$c \cdot f_{ctk}$		$\mu \cdot \sigma_n$		$\rho \cdot f_{yk} \cdot (\mu \cdot \sin\alpha + \cos\alpha)$	66	2.54	0.40	1.23
EC2+NA(D)	$c \cdot f_{ctk}$		$\mu \cdot \sigma_n$		$\rho \cdot f_{yk} \cdot (1.2 \cdot \mu \cdot \sin\alpha + \cos\alpha)$	66	2.27	0.40	1.11
prEC2:2018	$c \cdot f_{ck}^{1/2}$		$\mu \cdot \sigma_n$		$\rho \cdot f_{yd} \cdot (\mu_v \cdot \sin\alpha + \cos\alpha)$	66	2.46	0.38	1.23
(toppings)[1]	$c \cdot f_{ck}^{1/2}$		$\mu \cdot \sigma_n$		$k_t \cdot \rho \cdot \mu_v \cdot f_{yk} + k_t \cdot \rho \cdot \sqrt{f_{yk} \cdot f_{ck}}$	66	3.65	0.43	1.69
MC2010	$c \cdot f_{ck}^{1/3}$		$\mu \cdot \sigma_n$		$\mu \cdot \rho \cdot \kappa_1 \cdot f_{yk} + \kappa_2 \cdot \rho \cdot \sqrt{f_{yk} \cdot f_{ck}}$	66	3.91	0.44	1.76
ACI 318	τ_{adh} = const.[2] τ_{adh} = const.[3]		$\mu \cdot \sigma_n$		– $\rho \cdot f_{yk} \cdot (\mu \cdot \sin\alpha + \cos\alpha)$[4]	66	5.65	0.50	2.29
(neglecting the limitation with design for vertical shear for $\tau_{test} \geq 3.45$ N/mm²)							2.01	0.27	1.04
AASHTO	τ_{adh} = const.		$\mu \cdot \sigma_n$		$\rho \cdot f_{yk} \cdot (\mu \cdot \sin\alpha + \cos\alpha)$	66	2.82	0.42	1.33

X_m: mean value τ_{Rki}/τ_{calc}, COV: coefficient of variation, $X_{5\%}$: characteristic 5 % quantile ratio, [1]: no tests with concrete toppings which do not provide sufficient anchorage – evaluation for complete selected database; [2]: interfaces not intentionally roughened; [3]: interfaces intentionally roughened, [4]: interfaces intentionally roughened and with an applied shear stress ≥ 3.45 N/mm² the adhesive term is neglected and the design follows the design for vertical interfaces (s. Chapter 3.3.6 and 6.3.4)

Compared to small size tests with interface reinforcement, mean value and coefficient of variation are larger for the evaluation with beam and slab specimens. As mentioned for the evaluation of database E with beams and slabs without interface reinforcement, the larger scatter of test results might also be affected by additional influencing factors. Therefore, influence parameters considered in the design equations as well as other structural influences are assessed in the following. In the evaluated database, only three specimens were prestressed and showed no influence on the interface shear resistance.

Regarding interface roughness, the roughness depth was determined for only six specimens.

Table 6-14: Evaluation of database F-1 with τ_{test}/τ_{Rki} isolated for interface classification

	Interface classification	Coefficient of adhesion	Coefficient of friction μ	No. of tests	X_m	COV	$X_{5\%}$
EC2:2004 [EC2]	very smooth	0.025	0.5				
	smooth	0.2	0.6	15	2.62	0.48	1.04
	rough	0.4	0.7	51	2.52	0.38	1.26
	very rough	(1)					
EC2+NA(D) [EC2NAD]	very smooth	0	0.5				
	smooth	0.2	0.6	15	2.29	0.49	0.89
	rough	0.4	0.7	46	2.24	0.36	1.16
	very rough	0.5	0.9	5	2.68	0.52	0.75
prEC2:2018 [prEC2:18]	very smooth	0.0095	0.5				
	smooth	0.075	0.6	15	2.55	0.47	1.03
	rough	0.15	0.7	46	2.40	0.35	1.27
	very rough	0.19	0.9	5	2.44	0.38	0.96
prEC2:2018 (toppings)	very smooth	–	0.5 (k_f/k_t=0/1.5)				
	smooth	–	0.6 (k_f/k_t=0.5/1.5)	15	3.86	0.58	1.26
	rough	0.035	0.7 (k_f/k_t=0.5/0.9)	46	3.60	0.38	1.82
	very rough	0.07	0.9 (k_f/k_t=0.5/0.9)	5	3.69	0.43	1.30
MC 2010 [MC10]	very smooth	–	0.5 (k_1/k_2=0/1.5)				
	smooth	–	0.6 (k_1/k_2=0.5/1.1)	15	3.86	0.58	1.26
	rough	0.1	0.7 (k_1/k_2=0.5/0.9)	46	3.90	0.39	1.91
	very rough	0.2	0.8(2) / 1.0(3) (k_1/k_2=0.5/0.9)	5	4.28	0.53	1.19
ACI318 [ACI318]	not roughened	0.56 N/mm²	–	61	5.14	0.50	2.06
	roughened	1.76 N/mm²(4)	0.6(4) / 1.0(5)	5	6.75	1.03	0.64
AASHTO [AA-L]	not roughened	0.52 N/mm²	0.6	61	2.90	0.40	1.41
	roughened	1.66 N/mm²	1.0	5	1.80	0.38	0.72

X_m: mean value τ_{Rki}/τ_{calc}, COV: coefficient of variation, $X_{5\%}$: characteristic 5 % quantile ratio, (1): very rough surfaces correspond to rough surfaces (2): for $f_{ck} \geq 20$ N/mm²; (3): $f_{ck} \geq 35$ N/mm²; k_f and k_1: coefficient considering the clamping effect; k_t and k_2: coefficient considering the effect of dowel action; (4) for applied shear stress < 3.45 N/mm², for applied shear stress ≥ 3.45 N/mm² τ_{adh} = 0; (5) for applied shear stress ≥ 3.45 N/mm²

Influence of tensile strength

To assess the effect of tensile strength on the interface resistance, Figure 6-26 shows the related interface resistance over the tensile strength according to the evaluation with

considering the adhesive resistance by the square root of the characteristic concrete compressive strength according to [prEC2:18] and by constant adhesive strength according to [AA-L].

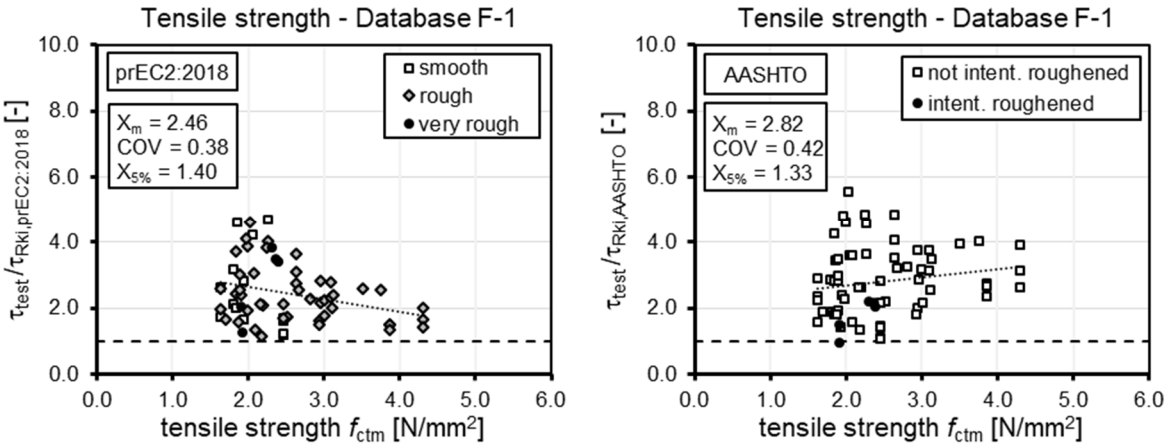

Figure 6-26: Influence of tensile strength on the related resistance according to [prEC2:18] and [AA-L] regarding tensile strength for database F-1 (66 tests)

As determined for the small size databases as well as for the database with beam and slab specimens without interface reinforcement, the interface resistance decreases with increasing tensile strength for the evaluation according to [prEC2:18]. In contrast, defining the adhesive term as a constant, leads to a slight increase of interface resistance with increasing tensile strength.

Influence of reinforcement ratio

The term of interface reinforcement ratio is generally described by the clamping effect based on shear friction theory. Only [prEC2:18] for concrete toppings and [MC10] formulate a combination of clamping effect and dowel action. The influence of interface reinforcement ratio on the ratio of experimental and calculated interface resistance according to [prEC2:18], [EC2NAD], [MC10] and [AA-L] are shown in Figure 6-27.

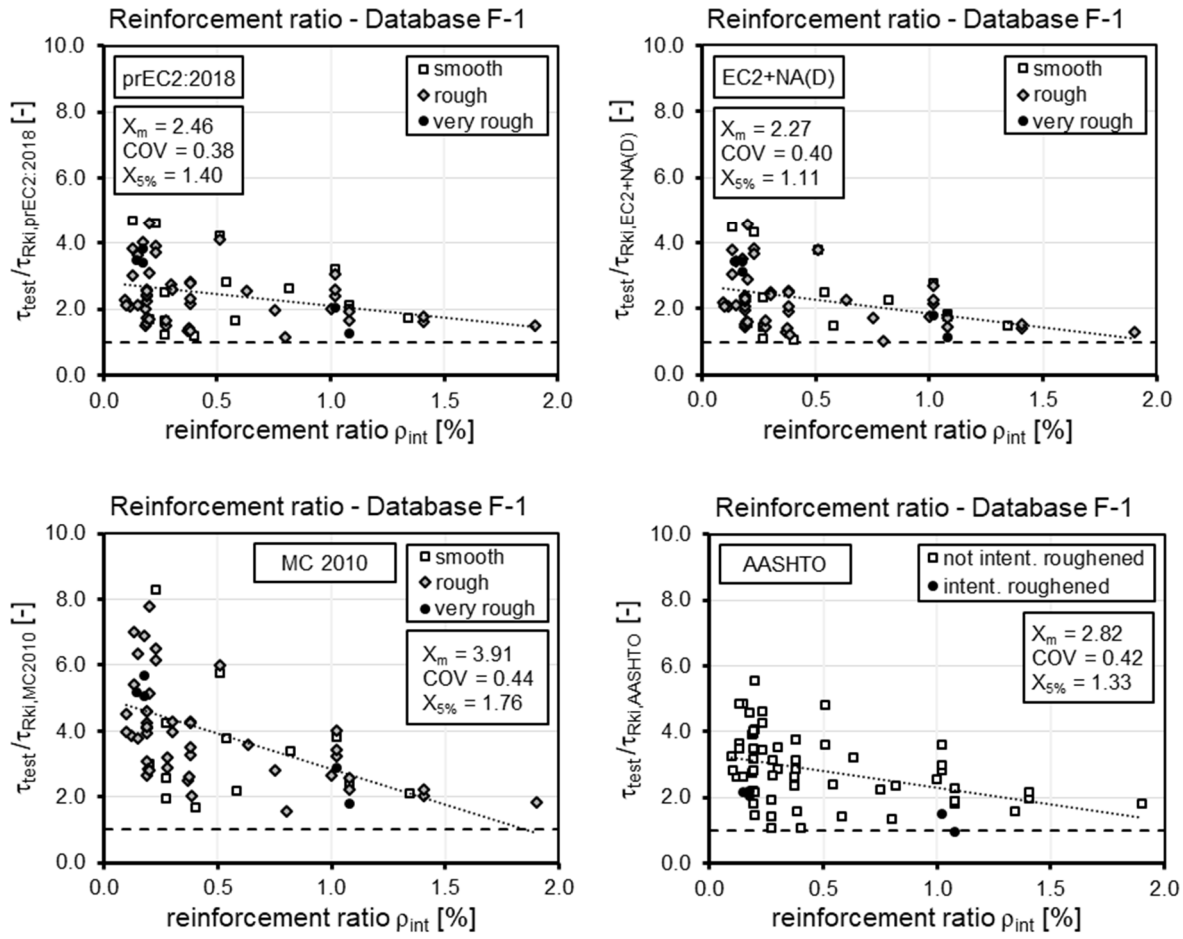

Figure 6-27: Influence of reinforcement ratio on the related resistance according to [prEC2:18], [EC2NAD], [MC10] and [AA-L] for database F-1 (66 tests)

For all codes, a decrease of referred interface resistance with increasing reinforcement ratio can be determined. Compared to [prEC2:18], the increase of the reinforcement term by the factor 1.2 according to [EC2NAD] leads to slightly smaller referred interface resistances. The evaluation considering dowel action according to [MC10] shows larger scattering with high underestimations of test data, especially for low interface reinforcement ratios. Compared to the evaluation of [prEC2:18] and [EC2NAD], the assumption of constant adhesive terms combined with the different roughness classifications according to [AA-L] leads to similar distribution of test data, but with generally lower calculated resistances, especially for small interface reinforcement ratios.

Influence of shear slenderness

The influence of shear slenderness on the ratio of experimental to calculated interface shear resistance according to [prEC2:18] is shown in Figure 6-28. In accordance with the assessment of database E with beams and slabs without interface reinforcement, a decrease of interface shear strength with increasing shear slenderness can be determined.

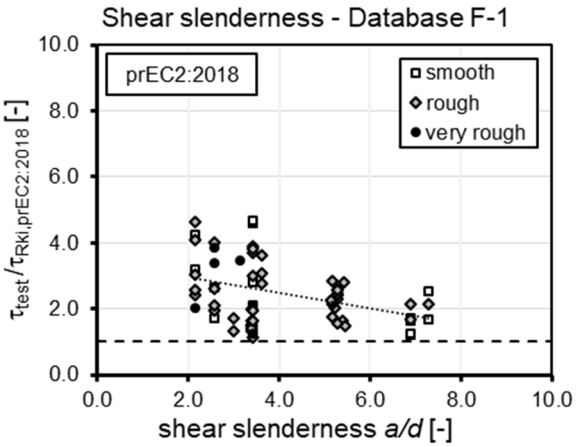

Figure 6-28: Influence of shear slenderness on the related resistance according to [prEC2:18] for database F-1 (66 tests)

Influence of interface location and dimension

The influence of the location of the interface in the cross section is shown in Figure 6-29 (left) by depicting the related interface resistance according to [prEC2:18] over the ratio of heigth of the insitu concrete layer h_{insitu} to the total heigth of the cross section h_{total}. In accordance to the evaluation of database E with beams and slabs without interface reinforcement, the interface resistance decreases with increasing heigth of the insitu concrete layer. Thus, for interface locations at the bottom of the cross section, smaller interface resistances were determined. Regarding the influence of interface width (Figure 6-29 (right)), most specimens were conducted as T-beams and only two beam and two slab specimens with wide interfaces were part of the database evaluation. However, for interfaces with large interface dimension, comparably low interface resistances were determined.

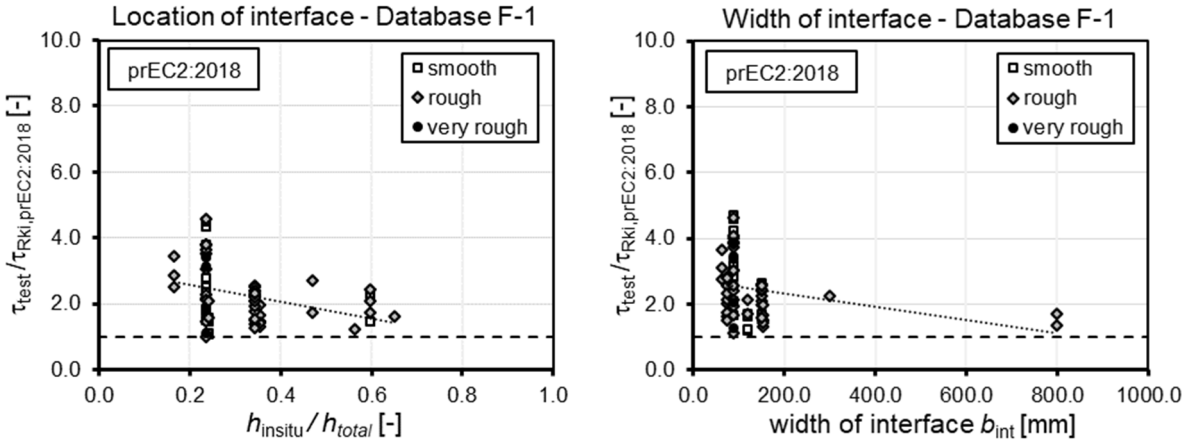

Figure 6-29: Influence of location and width of interface on the related resistance according to [prEC2:18] for database F-1 (66 tests)y

Evaluation of Database F-2 with lattice girders

To evaluate lattice girders as interface reinforcement, eight specimens could be evaluated. Two test series were conducted by [Zil08] and [Fur11] to investigate the effect of lattice girder diagonals declining towards the support. To calculate the interface resistance, these diagonals cannot be accounted as interface reinforcement. In the test programmes, either declining or inclining diagonals were removed from the lattice girders. Thus, only specimens with removed diagonals declining towards the support could be evaluated. The eight slabs had concrete compressive strength of precast element and insitu concrete layer between f_{ck} = 26 – 32 N/mm² and reinforcement ratios between ρ_{int} = 0.17 – 0.38 %. Six slabs had smooth interfaces and two slabs had rough interfaces. The design of semi-precast slabs follows the general technical approvals of lattice girders and the interface shear design is in accordance with the regulations of [EC2NAD]. Evaluating the eight specimens according to the [EC2NAD] provisions by comparing experimental to calculated interface shear resistance, gives a mean value of X_m = 1.62, a coefficient of variation COV = 0.27 and a characteristic 5 % quantile ratio of $X_{5\%}$ = 0.92. Evaluating the tests with the European design equations leads to statistical values summarised in Table 6-15. The evaluations show a quite large scatter for the eight slabs with characteristic 5 % quantile ratios slightly deceeding $X_{5\%}$ = 1.0, which might be influenced by the high number of specimens with removed lattice girder diagonals for evaluation. In accordance with the evaluation of stirrups as interface reinforcement, the design expression of [MC10] gives the most conservative estimation with very high mean value but a comparable range of scatter.

Table 6-15: Statistic evaluation of beam and slab specimens with lattice girders as interface reinforcement in database F-2 with τ_{test}/τ_{Rki}

Code τ_{Rki} =	τ_{adh}	+	τ_{fric}	+	τ_{reinf}	Σ	X_m	COV	$X_{5\%}$
EC2:2004	$c \cdot f_{ctk}$		$\mu \cdot \sigma_n$		$\rho \cdot f_{yk} \cdot (\mu \cdot \sin\alpha + \cos\alpha)$	8	1.74	0.27	0.99
EC2+NA(D)	$c \cdot f_{ctk}$		$\mu \cdot \sigma_n$		$\rho \cdot f_{yk} \cdot (1.2 \cdot \mu \cdot \sin\alpha + \cos\alpha)$	8	1.62	0.27	0.92
prEC2:2018	$c \cdot f_{ck}^{1/2}$		$\mu \cdot \sigma_n$		$\rho \cdot f_{yd} \cdot (\mu_v \cdot \sin\alpha + \cos\alpha)$	8	1.66	0.29	0.90
MC2010	$c \cdot f_{ck}^{1/3}$		$\mu \cdot \sigma_n$		$\mu \cdot \rho \cdot \kappa_1 \cdot f_{yk} + \kappa_2 \cdot \rho \cdot \sqrt{f_{yk} \cdot f_{ck}}$	8	3.90	0.25	2.32

X_m: mean value τ_{Rki}/τ_{calc}, COV: coefficient of variation, $X_{5\%}$: characteristic 5 % quantile ratio

6.4.4 Database G: Fatigue without interface reinforcement

To assess the effect of cyclic loading on the load bearing behaviour of composite beams and slabs without interface reinforcement, six specimens could be evaluated in database G. The six specimens were reported in [Sch96a] and [Chu76] and included two slabs with smooth interfaces and four prestressed T-beams with rough interfaces (s. Chapter 4.3.4). The characteristic concrete compressive strength varied between

f_{ck} = 26 – 44 N/mm² for both, precast element and insitu concrete. The tests were conducted in four-point bending tests with a shear slenderness of a/d = 3.0 for the slabs and 3.6 for the T-beams.

In accordance with the evaluation of small size tests without interface reinforcement under cyclic loading, only the adhesive terms of the design equations were considered. Since the regulations in [ACI318] and [AA-L] do not include considerations of cyclic loading for interface shear design, both codes could not be evaluated. The regulations in [EC2], [prEC2:18] and [MC10] reduce the coefficient of adhesion to 50 % with $c_{fat} = 0.5 \cdot c_{stat}$ for fatigue, whereas [EC2NAD] defines $c_{fat} = 0$ and thus, neglects a fatigue resistance by adhesion.

For the 6 fatigue tests, the comparison of static characteristic interface shear strength calculated according to [EC2] and [MC10] with $\tau_{Rki,calc} = c \cdot f_{ctk}$ (both expressions include similar coefficients of adhesion for smooth and rough interfaces) and [prEC2:18] with $\tau_{Rki,calc} = c \cdot f_{ck}^{1/2}$, differ only by 1 %. Thus, only results were determined by [EC2] and [MC10] are presented in the following.

The fatigue behaviour of concrete has a strong dependence on the applied mean load level. Therefore, Figure 6-30 (left) shows the maximum applied shear stress and minimum shear stress related to the calculated static adhesive strength according to [EC2] and [MC10]. The fatigue tests of the T-beams with rough interfaces were terminated after N = 1.0 mil. load cycles and the fatigue tests with slabs were terminated after N = 2.0 mil. load cycles. Two specimens with rough interfaces and a high applied load level with maximum loads of about 400 % of the calculated characteristic adhesive strength failed prior reaching the reference number of load cycles. The applied maximum load generally exceeded the calculated adhesive resistance by between 170 and 417 % and the minimum loads between 70 and 90 % of the calculated characteristic resistance.

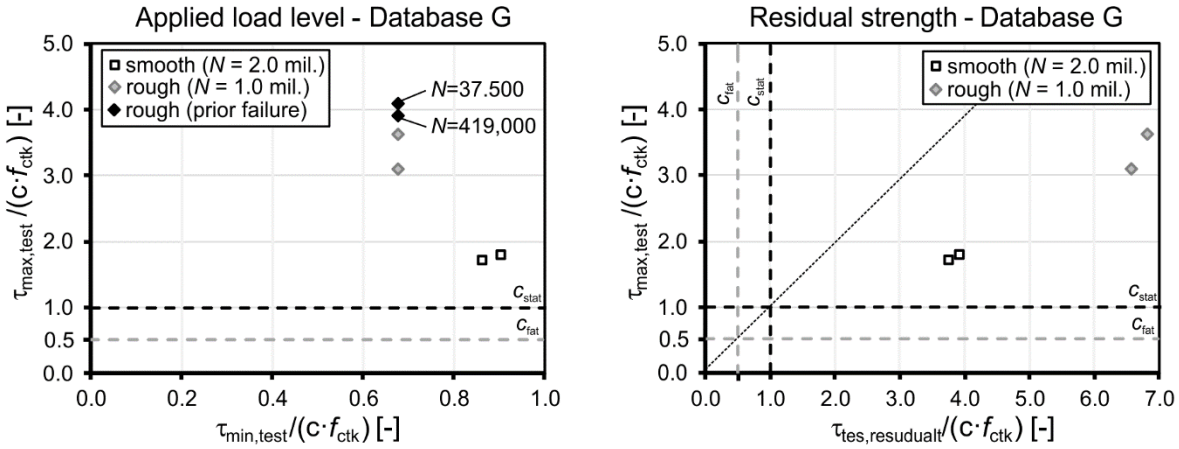

Figure 6-30: Applied load level related to calculated characteristic adhesive strength (left) and residual resistance related to calculated characteristic adhesive strength (right)

For specimens which reached the reference number of load cycles, the static residual strength was determined. As shown in Figure 6-30 (right), the residual resistances after the fatigue loading could be determined to be between 370 % for slabs with smooth interfaces and about 660 % for T-beams with rough interfaces. However, four of the six tests achieved suitable number of load cycles with maximum stress exceeding the defined limit of 50 % of the calculated static resistance by a multiple.

6.4.5 Database H: Fatigue with interface reinforcement

Database H-1: Fatigue of composite beams and slabs with stirrups

To assess the fatigue regulations for interface shear in beams and slabs with stirrups as interface reinforcement, 44 specimens could be evaluated in database H-1. The distributions of the evaluated tests regarding interface classification, reinforcement ratio, characteristic concrete compressive strength of precast and insitu concrete as well as the minimum concrete strength for design are shown in Figure 6-31.

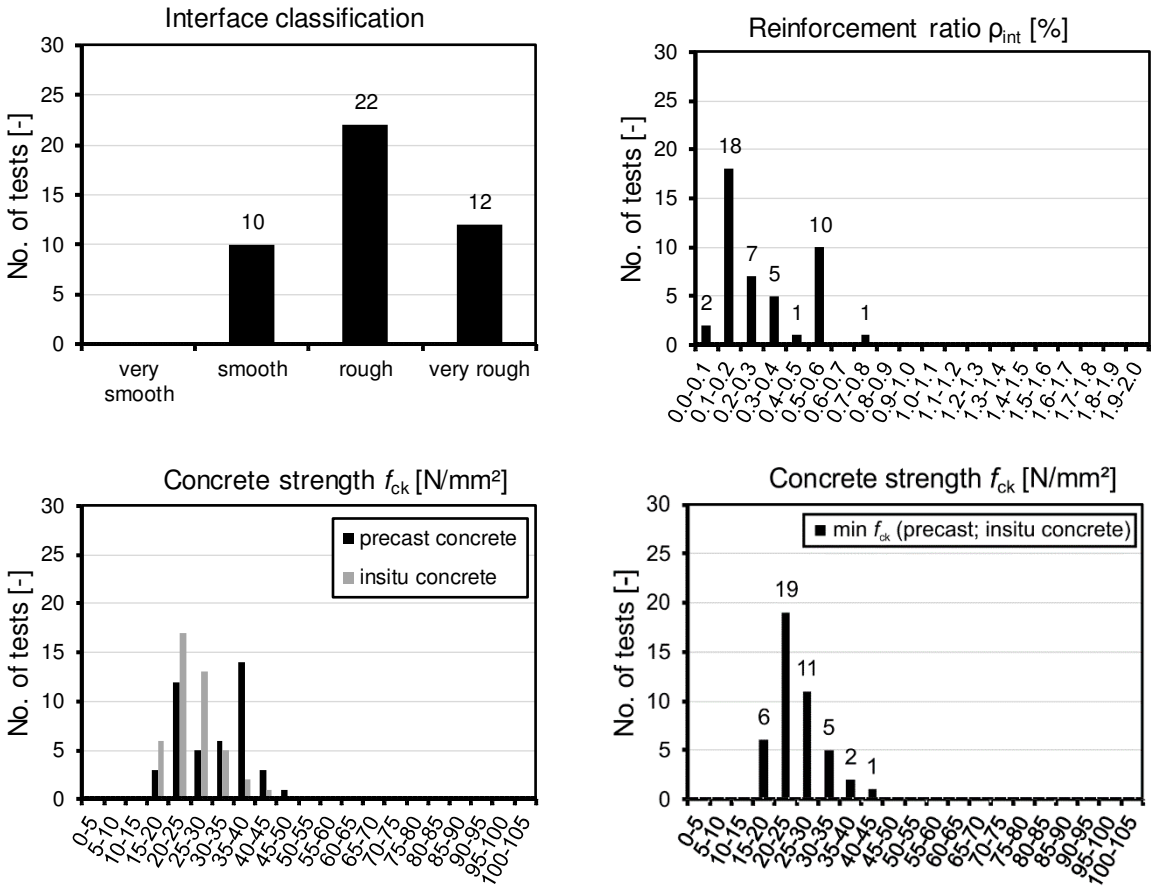

Figure 6-31: Distribution of 44 beam and slab specimens with stirrups as interface reinforcement in database H-1

The fatigue strength of reinforced concrete members depends on the applied load level. In this context, Figure 6-32 (left) shows the applied maximum fatigue stress as well as

the applied minimum fatigue stress related to the calculated static resistance according to the design expression of [prEC2:18]. The applied maximum loads varied between 55 % and 230 % of the calculated static interface resistance, whereas the applied minimum stress varied between 10 % and 70 % of the static calculated strength. From the 44 evaluated tests, eight specimens failed prior reaching the reference number of load cycles, which was defined between N = 1.0 mil. and 2.0 mil. load cycles, depending on test programme. Most specimens in the database with rough and very rough interfaces were T-beams, whereas all specimens with smooth interfaces and only two specimens with rough interfaces were slabs. All prestressed tests had a defined reference life length of N = 1.0 mil. load cycles. However, fatigue failure only occurred for the T-beams with rough and very rough interfaces and for both, high and low applied load levels.

After reaching the reference number of load cycles without fatigue failure, the static residual resistance was tested for all specimens. Figure 6-32 (right) shows the related maximum strength over the ratio of residual strength and calculated static resistance. For all specimens, at least the residual strength in accordance with the static resistance could be achieved. Especially for high applied maximum fatigue stresses, high residual strengths between 300 and 400 % of the calculated shear strength were determined.

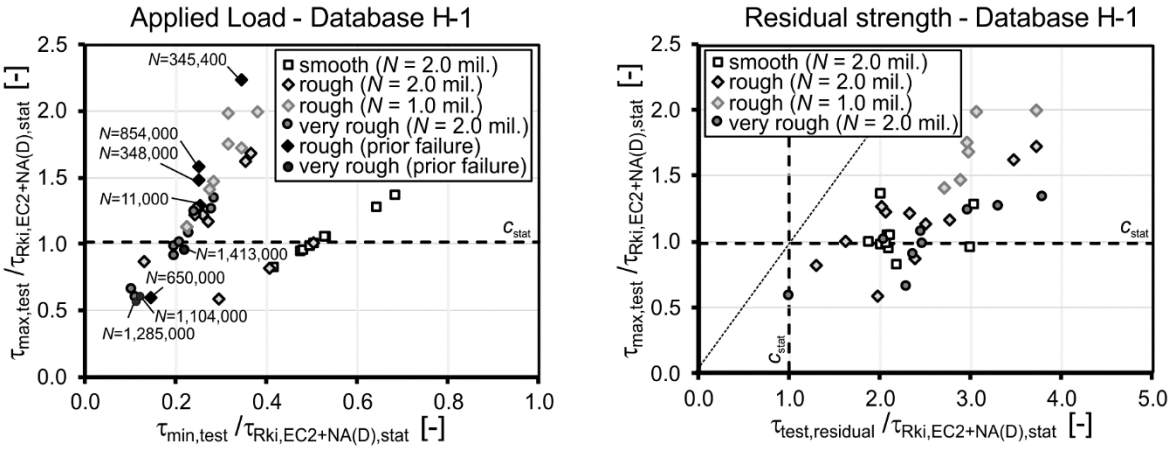

Figure 6-32: Applied load level related to calculated characteristic static resistance according to [prEC2:18] (left) and related maximum applied fatigue load over the ratio of residual strength and maximum

The interface shear design for fatigue according to the European provisions generally follow the design for monotonic loading. For the design at ultimate limit state, the provisions of [EC2] and [MC10] for rigid bond reduce the term of adhesion to $c_{fat} = 0.5 \cdot c_{stat}$ and [EC2NAD] neglects the adhesive term by $c_{fat} = 0$. The provisions of [MC10] for non-rigid bond reduce the static interface shear resistance to 40 %.

The residual resistances strongly depend on the applied fatigue load and the resulting state of fracture. However, to evaluate the residual resistance after cyclic loading

(N = 1.0 mil. and N = 2.0 mil. load cycles, respectively), Figure 6-33 shows the experimental residual resistances related to the calculated fatigue resistances according to [EC2] and [EC2NAD] over the interface reinforcement ratio.

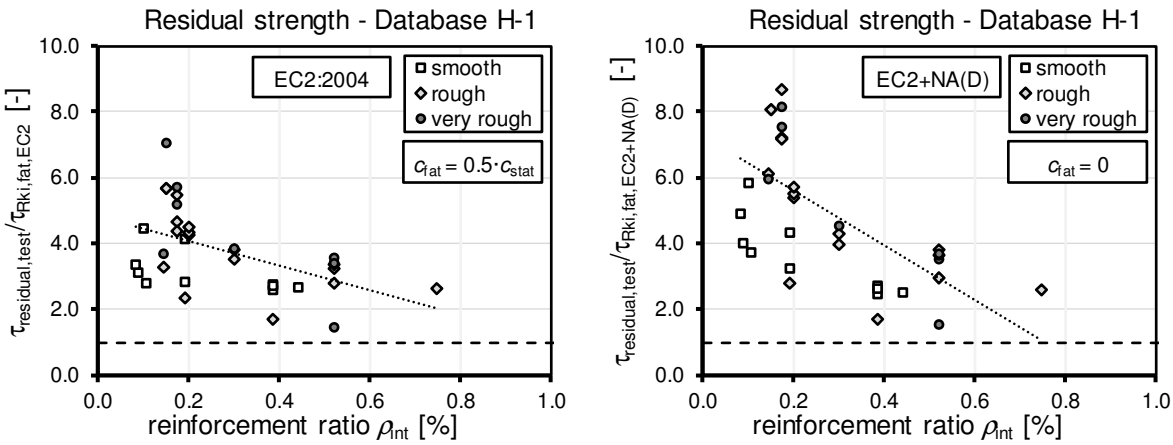

Figure 6-33: Influence of interface reinforcement ratio on the residual resistance after fatigue loading according to [EC2] and [EC2NAD]

For the term of interface reinforcement, the full characteristic yield strength was assumed for evaluation. The expression with 50 % of the adhesive resistance according to [EC2] shows a decrease of related residual resistance with decreasing interface reinforcement ratio. Especially for small interface reinforcement ratios, the calculated fatigue resistance strongly underestimated the experimental resistance. The expression of [EC2NAD] with neglecting the term of adhesion and increasing the term of reinforcement by the factor 1.2 show a large scattering of test data. However, all experimental residual strengths exceed the calculated fatigue resistance of both codes.

Since the [MC10] expression decrease the interface shear resistance for fatigue to 40 % of the static resistance, Figure 6-34 shows the experimental residual strength related to the calculated static resistance over the interface reinforcement ratio. Regarding the residual resistance, the reduction to 40 % of the static resistance (grey line) depicts a very low fatigue limit considering the evaluated tests.

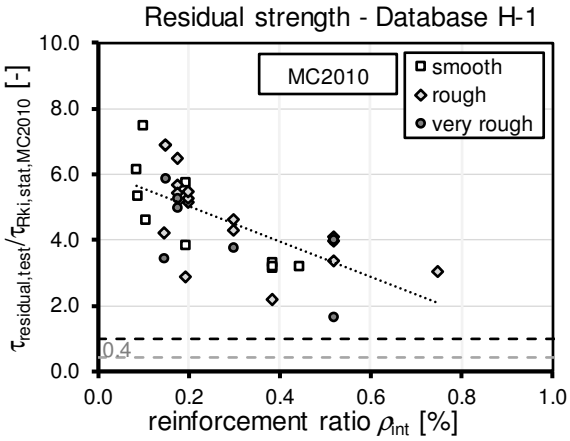

Figure 6-34: Influence of interface reinforcement ratio on residual strength according to [MC10]

The presented evaluation regarding residual strength and interface reinforcement ratio can only be assessed qualitatively. As shown in Database F-1 (beam and slab specimens with interface reinforcement under monotonic loading conditions), the evaluations show a general decrease of related interface shear resistance with increasing interface reinforcement ratio for monotonic loading. Additionally, interface resistances as well as test results subjected to cyclic load show very high scatter.

For design of reinforced concrete members under fatigue loading conditions, the stress range in the reinforcement must be verified. Therefore, the approved stress range in the reinforcement bars is defined by fatigue-strength curves (S-N-curves) depending on the number of load cycles. For straight and bent bars, the S-N-curve in the European Codes are defined with a characteristic stress range of $\Delta\sigma_{Rsk} = 175$ N/mm² for $N = 1.0$ mil. load cycles and inclinations of $k_1 = 5$ for $N < 1.0$ mil. and $k_2 = 9$ for $N > 1.0$ mil. load cycles. For bent bars with a ratio of mandrel diameter D to bar diameter Ø of $D/Ø < 25$, the stress range must be reduced by a reduction factor $\xi_1 = 0.35 + 0.026D/Ø$. For stirrups as shear reinforcement, this reduction can be omitted if the bar diameter deceeds $Ø \leq 16$ mm and the stirrup's height exceeds 600 mm. Even though the stirrups in the evaluated data did not exceed 600 mm, generally no details were provided regarding mandrel diameter in the test reports. Thus, the reduction of stress range was omitted for evaluation. To assess the design expressions by the tests in the database, the stress ranges in the stirrup bars were calculated considering the applied stress range in the fatigue tests and the fatigue design expression according to [EC2] with a reduction of adhesive strength to 50 %, the expression of [EC2NAD] by neglecting the adhesive strength and the expression of [prEC2:18] by omitting the adhesive strength and reducing the calculated stress range by a factor 0.45, considering the flatter inclination of compression strut (s. Chapter 3.3.4). The ratio of calculated stress range $\Delta\sigma_{test,Rki}$ and approved stress range $\Delta\sigma_{app}$ according to the S-N-curves defined in [EC2], [EC2NAD] and [prEC2:18] over the borne number of load cycles N are depicted in Figure 6-35.

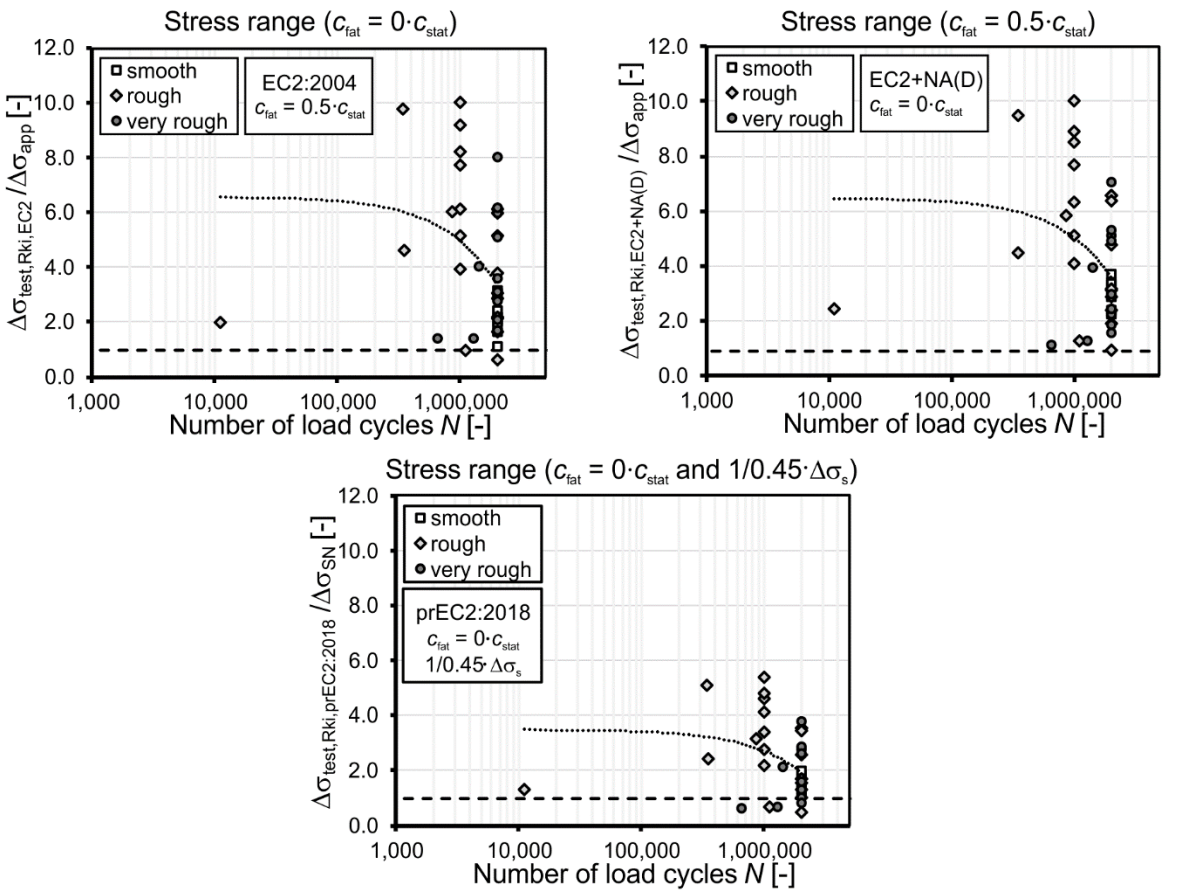

Figure 6-35: Verification of stress range in the interface reinforcement according to [EC2] [EC2NAD] and [prEC2:18]

Compared to the expression in [EC2] with 50 % of the adhesive strength being effective for fatigue, omitting the adhesive strength according to [EC2NAD] yields to slightly larger stress ranges. For both design expressions, the applied stress ranges exceed the approved stress ranges for almost all fatigue tests. Only for one T-beam with a rough interface, the approved stress range exceeds the calculated stress range. However, this particular specimen did not fail due to fatigue loading but due to static residual resistance. Considering the effect of a flatter inclination of compression strut in accordance to [prEC2:18] gives the smallest calculated shear stresses. However, three specimens, which failed prior reaching the reference number of load cycles, showed smaller calculated stress ranges than the approved stress ranges and thus, may lead to an unsafe estimation.

Database H-2: Fatigue of semi-precast slabs with lattice girders

Database H-2 holds a number of 47 fatigue tests with lattice girders in semi-precast slabs. The design regulations for the approved lattice girders for fatigue follow the technical approvals (TA) of the lattice girders, which are based on [EC2NAD]. The verification of stress range in the lattice girders follows a modified expression with an approved stress range, which is limited to $\Delta\sigma_{Rsk}$ = 92 N/mm² for N = 2.0 mil. load cycles.

The evaluation with the modified design expression according to the technical approvals (TA), as well as the evaluation according to [EC2] and [EC2NAD] with the approved stress range and with derived S-N-curves for lattice girders are presented in Chapter 4. The evaluations distinguishing between interface roughnesses as well as the evaluation according to the regulations in [prEC2:18] can be found in Annex B.2.7.

6.5 Summary and assessment of databases

In the previous chapter, databases with results from experimental investigations were developed and evaluated to assess the interface shear design expressions defined in Eurocode 2 [EC2], EC2+NA(D) [EC2NAD], prEC2:2018 [prEC2:18], MC2010 [MC10], ACI 318-14 [ACI318] and AASHTO LFRD [AA-L]. All design expressions define the interface shear resistance by terms of adhesion, friction due to normal stress and due to clamping of the interface reinforcement. The formulations in [EC2], [EC2NAD], [prEC2:18] and [MC10] describe the adhesive term depending on the concrete strength, whereas [ACI318] and [AA-L] consider constant adhesive strengths depending on roughness classification. For the reinforcement term, the equations of [MC10] and [prEC2:18] for toppings introduce an additional term of dowel action. Regarding interface classification, the European codes classify the interface in roughness classes as very smooth, smooth, rough, very rough and keyed surfaces, whereas the American Codes only distinguish between intentionally and not intentionally roughened surfaces.

The test results in the databases were achieved by small size tests as well as beam and slab specimens under monotonic and cyclic loading conditions. The allocations of the evaluated databases for specimens with adhesion, friction induced by normal stress and by clamping of the reinforcement with corresponding number of tests are summarised in Table 6-16. An evaluation of small size tests with interface reinforcement under cyclic loading was not possible since no evaluable tests could be found in literature.

Table 6-16: Overview of databases to assess interface shear design equations

	Small size tests			Beam and slab specimens		
	DB	Evaluation	No.	DB	Evaluation	No.
monotonic	A-1	τ_{adh}	83	E	$\tau_{adh} + (\tau_{fric})$	30
	A-2	$\tau_{adh} + \tau_{fric}$	145	F-1	$\tau_{adh} + (\tau_{fric}) + \tau_{reinf\ (stirrups)}$	66
	B	$\tau_{adh} + \tau_{reinf}$	266	F-2	$\tau_{adh} + (\tau_{fric}) + \tau_{reinf\ (LG)}$	8
	AB	$\tau_{adh} + \tau_{fric} + \tau_{reinf}$	39			
cyclic	C	$\Delta\tau_{adh}$	20	G	$\Delta\tau_{adh} + (\Delta\tau_{fric})$	6
	D	$\Delta\tau_{adh} + \Delta\tau_{reinf}$	0	H-1	$\Delta\tau_{adh} + (\Delta\tau_{fric}) + \Delta\tau_{reinf\ (stirrups)}$	44
				H-2	$\Delta\tau_{adh} + (\Delta\tau_{fric}) + \Delta\tau_{reinf\ (LG)}$	46

DB: database; τ_{adh}: adhesion; τ_{fric}: friction due to normal stress; τ_{reinf}: reinforcement; Δ: cyclic loading; LG: lattice girders

By comparing the experimental ultimate shear stress to the calculated characteristic shear resistance according to the evaluated codes, large ranges of scatter were observed for all databases. The large scatter developed not only due to the consideration of different test series with different boundary condition regarding test setup and interface preparation, but could also be determined for isolated evaluations of single test series. Furthermore, the classification of interface roughness in some test reports were only described qualitatively and thus, had to be assigned in the defined roughness classes (e.g. surfaces left as cast have a smooth surface classification but can exhibit very different roughness profiles and thus, different bond behaviours).

The evaluations of databases led to the following conclusions:

- Database A-1: The isolated evaluation of adhesive strength showed high mean values and high coefficients of variation for all codes, where the scatter of test data decreased with increasing interface roughness. However, due to the high mean values, characteristic 5 % quantile ratios with $X_{5\%} > 1.0$ were achieved. By defining the concrete tensile strength to be proportional to the square root of the characteristic concrete compressive strength as defined in [prEC2:18], the lowest coefficient of variation was determined. The lowest mean values, but highest range of scatter showed the evaluation with [AA-L], which defines constant adhesive strengths and only distinguish between interfaces not intentionally roughened and intentionally roughened. For the tests in Database A-1, no considerable influence of interface area and test setup was determined.
- Database A-2: Compared to database A-1, the evaluation of small size tests with externally applied normal stress resulted in lower mean values and lower coefficients of variation but with characteristic 5 % quantile ratios still exceeding $X_{5\%} > 1.0$. The scatter of test data was also increasing with decreasing interface roughness and the evaluations of the American codes led to the lowest mean values and the highest coefficients of variation.
- Database B: The evaluations of small size tests with interface reinforcement according to the European design expressions with terms of adhesion and clamping effect of reinforcement showed a better agreement with the test data due to lower mean values but similar coefficients of variation compared to the evaluation of specimens with normal stress, which results in 5 % characteristic ratios slightly deceeding the target value 1.0. In contrast to evaluations without interface reinforcement, the scatter increases with increasing interface roughness. The combination of clamping effect and dowel action in the reinforcement term according to [prEC2:18] for toppings and [MC10] gave a more conservative estimation of interface resistance with larger coefficients of variation. The highest scatter was determined by the American Codes with insufficient characteristic 5 % quantile ratios.

- Database AB: The evaluation of specimens with normal stress and reinforcement generally confirms the evaluation of database B with interface reinforcement.
- Database C: Small size tests without interface reinforcement under cyclic loading were generally conducted by applying high load levels, where the maximum loads exceeded the static calculated interface resistances. Only three out of 20 tests failed prior reaching the reference number of load cycles and for the remaining tests, the determined static residual resistances exceeded the static interface resistances significantly. Thus, the limited adhesive strength of 50 % for fatigue according to [EC2], [prEC2:18] and [MC10] gives an estimation on the safe side and neglecting the term of adhesion according to [EC2NAD] leads to a conservative estimation for fatigue. Since the American codes do not provide special regulations for interface fatigue, the codes were not evaluated.
- Database E: The evaluations of composite beam and slab specimens without interface reinforcement yield to conservative estimations for interface shear resistance with large coefficients of variation for the related test data. Besides the large scatter of the interface shear resistance itself, the large scatter of test results may be explained by the more complex stress state at the interface, the different location of interfaces in the cross section, the different width of interfaces in beams and slabs, as well as further influencing factors for bending and shear in structural members (e.g. shear slenderness). For small interface widths, small insitu concrete layers at the top of the cross section as well as small shear slendernesses, generally higher experimental interface resistances could be determined.
- Database F: If reinforcement is applied along the interface, the evaluation of structural member tests showed a better agreement of experimental and calculated interface resistance with smaller mean value and coefficient of variation. Since the characteristic 5 % quantile ratios exceeded $X_{5\%} \geq 1.0$ for all codes, all design expressions can be considered safe. Increasing the term of reinforcement by the factor 1.2 according to [EC2NAD] yield to a similar variation but smaller mean value compared to the evaluation of the [EC2] and [prEC2:18]. The additional term of dowel action according to [prEC2:18] for toppings and [MC10] led to a more conservative evaluation with higher mean values and higher coefficients of variation, which is in accordance to the evaluation with small size tests. The most conservative evaluation gives the approach according to [ACI318].
- Database G: The six fatigue tests with beam and slab specimens without interface reinforcement were subjected to high load levels with maximum fatigue loads exceeding the static interface resistance. However, only two out of six specimens failed prior reaching the reference number of load cycles. For the four tests which reached the reference number of load cycles, the static residual stress was a multiple of the static calculated interface shear resistance.

- Database H: For the 44 structural member tests with stirrups as interface reinforcement under cyclic loading conditions, previous fatigue failure could only be observed for eight specimens with rough and very rough interfaces. If high load levels were applied, the test specimens reaching the reference number of load cycles endured high residual loads. The evaluation of calculated stress ranges in the interface reinforcement bars showed a conservative, but safe estimation of the approved stress ranges for the evaluation according to [EC2] and [EC2NAD]. The evaluation with the [prEC2:18] expression led to a better overall agreement of applied and approved stress ranges but to an unsafe estimation for four specimens with prior fatigue failure. For semi-precast slabs with lattice girders as interface reinforcement, the evaluation is presented in Chapter 5.4.6.

The results of the database evaluation in this chapter are only presented for selected influencing parameters and codes. An extensive compilation of evaluation can be found in Annex B.

7 Design proposal for horizontal interface shear

7.1 Introduction

To quantify the shear resistance of concrete interfaces, model concepts were derived based on experimental investigations and theoretical considerations. The design expressions according to the presented codes are based on shear friction theory, which describes the interface resistance due to clamping effect of reinforcement (s. Chapter 2.3). Modifications based on *Mohr-Coulomb* analogy combine the load bearing mechanism of shear friction theory with the load bearing mechanisms of adhesion and friction due to externally applied normal stress. Due to superposition of the separate load resistance terms, an isolated consideration of each mechanism in structural members is hardly possible. Therefore, the coefficients of adhesion as well as the coefficient of friction must be calibrated using isolated small size tests with considering both, interface resistance and interaction of resistance terms.

The coefficients of adhesion and friction defined in the presented codes were derived using different databases with different test series. As shown in Chapter 6, the results of small size tests and structural members differ significantly. For all evaluated databases, large ranges of scatter were determined and the defined roughness coefficients in the evaluated codes give conservative estimations for interface resistance compared to test results, especially for interfaces in beam and slab specimens. Comparing the database evaluations, the draft for the next Eurocode 2 [prEC2:18], which defines the load bearing resistance of adhesion to be proportional to the square root of the characteristic concrete compressive strength, gives the best overall agreement of test data. However, the evaluated ratios of experimental to calculated interface resistances still shows a conservative estimation of interfaces resistance with large scattering, which bares potential for improvements regarding efficiency and level of reliability for the interface shear design equation.

To improve the interface shear design expression in terms of efficiency and reliability, a modified design equation is developed in this chapter. The proposed design equation is based on the regulations of Eurocode 2, but defining the load bearing resistance of adhesion to be proportional to the cubic root of the characteristic concrete compression strength. To account for the different interface roughnesses, the coefficients of adhesion and friction have a major influence on the range of scatter and safety level of the design approaches. In this context, the coefficients are determined and calibrated individually by using isolated databases with small size tests. To account for a sufficient level of safety, the design proposals introduce partial safety factors to the characteristic design approaches. The partial safety factors for materials in [EC2] and [prEC2:18] are defined as $\gamma_c = 1.5$ for concrete and $\gamma_s = 1.15$ for reinforcing steel. Due to the high scattering of interface shear resistance, an unadjusted adoption of these partial safety factors for the

term of adhesion and the term of reinforcement is questionable. Thus, partial safety factors for adhesion and reinforcement are derived, considering model uncertainty as well as uncertainty of material and geometry. To verify the applicability of the proposed design expression for structural members, the approach is validated systematically by comparing test results of structural members to the calculated interface shear resistance. To capture the larger interface dimension of structural members compared to small size tests, a factor considering the influence of the structure's dimension for adhesion is derived. For fatigue, this chapter defines a maximum fatigue load for concrete interfaces without interface reinforcement to be applied for design. For concrete interfaces with reinforcement, the verification of stress range in the reinforcement bars is revised and modified.

The following chapter presents the derivations and validations of roughness coefficients and partial safety factor for the proposed modified interface shear equation as well as for the approach according to the draft of the next Eurocode 2 [prEC2:18].

7.2 Safety concept according to EC0

7.2.1 Introduction

To transfer model concepts to design concepts, Eurocode 0 [EC0] defines a semi-probabilistic safety concept which applies partial safety factors to characteristic values. To achieve a sufficient level of safety, a reliability index β must be fulfilled for design. In contrast to high-order statistic procedures (Level II and III), which explicitly compare the existing reliability index to the required reliability index, the Level I procedure in [EC0] achieves the required safety level by applying partial safety factors to characteristic equations. By using Level II and III procedures, partial safety factors can be determined and calibrated considering the uncertainties of model concept as well as scatter of material and geometrical properties. For design, the determined partial safety factors can be applied by Level I procedures. In the following, the fundamentals of reliability for engineering structures and procedures to derive design values for structural resistances according to [EC0] are presented.

7.2.2 Fundamentals of Reliability

For design verification, the inequation comparing applied effects of action E to resistance R must be fulfilled following Eq. (7-1).

$$E \leq R \tag{7-1}$$

With probabilistic methods, the required level of safety of the stochastic functions of actions must be ensured. Assuming that effects of action E and resistance R can be described by stochastic independent normal distributions without confinement, the overlapping areas of both curves depict the range where loading exceed resistance. Since

overlapping areas cannot be prevented by decreasing actions or increasing resistance, a sufficient distance of both distribution densities must be determined by probabilistic methods.

Considering action E and resistance R with normal distributed density functions and the corresponding mean values μ_E and μ_R as well as standard deviations σ_E and σ_R as shown in Figure 7-1 (a), the central safety zone is defined as the area between the mean values of action and resistance. The corresponding nominal safety zone is the distance between the characteristic values of action E_k and resistance R_k, which are influenced by their scatter. Assuming a normal distribution, the characteristic values of action and resistance can be calculated using quantile factors for action $K_{p,E}$ and resistance $K_{p,R}$, respectively (Eqs. (7-2) and (7-3)).

$$E_k = \mu_E + K_{p,E} \cdot \sigma_E \tag{7-2}$$

$$R_k = \mu_R + K_{p,R} \cdot \sigma_R \tag{7-3}$$

To define the range of failure, a limit state function $G = R - E$ is introduced. Thus, the central safety zone of the limit state function corresponds to the distance between $g = 0$ and the mean value μ_G (Figure 7-1 (c)).

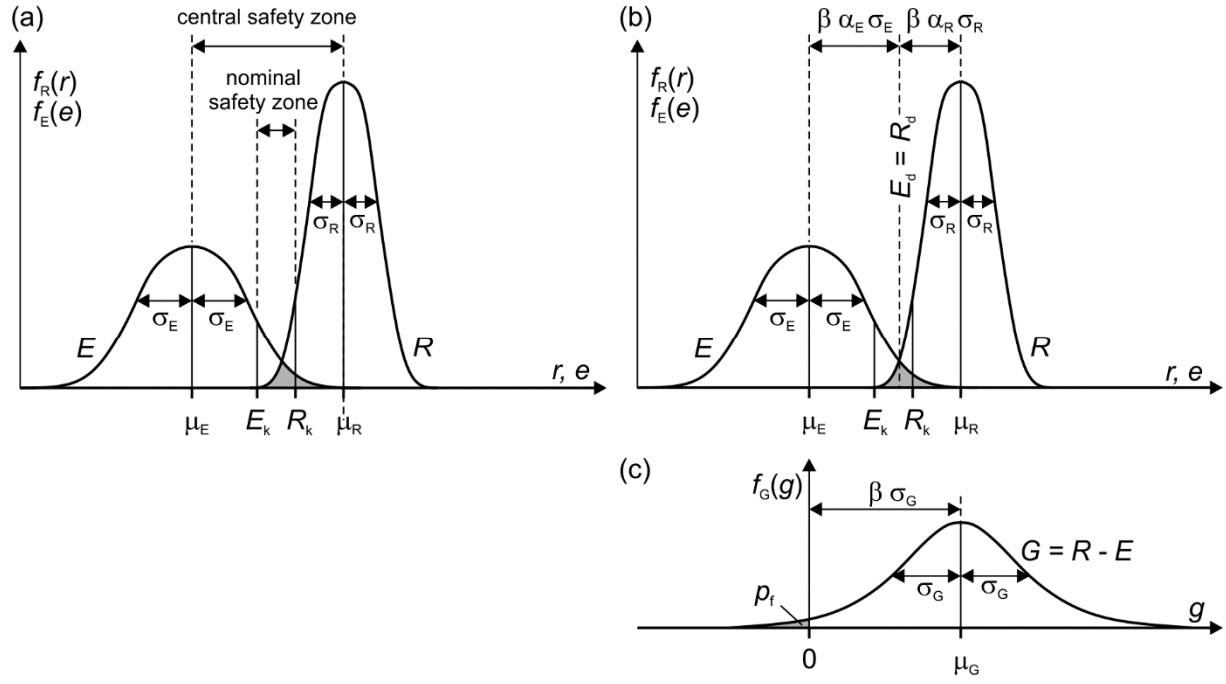

Figure 7-1: Density functions with definitions of safety zones (a), definition of reliability index β for action E and resistance R distributions (b) and limit state function G (c) according to [Zil10]

The correlation between effects of action, resistance and limit state function regarding mean value and standard deviation follow Eqs. (7-4) and (7-5) (Figure 7-1 (b) and (c)).

$$\mu_G = \mu_R - \mu_E \tag{7-4}$$

$$\sigma_G = \sqrt{\sigma_R^2 + \sigma_E^2} \tag{7-5}$$

The description of the central zone for the limit state function can be assessed by a multiple of the standard deviation σ_G with the reliability index β, which corresponds to the inverse coefficient of variation of the limit state function (Eq. (7-6)) [Zil10].

$$\beta = \frac{\mu_G}{\sigma_G} \tag{7-6}$$

The failure probability in a certain time period p_f is therefore the area underneath the limit state function in the range $G \leq 0$ ((Figure 7-1 (c)) and correlates with the reliability index β as shown in Eq. (7-7).

$$p_f = \int_{-\infty}^{0} f_G(g)\, dg = \Phi \cdot \left(-\frac{\mu_G}{\sigma_G}\right) = \Phi \cdot (-\beta) \tag{7-7}$$

With

Φ cumulative distribution function of standardised normal distribution

The failure probability factor p_f accounts for the level of probability and implies, that failure occurs in 10^i instances. The correlation of failure probability p_f and reliability index β according to [EC0] is summarised in Table 7-1.

Table 7-1: Correlation between failure probability and reliability index according to [EC0]

p_f	10^{-1}	10^{-2}	10^{-3}	10^{-4}	10^{-5}	10^{-6}	10^{-7}
β	1.28	2.32	3.09	3.72	4.27	4.75	5.20

For defining a required level of safety for design, [EC0] introduces three reliability classes which depend on the assumed consequences of failure. Therefore, [EC0] distinguishes between high, medium and low consequences regarding loss of human life, economic, social or environmental impact. Table 7-2 summarises the recommended minimum values of reliability index β, depending on reliability class and reference period.

Table 7-2: Recommended reliability index β according to [EC0] depending on reliability classes and reference period

Reliability class	Consequence class	Minimum value for β	
		1 year	50 years
RC3	high consequences	5.2	4.3
RC2	medium consequences	4.7	3.8
RC1	low consequences	4.2	3.3

For concrete structures with a reliability class of RC2 and medium consequences, the recommended minimum reliability index for verification at ultimate limit state is $\beta = 3.8$. For fatigue, the recommended range is $\beta = 1.5 – 3.8$, depending on accessibility, potential of maintenance and tolerance of fracture.

As shown in Figure 7-1 (b) and (c), the reliability index is applied to effects of action, resistance as well as limit state function. Since the correlation between standard deviation of limit state function and standard deviation of effects of action and resistance is non-linear, weighting factors for action and resistance α_E and α_R are introduced to account for the rate of influence on the failure probability. Thus, combining Eq. (7-5) and (7-6) yield to the modified expression of the central safety zone for the limit state function according to Eq. (7-8).

$$\mu_G = \beta \cdot \sigma_G = \beta \cdot \sqrt{\sigma_R{}^2 + \sigma_E{}^2} = \beta \cdot \alpha_R \cdot \sigma_R + \beta \cdot \alpha_E \cdot \sigma_E \tag{7-8}$$

The weighting factors α_E and α_R are directly connected to the standard deviation of both, action and resistance and thus, describe the influence of E and R on the failure probability. The recommended values in [EC0] are $\alpha_E = – 0.7$ and $\alpha_R = 0.8$.

Fulfilling the safety concepts of [EC0] with $E_d \leq R_d$, rearranging Eq. (7-8) gives the general design equation for limit state (Eq. (7-9)).

$$R_d = E_d \leftrightarrow \mu_R – \beta \cdot \alpha_R \cdot \sigma_R = \mu_E – \beta \cdot \alpha_E \cdot \sigma_E \tag{7-9}$$

To derive partial safety factors for effects of action γ_E and resistance γ_R to achieve a sufficient level of safety, the characteristic expressions are referred to the design expressions (Eq. (7-10) and (7-11)).

$$\gamma_E = E_k/E_d \tag{7-10}$$

$$\gamma_R = R_k/R_d \tag{7-11}$$

The partial safety factor for resistance $\gamma_R = \gamma_M$ considers the partial safety factor of materials γ_m and the partial safety factor of the model equation γ_{Rd} and is defined to be $\gamma_M = \gamma_m \cdot \gamma_{Rd}$ [EC0].

7.2.3 Derivation of design values

[EC0] Annex D provides two methods for deriving and applying partial safety factors. The first procedure allows a determination of design values for material parameters (e.g. material strength specified by material testing), either by applying a partial safety factor specified depending on the material to a characteristic value, or by direct determination of design values with implicitly considering the required reliability. The second procedure provides a probabilistic evaluation method which intends to be the basis for calibrating resistance models and for deriving safety factors.

In the first procedure, the design value X_d can be determined by the characteristic value X_k divided by the partial safety factor for the material γ_m following Eq. (7-12) for a normal distribution.

$$X_d = \eta_d \cdot \frac{X_{k(n)}}{\gamma_m} = \frac{\eta_d}{\gamma_m} \cdot m_x \cdot \{1 - k_n \cdot V_x\} \tag{7-12}$$

The characteristic value X_k describes the 5 % quantile ratio of the mean value m_x of test data, the quantile factors k_n depend on number of test data ($k_n = 1.64$ for $n \geq 100$ tests) and the coefficient of variation V_x is a parameter of scatter. The conversion factor η_d accounts for relevant parameters of test procedure (e.g. volume and scale effects).

To directly obtain design values, the required level of reliability is implemented by defining quantile factors $k_{d,n}$, which account for a 0.1 % quantile ratio and can be calculated by considering a defined reliability index $\beta = 3.8$ and a weighting factor for resistance $\alpha_R = 0.8$ according to Eq. (7-13).

$$k_{d,n} = \beta \cdot \alpha_R = 3.8 \cdot 0.8 = 3.04 \tag{7-13}$$

The design value X_d can then be directly determined by mean value of test results m_x and corresponding coefficient of variation V_x assuming a normal distribution according to Eq. (7-14).

$$X_d = \eta_d \cdot m_x \cdot \{1 - k_{d,n} \cdot V_x\} \tag{7-14}$$

If the test data underlies the assumption of a log-normal distribution, the calculation of design values follows Eq. (7-15), where m_y describes the mean value and s_y the standard deviation of the logarithmised test data $\ln(x_i)$.

$$X_d = \eta_d/\gamma_m \cdot \exp(m_y - k_n \cdot s_y) \text{ or } X_d = \eta_d \cdot \exp(m_y - k_{d,n} \cdot s_y) \tag{7-15}$$

The expressions for direct determination of characteristic and design values are based on the Bayesian Procedure which use uncertain prior distributions and lead to similar results compared to classical statistic methods with a confidence level of 75 %.

The second procedure to determine partial safety factors for design models according to [EC0] Annex D provides a probabilistic evaluation method which verifies the failure probability by approximating the results of a non-linear limit state function by assuming normal- or log-normal distributed random variables. The Mean-Value First-Order Second-Moments (MVFOSM) Method is the basis of the probabilistic evaluation. Therefore, the basis variables of the design approach are described by the first and second statistic moment of their distribution functions (i.e. their mean value X_m and their variance σ_i^2). An extensive description of the MVFOSM Method can be found in e.g. [Ric09]. This procedure accounts for the Level II statistic procedures and can therefore

be used to determine partial safety factors to be applied within Level I procedures [Ric09].

The calculation procedure of characteristic and design values with corresponding partial safety factors according to [EC0] Annex D is summarised in Table 7-3.

Table 7-3: Calculation of characteristic and design values according to [EC0]

Step 1	Determination of model equation	
	$r_t = g_{rt}(\underline{X})$	
Step 2	Comparison of theoretical values r_{ti} and experimental values r_{ei}	
Step 3	Estimation of mean value correlation	
	$r_m = b \cdot r_t(\underline{X}_m) = b \cdot g_{rt}(\underline{X}_m) \cdot \delta$	with $b = \frac{\Sigma\, r_{ei} \cdot r_{ti}}{\Sigma\, r_{ti}^2}$ and $\delta_i = \frac{r_{ei}}{b \cdot r_{ti}}$
Step 4	Estimation of COV for the error term δ	
	$V_\delta = \sqrt{\exp(s_\Delta^2) - 1}$	with $\Delta_i = \ln(\delta_i)$, $\overline{\Delta} = \frac{1}{n}\sum_{i=1}^{n} \Delta_i$, $s_\Delta^2 = \frac{1}{n-1}\sum_{i=1}^{n} (\Delta_i - \overline{\Delta})^2$
Step 5	Control of compatability	
Step 6	Estimation of COV for basis variables	
	$V_{rt} = \frac{1}{g_{rt}^2(X_m)} \sum_{i=1}^{j} \left(\frac{\delta g_{rt}}{\delta X_i} \cdot \sigma_i \right)^2$	
Step 7	Calculation of weighting factors	
	$\alpha_{rt} = \frac{Q_{rt}}{Q_r}$ and $\alpha_\delta = \frac{Q_\delta}{Q}$	with $Q_{rt} = \sqrt{\ln(V_{rt}^2 + 1)}$, $Q_\delta = \sqrt{\ln(V_\delta^2 + 1)}$, $Q_r = \sqrt{\ln(V_r^2 + 1)}$, $V_r^2 = V_{rt}^2 + V_\delta^2$
Step 8a	Determination of characteristic value	
	$r_k = b \cdot g_{rt}(X_m) \cdot \exp(-k_\infty Q - 0.5Q^2)$	
Step 8b	Determination of design value	
	$r_d = b \cdot g_{rt}(X_m) \cdot \exp(-k_\infty \cdot \alpha_{Rt} \cdot Q_{rt} - k_{d,n} \cdot \alpha_\delta \cdot Q_\delta - 0.5Q^2)$	
Step 9	Determination of partial safety factors	
	$\gamma_M = \frac{r_k}{r_d}$	

COV: coefficient of variation; r_t: theoretical resistance function; $g_{rt}(\underline{X})$: resistance function of basis variables; $\underline{X}$ and X_i: basis variables; X_m: mean value of basis variables; r_{ti}: theoretical values calculated with basis parameters of test i; r_{ei}: experimental value of test i; r_m: mean expression of resistance function; b: mean value correction; δ_i: observed error term for test specimen; V_δ: COV for error term δ; Δ_i: logarithmized estimated error term; $\overline{\Delta}$: mean value of log. estimated error; s_Δ: standard deviation of log. error term; V_{rt}: COV of basis variables; σ_i: standard deviation of basis variables; V_r: COV of error term; Q_r: standard deviation of log. of resistance function; α_{rt}: weighting factor for basis variables, α_δ: weighting factor for error term; r_k: characteristic value of resistance function, r_d: design value of resistance function; γ_M: partial safety factor of resistance function.

Following this procedure, a resistance function $r_t = g_{rt}(\underline{X})$ must be defined for the design model which includes all relevant basis variables $\underline{X}$ with an influence on the considered limit state. For comparison of design model and experimental data, the theoretical resistance of each test r_{ti}, considering all influencing parameters, must be compared to the experimental resistance r_{ei}. The observed error term for the test specimen δ_i with corresponding coefficient of variation V_δ may be determined by mean value correlation of resistance and experimental data. By verification of compatibility between resistance function and experimental results, the design approach should be adjusted, or the test results should be allocated in sub-groups to minimise the scattering influence of unconsidered parameters. To determine the coefficient of variation V_r, the variation of resistance function V_δ as well as the variation of basis variables V_{rt} must be applied. The variation of basis variables should be determined by the experimental test data or literature. By combining resistance function, mean value correlation, coefficients of variation and weighting factors for model approach and basis variables, the characteristic level as well as design level of resistance function may be determined. The characteristic level of the resistance function is based on the 5 % quantiles with $k_\infty = 1.64$ for the basis variables as well as k_n for the variation of resistance function depending on number experimental results. Using the characteristic formulation for design, commonly accepted partial safety factors may be applied to the approach. For the direct determination of design level for the resistance function, the derivation is based on the 0.1 % quantiles with $k_{d,\infty} = \beta \cdot \alpha_R = 3.8 \cdot 0.8 = 3.04$. Thus, a partial safety factor γ_M for the design approach can be determined, considering model uncertainty as well as uncertainties of materials and must be applied on the characteristic approach of the design equation.

7.3 Derivation of roughness coefficients and design values

7.3.1 Introduction

To develop an improved design expression for longitudinal interface shear based on the regulations according to [EC2], the coefficients of adhesion and friction have a major influence on the calculated interface shear resistance. An isolated observation of load resistance terms of adhesion and friction with their corresponding coefficients is not feasible by considering the comprehensive test data of experimental investigations. The effect of each load resistance term strongly depends on the applied test parameters and boundary conditions and interacts with the remaining load resistance terms. In this context, the available test data must be classified to investigate the effect of each resistance term mostly independent. The derived coefficients can then be validated using the comprehensive database.

A simple determination of the interface shear coefficients does not necessarily involve a sufficient level of reliability for design. Therefore, partial safety factors for the term of adhesion and transverse reinforcement can be derived to ensure a safe estimation of the design approach. The procedure of deriving partial safety factors according to [EC0]

Annex D is recommended for assessing the safety level of strength-based models which were derived with experimental test results. The provided procedure is limited to product-based resistance functions, which does not apply to the entire shear friction equation. However, the isolated interface resistance terms are product based and thus, isolated partial safety factors can be derived. Even though the probability of failure cannot be determined by this method, using the recommended reliability index $\beta = 3.8$ and the weighting factor for resistance $\alpha_R = 0.8$ is a generally excepted method to derive safety factors.

As a bases for developing an improved design expression, a limit state function must be defined. For longitudinal interface shear, Eq. (7-16) is defined in accordance to [EC2] and [prEC2:18].

$$\beta \cdot V_{Edi} = \beta \cdot \tau_{Edi} \cdot b_{int} \cdot z \leq V_{Rdi} = \tau_{Rdi} \cdot b_{int} \cdot z \tag{7-16}$$

For the resistance function, the design expression according to the development for Eurocode 2 [prEC2:18] showed the best overall accordance in the evaluated databases in Chapter 6. The interface shear equation therefore follows Eq. (7-17) (s. Chapter 3.3.4).

$$V_{Rdi} = (c \cdot \frac{f_{ck}^{\frac{1}{2}}}{\gamma_c} + \mu \cdot \sigma_n + \rho_{int} \cdot \frac{f_{yk}}{\gamma_s} \cdot (\mu \cdot \sin\alpha + \cos\alpha)) \cdot b_{int} \cdot z \tag{7-17}$$

The coefficients of adhesion c and friction μ as well as the results of database evaluations by comparing experimental results to the characteristic design expression τ_{test}/τ_{Rk} for the databases with small size tests without interface reinforcement and normal stress (database A), small size tests with interface reinforcement (database B), beam and slab specimens without interface reinforcement (database E) and beam and slab specimens with stirrups as interface reinforcement (database F) are summarised in Table 7-4 (s. Chapter 6.3 and 6.4). For design, the partial safety factors are defined to $\gamma_c = 1.5$ for concrete and $\gamma_s = 1.15$ for reinforcing steel [prEC2:18].

Table 7-4: Coefficients of adhesion and friction (left) and database evaluation for τ_{test}/τ_{Rk} according to the evaluation of [prEC2:18] (right)

Interface	c	μ	Database:	small size tests		slabs and beams	
				A (Table 6-4)	B (Table 6-9)	E (Table 6-11)	F (Table 6-14)
vs	0.0095	0.5	No.	83	266	30	66
s	0.075	0.6	X_m	3.06	1.56	4.35	2.46
r	0.15	0.7	COV	0.37	0.31	0.51	0.38
vr	0.19	0.9	$X_{5\%}$	1.57	0.91	1.70	1.23

vs: very smooth; s: smooth; r: rough; vr: very rough; A: small size tests without interface reinforcement; B: small size tests with interface reinforcement, E: structural member tests without interface reinforcement, F: structural member tests with interface reinforcement

Comparison calculations show an improved estimation of test data by defining the concrete tensile strength to be proportional to the cubic root of the characteristic concrete compression strength $f_{ck}^{1/3}$. Thus, the bases of the target design expression with partial safety factors for adhesion γ_{adh} and friction γ_{fric} and characteristic coefficients of adhesion c_k and friction μ_k gives Eq. (7-18).

$$V_{Rdi} = (c_k \cdot \frac{f_{ck}^{\frac{1}{3}}}{\gamma_{adh}} + \mu_k \cdot \sigma_n + \rho_{int} \cdot \frac{f_{yk}}{\gamma_{fric}} \cdot (\mu_k \cdot \sin\alpha + \cos\alpha)) \cdot b_{int} \cdot z \tag{7-18}$$

For interface shear design of longitudinal shear in beam and slab structures, the term of friction has a minor effect on the shear resistance, since normal compressive stress along the interface of the structure's axis are generally induces by self-weight of insitu concrete, which is comparatively small compared to resistance of adhesion and reinforcement. However, the coefficient of friction accounts for the term of normal stress and reinforcement. Thus, the focus of deriving coefficients of friction in these investigations is the determination of a friction factor for reinforcement, but with controlling the effect on the term of normal stress. In the following, the coefficient of adhesion c_k and partial safety factor for adhesion γ_{adh} as well as the friction coefficient μ_k and partial safety factor for friction γ_{fric} are derived using selected databases. For an application of the design formulation within the design concept of Eurocode 2, the derived roughness coefficients and partial safety factors were implemented for a consistent design with partial safety factors of concrete and steel as shown in Eq. (7-19).

$$V_{Rdi} = (c \cdot \frac{f_{ck}^{\frac{1}{3}}}{\gamma_c} + \mu \cdot \sigma_n + \rho_{int} \cdot \frac{f_{yk}}{\gamma_s} \cdot (\mu \cdot \sin\alpha + \cos\alpha)) \cdot b_{int} \cdot z \tag{7-19}$$

7.3.2 Calibration of adhesive term

The bases of experimental data for calibration of coefficients of adhesion and derivation of a partial safety factor was database A-1 with 83 small size tests without interface reinforcement and normal stress. To consider the interface classification, roughness classes were defined in accordance to the database evaluation in Chapter 6 as very smooth, smooth, rough and very rough. To follow the probabilistic procedure of [EC0] Annex D, the adhesive term must be expressed on mean level. Since the concrete tensile strength is defined to be proportional to the cubic root of the characteristic concrete compressive strength, a transformation of characteristic concrete compressive strength to mean concrete compressive strength with $f_{cm} = f_{ck} + 8$ or $f_{cm} = f_{ck} + 4$ under laboratory conditions is not possible offhand (s. Chapter 6.2.3). Thus, the coefficients of adhesion were calibrated to achieve a mean value of $X_m = 1.0$ for each roughness class (c_m). This is in accordance to [EC0] Annex D, where test data can be allocated to reduce the range of scatter. Figure 7-2 (left) shows the determined mean coefficients of adhesion for 64 smooth specimens (s) with $c_m = 0.41$, 8 rough specimens (r) with $c_m = 0.87$ and 11 very

rough (vr) specimens with $c_m = 1.01$. Since no specimens were tested with very smooth specimens, a consideration of very smooth surfaces was not possible at this stage.

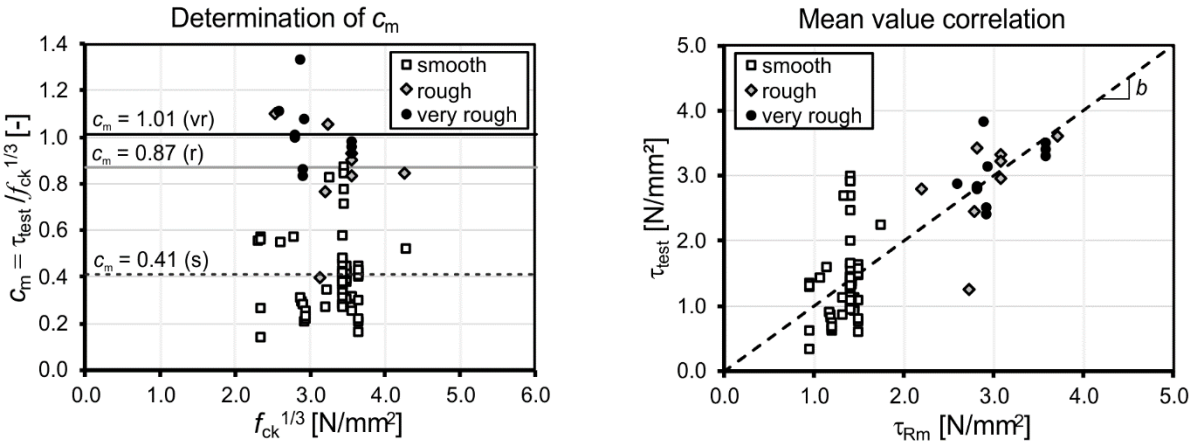

Figure 7-2: Determination of coefficient of adhesion for mean evaluation (left) and mean value correlation of experimental and theoretical data (right)

According to [EC0] Annex D, the influence of the variation of basis variables as well as model uncertainties are considered to derive partial safety factors. For the adhesive resistance in the interface shear equation, the basis variables are the concrete compressive strength f_{ck}, the width of the interface b_{int} and the lever arm of internal forces z (Eq. (7-20)).

$$V_{Rmi,adh} = c_m \cdot f_{ck}^{1/3} \cdot b_{int} \cdot 0.9 \cdot d \tag{7-20}$$

Even though the interface shear force for small size specimens is determined by the area of the interface, expressed by $A_{int} = b_{int} \cdot h_{int}$, the expression for composite action with $b_{int} \cdot z$ and $z = 0.9 \cdot d$ is chosen to derive partial safety factors, since the effective depth d underlies higher scatter compared to structural dimensions. The coefficients of adhesion c_m accounts as model uncertainty and gives the corresponding coefficient of variations for the resistance function. To determine the coefficients of variation of the basis variables, the partial derivatives are summarised in Table 7-5.

Table 7-5: Basis variables and corresponding partial derivatives for adhesive term

Basis variable X_i	f_{ck}	b_{int}	d
$\frac{\delta V_{Rmi,adh}}{\delta X_i}$	$\frac{1}{3 \cdot f_{ck}} \cdot V_{Rmi,adh}$	$\frac{1}{b_{int}} \cdot V_{Rmi,adh}$	$\frac{1}{d} \cdot V_{Rmi,adh}$

Since the uncertainties of the basis variables cannot be particularly determined by the test databases for interface shear, the information of standard deviation can be achieved from codes or other literature. For the concrete compressive strength, [EC2] defines a constant standard deviation of $\sigma_i = 4.9$ N/mm², which leads to a coefficient of variation depending on the concrete strength with $V_{rt,fck} = 4.9/f_{cm}$ (s. Chapter 6.2.3 and Eq. (6-8)). Thus, the coefficient of variation decreases with increasing compression strength. A

concrete strength of f_{cm} = 20 N/mm² as lower limit of concrete strength therefore gives a COV of 0.24, whereas a concrete strength of f_{cm} = 60 N/mm² gives a COV of 0.08. As stated in [Her17], the coefficients of variation for concrete compressive strength defined in literature vary between 0.15 and 0.18. To capture the large scatter for low concrete classes, a COV of 0.24 is assumed for derivation of partial safety factors for adhesion. In accordance to [Her17], the standard deviation of the width of the interface b_{int} is assumed to 4 mm. For the standard deviation of the effective depth, [Voi14] provides a summary of several approaches from literature which vary between 4.5 mm and 17.5 mm. For beams and slabs, [Han04] proposes a standard deviation of 5.5 mm for precast elements and 12.5 mm for insitu concrete. Thus, a standard deviation of 9 mm is assumed as a mean for the effective depth.

The calculation procedure to determine the partial safety factor of adhesion based on the mean value correlation with coefficients of adhesion c_m and mean value correction b (Figure 7-2 (right)) is summarised in Table 7-6 for basis variables randomly chosen. The determined partial safety factor for adhesion is γ_{adh} = 2.30. Due to the high measure of scattering of the model equation itself, the uncertainties of the basis variables have a minor influence on the partial safety factor. Thus, the derived partial safety factor for adhesion can be applied to the range of basis variables applicable in practice.

Table 7-6: Calculation of partial safety factor for adhesion according to [EC0] Annex D

Basis variable X_i	X_m	σ_i	COV	$\frac{\delta V_{Rmi,adh}}{\delta X_i}$	$\left(\frac{\delta V_{Rmi,adh}}{\delta X_i}\cdot\sigma_i\right)^2$
f_{ck}	25 N/mm²	4.9 N/mm²	0.24	0.013	0.0042
b_{int}	250 mm	4.0 mm	0.016	0.004	0.0003
d	300 mm	9.0 mm	0.03	0.003	0.0009
				Σ =	0.0054
V_r = 0.65359		V_δ = 0.65360		V_{rt} = 0.00037	
Q_r = 0.59641		Q_δ = 0.59641		Q_{rt} = 0.00033	
γ_{adh} = 2.30		α_δ = 0.99999		α_{rt} = 0.00055	

To apply the partial safety factor to the interface shear equation, the expression of adhesion must be transferred to characteristic level. According to [EC2], the conversion of mean concrete tensile strength to characteristic concrete tensile strength is performed by assuming a reduction to the characteristic 5 % quantile ratio with 70 % of the mean value with $f_{ctk,0.05} = 0.7 \cdot f_{ctm}$. Since the adhesive strength correlates with the concrete tensile strength, a similar reduction of the mean coefficients of adhesion c_m to the characteristic value c_k is assumed with $c_k = 0.7 \cdot c_m$. The determined coefficients of adhesion are summarised in Table 7-7.

The derived partial safety factor for adhesion γ_{adh} = 2.30 captures the partial safety factors for model uncertainty and concrete. Thus, $\gamma_{adh} = \gamma_{Rd,adh} \cdot \gamma_c$ with $\gamma_{Rd,adh}$ for model

uncertainty and γ_c for concrete applies. To verify the design expression based on the partial safety factors defined in [EC2] with $\gamma_c = 1.5$, the model uncertainty develops to $\gamma_{Rd} = \gamma_{adh,}/\gamma_c = 1.53$. Implementing the error term to the derived characteristic c_k-values yields to the values $c = c_k/1.53$ for design. The corresponding c-values for the design expression for the adhesive term (Eq. (7-21)) are summarised in Table 7-7.

$$\tau_{Rd,adh} = \frac{c_k \cdot f_{ck}^{\frac{1}{3}}}{\gamma_{adh}} = \frac{c_k}{\gamma_{Rd,adh}} \cdot \frac{f_{ck}^{\frac{1}{3}}}{\gamma_c} = c \cdot \frac{f_{ck}^{\frac{1}{3}}}{\gamma_c} \text{ with } \gamma_c = 1.5 \tag{7-21}$$

Evaluating database A-1 (small size tests without interface reinforcement and normal stress) by comparing experimental test data to the calculated characteristic interface shear resistance according to Eq. (7-21) with coefficient of adhesion c according to Table 7-7 without considering the partial safety factor leads to the statistical data as summarised in Table 7-7.

Table 7-7: Coefficients of adhesion (left) and evaluation of database A-1 with the modified approach for adhesion

Interface	c_m	c_k	c	Evaluation of database A-1	
very smooth (1)	–	–	–	No.	83
smooth	0.41	0.29	0.19	X_m	2.20
rough	0.87	0.61	0.39	COV	0.37
very rough	1.01	0.70	0.46	$X_{5\%}$	1.14

X_m: mean value τ_{Rki}/τ_{calc}, COV: coefficient of variation, $X_{5\%}$: characteristic 5 % quantile ratio, (1): no very smooth specimens in database – no determination possible at this stage

Compared to the database evaluation with the approach according to [prEC2:18] as summarised in Table 7-4, the evaluation with the modified expression and derived coefficients of adhesion yields to an improved characteristic 5 % quantile ratio of 27 % with similar coefficient of variation.

7.3.3 Calibration reinforcement term

For the calibration of the coefficients of friction μ and derivation of partial safety factors for the reinforcement term of the interface shear equation, test data of small size tests with interface reinforcement but without externally applied normal stress (database B) were the basis for investigation. Due to the interaction of load bearing resistances of adhesion and reinforcement according to the basis function, an isolated observations of the magnitude of reinforcement resistance is not possible offhand. For some specimens in the database, bondbreaker was used to prevent adhesive bond between the concrete layers. For these specimens, it can be assumed that interface shear resistance only develops by clamping of reinforcement. Thus, for the modification of friction factors as well as for the derivation of partial safety factors, a number of 48 tests could be seper-

ated. Following the procedure according to [EC0] Annex D, the basis function of reinforcement term on mean level gives Eq. (7-22). Since the inclination of the interface reinforcement was $\alpha = 90°$ for all evaluated specimens, the term accounting for inclined reinforcement was not considered.

$$V_{Rmi,reinf} = (\mu_m \cdot \rho_{int} \cdot f_{ym}) \cdot b_{int} \cdot z \tag{7-22}$$

To provide the basis function on mean level, the coefficients of friction were calibrated to fulfil $X_m = 1.0$ for each roughness class. Figure 7-3 (left) shows the determined mean coefficients of friction μ_m for 13 very smooth (vs), 27 smooth (s) and 8 rough (r) specimens. Since no specimens were tested with very rough surfaces, a consideration of very rough interfaces was not possible at this stage.

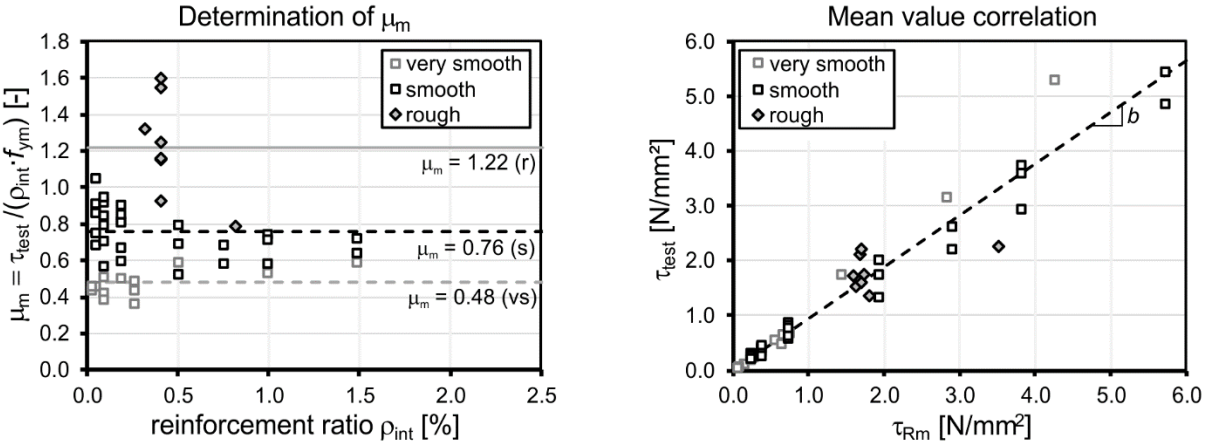

Figure 7-3: Determination of coefficient of friction for mean evaluation (left) and mean value correlation of experimental and theoretical data (right)

In the next step, the mean value equation must be regarded considering all basis variables. Therefore, the interface reinforcement ratio can be expressed by the area of interface reinforcement $A_{s,int}$ and the area if the interface A_{int} with $\rho_{int} = A_{s,int}/(b_{int} \cdot h_{int})$. Assuming the interface reinforcement equally spaced in transverse and longitudinal direction, the expression can be rewritten as $\rho_{int} = A_{s,bar}/(s_{bar}^2)$ with the area of each bar $A_{s,bar}$ with a spacing s_{bar}. As mentioned within the derivation of coefficients of adhesion, the scatter of the interface width in the small size tests was substituted by the scatter of the effective depth to account for the higher variation of effective depth compared to structural dimensions. The corresponding expression of interface shear force for determining partial safety factors gives Eq. (7-23). The coefficients of friction μ_m accounts for model uncertainty which gives the corresponding coefficient of variations of the resistance function.

$$V_{Rmi,reinf} = (\mu_m \cdot A_{s,bar}/(s_{bar})^2 \cdot f_{ym}) \cdot b_{int} \cdot 0.9 \cdot d \tag{7-23}$$

To determine the coefficients of variation of the basis variables, the partial derivatives are summarised in Table 7-8.

Table 7-8: Basis variables and corresponding partial derivatives for adhesive term

Basis variable X_i	$A_{s,bar}$	s_{bar}	f_{ym}	b_{int}	d
$\frac{\delta V_{Rmi,reinf}}{\delta X_i}$	$\frac{1}{A_{s,bar}} \cdot V_{Rmi,reinf}$	$-\frac{2}{s_{bar}} \cdot V_{Rmi,reif}$	$\frac{1}{f_{ym}} \cdot V_{Rmi,reinf}$	$\frac{1}{b_{int}} \cdot V_{Rmi,reinf}$	$\frac{1}{d} \cdot V_{Rmi,reinf}$

To consider the uncertainties of basis variables, the standard deviations must be defined particularly. For the area of interface reinforcement bar, a COV of 0.06 is assumed for stirrups in accordance to [Moo76] and [Voi14]. The variation of the spacing of the bars is assumed with a constant standard deviation of 4 mm [Her17]. [Voi14] summarises several approaches of defining the variation of reinforcement strength. For reinforcing steel B500 with a characteristic yield strength of 550 N/mm², [Vis95] proposes a coefficient of variation of 0.06, which was adopted for derivation. For interface width b_{int} and effective depth d, constant standard deviations were defined in accordance to the derivation of adhesive term to 4 mm for b_{int} and 9 mm for d.

The calculation procedure to determine the partial safety factor of reinforcement based on the mean value correlation with coefficients of friction μ_m and mean value correction b (Figure 7-3 (right)) is summarised in Table 7-9 for basis variables randomly chosen.

Table 7-9: Calculation of partial safety factor for reinforcement according to [EC0]

Basis variable X_i	X_m	σ_i	COV	$\frac{\delta V_{Rmi,adh}}{\delta X_i}$	$\left(\frac{\delta V_{Rmi,adh}}{\delta X_i} \cdot \sigma_i\right)^2$
$A_{s,bar}$	10 mm	0.6 mm	0.06	0.1	0.0036
s_{bar}	200 mm	4.0 mm	0.02	0.01	0.0016
f_{ym}	550 mm	33 N/mm²	0.06	0.002	0.0036
b_{int}	250 mm	4.0 mm	0.016	0.004	0.0003
d	300 mm	9.0 mm	0.03	0.003	0.0009
				Σ =	0.0100
V_{rt} = 0.00128		V_δ = 0.44002		V_r = 0.44021	
Q_{rt} = 0.01278		Q_δ = 0.42070		Q_r = 0.42087	
α_{rt} = 0.03038		α_δ = 0.99961		γ_{fric} = 1.80	

The determined partial safety factor for adhesion is $\gamma_{fric} = 1.80$. Even though the measure of scatter for the reinforcement term is smaller compared to the evaluation of adhesive term, the uncertainties of the model equation have a major influence on the determined partial safety factor. Thus, varying the basis variables does not affect the partial safety factor.

To apply the partial safety factor to the interface shear equation, the expression of reinforcement must be transferred to characteristic level. For reinforcement, [EC2] provides the characteristic value of yield strength to be 91 % of the mean yield strength with

$f_{ym} = 1.1 \cdot f_{yk}$. Thus, the transformation from mean to characteristic level follows a reduction of 91 % expressed by defining the characteristic yield strength of reinforcement with similar coefficients of friction $\mu_m = \mu_k$. The determined coefficients of friction are summarised in Table 7-10.

The derived partial safety factor for friction $\gamma_{fric} = 1.80$ captures the partial safety factors for model uncertainty and reinforcement. Thus, $\gamma_{fric} = \gamma_{Rd,reinf} \cdot \gamma_s$ with $\gamma_{Rd,reinf}$ for model uncertainty and γ_s for reinforcement applies. To verify the design expression based on the partial safety factors defined in [EC2] with $\gamma_s = 1.15$, the model uncertainty develops to $\gamma_{Rd,reinf} = \gamma_{fric}/\gamma_s = 1.57$. Implementing the model uncertainty to the derived coefficients of friction yields to the design values $\mu = \mu_k/1.57$. The corresponding friction factors for the design expression of the reinforcement term as shown in Eq. (7-24), are summarised in Table 7-10.

$$\tau_{Rd,fric} = \mu_k \cdot \rho_{int} \cdot \frac{f_{yk}}{\gamma_{fric}} = \frac{\mu_k}{\gamma_{Rd,fric}} \cdot \rho_{int} \cdot \frac{f_{yk}}{\gamma_s} = \mu \cdot \rho_{int} \cdot \frac{f_{yk}}{\gamma_s} \text{ with } \gamma_s = 1.15 \qquad (7\text{-}24)$$

Evaluating database B for small size specimens with interface reinforcement and impaired adhesive bond by comparing experimental test data to the calculated characteristic interface shear resistance according to Eq. (7-24) with coefficient of friction μ according to Table 7-10 (left) and without considering the partial safety factor leads to the statistical data as summarised in Table 7-10 (right).

Table 7-10: Coefficients of friction (left) and evaluation of database B (small size tests with interface reinforcement) with the modified approach for reinforcement (right)

Interface	$\mu_m = \mu_k$	μ	Evaluation of database B (bondbreaker)	
very smooth	0.48	0.31	No.	48
smooth	0.76	0.48	X_m	1.72
rough	1.22	0.78	COV	0.18
very rough (1)	–	–	$X_{5\%}$	1.26

X_m: mean value τ_{Rki}/τ_{calc}, COV: coefficient of variation, $X_{5\%}$: characteristic 5 % quantile ratio, (1): no very rough specimens in database – no determination possible at this stage

To verify the determined coefficients of friction combined with the coefficients of adhesion using the small size tests with interface reinforcement and without bondbreaker (database B), the experimental shear stress is related to the characteristic interface shear resistance considering term of adhesion and reinforcement. Due to missing data for deriving a coefficient of adhesion for very smooth interfaces as well as a coefficient of friction for very rough interfaces, the coefficients must be calibrated using the complete database. For very rough interfaces, the friction factor was calibrated to achieve a mean value of $X_m = 1.0$ for an evaluation on mean level using 36 specimens with interface reinforcement and very rough surfaces. To determine a coefficient of adhesion for very smooth surfaces, no specimens with interface reinforcement and without bondbreaker

were available. Thus, a coefficient of adhesion of 0.025 is assumed in accordance to [EC2] and [MC10]. A verification of the determined coefficient of adhesion using small size tests with very smooth interfaces and applied normal stress shows an overestimation of the derived coefficients of adhesion and friction. However, due to lack of test data, the estimation seems reasonable. The roughness coefficients and the corresponding statistical results of evaluating complete database B is summarised in Table 7-11. The evaluation shows a characteristic 5 % quantile ratio of $X_{5\%} = 0.90$, which deceed the required value of 1.0 about 10 %. However, the evaluated small size specimens were subjected to concentrated shear loads with small interface areas as well as small numbers of interface reinforcement bars. For interfaces in beam and slab specimens, interface shear develops due to composite action with larger interfaces and larger numbers of interface bars. Due to potential of load redistribution, a sudden failure of all interface reinforcement bars is unlikely. Thus, the small deviation for the evaluation using this adverse condition can be accepted for terms of calibration.

Table 7-11: Coefficients of adhesion and friction (left) and evaluation of database B with the modified approach (right)

Interface	c	μ	Evaluation of database B	
very smooth	0.025[(1)]	0.31	No.	266
smooth	0.19	0.48	X_m	1.48
rough	0.39	0.78	COV	0.28
very rough	0.46	0.80[(2)]	$X_{5\%}$	0.90

X_m: mean value τ_{Rki}/τ_{calc}, COV: coefficient of variation, $X_{5\%}$: characteristic 5 % quantile ratio, [(1)]: assumed based on [EC2] and [MC10] and validated using tests with normal stress; [(2)]: subsequently derived

7.3.4 Revision of friction coefficient for normal stress

Even though the load resistance term of friction due to externally applied normal stress has a minor influence on the interface shear strength of beam and slab structures, the coefficient of friction also applies to the resistance term of normal stress. To separately investigate the influence of friction due to normal stress, an isolated investigation is not possible, since no tests with impaired adhesive bond and externally applied normal stress are available in the database. To verify the derived coefficient of friction for the term normal stress, database A-2 with small size specimens without interface reinforcement but with applied normal stress was evaluated. Applying the derived coefficients of adhesion and friction as summarised in Table 7-11 (left), the evaluation of 145 specimen leads to a mean value $X_m = 2.58$, a COV = 0.31 and a characteristic 5 % quantile ratio of $X_{5\%} = 1.49$, which gives a conservative but safe estimation of test results.

7.4 Validation of design approach

7.4.1 Introduction

The modified design approach with the derived coefficients of adhesion and friction are determined by databases with small size tests with concentrated load application and comparably small interfaces. For beam and slab specimens with concrete cast at different times, the longitudinal interface shear develops due to composite action and correlates with load bearing mechanisms of bending and shear. Thus, the proposed design expression must be validated by databases with composite beam and slab specimens with and without interface reinforcement. To capture the larger interface dimension of structural members compared to small size tests, a factor considering the influence of interface width on the adhesive strength is derived.

7.4.2 Validation of beams and slabs without interface reinforcement

To validate the modified design approach with the derived roughness coefficients, database E with composite beam and slab specimens without interface reinforcement was evaluated by comparing the experimental interface shear strength to the calculated characteristic interface resistance. Database E with 30 specimens holds specimens with 10 smooth, 16 rough and 4 very rough interfaces. The proposed characteristic expression follows Eq. (7-25) with the roughness coefficients summarised in Table 7-12 (left).

$$\tau_{Rki,prop} = c \cdot f_{ck}^{1/3} + \mu \cdot \sigma_n \tag{7-25}$$

For the evaluated test data, the resistance term of normal stress is only affected by the self-weight of insitu concrete and thus, has a minor effect on the interface resistance. The mean value X_m, coefficient of variation COV and characteristic 5 % quantile ratio $X_{5\%}$ resulting from the database evaluation are summarised in Table 7-12. For comparison, the statistical values of the evaluation with the [prEC2:18] approach are opposed. Compared to the [prEC2:18] evaluation, the range of scatter could be reduced about 6 % to COV = 0.48, combined with a reduced mean value to 65 % with $X_m = 2.86$. The corresponding $X_{5\%} = 1.17$ shows a reduction of 31 % and gives a safe and more economic estimation for design.

Table 7-12: Coefficients of adhesion and friction for design proposal (left) and results of evaluation of Database E with proposed design expression and [prEC2:18] (right)

Interface	c	μ		Proposal	prEC2:2018
very smooth	0.025	0.31	No.	30	30
smooth	0.19	0.48	X_m	2.86	4.35
rough	0.39	0.78	COV	0.48	0.51
very rough	0.46	0.80	$X_{5\%}$	1.17	1.70

X_m: mean value τ_{Rki}/τ_{calc}, COV: coefficient of variation, $X_{5\%}$: characteristic 5 % quantile ratio

The comparison of the related interface resistance over the influence of characteristic concrete strength according to the proposed approach and the approach according to [prEC2:18] is shown in Figure 7-4. It can be seen, that the proposed design approach generally increases the calculated interface resistances for all interface roughnesses. For smooth interfaces, the determined coefficient of adhesion still overestimates the experimental resistances. For rough interfaces, the determined coefficient gives a good estimation for eight specimens, which pattern the lower bound of test data in Figure 7-4 (left). However, the remaining eight specimens with rough surfaces show higher experimental interface resistances with a large scatter. The four specimens with rough interfaces were conducted with small concrete strengths. With the derived coefficient of adhesion, a better agreement of experimental and calculated test data as well as a reduction of scatter can be achieved. For the overall test data, defining the tensile strength to be proportional to the cubic root of the characteristic concrete strength shows a better estimation of the adhesive term compared to the square root as defined in [prEC2:18].

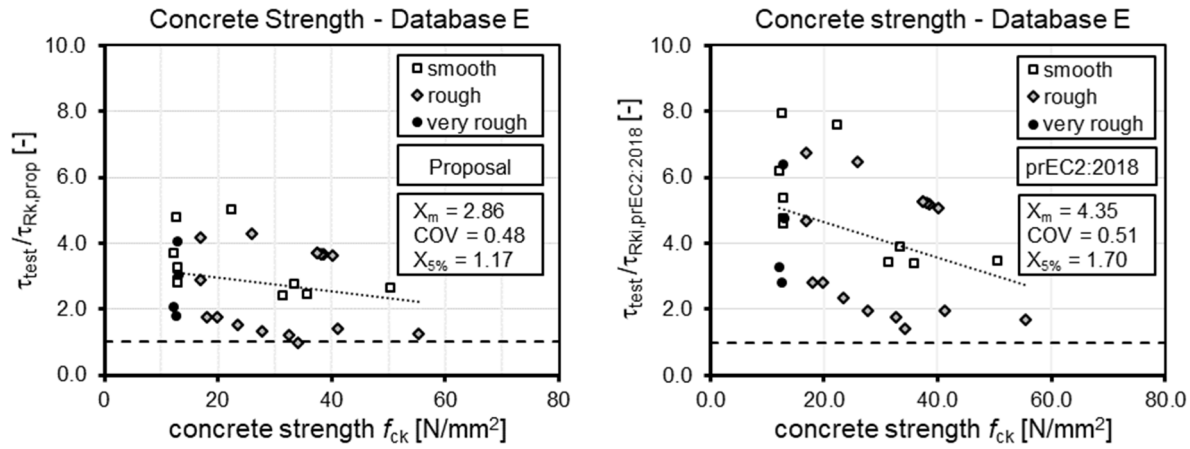

Figure 7-4: Database E (structural members without reinforcement): Influence of concrete strength according to proposal and [prEC2:18]

As mentioned in Chapter 6.4.2, the comparison of experimental to calculated interface resistance for beam and slab specimens without interface reinforcement show a decrease of experimental interface resistance with increasing width of interface. This effect can also be determined by applying the proposed design approach as shown in Figure 7-5 (left). Especially for small interfaces, higher experimental interface resistances could be achieved for smooth and rough surfaces. The decrease of interface resistance with increasing interface width might be caused by the higher potential of blemishes in the bond development along the interface which leads to a higher possibility of fracture. Specimens with rough interfaces pattern the lower bound of test data, whereas specimens with smooth interfaces pattern the upper bound of test data. Since all specimens with very rough interfaces had an interface width of b_{int} = 150 mm, no influence of interface width could be determined. As shown in Figure 7-5 (right), an influence of the length of the interface, defined as effective shear length between load application and

support for simply supported beams and slabs with single loads, could not be determined.

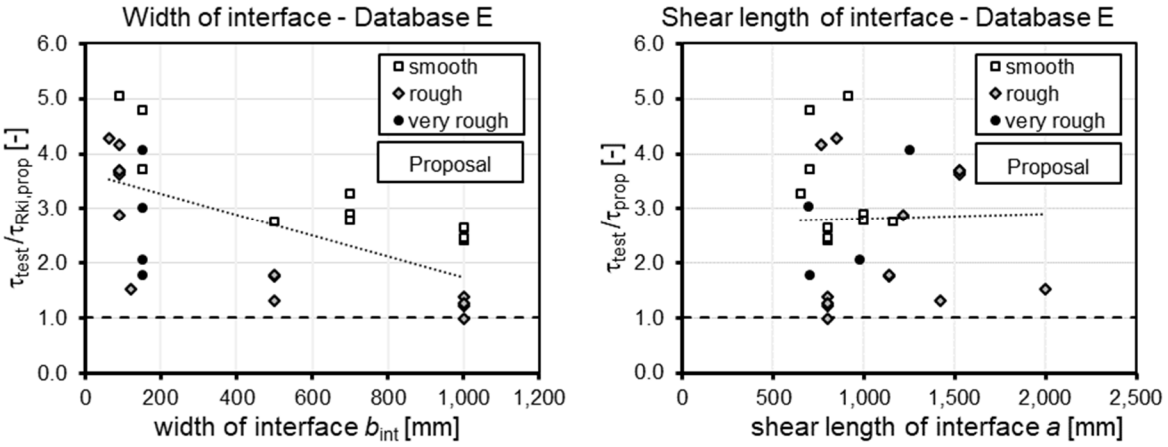

Figure 7-5: Database E (structural members without reinforcement): Influence of interface dimensions

7.4.3 Validation of beams and slabs with interface reinforcement

To verify the derived coefficients of adhesion and friction for beam and slab specimens with interface reinforcement, database F-1 was evaluated by referring the experimental interface resistance to the characteristic expression of the design approach following Eq. (7-26). The database holds 66 specimens with stirrups as interface reinforcement and includes 15 specimens with smooth, 46 with rough and 5 with very rough interfaces. The applied coefficients of adhesion and friction are summarised in Table 7-13 (left).

$$\tau_{Rki,prop} = c \cdot f_{ck}^{1/3} + \mu \cdot \sigma_n + \rho_{int} \cdot f_{yk} \cdot (\mu \cdot \sin\alpha + \cos\alpha) \tag{7-26}$$

The statistic values of the database evaluation with mean value X_m, coefficient of variation COV and characteristic 5 % quantile ratio $X_{5\%}$ for an evaluation with the proposed design expression and the expression according to [prEC2:18] are shown in Table 7-13 (right). To compare the proposed equation to the [prEC2:18] approach, the corresponding statistic evaluation data is shown in Table 7-13. As mentioned in context of the verification of beam and slabs without interface reinforcement, the resistance term of normal stress has a minor effect on the interface resistance. Compared to the [prEC2:18] approach, the evaluation with the new approach results in a reduction of mean value about 15 % to $X_m = 2.01$ and a reduction of coefficient of variation about 5 % to COV = 0.36, with a corresponding decreased characteristic 5 % quantile ratio about 15% of $X_{5\%} = 1.05$.

Table 7-13: Coefficients of adhesion and friction for design proposal (left) and results of evaluation of Database F-1 (structural members with interface reinforcement) with design proposal and [prEC2:18] (right)

Interface	c	μ		Proposal	prEC2:2018
very smooth	0.025	0.31	No.	66	66
smooth	0.19	0.48	X_m	2.01	2.46
rough	0.39	0.78	COV	0.36	0.38
very rough	0.46	0.80	$X_{5\%}$	1.05	1.23

X_m: mean value τ_{Rki}/τ_{calc}, COV: coefficient of variation, $X_{5\%}$: characteristic 5 % quantile ratio

The comparison of the influence of concrete strength and interface reinforcement ratio on the related interface resistance according to the modified design expression and [prEC2:18] is shown in Figure 7-6.

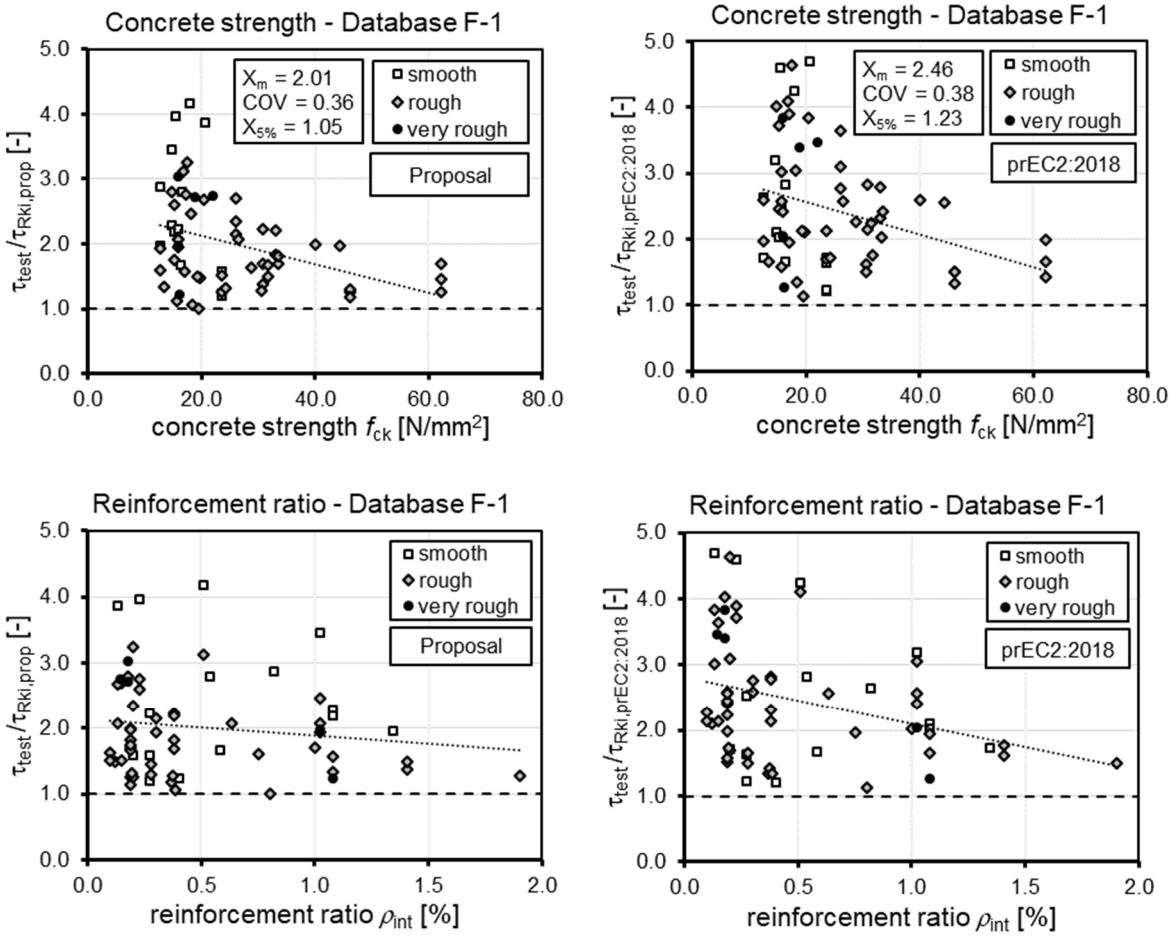

Figure 7-6: Database F-1 (structural members with reinforcement): Influence of concrete strength and interface reinforcement ratio according to design proposal and [prEC2:18]

Confirming the statistical data, the proposed interface shear approach generally gives higher interface resistances. By comparing the influence of the characteristic concrete strength, the approach considering the adhesive strength by the cubic root gives a

slightly flatter trend line than the [prEC2:18] approach with the square root of the concrete strength (Figure 7-6, top). The interaction of adhesive and reinforcement term can be expressed by comparing the influence of the interface reinforcement ratio (Figure 7-6, bottom). For smooth interfaces, the coefficient of friction of the proposed equation is defined to be lower compared to the [prEC2:18] approach. For small reinforcement ratios, the adhesive strength is the governing resistance term, which leads to higher calculated interface shear resistances. With increasing reinforcement ratio, the reinforcement term becomes the governing resistance and thus, smaller calculated interface resistance are achieved compared to [prEC2:18]. For rough interfaces, both resistance terms are introduced with higher roughness coefficients, which lead to higher calculated interface resistances for all test data. Even though a smaller friction coefficient is defined for very rough surfaces, higher interface resistances could be achieved for the very rough specimens with interface reinforcement ratios between $\rho_{int} = 0.18 – 1.1$ %.

Considering the influence of interface width, most specimens had small interfaces and only two specimens with large interfaces and rough surfaces could be evaluated (Figure 7-7). However, the two specimens with 800 mm interface width and low concrete strength ($f_{ck} = 18 – 24$ N/mm²) and low interface reinforcement ratios ($\rho_{int} = 0.19 – 0.39$ %) show interface resistances at the lower bound of test data. Thus, an influence of interfaces width on adhesive strength can also be assumed for interfaces with interface reinforcement.

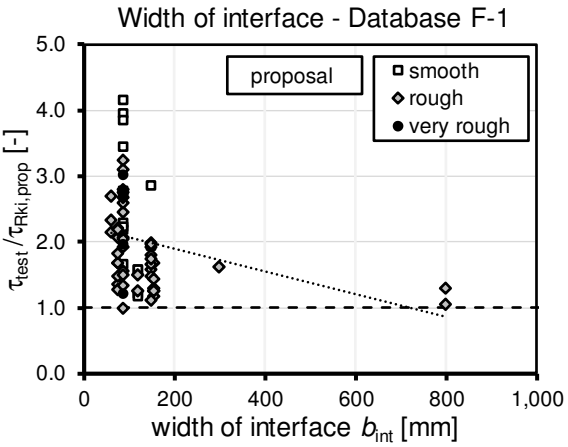

Figure 7-7: Database F-1 (structural members with reinforcement): Influence of interface width

7.4.4 Consideration of interface dimensions

The evaluation of database E with beam and slab specimens without interface reinforcement shows a decrease of experimental interface resistance with increasing width of interface. To improve the range of scatter for database evaluation, a parameter is derived considering the influence of interface width. In this context, Figure 7-8 (left) shows the development of related interface resistance according to the proposed equation with increasing interface dimension, separately for smooth and rough interfaces.

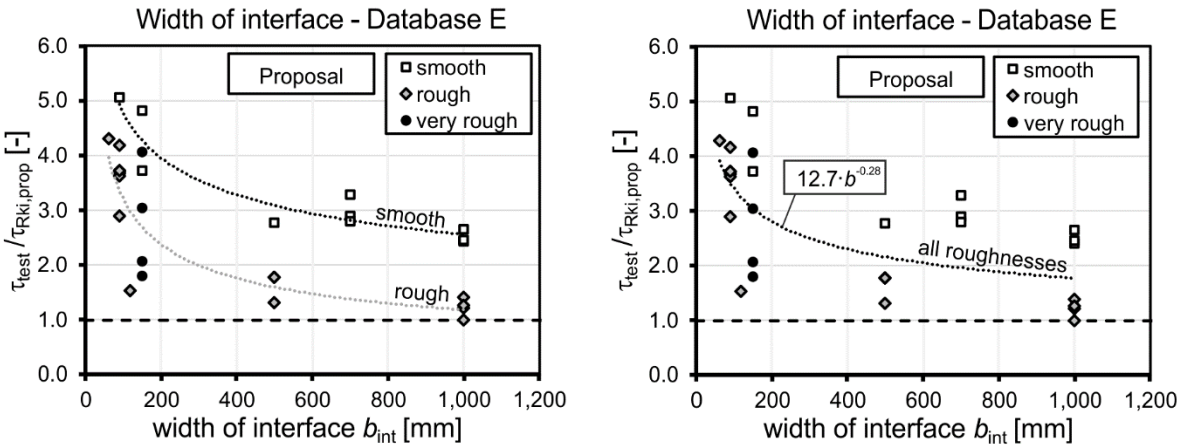

Figure 7-8: Database E (structural members without reinforcement): Influence of interface width for smooth and rough surfaces (left) and influence of interface width for all interface roughnesses (right)

For both interface classifications, the trendlines can be defined as power functions. For very rough interface, all specimens were conducted with b_{int} =150 mm. Thus, no trendline could be developed for very rough interface. To capture the development for all interface classes, the decreasing characteristic interface resistance can be described by the function as shown in Figure 7-8 (right). Applying this relation to the characteristic interface shear equation would lead to a mean value of X_m = 1.03 and a coefficient of variation of COV = 0.37, which therefore effects range of scatter as well as safety level of the design approach.

To only capture the influence of interface width on the range of scatter without effecting the level of safety, the test data was evaluated with the interface shear expression on mean level. Therefore, the mean coefficients of adhesion c_m and friction μ_m derived in Chapter 7.3.2 and 7.3.3 were applied to the design equation. The corresponding power function is shown in Figure 7-9 (left).

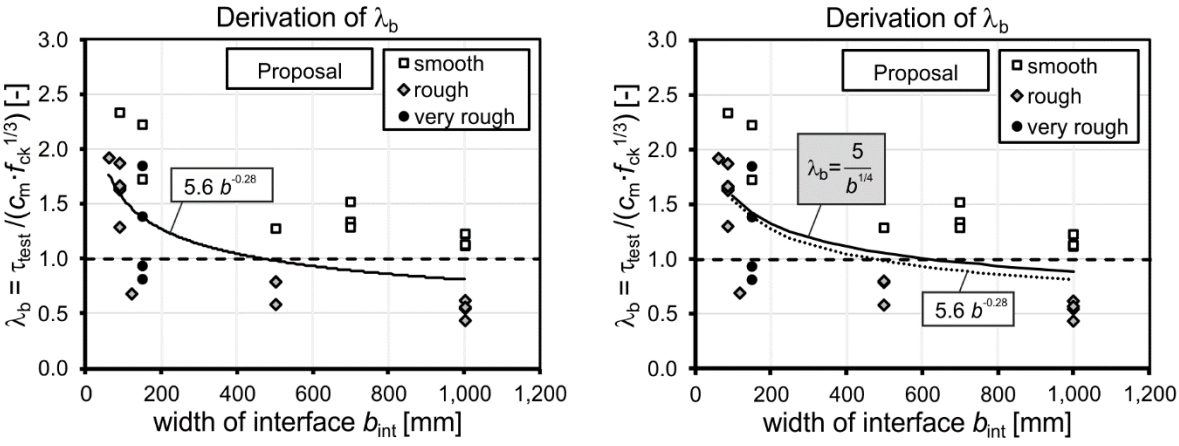

Figure 7-9: Determination of coefficient to consider the influence of width of interface

For applying the coefficient considering the influence of interface width on the adhesive term for database evaluation, the coefficient was defined as λ_b following Eq. (7-27). Compared to the best fit power function, the deviation of the expressions is about 3 % for small interfaces and 9 % for large interfaces (Figure 7-9 (right)).

$$\lambda_b = \frac{5}{b^{\frac{1}{4}}} \tag{7-27}$$

Applying this expression to the resistance function, the modified design expression follows Eq. (7-28).

$$\tau_{Rki,prop} = c \cdot f_{ck}^{\frac{1}{3}} \cdot \lambda_b + \mu \cdot \sigma_n \tag{7-28}$$

For small interfaces, regularly applied in e.g. T-beams or π-slabs, the factor leads to higher interface resistances. A beam with an interface of e.g. 300 mm would therefore gain an increased interface resistance of 20 %. For large interfaces in slab specimens, the interface width for verification is defined to be limited to b_{int} = 1.0 m. The interface resistance therefore decreases about 11 % compared to the initial resistance.

Applying the characteristic modified design expression with the derived coefficient of interface width λ_b to database E gives an evaluation of related interface resistance as summarised in Table 7-14. For comparison, Table 7-14 also holds the statistical evaluation data of the evaluation with the proposed design expression without the coefficient of interface width (Chapter 7.4.2) and of the [prEC2:18] expression (Chapter 6.4.2). Compared to the proposed expression without considering the interface width, the evaluation according to Eq. (7-28) yields in a decrease of mean value about 23 % to X_m = 2.20 with a decreased coefficient of variation about 23 % to COV = 0.37 and a corresponding characteristic 5 % quantile ratio of $X_{5\%}$ = 1.12. This large decrease of mean value and coefficient of variation was expected since the coefficient of interface width was derived with the test data in database E.

Table 7-14: Results of evaluation of Database E with new proposals and [prEC2:18]

Database E	Proposal λ_b	Proposal	prEC2:2018
No.	30	30	30
X_m	2.20	2.86	4.35
COV	0.37	0.48	0.51
$X_{5\%}$	1.12	1.17	1.70

X_m: mean value τ_{Rki}/τ_{calc}, COV: coefficient of variation, $X_{5\%}$: characteristic 5 % quantile ratio

The influence of concrete strength and interface width on the database evaluation of database E according to the modified expression including λ_b is shown in Figure 7-10. By applying the coefficient λ_b, the influence of concrete strength is affected indirectly

and gives a flatter trendline. The influence of interface dimension is now depicted trend free. Interfaces with smooth interfaces form the upper bound of test results whereas rough surfaces form the lower bound of test data.

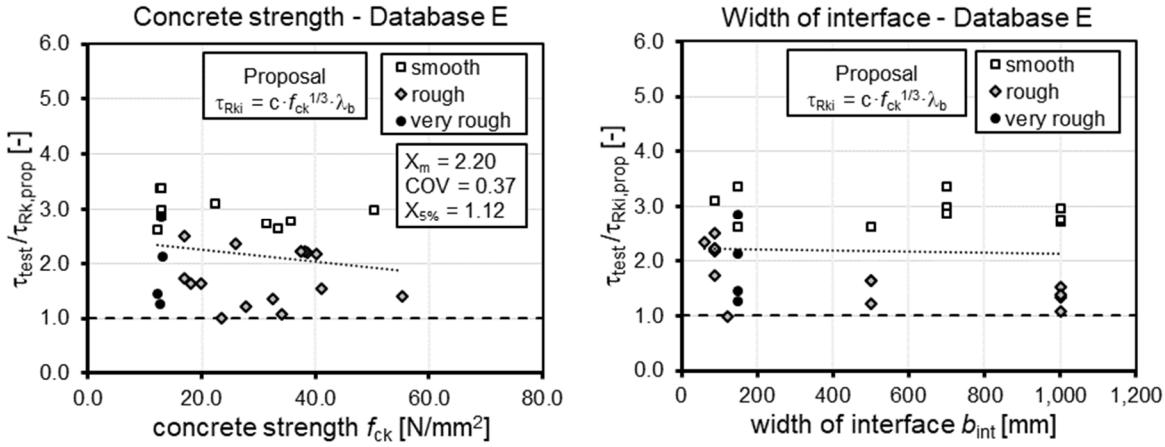

Figure 7-10: Database E (structural members without reinforcement): Influence of concrete strength and interface width design proposal including the coefficient of interface width λ_b

For smooth surfaces, the database evaluation shows an underestimation of experimental test data, independent from concrete strength and interface width. Since the bond development, especially for smooth surfaces with interfaces left as cast or additionally smoothened depict a critical range, a more conservative estimation of interface resistance seems reasonable. The calculated interface resistance of rough surfaces shows a better agreement with the experimental resistance for most specimens. Only for small interface widths, the experimental resistance exceeds the calculated resistance by its multiple.

For interfaces with interface reinforcement, considering the coefficient of interface width λ_b for the adhesive resistance yields to the characteristic interface design expression following Eq. (7-29).

$$\tau_{Rki,prop} = c \cdot f_{ck}^{1/3} \cdot \lambda_b + \mu \cdot \sigma_n + \rho_{int} \cdot f_{yk} \cdot (\mu \cdot \sin\alpha + \cos\alpha) \quad (7\text{-}29)$$

For applying this expression to the experimental data in Database F-1 with beam and slab specimens with interface reinforcement, the statistical evaluation data is shown in Table 7-15. For comparison, mean value X_m, coefficient of variation COV and characteristic 5 % quantile ratio $X_{5\%}$ of the database evaluation according the proposed expression without considering the effect of interface width (Chapter 7.4.3) and according to [prEC2:18] (Chapter 7) are added to Table 7-15.

Table 7-15: Results of evaluation of Database F-1 with new proposals and [prEC2:18]

Database F-1	Proposal λ_b	Proposal	prEC2:2018
No.	66	66	66
X_m	1.67	2.01	2.46
COV	0.31	0.36	0.38
$X_{5\%}$	0.95	1.05	1.23

X_m: mean value τ_{Rki}/τ_{calc}, COV: coefficient of variation, $X_{5\%}$: characteristic 5 % quantile ratio

Compared to the proposed expression without considering the influence of interface width, the mean value of the ratio of experimental to calculated interface resistance could be reduced about 17 % to $X_m = 1.67$ and the scatter could be reduced about 14% to COV = 0.31. The corresponding characteristic 5 % quantile ratio gives $X_{5\%} = 0.95$, which deceed the estimated value of $X_{5\%} = 1.00$ by 5 %. Regarding the effect of the coefficient of interface width on the evaluated data, it must be mentioned that most specimens in database F-1 were conducted with small interfaces and dimensions between $b_{int} = 75$ and 150 mm, partially due to application of brass or foil to decrease the effective area of bond in the interface. For these very small areas of interface, the coefficient of interface width gives an increased adhesive resistance between 43 and 70 %. In practice however, interfaces in precast beams or between beams and slabs are regularly larger. For more practical, but still small interface width of e.g. $b_{int} = 250$ mm, the increase of adhesive term would therefore be 26 %. Additionally, it must be mentioned that only three specimens were conducted with larger interface widths between 250 and 800 mm were tested. Thus, a decrease of interface resistance with increasing interface width can only be assumed.

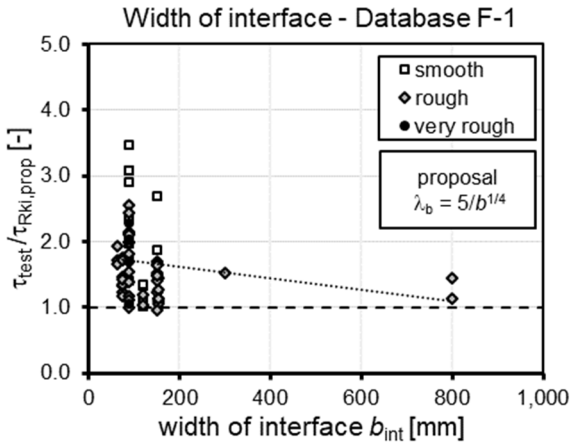

Figure 7-11: Database F-1 (structural members with reinforcement): Influence of interface width with modified design approach including the coefficient of interface λ_b

However, Figure 7-11 still shows an overestimation of calculated interface resistance for a large number of small interfaces. On the other hand, for the two specimens with

large interface widths of b_{int} = 800 mm and interface reinforcement, the adhesive resistance is reduced about 6 %. The calculated resistance exceeds the experimental resistance for only one specimen with an interface width of b_{int} = 150 mm. Thus, the small lower deviation of $X_{5\%}$ is mainly influenced by the large range of scatter, combined with the decrease of mean value for small interfaces and can therefore be accepted.

The magnitude of the influence of the interface width on the adhesive term of the interface resistance depends on concrete strength and reinforcement ratio. Due to the superposition of the adhesive resistance and the reinforcement resistance, an isolated consideration of both terms is not possible. Thus, Figure 7-12 shows the influence of concrete strength (left) and reinforcement ratio (right) on the related interface resistance. For high concrete strengths and small reinforcement ratios, the coefficient of interface width has a large effect on the interface shear resistance, whereas for small concrete strengths and high reinforcement ratios, the effect of the interface width is small.

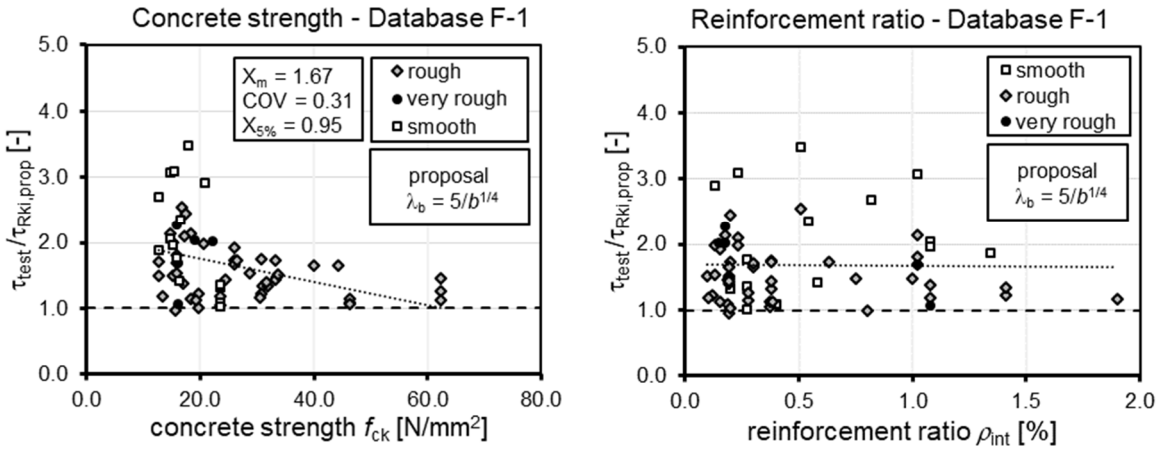

Figure 7-12: Database F-1 (structural members with reinforcement): Influence of concrete strength and reinforcement ratio with design proposal and coefficient of interface width λ_b

In contrast to the evaluation of beams and slabs without interface reinforcement, no bound of interface class can be determined by the specimens with interface reinforcement. Even though six specimens with smooth interfaces form the upper bound of related test data, the remaining tests scatter along the distribution of all test data. Whereas the related interface resistance still decreases with increasing interface width, the formulation describes the influence of the interface reinforcement almost trend free.

7.5 Proposal of design expression for interface shear

7.5.1 Introduction

In the previous chapters, a modified design expression for horizontal interface shear in beam and slab specimens was determined. The roughness coefficients considering the effect of interface surface were derived using selected databases. To consider the influence of interface width on the load bearing resistance of the adhesive term, an additional

parameter λ_b was derived. In this chapter, the modified interface shear equation is finalised and formulated to be adapted for design. Additionally, roughness coefficients are derived for the design equations of [prEC2:18] and the fatigue verification for interface shear is reviewed and revised.

7.5.2 Modified design proposal

The bases of the modified design expression for interface shear is the characteristic equation as shown in Chapter 7.4.4, Eq. (7-29). Compared to the evaluated codes in Chapter 6.4, the evaluation of databases with beam and slab specimens with and without interface reinforcement showed the best agreement of calculated and experimental interface resistance. Due to the high range of scatter, the coefficients of adhesion and friction were defined to guarantee a safe estimation for design.

As mentioned in Chapter 7.4.4, the coefficient of interface width λ_b was derived to consider the interface dimension without effecting the level of safety. Based on test results, the interface resistance is therefore increased for small interfaces and decreased for large interfaces as shown in Figure 7-13. Considering the range of application in practice, the adhesive resistance increases about 20 % for interface dimensions starting from b_{int} = 300 mm for beams and decreases about 11 % for slabs with b_{int} = 1000 mm. For an implementation of λ_b, it must be considered that for derivation of λ_b, only test data with varying interface width were available for smooth and rough interfaces. For very rough surfaces, only interface dimensions of 150 mm were tested and no specimens with very smooth surfaces were part of the databases. To cover the interface shear design of beam and slab specimens, an application of the minimum value to the design expression would lead to a general decrease of interface resistance and thus, to a large underestimation of interface resistance, especially for small interfaces. Therefore, the coefficient of interface width is defined to be λ_b = 1.0 for design. This corresponds to and interface width of b_{int} = 625 mm which can, in context of derivation of design equation, be defined as the mean interface width of beams and slabs for design.

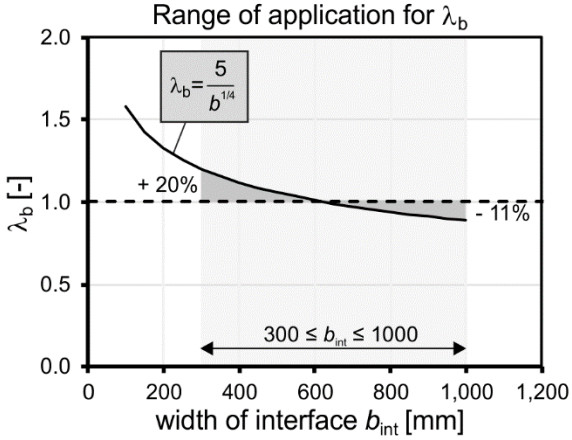

Figure 7-13: Influence of coefficient of interface width λ_b for practical range of application

The proposed design expression for interface shear stress in beam and slab specimens with $\lambda_b = 1.0$ therefore follows Eq. (7-30) with the coefficients of adhesion c and friction μ as summarised in Table 7-16.

Table 7-16: Roughness coefficients for proposed interface design expression

Interface	c	μ
very smooth	0.025	0.31
smooth	0.19	0.48
rough	0.39	0.78
very rough	0.46	0.80

$$\tau_{Rdi} = c \cdot \frac{f_{ck}^{\frac{1}{3}}}{\gamma_c} + \mu \cdot \sigma_n + \rho_{int} \cdot \frac{f_{yk}}{\gamma_s} \cdot (\mu \cdot \sin\alpha + \cos\alpha) \leq 0.5 \cdot \nu \cdot f_{cd} \tag{7-30}$$

With

γ_c partial safety factor for concrete $\gamma_c = 1.5$

γ_s partial safety factor for reinforcement with $\gamma_s = 1.15$

ν strength reduction factor

In accordance with [prEC2:18], the upper limit of shear resistance is defined by reducing the design concrete compressive strength by a strength reduction factor and the factor 0.5. This can be applied for angles of compression strut between $0 \leq \cot\theta \leq 2.5$ in ordinary reinforced members without normal force.

7.5.3 Modified approach for prEC2:2018

The presented modified interface design expression defined the adhesive resistance by the cubic root of the characteristic concrete compressive strength, whereas the approach according to [prEC2:18] defines the adhesive resistance by terms of the square root of the characteristic concrete compressive strength. The coefficients of adhesion defined in [prEC2:18] were derived by recalculating the coefficients defined in [EC2] to the $f_{ck}^{1/2}$ expression. In context of the revision process of roughness coefficients in this thesis, the coefficients of adhesion and partial safety factors for the [prEC2:18] approach were derived and validated following the procedure presented in Chapter 7.3 and 7.4.

For the resistance term of adhesion, the mean coefficients of adhesion were determined by database A-1 with small size tests without interface reinforcement and normal stress to achieve a mean value of $X_m = 1.0$ for each roughness class. The corresponding coefficients c_m are shown in Figure 7-14 (left).

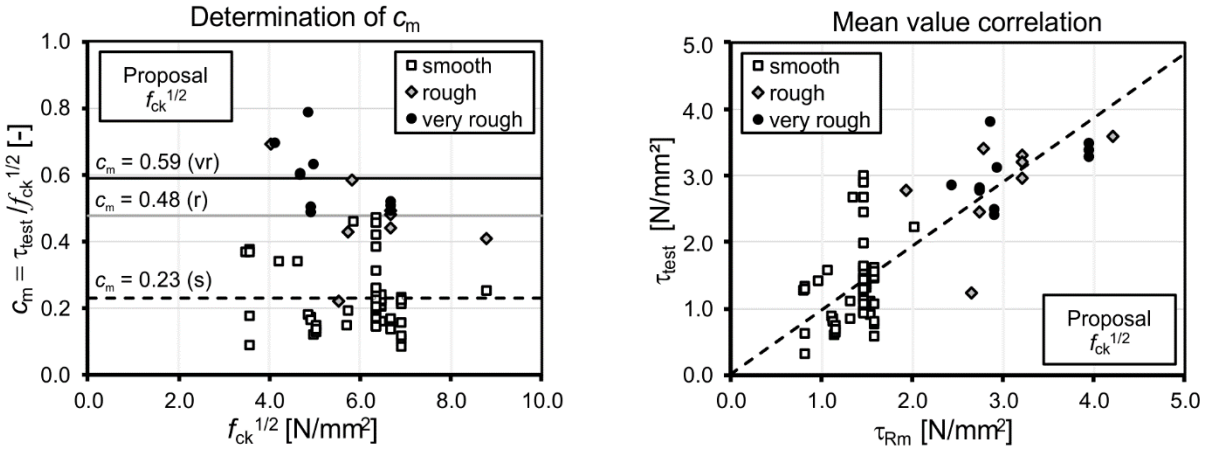

Figure 7-14: Determination of coefficient of adhesion for mean evaluation (left) and mean value correlation of experimental and theoretical data (right) for the [prEC2:18] approach

To derive a partial safety factor for adhesion, Eq. (7-31) shows the resistance equation including all basis variables.

$$V_{\mathrm{Rmi,adh}} = c_{\mathrm{m}} \cdot f_{\mathrm{ck}}^{1/2} \cdot b_{\mathrm{int}} \cdot 0.9 \cdot d \tag{7-31}$$

To determine the coefficients of variation of the basis variables, the partial derivatives are summarised in Table 7-17.

Table 7-17: Basis variables and corresponding partial derivatives for adhesive term for the [prEC2:18] approach

Basis variable X_i	f_{ck}	b_{int}	d
$\frac{\delta V_{\mathrm{Rmi,adh}}}{\delta X_i}$	$\frac{1}{2 \cdot f_{ck}} \cdot V_{\mathrm{Rmi,adh}}$	$\frac{1}{b_{int}} \cdot V_{\mathrm{Rmi,adh}}$	$\frac{1}{d} \cdot V_{\mathrm{Rmi,adh}}$

The calculation procedure to determine a partial safety factor for adhesion follows the procedure of [EC0], Annex D and the assumption of variation of basis variables as presented in Chapter 7.3.2 is summarised in Table 7-18.

The corresponding partial safety factor was determined to $\gamma_{adh} = 2.31$. For applying the partial safety factor to the characteristic approach of the design expression, the mean coefficients of adhesion were transferred to characteristic coefficients with $c_k = 0.7 \cdot c_m$ (Table 7-19, left). In the next step, the deviation of partial safety factor of adhesion to partial safety factor of concrete was implemented to the coefficients of adhesion as shown in Eq. (7-32).

Table 7-18: Calculation of partial safety factor for adhesion according to [EC0] Annex D for the [prEC2:18] approach

Basis variable X_i	X_m	σ_i	COV	$\frac{\delta V_{Rmi,adh}}{\delta X_i}$	$\left(\frac{\delta V_{Rmi,adh}}{\delta X_i}\cdot\sigma_i\right)^2$
f_{ck}	25 N/mm²	4.9 N/mm²	0.24	0.020	0.0096
b_{int}	250 mm	4.0 mm	0.016	0.004	0.0003
d	300 mm	9.0 mm	0.03	0.003	0.0009
				Σ =	0.0108
V_r = 0.65620		V_δ = 0.65620		V_{rt} = 0.00046	
Q_r = 0.59841		Q_δ = 0.59841		Q_{rt} = 0.00046	
γ_{adh} = 2.31		α_δ = 0.99999		α_{rt} = 0.00077	

$$\tau_{Rd,adh} = \frac{c_k \cdot f_{ck}^{\frac{1}{2}}}{\gamma_{adh}} = \frac{c_k \cdot f_{ck}^{\frac{1}{2}}}{\gamma_{Rd,adh} \cdot \gamma_c} = c \cdot \frac{f_{ck}^{\frac{1}{2}}}{\gamma_c} \text{ with } \gamma_c = 1.5 \tag{7-32}$$

With γ_{adh} = 2.31 and γ_c = 1.5, the model uncertainty implantation factor corresponds to $\gamma_{Rd} = \gamma_{adh,adh}/\gamma_c$ = 1.54. Implementing the measure of scatter to the derived characteristic c_k-values yields to the values $c = c_k/1.54$ for design. The corresponding c-values are summarised in Table 7-19 (left).

Table 7-19: Modified coefficients of adhesion (left) and database evaluation for the [prEC2:18] approach (right)

Interface	c_m	c_k	c	Evaluation of database A-1	
very smooth [1]	–	–	–	No.	83
smooth	0.23	0.16	0.11	X_m	2.09
rough	0.48	0.33	0.22	COV	0.37
very rough	0.59	0.41	0.27	$X_{5\%}$	1.08

[1]: no very smooth specimens in database – no determination possible at this stage

Evaluating database A-1 by comparing experimental test data to the calculated characteristic interface shear resistance according to Eq. (7-32) with coefficient of adhesion c according to Table 7-19 (left) without considering the partial safety factor leads to the statistical data as summarised in Table 7-19 (right). Compared to the [prEC2:18] approach, the derived coefficients of adhesion give a decrease of mean value about 30 % and an unchanged coefficient of variation. The corresponding characteristic 5 % quantile ratio decreases about 31 %.

The derivation of coefficient of friction and the partial safety factor for reinforcement in Chapter 7.3.3 was based on experimental data with bondbreaker and the assumption of no effective adhesive bond between the concrete layers. Thus, the derived coefficients

of friction are independent of the adhesive resistance and can therefore be adopted for the [prEC2:18] expression. However, to verify the interaction of the derived coefficients of adhesion with the coefficients of friction, database B with small size tests with interface reinforcement, database E with beam and slab specimens without interface reinforcement and database F-1 with beam and slab specimens with interface reinforcement were evaluated by comparing experimental and calculated characteristic resistance. The coefficients of adhesion and friction as well as the results of the database evaluation are shown in Table 7-20.

Table 7-20: Modified coefficients of adhesion and friction (left) with database evaluation for the modified [prEC2:18] approach (right)

Interface	c	μ		Database B	Database E	Database F-1
very smooth	0.01[(1)]	0.31	No.	266	30	66
smooth	0.11	0.48	X_m	1.48	2.98	2.07
rough	0.22	0.78	COV	0.27	0.51	0.37
very rough	0.27	0.80[(2)]	$X_{5\%}$	0.92	1.17	1.05

X_m: mean value τ_{Rki}/τ_{calc}, COV: coefficient of variation, $X_{5\%}$: characteristic 5 % quantile ratio, [(1)]: assumed based on [prEC2:18] and validated using tests with normal stress; [(2)]: subsequently derived

Compared to the database evaluation with the approach according to [prEC2:18], the evaluation with the modified coefficient of adhesion and friction yields to an overall improvement of mean value and coefficient of variation. The lower deviation of the database B evaluation with small size tests with interface reinforcement is in accordance with Chapter 7.3.3. Due to concentrated load application, small interfaces with small numbers of reinforcement bar, database B depicts an adverse case for evaluation. Thus, a small lower deviation of 8 % to the reference value $X_{5\%} = 1.0$ can be accepted. The evaluation of database E gives a 31 % lower mean value with unchanged coefficient of variation. For database F-1, the mean value decreases about 16 % and the coefficient of variation reduces about 3 % with a corresponding reduction of characteristic 5 % quantile ratio about 15 %.

7.5.4 Proposal for fatigue

For fatigue, the verification of concrete interfaces distinguishes between interfaces with interface reinforcement and interfaces without interface reinforcement. The applied shear stress of the cyclic loading is therefore based on the frequent load combination. For interfaces without interface reinforcement, the maximum of the applied shear stress must be limited. Thus, the maximum applied fatigue strength can be calculated according Eq. (7-33) with $\gamma_{c,fat} = 1.5$.

$$\tau_{max,Rdi} = 0.5 \cdot c \cdot \frac{f_{ck}^{\frac{1}{3}}}{\gamma_{c,fat}} + \mu \cdot \sigma_n \tag{7-33}$$

The reduction of the adhesive strength to 50 % under monotonic loading conditions is based on the regulations defined in [EC2], [prEC2:18] and [MC10], which are based on the results of experimental investigations where no considerable interface displacement could be determined for applied maximum stress about 50 % of the static resistance (s. Chapter 4.2.5).

For validating the expressions, only six tests with beam and slabs under cyclic loading conditions could be evaluated. As mentioned in Chapter 0, the applied maximum resistances exceeded the calculated static interface resistances according to [EC2], [prEC2:18] and [MC10] by their multiple. This also applies to the modified design expression and the modified [prEC2:18] approach with exceeding the static interface resistance between 125 % and 260 %. The tested residual resistance after reaching the reference number of load cycles exceeded the static interface resistance between 275 % and 435 %. Thus, the defined limitation for fatigue gives a safe estimation of applied maximum shear stress for interface shear.

For concrete interfaces with interface reinforcement, the verification follows a limitation of the characteristic stress range $\Delta\sigma_{Rsk}$ in the reinforcement bars with a partial safety factor of steel for fatigue of $\gamma_{s,fat} = 1.15$. Therefore, the applied stress range $\Delta\tau_{Ed}$ is calculated based on the frequent load combination. According to [EC2], 50 % of the adhesive strength can be accounted for fatigue, whereas [EC2NAD] omits the adhesive resistance. The regulations in [prEC2:18] neglects the adhesive resistance and a reduced inclination of compression strut from 45° to 25° is assumed. By assuming that the compression strut declines with a flatter inclination, more stirrups can be activated. The favourable effect of the flatter inclination is considered by a reduction factor of $1/\cot\theta \approx 0.45$ with $\theta = 25°$.

To define a fatigue verification for interface reinforcement, the applied stress ranges in the beam and slab specimens of database H-1 were calculated based on the modified interface shear equation with the fatigue provisions of [EC2NAD], [EC2] and [prEC2:18] (Figure 7-15). For evaluation, the term of normal stress and partial safety factors were not considered. For comparison, the ratio of calculated stress ranges to approved stress ranges according to the S-N curves defined in [EC2] are depicted over the borne number of load cycles in Figure 7-15.

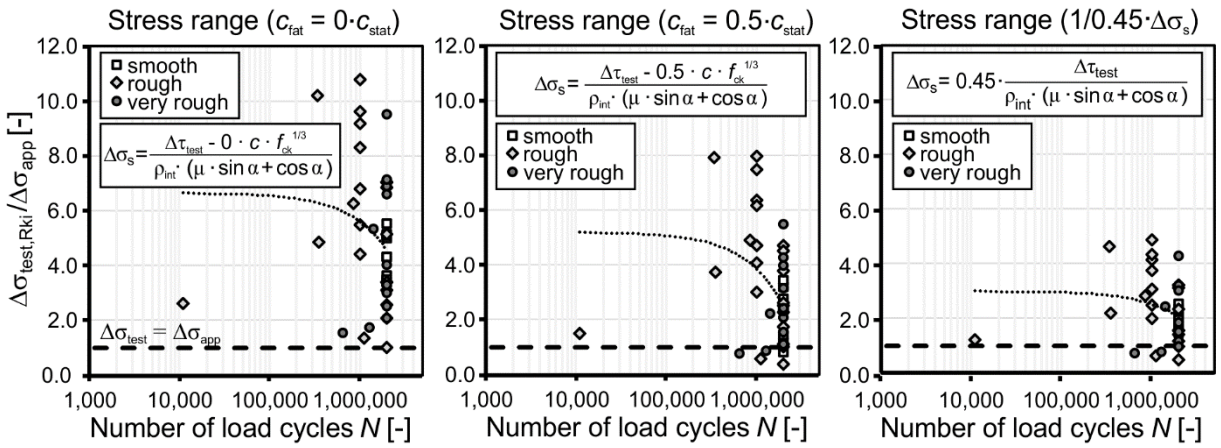

Figure 7-15: Comparison of calculated and approved stress ranges

In accordance with [EC2NAD], the adhesive resistance was not considered ($c_{fat} = 0 \cdot c_{stat}$) in Figure 7-15 (left), which shows an underestimation of approved stress ranges compared to the applied stress ranges with a high range of scatter, especially for high numbers of borne load cycles. Reducing the applied stress range to 50 % of the static adhesive term in accordance to [EC2] (Figure 7-15, (middle)) leads to a general reduction of applied stress ranges, but still shows high scattering. The approved stress ranges deceed the approved stress range for three specimens with prior fatigue failure and two specimens which reached the reference number of load cycles. Thus, assuming 50 % of the adhesive strength for verifying the stress range may lead to a somehow unsafe estimation. Neglecting the adhesive term and assuming a reduced inclination of compression strut in accordance to [prEC2:18] (Figure 7-15, (right)) leads to a decrease of scatter but to an overestimation of stress range for three specimens with fatigue failure.

Since the fatigue verification based on the [prEC2:18] regulations show the smallest range of scatter, the expression was modified to achieve a safe estimation of stress range resistance for interface reinforcement. Therefore, it was assumed that the inclination of compression strut results in $\theta = 30°$, which corresponds to a reduction factor of $1/\cot\theta \approx 0.6$. A reduction factor of 0.6 has been defined in previous design regulations of DIN 1045:88 [D1045] for fatigue of interface reinforcement and has been adopted for the verification of lattice girders in the general technical approvals (e.g. [DZ-93][DZ-38]). Comparison calculations with semi-precast slabs with lattice girder under cyclic loading condition in Chapter 5.4.6 show the best accordance of calculated shear stress to approved stress ranges compared to the design expression of [EC2NAD] and [EC2]. Adopting this assumption to the fatigue verification of interface reinforcement according to the modified design expression and neglecting the term of adhesion, leads to the expression in Eq. (7-34). Accordingly, the calculation of stress range with omitting the term of normal stress follows Eq. (7-35).

$$\Delta\tau_{Rdi} = \mu \cdot \sigma_n + \frac{1}{0.6} \cdot \rho_{int} \cdot \frac{\Delta\sigma_{Rsk}}{\gamma_{s,fat}} (\mu \cdot \sin\alpha + \cos\alpha) \tag{7-34}$$

$$\frac{\Delta\sigma_s}{\gamma_{s,fat}} = 0.6 \cdot \frac{\Delta\tau_{Ed}}{\rho_{int} \cdot (\mu \cdot \sin\alpha + \cos\alpha)} \tag{7-35}$$

The evaluation of calculated stress range according to Eq. (7-35) without considering partial safety factors, related to the approved characteristic stress ranges is shown in Figure 7-16. It can be seen, that the factor 0.6 still leads to a reduced range of scatter for the evaluated test data, but only one test with prior fatigue failure and one test which reached the reference number of load cycles deceed the approved stress range. Combined with the improved scatter of test data, the proposed expression presents a sufficient approach for fatigue design of interface reinforcement.

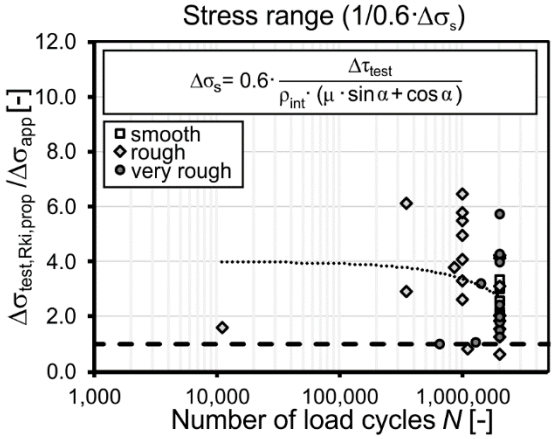

Figure 7-16: Comparison of calculated to approved stress range according to the proposed fatigue verification

For the verification of semi-precast slabs with lattice girders, database H-2 was evaluated with the proposed fatigue equation and considering all interface roughnesses. The calculated characteristic stress range was related to the approved stress range according to the S-N-curves derived in Chapter 4 and plotted over the borne number of load cycles (Figure 7-17). It can be seen, that the proposed fatigue verification shows a good agreement of applied and approved stress ranges for the specimens in database H-2 for all borne number of load cycles.

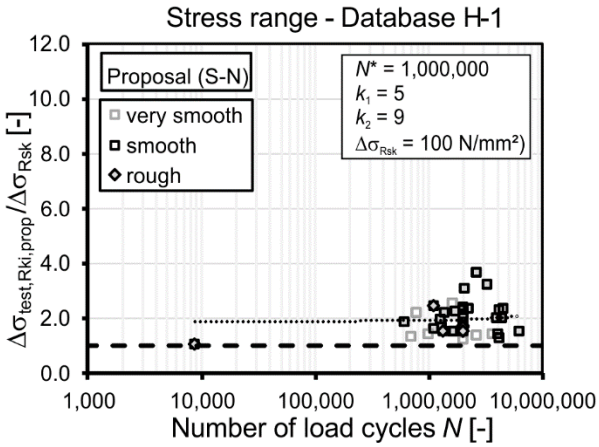

Figure 7-17: Comparison of calculated to approved stress range according to the proposed fatigue verification for database H-2 with semi-precast slabs with lattice girders

7.6 Summary

In the previous chapter, a modified interface shear design equation was proposed based on the design regulations according to the draft for the new Eurocode 2 [prEC2:18]. The design equation describes the interface shear resistance based on the model concepts of *Mohr-Coulomb* combined with shear friction theory by terms of adhesion, friction induced by externally applied normal stress and by clamping of the interface reinforcement. The resistance term of adhesion is defined to be proportional to the cubic root of the characteristic concrete compressive strength, which shows a better accordance to results of experimental investigations than the approach of the square root of the concrete compressive strength as defined in [prEC2:18]. To capture the influence of interface roughness, the coefficients of adhesion and friction were derived using isolated test data. The coefficient of adhesion was derived by small size tests without normal stress and interface reinforcement and the coefficient of friction was derived by small size tests with interface reinforcement and impaired bond conditions to prevent adhesive bond. To account for a sufficient level of reliability, partial safety factors were derived for adhesion and friction using the probabilistic evaluation method according to [EC0], Annex D. The derived partial safety factors for adhesion is $\gamma_{adh} = 2.30$ and for friction $\gamma_{adh} = 1.80$. For design, the coefficients of adhesion and friction were adjusted to provide a design procedure based on the safety concept of [prEC2:18] with the partial safety factors $\gamma_c = 1.5$ for concrete and $\gamma_s = 1.15$ for reinforcing steel. To verify the applicability of the design approach to structural members, the design approach was validated systematically using databases with beam and slab specimens with and without interface reinforcement. Compared to small size tests, the database evaluation shows a decrease of interface resistance with increasing interface width for the adhesive term. Thus, a coefficient of interface width for the adhesive term is derived, which show a better agreement of experimental and calculated resistance. Especially for small interface dimensions, the interface resistance increase. However, for the practical range of interface width, the coefficient of interface width yields to a small increase for small interfaces in

beams and a small decrease for large interfaces in slabs. Thus, for practical reasons, the influence of interface width can be omitted for design.

To implement the presented procedure to the adhesive resistance term as defined in the expression of [prEC2:18], roughness coefficients of adhesion were derived for the approach describing the adhesive resistance to be proportional to the square root of the characteristic concrete compressive strength.

Table 7-21 summarises the results of the database evaluation of database E with 30 beam and slabs specimens without interface reinforcement by comparing the experimental resistance to the calculated characteristic interface resistance. Therefore, mean value X_m, coefficient of variation COV and characteristic 5 % quantile ratio $X_{5\%}$ according to the modified approach considering the coefficient of interface width λ_b, to the modified design proposal without λ_b, to the modified approach of [prEC2:18] and [prEC2:18] are compared.

Table 7-21: Overview of database evaluation of database E (30 beam and slabs specimens without interface reinforcement)

τ_{test}/τ_{Rki}	Modified approach considering interface width λ_b	Modified design proposal	Modified prEC2:2018	prEC2:2018
X_m	2.20	2.86	2.98	4.35
COV	0.37	0.48	0.51	0.51
$X_{5\%}$	1.12	1.17	1.17	1.70

X_m: mean value τ_{Rki}/τ_{calc}, COV: coefficient of variation, $X_{5\%}$: characteristic 5 % quantile ratio

For beam and slab specimens with stirrups as interface reinforcement, Table 7-22 summarises the results of the database evaluation of database F-1 with 66 specimens.

Table 7-22: Overview of database evaluation of database F-1 (66 beam and slabs specimens with stirrups as interface reinforcement)

τ_{test}/τ_{Rki}	Modified approach considering interface width λ_b	Modified design proposal	Modified prEC2:2018	prEC2:2018
X_m	1.67	2.01	2.07	2.46
COV	0.31	0.36	0.37	0.38
$X_{5\%}$	0.95	1.05	1.05	1.23

X_m: mean value τ_{Rki}/τ_{calc}, COV: coefficient of variation, $X_{5\%}$: characteristic 5 % quantile ratio

The proposed modified design expression improves the interface shear design with reduced mean value and coefficient of variation compared to the design codes evaluated in Chapter 6. The corresponding characteristic 5 % quantile ratio show a safe and more efficient estimation of experimental test data by the characteristic design approaches.

For the fatigue verification of interfaces without interface reinforcement, the adhesive resistance is reduced to 50 % of the static adhesive strength in accordance to [prEC2:18]. For the verification of stress range in the interface reinforcement for reinforced interfaces under cyclic loading conditions, the load resistance term was omitted. The favourable effect of a flatter inclination of compression strut is considered by a reduction factor of $1/\cot\theta \approx 0.6$ with $\theta = 30°$. The comparison of calculated stress ranges from fatigue tests and approved stress ranges from S-N-curves show a better agreement compared to the fatigue regulations in the current European codes for both, stirrups as lattice girders as interface reinforcement.

8 Conclusion and Outlook

8.1 Conclusion

Horizontal interfaces between concrete cast at different times in composite beam and slab structures commonly occur in building practice due to section wise concrete casting or in precast construction. To achieve a quasi-monolithic load bearing behaviour of the composite structure, shear transfer across the interface must be ensured to verify the bending resistance. In literature, five important mechanisms exist to describe interface shear transfer. Starting with shear friction theory, which defined interface shear resistance by the clamping effect of the interface reinforcement, further modifications were proposed considering adhesive resistance, concrete strength, aggregate interlock, and dowel action. In construction practice, the design regulations of Eurocode 2, Eurocode 2 with the National Annex of Germany, the draft for the next Eurocode 2, ACI 318-14 and AASHTO LFRD simplify interface shear resistance with terms for adhesion, friction induced by normal stress, and friction induced by clamping of interface reinforcement. The regulations of Model Code 2010 and the new approach of Eurocode 2 for concrete toppings extend the resistance term of interface reinforcement by additionally considering the effect of dowel action. Various test programmes were conducted by researchers to develop and verify these design regulations. The test programmes included small size and structural member tests and covered concrete interfaces with and without normal stress and interface reinforcement, as well as monotonic and cyclic loading conditions. Even though the aforementioned design regulations were built upon similar theoretical considerations, different regulations result in calculated interface resistances that differ up to several orders of magnitude.

The objective of this thesis was to revise and assess the aforementioned interface shear regulations and to develop an improved design formulation in terms of efficiency and level of safety for monotonic and cyclic loading conditions. In order to assess the considered design equations, databases were compiled based on comprehensive literature research and own experimental investigations. The databases comprise 553 small size tests and 201 composite beam and slab structures. For both test setups, the influences of load resistance terms (interfaces without normal stress and interface reinforcement for adhesion, interfaces with externally applied normal stress and interfaces with reinforcement) and loading conditions (monotonic and cyclic loading) were evaluated separately. The comparison between experimental ultimate interface strength and calculated characteristic interface shear resistance was utilised to assess efficiency and level of safety of the design equations. For all evaluated design equations and databases, high scatter were observed. The roughness classifications and definitions of adhesive resistance by terms of concrete strength, as defined in European codes, yield better agreement of test data compared to the American codes, which define constant adhesive strengths for interfaces intentionally roughened and not intentionally roughened. As expected, struc-

tural member tests show more scatter compared to small size tests. The largest coefficients of variation (magnitude of scatter) were determined for interfaces without interface reinforcement and normal stress. With increasing interface roughness, the scatter of related test data decreases. For specimens with interface reinforcement, the range of scatter decreases for both, small size tests and structural member tests. The additional load bearing resistance of dowel action according to Model Code 2010 gives a more conservative estimation of shear resistance. However, the combination of high coefficients of variation for beam and slab specimens, COV = 0.51 – 0.64 (no interface reinforcement) and COV = 0.38 – 0.44 (interface reinforcement), and high mean values, X_m = 4.35 – 4.86 (no interface reinforcement) and X_m = 2.27 – 3.91 (with interface reinforcement), results in 5 % quantile ratios about $X_{5\%}$ = 1.70 (no interface reinforcement) and X_m = 1.11 – 1.76 (interface reinforcement). Thus, the design expressions give a safe but conservative estimation of interface resistance.

In the evaluated test data, the related interface resistance decreases with increasing concrete strength. Defining the adhesive resistance by terms of the square root of the characteristic concrete compressive strength according to the new draft for Eurocode 2 gave the best agreement with the test data. For the resistance of interface reinforcement, the expression of the clamping effect showed a better agreement of test data compared to the expressions with an additional term for dowel action. Further parameters like shear slenderness and prestressing of precast concrete showed no significant effect, due to very high scatter. Whereas no influence of interface dimensions was determined for small size tests, a decrease of interface resistance was observed for increasing interface width in structural members.

Specimens subjected to cyclic loading were only evaluated with the European Codes because the American Codes do not provide regulations for fatigue in concrete interfaces. Reducing the adhesive resistance to 50 % of the static resistance gives a safe estimation for interfaces without interface reinforcement. To verify the stress range in the interface reinforcement, the assumption of a reduced adhesive resistance gives a conservative but safe estimation of approved stress ranges. Neglecting the adhesive resistance and assuming a flatter inclination of the compression strut of 25° results in smaller calculated stress ranges which may lead to somehow unsafe estimations.

A modified interface shear design expression was proposed for efficient and safe estimation of interface resistance. The proposed equation is based on the design concept for the next Eurocode 2, but defines the adhesive resistance as a function of the cubic root of the characteristic concrete compressive strength. The coefficients of adhesion and friction were derived separately using isolated databases. To account for a sufficient level of safety, partial safety factors for adhesion and friction were derived by means of probabilistic evaluation methods in accordance to Eurocode 0. An additional coefficient of interface width was derived for the adhesive resistance term to account for the inverse

relationship between interface width and interface shear resistance for structural members. The proposed equation was validated with experimental test results of structural members without interface reinforcement and improves the ratio of experimental to calculated characteristic resistance by 23 % (mean value $X_m = 2.20$, coefficient of variation COV = 0.37). For structural members with interface reinforcement, the proposed design expression also improves the ratio of experimental to calculated characteristic resistance by 17 % (mean value $X_m = 1.67$) and 14 % (coefficient of variation COV = 0.31), respectively. In order to apply the proposed interface shear expression in building practice, additional roughness coefficients and partial safety factors were derived for the draft of the next Eurocode 2. Furthermore, the partial safety factors and the coefficient of interface width were simplified for the common design expression.

To extend the understanding of monotonically loaded interfaces to cyclic loading conditions, a new experimental programme on the fatigue behaviour of semi-precast slabs with lattice girders as interface reinforcement was conducted. The test parameters of the 14 slab specimens with two sub-tests were interface roughness, slab thickness, interface reinforcement ratio and concrete strength. Besides higher scatter in fatigue test data compared to static tests, influences of interface roughness, interface reinforcement ratio, slab thickness, and steel strains in the lattice girders were observed. Even though the determined stress ranges in the lattice girders were considerably higher compared to the approved stress range according to the technical approvals, the fatigue design regulations of lattice girders were generally confirmed. With S-N-curves for lattice girders derived from small size tests, the range of application of semi-precast slabs for fatigue was extended and a better agreement of calculated stress ranges with test data was achieved.

For the fatigue verification of stress range in the interface reinforcement, the design concept of the next generation of Eurocode 2 was revised and adjusted by applying the roughness coefficients of the proposed design expression. Furthermore, a steeper inclination of compressive strut of 30° is assumed based on the own experimental investigations with lattice girders. The comparison of calculated stress ranges in fatigue tests and approved stress ranges showed a better agreement and safe estimation.

8.2 Future research

Past research has significantly contributed to the understanding of horizontal shear stress in composite beam and slab structures. Nevertheless, further research is needed in order to advance current knowledge. Some major topics for future research are:

- Interfaces in continuous beams and slabs: The design regulations for interface shear were derived by small size tests and simply supported structural member tests. For continuous beams and slabs, higher interface shear resistances can be

expected due to restraints for horizontal displacement in the area of the mid-supports. The influence of the structural system for monotonic and cyclic loading conditions is still outstanding and needs to be investigated.

- Influence of interface location in the cross section: Interface failure in simply supported composite beam and slab structures generally occurs after flexural cracks start from the bottom of the cross section and develop to shear cracks. In case of insufficient interface resistance, the shear cracks proceed along the interface. Whereas interfaces in composite slabs are generally located at the bottom of the cross section, interfaces in beam-slab connections in T-beams are commonly located at the top of the cross section. Thus, for simply supported beams, higher interface resistances can be expected in T-beams. The influence of interface location on interface resistance as well as the effect of the reverse crack development at mid-supports in continuous structures requires further investigations.

- Influence of interface width: The database evaluation showed an increase of interface resistance with increasing interface width for structural members, which might be constituted by the higher potential of blemished in the interface. This effect was captured by an empirical coefficient of interface width in the own proposal. To verify this inverse relationship, systematic test series with varying interface width combined with varying interface roughnesses are necessary.

- Verification of comprehensive roughness coefficients: The roughness coefficients for the proposed design equation were derived by databases with small size tests. For the determination of the coefficient of adhesion, no specimens with very smooth surfaces could be evaluated. For the friction coefficient, no specimens with very rough surfaces and impaired bond were available in the databases. Thus, the corresponding coefficients were extrapolated based on existing regulations and validated with existing test data. To verify the extrapolated coefficients, appropriate test data is necessary to ensure an efficient and safe design.

- Transferability of small size and structural member tests: Interface shear in small size tests is localised to small interfaces with concentrated load application, whereas interface shear in beam and slab structures develops due to composite action. However, compared to structural member tests, small size tests present an efficient method to investigate the influence of several parameters on interface shear resistance. To minimise the scatter of tests results, consistent test series with small size tests and structural member tests can be conducted with similar interface roughness to investigate the transferability of the different test setups considering influences of e.g. different stress states or size effects.

References

[AA-L] AASHTO LFRD Bridge Design Specifications, American Association of State Highway and Transportation Officials, 7. Edition, 2014.

[AA-S] AASHTO Standard Specifications for Highways Bridges. American Association of State Highway and Transportation Officials, 17. Edition, 2002.

[Abe72] ABELES, P.W.; BROWN, E.I., HU, C.H.: Tests of composite concrete beams with prestressed planks. Materiaux et Construction, Vol. 5, No. 25, pp. 31–41, 1972.

[ACI318] ACI 318-14: Building Code Requirements for Structural Concrete. American Concrete Institute, 2015.

[Ack92] ACKERMANN, G.; BURKHARDT, M.: Tragverhalten von bewehrten Verbundfugen bei Fertigteilen und Ortbeton in den Grenzzuständen der Tragfähigkeit und Gebrauchstauglichkeit. Beton und Stahlbetonbau, Vol. 87, Issue 7, S. 165 – 170, 1992.

[Alb14] ALBRECHT, C.: Bemessung von Stahlbetondecken mit abgeflachten rotationssymmetrischen Hohlkörpern und ein Beitrag zum besseren Verständnis der Querkrafttragfähigkeit. PhD Thesis, Institute of Structural Concrete, Technische Universität Kaiserslautern, 2014.

[Ann90] ANNAMALAI, G.; R.C. BROWN: Shear-Transfer Behavior of Post-Tensioned Grouted Shear-Key Connections in Precast Concrete-Framed Structures. ACI Structural Journal, Vol. 87, No. 1, pp.: 53-59, 1990.

[And60] ANDERSON, A.R.: Composite designs in precast and cast-in-place concrete, Progressive Architecture, Vol. 41, No. 9, pp. 172-179, September 1960.

[Bad65] BADOUX, J.C.: Horizontal shear connection in composite concrete beams under repeated loading. PhD Thesis, Lehigh University, 1965.

[Bad67] BADOUX, J.C.; HULSBOS, C.L.: Horizontal shear connection in composite concrete beams under repeated loads. Journal of the American Concrete Institute, Vol. 64, No. 12, pp. 811-819, December 1967.

[Ban05] BANTA, T.E.: Horizontal shear transfer between ultra high performance concrete and lightweight concrete. PhD-Thesis, Virginia Polytechnic Institute and State University, 2005

[Bar17] BARBOSA A, TREJO, D.; NIELSON, D.: Effect of High-Strength Reinforcement Steel on Shear Friction Behavior. Journal of Bridge Engineering, Vol. 22, No. 8, 2017.

[Bas89] BASS, R. A.; R. L. CARRASQUILLO; J. O. JIRSA: Shear Transfer Across New and Existing Concrete Interfaces. ACI Structural Journal, Vol. 86, No. 4, pp.: 383-393, 1989.

[Bec73] BECK, H.; MEHLHORN, G.; STAUDER, W.; SCHWING, H.: Zusammenwirken von einzelnen Fertigteilen als großflächige Scheibe. Deutscher Ausschuss für Stahlbeton DAfStb, Issue 224, Beuth Verlag, 1973.

[Ber89] BERTRAM, D.; BUNKE, N.: Erläuterungen zu DIN 1045 Beton und Stahlbeton, Ausgabe 07.88. Deutscher Ausschuss für Stahlbeton DAfStb, Issue 400, Beuth Verlag, Berlin, 1989.

[Beu05] BEUSHAUSEN, H.: Long-term performance of bonded concrete overlays subjected to differential shrinkage. PhD Thesis, University of Cape Town, South Africa, 2005.

[Bir66] BIRKELAND, P.W.; BIRKELAND, H.W.: Connections in Precast Concrete Construction. Journal of the American Concrete Institute, Title no. 63-15, pp. 345-367, March, 1966.

[BIR68] BIRKELAND, H.W.: Precast and prestressed concrete. Class notes for course, University of British Columbia, 1968.

[Blo89] BLOCK, M.: Spritzbeton auf carbonisiertem Beton – Haftzugfestigkeit bei nachträglich ergänzten Querschnitten. Beton, No. 7, S. 299-302, 1989.

[Blo98] BLOCK, M.: Oberflächenrauheut und Haftverbund – Spritzbetonverstärkte Bauteile. Beton, No. 2, S. 74-79, 1998.

[Blo03] BLOCK, K.; DREIER, F.: Das Ermüdungsverhalten von Dübelbefestigungen. Deutscher Ausschuss für Stahlbeton DAfStb, Issue 541, Beuth Verlag, Berlin, 2003.

[Bux86] BUXBAUM, O.: Betriebsfestigkeit – Sichere und wirtschaftliche Bemessung schwingbruchgefährdeter Bauteile. Verlag Stahleisen, 1986.

[Che88] CHEN, W.F.; HAN, D.J.: Plasticity for Structural Engineers. Springer Verlag, New York, 1998.

[Cho99] CHOI, D.U.; JIRSA, J.O.; FOWLER, D.W.: Shear Transfer across Interface between New and Existing Concretes Using Large Powder-Driven Nails. ACI Structural Journal, Title no. 96-S20, pp. 183-192 March-April, 1999.

[Chu76] CHUNG, H.W.; CHUNG, T.Y.: Prestressed concrete composite beams under repeated loading. ACI Journal, Title No. 73.24, pp. 291-295, May 1976.

[D488] DIN 488-1:2009-08: Betonstahl – Teil1: Stahlsorten, Eigenschaften, Kennzeichnungen. Deutsches Institut für Normung (DIN), German version, Beuth Verlag, Berlin, 2009.

[D1045] DIN 1045:88: Beton- und Stahlbeton, Bemessung und Ausführung. Deutsches Institut für Normung (DIN), German version, Beuth Verlag, Berlin, 1988.

[D1045-1] DIN 1045-1:2008-08: Tragwerke aus Beton, Stahlbeton und Spannbeton – Teil 1: Bemessung und Konstruktion. Deutsches Institut für Normung (DIN), German version, Beuth Verlag, Berlin, 1988.

[D1766] DIN EN 1766:2017-06: Produkte und Systeme für den Schutz und die Instandsetzung von Betontragwerken – Prüfverfahren – Referenzbetone für Prüfungen. Deutsches Institut für Normung (DIN), German version, Beuth Verlag, Berlin, 2017.

[D4287] DIN EN ISO 4287:2010-07: Geometrische Produktspezifikationen (GPS) – Oberflächenbeschaffenheit: Tastschnittverfahren – Benennung, Definition und Kenngrößen der Oberflächenbeschaffenheit. DIN Deutsches Institut für Normung (DIN), German version, Beuth Verlag, Berlin, 2010.

[D13036] DIN EN 13036-1:2010-10: Oberflächeneigenschaften von Straßen und Flugplätzen – Prüfverfahren – Teil 1: Messungen der Makrotexturtiefe der Fahrbahnoberfläche mit Hilfe eines volumetrischen Verfahrens. DIN Deutsches Institut für Normung (DIN), German version, Beuth Verlag, Berlin, 2010.

[D13473] DIN EN ISO 13473-1:2004-07: Charakterisierung der Textur von Fahrbahnbelägen unter Verwendung von Oberflächenprofilen – Teil 1: Bestimmung der mittleren Profiltiefe. Deutsches Institut für Normung (DIN), German version, Beuth Verlag, Berlin, 2004.

[D15630] DIN EN ISO 15630-1:2011-02: Stähle für die Bewehrung und das Vorspannen von Beton Prüfverfahren – Teil 1: Bewehrungsstäbe, -walzdraht und -draht. Deutsches Institut für Normung (DIN), German version, Beuth Verlag, Berlin, 2011.

[D50100] DIN 50100:2016-12: Schwingfestigkeitsversuch – Durchführung und Auswertung von zyklischen Versuchen mit konstanter Lastamplitude für metallische Werkstoffproben und Bauteile. Werkstoffprüfung Dauerschwingversuch, Begriffe, Zeichen, Durchführung, Auswertung. Deutsches Institut für Normung (DIN), German version, Beuth Verlag, Berlin, 2016.

[DA600] DEUTSCHER AUSSCHUSS FÜR STAHLBETON: Erläuterungen zu DIN EN 1992-1-1 und DIN EN 1992-1-1/NA (Eurocode 2). DAfStb, Issue 600, Beuth Verlag, Berlin, 2012.

[Das82] DASCHNER, F.; KUPFER, H.: Versuche zur Schubkraftübertragung in Rissen von Normal- und Leichtbeton. Der Bauingenieur, Vol. 57, pp. 57-60, 1982.

[Das86a] DASCHNER, F.: Versuche zur notwendigen Schubbewehrung zwischen Betonfertigteilen und Ortbeton; Deutscher Ausschuss für Stahlbeton DAfStb, Issue 372, Ernst & Sohn Verlag, Berlin, 1986.

[Das86b] DASCHNER, F.; NISSEN, I.; KUPFER, H: Verminderte Schubdeckung in Stahlbeton und Spannbetonträgern mit Fugen parallel zur Tragrichtung unter Berücksichtigung nicht vorwiegend ruhender Lasten. Deutscher Ausschuss für Stahlbeton DAfStb, Issue 372, Ernst & Sohn Verlag, Berlin, 1986.

[DRi96] DEUTSCHER AUSSCHUSS FÜR STAHLBETON: Richtlinie zur Verwendung von Flugasche nach DIN EN 450 im Betonbau. Beuth Verlag, 1996.

[DZ-93] DIBt Z-15.1-93: Filigran-EQ-Gitterträger für Fertigplatten mit statisch mitwirkender Ortbetonschicht. Allgemeine bauaufsichtliche Zulassung, Deutsches Institut für Bautechnik, Berlin, 2014.

[DZ-38] DIBt Z-15.1-38: Kaiser-Omnia-Träger KTS für Fertigplatten mit statisch mitwirkender Ortbetonschicht. Allgemeine bauaufsichtliche Zulassung, Deutsches Institut für Bautechnik, Berlin, 2015.

[DZ-136] DIBt Z-15.1-136: Kaiser-Omnia-Träger KT 100 für Fertigplatten mit statisch mitwirkender Ortbetonschicht (MONTAQUICK-Fertigplatten). Allgemeine bauaufsichtliche Zulassung, Deutsches Institut für Bautechnik, Berlin, 2014.

[DZ-40] DIBt Z-15.2-40: Filigran-EQ-Gitterträger für Filigran-Elementwände. Allgemeine bauaufsichtliche Zulassung, Deutsches Institut für Bautechnik, Berlin, 2015.

[DZ-100] DIBt Z-15.2-100: Kaiser-Omnia-Plattenwand mit Kaiser Gitterträgern KT 800, KT 900 oder KTE. Allgemeine bauaufsichtliche Zulassung, Deutsches Institut für Bautechnik, Berlin, 2015.

[DZ-9] DIBt Z-15.2-9: Gitterträger KTW 200 oder KTW 300 für Kaiser-Omnia-Plattenwände. Allgemeine bauaufsichtliche Zulassung, Deutsches Institut für Bautechnik, Berlin, 2014.

[Dub95] DUBBEL, H.: Taschenbuch für den Maschinenbau, Springer Verlag, Berlin, 1995.

[Dul72] DULACSKA, H.: Dowel Action of Reinforcement Crossing Cracks in Concrete. ACI Journal Proceedings, Vol. 69, pp. 754-757, 1972.

[EC0] DIN EN 1990:2010-12: Eurocode: Grundlagen der Tragwerksplanung. Deutsches Institut für Normung (DIN), German version, Beuth Verlag, Berlin, 2010.

[EC2] EN 1992-1-1:2004: Eurocode 2: Design of concrete structures – Part 1-1: General rules and rules for buildings. European Committee for Standardization (CEN), Brussels, 2004.

[EC2NAD] DIN EN 1992-1-1/NA:2013-04: Nationaler Anhang – National festgelegte Parameter – Eurocode 2: Bemessung und Konstruktion von Stahlbeton- und Spannbetontragwerken – Teil 1-1: Allgemeine Bemessungsregeln und Regeln für den Hochbau. Deutsches Institut für Normung (DIN), German version, Beuth Verlag, Berlin, 2013.

[prEC2:18] prEN 1992-1-1:2018: Eurocode 2: Design of concrete structures – Part 1-1: General rules, rules for buildings, bridges and civil engineering structures. Final draft of April 2018 by PT.SC2.T1, 2018. (unpublished)

[Fin16] FINGERLOOS, F.; HEGGER, J.; ZILCH, K.: Eurocode 2 für Deutschland – DIN EN 1992-1-1 Bemessung von Stahlbeton- und Spannbetontragwerken – Teil 1-1: Allgemeine Bemessungsregeln für den Hochbau mit nationalem Anhang – Kommentierte und Konsolidierte Fassung. Ernst & Sohn und Beuth Verlag, Berlin, 2011.

[Fra59] FRANZ, G.: Versuche über die Querkraftaufnahme in Fugen von Spannbetonträgern aus Fertigteilen. Beton- und Stahlbetonbau, Vol. 54, Issue 6, pp. 137-140, 1959.

[Fur11] FURCHE, J.; KLUG, Y.: Gitterträger als Querkraft und Verbundbewehrung. 9. Tagung Betonbauteile – Neue Normen und Werkstoffe im Betonbau, HTWK Leipzig, 2011.

[Fur14] FURCHE, J.; BAUMEISTER, U.: Flachdecken in Elementbauweise mit Gitterträgern – Hinweise zur Anwendung nach Eurocode 2. Beton- und Stahlbetonbau 109, Issue 11, pp. 783-792, 2014.

[Fur16] FURCHE, J.; BAUMEISTER, U.: Elementbauweise mit Gitterträgern nach Eurocode 2. Sonderdruck Betonkalender 2016, Ernst & Sohn Verlag, 2016.

[Fur19] FURCHE, J.; BAUMEISETER, U.; KUMMEROW, A.; HILLEBRAND, M.: Durchstanzen bei Ermüdungsbeanspruchung. Beton- und Stahlbetonbau 114, Issue 8, pp. 557 - 564, 2019.

[Gas64] GASTON, J.R.; KRIZ, L.B.: Connections in precast concrete structures – scarf joints. PCI Journal, Vol. 9, No. 3, pp. 37-59, 1964.

[Goh00] GOHNERT, M.: Proposed theory to determine the horizontal shear between composite precast and in situ concrete. Cement & Concrete Composites, Vol. 22, pp. 469-476, 2000.

[Goh03] GOHNERT, M.: Horizontal shear transfer across a roughened surface, Cement and Concrete Composites, Vol. 25, No. 3, pp. 379-385, 2003.

[Hai06] HAIBACH, E.: Betriebsfestigkeit – Verfahren und Daten zur Bauteilberechnung. Springer Verlag, Berlin, 2006.

[Han60] HANSON, N.W.: Precast-Prestressed Concrete Bridges 2. Horizontal Shear connections. Portland Cement Association, Research and Development Laboratories, Bulletin D35, Vol. 2, No. 2, pp. 38-58, 1960.

[Han04] HANSEN, M: Zur Auswirkung von Überwachungsmaßnahmen auf die Zuverlässigkeit von Betonbauteilen. Research report, Institut of structural concrete, Leibniz University Hannover, 2004.

[Har12] HARRIES, K. A.; ZENO, G.; SHAHROOZ, B.: Toward an Improved Understanding of Shear-Friction Behavior. ACI Structural Journal, Vol. 109, Issue 6, 2012.

[Heg99] HEGGER, J.; GÖRTZ, S.: Überprüfung und Vereinheitlichung der Bemessungsansätze für querkraftbeanspruchte Stahlbeton- und Spannbetonbauteile aus normalfestem und hochfestem Beton nach DIN 1045-1. Kapitel 6: Querkrafttragfähigkeit von monolithischen und nachträglich ergänzten Bauteilen mit und ohne Querkraftbewehrung. Research report, DIBt – Research project IV 1-5-876/98, 1999.

[Heg03] HEGGER, J.; GÖRTZ, S.: Nachträglich ergänzte Querschnitte mit horizontaler Fuge nach DIN 1045-1. Beton- und Stahlbetonbau 98, Issue 5, pp. 277-284, Berlin, 2003.

[Heg17] HEGGER, J.; WIENEKE, K.: Abschlussbericht zum IGF-Forschungsvorhaben 18407 N/1 „Ermüdung von Elementdecken mit Gitterträgern“. Institute of Structural Concrete, RWTH Aachen University, 2017.

[Her17] HERBRAND, M.: Shear Strength Models for Reinforced and Prestressed Concrete Members. PhD Thesis, Institut of Structural Concrete, RWTH Aachen University, 2017.

[Hil19] HILLEBRAND, M.; HEGGER, J.: Ermüdungsversuche an profilierten Spannbetonträgern unter Querkraftbeanspruchung. Beton und Stahlbetonbau 114, Issue 8, pp. 565-574, 2019.

[Hof69] HOFBECK, J.A.; IBRAHIM, I.O.; MATTOCK, A.H.: Shear transfer in Reinforced Concrete. ACI Journal, Title no. 66-13, pp. 119-128, 1969.

[Hoh04] HOHBERG, R.: Zum Ermüdungsverhalten von Beton. PhD Thesis, Technische Universität Berlin, 2004.

[Hol79] HOLMEN, J.O.: Fatigue of concrete by constant and variable amplitude loading. PhD Thesis, University of Trondheim, 1979.

[JOI00] JOINT COMMITTEE ON STRUCTURAL SAFETY: Probabilistic Model Code. Technical University of Denmark, Lyngby, 2000.

[Kah02] KAHN, L.F.; MITCHELL, A.D.: Shear friction tests with high-strength concrete. ACI Structural Journal, Vol. 99, No. 1, pp. 98-103, 2002.

[Kah04] KAHN, L.F.; SLAPKUS, A.: Interface Shear in High Strength Composite T-Beams. PCI Journal, Vol. 49, Issue 4, pp. 102-110, 2004.

[Kau71] KAUFMANN, N.: *Das Sandflächenverfahren*. Straßenbautechnik 24, No. 3, S. 131-135, 1971.

[Kes02] KESSLER-KRAMER, C.: Zugtragverhalten von Beton unter Ermüdungsbeanspruchung. PhD Thesis, Institute of Concrete Structures and Building Materials, Karlsruhe Institute of Technology, 2002.

[Kön94] KÖNIG, G.; DANIELEWCZ, I.: Ermüdungsfestigkeit von Stahlbeton und Spannbetonbauteilen mit Erläuterungen zu den Nachweisen gemäß CEB-FIP Model Code 90. Deutscher Ausschuss für Stahlbeton DAfStb, Issue 439, Beuth Verlag, Berlin, 1994.

[Krc16] KRC, K.; WERMAGER, S.; SNEED, L.H.; MEINHEIT, D.: Examination of the effective coefficient of friction for shear friction design. PCI Journal, November-December, pp. 44-67, 2016.

[Len12] LENZ, P.: Beton-Beton-Verbund Potentiale für Schubfugen. PhD Thesis, Chair of Concrete Structures, Technical University of Munich, 2012.

[Leo84] LEONHARDT, F.; MÖNNING, E.: Vorlesungen über Massivbau – Teil 1: Grundlagen zur Bemessung im Stahlbetonbau. Springer Verlag, 3. Edition, Berlin, 1984.

[Lin06_1] LINDIG, V.: Stahlbeton-Verbundkonstruktionen – Ein Bemessungskonzept für schubbeanspruchte Fugen, Teil 1: Korrelation zwischen Simulation und Bemessung. Beton- und Stahlbetonbau 101, Issue 11; Ernst & Sohn Verlag, Berlin, 2006.

[Loo78] LOOV, R.E.: Design of precast connections. Paper presented at a seminar organized by Compa International Pte, Ltd, 8 p., Singapore, September 1978.

[Loo94] LOOV, R.E.; PATNAIK, A.K.: Horizontal shear strength of composite concrete beams with a rough interface. PCI Journal, Vol. 39, No. 1, pp. 48-69, January-February, 1994.

[Mai98] MAINZ, J.; ZILCH, K.: Schubtragverhalten von Betonergänzungen an nachträglich aufgerauhten Oberflächen bei Sanierungs- und Ertüchigungsmaßnahmen. Research report, Chair of Concrete Structures, Technical University of Munich, 1998.

[Mas68] MAST, R.F.: Auxiliary reinforcement in precast concrete connections, American Society of Civil Engineers, Journal of the Structural Division, Vol. 94, No. ST6, pp. 1485-1504, June, 1968.

[Mau10a] MAURER, R.; BLOCK, K.; DREIER, F.: Ermüdungsfestigkeit von Betonstahl – Bestimmung mit dem Interaktiven Verfahren. Bauingenieur 85, No. 1, S.17-28, 2010.

[Mau10b] MAURER, R.; DREIER, F.; MACHOCZEK, D.; HEEKE, G.: Bestimmung der Ermüdungsfestigkeit von einbetoniertem Betonstahl mit dem Interaktiven Verfahren. Fraunhofer IRB Verlag, Stuttgart, 2010.

[Mat61] MATTOCK, A.H.; KAAR, P.H.: Precast-prestressed concrete bridges, 4. Shear tests of continuous girders, Journal of the PCA R&D Laboratories, Vol. 3, No. 1, pp. 19-46, January, 1961.

[Mat72] MATTOCK, A.H.; HAWKINS, N.M.: Shear transfer in reinforced concrete – recent research. PCI Journal, Vol. 17, No. 2, pp. 55-75, March-April, 1972.

[Mat74] MATTOCK, A.H.: Shear transfer in concrete having reinforcement at an angle to the shear plane. American Concrete Institute, Special Publication 42-2, pp. 17-42, January, 1974.

[Mat75] MATTOCK, A.H.; JOHAL, L.; CHOW, H.C.: Shear transfer in reinforced concrete with moment or tension acting across the shear plane. PCI Journal, Vol. 20, No. 4, pp. 76-93, July-August, 1975.

[Mat76] MATTOCK, A.H.; LI, W.K.; WANG, T.C.: Shear transfer in lightweight reinforced concrete. PCI Journal, Vol. 21, No. 1, pp. 20-39, January-February. 1976.

[Mat81] MATTOCK, A.H.: Cyclic shear transfer and type of interface. American Society of Civil Engineers, Journal of the Structural Division, Vol. 107, No. ST10, pp. 1945-1964, October, 1981.

[Mat88] MATTOCK, A.H.: Reader comments of paper Influence of concrete strength and load history on the shear friction capacity of concrete members. Published in PCI Journal, Vol. 32, No. 1, pp. 66-84, January-February, 1987 by Walraven *et al.;* PCI Journal, Vol. 33, No. 1, pp. 165-166, January-February, 1988.

[Mat01] MATTOCK, A.H.: Shear Friction and High Strength Concrete. ACI Structural Journal, V.98, No.1, Jan-Feb., pp. 50-59, 2001.

[MC78] CEB FIP: Model Code 1978 Revision Process. International Federation for Structural Concrete, 1978.

[MC90] CEB-FIP: Model Code 1990 Design Code. Euro-International Committee for Concrete, Thomas Telford, 1993.

[MC10] CEB FIP: Model Code 2010 Final Draft. International Federation for Structural Concrete, September, 2011.

[Meh77] MEHLHORN, G.; SCHWING, H.; BERG, K.R.: Versuche zur Schubtragfähigkeit verzahnter Fugen. Deutscher Ausschuss für Stahlbeton DAfStb, Issue 288, 1977.

[Mell08] MELLMANN, G.; OPPAT, K.: Maß für Maß: Rautiefen Bestimmung von Betonoberflächen mittels Lasermessverfahren. Bautenschutz und Bausanierung, Vol. 31, Issue 2, pp. 30-32, 2008.

[Men92] MENN, C.; BRENNI, P.; KELLER, T.; PELLEGRINELLI, L.: Verbindungen von altem und neuem Beton. Research Report, Institute of Structural Engineering, ETH Zürich, 1992.

[Moh15a] MOHAMED, M.E.; IBRAHIM, I.S.; ABDULLAH, R.; RAHMA, A.B. ABD; KUEH, A.B.H; USMAN, J.: Friction and cohesion coefficients of composite concrete to concrete bond. Cement and Concrete Composites, Vol. 56, pp. 1-14, 2015.

[Moh15b] MOHAMED, M.E.; IBRAHIM, I.S.: Interface shear strength of concrete- to concrete bond with and without projecting steel reinforcement. Journal Teknologi (Science & Engineering), Vol. 75, Issue 1, pp. 169-172, 2015.

[Moo76] MOOSECKER, W.: Zur Bemessung der Schubbewehrung von Stahlbetonbalken mit möglichstgleichmäßiger Zuverlässigkeit. Deutscher Ausschuss für Stahlbeton DAfStb, Issue 307, Ernst&Sohn Verlag, Berlin, 1979.

[Mör27] MÖRSCH, E.: Die Schubsicherung von Eisenbetonbalken. Beton und Eisen, No. 2, pp. 27-35, 1927.

[Mül09] MÜLLER, A.: Zum Zug- und Schubtragverhalten von Betonfugen. PhD Thesis, Chair of Concrete Structures, Technical University of Munich, 2009.

[Nie11] NIELSEN, M.P.; HOANG, L.C.: Limit Analysis and Concrete Plasticity. 3. Edition, CRC Press, Boca Raton, 2011.

[Nis62] NISSEN, L.: Rissverzahnung des Betons - Gegenseitige Rissuferverschiebung und übertragene Kräfte. PhD Thesis, Chair of Concrete Structures, Technical University of Munich, 1987.

[Nis86] NISSEN, I.; DASCHNER, F.; KUPFER, H.: Verminderte Schubdeckung in Stahlbeton und Spannbetonträgern mit Fugen parallel zur Tragrichtung unter Berücksichtigung nicht vorwiegend ruhender Lasten. Deutscher Ausschuss für Stahlbeton DAfStb, Issue 372, Ernst & Sohn Verlag, Berlin, 1986.

[Nür82] NÜRNBERGER, U.: Schwingfestigkeitsverhalten von Betonstählen. IHBV Reports Vol. 37, Lausanne, 1982.

[Pap02] PAPANICOLAOU, C.G.; TRIANTAFILLOU, T.C.: Shear transfer capacity along pumice aggregate concrete and high-performance concrete interfaces. Materials and Structures, Vol. 35, No. 4, pp. 237-245, May, 2002.

[Pat92] PATNAIK, A.H.: Horizontal shear strength of composite concrete beams with a rough interface. PhD Thesis, Department of Civil Engineering, University of Calgary, 1992.

[Pau74] PAULAY, T.; PARK, R.; PHILLIPS, M. H.: Horizontal Construction Joints in Cast in Place Reinforced Concrete. ACI-Special Publication, SP-42 Shear in Reinforced Concrete, pp. 599-616, 1974.

[Pru88] PRUIJSSERS, A.F.: Aggregate interlock and Dowel Action under monotonic and cyclic loading. PhD Thesis, Department of Engineering Structures, University of Technology Delft, 1998.

[Ran97] RANDL, N.: Untersuchungen zur Kraftübertragung zwischen Alt- und Neubeton bei unterschiedlichen Fugenrauhigkeiten. PhD-Thesis, Faculty of Civil Engineering and Architecture, University Innsbruck, 1997.

[Ran05] RANDL, N.; MÜNGER, F.; WICKE, M.: Verstärkung von Brückentragwerken durch Aufbeton. Bauingenieur, Issue 4, pp. 207-214, 2005.

[Ran08] RANDL, N.; ZILCH, K.; MÜLLER, A.: Bemessung nachträglich ergänzter Betonbauteile mit längsschubbeanspruchter Fuge. Beton- und Stahlbetonbau 103, Issue 7, pp. 482-497, 2008.

[Ran13] RANDL, N.: Design recommendations for interface shear transfer in fib Model Code 2010. Structural Concrete 14, No. 3, Ernst & Sohn Verlag, 2013.

[Ran14] RANDL, N.; SIMON, C.: Static and dynamic testing of RC-slabs with high strength concrete overlay. Construction Materials and Structures, S.O. Ekoli et al. (Eds), IOS Press, pp. 980-988, 2014.

[Ran15] RANDL, N.; STEINER, M.: Hochfester Beton als Aufbeton im Bestand und als monolithische Deckschicht im Neubau- Aufbetonschichten. Research Report, Kärnten University of Applied Science, 2015.

[Rat77] RATHS, C.H.: Reader comments of paper Design proposals for reinforced concrete corbels. PCI Journal, Vol. 21, No. 3, pp. 18-42, May-June, 1976 by Mattock, A., PCI Journal, Vol. 22, No. 2, pp. 93- 98, March-April, 1977.

[Reh80] REHM, G.; ELIGEHAUSEN, R.; PAUL. F.: Verbundbewehrung in Fugen von Platten ohne Schubbewehrung. Research Project, University Stuttgart, 1980.

[Reh81] REHM, G.; HARRE, W.; RUSSWURM, D.: Untersuchungen über die Schwingfestigkeit geschweißter Betonstahlverbindung Teil 1 Schwingfestigkeitsversuche. Deutscher Ausschuss für Stahlbeton DAfStb, Issue 317, Beuth Verlag, Berlin, 1981.

[Rei04] REINECKE, R.: Haftverbund und Rissverzahnung in unbewehrten Betonschubfugen. PhD Thesis, Chair of Concrete Structures, Technical University of Munich, 2004.

[Rei12] REINECK, K.H.; KUCHMA, D.A.; FITIK, B.: Erweiterte Datenbanken zur Überprüfung der Querkraftbemessung für Konstruktionsbauteile mit und ohne Bügel, Deutscher Ausschuss für Stahlbeton DAfStb, Issue 597, Beuth Verlag, Berlin, 2012.

[Ric09] RICKER, M.: Zur Zuverlässigkeit der Bemessung gegen Durchstanzen bei Einzelfundamenten. PhD Thesis, Institute of Structural Concrete, RWTH Aachen University, 2009.

[Ril94] RILEM TECHNICAL COMMITTEE 36-RDL: Long term random dynamic loading of concrete structures. Materials and Structures – research and testing 17, No. 97, pp. 1–28, 1994.

[Sae64] SAEMANN, J.C.; WASHA, G.W.: Horizontal shear connections between precast beams and cast-in-place slabs. Journal of the American Concrete Institute, Vol. 61, No. 11, pp. 1383-1409, November, 1964.

[San06] SANTOS, P.M.D.; JULIO, E.N.B.S.: Correlations between concrete-to-concrete bond strength and the roughness of the substrate surface. Construction and Building Materials 21, pp. 1688-1695, 2006.

[San09] SANTOS, P.M.D.: Assessment of the Shear Strength between Concrete Layers. PhD Thesis, University of Coimbra, 2009.

[San10] SANTOS, P.M.D; JULIO, E.N.B.S.: Comparison of Methods for Texture Assessment of Concrete Surfaces. ACI Materials Journal, pp. 433-440, September-October, 2010.

[San13] SANTOS, P.M.D; JULIO, E.N.B.S.: A state-of-the-art review on roughness quantification methods for concrete surfaces. Construction and Building Materials 38, pp. 912-923, 2013.

[Sch96a] SCHÄFER, H. G.; SCHMIDT-KEHLE, W.: Zum Schubtragverhalten von Fertigplatten mit Ortbetonergänzung. Deutscher Ausschuss für Stahlbeton DAfStb, issue 456, Beuth Verlag, Berlin 1996.

[Sch96b] SCHÄFER, H. G.; BLOCK, K.; DRELL, R..: Oberflächenrauheit und Haftverbund. Deutscher Ausschuss für Stahlbeton DAfStb, issue 456, Beuth Verlag, Berlin 1996.

[Sch96c] SCHÄFER, H. G.; SCHMIDT-KEHLE, W.: Zur Oberflächenrauheit von Fertigplatten mit Ortbetonergänzung. Deutscher Ausschuss für Stahlbeton DAfStb, issue 456, Beuth Verlag, Berlin 1996.

[Sch96d] SCHÄFER, H. G.; SCHMIDT-KEHLE, W.: Ortbetonergänzte Fertigteilbalken mit profilierter Anschlussfuge unter hoher Querkraftbeanspruchung. Deutscher Ausschuss für Stahlbeton DAfStb, issue 456, Beuth Verlag, Berlin 1996.

[Sch81] SCHIEßL, P.; SCHWARZKOPF, M.: Montaquick Fertigteildecken mit statischer Ortbetonschicht bei dynamischer Beanspruchung. Research report - test series 1, Institut für Betonstahl und Stahlbeton e.V., Munich, 1981.

[Sch82] SCHIEßL, P.; SCHWARZKOPF, M.: Montaquick Fertigteildecken mit statischer Ortbetonschicht bei dynamischer Beanspruchung. Research report test series 2, Institut für Betonstahl und Stahlbeton e.V., Munich, 1982.

[Sch83] SCHIEßL, P.; SCHWARZKOPF, M.: Montaquick Fertigteildecken mit statischer Ortbetonschicht bei dynamischer Beanspruchung. Research report test series 3, Institut für Betonstahl und Stahlbeton e.V., Munich, 1983.

[Sch85] SCHIEßL, P.; SCHWARZKOPF, M.: Kaiser Omnia-Träger KTS für Fertigplatten mit statisch mitwirkender Ortbetonschickt bei dynamischer Beanspruchung. Research report, Institit für Betonstahl und Stahlbetonbau e.V., Munich, 1985.

[Sch17] SCHULZ, R.R.: Fortschritte bei der Rauigkeitsbewertung von Betonoberflächen. Beton, Issue 4, pp. 44-48, 2017.

[Sco10] SCOTT, J.: Interface shear strength in lightweight concrete bridge girders. M.Sc. Thesis, Virginia Polytechnic Institute and State University, 2010.

[Sha78] SHAIKH, A.F.: Proposed revisions to shear-friction provisions. PCI Journal, Vol. 23, No. 2, pp. 12-21, March-April, 1978.

[Sha14] SHAW, D.; SNEED, L.: Interface Shear Transfer of Lightweight Aggregate Concretes Cast at Different Times. PCI Journal, Vol. 59, No. 3, pp. 130-144, 2014.

[Sne16] SNEED, L. H.; KRC, K.; WERMAGER, S.; MEINHEIT, D.: Interface Shear Transfer of Lightweight-Aggregate Concretes. PCI Journal, Vol. 61, No. 2, pp. 38-55, 2016.

[Sol17] SOLTANI, M.; ROSS, B.E.: Database evaluation of interface shear transfer in reinforced concrete members. ACI Structural journal, pp. 383-394, March-April, 2017.

[Tas87] TASSIOS, T.P.; VINTZELEOU, E.N.: Concrete to concrete friction. Journal of Structural Engineering 113, Issue 4, pp. 832-849, 1987.

[Tew14] TEWORTE, F.: Zum Querkrafttragverhalten von Spannbetonträgern unter Ermüdungsbeanspruchung. PhD Thesis, Institute of Structural Concrete, RWTH Aachen University, 2014.

[Tso89] TSOUKANTAS, S.G.; TASSIOS, T.P.: Shear resistance of connections between reinforced concrete linear precast elements. ACI Structural Journal, Vol. 86, No. 3, pp. 242-249, May-June, 1989.

[Val99] VALLUVAN, R., KREGER, M. E.; JIRSA, J. O.: Evaluation of ACI 318-95 Shear-Friction Provisions. ACI Structural Journal, Vol. 96, Issue 4, pp. 473-482, 1999.

[Vis95] VISMANN, U.: Zuverlässigkeitstheoretische Verifikation von Bemessungskriterien im Stahlbetonbau. Reports from Structural Engineering 4/95, Chair of Concrete Structures, Technical University of Munich, 1995.

[Vog17] VOGLER, N.; GLUTH, G.J.G.; OPPAT, K.; KÜHNE, H.-C.: Charakterisierung von Bauteiloberflächen – Rautiefenbestimmung mittels konventioneller und laserbasierter Verfahren. Bauingenieur, Issue3, pp. 97-104, 2017.

[Voi14] VOIGT, J.: Beitrag zur Bestimmung der Tragfähigkeit bestehender Stahlbetonkonstruktionen auf Grundlage der Systemzuverlässigkeit. PhD Thesis, Faculty of Civil Engineering, University Siegen, 2014.

[Wal81] WALRAVEN, J.C.: Fundamental analysis of aggregate interlock. Journal of the Structural Division, Vol. 107, No. ST11, pp. 2245-2270, November, 1981.

[Wal87] WALRAVEN, J.; FRÉNAY, J.; PRUIJSSERS, A.: Influence of concrete strength and load history on the shear friction capacity of concrete members, PCI Journal, Vol. 32, No. 1, pp. 66-84, January-February, 1987.

[Web89] WEBER, J.W.; SCHMIDT, R.: Zulassungsversuche für den Filigran EQ-Träger unter dynamischer Beanspruchung. Test report, Institute of Building Materials Science, RWTH Aachen University, 1989.

[Web95] WEBER, J.W.; LEIßNER, J.; WEYERT, R.: Zulassungsversuche für die Kaiser-Omnia-Plattenwand mit Gitterträgern KTW 100 oder KTW 30 bei dynamischer Belastung. Research report; Institute of Building Materials Science, RWTH Aachen University, 1995.

[Wie17a] WIENEKE K; CLAßEN, M.; HEGGER, J.: Elementdecken mit Gitterträgern unter zyklischer Belastung. Beton- und Stahlbetonbau 112, Issue 9, pp. 579-588, 2017.

[Wie17b] WIENEKE, K; VAN ELTEN, L.; CLAßEN, M.; HEGGER, J.: Ermüdung von Elementdecken mit Gitterträgern: Wöhlerlinien für Gitterträger. Beton- und Stahlbetonbau 112, Issue 11, pp. 723-722, 2017.

[Wie18] WIENEKE, K.; HERBRAND, M.; VOGLER, N., SCHWERMANN, R.; BLANKENBACH, J.: Messerverfahren zur Bestimmung der Rautiefe von Betonoberflächen. Bauingenieur, Vol. 93, pp. 365-376, September, 2018.

[Wil17] WILLIAMS, C.S.; MASSEY, J.B.; BAYRAK, O.; JIRSA, J.O.: Investigation of Interface Shear Transfer Using Push-Through Tests. ACI Structural Journal, Vol. 114, Issue 1, pp. 173-185, 2017.

[Win13] WINGENFELD, D.R.: Fügetechnische Konstruktionslösungen für Bauteile aus ultrahochfestem Beton (UHPC). PhD Thesis, Chair of Concrete Structures, Technical University of Munich, 2013.

[Zel61] ZELGER, C.; RÜSCH, H.: Der Einfluß von Fugen auf die Festigkeit von Fertigteilschalen. Beton- und Stahlbetonbau, No. 10, 1961.

[Zen09] ZENO, G.A.: Use of High-Strength Steel Reinforcement in Shear Friction Applications. PhD Thesis, University of Pittsburgh, Pittsburgh, 2009.

[Zil03] ZILCH, K.; ZEHETMAIER, G.; RUSSWURM, D.: Zum Ermüdungsnachweis bei Stahlbeton- und Spannbetonbauteilen. Deutscher Ausschuss für Stahlbeton DAfStb, Issue 525, Beuth Verlag, Berlin, 2003.

[Zil04] ZILCH, K.; MÜLLER, A.: Experimentelle Untersuchungen zum Ermüdungstragverhalten von unbewehrten Schubfugen an Nachträglich ergänzten Bauteilen, Research Report, Chair of Concrete Structures, Technical University of Munich, 2004.

[Zil04a] ZILCH, K.; ZEHETMAIER, G.; GLÄSER, C.: Ermüdungsnachweis bei Massivbrücken. Betonkalender 2004, Part 1, Ernst & Sohn Verlag, Berlin, 2004.

[Zil06] ZILCH, K.; MÜLLER, A.: Grundlagen und Anwendungsregeln der Bemessung von Fugen nach EN 1992-1-1. Research Report, Chair of concrete structures, Technical University of Munich, 2006.

[Zil08] ZILCH, K.; LENZ, P.; MÜLLER, A.: Zum Einfluss einer zum Auflager hin fallender Verbundbewehrung auf die Schubkraftübertragung in Fugen. Chair of concrete structures, Technical University of Munich, 2008.

[Zil10] ZILCH, K.; ZEHETMAIER, G.: Bemessung im konstruktiven Betonbau. Springer Verlag, 2. Edition, Springer Verlag, 2010.

[ZTV03] BASt BUNDESANSTALT FÜR STRAßENBAU: ZTV-ING Zusätzliche Technische Vertragsbedingungen und Richtlinien für Ingenieurbauten – Teil 1: Allgemeines – Abschnitt 3: Prüfung während der Ausführung. Verkehrsblatt-Verlag, Dortmund, January, 2003.

Annex

Table of contents

Annex A Own investigations

A.1 Test matrix

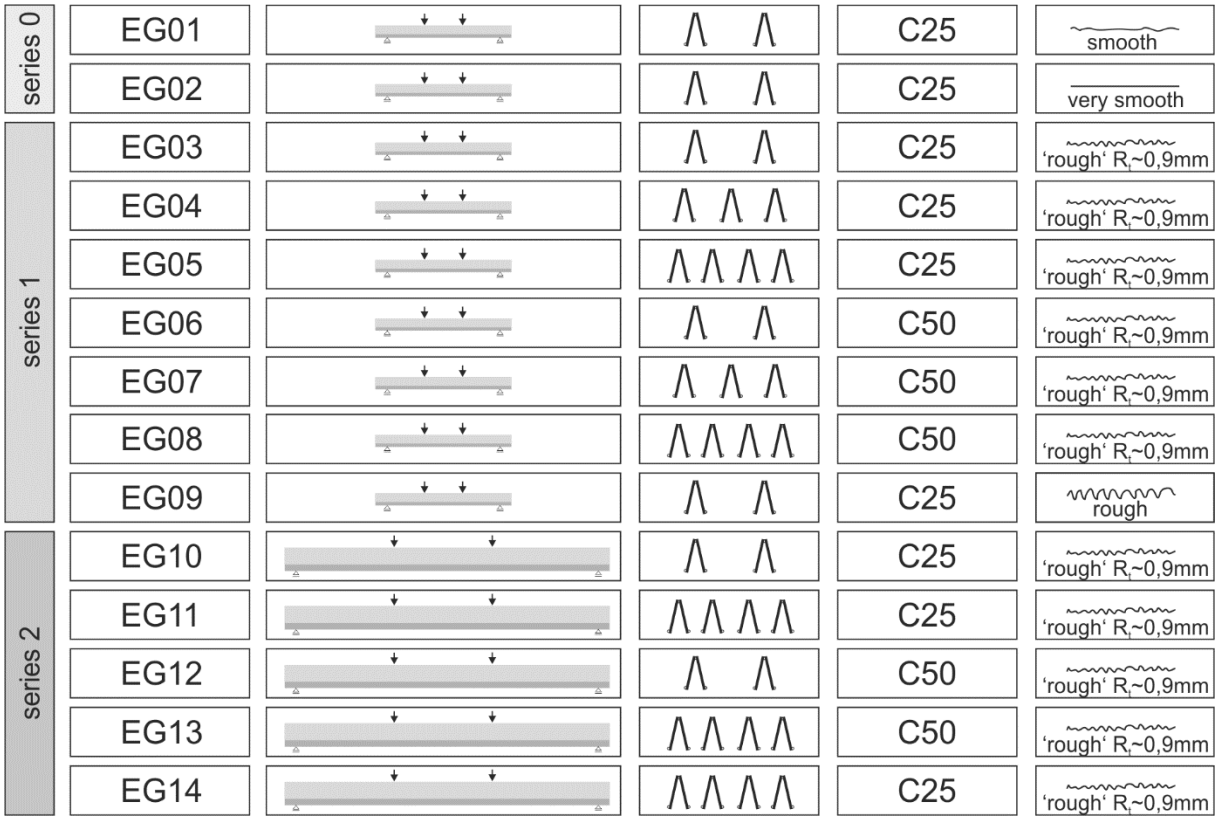

Figure A-1: Test matrix

A.2 Material properties

A.2.1 Concrete

Table A-1: Concrete composition of precast slab and insitu concrete

	cement		aggregates [mm]			water		flow spread	date
	CEM I [-]	Menge [kg/m³]	0-2 [kg/m³]	2-8 [kg/m³]	8-16 [kg/m³]	amount [kg/m³]	w/z [-]	[cm]	[-]
EG01, EG02									
precast	52,5R	280	grading curve AB16			172	0,60	-	04.05.2015
insitu	52,5R	280	787	637	450	200	0,71	52	08.05.2015
EG03, EG04, EG05									
precast	52,5R	260	814	659	465	182	0,70	-	27.08.2015
insitu	52,5R	260	814	659	465	182	0,70	-	08.09.2015
EG06, EG07, EG08									
precast	52,5R	400	748	438	638	180	0,45	45	26.11.2015
insitu	52,5R	400	748	392	641	170	0,43	45	11.12.2015
EG09, EG14									
precast	52,5R	260	814	659	465	182	0,70	46	07.03.2016
insitu	52,5R	270	758	474	663	175	0,65	50	17.03.2016
EG10, EG11									
precast	52,5R	270	758	474	663	184	0,68	46	08.10.2015
insitu	52,5R	270	758	474	663	186	0,65	50	22.10.2015
EG12, EG13									
precast	52,5R	400	748	438	638	180	0,45	49	07.12.2015
insitu	52,5R	400	748	392	641	170	0,43	52	17.12.2015

Table A-2: Mean values of concrete strength of precast slab and insitu concrete

Test		Testing age [d]	$f_{c,cyl}$ [N/mm²]	$f_{c,cube}$ [N/mm²]	$f_{ct,flex}$ [N/mm²]	$f_{ct,sp}$ [N/mm²]	$f_{c,cube,28d}$ [N/mm²]	E_c [N/mm²]
EG01	pre	53	25,3[1]	41,7[1]	3,6[1]	2,9[1]	39,9[1]	26583[1]
	in	49	35,6[1]	45,3[1]	3,9[2]	3,0[1]	41,8[1]	20641[1]
EG02	pre	71	25,6	42,5	4,4	3,0	39,9	27396
	in	67	33,9	41,6	3,9[2]	3,2	41,8	27077
EG03	pre	32	27,7	39,6	-	2,7	42,3	24695
	in	20	33,2	38,1	2,8	2,8	44,3	26043
EG04	pre	40	27,9[1]	40,3[1]	-	2,7[1]	42,3[1]	24546[1]
	in	29	34,0[1]	39,1[1]	3,1[1]	2, 8[1]	44,3[1]	26017[1]
EG05	pre	53	28,2[1]	41,5[1]	-	2,7[1]	42,3[1]	24304[1]
	in	42	35,2[1]	40,6[1]	3,4[1]	2,9[1]	44,3[1]	25980[1]
EG06	pre	109[2]	51,1[2]	68,8[2]	-	3,6[2]	72,1[2]	29401[2]
	in	95[2]	61,3[2]	76,0[2]	-	4,3[2]	70,9[2]	28343[2]
EG07	pre	112	51,1[1]	68,7[1]	-	3,6[1]	72,1[1]	29378
	in	97	61,3[2]	75,8[1]	-	4,3[1]	70,9[2]	28343[2]
EG08	pre	130	51,4[1]	68,7[1]	-	3,6[1]	72,1[1]	29242[1]
	in	115	61,3[2]	74,2	-	4,1[1]	70,9[2]	28343[2]
EG09	pre	42	32,9	37,7	4,6[2]	2,9	43,3	25079
	in	32	34,4	40,8	-	3,1	41,2	23157
EG10	pre	40	36,0	43,3	3,8	3,4	43,5	22157
	in	26	32,0	39,1	3,6	2,8	43,8	22960
EG11	pre	88	37,2	45,1	4,3[1]	2,8	43,5	20366
	in	74	36,0	42,9	3,9[1]	3,0	43,8	24509
EG12	pre	37	48,6	65,2	4,1[2]	3,4	68,9	29935
	in	27	55,6	72,3	5,6[2]	4,0	68,4	29335
EG13	pre	73	49,0[1]	67,5[1]	4,1[2]	3,7[1]	68,9[2]	30577[1]
	in	63	56,8[1]	72,8[1]	5,6[2]	3,9[1]	68,4[2]	29376[1]
EG14	pre	94	31,5	37,4	3,8	2,7[1]	43,3	24748
	in	84	34,8	39,3	-	3,1	41,2	22652

pre: precast slab; in: insitu concrete; [1]: linearly interpolated; [2]: no interpolation possible – values adopted from testig date; $f_{c,cyl}$: cylinder compressive strength; $f_{c,cube}$: cube compressive strength; $f_{ct,flex}$: flexural tensile strength; $f_{ct,sp}$: splitting tensile strength; $f_{c,cube,28d}$: cube compressive strength after 28 days; E_c: young's modulus

A.2.2 Reinforcement

Table A-3: Steel properties of lattice girders

		Ø [mm]	A_0 [mm²]	f_y [MPa]	f_t [MPa]	A_{10} [%]	A_{gt} [%]	E_s [MPa]
KTS 100	U	5	19,63	597	643	-	3,90	211930
	D	7	38,48	554	603	-	5,15	207730
	L	5	19,63	570	623	-	3,55	217699
EQ 30	U	5,1	20,43	597	648	-	-	211791
	D	7	38,48	554	609	-	-	209811
	L	5,1	20,43	589	642	-	-	207856

U: upper chord; D: diagonal; L: lower chord; Ø: diameter; A_0: initial cross section; f_y: 0,2%-yiled strength; f_t: tensile strength; A_{10}: failure strain; A_{gt}: stain at ultimate load; E_s: youngs's modulus

Table A-4: Steel properties of longitudinal reinforcement

	Ø [mm]	A_0 [mm²]	f_y [MPa]	f_t [MPa]	A_{10} [%]	A_{gt} [%]	E_s [MPa]
EG01/ EG02	20,2	319,47	954	1160	-	-	193277
EG03 - EG14	20,2	319,27	939	1135	-	-	195293

Ø: diameter; A_0: initial cross section; f_y: 0,2%-yiled strength; f_t: tensile strength; A_{10}: failure strain; A_{gt}: stain at ultimate load; E_s: youngs's modulus

A.3 Reinforcement and formwork details

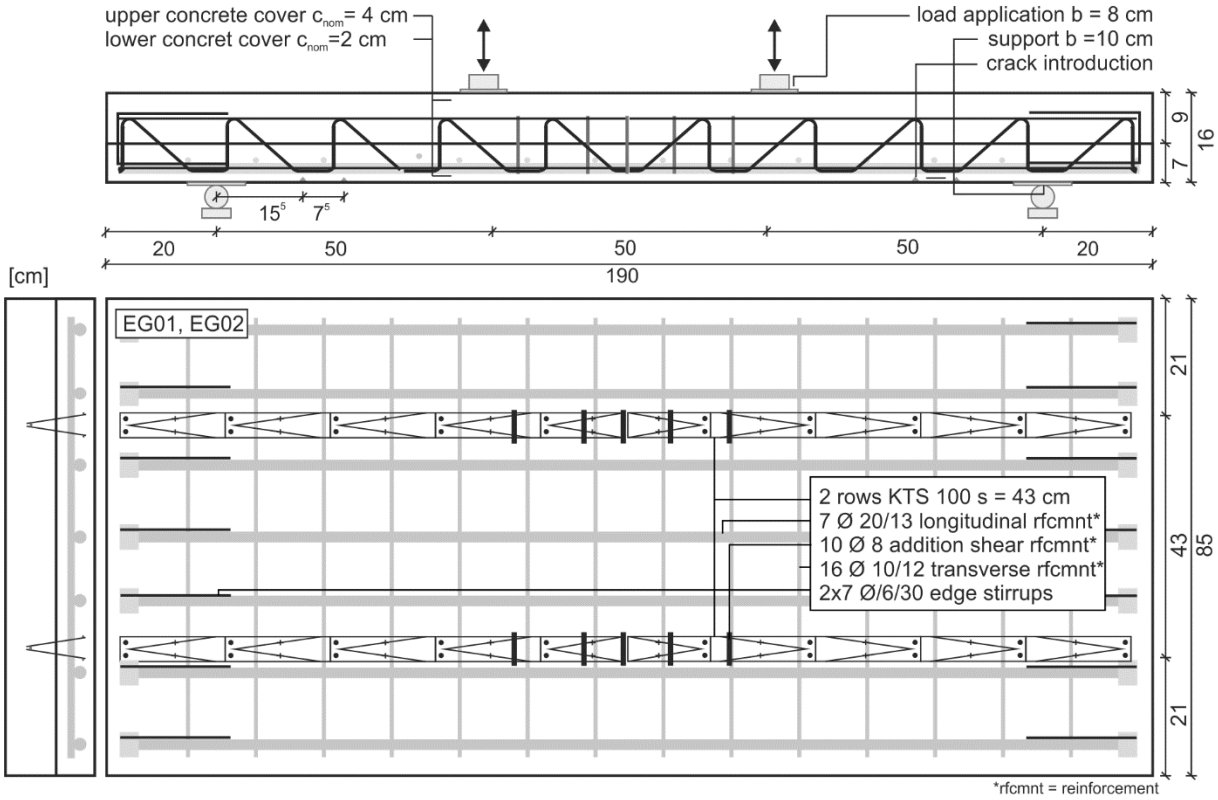

Figure A-2: Reinforcement and formwork detail of specimens EG01 and EG02

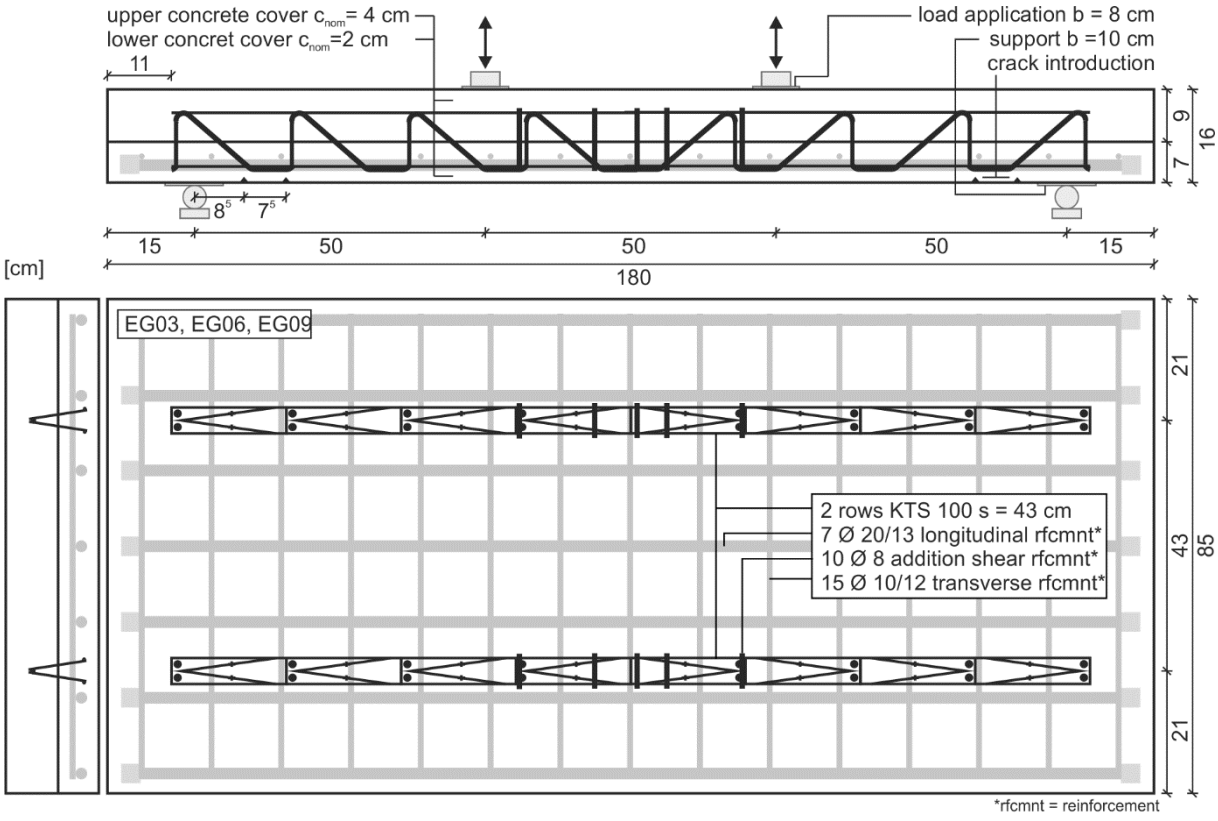

Figure A-3: Reinforcement and formwork detail of specimens EG03, EG06 and EG9

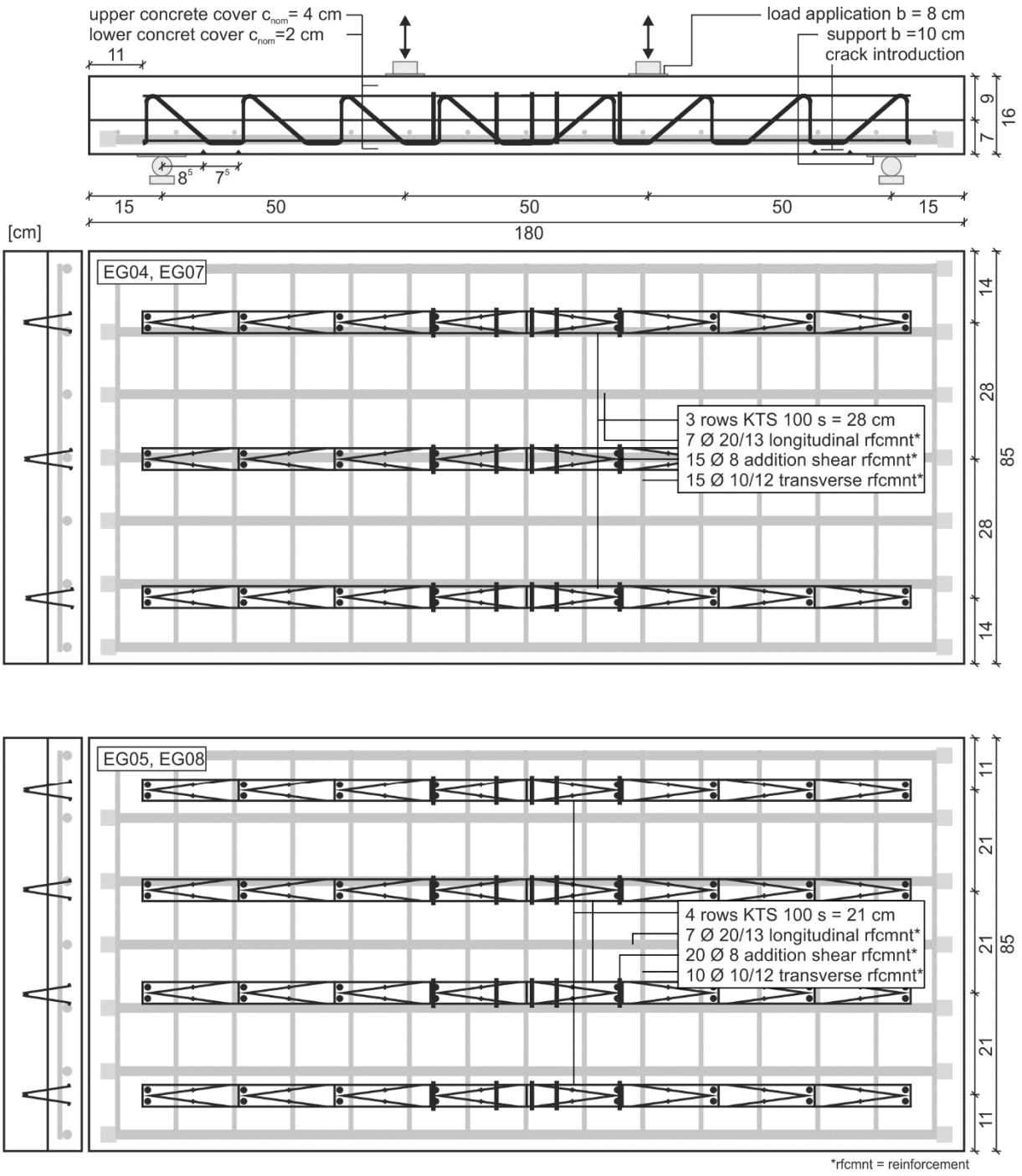

Figure A-4: Reinforcement and formwork detail of specimens EG04 and EG07 as well as EG05 and EG08

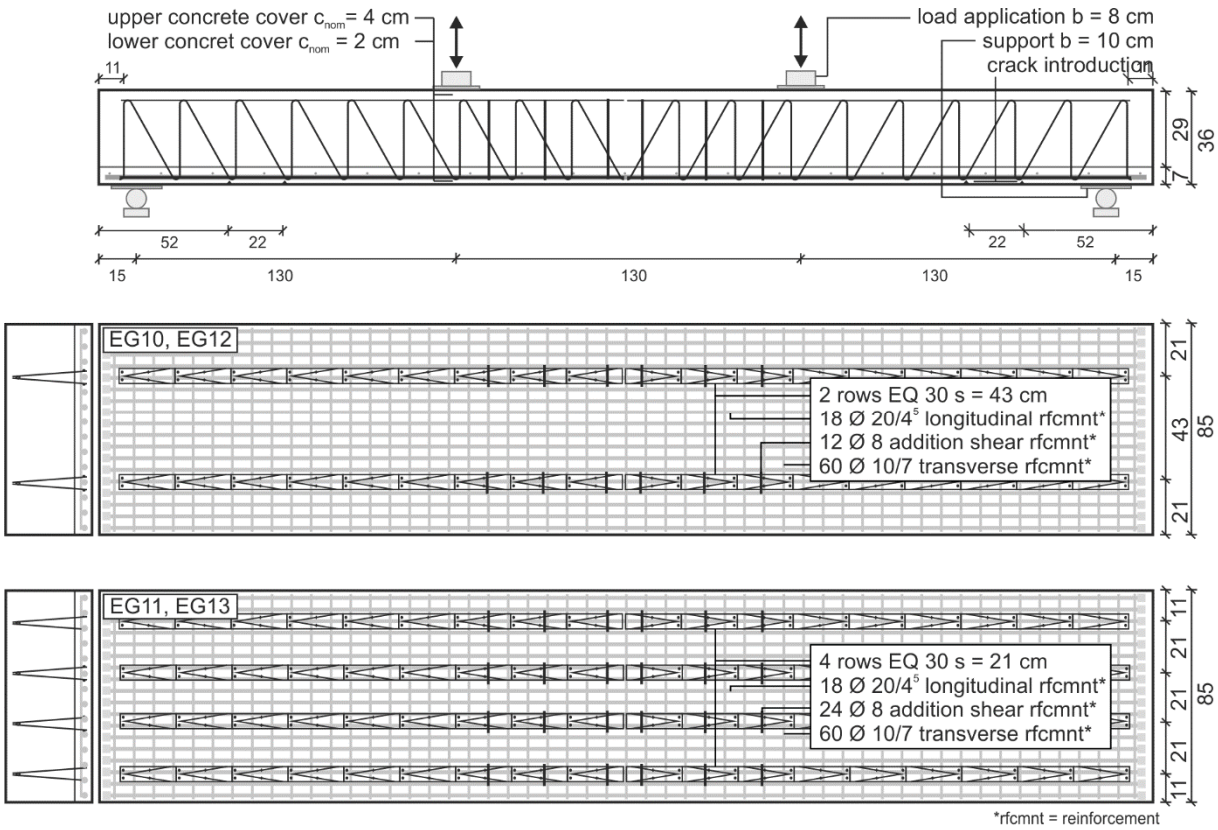

Figure A-5: Reinforcement and formwork detail of specimens EG10, EG11, EG12 and EG13

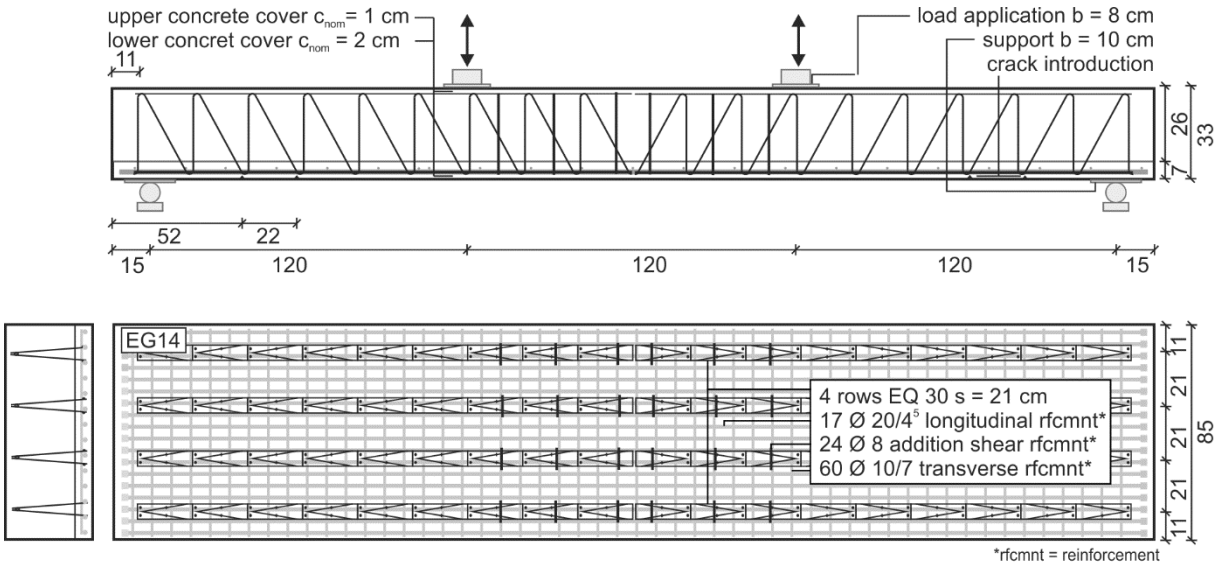

Figure A-6: Reinforcement and formwork detail of specimens EG10, EG11, EG12 and EG14

A.4 Applied load history

Table A-5: Load history of test specimen EG01

EG01	$V_{max,test}$ [kN]	$\frac{V_{max,test}}{V_{stat,calc}}$ [-]	ΔV [kN]	$\frac{\Delta V_{test}}{V_{max,test}}$ [-]	N [-]
sub-test I	116	0.80	35	0.30	0 – 1.500.000
	116	0.80	58	0.50	1,500,000 – 2,000,000
	126	0.87	68	0.54	2,000,000 – 2,500,000
	129	0.89	71	0.55	2,500,000 – 3,000,000
	136	0.94	78	0.57	3,000,000 – 3,500,000
	144	1.00	86	0.60	3,500,000 – 3,750,000
	152	1.05	94	0.62	3,750,000 – 4,000,000
	162	1.12	104	0.65	4,000,000 – 4,180,000*
sub-test II	162	1.12	104	0.65	4,180,000 – 4,180,350*

$V_{max,test}$: maximum applied shear force in test; $V_{stat,calc} = V_{Rm,i,smooth}$: calculated static shear force; ΔV_{test}: maximum applied shear force in test; *: load cycles of ultimate fatigue load

Table A-6: Load history of test specimen EG02

EG02	$V_{max,test}$ [kN]	$\frac{V_{max,test}}{V_{stat,calc}}$ [-]	ΔV_{test} [kN]	$\frac{\Delta V_{test}}{V_{max,test}}$ [-]	N [-]
sub-test I	116	0.80	35	0.30	0 – 1.500.000
	116	0.80	58	0.50	1,500,000 – 2,660,000*
sub-test II	116	0.80	58	0.50	2,660,000 – 3,590,000*

$V_{max,test}$: maximum applied shear force in test; $V_{stat,calc} = V_{Rm,i,smooth}$: calculated static shear force; ΔV_{test}: maximum applied shear force in test; *: load cycles of ultimate fatigue load

Table A-7: Load history of test specimen EG03

EG03	$V_{max,test}$ [kN]	$\frac{V_{max,test}}{V_{stat,calc}}$ [-]	ΔV_{test} [kN]	$\frac{\Delta V_{test}}{V_{max,test}}$ [-]	N [-]
sub-test I	152	0.70	90	0.65	0 – 2,075,444*
sub-test II	152	0.70	90	0.65	2,075,000 – 3,250,000*

$V_{max,test}$: maximum applied shear force in test; $V_{stat,calc} = V_{Rm,i,rough}$: calculated static shear force; ΔV_{test}: maximum applied shear force in test; *: load cycles of ultimate fatigue load

Table A-8: Load history of test specimen EG04

EG04	$V_{max,test}$ [kN]	$\frac{V_{max,test}}{V_{stat,calc}}$ [-]	ΔV_{test} [kN]	$\frac{\Delta V_{test}}{V_{max,test}}$ [-]	N [-]
sub-test I	165	0.60	82.5	0.55	0 – 3,000,000
	165	0.60	97.5	0.65	3,000,000 – 4,000,000
	165	0.60	112.5	0.75	4,000,000 – 4,363,000*
sub-test II	260(1)				

$V_{max,test}$: maximum applied shear force in test; $V_{stat,calc} = V_{Rm,sy}$: calculated static shear force; ΔV_{test}: maximum applied shear force in test; *: load cycles of ultimate fatigue load; (1): no fatigue sub-test II due to processed fracture of second side – static residual capacity

Table A-9: Load history of test specimen EG05

EG05	$V_{max,test}$ [kN]	$\frac{V_{max,test}}{V_{stat,calc}}$ [-]	ΔV_{test} [kN]	$\frac{\Delta V_{test}}{V_{max,test}}$ [-]	N [-]
sub-test I	226	0.60	113	0.53	0 – 27,000*
sub-test II	271(1)				

$V_{max,test}$: maximum applied shear force in test; $V_{stat,calc} = V_{Rm,max}$: calculated static shear force; ΔV_{test}: maximum applied shear force in test; *: load cycles of ultimate fatigue load; (1): no fatigue sub-test II due to processed fracture of second side – static residual capacity

Table A-10: Load history of test specimen EG06

EG06	$V_{max,test}$ [kN]	$\frac{V_{max,test}}{V_{stat,calc}}$ [-]	ΔV_{test} [kN]	$\frac{\Delta V_{test}}{V_{max,test}}$ [-]	N [-]
sub-test I	172	0.70	105	0.65	0 – 2,250,000
	197	0.80	120	0.65	2,250,000 – 2,604,000*
sub-test II	197	0.80	120	0.65	2,604,000 – 2,615,000*

$V_{max,test}$: maximum applied shear force in test; $V_{stat,calc} = V_{Rm,i,rough}$: calculated static shear force; ΔV_{test}: maximum applied shear force in test; *: load cycles of ultimate fatigue load

Table A-11: Load history of test specimen EG07

EG07	$V_{max,test}$ [kN]	$\frac{V_{max,test}}{V_{stat,calc}}$ [-]	ΔV_{test} [kN]	$\frac{\Delta V_{test}}{V_{max,test}}$ [-]	N [-]
sub-test I	172	0.60	87.5	0.55	0 – 2,000,000
	172	0.60	105	0.65	2,000,000 – 3,000,000
	172	0.60	120	0.75	3,000,000 – 4,000,000
	197	0.70	120	0.75	4,000,000 – 4,033,000*
sub-test II	197	0.70	120	0.75	4,033,000 – 6,283,000*

$V_{max,test}$: maximum applied shear force in test; $V_{stat,calc} = V_{Rm,sy}$: calculated static shear force; ΔV_{test}: maximum applied shear force in test; *: load cycles of ultimate fatigue load

Table A-12: Load history of test specimen EG08

EG08	$V_{max,test}$ [kN]	$\frac{V_{max,test}}{V_{stat,calc}}$ [-]	ΔV_{test} [kN]	$\frac{\Delta V_{test}}{V_{max,test}}$ [-]	N [-]
sub-test I	215	0.60	110	0.55	0 – 2,000,000
	215	0.60	132.5	0.65	2,000,000 – 3,000,000
	215	0.60	152.5	0.75	3,000,000 – 3,951,703*
sub-test II	(2)				

$V_{max,test}$: maximum applied shear force in test; $V_{stat,calc} = V_{Rm,max}$: calculated static shear force; ΔV_{test}: maximum applied shear force in test; *: load cycles of ultimate fatigue load; (2): no sub-test II due to processed fracture of second side

Table A-13: Load history of test specimen EG09

EG09	$V_{max,test}$ [kN]	$\frac{V_{max,test}}{V_{stat,calc}}$ [-]	ΔV [kN]	$\frac{\Delta V_{test}}{V_{max,test}}$ [-]	N [-]
sub-test I	155	0.70	92.5	0.65	0 – 8,700*
sub-test II	155	0.70	60	0.45	8,700 – 1,095,000*

$V_{max,test}$: maximum applied shear force in test; $V_{stat,calc} = V_{Rm,I,rough}$: calculated static shear force; ΔV_{test}: maximum applied shear force in test; *: load cycles of ultimate fatigue load

Table A-14: Load history of test specimen EG10

EG10	$V_{max,test}$ [kN]	$\frac{V_{max,test}}{V_{stat,calc}}$ [-]	ΔV_{test} [kN]	$\frac{\Delta V_{test}}{V_{max,test}}$ [-]	N [-]
sub-test I	282	0.5	150	0.6	0 – 2,000,000
	372	0.7	225	0.9	2,000,000 – 2,001,000
sub-test II	(2)				

$V_{max,test}$: maximum applied shear force in test; $V_{stat,calc} = V_{Rm,i,smooth}$: calculated static shear force; ΔV_{test}: maximum applied shear force in test; *: load cycles of ultimate fatigue load; (2): no sub-test II due to processed fracture of second side

Table A-15: Load history of test specimen EG11

EG11	$V_{max,test}$ [kN]	$\frac{V_{max,test}}{V_{stat,calc}}$ [-]	ΔV_{test} [kN]	$\frac{\Delta V_{test}}{V_{max,test}}$ [-]	N [-]
sub-test I	537	0.55	195	0.40	0 – 310,000*
sub-test II	537	0.55	196	0.40	310,000 – 1,210,000*

$V_{max,test}$: maximum applied shear force in test; $V_{stat,calc} = V_{Rm,max}$: calculated static shear force; ΔV_{test}: maximum applied shear force in test; *: load cycles of ultimate fatigue load

Table A-16: Load history of test specimen EG12

EG12	$V_{max,test}$ [kN]	$\frac{V_{max,test}}{V_{stat,calc}}$ [-]	ΔV_{test} [kN]	$\frac{\Delta V_{test}}{V_{max,test}}$ [-]	N [-]
sub-test I	359	0.60	135	0.40	0 – 2,000,000
	359	0.60	197.5	0.60	2,000,000 – 3,375,000
	420	0.70	232.5	0.60	3,375,000 – 4,119,000*
sub-test II	420	0.70	232.5	0.60	4,119 – 4,465,000*

$V_{max,test}$: maximum applied shear force in test; $V_{stat,calc} = V_{Rm,i,rough}$: calculated static shear force; ΔV_{test}: maximum applied shear force in test; *: load cycles of ultimate fatigue load

Table AA-17: Load history of test specimen EG13

EG13	$V_{max,test}$ [kN]	$\frac{V_{max,test}}{V_{stat,calc}}$ [-]	ΔV_{test} [kN]	$\frac{\Delta V_{test}}{V_{max,test}}$ [-]	N [-]
sub-test I	519	0.55	165	0.40	0 – 435*
sub-test II	519	0.55	165	0.40	435 – 9,600*

$V_{max,test}$: maximum applied shear force in test; $V_{stat,calc} = V_{Rm,max}$: calculated static shear force; ΔV_{test}: maximum applied shear force in test; *: load cycles of ultimate fatigue load

Table A-18: Load history of test specimen EG14

EG14	$V_{max,test}$ [kN]	$\frac{V_{max,test}}{V_{stat,calc}}$ [-]	ΔV_{test} [kN]	$\frac{\Delta V_{test}}{V_{max,test}}$ [-]	N [-]
sub-test I	487	0.55	175,	0.40	0 – 1,626,488*
sub-test II	487	0.55	175	0.40	1,626,000 – 1,655,000*

$V_{max,test}$: maximum applied shear force in test; $V_{stat,calc} = V_{Rm,max}$: calculated static shear force; ΔV_{test}: maximum applied shear force in test; *: load cycles of ultimate fatigue load

A.5 Crack patterns

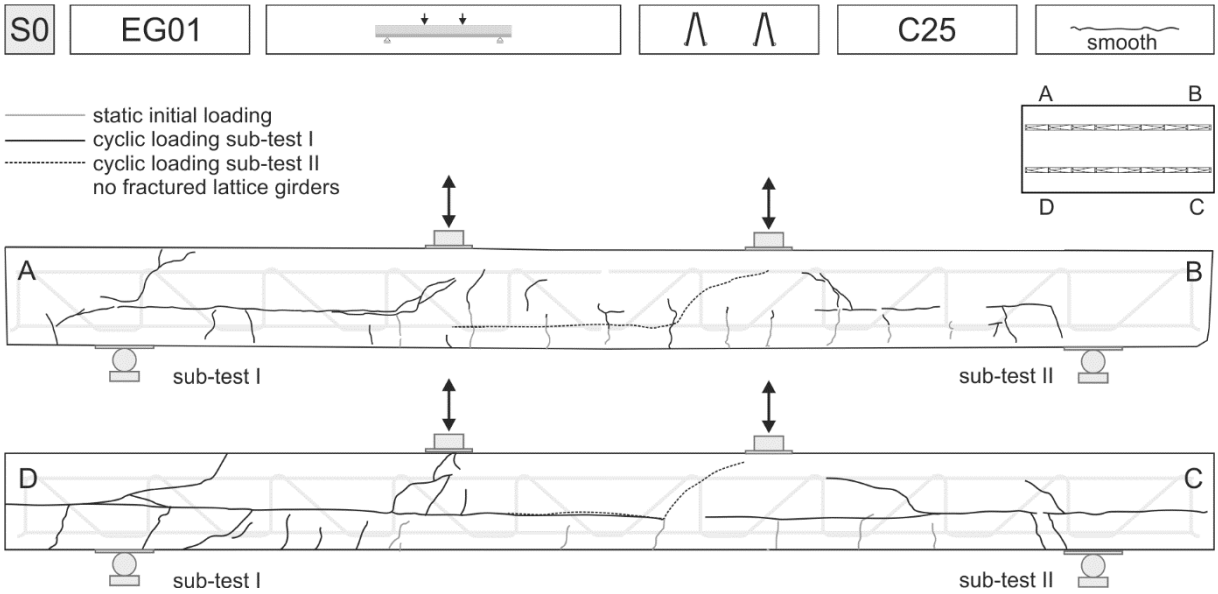

Figure A-7: Test parameters, crack patterns and lattice girder fractures of specimen EG01

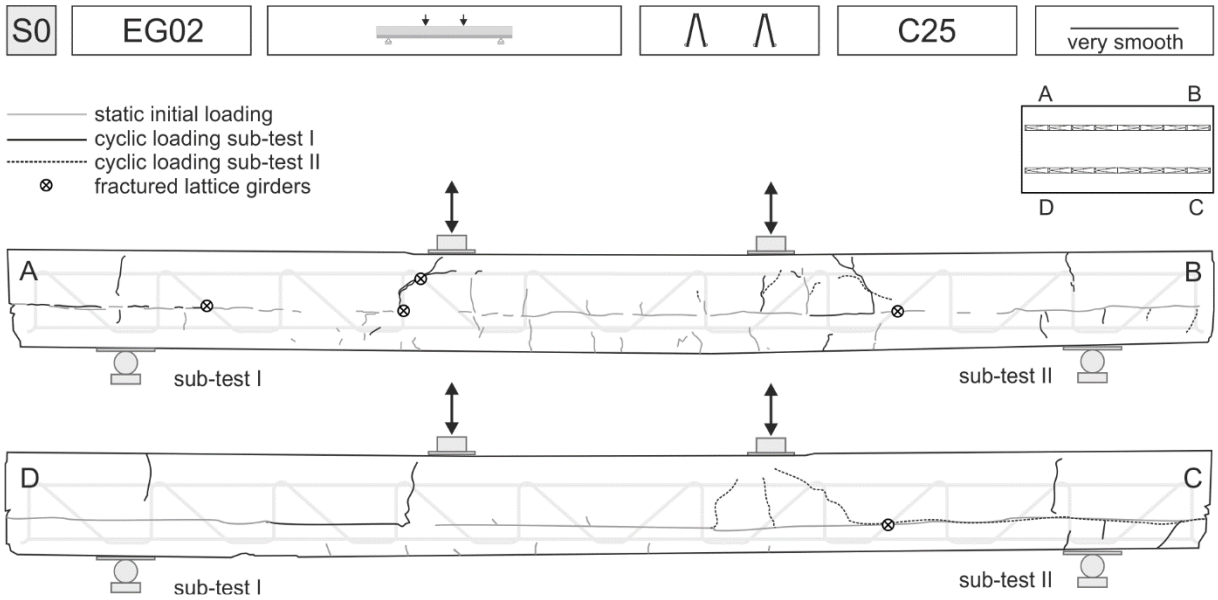

Figure A-8: Test parameters, crack patterns and lattice girder fractures of specimen EG02

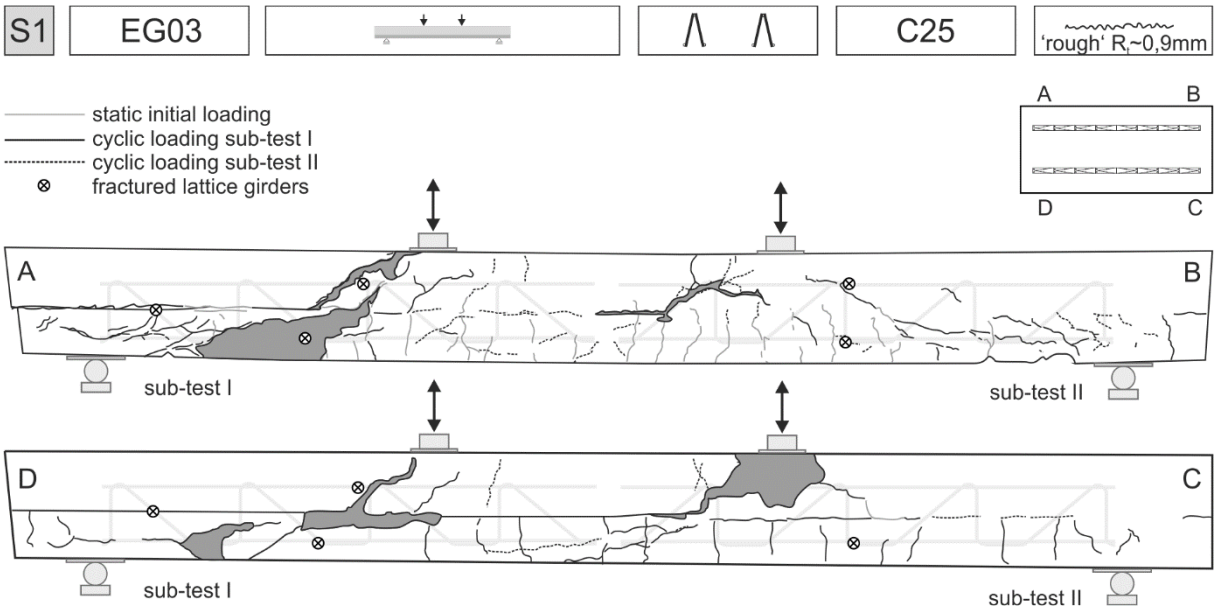

Figure A-9: Test parameters, crack patterns and lattice girder fractures of specimen EG03

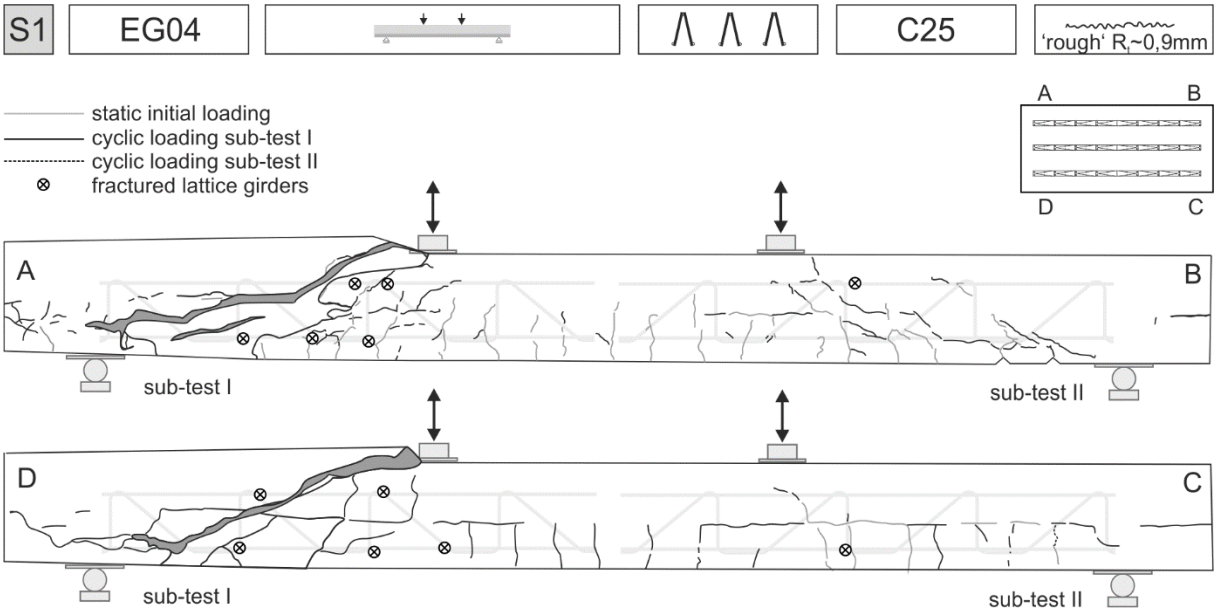

Figure A-10: Test parameters, crack patterns and lattice girder fractures of specimen EG04

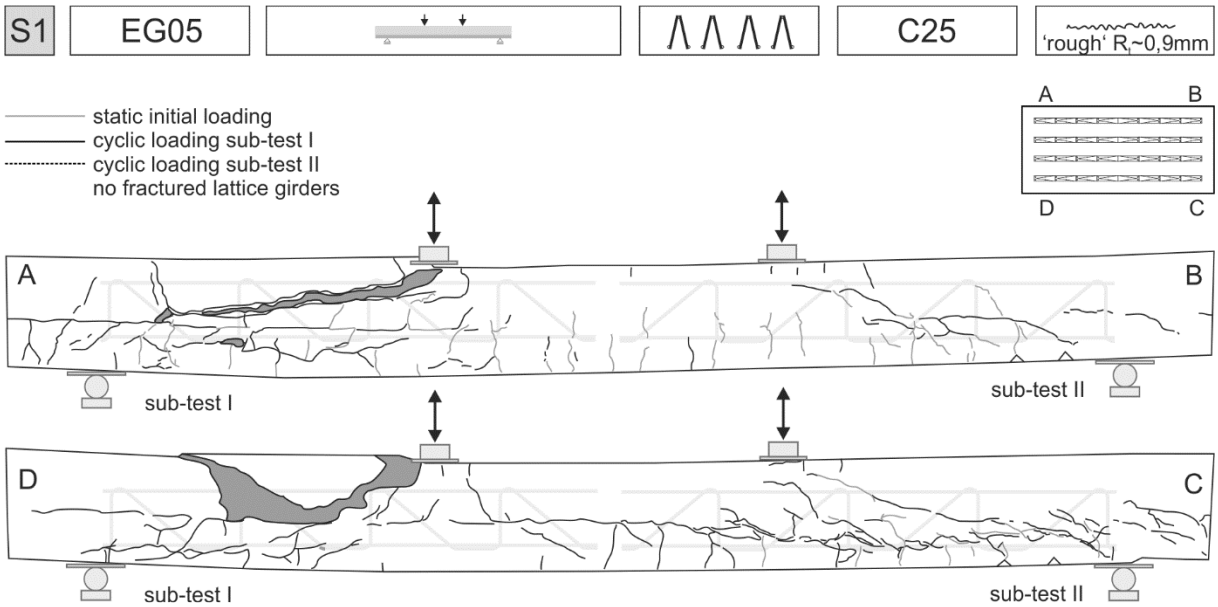

Figure A-11: Test parameters, crack patterns and lattice girder fractures of specimen EG05

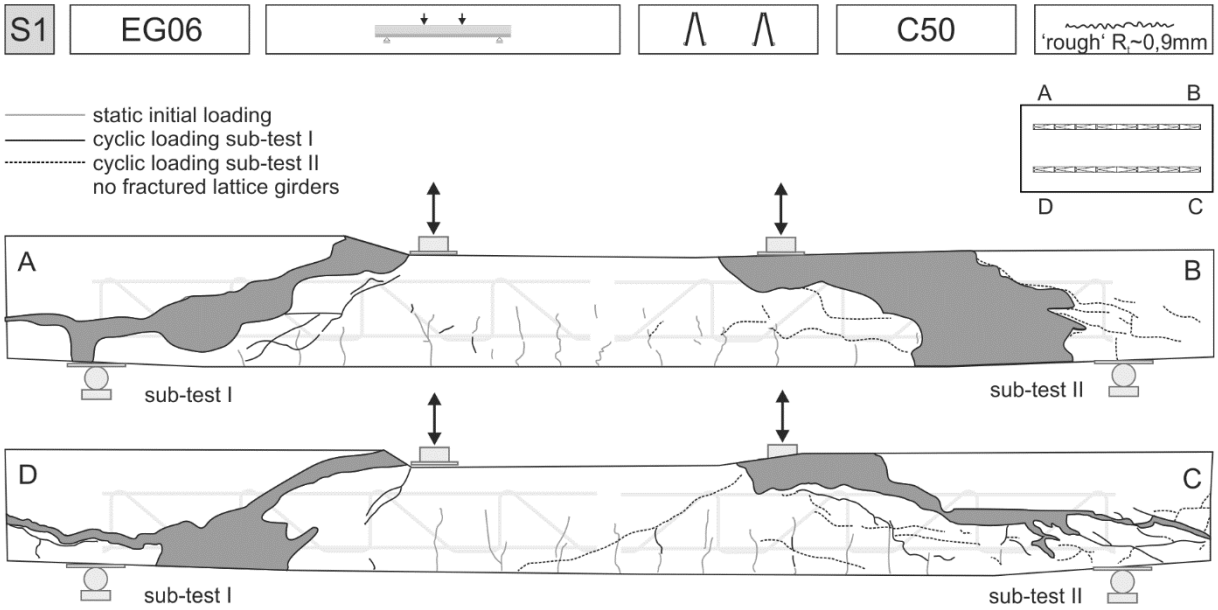

Figure A-12: Test parameters, crack patterns and lattice girder fractures of specimen EG06

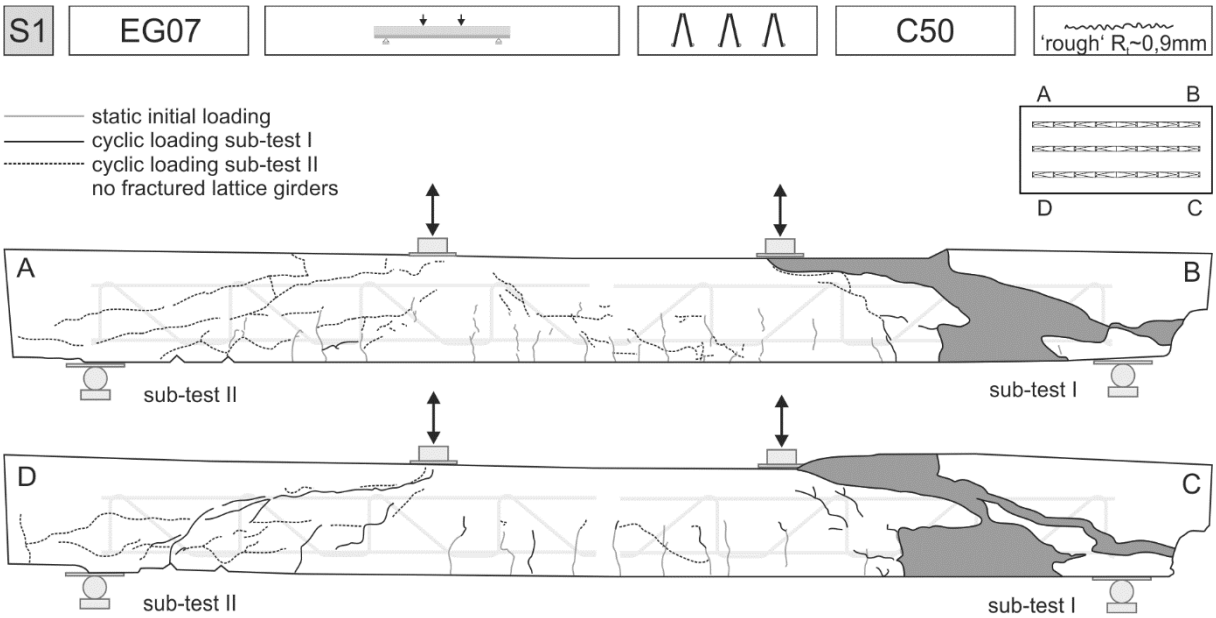

Figure A-13: Test parameters, crack patterns and lattice girder fractures of specimen EG07

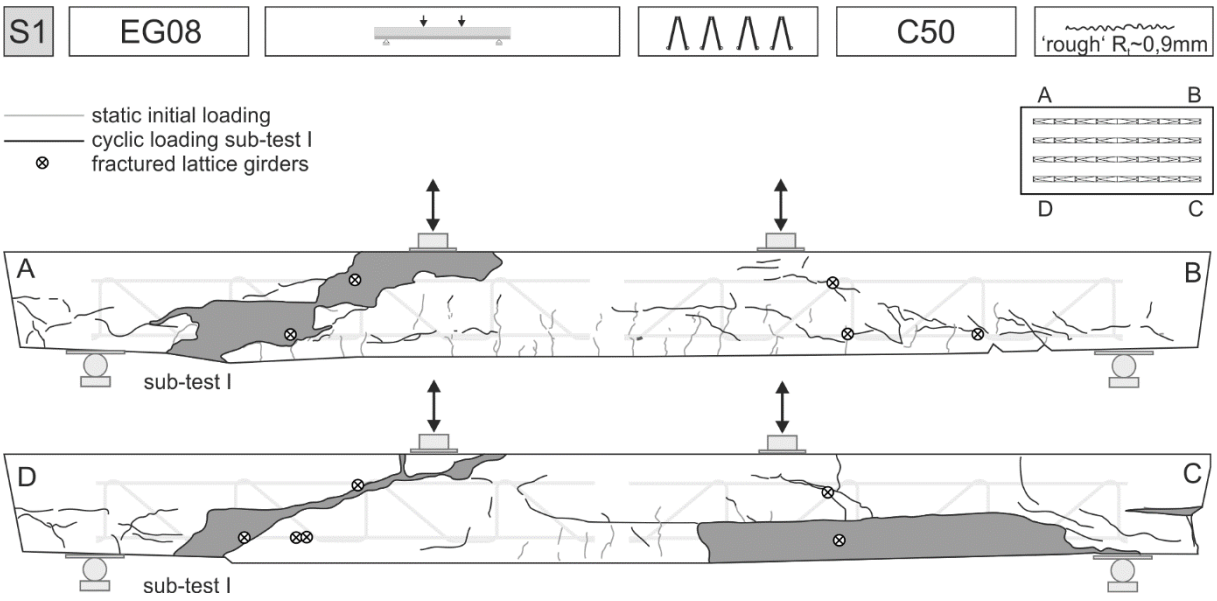

Figure A-14: Test parameters, crack patterns and lattice girder fractures of specimen EG08

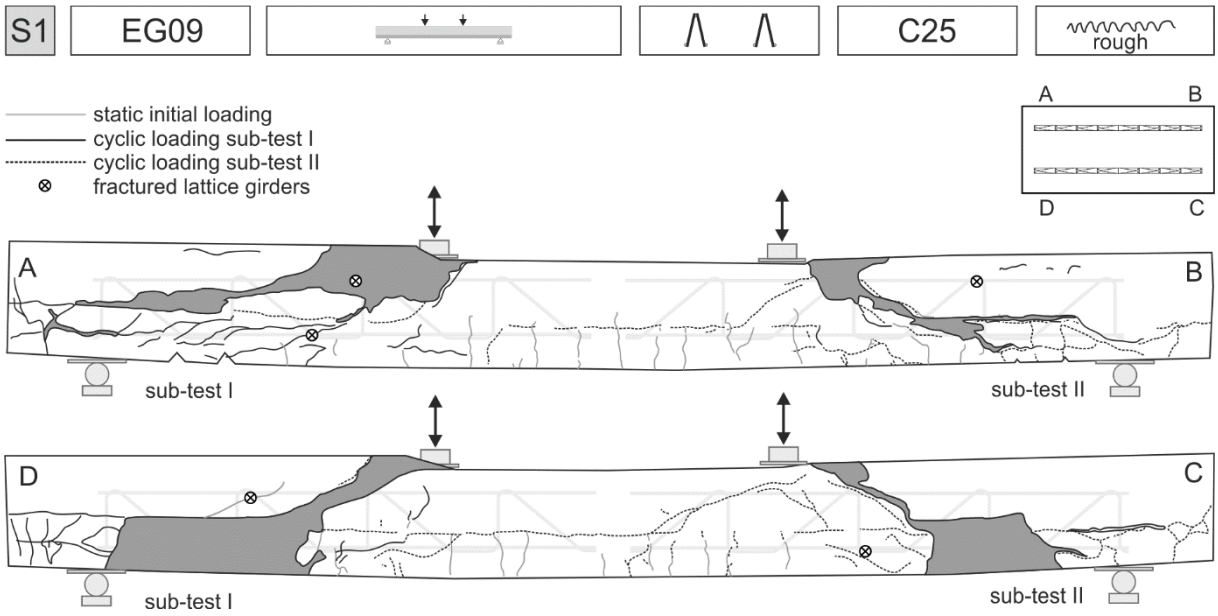

Figure A-15: Test parameters, crack patterns and lattice girder fractures of specimen EG09

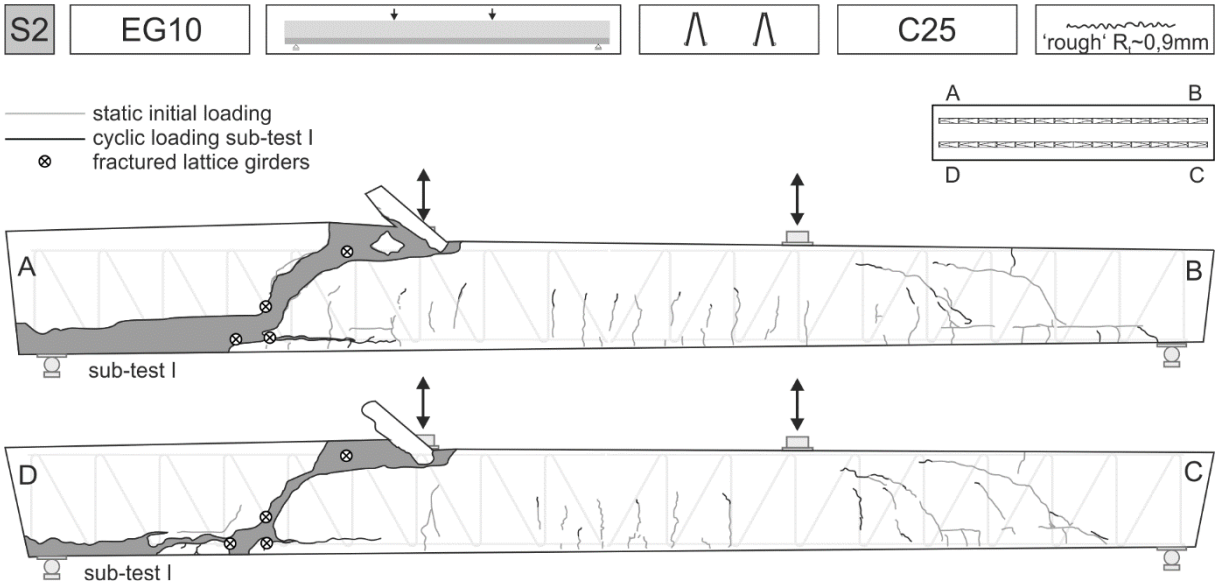

Figure A-16: Test parameters, crack patterns and lattice girder fractures of specimen EG10

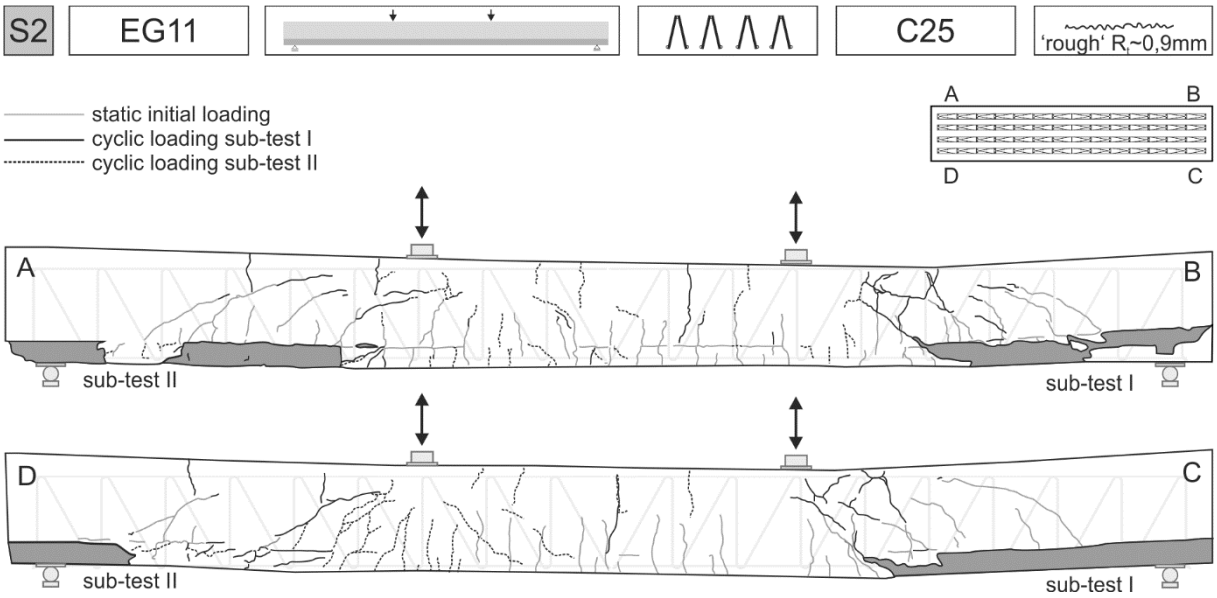

Figure A-17: Test parameters, crack patterns and lattice girder fractures of specimen EG11

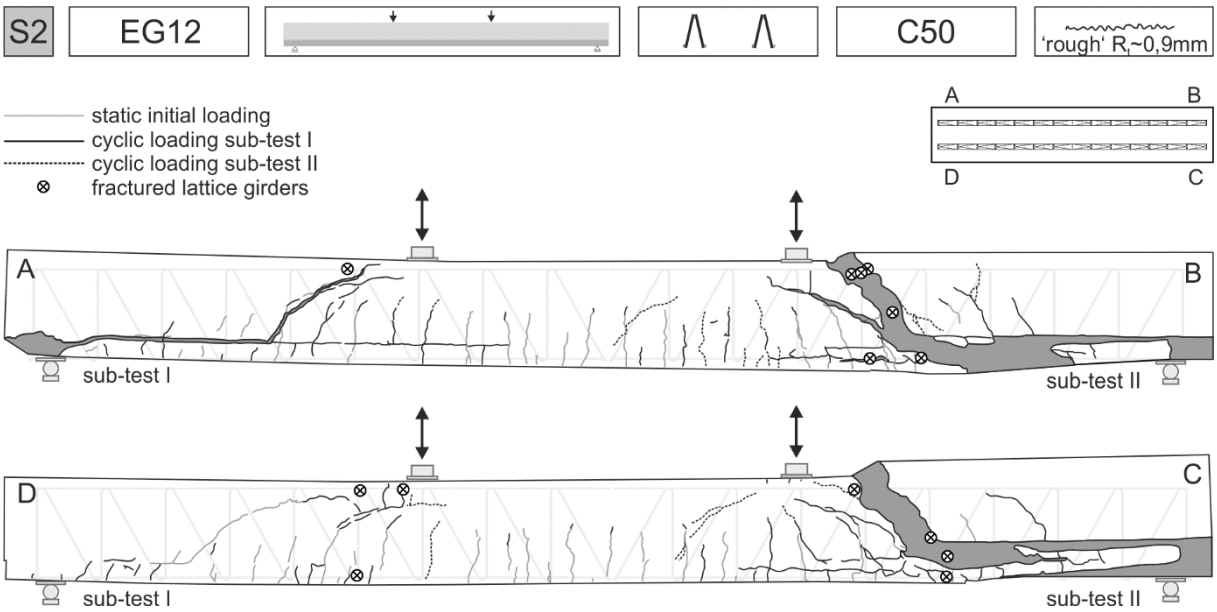

Figure A-18: Test parameters, crack patterns and lattice girder fractures of specimen EG12

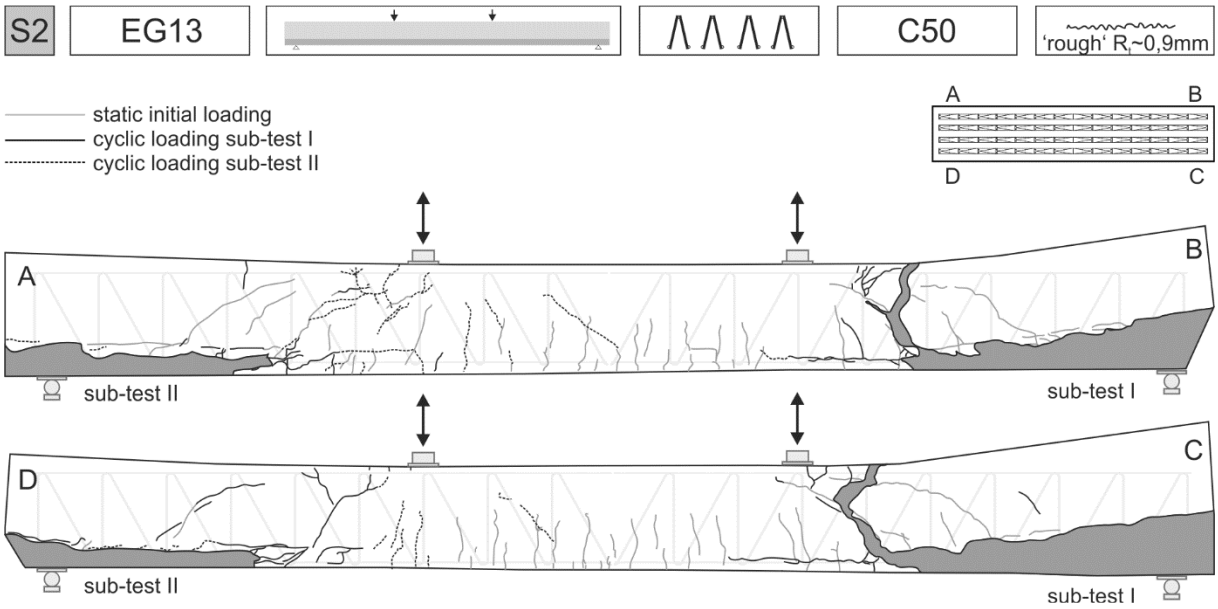

Figure A-19: Test parameters, crack patterns and lattice girder fractures of specimen EG13

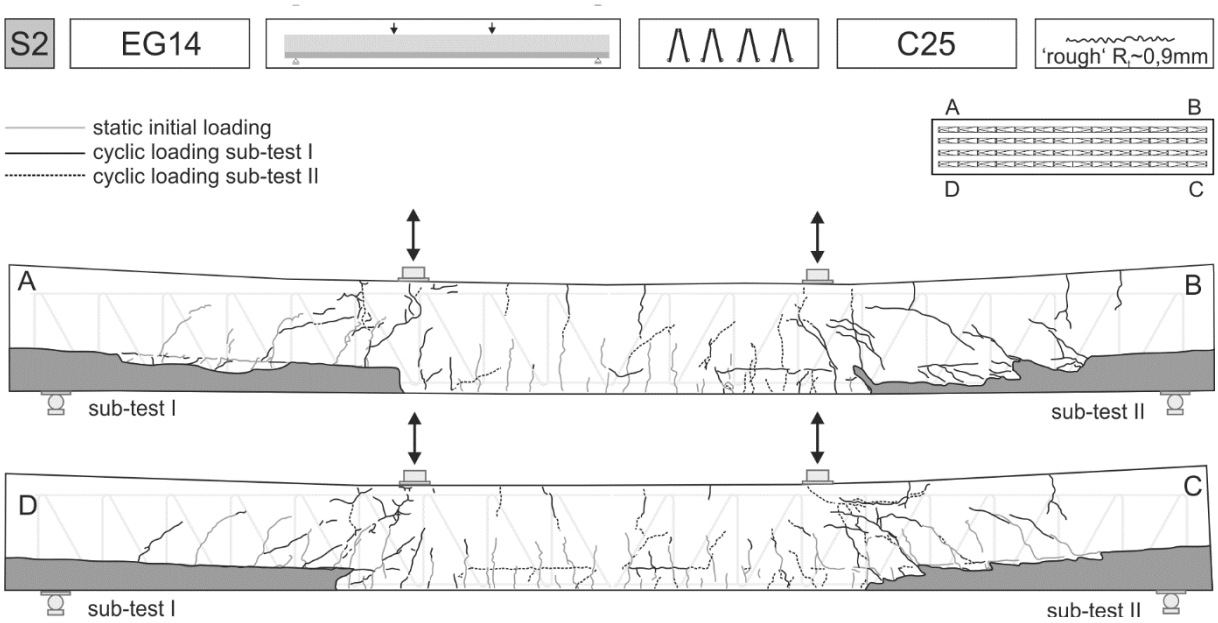

Figure A-20: Test parameters, crack patterns and lattice girder fractures of specimen EG14

Annex B Database

Annex B.1.1 and B.2.1 present the test setups and main test parameters for each test programme in the databases for small size tests as well as structural member tests. An extensive overview of test parameters and failure shear stresses for each test specimen within the test programmes are presents in the corresponding database in Annex B.1.2 – B.1.7 (small size tests) and B.2.2 – B.2.7 (structural member tests).

Notations

Databases

A-1	Database with small size tests without normal stress and interface reinforcement under monotonic loading
A-2	Database with small size tests with normal stress and without interface reinforcement under monotonic loading
B	Database with small size tests with interface reinforcement and without normal stress under monotonic loading
AB	Database with small size tests with normal stress and with interface reinforcement under monotonic loading
C	Database with small size tests without interface reinforcement under cyclic loading
D	Database with small size tests with interface reinforcement under cyclic loading
E	Database with beam and slab specimens without interface reinforcement under monotonic loading
F-1	Database with beam and slab specimens with stirrups as interface reinforcement under monotonic loading
F-2	Database with beam and slab specimens with lattice girders as interface reinforcement under monotonic loading
G	Database with beam and slab specimens without interface reinforcement under cyclic loading
H-1	Database with beam and slab specimens with stirrups as interface reinforcement under cyclic loading
H-2	Database with beam and slab specimens with lattice girders as interface reinforcement under cyclic loading

Interface classification

vs:	very smooth
s:	smooth
r:	rough
vr:	very rough
k:	keyed

Test setup

p-o:	push-off
m po:	modified push-off
co	corbel
m co:	modified corbel
p-th:	push-through
sw:	sliding wall

Test parameters

α	inclination of interface reinforcement
α_1	inclination of first lattice girder diagonal
α_2	inclination of second lattice girder diagonal
a_{int}	distance between load application and support
A_{int}	cross-sectional area of interface
b_{int}	width of interface
d	effective depth
$f_{cm,cyl,1}$	mean cylinder concrete compressive strength of first concrete layer
$f_{cm,cyl,2}$	mean cylinder concrete compressive strength of second concrete layer
$f_{ctm,1}$	mean concrete tensile strength of first concrete layer
$f_{ctm,2}$	mean concrete tensile strength of second concrete layer
$f_{ym,l}$	mean yield strength of longitudinal reinforcement
$f_{ym,int}$	mean yield strength of interface reinforcement
$f_{ym,int}$	mean yield strength of lattice girders
h_{LG}	height of lattice girders
h_{ins}	height of insitu concrete layer
h_{pre}	height of precast element
LG	lattice girder
l_{int}	length of interface
N	number of load cycles
n_{LG}	number of rows of lattice girders
ρ_{int}	interface reinforcement ratio
ρ_l	longitudinal reinforcement ratio
R_t	mean roughness depth
s_{LG}	transverse spacing of lattice girders
σ_n	applied normal stress
τ_{test}	tested shear stress
$\tau_{test,res}$	residual shear stress
$\tau_{test,max}$	maximum applied shear stress
$\Delta\tau_{test}$	applied shear stress range

B.1 Small size specimens

B.1.1 Overview of test reports in database

Autor:	Albrecht, C.	[Alb14]
Title:	Bemessung von Stahlbetondecken mit abgeflachten rotationssymmetrischen Hohlkörpern und ein Beitrag zum besseren Verständnis der Querkrafttragfähigkeit	
Source:	PhD-thesis, Institute of Structural Concrete, Technische Universität Kaiserslautern, 2014	

Test setup:

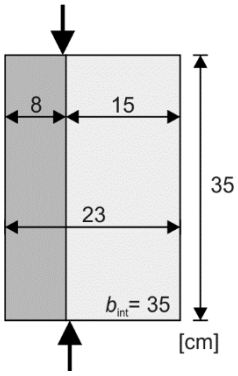

Nr. of tests	9
very smooth	–
smooth(1)	7
rough(2)	2
very rough	–
keyed	–

Normal stress: External prestressing

Interface reinforcement: –

(1): smooth: left as cast; (2): rough: fast screeding

Autor:	Annamalai, G.; Brown, R.C.	[Ann90]
Title:	Shear-Transfer Behavior of Post-Tensioned Grouted Shear-Key Connections in Pre-cast Concrete-Framed Structures	
Source:	ACI Structural Journal, Vol. 87, No. 1, pp.: 53-59, 1990	

Test setup:

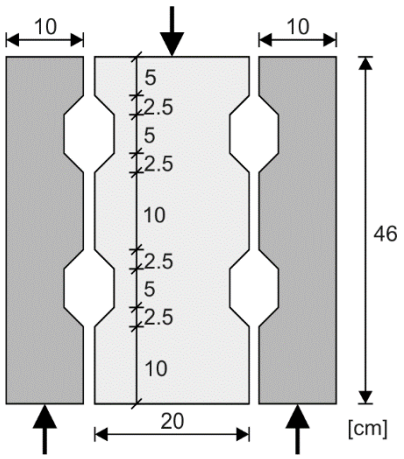

Nr. of tests	28
very smooth	–
smooth	–
rough	–
very rough	–
keyed(1)	28

Normal stress: External prestressing

Interface reinforcement: –

(1): grouted joint

Autor:	Banta, T.E.	[Ban05]
Title:	Horizontal shear transfer between ultra high performance concrete and lightweight concrete	
Source:	PhD-thesis, Virginia Polytechnic Institute and State University, 2005	

Test setup:

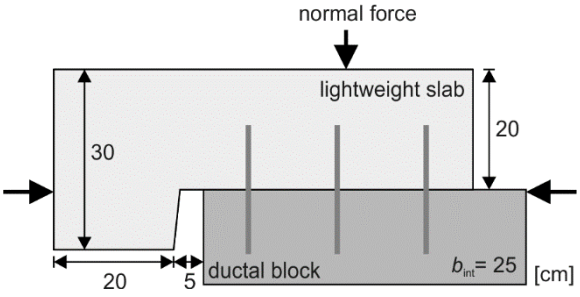

Nr. of tests	24
very smooth	–
smooth(1)	18
rough(2)	4
very rough	–
keyed	2

Normal stress: Was applied to simulate dead load of bridge deck

Interface reinforcement: 0, 1, 2, 4, 6 of Ø9.5 mm bars

(1): smooth: smoothened to prevent surface deformations; (2): rough: raked

Autor:	Barbosa A, Trejo, D.; Nielson, D.	[Bar17]
Title:	Effect of High-Strength Reinforcement Steel on Shear Friction Behavior	
Source:	Journal of Bridge Engineering, Vol. 22, No. 8, 2017	

Test setup:

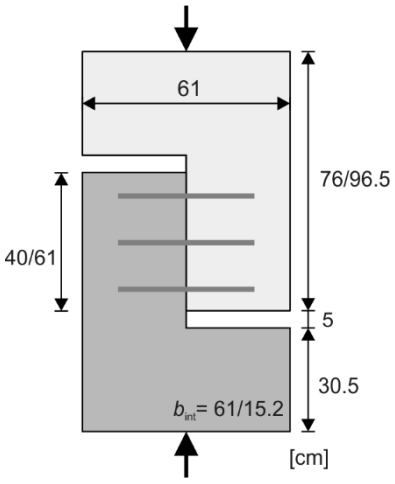

Nr. of tests	4
very smooth	–
smooth	–
rough(1)	4
very rough	–
keyed	–

Normal stress: –

Interface reinforcement: 3 and 4 rows of Ø12.7 and Ø15.9 mm stirrups

(1): rough: not intentionally roughened but with coarse aggregates

Autor:	Bass, R. A.; R. L. Carrasquillo; J. O. Jirsa	[Bas89]
Title:	Shear Transfer Across New and Existing Concrete Interfaces	
Source:	ACI Structural Journal Vol. 86, No. 4, pp.: 383-393, 1989	

Test setup:

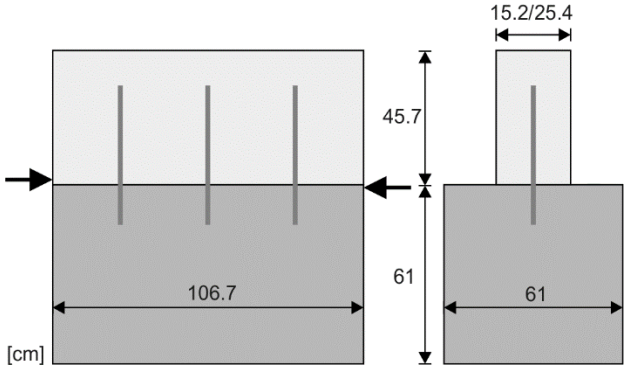

Nr. of tests	33
very smooth	–
smooth(1)	1
rough(2)	25
very rough(3)	4
keyed	3

Normal stress: –

Interface reinforcement: 2 – 6 dowels with Ø19 mm and between 7.6 – 30.5 mm embedment depth and 15.2 – 30.5 mm bar spacing

(1): smooth: untreated as cast; (2): rough: heavily sandblasted, (3): very rough: chipped

Autor:	Beck, H.; Mehlhorn, G.; Stauder, W.; Schwing, H.	[Bec73]
Title:	Zusammenwirken von einzelnen Fertigteilen als großflächige Scheibe	
Source:	Deutscher Ausschuss für Stahlbeton DAfStb, Issue 224, Beuth Verlag, 1973	

Test setup:

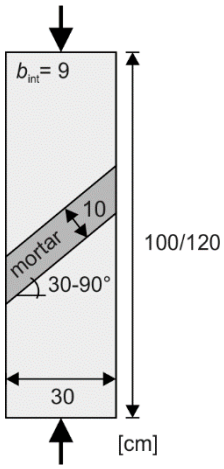

Nr. of tests	88
very smooth	–
smooth(1)	34
rough	–
very rough(2)	54
keyed	–

Normal stress: Constant ratio of shear and normal stress due to inclined interface

Interface reinforcement: –

(1): smooth: left as cast; (2): very rough: waved

Autor:	Choi, D.U.; Jirsa, J.O.; Fowler, D.W.	[Cho99]
Title:	Shear Transfer across Interface between New and Existing Concretes Using Large Powder-Driven Nails	
Source:	ACI Structural Journal, Title no. 96-S20, pp. 183-192 March-April, 1999	

Test setup:

Push off tests, no picture of test setup provided

Nr. of tests	44
very smooth	–
smooth(1)	14
rough(2)	30
very rough	–
keyed	–

Normal stress: Selfweight

Interface reinforcement: 0, 1, 2 large powder driven nails with Ø10 mm and 120 mm length

(1): smooth: lightly sandblasted, trowel finish, 12 specimens with bondbreaker; (2): rough: heavily sandblasted

Autor:	Daschner, F.	[Das86a]
Title:	Versuche zur notwendigen Schubbewehrung zwischen Betonfertigteilen und Ortbeton	
Source:	Deutscher Ausschuss für Stahlbeton DAfStb, Issue 372, Ernst & Sohn Verlag, Berlin, 1986	

Test setup:

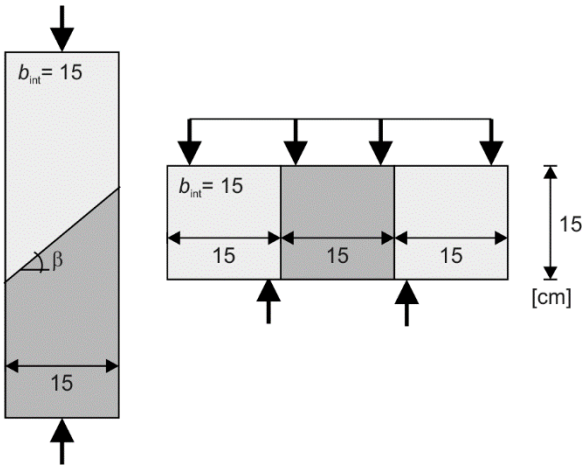

Nr. Of tests	172
very smooth(1)	18
smooth(2)	57
rough(3)	44
very rough(4)	53
keyed	–

56 modified push-off

116 push through

Normal stress: Modified push off: constant ratio of shear and normal stress due to inclined interface

Push-through: normal stress externally applied

Interface reinforcement: Push-through: 0, 1, 2, 3 and 4 stirrups Ø10 mm

(1): very smooth: cast against wood, (2): smooth: left as cast, additionally smoothened, (3): rough: raked, sandblasted, (4): very rough: triangular and rectangular shapes

Autor:	Dulacska, H.	[Dul72]
Title:	Dowel Action of Reinforcement Crossing Cracks in Concrete	
Source:	ACI Journal Proceedings, Vol. 69, pp. 754-757, 1972.	

Test setup:

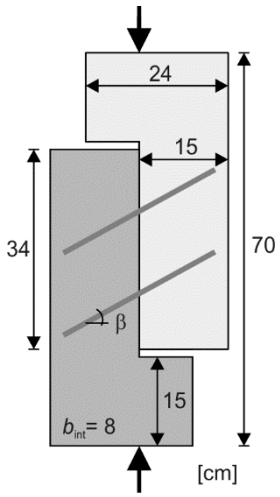

Nr. of tests	16
very smooth(1)	16
smooth	–
rough	–
very rough	–
keyed	–

Normal stress: Modified push off: constant ratio of shear and normal stress due to inclined interface

Push-through: normal stress externally applied

Interface reinforcement: 2 bars Ø6.5, Ø10 and Ø14 mm and inclinations β=10°, 20°, 30° and 40°

(1): very smooth: concrete separated sheet brass

Autor:	Franz, G.	[Fra59]
Title:	Versuche über die Querkraftaufnahme in Fugen von Spannbetonträgern aus Fertigteilen	
Source:	Beton- und Stahlbetonbau, Vol. 54, Issue 6, pp. 137-140, 1959.	

Test setup:

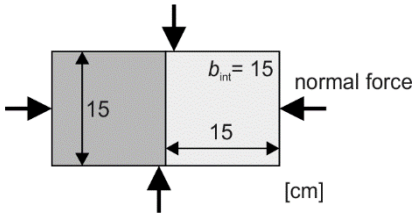

Nr. of tests	16
very smooth	12
smooth	–
rough	–
very rough	–
keyed	4

Normal stress: Applied by two external stressed steel bars

Interface reinforcement: –

Autor:	Gaston, J.R.; Kriz, L.B.	[Gas64]
Title:	Connections in precast concrete structures – scarf joints	
Source:	PCI Journal, Vol. 9, No. 3, pp. 37-59, 1964	

Test setup:

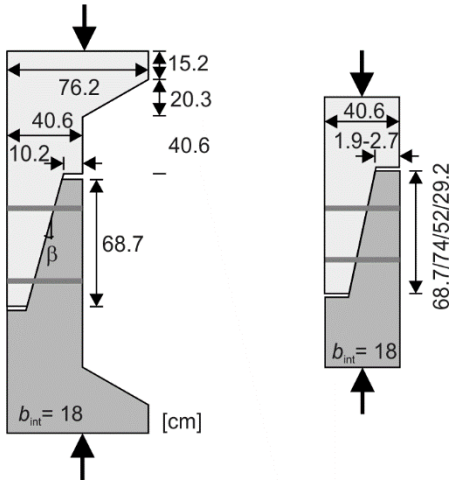

Nr. of tests	12
very smooth	–
smooth	–
rough(1)	12
very rough	–
keyed	–

Interface inclination β=45°, 25°, 15° and 11°

Normal stress: By prestressed bolts and inclined interface

Interface reinforcement: 2 prestressed bolts Ø28.6

(1): rough: no further classifications

Autor:	GOHNERT, M.	[Goh00]
Title:	Proposed theory to determine the horizontal shear between composite precast and in situ concrete	
Source:	Cement and Concrete Composites 22, 469-476, 2000	

Test setup:

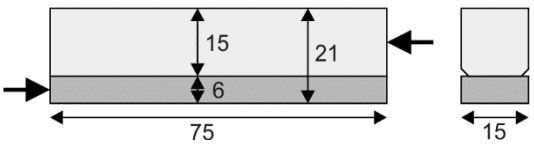

Nr. of tests	12
very smooth	–
smooth	–
rough(1)	12
very rough	–
keyed	–

Normal stress: –

Interface reinforcement: –

(1): rough: brushed surface

Autor: GOHNERT, M. [Goh03]

Title: Horizontal shear transfer across a roughened surface

Source: Cement and Concrete Composites, Vol. 25, No. 3, pp. 379-385, 2003

Test setup:

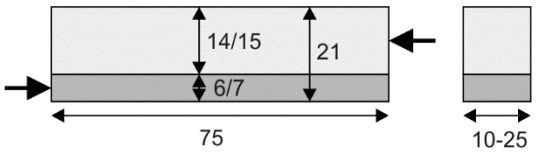

Nr. of tests	90
very smooth	–
smooth	–
rough(1)	30
very rough(2)	60
keyed	–

Normal stress: –

Interface reinforcement: –

(1): rough: brushed surface; (2): very rough: raked surface

Autor: Hanson, N.W.. [Han60]

Title: Precast-Prestressed Concrete Bridges 2. Horizontal Shear connections

Source: Portland Cement Association, Research and Development Laboratories, Bulletin D35, Vol. 2, No. 2, pp. 38-58, 1960

Test setup:

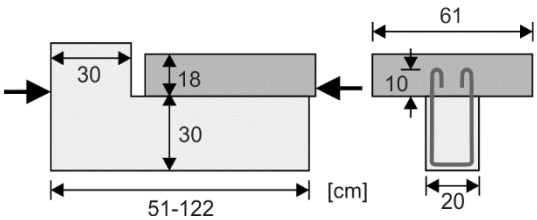

Nr. of tests	62
very smooth	–
smooth(1)	15
rough(2)	10
very rough(3)	21
keyed	16

Normal stress: –

Interface reinforcement: 0 and 2 Ø12.7 stirrups

(1): smooth: left as cast, trowelled, (2) rough: roughened by scrapping; (3): very rough: scrapped with a roughness amplitude of at least 6.4 mm

Autor:	Harries, K. A.; Zeno, G.; Shahrooz, B.	[Har12]
Title:	Toward an Improved Understanding of Shear-Friction Behavior	
Source:	ACI Structural Journal, Vol. 109, Issue 6, 2012	

Test setup:

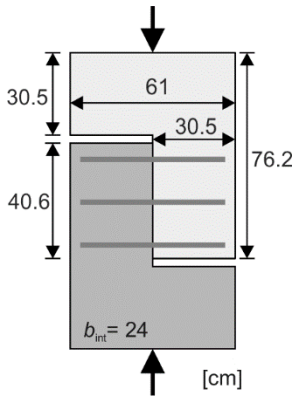

Nr. of tests	8
very smooth	–
smooth	–
rough	–
very rough(1)	8
keyed	–

Normal stress: –

Interface reinforcement: 3 Ø9.5 and Ø12.7 mm stirrups

(1): very rough: scrapped with a roughness amplitude of at least 6.4 mm

Autor:	Kahn, L.F.; Mitchell, A.D.	[Kah02]
Title:	Shear friction tests with high-strength concrete	
Source:	ACI Structural Journal, Vol. 99, No. 1, pp. 98-103, 2002	

Test setup:

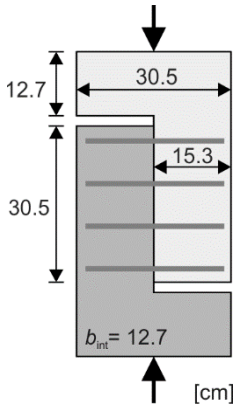

Nr. of tests	12
very smooth	–
smooth(1)	2
rough(2)	10
very rough	–
keyed	–

Normal stress: –

Interface reinforcement: 1, 2, 3 and 4 rows of Ø9.5 mm stirrups

(1): smooth: left as cast; (2): rough: roughened to an amplitude < 6.4 mm

Autor:	Mohamed, M.E.; Ibrahim, I.S.; Abdullah, R.; Rahma, A.B. Abd; Kueh, A.B.H; Usman, J.	[Moh15a]
Title:	Friction and cohesion coefficients of composite concrete to concrete bond	
Source:	Cement and Concrete Composites, Vol. 56, pp. 1-14, 2015	

Autor:	Mohamed, M.E.; Ibrahim, I.S.	[Moh15b]
Title:	Interface shear strength of concrete to concrete bond with and without projecting steel reinforcement	
Source:	Journal Teknologi (Science & Engineering), Vol. 75, Issue 1, pp. 169-172, 2015	

Test setup:

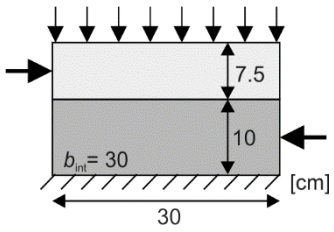

Nr. of tests	72
very smooth	–
smooth(1)	24
rough(2)	24
very rough(3)	12
keyed	12

Normal stress: Applied with 0, 0.5, 1, and 1.5 N/mm²

Interface reinforcement: 1, 2, 3 and 4 rows of Ø9.5 mm stirrups

(1): smooth: left as cast; (2): rough: longitudinal and transverse roughness profiles; (3): very rough: deep grove

Autor:	Papanicolaou, C.G.; Triantafillou, T.C.	[Pap02]
Title:	Shear transfer capacity along pumice aggregate concrete and high-performance concrete interfaces	
Source:	Materials and Structures, Vol. 35, No. 4, pp. 237-245, May, 2002	

Test setup:

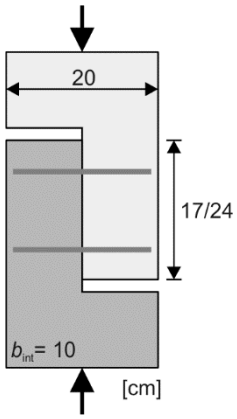

Nr. of tests	36
very smooth	–
smooth(1)	13
rough(2)	23
very rough	–
keyed	–

Normal stress: Applied with 0 and 1.0 N/mm²

Interface reinforcement: 0, 1 and 2 Ø8 mm bars

(1): smooth: smoothened with disk scanner; (2): rough: roughened by hammering

Autor:	Paulay, T.; Park, R.; Phillips, M. H. [Pau74]
Title:	Horizontal Construction Joints in Cast in Place Reinforced Concrete
Source:	ACI-Special Publication, SP-42 Shear in Reinforced Concrete, pp. 599-616, 1974

Test setup:

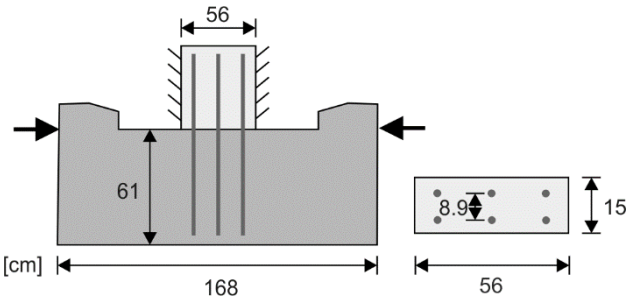

Nr. of tests	30
very smooth(1)	3
smooth(2)	10
rough(3)	13
very rough(4)	3
keyed	1

Normal stress: –

Interface reinforcement: 6 bars with Ø6.25, Ø9.5, Ø12.7 mm

(1): very smooth: finished with steel trowel; (2): smooth: sprayed with retarder and washed; (3): rough: scraped with steel trowel, brushed, (4): very rough: chipped with hammer

Autor:	Randl, N. [Ran97]
Title:	Untersuchungen zur Kraftübertragung zwischen Alt- und Neubeton bei unterschiedlichen Fugenrauhigkeiten
Source:	PhD-Thesis, Faculty of Civil Engineering and Architecture, University Innsbruck, 1997

Test setup:

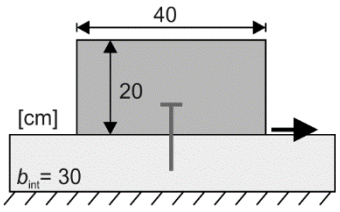

Nr. of tests	83
very smooth(1)	13
smooth(2)	34
rough(3)	36
very rough	–
keyed	–

Normal stress: –

Interface reinforcement: Subsequently applied dowel with Ø6, Ø12 and Ø20 mm

(1): very smooth: casted against formwork; (2): smooth: left as cast; (3): rough: sandblasted, (4): very rough: high pressure water

Autor:	Randl, N.; Steiner, M.	[Ran15]
Title:	Hochfester Beton als Aufbeton im Bestand und als monolithische Deckschicht im Neubau- Aufbetonschichten	
Source:	Research Report, Kärnten University of Applied Science, 2015	

Test setup:

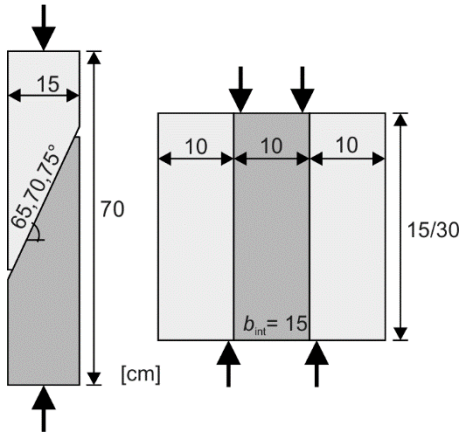

Nr. of tests	27
very smooth	–
smooth(1)	9
rough(2)	9
very rough(3)	9
keyed	–

18 modified push-off
9 push through

Normal stress: Modified push off: constant ratio of shear and normal stress due to inclined interface

Push through: –

Interface reinforcement: –

(1): smooth: slight high pressure water; (2): rough: medium high pressure water; (3): very rough: heavy high pressure water

Autor:	Reinecke, R..	[Rei04]
Title:	Haftverbund und Rissverzahnung in unbewehrten Betonschubfugen	
Source:	PhD Thesis, Chair of Concrete Structures, Technical University of Munich, 2004	

Test setup:

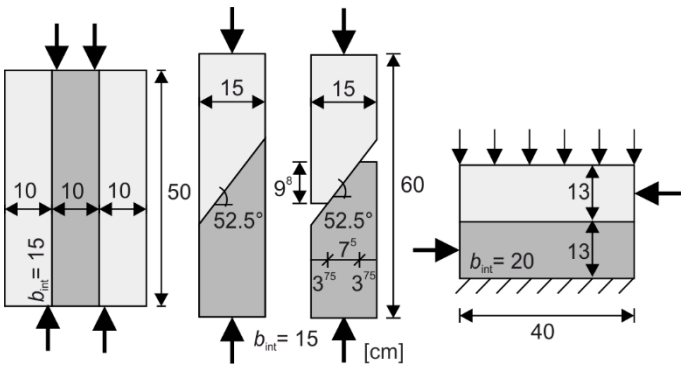

Nr. of tests	107
very smooth	13
smooth(1)	94
rough	–
very rough	–
keyed	–

49 push through
36 modified push-off
22 sliding walls

Normal stress: Modified push off: constant ratio of shear and normal stress due to inclined interface,

Sliding wall: externally applied

Interface reinforcement: –

(1): smooth: left as cast, sandblasted

Autor:	Scott, J.	[Sco10]
Title:	Interface shear strength in lightweight concrete bridge girders	
Source:	M.Sc. Thesis, Virginia Polytechnic Institute and State University, 2010	

Test setup:

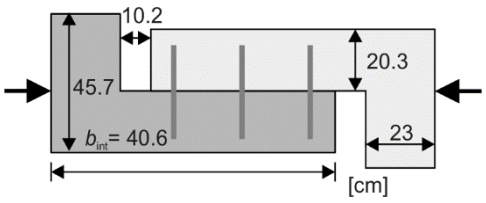

Nr. of tests	27
very smooth	–
smooth	–
rough(1)	27
very rough	–
keyed	–

Normal stress:	Simulated dead weight of concrete girder by a concrete block
Interface reinforcement:	1 and 3 stirrups with Ø9.5 and Ø12.7 mm

(1): rough: raked to an amplitude of 6.3 mm

Autor:	Shaw, D.; Sneed, L.	[Sha14]
Title:	Interface Shear Transfer of Lightweight Aggregate Concretes Cast at Different Times	
Source:	PCI Journal, Vol. 59, No. 3, pp. 130-144, 2014	

Test setup:

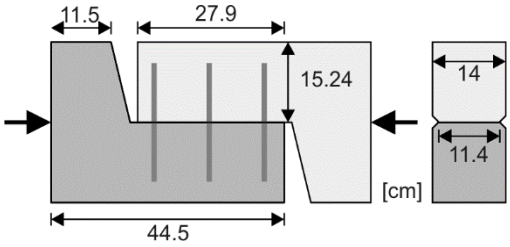

Nr. of tests	36
very smooth	–
smooth	18
rough	18
very rough	–
keyed	–

Normal stress:	–
Interface reinforcement:	3 stirrups with Ø9.5 mm

Autor:	Sneed, L. H.; Krc, K.; Wermager, S.; Meinheit, D..	[Sne16]
Title:	Interface Shear Transfer of Lightweight-Aggregate Concretes	
Source:	PCI Journal, Vol. 61, No. 2, pp. 38-55, 2016	

Test setup:

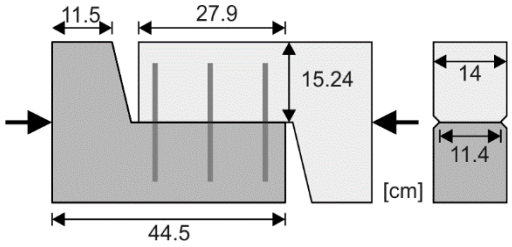

Nr. of tests	34
very smooth	–
smooth(1)	18
rough(2)	16
very rough	–
keyed	–

Normal stress: –

Interface reinforcement: 2, 3, 4 and 5 stirrups with Ø9.5 mm

(1): smooth: left as cast; (2): rough: scoring indentations

Autor:	Valluvan, R., Kreger, M. E.; Jirsa, J. O.	[Val99]
Title:	Evaluation of ACI 318-95 Shear-Friction Provisions	
Source:	ACI Structural Journal, Vol. 96, Issue 4, pp. 473-482, 1999	

Test setup:

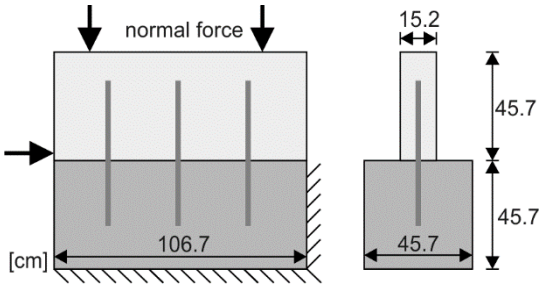

Nr. of tests	14
very smooth	–
smooth	–
rough(1)	14
very rough	–
keyed	–

Normal stress: External compressive stress by a self equilibrating vertical loading system with two steel tubes

Interface reinforcement: 3 and 6 dowels with Ø19 mm

(1): rough: sandblasted

Autor:	Williams, C.S.; Massey, J.B.; Bayrak, O.; Jirsa, J.O.	[Wil17]
Title:	Investigation of Interface Shear Transfer Using Push-Through Tests	
Source:	ACI Structural Journal, Vol. 114, Issue 1, pp. 173-185, 2017	

Test setup:

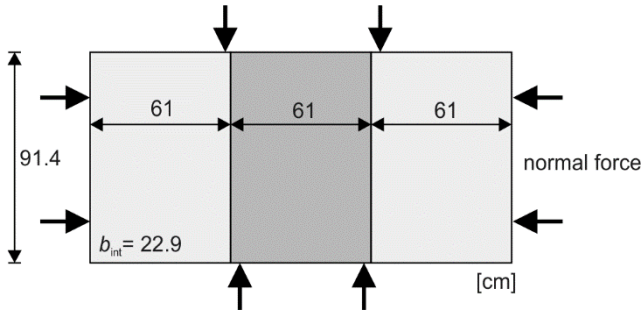

Nr. of tests	11
very smooth	–
smooth	1
rough	–
very rough	–
keyed	11

Normal stress:	Applied with diagonal post tensioned rods
Interface reinforcement:	0, 4 and 8 bars with Ø12.7 and Ø15.9 mm

Autor:	Zeno, G.A.	[Zen09]
Title:	Use of High-Strength Steel Reinforcement in Shear Friction Applications	
Source:	PhD Thesis, University of Pittsburgh, Pittsburgh, 2009	

Test setup:

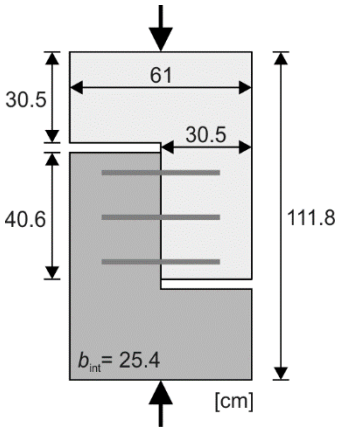

Nr. of tests	8
very smooth	
smooth	–
rough	–
very rough[(1)]	8
keyed	–

Normal stress:	–
Interface reinforcement:	3 stirrups with Ø9.5 and Ø12.7 mm

[(1)]: very rough: roughened to an amplitude of at least 6.3 mm

Autor:	Zilch, K.; Müller, A. [Zil04]
Title:	Experimentelle Untersuchungen zum Ermüdungstragverhalten von unbewehrten Schubfugen an Nachträglich ergänzten Bauteilen
Source:	Research Report, Chair of Concrete Structures, Technical University of Munich, 2004

Test setup:

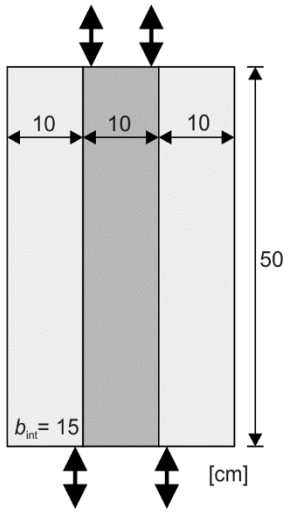

Nr. of tests	32
very smooth	
smooth(1)	16
rough(2)	16
very rough	–
keyed	–

8 monotonic loading
24 cyclic loading

Normal stress: –

Interface reinforcement: –

(1): smooth: slightly sandblasted; (2): rough: medium sandblasted

Table B-1: Overview of research reports with corresponding allocation of small size tests before filter

Complete database before filter																				
Nr.	Source	Nr. of tests	Database						Interface					Test-setup						
			A-1	A-2	B	AB	C	D	vs	s	r	vr	k	p-o	m p-o	co	m co	p-th	sw	
1	[Alb14]	9	5	4	-	-	-	-	-	7	2	-	-	9	-	-	-	-	-	
2	[Ann90]	28	2	26	-	-	-	-	-	2	-	-	26	-	-	-	-	28	-	
3	[Ban05]	24	-	12	-	12	-	-	-	18	4	-	2	24	-	-	-	-	-	
4	[Bar17]	4	-	-	4	-	-	-	-	-	4	-	-	4	-	-	-	-	-	
5	[Bas89]	33	-	-	33	-	-	-	-	1	25	4	3	-	-	-	-	-	33	
6	[Bec73]	88	-	88	0	-	-	-	-	34	-	54	-	-	88	-	-	-	-	
7	[Cho99]	44	-	12		32	-	-	-	14	30	-	-	44	-	-	-	-	-	
8	[Das86]	172	28	104	31	9	-	-	18	57	44	53	-	-	56	-	-	116		
9	[Dul72]	16	-	-	16	-	-	-	16	-	-	-	-	16	-	-	-	-	-	
10	[Fra59]	16	-	16	-	-	-	-	12	-	-	-	4	16	-	-	-	-	-	
11	[Gas64]	12	-	-	-	12	-	-	-	-	12	-	-	-	8	-	4	-	-	
12	[Goh00]	12	12	-	-	-	-	-	-	-	12	-	-	-	-	-	-	-	12	
13	[Goh03]	90	90	-	-	-	-	-	-	-	30	60	-	-	-	-	-	-	90	
14	[Han60]	62	18	-	44	-	-	-	-	15	10	21	16	62	-	-	-	-	-	
15	[Har12]	8	-	-	8	-	-	-	-	-	-	8	-	8	-	-	-	-	-	
16	[Kah02]	12	-	-	12	-	-	-	-	2	10	-	-	12	-	-	-	-	-	
17	[Meh77]	16	-	-	12	4	-	-	-	-	-	-	16	16	-	-	-	-	-	
18	[Moh15a] [Moh15b]	72	60	-	12	-	-	-	-	24	24	12	12	-	-	-	-	-	72	
19	[Pap02]	36	-	12	-	24	-	-	-	13	23	-	-	36	-	-	-	-		
20	[Pau74]	30	-	-	30	-	-	-	3	10	13	3	1	30	-	-	-	-		
21	[Ran97]	83	11	-	72	-	-	-	13	34	36	0	-	-	-	-	-		83	
22	[Ran15]	27	9	18	-	-	-	-	-	9	9	9	-	-	18	-	-	9	-	
23	[Rei04]	107	49	58	-	-	-	-	13	94	-	-	-	-	36	-	-	49	22	
24	[Sco10]	27	-	18	-	9	-	-	-	-	27	-	-	27	-	-	-	-	-	
25	[Sha14]	36	-	-	36	-	-	-	-	18	18	-	-	36	-	-	-	-	-	
26	[Sne16]	34	-	-	34	-	-	-	-	18	16	-	-	34	-	-	-	-	-	
27	[Val99]	14	-	-	5	9	-	-	-	-	14	-	-	-	-	-	-	-	14	
28	[Wil17]	11	-	1	-	10	-	-	-	1	-	-	10	-	-	-	-	11	-	
29	[Zen09]	8	-	-	8	-	-	-	-	-	-	8	-	8	-	-	-	-	-	
30	[Zil04]	32	8	-	-	-	24	-	-	16	16	-	-	-	-	-	-	32	-	

Table B-2: Overview of research reports with corresponding allocation of small size tests after filter

Selected database after filter																			
Nr.	Source	Nr. of tests	Database						Interface					Test-setup					
			A-1	A-2	B	AB	C	D	vs	s	r	vr	k	p-o	m p-o	co	m co	p-th	sw
1	[Alb14]	9	5	4	-	-	-	-	-	7	2	-	-	9	-	-	-	-	-
2	[Ann90]	-	-	-	-	-	-	-	-	-	-	-	-	-	-	-	-	-	-
3	[Ban05]	-	-	-	-		-	-	-	-	-	-		-	-	-	-	-	-
4	[Bar17]	4	-	-	4		-	-	-	-	4	-	-	4	-	-	-	-	-
5	[Bas89]	30	-	-	30		-	-	-	1	25	4	-	-	-	-	-	-	30
6	[Bec73]	-	-	-	-	-	-	-	-	-	-	-	-	-	-	-	-	-	-
7	[Cho99]	-	-	-	-	-	-	-	-	-	-	-	-	-	-	-	-		-
8	[Das86]	79	2	59	9	9	-	-	12	23	16	28	-	-	38	-	-	41	-
9	[Dul72]	-	-	-	-	-	-	-		-	-	-	-	-		-	-		-
10	[Fra59]	4	-	4	-	-	-	-	4	-	-	-	-	4	-	-	-	-	-
11	[Gas64]	8	-	-	-	8	-	-	-	-	8	-	-	-	8	-	-	-	-
12	[Goh00]	-	-	-	-	-	-	-	-	-	-	-	-	-	-	-	-	-	-
13	[Goh03]	-	-	-	-	-	-	-	-	-	-	-	-	-	-	-	-	-	-
14	[Han60]	46	16		30	-	-	-	-	15	10	21	-	46	-	-	-	-	-
15	[Har12]	8	-	-	8	-	-	-	-			8	-	8	-	-	-	-	-
16	[Kah02]	11	-	-	11	-	-	-	-	2	9		-	11	-	-	-	-	-
17	[Meh77]	-	-	-	-	-	-	-	-	-	-	-	-	-	-	-	-	-	-
18	[Moh15a] [Moh15b]	-	-	-	-	-	-	-	-	-	-	-	-	-	-	-	-	-	-
19	[Pap02]	-	-	-	-	-	-	-	-	-	-	-	-	-	-	-	-	-	-
20	[Pau74]	23	-	-	23	-	-	-	-	7	13	3	-	23	-	-	-	-	-
21	[Ran97]	71	-	-	71	-	-	-	13	28	30	-	-	-	-	-	-	-	71
22	[Ran15]	27	9	18	-	-	-	-	-	9	9	9	-	-	18	-	-	9	
23	[Rei04]	94	43	51	-	-	-	-	4	90	-	-	-	-	33	-	-	43	18
24	[Sco10]	27	-	18	-	9	-	-	-		27	-	-	27		-	-	-	-
25	[Sha14]	36	-		36	-	-	-	-	18	18	-	-	36	-	-	-	-	-
26	[Sne16]	34	-	-	34	-	-	-	-	18	16	-	-	34	-	-	-	-	-
27	[Val99]	7	-	-	2	5	-	-	-	-	7	-	-	-	-	-	-	-	7
28	[Wil17]	1	-	-	-	1	-	-	-	1	-	-	-	-	-	-	-	1	-
29	[Zen09]	8	-	-	8	-	-	-	-	-	-	8	-	8	-	-	-	-	-
30	[Zil04]	29	8	-	-	-	20	-	-	13	15	-	-	-	-	-	-	28	-

B.1.2 Database A-1: Adhesion

Table B-3: Database A-1 – Specimens Nr. 1 – 37

Nr. [-]	Source [-]	Specimen ID [-]	Test-setup [-]	Interface [-]	R_t [mm]	b_{int} [mm]	l_{int} [mm]	A_{int} [cm²]	$f_{cm,cyl,1}$ [N/mm²]	$f_{ctm,1}$ [N/mm²]	$f_{cm,cyl,2}$ [N/mm²]	$f_{ctm,2}$ [N/mm²]	τ_{test} [N/mm²]
1	[Alb14]	V-F-oH-oB-oS-g	push-off	smooth	0.73	350	350	1225	40.25	3.18	21.54	2.14	1.44
2	[Alb14]	V-O-oH-oB-oS-g	push-off	smooth	1.21	350	350	1225	22.44	2.29	16.57	1.52	1.34
3	[Alb14]	V-O-oH-oB-oS-s	push-off	smooth	-	350	350	1225	21.97	2.17	16.10	1.53	1.29
4	[Alb14]	V-O-oH-BK-oS-g	push-off	smooth	-	350	350	1225	22.44	2.29	16.57	1.52	1.31
5	[Alb14]	V-F-oH-oB-oS-r	push-off	rough	2.82	350	350	1225	40.12	3.17	20.16	2.02	2.79
6	[Das86]	52	push-through	smooth	-	150	150	225	33.93	2.89	16.63	1.63	0.63
7	[Das86]	53	push-through	smooth	-	150	150	225	33.93	2.89	16.63	1.63	0.33
8	[Han60]	BR12-1	push-off	very rough	-	203.2	304.8	619	34.20	2.91	20.96	1.98	2.87
9	[Han60]	BR12-2	push-off	very rough	-	203.2	304.8	619	36.82	3.08	27.44	2.46	3.83
10	[Han60]	BR12-3	push-off	very rough	-	203.2	304.8	619	36.34	3.04	28.61	2.54	3.14
11	[Han60]	BR12-4	push-off	very rough	-	203.2	304.8	619	34.40	2.92	28.13	2.51	2.41
12	[Han60]	BR12-5	push-off	very rough	-	203.2	304.8	619	34.40	2.92	28.13	2.51	2.50
13	[Han60]	BR12-6	push-off	very rough	-	203.2	304.8	619	34.82	2.95	25.65	2.33	2.83
14	[Han60]	BR12-7	push-off	very rough	-	203.2	304.8	619	34.82	2.95	25.65	2.33	2.81
15	[Han60]	BR12-8	push-off	very rough	-	203.2	304.8	619	34.82	2.95	25.65	2.33	2.79
16	[Han60]	B12-1	push-off	smooth	-	203.2	304.8	619	33.58	2.87	27.92	2.49	0.86
17	[Han60]	B12-2	push-off	smooth	-	203.2	304.8	619	35.65	3.00	25.23	2.30	1.59
18	[Han60]	B12-3	push-off	smooth	-	203.2	304.8	619	36.82	3.08	27.44	2.46	0.90
19	[Han60]	B12-4	push-off	smooth	-	203.2	304.8	619	37.71	3.13	28.61	2.54	0.62
20	[Han60]	B12-5	push-off	smooth	-	203.2	304.8	619	34.40	2.92	28.13	2.51	0.83
21	[Han60]	B24-1	push-off	smooth	-	203.2	609.6	1239	32.13	2.77	29.10	2.57	0.75
22	[Han60]	B24-2	push-off	smooth	-	203.2	609.6	1239	32.13	2.77	29.10	2.57	0.65
23	[Han60]	B24-3	push-off	smooth	-	203.2	609.6	1239	32.13	2.77	29.10	2.57	0.69
24	[Ran15]	S4	push-through	very rough	3.29	150	300	450	48.55	3.77	65.21	4.28	3.30
25	[Ran15]	S5	push-through	very rough	3.14	150	300	450	48.55	3.77	65.21	4.28	3.40
26	[Ran15]	S6	push-through	very rough	3.74	150	304	456	48.55	3.77	65.21	4.28	3.49
27	[Ran15]	S1	push-through	smooth	0.53	150	300	450	48.55	3.77	65.21	4.28	0.98
28	[Ran15]	S2	push-through	smooth	0.53	150	300	450	48.55	3.77	65.21	4.28	0.92
29	[Ran15]	S3	push-through	smooth	0.53	150	300	450	48.55	3.77	65.21	4.28	1.13
30	[Ran15]	S7	push-through	rough	1.93	150	300	450	48.55	3.77	65.21	4.28	3.31
31	[Ran15]	S8	push-through	rough	1.51	150	302	453	48.55	3.77	65.21	4.28	2.96
32	[Ran15]	S9	push-through	rough	1.77	150	298	447	48.55	3.77	65.21	4.28	3.21
33	[Rei04]	1	push-through	smooth	0.61	150	500	750	84.82	4.77	45.74	3.61	1.33
34	[Rei04]	2	push-through	smooth	0.57	150	500	750	84.82	4.77	45.74	3.61	1.37
35	[Rei04]	3	push-through	smooth	0.64	150	500	750	84.82	4.77	45.74	3.61	1.45
36	[Rei04]	4	push-through	smooth	0.56	150	500	750	84.82	4.77	51.56	3.94	0.77
37	[Rei04]	5	push-through	smooth	0.55	150	500	750	84.82	4.77	51.56	3.94	1.47

Table B-4: Database A-1 – Specimens Nr. 38 – 74

Nr. [-]	Source [-]	Specimen ID [-]	Test-setup [-]	Interface [-]	R_t [mm]	b_{int} [mm]	l_{int} [mm]	A_{int} [cm²]	$f_{cm,cyl,1}$ [N/mm²]	$f_{ctm,1}$ [N/mm²]	$f_{cm,cyl,2}$ [N/mm²]	$f_{ctm,2}$ [N/mm²]	τ_{test} [N/mm²]
38	[Rei04]	6	push-through	smooth	0.75	150	500	750	84.82	4.77	51.56	3.94	0.60
39	[Rei04]	7	push-through	smooth	0.55	150	500	750	84.82	4.77	44.07	3.51	0.96
40	[Rei04]	8	push-through	smooth	0.58	150	500	750	84.82	4.77	44.07	3.51	0.98
41	[Rei04]	9	push-through	smooth	0.55	150	500	750	84.82	4.77	44.07	3.51	1.19
42	[Rei04]	10	push-through	smooth	0.91	150	500	750	93.97	4.96	45.74	3.61	1.49
43	[Rei04]	11	push-through	smooth	0.98	150	500	750	93.97	4.96	45.74	3.61	1.49
44	[Rei04]	12	push-through	smooth	0.95	150	500	750	93.97	4.96	45.74	3.61	1.46
45	[Rei04]	13	push-through	smooth	0.84	150	500	750	93.97	4.96	51.56	3.94	1.53
46	[Rei04]	14	push-through	smooth	1.05	150	500	750	93.97	4.96	51.56	3.94	1.63
47	[Rei04]	15	push-through	smooth	0.88	150	500	750	93.97	4.96	51.56	3.94	1.09
48	[Rei04]	16	push-through	smooth	0.95	150	500	750	93.97	4.96	44.07	3.51	1.46
49	[Rei04]	17	push-through	smooth	0.8	150	500	750	93.97	4.96	44.07	3.51	1.46
50	[Rei04]	18	push-through	smooth	0.9	150	500	750	93.97	4.96	44.07	3.51	1.99
51	[Rei04]	19	push-through	smooth	0.75	150	500	750	80.66	4.67	45.74	3.61	1.48
52	[Rei04]	20	push-through	smooth	0.8	150	500	750	80.66	4.67	45.74	3.61	1.56
53	[Rei04]	21	push-through	smooth	0.73	150	500	750	80.66	4.67	45.74	3.61	1.06
54	[Rei04]	22	push-through	smooth	0.7	150	500	750	80.66	4.67	51.56	3.94	0.81
55	[Rei04]	23	push-through	smooth	0.58	150	500	750	80.66	4.67	51.56	3.94	1.49
56	[Rei04]	24	push-through	smooth	0.66	150	500	750	80.66	4.67	51.56	3.94	1.57
57	[Rei04]	25	push-through	smooth	0.81	150	500	750	80.66	4.67	44.07	3.51	1.43
58	[Rei04]	26	push-through	smooth	0.79	150	500	750	80.66	4.67	44.07	3.51	1.64
59	[Rei04]	27	push-through	smooth	0.73	150	500	750	80.66	4.67	44.07	3.51	1.15
60	[Rei04]	28	push-through	smooth	0.64	150	500	750	103.95	5.16	44.07	3.51	1.08
61	[Rei04]	29	push-through	smooth	0.67	150	500	750	103.95	5.16	44.07	3.51	1.37
62	[Rei04]	30	push-through	smooth	0.66	150	500	750	103.95	5.16	44.07	3.51	0.97
63	[Rei04]	31	push-through	smooth	0.66	150	500	750	103.95	5.16	44.07	3.51	0.94
64	[Rei04]	32	push-through	smooth	0.63	150	500	750	103.95	5.16	44.07	3.51	1.33
65	[Rei04]	34	push-through	smooth	0.69	150	500	750	103.95	5.16	44.07	3.51	1.26
66	[Rei04]	35	push-through	smooth	0.61	150	500	750	103.95	5.16	44.07	3.51	1.44
67	[Rei04]	36	push-through	smooth	0.72	150	500	750	103.95	5.16	44.07	3.51	1.29
68	[Rei04]	40	push-through	smooth	0.64	150	500	750	103.95	5.16	44.07	3.51	1.58
69	[Rei04]	41	push-through	smooth	0.61	150	500	750	103.95	5.16	44.07	3.51	1.31
70	[Rei04]	42	push-through	smooth	0.65	150	500	750	103.95	5.16	44.07	3.51	1.66
71	[Rei04]	44	push-through	smooth	0.46	150	500	750	44.32	3.53	76.34	4.57	2.92
72	[Rei04]	45	push-through	smooth	0.51	150	500	750	44.32	3.53	76.34	4.57	3.00
73	[Rei04]	46	push-through	smooth	0.63	150	500	750	44.32	3.53	76.34	4.57	2.46
74	[Rei04]	47	push-through	smooth	0.64	150	500	750	44.32	3.53	76.34	4.57	2.91

Table B-5: Database A-1 – Specimens Nr. 75 – 83

Nr. [-]	Source [-]	Specimen ID [-]	Test-setup [-]	Interface [-]	R_t [mm]	b_{int} [mm]	l_{int} [mm]	A_{int} [cm²]	$f_{cm,cyl,1}$ [N/mm²]	$f_{ctm,1}$ [N/mm²]	$f_{cm,cyl,2}$ [N/mm²]	$f_{ctm,2}$ [N/mm²]	τ_{test} [N/mm²]
75	[Rei04]	51	push-through	smooth	0.83	150	500	750	44.32	3.53	76.34	4.57	2.68
76	[Zil04]	HHH-W2	push-through	smooth	0.8	150	500	750	82.90	4.73	81.20	4.69	2.24
77	[Zil04]	NHN-W2	push-through	smooth	0.8	150	500	750	38.20	3.16	81.40	4.69	2.69
78	[Zil04]	HNH-W2	push-through	smooth	0.8	150	500	750	82.90	4.73	36.50	3.06	0.87
79	[Zil04]	NNN-W2	push-through	smooth	0.8	150	500	750	38.50	3.18	36.80	3.07	1.12
80	[Zil04]	HHH-R2	push-through	rough	1.5	150	500	750	82.90	4.73	81.10	4.68	3.60
81	[Zil04]	NHN-R2	push-through	rough	1.5	150	500	750	37.70	3.13	79.20	4.64	3.41
82	[Zil04]	HNH-R2	push-through	rough	1.5	150	500	750	82.80	4.72	34.60	2.93	1.24
83	[Zil04]	NNN-R2	push-through	rough	1.5	150	500	750	38.40	3.17	36.70	3.07	2.45

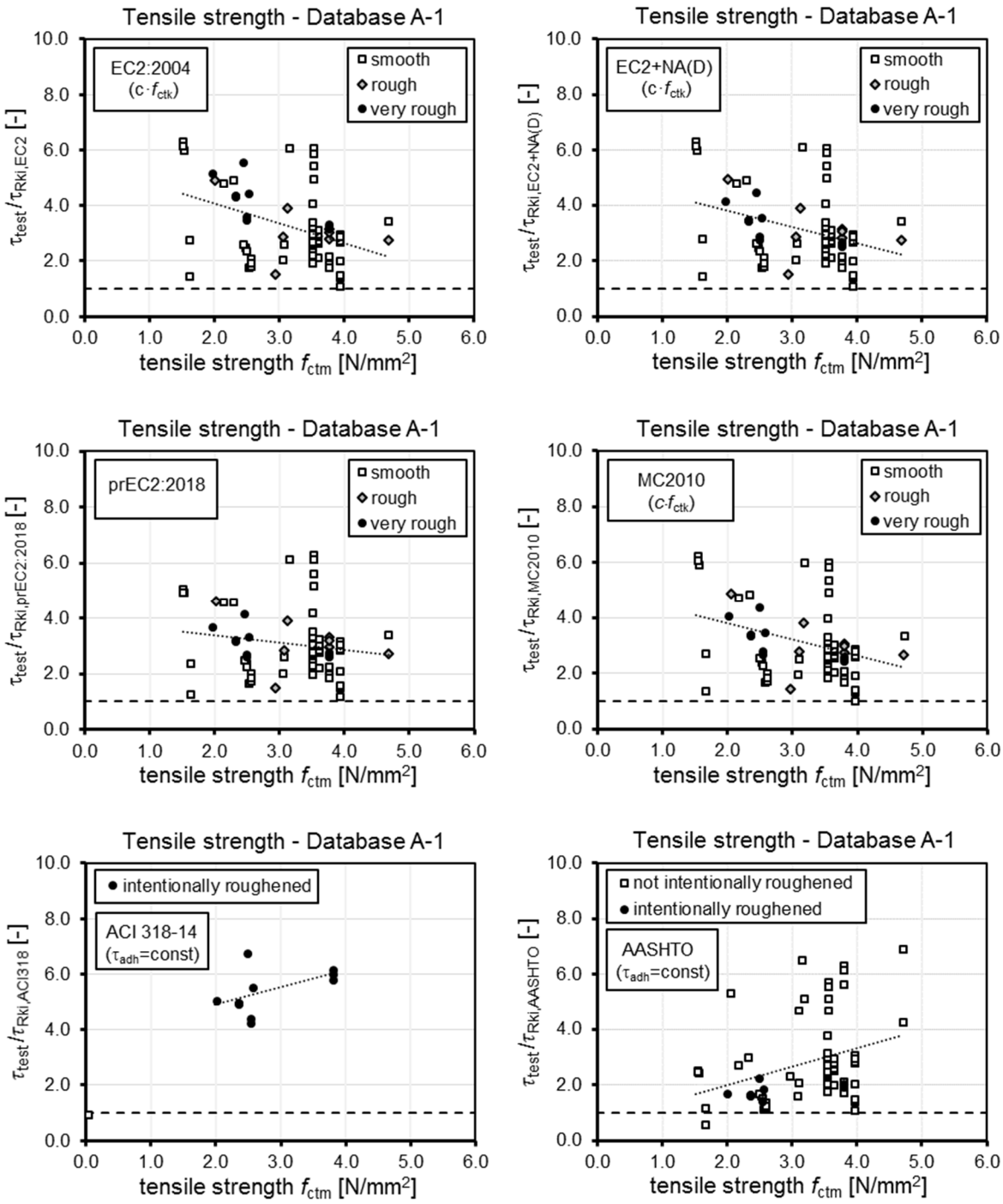

Figure B-1: Evaluation of tensile strength of database A-1 according to evaluated codes

B.1.3 Database A-2: Normal stress

Table B-6: Database A-2 – Specimens Nr. 1 – 37

Nr. [-]	Source [-]	Specimen ID [-]	Test-setup [-]	Interface [-]	R_t [mm]	b_{int} [mm]	l_{int} [mm]	A_{int} [cm²]	$f_{cm,cyl,1}$ [N/mm²]	$f_{ctm,1}$ [N/mm²]	$f_{cm,cyl,2}$ [N/mm²]	$f_{ctm,2}$ [N/mm²]	σ_n [N/mm²]	τ_{test} [N/mm²]
1	[Alb14]	V-F-oH-oB-mS-g	push-off	smooth	0.67	350	350	1225	40.18	3.17	20.85	2.08	2.48	4.25
2	[Alb14]	V-O-oH-oB-mS-g	push-off	smooth	1.49	350	350	1225	22.91	2.39	17.04	1.52	2.04	3.52
3	[Alb14]	V-O-oH-BK-mS-g	push-off	smooth	-	350	350	1225	22.91	2.39	17.04	1.52	2.03	3.48
4	[Alb14]	V-F-oH-oB-mS-r	push-off	rough	2.82	350	350	1225	40.12	3.17	20.16	2.02	2.77	4.84
5	[Das86]	112	modified push-off	very smooth	-	150	197	296	27.77	2.48	16.63	1.63	7.10	6.03
6	[Das86]	73	push-through	very rough	-	150	150	225	28.44	2.53	16.13	1.58	1.95	4.00
7	[Das86]	146	push-through	very rough	-	150	383	575	44.91	3.56	25.78	2.34	3.69	8.68
8	[Das86]	147	push-through	very rough	-	150	383	575	44.91	3.56	26.44	2.39	3.72	6.74
9	[Das86]	148	push-through	very rough	-	150	322	483	44.91	3.56	26.44	2.39	5.65	10.74
10	[Das86]	149	push-through	very rough	-	150	322	483	44.91	3.56	26.44	2.39	5.85	11.12
11	[Das86]	150	push-through	very rough	-	150	302	453	44.91	3.56	25.78	2.34	6.87	12.02
12	[Das86]	151	push-through	very rough	-	150	302	453	44.91	3.56	25.78	2.34	6.71	11.74
13	[Das86]	152	push-through	very rough	-	150	293	440	44.91	3.56	25.78	2.34	7.12	11.93
14	[Das86]	153	push-through	very rough	-	150	293	440	44.91	3.56	25.78	2.34	7.05	11.82
15	[Das86]	154	push-through	very rough	-	150	287	431	44.91	3.56	26.44	2.39	8.00	13.04
16	[Das86]	155	push-through	very rough	-	150	287	431	44.91	3.56	26.44	2.39	7.54	12.28
17	[Das86]	170	push-through	very rough	-	150	150	225	44.91	3.56	28.19	2.51	0.34	3.41
18	[Das86]	171	push-through	very rough	-	150	150	225	44.91	3.56	28.86	2.56	0.61	3.65
19	[Das86]	172	push-through	very rough	-	150	150	225	44.91	3.56	28.52	2.53	1.03	4.73
20	[Das86]	173	push-through	very rough	-	150	150	225	44.91	3.56	28.52	2.53	1.24	4.98
21	[Das86]	174	push-through	very rough	-	150	150	225	44.91	3.56	28.52	2.53	1.18	4.12
22	[Das86]	175	push-through	very rough	-	150	150	225	44.91	3.56	28.52	2.53	1.27	4.45
23	[Das86]	176	push-through	very rough	-	150	150	225	*44.91*	*3.56*	*28.86*	*2.56*	*1.82*	5.46
24	[Das86]	156	modified push-off	very rough	-	150	383	575	44.91	3.56	32.60	2.81	3.83	9.00
25	[Das86]	157	modified push-off	very rough	-	150	383	575	44.91	3.56	32.60	2.81	4.12	9.67
26	[Das86]	158	modified push-off	very rough	-	150	322	483	44.91	3.56	32.60	2.81	6.54	12.42
27	[Das86]	159	modified push-off	very rough	-	150	322	483	44.91	3.56	32.60	2.81	6.62	12.58
28	[Das86]	160	modified push-off	very rough	-	150	302	453	44.91	3.56	32.60	2.81	7.51	13.13
29	[Das86]	161	modified push-off	very rough	-	150	302	453	44.91	3.56	32.60	2.81	7.70	13.48
30	[Das86]	162	modified push-off	very rough	-	150	293	440	46.40	3.65	33.10	2.84	8.29	13.89
31	[Das86]	163	modified push-off	very rough	-	150	293	440	46.40	3.65	33.10	2.84	7.83	13.11
32	[Das86]	164	modified push-off	very rough	-	150	287	431	46.40	3.65	33.10	2.84	8.80	14.34
33	[Das86]	165	modified push-off	very rough	-	150	287	431	46.40	3.65	33.10	2.84	8.85	14.42
34	[Das86]	59	push-through	smooth	-	150	150	225	34.51	2.93	16.96	1.66	0.81	1.97
35	[Das86]	60	push-through	smooth	-	150	150	225	34.51	2.93	16.96	1.66	1.57	3.16
36	[Das86]	61	push-through	smooth	-	150	150	225	34.51	2.93	16.96	1.66	1.92	3.93
37	[Das86]	117	modified push-off	smooth	-	150	164	246	28.11	2.50	16.80	1.64	13.30	5.90

Table B-7: Database A-2 – Specimens Nr. 38 – 74

Nr. [-]	Source [-]	Specimen ID [-]	Test-setup [-]	Interface [-]	R_t [mm]	b_{int} [mm]	l_{int} [mm]	A_{int} [cm²]	$f_{cm,cyl,1}$ [N/mm²]	$f_{ctm,1}$ [N/mm²]	$f_{cm,cyl,2}$ [N/mm²]	$f_{ctm,2}$ [N/mm²]	σ_n [N/mm²]	τ_{test} [N/mm²]
38	[Das86]	129	modified push-off	smooth	-	150	164	246	27.94	2.49	17.05	1.66	13.37	5.94
39	[Das86]	118	modified push-off	smooth	-	150	197	296	27.77	2.48	16.63	1.63	8.80	7.50
40	[Das86]	130	modified push-off	smooth	-	150	197	296	27.94	2.49	17.05	1.66	9.19	7.81
41	[Das86]	140	modified push-off	smooth	-	150	234	351	25.78	2.34	16.96	1.66	4.30	5.16
42	[Das86]	141	modified push-off	smooth	-	150	234	351	25.78	2.34	16.96	1.66	3.66	4.63
43	[Das86]	119	modified push-off	smooth	-	150	251	377	27.77	2.48	16.63	1.63	4.42	5.94
44	[Das86]	131	modified push-off	smooth	-	150	249	374	27.94	2.49	17.05	1.66	5.24	6.96
45	[Das86]	142	modified push-off	smooth	-	150	246	369	25.78	2.34	16.96	1.66	3.27	4.25
46	[Das86]	143	modified push-off	smooth	-	150	246	369	25.78	2.34	16.38	1.61	3.34	4.34
47	[Das86]	144	modified push-off	smooth	-	150	270	405	25.78	2.34	16.38	1.61	2.22	3.32
48	[Das86]	145	modified push-off	smooth	-	150	272	408	25.78	2.34	16.38	1.61	2.63	3.97
49	[Das86]	120	modified push-off	smooth	-	150	291	437	27.77	2.48	16.63	1.63	2.82	4.68
50	[Das86]	132	modified push-off	smooth	-	150	287	431	28.44	2.53	17.30	1.68	4.08	6.64
51	[Das86]	121	modified push-off	smooth	-	150	339	509	27.77	2.48	16.63	1.63	1.77	3.59
52	[Das86]	133	modified push-off	smooth	-	150	339	509	27.94	2.49	17.05	1.66	2.25	4.56
53	[Das86]	124	modified push-off	very smooth	-	150	197	296	27.94	2.49	17.05	1.66	8.18	6.95
54	[Das86]	134	modified push-off	very smooth	-	150	223	335	25.78	2.34	16.96	1.66	2.66	2.92
55	[Das86]	135	modified push-off	very smooth	-	150	223	335	25.78	2.34	16.96	1.66	2.53	2.79
56	[Das86]	136	modified push-off	very smooth	-	150	229	344	25.78	2.34	16.38	1.61	1.95	2.24
57	[Das86]	137	modified push-off	very smooth	-	150	229	344	25.78	2.34	16.38	1.61	2.11	2.42
58	[Das86]	113	modified push-off	very smooth	-	150	251	377	27.77	2.48	16.63	1.63	2.03	2.73
59	[Das86]	125	modified push-off	very smooth	-	150	251	377	27.94	2.49	17.05	1.66	2.47	3.29
60	[Das86]	114	modified push-off	very smooth	-	150	274	411	27.77	2.48	16.63	1.63	1.60	2.44
61	[Das86]	126	modified push-off	very smooth	-	150	274	411	27.61	2.47	17.30	1.68	1.43	2.18
62	[Das86]	115	modified push-off	very smooth	-	150	300	450	27.77	2.48	16.63	1.63	1.18	2.04
63	[Das86]	127	modified push-off	very smooth	-	150	300	450	27.94	2.49	17.05	1.66	1.22	2.10
64	[Fra59]	1	push-off	very smooth	-	200	200	400	38.00	3.15	38.00	3.15	1.59	1.52
65	[Fra59]	2	push-off	very smooth	-	200	200	400	38.00	3.15	38.00	3.15	3.19	2.45
66	[Fra59]	3	push-off	very smooth	-	200	200	400	38.00	3.15	38.00	3.15	4.78	3.78
67	[Fra59]	4	push-off	very smooth	-	200	200	400	38.00	3.15	38.00	3.15	6.37	5.07
68	[Ran15]	70_4	modified push-off	very rough	3.98	150	343	515	48.55	3.77	65.21	4.28	5.87	16.12
69	[Ran15]	70_5	modified push-off	very rough	3.98	150	334	502	48.55	3.77	65.21	4.28	4.74	13.02
70	[Ran15]	70_6	modified push-off	very rough	4.38	150	342	513	48.55	3.77	65.21	4.28	5.17	14.02
71	[Ran15]	75_1	modified push-off	very rough	-	150	486	729	48.55	3.77	65.21	4.28	3.35	12.49
72	[Ran15]	75_3	modified push-off	very rough	3.43	150	477	715	48.55	3.77	65.21	4.28	3.39	12.65
73	[Ran15]	75_4	modified push-off	very rough	3.56	150	483	724	48.55	3.77	65.21	4.28	3.14	11.71
74	[Ran15]	65_1	modified push-off	Smooth	0.53	150	265	398	*48.55*	*3.77*	*65.21*	*4.28*	*7.89*	16.91

Table B-8: Database A-2 – Specimens Nr. 75 – 111

Nr. [-]	Source [-]	Specimen ID [-]	Test-setup [-]	Interface [-]	R_t [mm]	b_{int} [mm]	l_{int} [mm]	A_{int} [cm²]	$f_{cm,cyl,1}$ [N/mm²]	$f_{ctm,1}$ [N/mm²]	$f_{cm,cyl,2}$ [N/mm²]	$f_{ctm,2}$ [N/mm²]	σ_n [N/mm²]	τ_{test} [N/mm²]
75	[Ran15]	65_2	modified push-off	Smooth	0.53	150	262	393	48.55	3.77	65.21	4.28	7.86	16.85
76	[Ran15]	65_3	modified push-off	Smooth	0.55	150	246	369	48.55	3.77	65.21	4.28	7.64	16.38
77	[Ran15]	70_1	modified push-off	Smooth	0.51	150	316	474	48.55	3.77	65.21	4.28	5.07	13.94
78	[Ran15]	70_2	modified push-off	Smooth	0.48	150	338	507	48.55	3.77	65.21	4.28	4.19	11.53
79	[Ran15]	70_3	modified push-off	Smooth	0.52	150	343	514	48.55	3.77	65.21	4.28	5.01	13.76
80	[Ran15]	65_4	modified push-off	rough	1.63	150	280	420	48.55	3.77	65.21	4.28	7.95	17.04
81	[Ran15]	65_5	modified push-off	rough	1.76	150	278	417	48.55	3.77	65.21	4.28	7.93	17.00
82	[Ran15]	65_6	modified push-off	rough	1.63	150	266	400	48.55	3.77	65.21	4.28	8.14	17.46
83	[Ran15]	75_2	modified push-off	rough	1.93	150	479	719	48.55	3.77	65.21	4.28	3.07	11.45
84	[Ran15]	75_5	modified push-off	rough	2.01	150	478	717	48.55	3.77	65.21	4.28	3.41	12.74
85	[Ran15]	75_6	modified push-off	rough	1.64	150	479	719	48.55	3.77	65.21	4.28	2.94	10.96
86	[Rei04]	79	modified push-off	very smooth	-	150	246	370	103.95	5.16	44.07	3.51	8.56	11.16
87	[Rei04]	80	modified push-off	very smooth	-	150	246	370	103.95	5.16	44.07	3.51	15.94	20.78
88	[Rei04]	81	modified push-off	very smooth	-	150	246	370	103.95	5.16	44.07	3.51	15.45	20.13
89	[Rei04]	100	push-off/sliding wall	very smooth	0.05	200	400	800	95.05	4.99	44.32	3.53	6.00	4.72
90	[Rei04]	52	modified push-off	smooth	0.88	150	246	370	84.82	4.77	45.74	3.61	12.37	16.12
91	[Rei04]	53	modified push-off	smooth	0.75	150	246	370	84.82	4.77	45.74	3.61	13.64	17.78
92	[Rei04]	54	modified push-off	smooth	0.67	150	246	370	84.82	4.77	45.74	3.61	15.55	20.26
93	[Rei04]	55	modified push-off	smooth	0.96	150	246	370	84.82	4.77	51.56	3.94	14.98	19.52
94	[Rei04]	56	modified push-off	smooth	0.81	150	246	370	84.82	4.77	51.56	3.94	11.97	15.60
95	[Rei04]	57	modified push-off	smooth	0.77	150	246	370	84.82	4.77	51.56	3.94	13.94	18.17
96	[Rei04]	58	modified push-off	smooth	0.87	150	246	370	84.82	4.77	44.07	3.51	15.31	19.95
97	[Rei04]	59	modified push-off	smooth	0.80	150	246	370	84.82	4.77	44.07	3.51	15.72	20.49
98	[Rei04]	60	modified push-off	smooth	0.77	150	246	370	84.82	4.77	44.07	3.51	15.33	19.98
99	[Rei04]	61	modified push-off	smooth	0.84	150	246	370	93.97	4.96	45.74	3.61	15.56	20.28
100	[Rei04]	62	modified push-off	smooth	0.88	150	246	370	93.97	4.96	45.74	3.61	15.98	20.83
101	[Rei04]	63	modified push-off	smooth	0.87	150	246	370	93.97	4.96	45.74	3.61	15.33	19.98
102	[Rei04]	64	modified push-off	smooth	0.81	150	246	370	93.97	4.96	51.56	3.94	15.16	19.76
103	[Rei04]	65	modified push-off	smooth	0.96	150	246	370	93.97	4.96	51.56	3.94	13.19	17.19
104	[Rei04]	66	modified push-off	smooth	0.70	150	246	370	93.97	4.96	51.56	3.94	15.27	19.91
105	[Rei04]	67	modified push-off	smooth	0.75	150	246	370	93.97	4.96	44.07	3.51	15.86	20.67
106	[Rei04]	68	modified push-off	smooth	1.05	150	246	370	93.97	4.96	44.07	3.51	15.37	20.03
107	[Rei04]	69	modified push-off	smooth	0.87	150	246	370	93.97	4.96	44.07	3.51	14.47	18.86
108	[Rei04]	70	modified push-off	smooth	0.66	150	246	370	80.66	4.67	45.74	3.61	15.87	20.68
109	[Rei04]	71	modified push-off	smooth	0.10	150	246	370	80.66	4.67	45.74	3.61	16.02	20.87
110	[Rei04]	72	modified push-off	smooth	0.81	150	246	370	80.66	4.67	45.74	3.61	15.74	20.51
111	[Rei04]	73	modified push-off	smooth	0.84	150	246	370	80.66	4.67	51.56	3.94	16.29	21.22

Table B-9: Database A-2 – Specimens Nr. 112 – 145

Nr. [-]	Source [-]	Specimen ID [-]	Test-setup [-]	Interface [-]	R_t [mm]	b_{int} [mm]	l_{int} [mm]	A_{int} [cm²]	$f_{cm,cyl.1}$ [N/mm²]	$f_{ctm.1}$ [N/mm²]	$f_{cm,cyl.2}$ [N/mm²]	$f_{ctm.2}$ [N/mm²]	σ_n [N/mm²]	τ_{test} [N/mm²]
112	[Rei04]	74	modified push-off	smooth	0.79	150	246	370	80.66	4.67	51.56	3.94	13.69	17.84
113	[Rei04]	75	modified push-off	smooth	0.73	150	246	370	80.66	4.67	51.56	3.94	16.66	21.71
114	[Rei04]	76	modified push-off	smooth	0.72	150	246	370	80.66	4.67	44.07	3.51	16.04	20.90
115	[Rei04]	77	modified push-off	smooth	0.75	150	246	370	80.66	4.67	44.07	3.51	15.80	20.58
116	[Rei04]	78	modified push-off	smooth	0.86	150	246	370	80.66	4.67	44.07	3.51	14.57	18.98
117	[Rei04]	85	modified push-off	smooth	0.75	150	123	185	103.95	5.16	44.07	3.51	15.75	20.52
118	[Rei04]	86	modified push-off	smooth	0.67	150	123	185	103.95	5.16	44.07	3.51	14.46	18.85
119	[Rei04]	87	modified push-off	smooth	0.65	150	123	185	103.95	5.16	44.07	3.51	19.53	25.46
120	[Rei04]	88	push-off/sliding wall	smooth	0.63	200	400	800	95.05	4.99	44.32	3.53	3.50	6.47
121	[Rei04]	89	push-off/sliding wall	smooth	0.63	200	400	800	95.05	4.99	44.32	3.53	3.50	6.70
122	[Rei04]	90	push-off/sliding wall	smooth	0.63	200	400	800	95.05	4.99	44.32	3.53	3.50	6.65
123	[Rei04]	92	push-off/sliding wall	smooth	0.63	200	400	800	95.05	4.99	44.32	3.53	6.00	10.05
124	[Rei04]	93	push-off/sliding wall	smooth	0.63	200	400	800	95.05	4.99	44.32	3.53	6.00	10.31
125	[Rei04]	94	push-off/sliding wall	smooth	0.87	200	400	800	95.05	4.99	44.32	3.53	3.50	7.29
126	[Rei04]	95	push-off/sliding wall	smooth	0.86	200	400	800	95.05	4.99	44.32	3.53	3.50	7.27
127	[Rei04]	96	push-off/sliding wall	smooth	0.90	200	400	800	95.05	4.99	44.32	3.53	3.50	7.55
128	[Rei04]	97	push-off/sliding wall	smooth	0.87	200	400	800	95.05	4.99	44.32	3.53	6.00	10.45
129	[Rei04]	98	push-off/sliding wall	smooth	0.72	200	400	800	95.05	4.99	44.32	3.53	3.50	7.25
130	[Rei04]	99	push-off/sliding wall	smooth	0.86	200	400	800	95.05	4.99	44.32	3.53	3.50	3.06
131	[Rei04]	104	push-off/sliding wall	smooth	0.64	200	400	800	45.90	3.62	44.32	3.53	3.50	6.70
132	[Rei04]	105	push-off/sliding wall	smooth	0.65	200	400	800	45.90	3.62	44.32	3.53	3.50	7.05
133	[Rei04]	106	push-off/sliding wall	smooth	0.64	200	400	800	45.90	3.62	44.32	3.53	6.00	9.35
134	[Rei04]	107	push-off/sliding wall	smooth	0.70	200	400	800	45.90	3.62	96.46	5.01	3.50	10.46
135	[Rei04]	108	push-off/sliding wall	smooth	0.63	200	400	800	45.90	3.62	96.46	5.01	6.00	14.15
136	[Rei04]	109	push-off/sliding wall	smooth	0.67	200	400	800	45.90	3.62	96.46	5.01	6.00	15.93
137	[Sco10]	LL-0-A	push-off	rough	-	406	610	2477	43.09	3.46	76.53	4.57	0.05	2.36
138	[Sco10]	LL-0-B	push-off	rough	-	406	610	2477	43.09	3.46	76.53	4.57	0.05	2.50
139	[Sco10]	LL-0-C	push-off	rough	-	406	610	2477	43.09	3.46	76.53	4.57	0.05	3.18
140	[Sco10]	NN-0-A	push-off	rough	-	406	610	2477	42.40	3.41	53.64	4.05	0.05	2.73
141	[Sco10]	NN-0-B	push-off	rough	-	406	610	2477	42.40	3.41	53.64	4.05	0.05	2.85
142	[Sco10]	NN-0-C	push-off	rough	-	406	610	2477	42.40	3.41	53.64	4.05	0.05	2.78
143	[Sco10]	NL-0-A	push-off	rough	-	406	610	2477	43.09	3.46	53.64	4.05	0.05	3.32
144	[Sco10]	NL-0-B	push-off	rough	-	406	610	2477	43.09	3.46	53.64	4.05	0.05	2.34
145	[Sco10]	NL-0-C	push-off	rough	-	406	610	2477	43.09	3.46	53.64	4.05	0.05	3.51

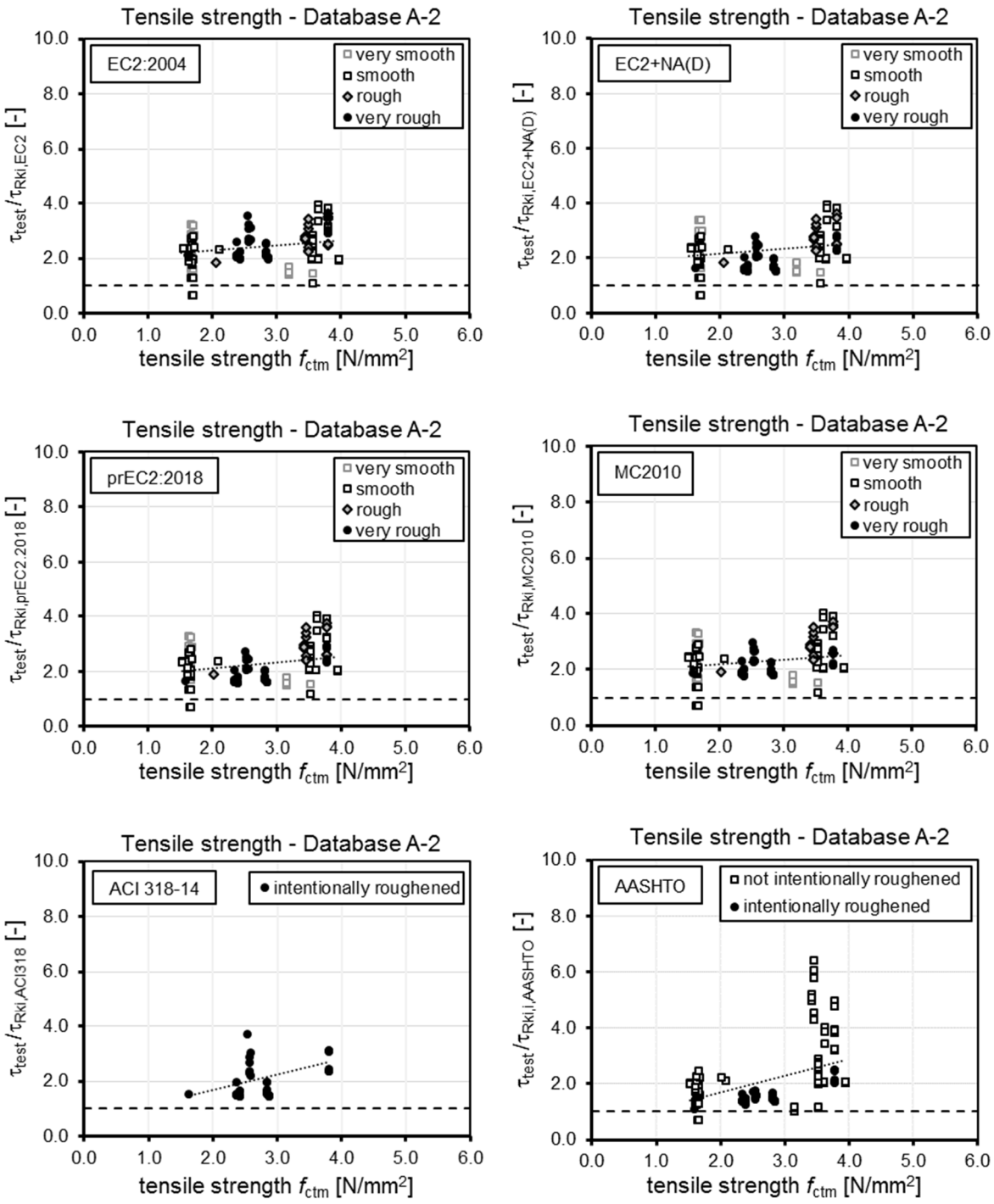

Figure B-2: Evaluation of tensile strength of database A-2 according to evaluated codes

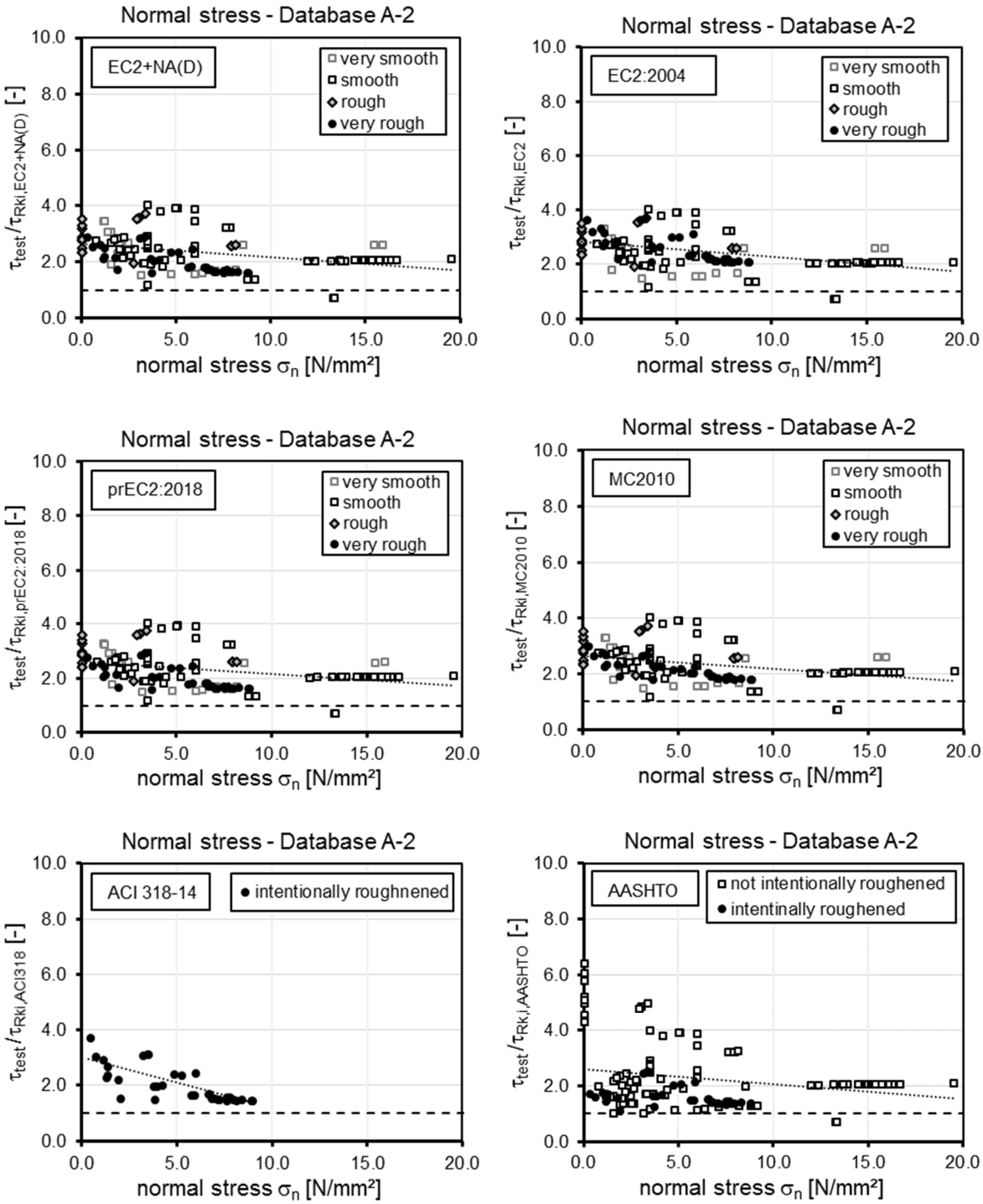

Figure B-3: Evaluation of normal stress of database A-2 according to evaluated codes

B.1.4 Database B: Reinforcement

Table B-10: Database B – Specimens Nr. 1 – 37

Nr. [-]	Source [-]	Specimen ID [-]	Test-setup [-]	Interface [-]	R_t [mm]	b_{int} [mm]	l_{int} [mm]	A_{int} [cm²]	$f_{cm,cyl.1}$ [N/mm²]	$f_{ctm.1}$ [N/mm²]	$f_{cm,cyl.2}$ [N/mm²]	$f_{ctm.2}$ [N/mm²]	ρ_{int} [%]	α [-]	$f_{ym,int}$ [N/mm²]	τ_{test} [N/mm²]
1	[Bar17]	4G60	rough	push-off	-	610	405	2471	35	2.97	29.90	2.63	0.488	90	475	4.73
2	[Bar17]	4G80	rough	push-off	-	610	405	2471	35	2.94	28.90	2.56	0.488	90	475	4.72
3	[Bar17]	5G60	rough	push-off	-	610	405	2471	36	3.02	29.80	2.62	0.430	90	604	4.95
4	[Bar17]	5G80	rough	push-off	-	610	405	2471	36	3.04	28.60	2.54	0.430	90	604	5.40
5	[Bas89]	12A	very rough	push-off/sliding wall	6.40	254	1067	2710	19	1.82	27.44	2.46	0.316	90	414	1.94
6	[Bas89]	18A	very rough	push-off/sliding wall	6.40	254	1067	2710	19	1.82	27.23	2.44	0.316	90	414	1.94
7	[Bas89]	21A	very rough	push-off/sliding wall	6.40	254	1067	2710	29	2.54	25.51	2.32	0.316	90	414	1.89
8	[Bas89]	20B	very rough	push-off/sliding wall	6.40	254	1067	2710	19	1.79	25.51	2.32	0.316	90	414	1.23
9	[Bas89]	14A	smooth	push-off/sliding wall	-	254	1067	2710	19	1.82	27.23	2.44	0.316	90	414	1.48
10	[Bas89]	1A	rough	push-off/sliding wall	3.20	254	1067	2710	21	2.01	24.13	2.22	0.316	90	414	2.38
11	[Bas89]	2A	rough	push-off/sliding wall	3.20	254	1067	2710	21	2.01	24.82	2.27	0.316	90	414	2.51
12	[Bas89]	3A	rough	push-off/sliding wall	3.20	254	1067	2710	21	2.01	24.82	2.27	0.316	90	414	2.50
13	[Bas89]	4A	rough	push-off/sliding wall	3.20	254	1067	2710	21	2.01	24.82	2.27	0.316	90	414	2.71
14	[Bas89]	5A	rough	push-off/sliding wall	3.20	254	1067	2710	21	2.01	24.82	2.27	0.316	90	414	2.46
15	[Bas89]	6A	rough	push-off/sliding wall	3.20	254	1067	2710	21	2.01	24.82	2.27	0.316	90	414	2.71
16	[Bas89]	7A	rough	push-off/sliding wall	3.20	254	1067	2710	21	2.01	24.82	2.27	0.210	90	414	2.17
17	[Bas89]	8A	rough	push-off/sliding wall	3.20	254	1067	2710	21	2.01	26.54	2.39	0.631	90	414	3.45
18	[Bas89]	9A	rough	push-off/sliding wall	3.20	254	1067	2710	21	2.01	26.54	2.39	0.316	90	414	3.12
19	[Bas89]	10A	rough	push-off/sliding wall	3.20	254	1067	2710	21	2.01	26.54	2.39	0.316	90	414	2.13
20	[Bas89]	11A	rough	push-off/sliding wall	3.20	254	1067	2710	19	1.79	25.51	2.32	0.316	90	414	1.71
21	[Bas89]	15A	rough	push-off/sliding wall	3.20	254	1067	2710	19	1.82	27.23	2.44	0.316	90	414	1.44
22	[Bas89]	16A	rough	push-off/sliding wall	3.20	254	1067	2710	19	1.82	27.23	2.44	0.316	90	414	1.72
23	[Bas89]	17A	rough	push-off/sliding wall	3.20	254	1067	2710	19	1.79	25.51	2.32	0.316	90	414	2.05
24	[Bas89]	20A	rough	push-off/sliding wall	3.20	254	1067	2710	20	1.89	24.61	2.26	0.316	90	414	2.20
25	[Bas89]	23A	rough	push-off/sliding wall	3.20	254	1067	2710	30	2.61	27.23	2.44	0.316	90	414	2.22
26	[Bas89]	24A	rough	push-off/sliding wall	3.20	254	1067	2710	30	2.61	27.23	2.44	0.316	90	414	2.63
27	[Bas89]	1B	rough	push-off/sliding wall	3.20	152	1067	1626	22	2.07	24.61	2.26	0.526	90	414	2.79
28	[Bas89]	2B	rough	push-off/sliding wall	3.20	254	1067	2710	22	2.07	24.55	2.25	0.316	90	414	2.46
29	[Bas89]	3B	rough	push-off/sliding wall	3.20	254	1067	2710	22	2.07	24.55	2.25	0.316	90	414	2.66
30	[Bas89]	4B	rough	push-off/sliding wall	3.20	254	1067	2710	22	2.07	24.61	2.26	0.210	90	414	2.25
31	[Bas89]	5B	rough	push-off/sliding wall	3.20	254	1067	2710	22	2.07	34.75	2.94	0.316	90	414	2.73
32	[Bas89]	6B	rough	push-off/sliding wall	3.20	254	1067	2710	22	2.07	34.75	2.94	0.316	90	414	2.82
33	[Bas89]	17B	rough	push-off/sliding wall	3.20	254	1067	2710	20	1.89	24.61	2.26	0.316	90	414	2.48
34	[Bas89]	21B	rough	push-off/sliding wall	3.20	254	1067	2710	30	2.61	24.61	2.26	0.316	90	414	2.17
35	[Das86]	37	smooth	push-through	-	150	150	225	27	2.40	17.88	1.73	1.005	90	450	3.42
36	[Das86]	38	smooth	push-through	-	150	150	225	27	2.40	17.88	1.73	1.005	90	450	3.49
37	[Das86]	39	rough	push-through	-	150	150	225	27	2.40	17.88	1.73	0.251	90	450	2.18

Table B-11: Database B – Specimens Nr. 38 – 74

Nr. [-]	Source [-]	Specimen ID [-]	Test-setup [-]	Interface [-]	R_t [mm]	b_{int} [mm]	l_{int} [mm]	A_{int} [cm²]	$f_{cm,cyl,1}$ [N/mm²]	$f_{ctm,1}$ [N/mm²]	$f_{cm,cyl,2}$ [N/mm²]	$f_{ctm,2}$ [N/mm²]	ρ_{int} [%]	α [-]	$f_{ym,int}$ [N/mm²]	τ_{test} [N/mm²]
38	[Das86]	40	rough	push-through	-	150	150	225	27	2.40	17.88	1.73	0.251	90	450	2.94
39	[Das86]	35	rough	push-through	-	150	150	225	27	2.40	17.88	1.73	1.005	90	450	5.34
40	[Das86]	36	rough	push-through	-	150	150	225	27	2.40	17.88	1.73	1.005	90	450	5.15
41	[Das86]	98	rough	push-through	-	150	150	225	26	2.33	16.13	1.58	0.503	90	548	3.23
42	[Das86]	99	rough	push-through	-	150	150	225	26	2.33	16.13	1.58	0.503	90	532	3.08
43	[Das86]	100	rough	push-through	-	150	150	225	26	2.33	16.13	1.58	0.503	90	548	2.92
44	[Han60]	BRS6-1	very rough	push-off	-	203	152	310	32	2.75	24.13	2.22	0.818	90	345	4.69
45	[Han60]	BRS6-2	very rough	push-off	-	203	152	310	37	3.07	22.34	2.09	0.818	90	345	2.72
46	[Han60]	BRS6-3	very rough	push-off	-	203	152	310	37	3.07	25.51	2.32	0.818	90	352	4.41
47	[Han60]	BRS12-1	very rough	push-off	-	203	305	619	39	3.22	28.48	2.53	0.409	90	334	3.38
48	[Han60]	BRS12-2	very rough	push-off	-	203	305	619	34	2.91	24.68	2.26	0.409	90	324	3.14
49	[Han60]	BRS12-3	very rough	push-off	-	203	305	619	28	2.51	22.82	2.12	0.409	90	352	2.41
50	[Han60]	BRS12-4	very rough	push-off	-	203	305	619	28	2.51	22.82	2.12	0.409	90	352	2.45
51	[Han60]	BRS12-6	very rough	push-off	-	203	305	619	30	2.66	27.30	2.45	0.409	90	345	2.52
52	[Han60]	BRS12-8	very rough	push-off	-	203	305	619	30	2.66	27.30	2.45	0.409	90	345	3.03
53	[Han60]	BRS24-1	very rough	push-off	-	203	610	1239	40	3.25	24.41	2.24	0.409	90	338	3.22
54	[Han60]	BRS24-2	very rough	push-off	-	203	610	1239	32	2.75	23.65	2.18	0.409	90	359	2.38
55	[Han60]	BRS24-3	very rough	push-off	-	203	610	1239	34	2.93	23.58	2.18	0.614	90	345	2.76
56	[Han60]	BRS24-4	very rough	push-off	-	203	610	1239	42	3.37	24.20	2.23	0.614	90	345	3.07
57	[Han60]	BS6-1	smooth	push-off	-	203	152	310	37	3.07	22.34	2.09	0.818	90	345	1.08
58	[Han60]	BS6-2	smooth	push-off	-	203	152	310	37	3.07	22.34	2.09	0.818	90	345	1.55
59	[Han60]	BS6-3	smooth	push-off	-	203	152	310	35	2.96	25.51	2.32	0.818	90	345	1.59
60	[Han60]	BS6-4	smooth	push-off	-	203	152	310	35	2.96	25.51	2.32	0.818	90	345	1.48
61	[Han60]	BS6-5	smooth	push-off	-	203	152	310	35	2.96	25.51	2.32	0.818	90	345	1.66
62	[Han60]	BS12-1	smooth	push-off	-	203	305	619	34	2.87	27.92	2.49	0.409	90	346	1.14
63	[Han60]	BS12-2	smooth	push-off	-	203	305	619	36	3.00	25.23	2.30	0.409	90	346	0.76
64	[Han60]	BRS12-5	rough	push-off	-	203	305	619	28	2.51	22.82	2.12	0.409	90	352	2.14
65	[Han60]	BRS12-7	rough	push-off	-	203	305	619	30	2.66	27.30	2.45	0.409	90	345	3.17
66	[Han60]	RS6-1	rough	push-off	-	203	152	310	32	2.76	24.13	2.22	0.818	90	345	1.72
67	[Han60]	RS6-2	rough	push-off	-	203	152	310	37	3.07	25.51	2.32	0.818	90	352	2.26
68	[Han60]	RS12-1	rough	push-off	-	203	305	619	39	3.22	28.48	2.53	0.409	90	334	2.12
69	[Han60]	RS12-2	rough	push-off	-	203	305	619	34	2.92	24.68	2.26	0.409	90	324	1.53
70	[Han60]	RS24-1	rough	push-off	-	203	610	1239	40	3.25	24.41	2.24	0.409	90	338	1.60
71	[Han60]	RS24-2	rough	push-off	-	203	610	1239	32	2.75	23.65	2.18	0.409	90	359	1.36
72	[Han60]	RS24-3	rough	push-off	-	203	610	1239	34	2.93	23.58	2.18	0.409	90	345	1.76
73	[Han60]	RS24-4	rough	push-off	-	203	610	1239	42	3.37	24.20	2.23	0.409	90	338	2.21
74	[Har12]	615-3 A	very rough	push-off	-	254	406	1032	49	3.80	40.00	3.27	0.412	90	464	4.85

Table B-12: Database B – Specimens Nr. 75 – 111

Nr. [-]	Source [-]	Specimen ID [-]	Test-setup [-]	Interface [-]	R_t [mm]	b_{int} [mm]	l_{int} [mm]	A_{int} [cm²]	$f_{cm,cyl,1}$ [N/mm²]	$f_{ctm,1}$ [N/mm²]	$f_{cm,cyl,2}$ [N/mm²]	$f_{ctm,2}$ [N/mm²]	ρ_{int} [%]	α [-]	$f_{ym,int}$ [N/mm²]	τ_{test} [N/mm²]
75	[Har12]	615-3 B	very rough	push-off	-	254	406	1032	49	3.80	40.00	3.27	0.412	90	464	4.16
76	[Har12]	615-4 A	very rough	push-off	-	254	406	1032	49	3.80	40.00	3.27	0.736	90	424	4.93
77	[Har12]	615-4 B	very rough	push-off	-	254	406	1032	49	3.80	40.00	3.27	0.736	90	424	5.56
78	[Har12]	1035-3 A	very rough	push-off	-	254	406	1032	49	3.80	40.00	3.27	0.412	90	897	3.88
79	[Har12]	1035-3 B	very rough	push-off	-	254	406	1032	49	3.80	40.00	3.27	0.412	90	897	4.52
80	[Har12]	1035-4 A	very rough	push-off	-	254	406	1032	49	3.80	40.00	3.27	0.736	90	966	5.85
81	[Har12]	1035-4 A	very rough	push-off	-	254	406	1032	49	3.80	40.00	3.27	0.736	90	966	4.89
82	[Kah02]	SF-7-1-CJ	rough	push-off	-	127	305	387	81	4.68	80.90	4.68	0.368	90	572	6.17
83	[Kah02]	SF-7-2-CJ	rough	push-off	-	127	305	387	81	4.68	80.90	4.68	0.736	90	572	9.37
84	[Kah02]	SF-7-3-CJ	rough	push-off	-	127	305	387	86	4.79	85.98	4.79	1.104	90	572	12.59
85	[Kah02]	SF-7-4-CJ	rough	push-off	-	127	305	387	86	4.79	85.98	4.79	1.473	90	572	15.15
86	[Kah02]	SF-10-1-CJ	smooth	push-off	-	127	305	387	99	5.06	98.77	5.06	0.368	90	572	3.62
87	[Kah02]	SF-10-2-CJ	smooth	push-off	-	127	305	387	83	4.73	83.10	4.73	0.736	90	572	5.63
88	[Kah02]	SF-10-3-CJ	rough	push-off	-	127	305	387	89	4.87	89.31	4.87	1.104	90	572	13.01
89	[Kah02]	SF-10-4-CJ	rough	push-off	-	127	305	387	89	4.87	89.31	4.87	1.473	90	572	14.39
90	[Kah02]	SF-14-2-CJ	rough	push-off	-	127	305	387	102	5.12	101.74	5.12	0.736	90	572	11.33
91	[Kah02]	SF-14-3-CJ	rough	push-off	-	127	305	387	105	5.18	104.92	5.18	1.104	90	572	15.38
92	[Kah02]	SF-14-4-CJ	rough	push-off	-	127	305	387	105	5.18	104.92	5.18	1.473	90	572	17.48
93	[Pau74]	ZB01	very rough	push-off	-	152	406	619	28	2.51	27.10	2.43	0.690	90	320	4.17
94	[Pau74]	WB01	very rough	push-off	-	152	406	619	28	2.51	27.10	2.43	0.690	90	320	4.97
95	[Pau74]	SB01	very rough	push-off	-	152	406	619	28	2.51	27.10	2.43	0.690	90	320	5.24
96	[Pau74]	TB01	smooth	push-off	-	152	406	619	28	2.51	27.10	2.43	0.690	90	320	2.39
97	[Pau74]	TA02	smooth	push-off	-	152	406	619	27	2.43	23.99	2.21	0.307	90	320	1.45
98	[Pau74]	TB02	smooth	push-off	-	152	406	619	27	2.43	23.99	2.21	0.690	90	320	2.78
99	[Pau74]	TC02	smooth	push-off	-	152	406	619	27	2.43	23.99	2.21	1.227	90	320	4.24
100	[Pau74]	TAM1	smooth	push-off	-	152	406	619	30	2.63	20.13	1.92	0.307	90	320	2.24
101	[Pau74]	TBM1	smooth	push-off	-	152	406	619	30	2.63	20.13	1.92	0.690	90	320	3.45
102	[Pau74]	TCM1	smooth	push-off	-	152	406	619	30	2.63	20.13	1.92	1.227	90	320	2.72
103	[Pau74]	RA01X	rough	push-off	-	152	406	619	20	1.93	28.20	2.51	0.307	90	320	1.48
104	[Pau74]	RB01X	rough	push-off	-	152	406	619	20	1.93	28.20	2.51	0.690	90	320	3.28
105	[Pau74]	RC01X	rough	push-off	-	152	406	619	20	1.93	28.20	2.51	1.227	90	320	4.45
106	[Pau74]	RB01	rough	push-off	-	152	406	619	28	2.51	27.10	2.43	0.690	90	320	4.03
107	[Pau74]	RA01	rough	push-off	-	152	406	619	27	2.43	23.99	2.21	0.307	90	320	3.59
108	[Pau74]	RA02	rough	push-off	-	152	406	619	27	2.43	23.99	2.21	0.307	90	320	3.66
109	[Pau74]	RB02	rough	push-off	-	152	406	619	27	2.43	23.99	2.21	0.690	90	320	4.10
110	[Pau74]	RC02	rough	push-off	-	152	406	619	27	2.43	23.99	2.21	1.227	90	320	6.48
111	[Pau74]	RAM1	rough	push-off	-	152	406	619	24	2.21	29.99	2.63	0.307	90	320	3.45

Table B-13: Database B – Specimens Nr. 112 – 148

Nr. [-]	Source [-]	Specimen ID [-]	Test-setup [-]	Interface [-]	R_t [mm]	b_{int} [mm]	l_{int} [mm]	A_{int} [cm²]	$f_{cm,cyl,1}$ [N/mm²]	$f_{ctm,1}$ [N/mm²]	$f_{cm,cyl,2}$ [N/mm²]	$f_{ctm,2}$ [N/mm²]	ρ_{int} [%]	α [-]	$f_{ym,int}$ [N/mm²]	τ_{test} [N/mm²]
112	[Pau74]	RBM1	rough	push-off	-	152	406	619	24	2.21	29.99	2.63	0.690	90	320	4.69
113	[Pau74]	RBM2	rough	push-off	-	152	406	619	24	2.21	29.99	2.63	0.690	90	320	4.62
114	[Pau74]	RCM1	rough	push-off	-	152	406	619	24	2.21	29.99	2.63	1.227	90	320	4.83
115	[Pau74]	RCM2	rough	push-off	-	152	406	619	24	2.21	29.99	2.63	1.227	90	320	4.83
116	[Ran97]	55	very smooth	push-off/sliding wall	-	300	400	1200	45	3.56	36.17	3.03	0.047	90	653	0.13
117	[Ran97]	56	very smooth	push-off/sliding wall	-	300	400	1200	45	3.56	36.17	3.03	0.094	90	600	0.24
118	[Ran97]	57	very smooth	push-off/sliding wall	-	300	400	1200	45	3.56	36.17	3.03	0.188	90	600	0.57
119	[Ran97]	58	very smooth	push-off/sliding wall	-	300	400	1200	45	3.56	36.17	3.03	0.262	90	600	0.69
120	[Ran97]	59	very smooth	push-off/sliding wall	-	113	400	452	45	3.56	36.17	3.03	0.500	90	600	1.76
121	[Ran97]	60	very smooth	push-off/sliding wall	-	57	400	228	45	3.56	36.17	3.03	0.992	90	600	3.18
122	[Ran97]	61	very smooth	push-off/sliding wall	-	57	400	228	45	3.56	36.17	3.03	1.488	90	600	5.31
123	[Ran97]	62	very smooth	push-off/sliding wall	-	300	400	1200	45	3.56	36.17	3.03	0.024	90	653	0.07
124	[Ran97]	63	very smooth	push-off/sliding wall	-	300	400	1200	45	3.56	36.17	3.03	0.094	90	600	0.29
125	[Ran97]	64	very smooth	push-off/sliding wall	-	300	400	1200	45	3.56	36.17	3.03	0.262	90	524	0.67
126	[Ran97]	81	very smooth	push-off/sliding wall	-	300	400	1200	19	1.79	16.47	1.61	0.024	90	653	0.05
127	[Ran97]	82	very smooth	push-off/sliding wall	-	300	400	1200	19	1.79	16.47	1.61	0.094	90	508	0.19
128	[Ran97]	83	very smooth	push-off/sliding wall	-	300	400	1200	19	1.79	16.47	1.61	0.262	90	508	0.48
129	[Ran97]	29	smooth	push-off/sliding wall	0.50	300	400	1200	38	3.12	35.26	2.98	0.047	90	653	0.32
130	[Ran97]	30	smooth	push-off/sliding wall	0.50	300	400	1200	38	3.12	35.26	2.98	0.047	90	653	0.28
131	[Ran97]	31	smooth	push-off/sliding wall	0.50	300	400	1200	38	3.12	35.26	2.98	0.047	90	653	0.27
132	[Ran97]	32	smooth	push-off/sliding wall	0.50	300	400	1200	38	3.12	35.26	2.98	0.094	90	508	0.41
133	[Ran97]	33	smooth	push-off/sliding wall	0.50	300	400	1200	38	3.12	35.26	2.98	0.094	90	508	0.38
134	[Ran97]	34	smooth	push-off/sliding wall	0.50	300	400	1200	38	3.12	35.26	2.98	0.094	90	508	0.44
135	[Ran97]	35	smooth	push-off/sliding wall	0.50	300	400	1200	38	3.12	35.26	2.98	0.188	90	508	0.87
136	[Ran97]	36	smooth	push-off/sliding wall	0.50	300	400	1200	38	3.12	35.26	2.98	0.188	90	508	0.78
137	[Ran97]	37	smooth	push-off/sliding wall	0.50	300	400	1200	38	3.12	35.26	2.98	0.188	90	508	0.82
138	[Ran97]	38	smooth	push-off/sliding wall	0.50	113	400	452	38	3.12	35.26	2.98	0.500	90	508	1.76
139	[Ran97]	39	smooth	push-off/sliding wall	0.50	75	400	300	38	3.12	35.26	2.98	0.754	90	508	2.63
140	[Ran97]	40	smooth	push-off/sliding wall	0.50	57	400	228	38	3.12	35.26	2.98	0.992	90	508	3.74
141	[Ran97]	41	smooth	push-off/sliding wall	0.50	57	400	228	38	3.12	35.26	2.98	1.488	90	508	5.45
142	[Ran97]	45	smooth	push-off/sliding wall	0.14	300	400	1200	34	2.87	34.84	2.95	0.047	90	653	0.23
143	[Ran97]	46	smooth	push-off/sliding wall	0.14	300	400	1200	34	2.87	34.84	2.95	0.047	90	653	0.21
144	[Ran97]	47	smooth	push-off/sliding wall	0.14	300	400	1200	34	2.87	34.84	2.95	0.094	90	508	0.34
145	[Ran97]	48	smooth	push-off/sliding wall	0.14	300	400	1200	34	2.87	34.84	2.95	0.094	90	508	0.27
146	[Ran97]	49	smooth	push-off/sliding wall	0.14	300	400	1200	34	2.87	34.84	2.95	0.188	90	508	0.58
147	[Ran97]	50	smooth	push-off/sliding wall	0.14	300	400	1200	34	2.87	34.84	2.95	0.188	90	508	0.64
148	[Ran97]	51	smooth	push-off/sliding wall	0.14	113	400	452	34	2.87	34.84	2.95	0.500	90	508	1.33

Table B-14: Database B – Specimens Nr. 149 – 185

Nr. [-]	Source [-]	Specimen ID [-]	Test-setup [-]	Interface [-]	R_t [mm]	b_{int} [mm]	l_{int} [mm]	A_{int} [cm²]	$f_{cm,cyl,1}$ [N/mm²]	$f_{ctm,1}$ [N/mm²]	$f_{cm,cyl,2}$ [N/mm²]	$f_{ctm,2}$ [N/mm²]	ρ_{int} [%]	α [-]	$f_{ym,int}$ [N/mm²]	τ_{test} [N/mm²]
149	[Ran97]	52	smooth	push-off/sliding wall	0.14	75	400	300	34	2.87	34.84	2.95	0.754	90	508	2.22
150	[Ran97]	53	smooth	push-off/sliding wall	0.14	57	400	228	34	2.87	34.84	2.95	0.992	90	508	2.95
151	[Ran97]	54	smooth	push-off/sliding wall	0.14	57	400	228	34	2.87	34.84	2.95	1.488	90	508	4.20
152	[Ran97]	73	smooth	push-off/sliding wall	0.50	300	400	1200	19	1.79	21.45	2.02	0.094	90	508	0.46
153	[Ran97]	74	smooth	push-off/sliding wall	0.50	300	400	1200	19	1.79	21.45	2.02	0.188	90	508	0.78
154	[Ran97]	75	smooth	push-off/sliding wall	0.50	113	400	452	19	1.79	21.45	2.02	0.500	90	508	2.02
155	[Ran97]	76	smooth	push-off/sliding wall	0.50	57	400	228	19	1.79	21.45	2.02	0.992	90	508	3.60
156	[Ran97]	77	smooth	push-off/sliding wall	0.50	57	400	228	19	1.79	21.45	2.02	1.488	90	508	4.87
157	[Ran97]	1	rough	push-off/sliding wall	2.70	300	400	1200	38	3.12	36.84	3.08	0.094	90	508	2.74
158	[Ran97]	2	rough	push-off/sliding wall	2.70	300	400	1200	38	3.12	36.84	3.08	0.094	90	508	2.19
159	[Ran97]	3	rough	push-off/sliding wall	2.70	300	400	1200	38	3.12	36.84	3.08	0.094	90	508	3.03
160	[Ran97]	4	rough	push-off/sliding wall	2.70	300	400	1200	38	3.12	36.84	3.08	0.094	90	508	2.03
161	[Ran97]	5	rough	push-off/sliding wall	2.70	300	400	1200	38	3.12	36.84	3.08	0.094	90	508	1.34
162	[Ran97]	6	rough	push-off/sliding wall	2.70	250	400	1000	38	3.12	36.84	3.08	0.226	90	508	3.81
163	[Ran97]	7	rough	push-off/sliding wall	2.70	250	400	1000	38	3.12	36.84	3.08	0.226	90	508	3.60
164	[Ran97]	8	rough	push-off/sliding wall	2.70	250	400	1000	38	3.12	36.84	3.08	0.226	90	508	3.74
165	[Ran97]	9	rough	push-off/sliding wall	2.70	250	400	1000	38	3.12	36.84	3.08	0.226	90	508	2.04
166	[Ran97]	10	rough	push-off/sliding wall	2.70	250	400	1000	38	3.12	36.84	3.08	0.226	90	508	1.78
167	[Ran97]	12	rough	push-off/sliding wall	2.70	113	400	452	38	3.12	36.84	3.08	0.500	90	508	5.55
168	[Ran97]	13	rough	push-off/sliding wall	2.70	113	400	452	38	3.12	36.84	3.08	0.500	90	508	5.33
169	[Ran97]	14	rough	push-off/sliding wall	2.70	113	400	452	38	3.12	36.84	3.08	0.500	90	508	3.79
170	[Ran97]	15	rough	push-off/sliding wall	2.70	113	400	452	38	3.12	36.84	3.08	0.500	90	508	4.38
171	[Ran97]	16	rough	push-off/sliding wall	2.70	57	400	228	38	3.12	36.84	3.08	0.992	90	508	8.72
172	[Ran97]	17	rough	push-off/sliding wall	2.70	57	400	228	38	3.12	36.84	3.08	0.992	90	508	8.77
173	[Ran97]	18	rough	push-off/sliding wall	2.70	57	400	228	38	3.12	36.84	3.08	0.992	90	508	8.52
174	[Ran97]	21	rough	push-off/sliding wall	2.70	300	400	1200	38	3.12	33.43	2.86	0.047	90	653	2.20
175	[Ran97]	22	rough	push-off/sliding wall	2.70	300	400	1200	38	3.12	33.43	2.86	0.047	90	653	2.07
176	[Ran97]	23	rough	push-off/sliding wall	2.70	300	400	1200	38	3.12	33.43	2.86	0.094	90	508	2.25
177	[Ran97]	24	rough	push-off/sliding wall	2.70	300	400	1200	38	3.12	33.43	2.86	0.094	90	508	2.39
178	[Ran97]	25	rough	push-off/sliding wall	2.70	250	400	1000	38	3.12	33.43	2.86	0.226	90	508	2.24
179	[Ran97]	26	rough	push-off/sliding wall	2.70	250	400	1000	38	3.12	33.43	2.86	0.226	90	508	2.36
180	[Ran97]	27	rough	push-off/sliding wall	2.70	75	400	300	38	3.12	33.43	2.86	0.754	90	508	5.00
181	[Ran97]	28	rough	push-off/sliding wall	2.70	57	400	228	38	3.12	33.43	2.86	1.488	90	508	8.67
182	[Ran97]	65	rough	push-off/sliding wall	2.70	300	400	1200	19	1.79	21.45	2.02	0.094	90	508	1.68
183	[Ran97]	66	rough	push-off/sliding wall	2.70	300	400	1200	19	1.79	21.45	2.02	0.188	90	508	1.81
184	[Ran97]	67	rough	push-off/sliding wall	2.70	113	400	452	19	1.79	21.45	2.02	0.500	90	508	3.33
185	[Ran97]	68	rough	push-off/sliding wall	2.70	57	400	228	19	1.79	21.45	2.02	0.992	90	508	5.13

Table B-15: Database B – Specimens Nr. 186 – 222

Nr. [-]	Source [-]	Specimen ID [-]	Test-setup [-]	Interface [-]	R_t [mm]	b_{int} [mm]	l_{int} [mm]	A_{int} [cm²]	$f_{cm,cyl,1}$ [N/mm²]	$f_{ctm,1}$ [N/mm²]	$f_{cm,cyl,2}$ [N/mm²]	$f_{ctm,2}$ [N/mm²]	ρ_{int} [%]	α [-]	$f_{ym,int}$ [N/mm²]	τ_{test} [N/mm²]
186	[Ran97]	69	rough	push-off/sliding wall	2.70	57	400	228	19	1.79	21.45	2.02	1.488	90	508	7.46
187	[Sha14]	N-5-S-4	smooth	push-off	-	114	279	319	34	2.90	33.51	2.90	1.339	90	457	4.53
188	[Sha14]	N-5-S-5	smooth	push-off	-	114	279	319	34	2.90	33.51	2.90	1.339	90	457	4.80
189	[Sha14]	N-5-S-6	smooth	push-off	-	114	279	319	34	2.90	33.51	2.90	1.339	90	457	5.42
190	[Sha14]	N-8-S-1	smooth	push-off	-	114	279	319	52	3.72	52.06	3.72	1.339	90	457	9.08
191	[Sha14]	N-8-S-2	smooth	push-off	-	114	279	319	52	3.72	52.06	3.72	1.339	90	457	7.38
192	[Sha14]	N-8-S-3	smooth	push-off	-	114	279	319	52	3.72	52.06	3.72	1.339	90	457	7.66
193	[Sha14]	S-5-S-1	smooth	push-off	-	114	279	319	31	2.21	31.37	2.21	1.339	90	457	5.33
194	[Sha14]	S-5-S-2	smooth	push-off	-	114	279	319	31	2.21	31.37	2.21	1.339	90	457	4.72
195	[Sha14]	S-5-S-3	smooth	push-off	-	114	279	319	31	2.21	31.37	2.21	1.339	90	457	5.51
196	[Sha14]	S-8-S-1	smooth	push-off	-	114	279	319	50	3.52	49.64	3.52	1.339	90	457	9.28
197	[Sha14]	S-8-S-2	smooth	push-off	-	114	279	319	50	3.52	49.64	3.52	1.339	90	457	8.01
198	[Sha14]	S-8-S-3	smooth	push-off	-	114	279	319	50	3.52	49.64	3.52	1.339	90	457	8.15
199	[Sha14]	A-5-S-1	smooth	push-off	-	114	279	319	42	3.52	41.92	3.52	1.339	90	457	5.74
200	[Sha14]	A-5-S-2	smooth	push-off	-	114	279	319	42	3.52	41.92	3.52	1.339	90	457	5.55
201	[Sha14]	A-5-S-3	smooth	push-off	-	114	279	319	42	3.52	41.92	3.52	1.339	90	457	5.43
202	[Sha14]	A-8-S-1	smooth	push-off	-	114	279	319	54	3.59	54.09	3.59	1.339	90	457	6.38
203	[Sha14]	A-8-S-2	smooth	push-off	-	114	279	319	54	3.59	54.09	3.59	1.339	90	457	6.65
204	[Sha14]	A-8-S-3	smooth	push-off	-	114	279	319	54	3.59	54.09	3.59	1.339	90	457	7.16
205	[Sha14]	N-5-R-4	rough	push-off	-	114	279	319	34	2.90	33.51	6.00	1.339	90	457	8.17
206	[Sha14]	N-5-R-5	rough	push-off	-	114	279	319	34	2.90	33.51	2.90	1.339	90	457	7.39
207	[Sha14]	N-5-R-6	rough	push-off	-	114	279	319	34	2.90	33.51	2.90	1.339	90	457	7.40
208	[Sha14]	N-8-R-1	rough	push-off	-	114	279	319	52	3.72	52.06	3.72	1.339	90	457	10.25
209	[Sha14]	N-8-R-2	rough	push-off	-	114	279	319	52	3.72	52.06	3.72	1.339	90	457	7.76
210	[Sha14]	N-8-R-3	rough	push-off	-	114	279	319	52	3.72	52.06	3.72	1.339	90	457	8.88
211	[Sha14]	S-5-R-1	rough	push-off	-	114	279	319	31	2.21	31.37	2.21	1.339	90	457	7.12
212	[Sha14]	S-5-R-2	rough	push-off	-	114	279	319	31	2.21	31.37	2.21	1.339	90	457	6.97
213	[Sha14]	S-5-R-3	rough	push-off	-	114	279	319	31	2.21	31.37	2.21	1.339	90	457	8.84
214	[Sha14]	S-8-R-1	rough	push-off	-	114	279	319	50	3.52	49.64	3.52	1.339	90	457	9.97
215	[Sha14]	S-8-R-2	rough	push-off	-	114	279	319	50	3.52	49.64	3.52	1.339	90	457	9.33
216	[Sha14]	S-8-R-3	rough	push-off	-	114	279	319	50	3.52	49.64	3.52	1.339	90	457	9.23
217	[Sha14]	A-5-R-1	rough	push-off	-	114	279	319	42	3.52	41.92	3.52	1.339	90	457	6.70
218	[Sha14]	A-5-R-2	rough	push-off	-	114	279	319	42	3.52	41.92	3.52	1.339	90	457	7.31
219	[Sha14]	A-5-R-3	rough	push-off	-	114	279	319	42	3.52	41.92	3.52	1.339	90	457	7.12
220	[Sha14]	A-8-R-1	rough	push-off	-	114	279	319	54	3.59	54.09	3.59	1.339	90	457	8.55
221	[Sha14]	A-8-R-2	rough	push-off	-	114	279	319	54	3.59	54.09	3.59	1.339	90	457	8.85
222	[Sha14]	A-8-R-3	rough	push-off	-	114	279	319	54	3.59	54.09	3.59	1.339	90	457	8.88

Table B-16: Database B – Specimens Nr. 223 – 259

Nr. [-]	Source [-]	Specimen ID [-]	Test-setup [-]	Interface [-]	R_t [mm]	b_{int} [mm]	l_{int} [mm]	A_{int} [cm²]	$f_{cm,cyl,1}$ [N/mm²]	$f_{ctm,1}$ [N/mm²]	$f_{cm,cyl,2}$ [N/mm²]	$f_{ctm,2}$ [N/mm²]	ρ_{int} [%]	α [-]	$f_{ym,int}$ [N/mm²]	τ_{test} [N/mm²]
223	[Sne16]	-SL-CJ-13-S	smooth	push-off	-	114	279	319	38	3.54	38.40	3.54	1.339	90	516	5.47
224	[Sne16]	-SL-CJ-13-S	smooth	push-off	-	114	279	319	38	3.54	38.40	3.54	1.339	90	517	6.75
225	[Sne16]	-CL-CJ-13-S	smooth	push-off	-	114	279	319	32	2.23	31.99	2.23	1.339	90	524	5.67
226	[Sne16]	-CL-CJ-13-S	smooth	push-off	-	114	279	319	32	2.23	31.99	2.23	1.339	90	525	5.59
227	[Sne16]	-SL-CJ-13-S	smooth	push-off	-	114	279	319	30	2.61	30.20	2.61	1.339	90	528	5.23
228	[Sne16]	-SL-CJ-13-S	smooth	push-off	-	114	279	319	30	2.61	30.20	2.61	1.339	90	529	5.37
229	[Sne16]	-CL-CJ-13-S	smooth	push-off	-	114	279	319	31	2.51	30.75	2.51	1.339	90	530	5.11
230	[Sne16]	-CL-CJ-13-S	smooth	push-off	-	114	279	319	31	2.51	30.75	2.51	1.339	90	531	5.16
231	[Sne16]	-SL-CJ-09-S	smooth	push-off	-	114	279	319	37	3.69	37.09	3.69	0.892	90	514	3.73
232	[Sne16]	-SL-CJ-09-S	smooth	push-off	-	114	279	319	37	3.69	37.09	3.69	0.892	90	515	4.51
233	[Sne16]	-SL-CJ-17-S	smooth	push-off	-	114	279	319	34	4.16	34.13	4.16	1.785	90	518	6.89
234	[Sne16]	-SL-CJ-17-S	smooth	push-off	-	114	279	319	34	4.16	34.13	4.16	1.785	90	519	7.82
235	[Sne16]	-SL-CJ-22-S	smooth	push-off	-	114	279	319	34	2.76	34.47	2.76	2.231	90	520	6.89
236	[Sne16]	-SL-CJ-22-S	smooth	push-off	-	114	279	319	34	2.76	34.47	2.76	2.231	90	521	7.82
237	[Sne16]	S-CL-CJ-9-S-	smooth	push-off	-	114	279	319	33	2.11	32.89	2.11	0.892	90	522	4.42
238	[Sne16]	S-CL-CJ-9-S-	smooth	push-off	-	114	279	319	33	2.11	32.89	2.11	0.892	90	523	5.25
239	[Sne16]	-CL-CJ-17-S	smooth	push-off	-	114	279	319	31	2.54	31.37	2.54	1.785	90	526	5.97
240	[Sne16]	-CL-CJ-17-S	smooth	push-off	-	114	279	319	31	2.54	31.37	2.54	1.785	90	527	6.77
241	[Sne16]	-SL-CJ-13-R	rough	push-off	-	114	279	319	38	3.54	38.40	3.54	1.339	90	500	8.74
242	[Sne16]	-SL-CJ-13-R	rough	push-off	-	114	279	319	38	3.54	38.40	3.54	1.339	90	501	8.22
243	[Sne16]	-CL-CJ-13-R	rough	push-off	-	114	279	319	32	2.23	31.99	2.23	1.339	90	508	7.03
244	[Sne16]	-CL-CJ-13-R	rough	push-off	-	114	279	319	32	2.23	31.99	2.23	1.339	90	509	6.49
245	[Sne16]	-SL-CJ-13-R	rough	push-off	-	114	279	319	30	2.61	30.20	2.61	1.339	90	510	6.44
246	[Sne16]	-SL-CJ-13-R	rough	push-off	-	114	279	319	30	2.61	30.20	2.61	1.339	90	511	6.49
247	[Sne16]	-CL-CJ-13-R	rough	push-off	-	114	279	319	31	2.51	30.75	2.51	1.339	90	512	5.79
248	[Sne16]	-CL-CJ-13-R	rough	push-off	-	114	279	319	31	2.51	30.75	2.51	1.339	90	513	6.06
249	[Sne16]	-SL-CJ-09-R	rough	push-off	-	114	279	319	37	3.69	37.09	3.69	0.892	90	498	6.83
250	[Sne16]	-SL-CJ-09-R	rough	push-off	-	114	279	319	37	3.69	37.09	3.69	0.892	90	499	6.99
251	[Sne16]	-SL-CJ-17-R	rough	push-off	-	114	279	319	34	4.16	34.13	4.16	1.785	90	502	8.63
252	[Sne16]	-SL-CJ-17-R	rough	push-off	-	114	279	319	34	4.16	34.13	4.16	1.785	90	503	9.02
253	[Sne16]	-SL-CJ-22-R	rough	push-off	-	114	279	319	34	2.76	34.47	2.76	2.231	90	504	8.92
254	[Sne16]	-SL-CJ-22-R	rough	push-off	-	114	279	319	34	2.76	34.47	2.76	2.231	90	505	7.97
255	[Sne16]	S-CL-CJ-9-R-	rough	push-off	-	114	279	319	33	2.11	32.89	2.11	0.892	90	506	5.13
256	[Sne16]	S-CL-CJ-9-R-	rough	push-off	-	114	279	319	33	2.11	32.89	2.11	0.892	90	507	5.94
257	[Val99]	B1	rough	push-off/sliding wall	-	102	813	826	24	2.22	41.37	3.35	1.035	90	476	6.05
258	[Val99]	B2	rough	push-off/sliding wall	-	102	813	826	24	2.22	41.37	3.35	2.071	90	476	6.96
259	[Zen09]	P615-3A	very rough	push-off	-	254	406	1032	40	3.26	49.09	3.80	0.414	90	464	4.82

Table B-17: Database B – Specimens Nr. 260 – 266

Nr. [-]	Source [-]	Specimen ID [-]	Test-setup [-]	Interface [-]	R_t [mm]	b_{int} [mm]	l_{int} [mm]	A_{int} [cm²]	$f_{cm,cyl,1}$ [N/mm²]	$f_{ctm,1}$ [N/mm²]	$f_{cm,cyl,2}$ [N/mm²]	$f_{ctm,2}$ [N/mm²]	ρ_{int} [%]	α [-]	$f_{ym,int}$ [N/mm²]	τ_{test} [N/mm²]
260	[Zen09]	P615-3B	very rough	push-off	-	254	406	1032	40	3.26	49.09	3.80	0.414	90	464	4.13
261	[Zen09]	P615-4A	very rough	push-off	-	254	406	1032	40	3.26	49.09	3.80	0.736	90	424	4.90
262	[Zen09]	P615-4B	very rough	push-off	-	254	406	1032	40	3.26	49.09	3.80	0.736	90	424	5.52
263	[Zen09]	P1035-3A	very rough	push-off	-	254	406	1032	40	3.26	49.09	3.80	0.414	90	897	3.85
264	[Zen09]	P1035-3B	very rough	push-off	-	254	406	1032	40	3.26	49.09	3.80	0.414	90	869	4.50
265	[Zen09]	P1035-4A	very rough	push-off	-	254	406	1032	40	3.26	49.09	3.80	0.736	90	966	5.81
266	[Zen09]	P1035-4B	very rough	push-off	-	254	406	1032	40	3.26	49.09	3.80	0.736	90	906	4.86

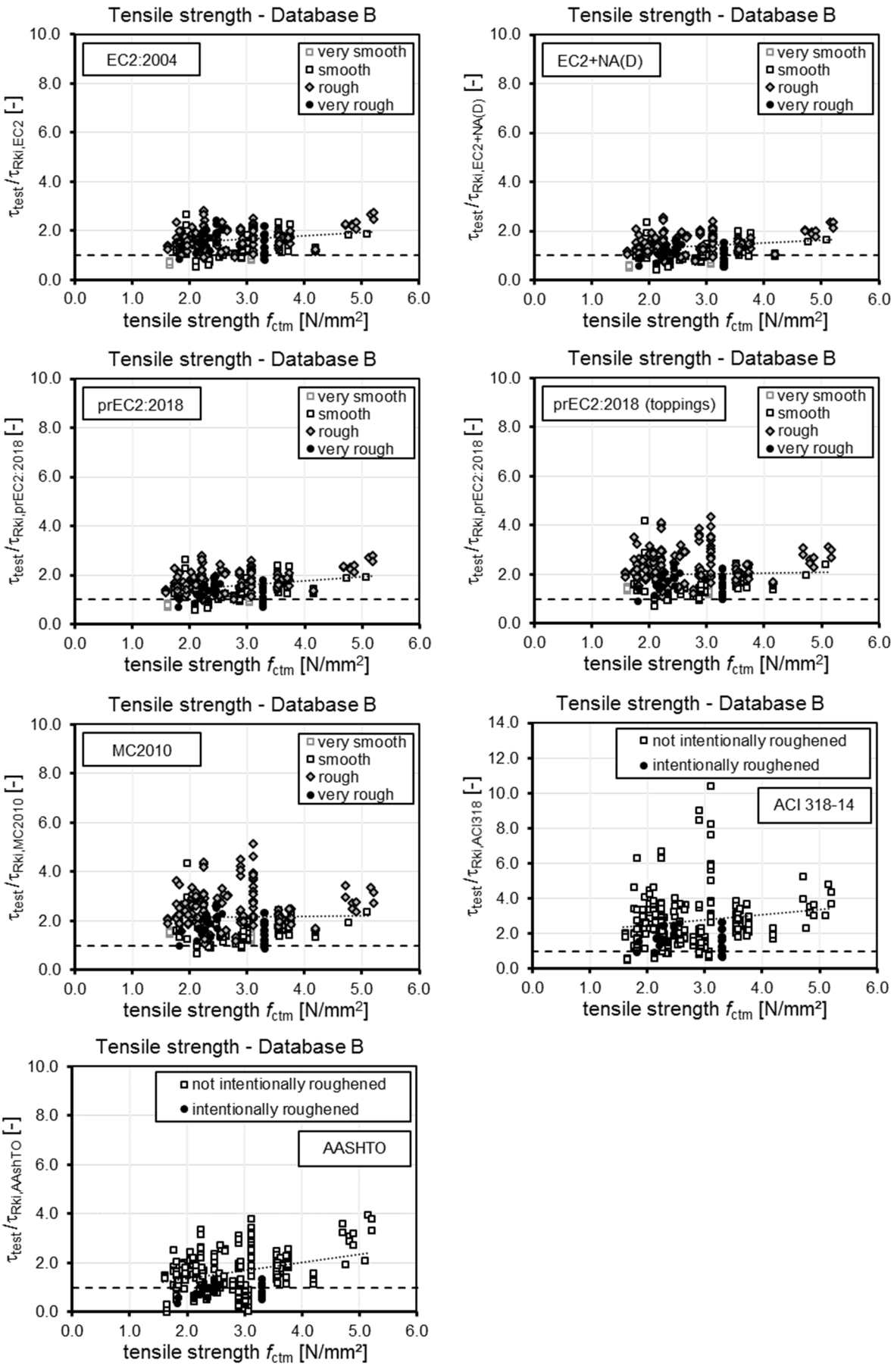

Figure B-4: Evaluation of tensile strength of database B according to evaluated codes

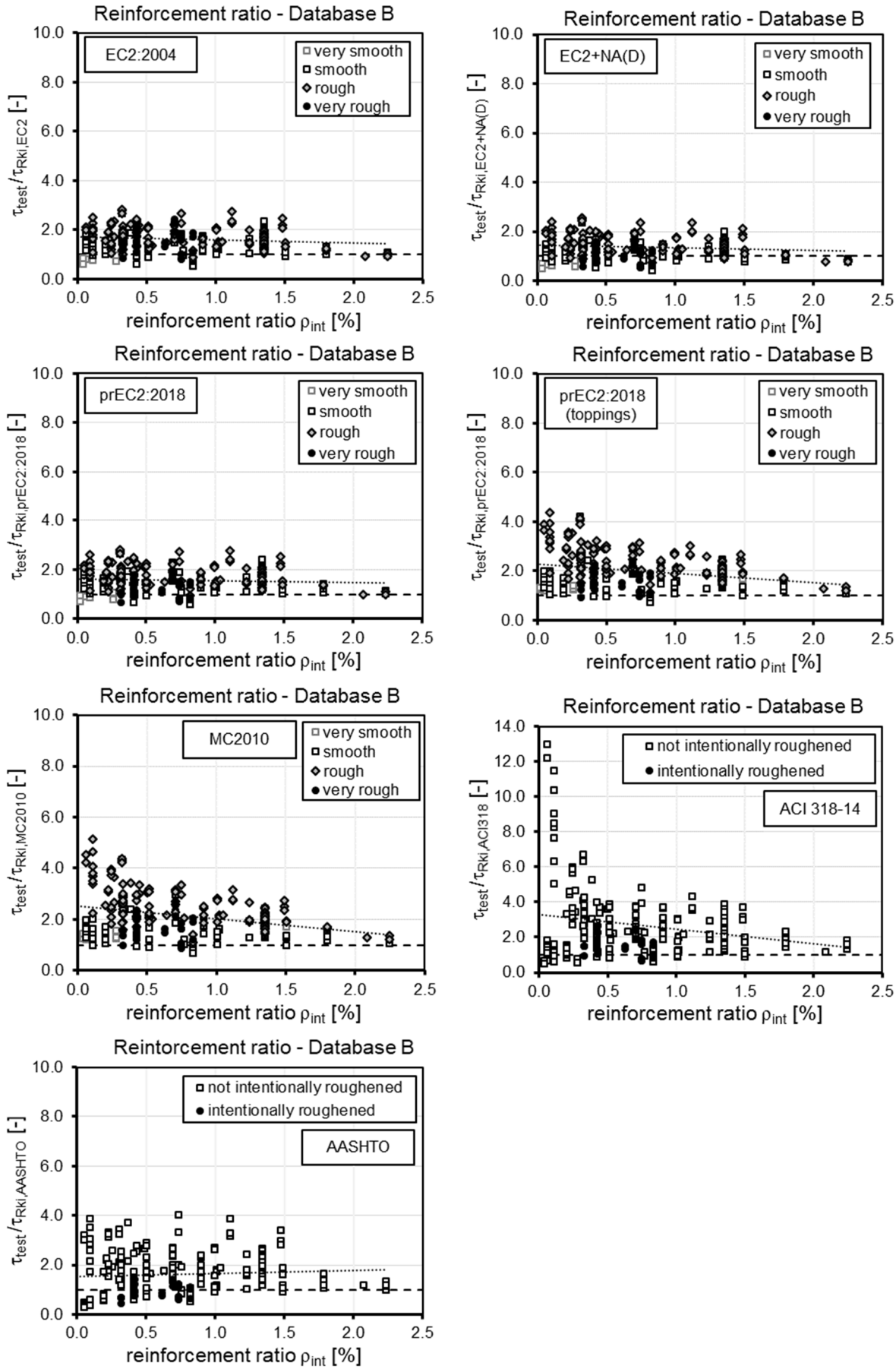

Figure B-5: Evaluation of interface reinforcement of database B according to evaluated codes

B.1.5 Database AB: Normal stress and reinforcement

Table B-18: Database AB – Specimens Nr. 1 – 37

Nr. [-]	Source [-]	Test ID [-]	Test-setup [-]	Interface [-]	b_{int} [mm]	l_{int} [mm]	A_{int} [cm²]	$f_{cm,cyl,1}$ [N/mm²]	$f_{ctm,1}$ [N/mm²]	$f_{cm,cyl,2}$ [N/mm²]	$f_{ctm,2}$ [N/mm²]	ρ_{int} [%]	α [-]	f_{ym} [N/mm²]	σ_n [N/mm²]	τ_{test} [N/mm²]
1	[Das86]	101	rough	push-through	150	150	225	25.61	2.33	16.13	1.58	0.50	90	586	0.55	3.14
2	[Das86]	102	rough	push-through	150	150	225	25.61	2.33	16.13	1.58	0.50	90	543	1.07	4.00
3	[Das86]	103	rough	push-through	150	150	225	25.61	2.33	16.13	1.58	0.50	90	535	0.42	3.27
4	[Das86]	104	rough	push-through	150	150	225	25.61	2.33	16.13	1.58	0.50	90	546	0.79	3.50
5	[Das86]	105	rough	push-through	150	150	225	25.61	2.33	16.13	1.58	0.50	90	542	1.55	4.58
6	[Das86]	106	rough	push-through	150	150	225	25.61	2.33	16.13	1.58	0.50	90	533	1.93	5.32
7	[Das86]	107	rough	push-through	150	150	225	25.61	2.33	16.13	1.58	0.50	90	549	0.29	3.66
8	[Das86]	108	rough	push-through	150	150	225	25.61	2.33	16.13	1.58	0.50	90	543	0.73	3.60
9	[Das86]	109	rough	push-through	150	150	225	25.61	2.33	16.13	1.58	0.50	90	551	1.42	4.52
10	[Gas64]	A-1	rough	modified push-off	178	673	1196	33.58	2.87	33.58	2.87	1.07	79	414	3.84	14.01
11	[Gas64]	A-2	rough	modified push-off	178	743	1321	28.54	2.53	28.54	2.53	0.97	75	414	3.78	10.61
12	[Gas64]	A-3	rough	modified push-off	178	631	1121	27.85	2.49	27.85	2.49	1.14	60	414	7.77	12.22
13	[Gas64]	A-4	rough	modified push-off	178	377	671	32.27	2.78	32.27	2.78	1.91	45	414	17.32	17.32
14	[Gas64]	A-1g	rough	modified push-off	178	673	1196	31.99	2.77	31.99	2.77	1.07	79	414	3.14	10.38
15	[Gas64]	A-2g	rough	modified push-off	178	743	1321	34.13	2.90	34.13	2.90	0.97	75	414	4.23	12.24
16	[Gas64]	A-3g	rough	modified push-off	178	631	1121	33.78	2.88	33.78	2.88	1.14	60	414	8.56	13.59
17	[Gas64]	A-4g	rough	modified push-off	178	377	671	27.44	2.46	27.44	2.46	1.91	45	414	16.86	16.86
18	[Sco10]	LL-1-A	rough	push-off	406	610	2477	43.09	3.46	76.53	4.57	0.10	90	414	0.05	4.32
19	[Sco10]	LL-1-B	rough	push-off	406	610	2477	43.09	3.46	76.53	4.57	0.10	90	414	0.05	2.62
20	[Sco10]	LL-1-C	rough	push-off	406	610	2477	43.09	3.46	75.84	4.56	0.10	90	414	0.05	3.35
21	[Sco10]	NN-1-A	rough	push-off	406	610	2477	42.40	3.41	53.64	4.05	0.10	90	414	0.05	2.19
22	[Sco10]	NN-1-B	rough	push-off	406	610	2477	42.40	3.41	53.64	4.05	0.10	90	414	0.05	2.52
23	[Sco10]	NN-1-C	rough	push-off	406	610	2477	42.40	3.41	53.64	4.05	0.10	90	414	0.05	3.09
24	[Sco10]	NL-1-A	rough	push-off	406	610	2477	43.09	3.46	53.64	4.05	0.10	90	414	0.05	3.02
25	[Sco10]	NL-1-B	rough	push-off	406	610	2477	43.09	3.46	53.64	4.05	0.10	90	414	0.05	3.12
26	[Sco10]	NL-1-C	rough	push-off	406	610	2477	43.09	3.46	53.64	4.05	0.10	90	414	0.05	3.26
27	[Sco10]	LL-3-A	rough	push-off	406	610	2477	39.51	3.24	76.53	4.57	0.48	90	414	0.05	3.59
28	[Sco10]	LL-3-B	rough	push-off	406	610	2477	39.51	3.24	76.53	4.57	0.48	90	414	0.05	3.98
29	[Sco10]	LL-3-C	rough	push-off	406	610	2477	39.51	3.24	76.53	4.57	0.48	90	414	0.05	4.10
30	[Sco10]	NN-3-A	rough	push-off	406	610	2477	42.40	3.41	53.64	4.05	0.48	90	414	0.05	3.48
31	[Sco10]	NN-3-B	rough	push-off	406	610	2477	42.40	3.41	53.64	4.05	0.48	90	414	0.05	3.89
32	[Sco10]	NN-3-C	rough	push-off	406	610	2477	42.40	3.41	53.64	4.05	0.48	90	414	0.05	4.09
33	[Sco10]	NL-3-A	rough	push-off	406	610	2477	39.51	3.24	53.64	4.05	0.48	90	414	0.05	4.32
34	[Sco10]	NL-3-B	rough	push-off	406	610	2477	39.51	3.24	53.64	4.05	0.48	90	414	0.05	4.25
35	[Sco10]	NL-3-C	rough	push-off	406	610	2477	39.51	3.24	53.64	4.05	0.48	90	414	0.05	3.26
36	[Val99]	B5	rough	push-off/sliding wal	102	813	826	24.13	2.22	41.37	3.35	1.04	90	476	6.90	14.13
37	[Val99]	B6	rough	push-off/sliding wal	102	813	826	24.13	2.22	41.37	3.35	2.07	90	476	6.90	14.67

Table B-19: Database AB – Specimens Nr. 38, 39

Nr. [-]	Source [-]	Test ID [-]	Test-setup [-]	Interface [-]	b_{int} [mm]	l_{int} [mm]	A_{int} [cm²]	$f_{cm,cyl,1}$ [N/mm²]	$f_{ctm,1}$ [N/mm²]	$f_{cm,cyl,2}$ [N/mm²]	$f_{ctm,2}$ [N/mm²]	ρ_{int} [%]	α [-]	f_{ym} [N/mm²]	σ_n [N/mm²]	τ_{test} [N/mm²]
38	[Val99]	B9	rough	push-off/sliding wal	102	813	826	24.13	2.22	41.37	3.35	1.04	90	476	2.41	8.94
39	[Wil17]	1-1	smooth	push-through	233	914	2132	65.91	5.79	61.50	6.07	0.24	90	453	3.40	4.98

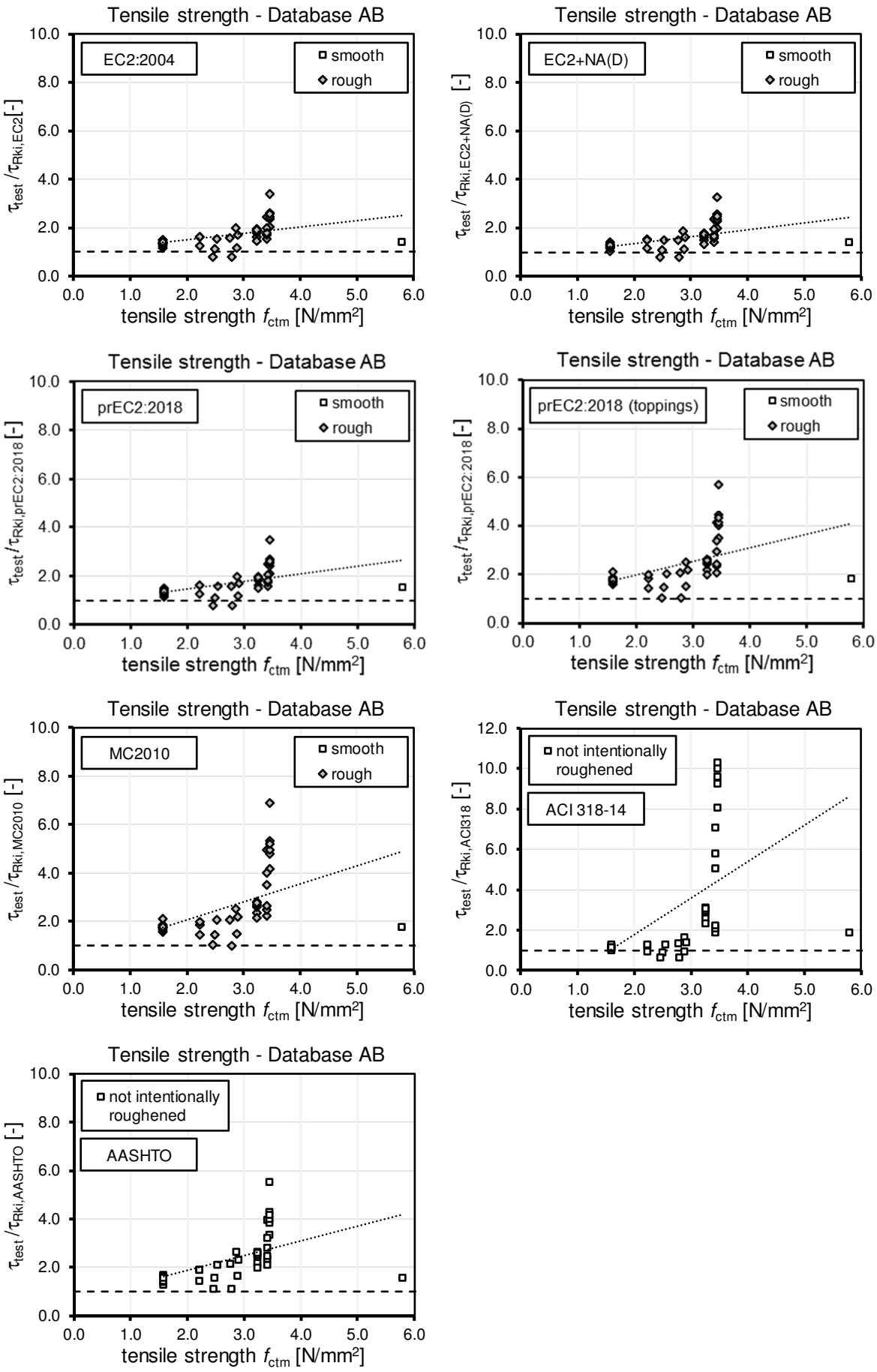

Figure B-6: Evaluation of tensile strength of database AB according to evaluated codes

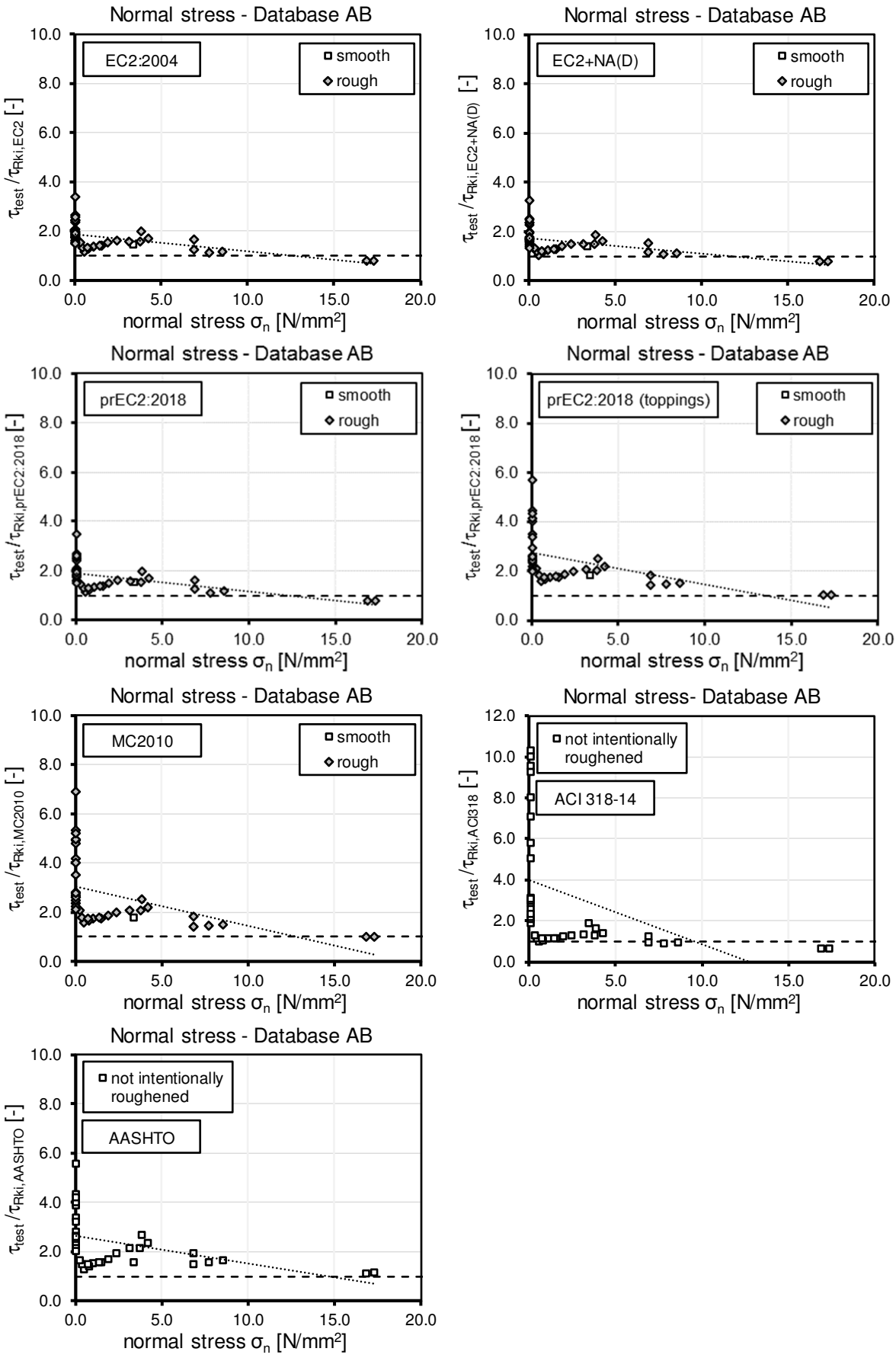

Figure B-7: Evaluation of normal stress of database AB according to evaluated codes

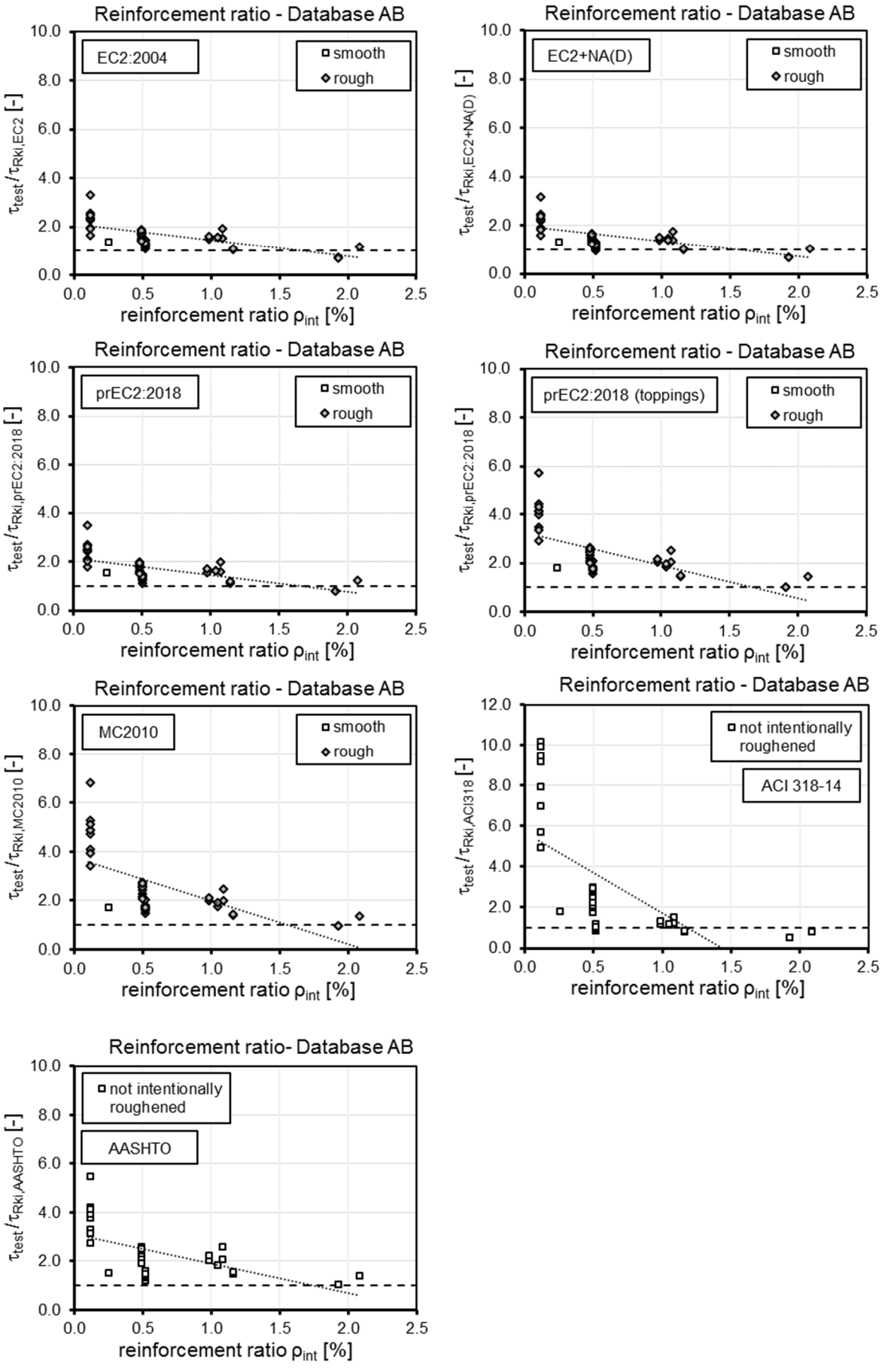

Figure B-8: Evaluation of reinforcement ratio of database AB according to evaluated codes

B.1.6 Database C: Adhesion - fatigue

Table B-20: Database C– Specimens Nr. 1 – 20

Nr. [-]	Source [-]	Test ID [-]	Test-setup [-]	Interface [-]	R_t [mm]	b_{int} [mm]	l_{int} [mm]	A_{int} [cm²]	$f_{cm,cyl,1}$ [N/mm²]	$f_{ctm,1}$ [N/mm²]	$f_{cm,cyl,2}$ [N/mm²]	$f_{ctm,2}$ [N/mm²]	$\tau_{test,max}$ [N/mm²]	$\Delta\tau_{test}$ [N/mm²]	N [-]	$\tau_{test,res}$ [N/mm²]
1	[Zil04]	HHH-W1	smooth	push-through	0.8	150	500	750	82.90	4.73	82.90	4.73	1.27	0.84	1000000	2.79
2	[Zil04]	HHH-W3	smooth	push-through	0.8	150	500	750	82.90	4.73	82.90	4.73	1.23	0.8	1000000	2.45
3	[Zil04]	HHH-W4	smooth	push-through	0.8	150	500	750	82.90	4.73	82.90	4.73	1.28	0.89	1000000	3.08
4	[Zil04]	NHN-W1	smooth	push-through	0.8	150	500	750	40.50	3.30	82.90	4.73	1.64	1.17	2000000	3.00
5	[Zil04]	NHN-W3	smooth	push-through	0.8	150	500	750	40.70	3.31	82.90	4.73	1.71	1.18	2000000	3.71
6	[Zil04]	HNH-W3	smooth	push-through	0.8	150	500	750	82.90	4.73	41.00	3.33	0.7	0.49	2000000	1.13
7	[Zil04]	HNH-W4	smooth	push-through	0.8	150	500	750	82.90	4.73	41.20	3.34	0.64	0.48	2000000	1.43
8	[Zil04]	NNN-W3	smooth	push-through	0.8	150	500	750	41.50	3.36	41.40	3.36	0.73	0.5	2000000	2.43
9	[Zil04]	NNN-W4	smooth	push-through	0.8	150	500	750	41.60	3.37	41.40	3.36	0.68	0.47	2000000	1.87
10	[Zil04]	HHH-R1	rough	push-through	1.5	150	500	750	82.90	4.73	82.40	4.71	2.21	1.48	101955	-
11	[Zil04]	HHH-R3	rough	push-through	1.5	150	500	750	82.90	4.73	82.60	4.72	2.16	1.32	1020	-
12	[Zil04]	HHH-R4	rough	push-through	1.5	150	500	750	82.90	4.73	82.90	4.73	2.01	1.37	1000000	4.04
13	[Zil04]	NHN-R1	rough	push-through	1.5	150	500	750	38.20	3.16	81.10	4.68	1.85	1.21	2000000	3.01
14	[Zil04]	NHN-R3	rough	push-through	1.5	150	500	750	38.50	3.18	82.20	4.71	1.81	1.18	2000000	3.47
15	[Zil04]	NHN-R4	rough	push-through	1.5	150	500	750	38.90	3.20	82.90	4.73	1.84	1.24	2000000	3.17
16	[Zil04]	HNH-R1	rough	push-through	1.5	150	500	750	82.90	4.73	38.20	3.16	0.8	0.48	2000000	1.47
17	[Zil04]	HNH-R3	rough	push-through	1.5	150	500	750	82.90	4.73	38.50	3.18	0.69	0.45	2000000	1.25
18	[Zil04]	HNH-R4	rough	push-through	1.5	150	500	750	82.80	4.72	38.80	3.20	0.77	0.4	2000000	1.19
19	[Zil04]	NNN-R1	rough	push-through	1.5	150	500	750	41.40	3.36	41.20	3.34	1.56	1.04	92	-
20	[Zil04]	NNN-R3	rough	push-through	1.5	150	500	750	41.50	3.36	41.30	3.35	1.47	1.02	2000000	2.72

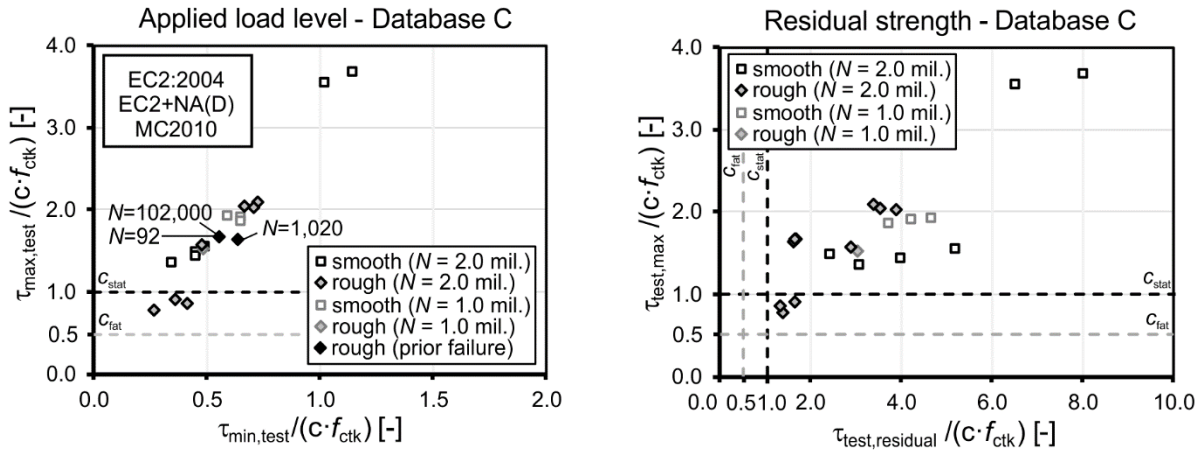

Figure B-9: Applied load level referred to calculated characteristic adhesive strength (left) and residual resistance referred to calculated characteristic adhesive strength (right) according to EC2, EC2+NA(D) and MC2010

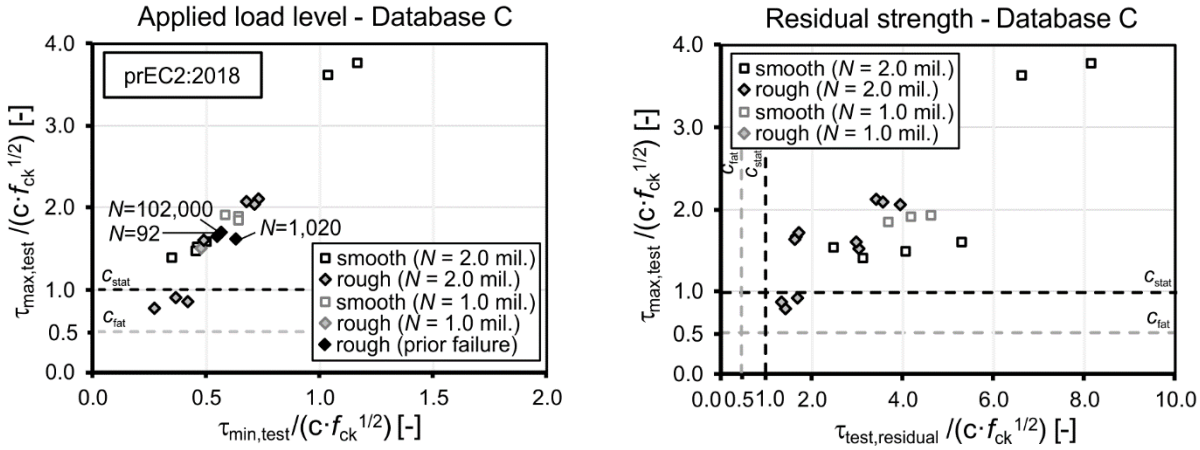

Figure B-10: Applied load level referred to calculated characteristic adhesive strength (left) and residual resistance referred to calculated characteristic adhesive strength (right) according to prEC2:2018

B.1.7 Database D: Reinforcement – fatigue

No small size tests with interface reinforcement in database which fulfilled the database filter conditions

B.2 Beam and slab specimens

B.2.1 Overview of test reports in database

Autor: Abeles, P.W.; Brown, E.I., Hu, C.H. [Han60]

Title: Tests of composite concrete beams with prestressed planks

Source: Materiaux et Construction, Vol. 5, No. 25, pp. 31–41, 1972

Test setup:

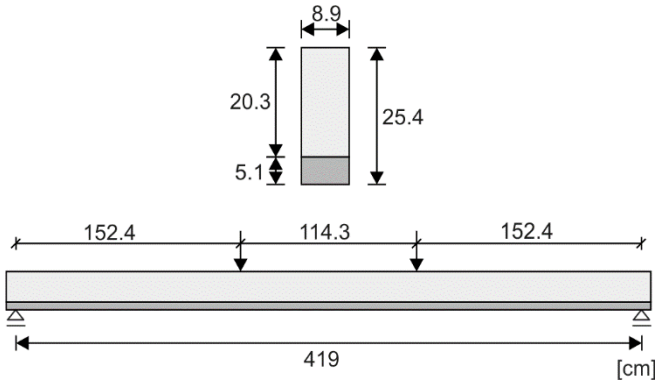

Nr. of tests	5
very smooth	–
smooth	–
rough(1)	5
very rough	–
keyed	–

Interface reinforcement: –

(1): rough: roughened by raking

Autor: BADOUX, J.C. [Bad65]

Title: Horizontal shear connection in composite concrete beams under repeated loading

Source: PhD Thesis, Lehigh University, 1965

Test setup:

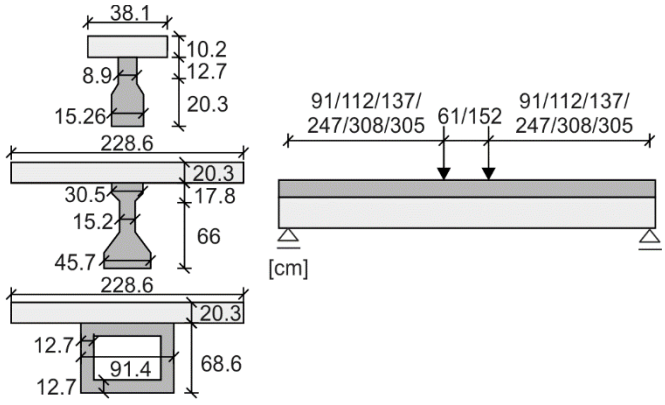

Nr. of tests	26
very smooth	–
smooth(1)	1
rough(2)	10
very rough(3)	15
keyed	–

Interface reinforcement: ρ_{sw} = 0.05, 0.145, 0.175, 0.3 and 0.52%
with Ø9.5 and Ø12.7 mm stirrups

(1): smooth: left as cast, (2): rough: lightly brushed; (3): very rough: raked

Autor:	Albrecht, C.	[Alb14]
Title:	Bemessung von Stahlbetondecken mit abgeflachten rotationssymmetrischen Hohlkörpern und ein Beitrag zum besseren Verständnis der Querkrafttragfähigkeit	
Source:	PhD Thesis, Institute of Structural Concrete, Technische Universität Kaiserslautern, 2014	

Test setup:

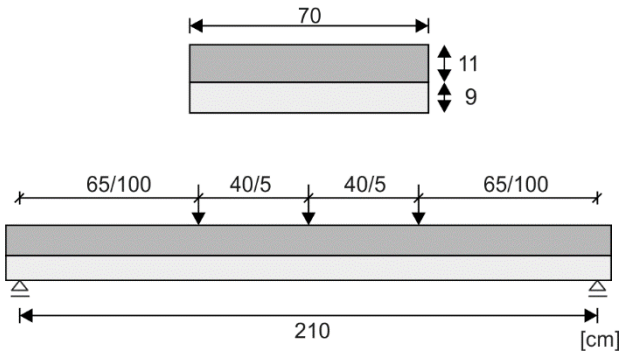

Nr. of tests	3
very smooth	–
smooth(1)	3
rough	–
very rough	–
keyed	–

Interface reinforcement: –

(1): smooth: left as cast

Autor:	Chung, H.W.; Chung, T.Y.	[Chu76]
Title:	Prestressed concrete composite beams under repeated loading	
Source:	ACI Journal, Title No. 73.24, pp. 291-295, May 1976	

Test setup:

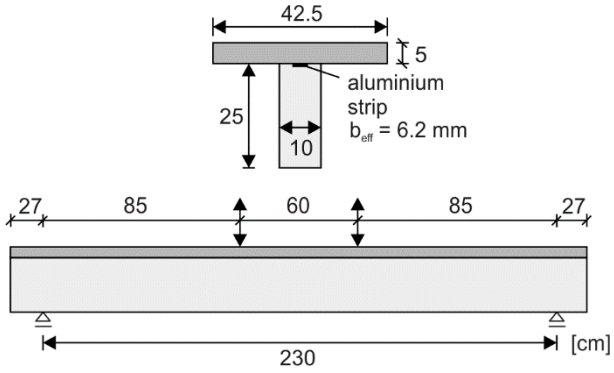

Nr. of tests	18
very smooth	–
smooth	–
rough(1)	18
very rough	–
keyed	–

4 monotonic tests
14 cyclic tests

Interface reinforcement: ρ_{sw} = 0, 0.15, 0.2, 0.3% with Ø5 mm stirrups

(1): rough: exposure of coarse aggregate

Autor: Daschner, F. [Das86a]

Title: Versuche zur notwendigen Schubbewehrung zwischen Betonfertigteilen und Ortbeton

Source: Deutscher Ausschuss für Stahlbeton DAfStb, Issue 372, Ernst & Sohn Verlag, Berlin, 1986

Test setup:

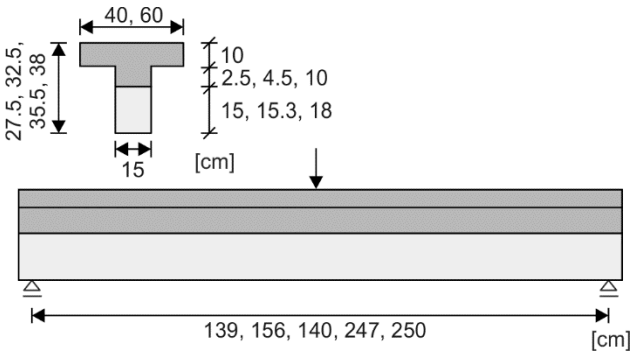

Nr. of tests	20
very smooth	–
smooth(1)	8
rough(2)	5
very rough(3)	5
keyed	–

Interface reinforcement: ρ_{sw} = 0, 0.12, 0.3, 0.75, 0.82, 1.34% with Ø6, Ø8 and Ø10 mm stirrups

(1): smooth: smoothened by trowel, left as cast; (2): rough: nail raked; (3): very rough; sawtooth

Autor: Daschner, F.; Nissen, I.; Kupfer, H. [Das86b]

Title: Verminderte Schubdeckung in Stahlbeton und Spannbetonträgern mit Fugen parallel zur Tragrichtung unter Berücksichtigung nicht vorwiegend ruhender Lasten

Source: Deutscher Ausschuss für Stahlbeton DAfStb, Issue 372, Ernst & Sohn Verlag, Berlin, 1986

Test setup:

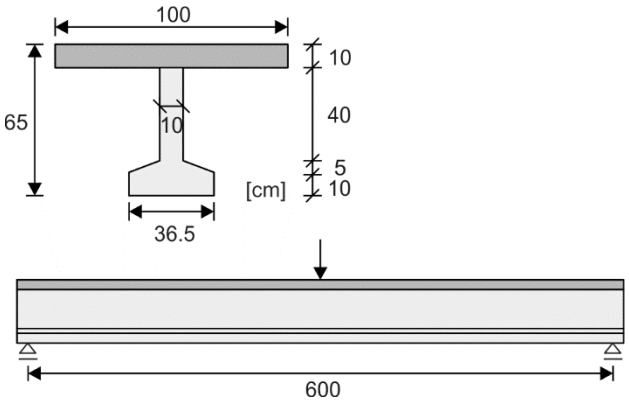

Nr. of tests	1
very smooth	–
smooth	–
rough(1)	1
very rough	–
keyed	–

Interface reinforcement: ρ_{sw} = 0.75 with Ø10 mm stirrups

(1): rough: exposure of coarse aggregate

Autor:	Furche, J.; Klug, Y.	[Fur11]
Title:	Gitterträger als Querkraft und Verbundbewehrung	
Source:	9. Tagung Betonbauteile – Neue Normen und Werkstoffe im Betonbau HTWK Leipzig, 2011	

Test setup:

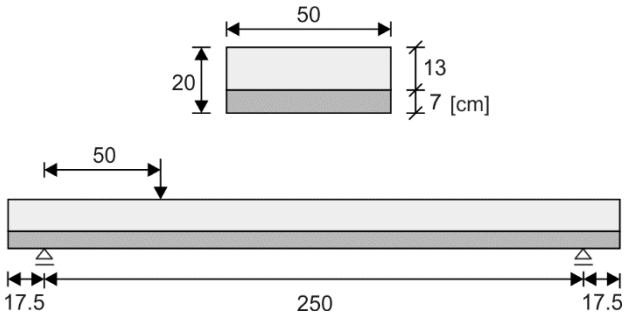

Nr. of tests	8
very smooth	–
smooth(1)	8
rough	–
very rough	–
keyed	–

Interface reinforcement: 3 rows of lattice girders E15 6/6/10

(1): smooth: left as cast

Autor:	GOHNERT, M.	[Goh00]
Title:	Proposed theory to determine the horizontal shear between composite precast and in situ concrete	
Source:	Cement & Concrete Composites, Vol. 22, pp. 469-476, 2000	

Test setup:

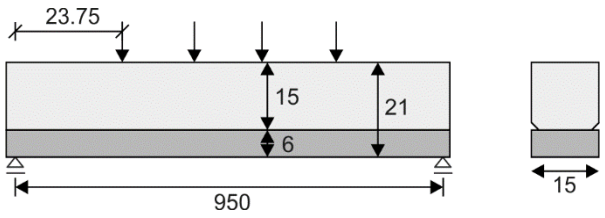

Nr. of tests	6
very smooth	–
smooth	–
rough(1)	6
very rough	–
keyed	–

Interface reinforcement: –-

(1): rough: brushed surface

Autor: Hanson, N.W. [Han60]

Title: Precast-Prestressed Concrete Bridges 2. Horizontal Shear connections

Source: Portland Cement Association, Research and Development Laboratories, Bulletin D35, Vol. 2, No. 2, pp. 38-58, 1960

Test setup:

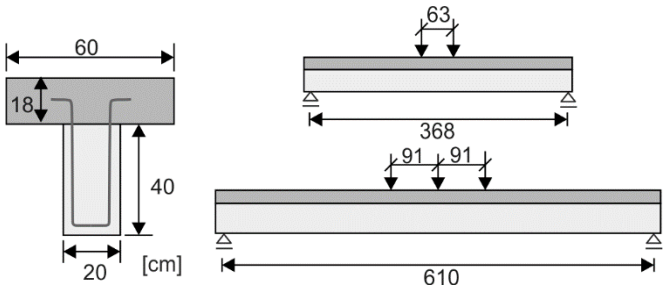

Nr. of tests	7
very smooth(1)	2
smooth(2)	2
rough	–
very rough(3)	3
keyed	–

Interface reinforcement: ρ_{sw} = 0.46% and 0.17% with Ø9.5 mm stirrups

(1): very smooth: smooth with applied bondbreaker; (2): smooth: left as cast, trowelled, (3): very rough: scrapped with a roughness amplitude of at least 6.4 mm

Autor: Hegger, J.; Will, N.; Bülte, S.; Görtz, S.; Schmidt, M. [Heg02]

Title: Vorgespannte Elementdecken aus hochfestem Beton

Source: Research report Nr. 75/2002, Institute of Strucutral Concrete, RWTH Aachen University, 2002

Test setup:

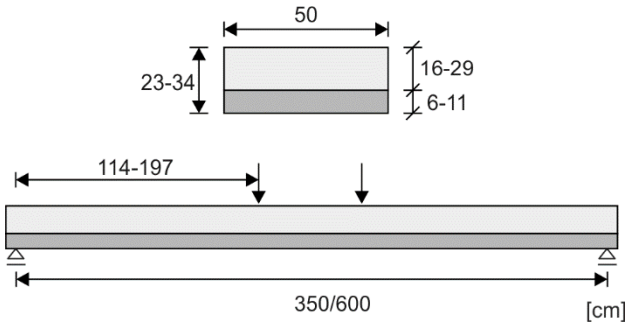

Nr. of tests	12
very smooth	–
smooth(1)	2
rough(2)	10
very rough(3)	–
keyed	–

prestressed

Interface reinforcement: ρ_{sw} = 0% (10 specimens) ρ_{sw} = 0.31% (2 specimens)

(1): smooth: left as cast; (2): rough: raked

Autor: Kahn, L.F.; Slapkus, A. [Kah04]

Title: Interface Shear in High Strength Composite T-Beams

Source: PCI Journal, Vol. 49, Issue 4, pp. 102-110, 2004

Test setup:

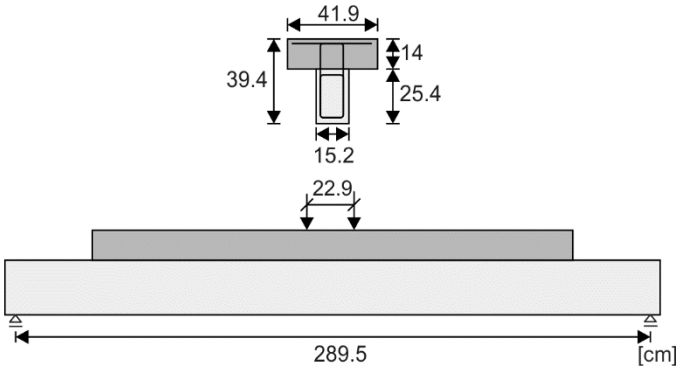

Nr. of tests	6
very smooth	–
smooth	–
rough(1)	6
very rough	–
keyed	–

Interface reinforcement: ρ_{sw} = 0.19, 0.28 and 0.38 % with Ø9.25 mm stirrups

(1): rough: protruded aggregated about 6 mm

Autor: Loov, R.E.; Patnaik, A.K. [Loo94]

Title: Horizontal shear strength of composite concrete beams with a rough interface

Source: PCI Journal, Vol. 39, No. 1, pp. 48-69, January-February, 1994

Test setup:

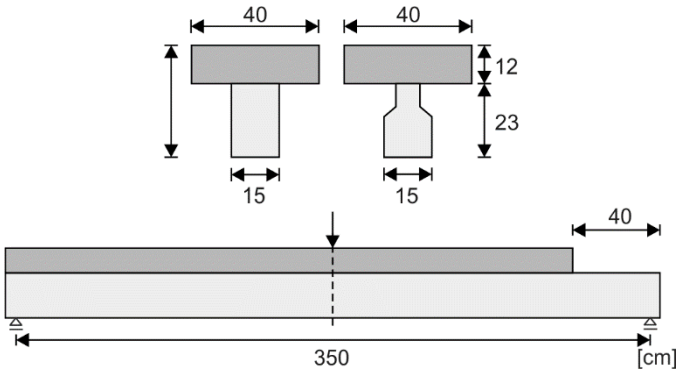

Nr. of tests	16
very smooth	–
smooth	–
rough(1)	16
very rough	–
keyed	–

Interface reinforcement: ρ_{sw} = 0.1 – 1.41 % with Ø9.25 mm stirrups

(1): rough: clean and free of laitance, with coarse aggregate protruding but firmly fixed in the matrix.

Autor:	Menn, C.; Brenni, P.; Keller, T.; Pellegrinelli, L.	[Men92]
Title:	Verbindungen von altem und neuem Beton	
Source:	Research Report, Institute of Structural Engineering, ETH Zürich, 1992	

Test setup:

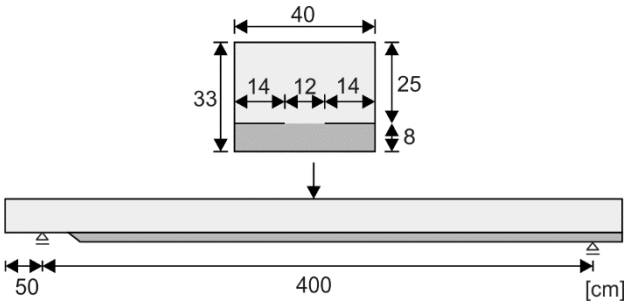

Nr. of tests	10
very smooth	–
smooth(1)	7
rough(2)	3
very rough	–
keyed	–

Interface reinforcement: ρ_{sw} = 0 (4 specimens), ρ_{sw} = 0.1 – 0.4 % with Ø10 mm stirrups (6 specimens)

(1): smooth: slightly roughened to a mean roughness depth of 0.6 – 0.9 mm; (2): rough: roughened to a mean roughness depth of 3 mm

Autor:	Müller, A.	[Mül09]
Title:	Zum Zug- und Schubtragverhalten von Betonfugen	
Source:	PhD Thesis, Chair of Concrete Structures, Technical University of Munich, 2009	

Test setup:

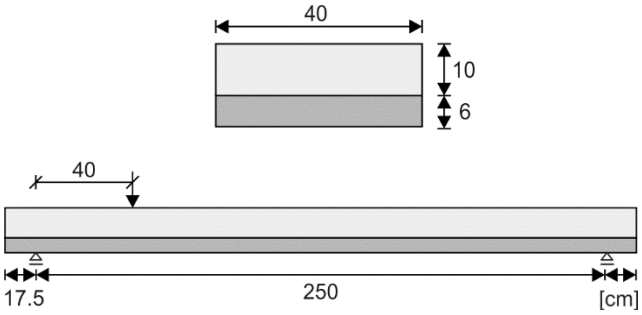

Nr. of tests	4
very smooth	–
smooth(1)	2
rough	–
very rough(2)	2
keyed	–

Interface reinforcement: –

(1): smooth: high pressure water to a mean roughness depth of 0.9 mm; (2): very rough: raked to a mean roughness depth of 3.5 mm

Autor:	Randl, N.; Simon, C.	[Ran14]
Title:	Static and dynamic testing of RC-slabs with high strength concrete overlay	
Source:	Construction Materials and Structures, S.O. Ekoli et al. (Eds), IOS Press, pp. 980-988, 2014	

Test setup:

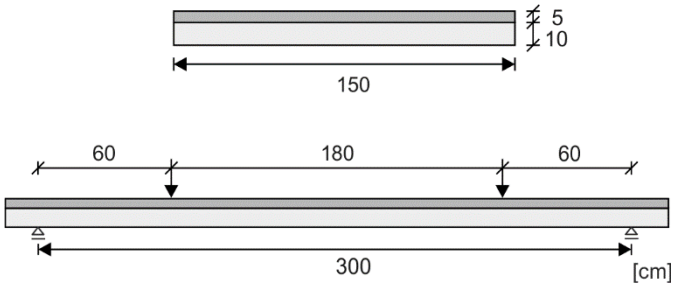

Nr. of tests	11
very smooth	–
smooth(1)	8
rough(2)	3
very rough	–
keyed	–

7 monotonic tests
4 cyclic tests

Interface reinforcement: No interface reinforcement (9 specimens), 72/144 studs (2 specimens)

(1): smooth: sandblasted; (2): rough: high pressure water

Autor:	Rehm, G.; Eligehausen, R.; Paul. F.	[Reh80]
Title:	Verbundbewehrung in Fugen von Platten ohne Schubbewehrung	
Source:	Research Project, University Stuttgart, 1980	

Test setup:

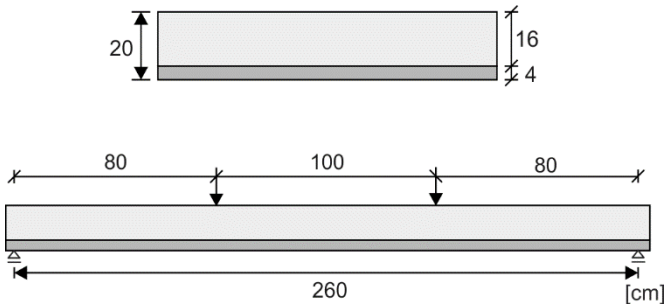

Nr. of tests	8
very smooth(1)	1
smooth(2)	3
rough(3)	4
very rough	–
keyed	–

Interface reinforcement: –

(1): very smooth: left as cast with bondbreaker; (2): smooth: left as cast; (3): rough: raked

Autor: Schäfer, H. G.; Schmidt-Kehle, W. [Sch96d]

Title: Ortbetonergänzte Fertigteilbalken mit profilierter Anschlussfuge unter hoher Querkraftbeanspruchung

Source: Deutscher Ausschuss für Stahlbeton DAfStb, issue 456, Beuth Verlag, Berlin 1996

Test setup:

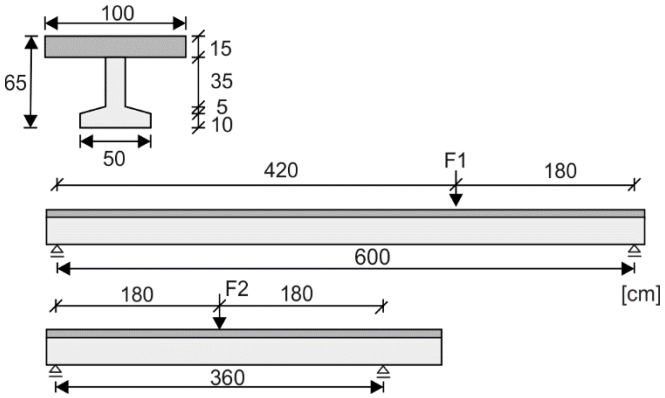

Nr. of tests	6
very smooth	–
smooth	–
rough	–
very rough	–
keyed	6

Interface reinforcement: ρ_{sw} = 0.21 and 0.41 % with Ø12 mm stirrups

Autor: Schäfer, H. G.; Schmidt-Kehle, W. [Sch96a]

Title: Zum Schubtragverhalten von Fertigplatten mit Ortbetonergänzung

Source: Deutscher Ausschuss für Stahlbeton DAfStb, issue 456, Beuth Verlag, Berlin 1996

Test setup:

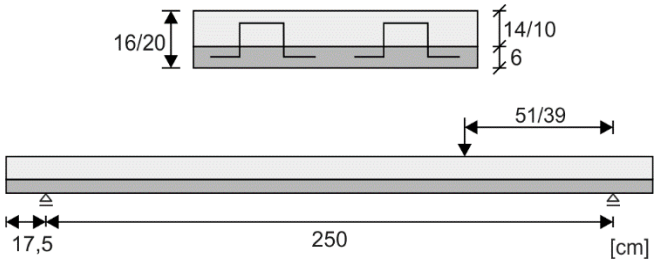

Nr. of tests	12
very smooth	–
smooth[(1)]	12
rough	–
very rough	–
keyed	–

Interface reinforcement: ρ_{sw} = 0.09 – 0.44 % with Ø7, 7.5, 8 and 9 mm stirrups

[(1)]: smooth: left as cast

Autor:	Schäfer, H. G.; Schmidt-Kehle, W. [Sch96c]
Title:	Zur Oberflächenrauheit von Fertigplatten mit Ortbetonergänzung
Source:	Deutscher Ausschuss für Stahlbeton DAfStb, issue 456, Beuth Verlag, Berlin 1996

Test setup:

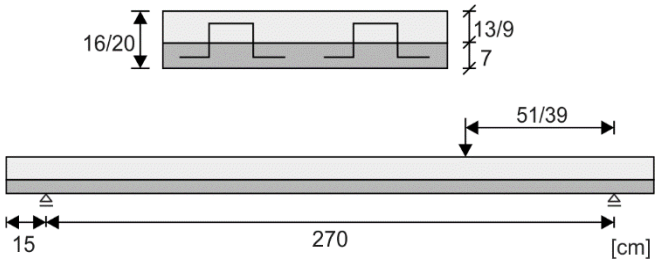

Nr. of tests	8
very smooth	–
smooth	–
rough(1)	4
very rough	–
keyed	4

Interface reinforcement: ρ_{sw} = 0.19 – 0.28 % with Ø7 mm stirrups

(1): rough: left as cast but with a roughness of > 1.5 mm

Autor:	Schießl, P.; Schwarzkopf, M. [Sch81], [Sch82], [Sch83]
Title:	Montaquick Fertigteildecken mit statischer Ortbetonschicht bei dynamischer Beanspruchung
Source:	Research report - test series 1 – 3, Institut für Betonstahl und Stahlbeton e.V., Munich, 1981, 1982, 1983.

Test setup:

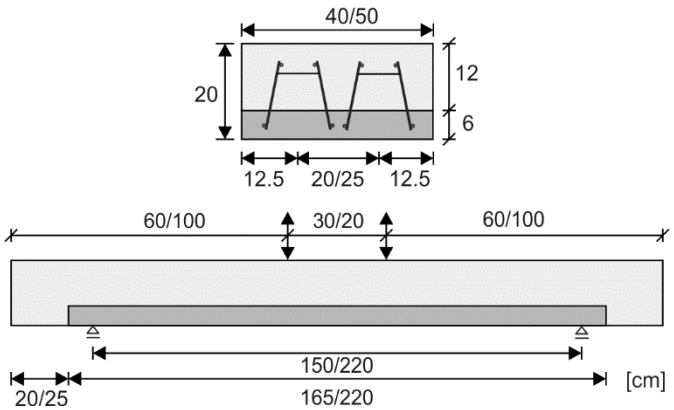

Nr. of tests	14
very smooth(1)	4
smooth(2)	7
rough(3)	3
very rough	–
keyed	–

14 cyclic tests

Interface reinforcement: 2 rows of lattice girders M-KT 116 8-6-6, 3 specimens with extra Ø8 mm stirrups with ρ_{sw} = 0.21 %

(1): very smooth: left as cast with bondbreaker; (2): smooth: left as cast; (3): rough: raked

Autor: Schießl, P.; Schwarzkopf, M. [Sch85]

Title: Kaiser Omnia-Träger KTS für Fertigplatten mit statisch mitwirkender Ortbetonschickt bei dynamischer Beanspruchung

Source: Research report, Institit für Betonstahl und Stahlbetonbau e.V., Munich, 1985

Test setup:

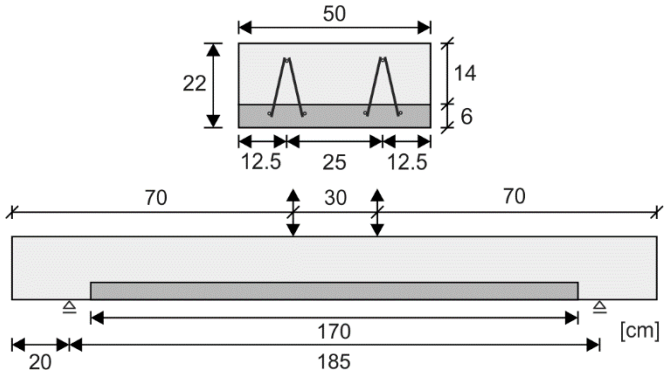

Nr. of tests	10
very smooth(1)	4
smooth(2)	4
rough(3)	2
very rough	–
keyed	–

10 cyclic tests

Interface reinforcement: 2 rows of lattice girders KTS 16 7-5-5

(1): very smooth: left as cast with bondbreaker; (2): smooth: left as cast; (3): rough: raked

Autor: SAEMANN, J.C.; WASHA, G.W. [Sae64]

Title: Horizontal shear connections between precast beams and cast-in-place slabs

Source: Journal of the American Concrete Institute, Vol. 61, No. 11, pp. 1383-1409, November, 1964

Test setup:

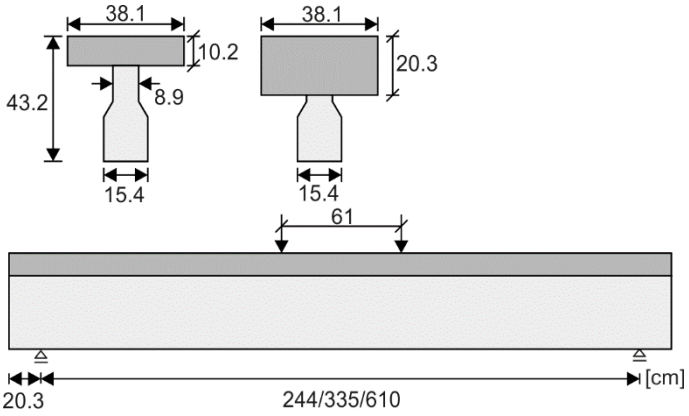

Nr. of tests	42
very smooth	–
smooth(1)	12
rough(2)	23
very rough(3)	4
keyed	3

Interface reinforcement: ρ_{sw} = 0 (2 specimens), ρ_{sw} = 0.06 – 1.12 % with Ø9.25 and 12.7 mm stirrups (40 specimens)

(1): smooth: screeding; (2): rough: brushed; (3): very rough: nail-raked

Autor:	Weber, J.W.; Schmidt, R.	[Web89]
Title:	Zulassungsversuche für den Filigran EQ-Träger unter dynamischer Beanspruchung	
Source:	Test report, Institute of Building Materials Science, RWTH Aachen University, 1989	

Test setup:

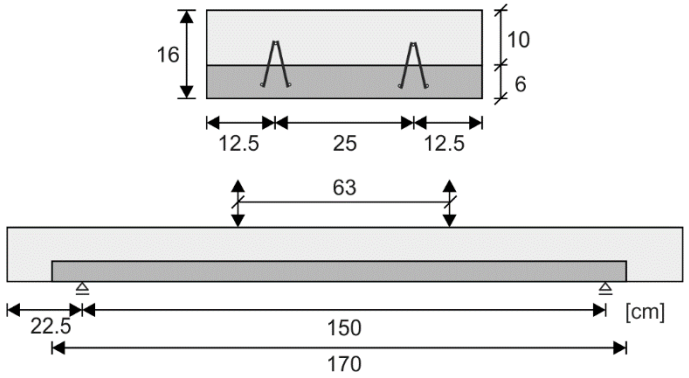

Nr. of tests	2
very smooth(1)	1
smooth(2)	1
rough	–
very rough	–
keyed	–

2 cyclic tests

Interface reinforcement: 2 rows of lattice girders EQ 10 7-5-5

(1): very smooth: left as cast with bondbreaker; (2): smooth: left as cast;

Autor:	Weber, J.W.; Leißner, J.; Weyert, R.	[Web95]
Title:	Zulassungsversuche für die Kaiser-Omnia-Plattenwand mit Gitterträgern KTW 100 oder KTW 30 bei dynamischer Belastung	
Source:	Research report; Institute of Building Materials Science, RWTH Aachen University, 1995	

Test setup:

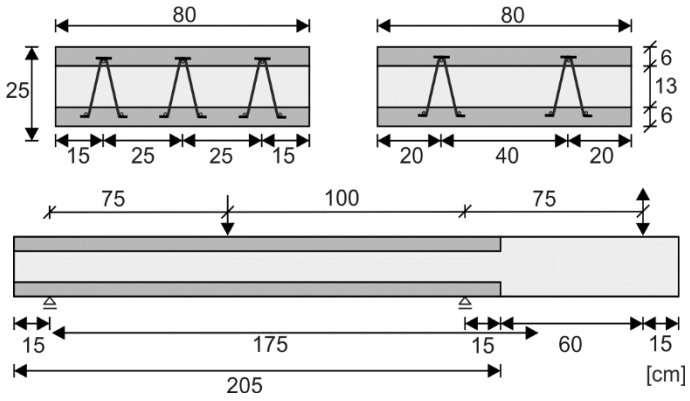

Nr. of tests	3
very smooth	–
smooth(1)	3
rough	–
very rough	–
keyed	–

3 cyclic tests

Interface reinforcement: 2 rows of lattice girders KTW 200 7-8-7

(1): smooth: left as cast

Autor: Wieneke K; Claßen, M.; Hegger, J. [Wie17a]

Title: Elementdecken mit Gitterträgern unter zyklischer Belastung

Source: Beton- und Stahlbetonbau 112, Issue 9, pp. 579-588, 2017

Test setup:

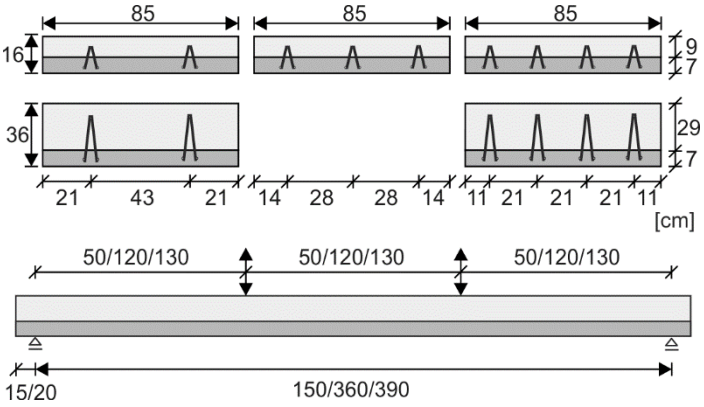

Nr. of tests	28
very smooth(1)	2
smooth(2)	24
rough(3)	2
very rough	–
keyed	–

28 cyclic tests

Interface reinforcement: 2, 3 and 4 rows of lattice girders EQ 30 7-5-5 and KTS 100 7-5-5

(1): very smooth: left as cast with bondbreaker; (2): smooth: left as cast; (3): rough: left as cast and slightly roughened

Autor: ZILCH, K.; LENZ, P.; MÜLLER, A. [Zil08]

Title: Zum Einfluss einer zum Auflager hin fallender Verbundbewehrung auf die Schubkraftübertragung in Fugen

Source: Chair of concrete structures, Technical University of Munich, 2008

Test setup:

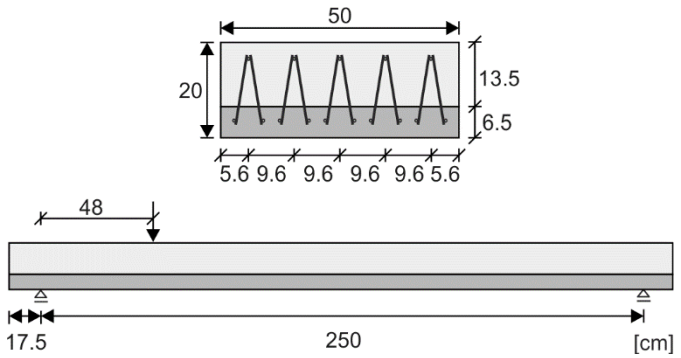

Nr. of tests	6
very smooth	–
smooth(1)	3
rough(2)	3
very rough	–
keyed	–

Interface reinforcement: 5 rows of lattice girders E 15 6-7-12

(1): smooth: left as cast; (2): rough: raked with steel-rake

Table B-21: Overview of research reports with corresponding allocation of tests with beam and slab specimens before filter

Complete database before filter																	
Nr.	Source	Nr. of tests	Database						Interface					Specimen Type			
			E	F	F-LG	G	H	H-LG	vs	s	r	vr	k	T-beam	beam	slab	prestressed
1	[Abe72]	10	10	-	-	-	-	-	-	-	6	4	-	-	10	-	10
2	[Alb14]	3	3	-	-	-	-	-	-	3	-	-	-	-	-	3	-
3	[Bar65]	29	1	4	-	1	23	-	-	2	10	17	-	29	-	-	-
4	[Chu76]	18	1	3	-	4	10	-	-	-	18	-	-	18	-	-	-
5	[Das86a]	20	11	9	-	-	-	-	-	8	7	5	-	20	-	-	18
6	[Das86b]	1	-	-	-	-	1	-	-	-	1	-	-	1	-	-	-
7	[Fur11]	8	2	-	6	-	-	-	-	8	-	-	-	-	-	8	-
8	[Goh00]	6	6	-	-	-	-	-	-	-	6	-	-	-	6	-	6
9	[Han06]	7	1	6	-	-	-	-	2	2	-	3	-	7	-	-	-
10	[Heg02]	12	10	2	-	-	-	-	-	2	10	-	-	-	-	12	12
11	[Kah04]	6	-	6	-	-	-	-	-	-	6	-	-	6	-	-	-
12	[Loo94]	16	-	16	-	-	-	-	-	-	16	-	-	16	-	-	-
13	[Men92]	10	4	6	-	-	-	-	-	7	3	-	-	-	10	-	-
14	[Mül09]	4	4	-	-	-	-	-	-	2	-	2	-	-	4	-	-
15	[Ran14]	11	5	2	-	4	-	-	-	8	3	-	-	-	-	11	-
16	[Reh80]	8	-	8	-	-	-	-	1	3	4	-	-	-	-	8	-
17	[Sch96d]	6	-	3	-	-	3	-	-	-	-	-	6	6	-	-	-
18	[Sch96a]	12	-	-	-	2	10	-	-	12	-	-	-	-	-	12	-
19	[Sch96c]	8	-	4	-	-	4	-	-	-	4	-	4	-	-	8	-
20	[Sch81]	5	-	-	-	-	-	5	-	5	-	-	-	-	-	5	-
21	[Sch82]	7	-	-	-	-	-	7	2	2	3	-	-	-	-	7	-
22	[Sch83]	2	-	-	-	-	-	2	2	-	-	-	-	-	-	2	-
23	[Sch85]	10	-	-	-	-	-	10	4	4	2	-	-	-	-	10	-
24	[Sae64]	42	2	40	-	-	-	-	-	12	23	4	3	42	-	-	-
25	[Web89]	2	-	-	-	-	-	2	1	1	-	-	-	-	-	2	-
26	[Web95]	3	-	-	-	-	-	3	-	3	-	-	-	-	-	3	-
27	[Wie17a]	28	-	-	-	-	-	28	2	24	2	-	-	-	-	28	-
28	[Zil08]	6	-	-	6	-	-	-	-	3	3	-	-	-	-	6	-

Table B-22: Overview of research reports with corresponding allocation of tests with beam and slab specimens after filter

Complete database before filter																	
Nr.	Source	Nr. of tests	Database						Interface					Specimen Type			
			E	F	F-LG	G	H	H-LG	vs	s	r	vr	k	T-beam	beam	slab	prestressed
1	[Abe72]	10	10	-	-	-	-	-	-	-	6	4	-	-	10	-	10
2	[Alb14]	3	3	-	-	-	-	-	-	3	-	-	-	-	-	3	-
3	[Bar65]	29	1	4	-	1	23	-	-	2	10	17	-	29	-	-	-
4	[Chu76]	18	1	3	-	4	10	-	-	-	18	-	-	18	-	-	-
5	[Das86a]	20	11	9	-	-	-	-	-	8	7	5	-	20	-	-	18
6	[Das86b]	1	-	-	-	-	1	-	-	-	1	-	-	1	-	-	-
7	[Fur11]	8	2	-	6	-	-	-	-	8	-	-	-	-	-	8	-
8	[Goh00]	6	6	-	-	-	-	-	-	-	6	-	-	-	6	-	6
9	[Han06]	7	1	6	-	-	-	-	2	2	-	3	-	7	-	-	-
10	[Heg02]	12	10	2	-	-	-	-	-	2	10	-	-	-	-	12	12
11	[Kah04]	6	-	6	-	-	-	-	-	-	6	-	-	6	-	-	-
12	[Loo94]	16	-	16	-	-	-	-	-	-	16	-	-	16	-	-	-
13	[Men92]	10	4	6	-	-	-	-	-	7	3	-	-	-	10	-	-
14	[Mül09]	4	4	-	-	-	-	-	-	2	-	2	-	-	4	-	-
15	[Ran14]	11	5	2	-	4	-	-	-	8	3	-	-	-	-	11	-
16	[Reh80]	8	8	-	-	-	-	-	1	3	4	-	-	-	-	8	-
17	[Sch96d]	6	-	3	-	-	3	-	-	-	-	-	6	6	-	-	-
18	[Sch96a]	12	-	-	-	2	10	-	-	12	-	-	-	-	-	12	-
19	[Sch96c]	8	-	4	-	-	4	-	-	-	4	-	4	-	-	8	-
20	[Sch81]	5	-	-	-	-	-	5	-	5	-	-	-	-	-	5	-
21	[Sch82]	7	-	-	-	-	-	7	2	2	3	-	-	-	-	7	-
22	[Sch83]	2	-	-	-	-	-	2	2	-	-	-	-	-	-	2	-
23	[Sch85]	10	-	-	-	-	-	10	4	4	2	-	-	-	-	10	-
24	[Sae64]	42	2	40	-	-	-	-	-	12	23	4	3	42	-	-	-
25	[Web89]	2	-	-	-	-	-	2	1	1	-	-	-	-	-	2	-
26	[Web95]	3	-	-	-	-	-	3	-	3	-	-	-	-	-	3	-
27	[Wie17a]	28	-	-	-	-	-	28	2	24	2	-	-	-	-	28	-
28	[Zil08]	6	-	-	6	-	-	-	-	3	3	-	-	-	-	6	-

B.2.2 Database E: Adhesion

Table B-23: Database E – Specimens Nr. 1 – 30

Nr. [-]	Source [-]	Test ID [-]	Interface [-]	Section [-]	b_{int} [mm]	a_{int} [mm]	d [mm]	h_{pre} [mm]	h_{ins} [mm]	ρ_l [%]	$f_{ym,l}$ [N/mm²]	$f_{cm,cyl,1}$ [N/mm²]	$f_{ctm,1}$ [N/mm²]	$f_{cm,cyl,2}$ [N/mm²]	$f_{ctm,2}$ [N/mm²]	τ_{test} [N/mm²]
1	[Abe72]	1(C1)	rough	beam	89	1524	229	51	203	0.006	1813	44.80	3.56	42.60	3.43	4.85
2	[Abe72]	2(C2)	rough	beam	89	1524	229	51	203	0.006	1813	44.80	3.56	41.40	3.36	4.85
3	[Abe72]	3(C3)	rough	beam	89	1524	229	51	203	0.006	1813	44.80	3.56	42.10	3.40	4.85
4	[Abe72]	4(S1)	rough	beam	89	1524	229	51	203	0.006	1813	44.80	3.56	44.10	3.51	4.85
5	[Abe72]	6(S3)	rough	beam	89	1524	229	51	203	0.006	1813	44.80	3.56	41.40	3.36	4.85
6	[Alb14]	V-O-OH-1	smooth	slab	700	650	170	90	110	0.026	1829	17.52	1.84	16.86	1.71	1.46
7	[Alb14]	V-O-OH-2	smooth	slab	700	1000	170	90	110	0.026	550	17.52	1.84	16.86	1.71	1.29
8	[Alb14]	V-O-OH-3	smooth	slab	700	1000	170	90	110	0.026	550	17.52	1.84	16.86	1.62	1.25
9	[Bar65]	0.4	smooth	t-beam	89	914	254	330	102	0.013	343	29.26	3.05	26.27	2.37	2.70
10	[Chu76]	A1	rough	t-beam	62	850	235	250	50	0.005	550	42.00	3.39	30.00	2.63	4.96
11	[Das86]	B 6_1	very rough	t-beam	150	700	323	153	200	0.029	485	26.61	2.40	16.63	1.63	1.93
12	[Das86]	B 6_2	very rough	t-beam	150	1250	323	153	200	0.029	485	27.44	2.46	16.88	1.65	4.40
13	[Das86]	B 7	very rough	t-beam	150	975	323	153	200	0.029	485	25.61	2.33	16.13	1.58	2.18
14	[Das86]	B 9	very rough	t-beam	150	695	323	153	200	0.029	485	24.53	2.25	17.13	1.67	3.30
15	[Das86]	B 4	smooth	t-beam	150	700	250	150	125	0.010	420	25.61	2.33	16.13	1.58	1.63
16	[Das86]	B 5	smooth	t-beam	150	700	295	180	145	0.014	420	26.61	2.40	16.63	1.63	2.13
17	[Heg02]	EQ09	smooth	slab	500	1160	300	80	260	0.000	1829	88.00	4.84	37.30	3.11	1.70
18	[Heg02]	EQ01	rough	slab	500	1140	240	80	200	0.623	1829	82.26	4.71	22.00	2.06	1.81
19	[Heg02]	EQ03	rough	slab	500	1420	200	80	160	0.655	1829	71.89	4.46	31.70	2.75	1.56
20	[Heg02]	EQ06	rough	slab	500	1140	280	110	200	0.468	1829	88.00	4.84	23.80	2.20	1.88
21	[Men92]	B2	rough	beam	120	2000	290	250	80	0.008	500	35.00	2.96	27.50	2.46	1.72
22	[Reh80]	2	smooth	slab	1000	800	175	40	160	0.011	650	35.43	2.99	58.21	4.07	1.45
23	[Reh80]	4	smooth	slab	1000	800	175	40	160	0.011	650	39.75	3.26	66.53	4.31	1.54
24	[Reh80]	6	smooth	slab	1000	800	175	40	160	0.011	650	61.62	4.17	54.39	3.95	1.86
25	[Reh80]	1	rough	slab	1000	800	175	40	160	0.011	650	36.59	3.06	56.80	4.03	1.52
26	[Reh80]	3	rough	slab	1000	800	175	40	160	0.011	650	45.15	3.58	50.14	3.86	1.88
27	[Reh80]	5	rough	slab	1000	800	175	40	160	0.011	650	63.37	4.22	59.37	4.11	1.88
28	[Reh80]	7	rough	slab	1000	800	175	40	160	0.011	650	38.17	3.16	59.62	4.11	1.25
29	[Sae64]	15C	rough	t-beam	88.9	1219	356	330	102	0.036	252	20.90	1.98	22.20	2.08	2.90
30	[Sae64]	16C	rough	t-beam	88.9	762	356	330	102	0.036	252	20.90	1.98	21.10	1.99	4.18

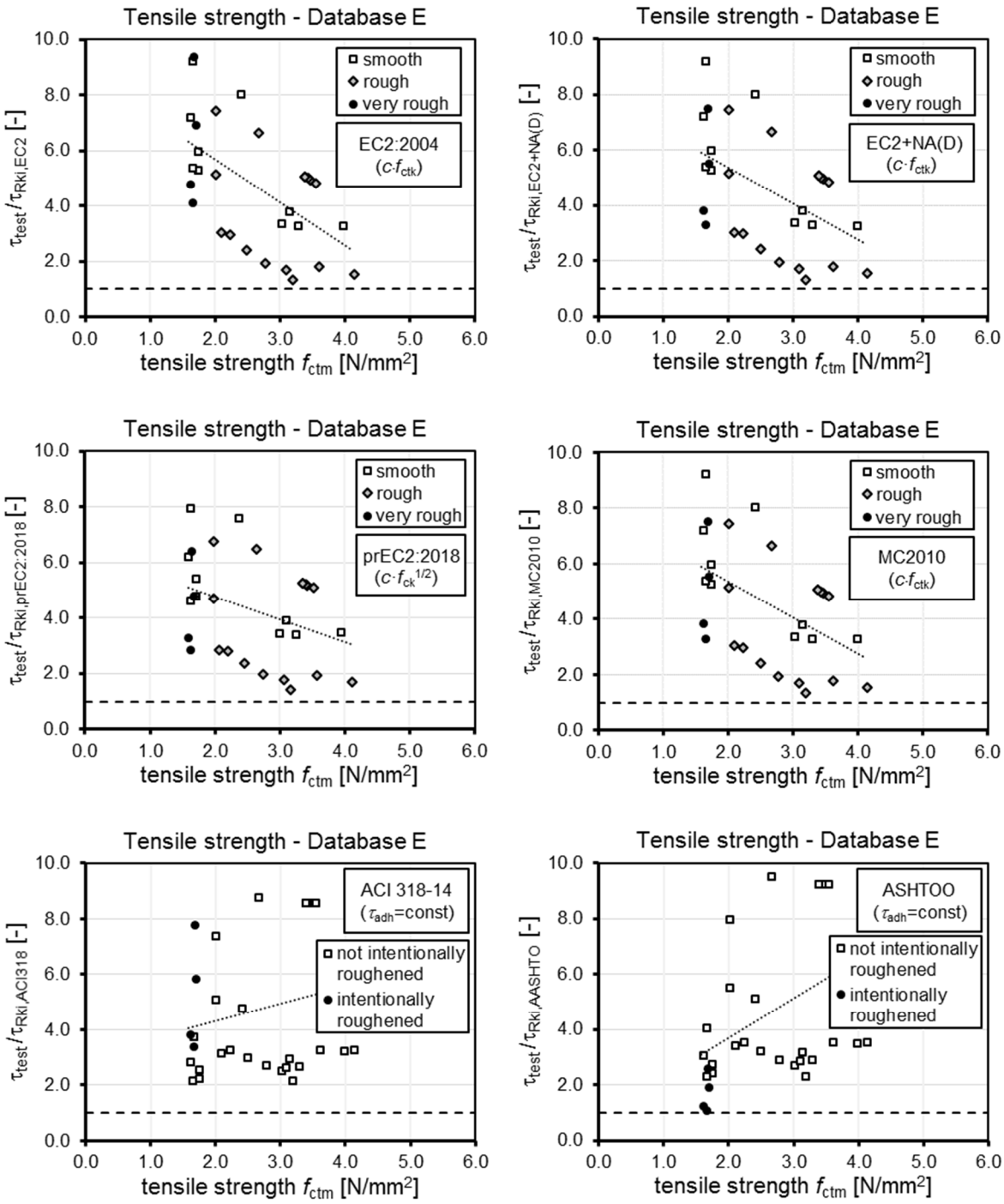

Figure B-11: Evaluation of tensile strength of database E according to the evaluated codes

B.2.3 Database F-1: Reinforcement (stirrups)

Table B-24: Database F-1 – Specimens Nr. 1 – 37 (a)

Nr. [-]	Source [-]	Test ID [-]	Interface [-]	Section [-]	b_{int} [mm]	a_{int} [mm]	h_{pre} [mm]	h_{ins} [mm]	$f_{cm,cyl,1}$ [N/mm²]	$f_{ctm,1}$ [N/mm²]	$f_{cm,cyl,2}$ [N/mm²]	$f_{ctm,2}$ [N/mm²]
1	[Bar65]	2.0	very rough	t-beam	89	914	330	102	19.88	2.31	23.79	2.64
2	[Bar65]	0.2	very rough	t-beam	89	914	330	102	22.94	2.39	25.11	2.74
3	[Bar65]	5.0	very rough	t-beam	89	1118	330	102	27.86	2.49	26.07	2.36
4	[Bar65]	1.0	rough	t-beam	89	914	330	102	18.70	2.27	18.72	2.40
5	[Chu76]	B1	rough	t-beam	62	850	250	50	42.00	3.39	30.00	2.63
6	[Chu76]	C1	rough	t-beam	62	850	250	50	42.00	3.39	30.00	2.63
7	[Chu76]	D1	rough	t-beam	62	850	250	50	42.00	3.39	30.00	2.63
8	[Das86a]	B 12_1	smooth	t-beam	150	930	155	230	24.12	2.22	16.63	1.63
9	[Das86a]	B 12_2	smooth	t-beam	150	930	155	230	24.12	2.22	16.63	1.63
10	[Das86a]	B 13_1	rough	t-beam	150	930	155	230	24.12	2.22	16.63	1.63
11	[Das86a]	B 13_2	rough	t-beam	150	930	155	230	24.12	2.22	16.63	1.63
12	[Das86a]	B 14	rough	t-beam	150	930	155	230	24.12	2.22	23.78	2.19
13	[Kah04]	7-5	rough	t-beam	154	1334	254	140	66.20	4.31	50.21	3.86
14	[Kah04]	7-7	rough	t-beam	154	1334	254	140	66.20	4.31	50.21	3.86
15	[Kah04]	7-9	rough	t-beam	154	1334	254	140	66.20	4.31	50.21	3.86
16	[Kah04]	11-5	rough	t-beam	154	1334	254	140	66.20	4.31	77.86	4.61
17	[Kah04]	11-7	rough	t-beam	154	1334	254	140	66.20	4.31	77.86	4.61
18	[Kah04]	11-9	rough	t-beam	154	1334	254	140	66.20	4.31	77.86	4.61
19	[Loo94]	1	rough	t-beam	75	1525	230	120	37.40	3.11	42.70	3.43
20	[Loo94]	2	rough	t-beam	75	1525	230	120	34.90	2.95	39.20	3.22
21	[Loo94]	3	rough	t-beam	75	1525	230	120	30.50	2.67	40.20	3.28
22	[Loo94]	4	rough	t-beam	75	1525	230	120	34.70	2.94	39.60	3.25
23	[Loo94]	5	rough	t-beam	75	1525	230	120	34.80	2.95	42.60	3.43
24	[Loo94]	6	rough	t-beam	75	1525	230	120	37.10	3.09	40.40	3.30
25	[Loo94]	7	rough	t-beam	75	1525	230	120	35.80	3.01	38.00	3.15
26	[Loo94]	8	rough	t-beam	150	1525	230	120	35.60	3.00	38.00	3.15
27	[Loo94]	9	rough	t-beam	75	1525	230	120	37.10	3.09	37.60	3.12
28	[Loo94]	10	rough	t-beam	150	1525	230	120	37.60	3.12	37.60	3.12
29	[Loo94]	11	rough	t-beam	300	1525	230	120	32.70	2.81	34.00	2.90
30	[Loo94]	12	rough	t-beam	75	1525	230	120	34.60	2.93	36.20	3.04
31	[Loo94]	13	rough	t-beam	150	1525	230	120	19.20	1.84	23.70	2.19
32	[Loo94]	14	rough	t-beam	150	1525	230	120	19.60	1.87	20.20	1.92
33	[Loo94]	15	rough	t-beam	150	1525	230	120	44.00	3.51	51.50	3.93
34	[Loo94]	16	rough	t-beam	150	1525	230	120	48.30	3.76	50.70	3.89
35	[Men92]	C1	smooth	beam	120	2000	250	80	35.00	2.96	27.50	2.46
36	[Men92]	C2	smooth	beam	120	2000	250	80	35.00	2.96	27.50	2.46
37	[Men92]	C3	smooth	beam	120	2000	250	80	35.00	2.96	27.50	2.46

Table B-25: Database F-1 – Specimens Nr. 1 – 37 (b)

Nr. [-]	Source [-]	Test ID [-]	Interface [-]	Section [-]	d [mm]	ρ_l [%]	$f_{ym,l}$ [N/mm²]	ρ_{int} [%]	α [-]	$f_{ym,int}$ [N/mm²]	τ_{test} [N/mm²]
1	[Bar65]	2.0	very rough	t-beam	356	0.029	345	0.18	90	366	4.93
2	[Bar65]	0.2	very rough	t-beam	356	0.029	345	0.18	90	366	4.60
3	[Bar65]	5.0	very rough	t-beam	355	0.008	343	0.15	90	366	4.61
4	[Bar65]	1.0	rough	t-beam	356	0.029	345	0.18	90	366	3.96
5	[Chu76]	B1	rough	t-beam	235	0.005	*	0.15	90	550	4.70
6	[Chu76]	C1	rough	t-beam	235	0.005	*	0.20	90	550	4.54
7	[Chu76]	D1	rough	t-beam	235	0.005	*	0.30	90	550	5.02
8	[Das86a]	B 12_1	smooth	t-beam	360	0.015	590	1.34	90	396	5.45
9	[Das86a]	B 12_2	smooth	t-beam	360	0.015	590	0.82	90	396	5.37
10	[Das86a]	B 13_1	rough	t-beam	360	0.015	590	0.75	90	458	5.38
11	[Das86a]	B 13_2	rough	t-beam	360	0.015	590	0.30	90	458	3.67
12	[Das86a]	B 14	rough	t-beam	360	0.015	590	0.12	90	478	2.16
13	[Kah04]	7-5	rough	t-beam	394	0.021	520	0.19	0	556	2.96
14	[Kah04]	7-7	rough	t-beam	394	0.021	520	0.28	0	556	3.64
15	[Kah04]	7-9	rough	t-beam	394	0.021	520	0.37	0	556	3.87
16	[Kah04]	11-5	rough	t-beam	394	0.021	520	0.19	0	556	4.23
17	[Kah04]	11-7	rough	t-beam	394	0.021	520	0.28	0	556	4.28
18	[Kah04]	11-9	rough	t-beam	394	0.021	520	0.37	0	556	4.36
19	[Loo94]	1	rough	t-beam	292	0.029	497	1.00	90	438	7.41
20	[Loo94]	2	rough	t-beam	295	0.029	454	0.38	90	438	4.07
21	[Loo94]	3	rough	t-beam	288	0.029	454	0.63	90	432	6.46
22	[Loo94]	4	rough	t-beam	282	0.030	334	1.41	90	430	7.59
23	[Loo94]	5	rough	t-beam	295	0.029	454	0.38	90	430	5.30
24	[Loo94]	6	rough	t-beam	281	0.030	454	0.38	90	428	5.30
25	[Loo94]	7	rough	t-beam	295	0.029	497	1.41	90	432	8.31
26	[Loo94]	8	rough	t-beam	295	0.026	454	0.19	90	407	2.99
27	[Loo94]	9	rough	t-beam	288	0.029	431	0.38	90	428	4.40
28	[Loo94]	10	rough	t-beam	288	0.027	431	0.19	90	409	3.29
29	[Loo94]	11	rough	t-beam	297	0.022	497	0.10	90	420	2.41
30	[Loo94]	12	rough	t-beam	280	0.030	455	1.90	90	408	8.62
31	[Loo94]	13	rough	t-beam	288	0.027	431	0.19	90	431	2.71
32	[Loo94]	14	rough	t-beam	288	0.027	431	0.19	90	431	1.76
33	[Loo94]	15	rough	t-beam	288	0.027	431	0.19	90	420	3.78
34	[Loo94]	16	rough	t-beam	288	0.027	431	0.19	90	420	3.86
35	[Men92]	C1	smooth	beam	290	0.008	500	0.20	90	500	1.56
36	[Men92]	C2	smooth	beam	290	0.008	500	0.27	90	500	1.80
37	[Men92]	C3	smooth	beam	290	0.008	500	0.40	90	500	1.76

Table B-26: Database F-1 – Specimens Nr. 38 – 66 (a)

Nr. [-]	Source [-]	Test ID [-]	Interface [-]	Section [-]	b_{int} [mm]	a_{int} [mm]	h_{pre} [mm]	h_{ins} [mm]	$f_{cm,cyl,1}$ [N/mm²]	$f_{ctm,1}$ [N/mm²]	$f_{cm,cyl,2}$ [N/mm²]	$f_{ctm,2}$ [N/mm²]
38	[Men92]	C4	smooth	beam	120	2000	250	80	35.00	2.96	27.50	2.46
39	[Men92]	C5	rough	beam	120	2000	250	80	35.00	2.96	27.50	2.46
40	[Men92]	C6	rough	beam	120	2000	250	80	35.00	2.96	27.50	2.46
41	[Sch96d]	16-2	rough	slab	800	360	70	90	44.05	3.51	22.34	2.09
42	[Sch96d]	18-1	rough	slab	800	480	70	130	50.92	3.90	28.34	2.52
43	[Sae64]	6A	very rough	t-beam	89	762	330	102	19.99	1.90	24.89	2.28
44	[Sae64]	8A	very rough	t-beam	89	1219	330	102	20.13	1.92	20.34	1.93
45	[Sae64]	1A	smooth	t-beam	89	762	330	102	19.72	1.88	18.68	1.80
46	[Sae64]	4A	smooth	t-beam	89	1219	330	102	19.37	1.85	18.75	1.80
47	[Sae64]	12A	smooth	t-beam	89	1219	330	102	21.17	2.00	19.24	1.84
48	[Sae64]	1C	smooth	t-beam	89	2591	330	102	21.79	2.04	20.34	1.93
49	[Sae64]	2C	smooth	t-beam	89	1219	330	102	20.48	1.94	22.75	2.12
50	[Sae64]	4C	smooth	t-beam	89	762	330	102	21.86	2.05	22.89	2.13
51	[Sae64]	6C	smooth	t-beam	89	2591	330	102	19.79	1.89	20.96	1.98
52	[Sae64]	7C	smooth	t-beam	89	1219	330	102	23.03	2.14	19.37	1.85
53	[Sae64]	3D	smooth	t-beam	89	1219	330	102	25.65	2.33	24.75	2.27
54	[Sae64]	2A	rough	t-beam	89	1219	330	102	17.44	1.70	18.48	1.78
55	[Sae64]	7A	rough	t-beam	89	762	330	102	19.93	1.90	21.03	1.99
56	[Sae64]	10A	rough	t-beam	89	762	330	102	21.10	1.99	19.79	1.89
57	[Sae64]	14B	rough	t-beam	89	1219	229	203	21.10	1.99	21.03	1.99
58	[Sae64]	15B	rough	t-beam	89	762	229	203	22.61	2.11	22.27	2.08
59	[Sae64]	3C	rough	t-beam	89	1219	330	102	21.24	2.00	21.17	2.00
60	[Sae64]	5C	rough	t-beam	89	762	330	102	20.82	1.97	22.48	2.10
61	[Sae64]	8C	rough	t-beam	89	1219	330	102	19.24	1.84	20.55	1.95
62	[Sae64]	10C	rough	t-beam	89	762	330	102	24.06	2.22	21.51	2.02
63	[Sae64]	11C	rough	t-beam	89	1219	330	102	20.34	1.93	19.79	1.89
64	[Sae64]	13C	rough	t-beam	89	1219	330	102	25.72	2.34	23.58	2.18
65	[Sae64]	1D	rough	t-beam	89	2591	330	102	24.27	2.23	23.30	2.16
66	[Sae64]	2D	rough	t-beam	89	1219	330	102	25.79	2.34	24.48	2.25

Table B-27: Database F-1 – Specimens Nr. 38 – 66 (b)

Nr. [-]	Source [-]	Test ID [-]	Interface [-]	Section [-]	d [mm]	ρ_l [%]	$f_{ym,l}$ [N/mm²]	ρ_{int} [%]	α [-]	$f_{ym,int}$ [N/mm²]	τ_{test} [N/mm²]
38	[Men92]	C4	smooth	beam	290	0.008	500	0.27	90	500	1.36
39	[Men92]	C5	rough	beam	290	0.008	500	0.10	90	500	2.23
40	[Men92]	C6	rough	beam	290	0.008	500	0.20	90	500	2.31
41	[Sch96d]	16-2	rough	slab	120	0.026	531	0.38	90	645	2.99
42	[Sch96d]	18-1	rough	slab	160	0.020	531	0.19	90	645	2.64
43	[Sae64]	6A	very rough	t-beam	356	0.036	252	1.02	90	294	6.57
44	[Sae64]	8A	very rough	t-beam	356	0.036	252	1.08	90	294	4.26
45	[Sae64]	1A	smooth	t-beam	356	0.036	252	1.02	90	294	6.14
46	[Sae64]	4A	smooth	t-beam	356	0.036	252	1.08	90	294	4.26
47	[Sae64]	12A	smooth	t-beam	356	0.036	252	1.08	90	294	4.10
48	[Sae64]	1C	smooth	t-beam	356	0.036	252	0.58	90	294	2.06
49	[Sae64]	2C	smooth	t-beam	356	0.036	252	0.54	90	294	3.30
50	[Sae64]	4C	smooth	t-beam	356	0.036	252	0.51	90	294	4.82
51	[Sae64]	6C	smooth	t-beam	356	0.036	252	0.27	90	294	1.85
52	[Sae64]	7C	smooth	t-beam	356	0.036	252	0.23	90	294	3.06
53	[Sae64]	3D	smooth	t-beam	356	0.036	252	0.13	90	370	2.84
54	[Sae64]	2A	rough	t-beam	356	0.036	252	1.08	90	294	4.26
55	[Sae64]	7A	rough	t-beam	356	0.036	252	1.02	90	294	6.04
56	[Sae64]	10A	rough	t-beam	356	0.036	252	1.02	90	294	6.44
57	[Sae64]	14B	rough	t-beam	356	0.027	252	1.08	90	294	5.14
58	[Sae64]	15B	rough	t-beam	356	0.027	252	1.02	90	294	7.78
59	[Sae64]	3C	rough	t-beam	356	0.036	252	0.23	90	294	4.10
60	[Sae64]	5C	rough	t-beam	356	0.036	252	0.51	90	294	6.44
61	[Sae64]	8C	rough	t-beam	356	0.036	252	0.23	90	294	3.78
62	[Sae64]	10C	rough	t-beam	356	0.036	252	0.20	90	294	4.65
63	[Sae64]	11C	rough	t-beam	356	0.036	252	0.13	90	370	2.73
64	[Sae64]	13C	rough	t-beam	356	0.036	252	0.80	90	370	2.90
65	[Sae64]	1D	rough	t-beam	356	0.036	252	0.15	90	370	2.17
66	[Sae64]	2D	rough	t-beam	356	0.036	252	0.13	90	370	3.78

* no information about yield strength in test report

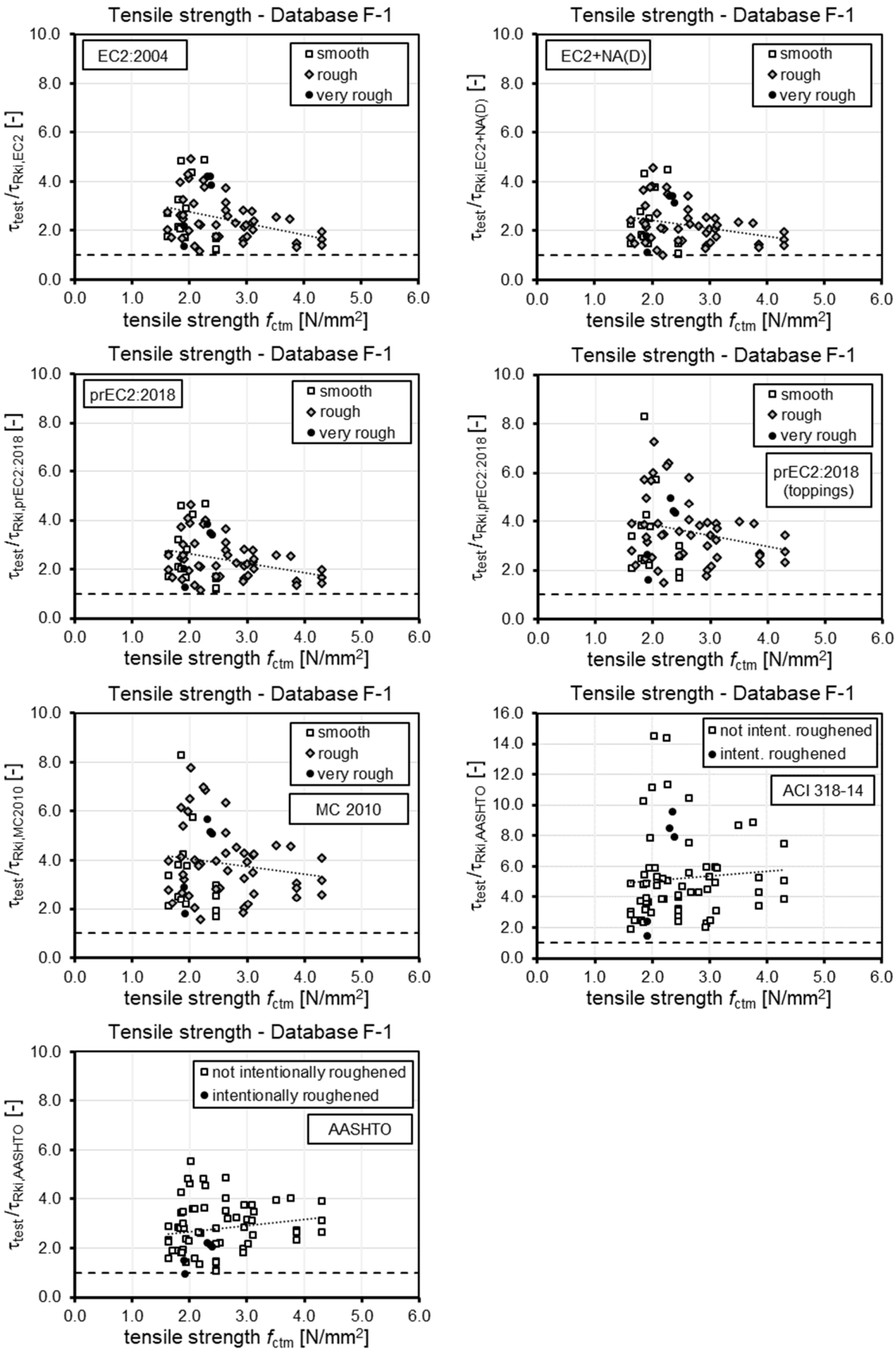

Figure B-12: Evaluation of tensile strength of database F-1 according to the evaluated codes

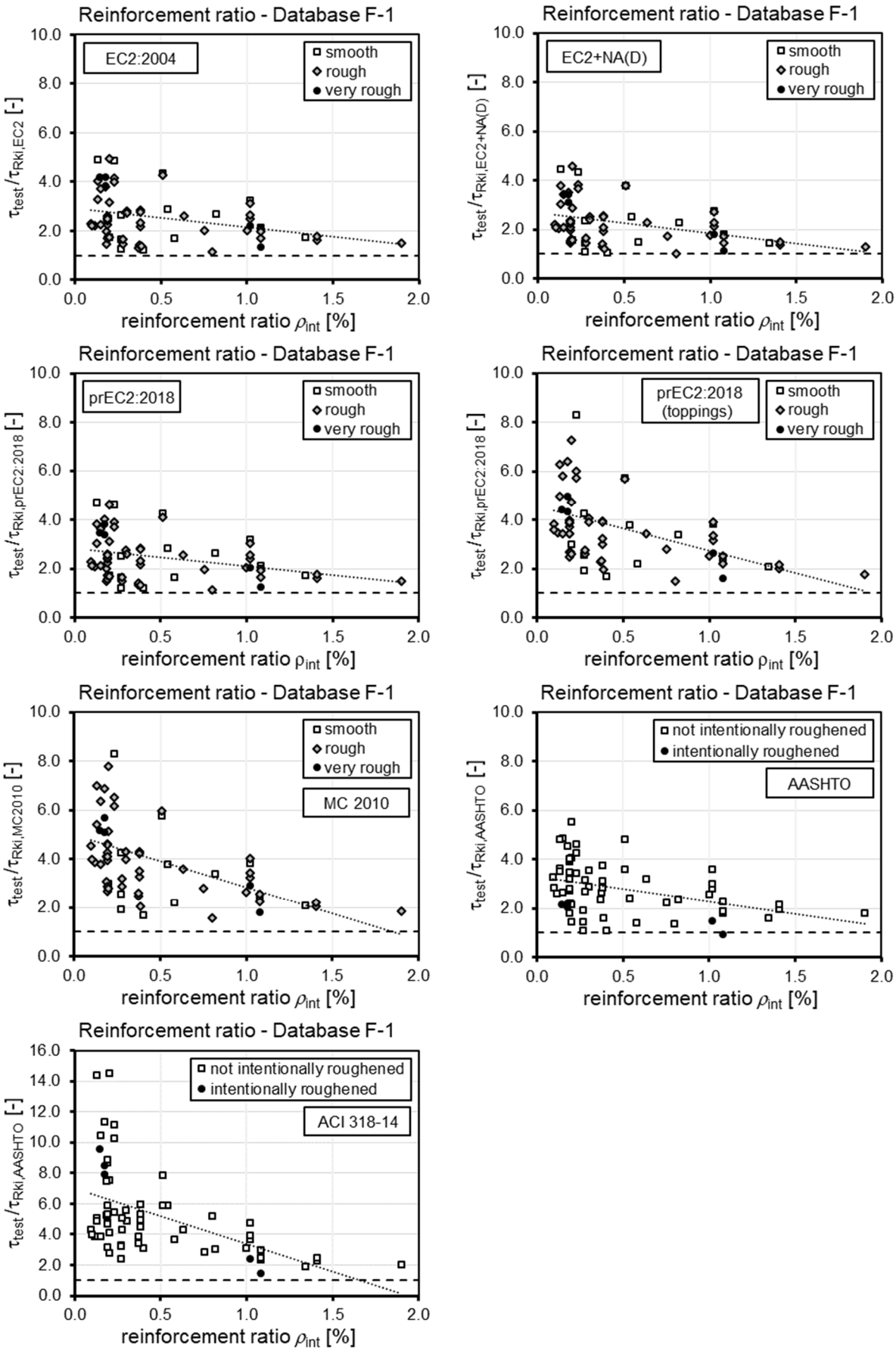

Figure B-13: Evaluation of interface reinforcement of database F-1 according to the evaluated codes

B.2.4 Database F-2: Reinforcement (lattice girders)

Table B-28: Database F-2 – Specimens Nr. 1 – 8 (a) and (b)

Nr. [-]	Source [-]	Test ID [-]	Interface [-]	Section [-]	b_{int} [mm]	a_{int} [mm]	h_{pre} [mm]	h_{ins} [mm]	$f_{cm,cyl,1}$ [N/mm²]	$f_{ctm,1}$ [N/mm²]	$f_{cm,cyl,2}$ [N/mm²]	$f_{ctm,2}$ [N/mm²]
1	[Fur11]	2-1	smooth	slab	500	500	70	130	28.26	1.89	35.80	1.98
2	[Fur11]	2-2	smooth	slab	500	500	70	130	28.26	1.89	35.80	1.98
3	[Fur11]	3-1	smooth	slab	500	500	70	130	28.26	1.89	35.80	1.98
4	[Fur11]	3-2	smooth	slab	500	500	70	130	28.26	1.89	35.80	1.98
5	[Zil08]	1	rough	slab	480	480	65	135	35.50	2.61	33.50	2.70
6	[Zil08]	2	smooth	slab	480	480	65	135	35.50	2.61	33.50	2.70
7	[Zil08]	3	rough	slab	480	480	65	135	35.50	2.61	33.50	2.70
8	[Zil08]	4	smooth	slab	480	480	65	135	35.50	2.61	33.50	2.70

Nr. [-]	Source [-]	Test ID [-]	Interface [-]	Section [-]	d [mm]	ρ_l [%]	$f_{ym,l}$ [N/mm²]	LG type [-]	h_{LG} [mm]	n_{LG} [-]	s_{LG} [mm]	ρ_{int} [%]	α_1 [-]	α_2 [-]	$f_{ym,LG}$ [N/mm²]	τ_{test} [N/mm²]
1	[Fur11]	2-1	smooth	slab	170	356	538	E15-6/6/10	150	3	145	0.002	56	124	520	1.19
2	[Fur11]	2-2	smooth	slab	170	356	538	E15-6/6/10	150	3	145	0.002	56	124	520	1.28
3	[Fur11]	3-1	smooth	slab	170	355	538	E15-6/6/10	150	3	145	0.002	56	-	520	2.41
4	[Fur11]	3-2	smooth	slab	170	356	538	E15-6/6/10	150	3	145	0.002	56	-	520	2.26
5	[Zil08]	1	rough	slab	165	235	534	E15-6/7/12	150	5	96	0.004	56	-	564	5.65
6	[Zil08]	2	smooth	slab	165	235	534	E15-6/7/12	150	5	96	0.004	56	124	564	4.73
7	[Zil08]	3	rough	slab	165	360	534	E15-6/7/12	150	5	96	0.004	56	-	564	5.53
8	[Zil08]	4	smooth	slab	165	235	534	E15-6/7/12	150	5	96	0.004	56	124	564	4.32

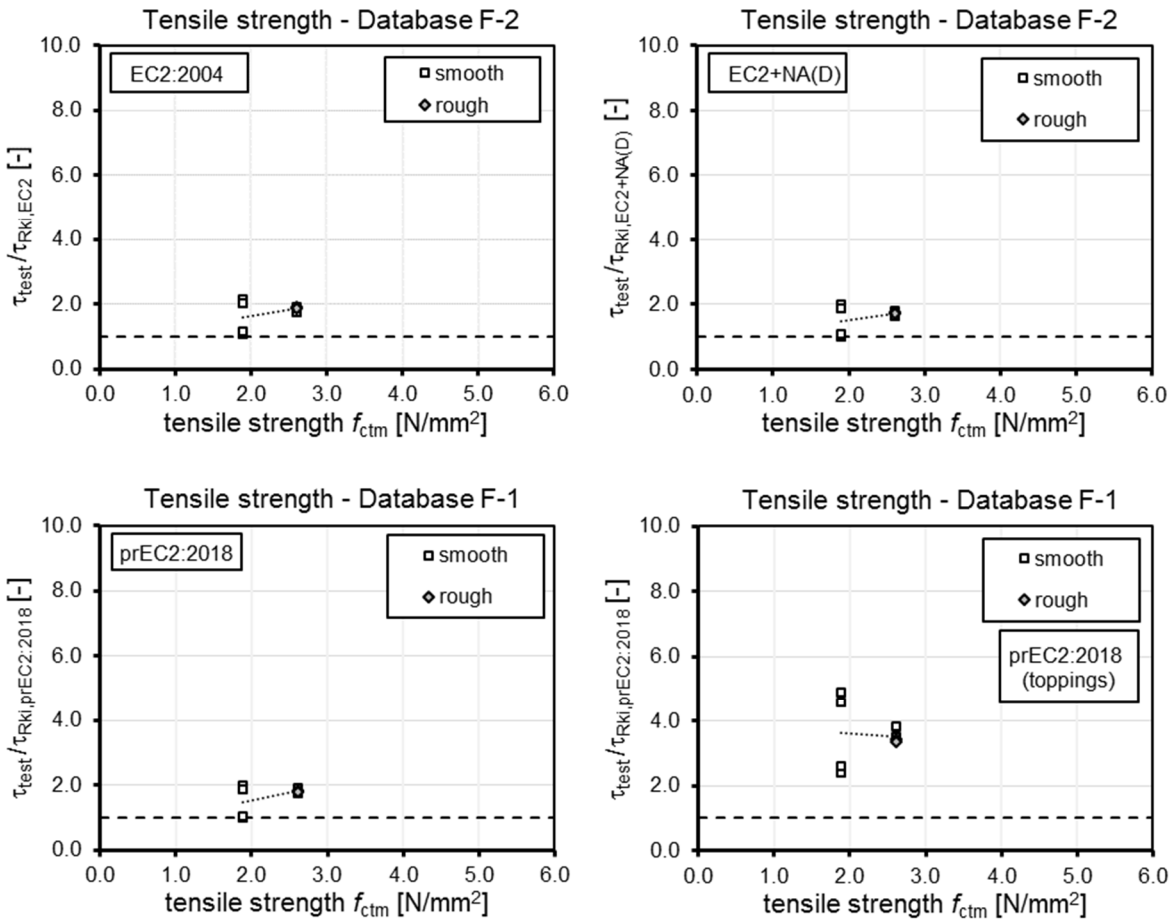

Figure B-14: Evaluation of tensile strength of database F-2 according to the evaluated codes

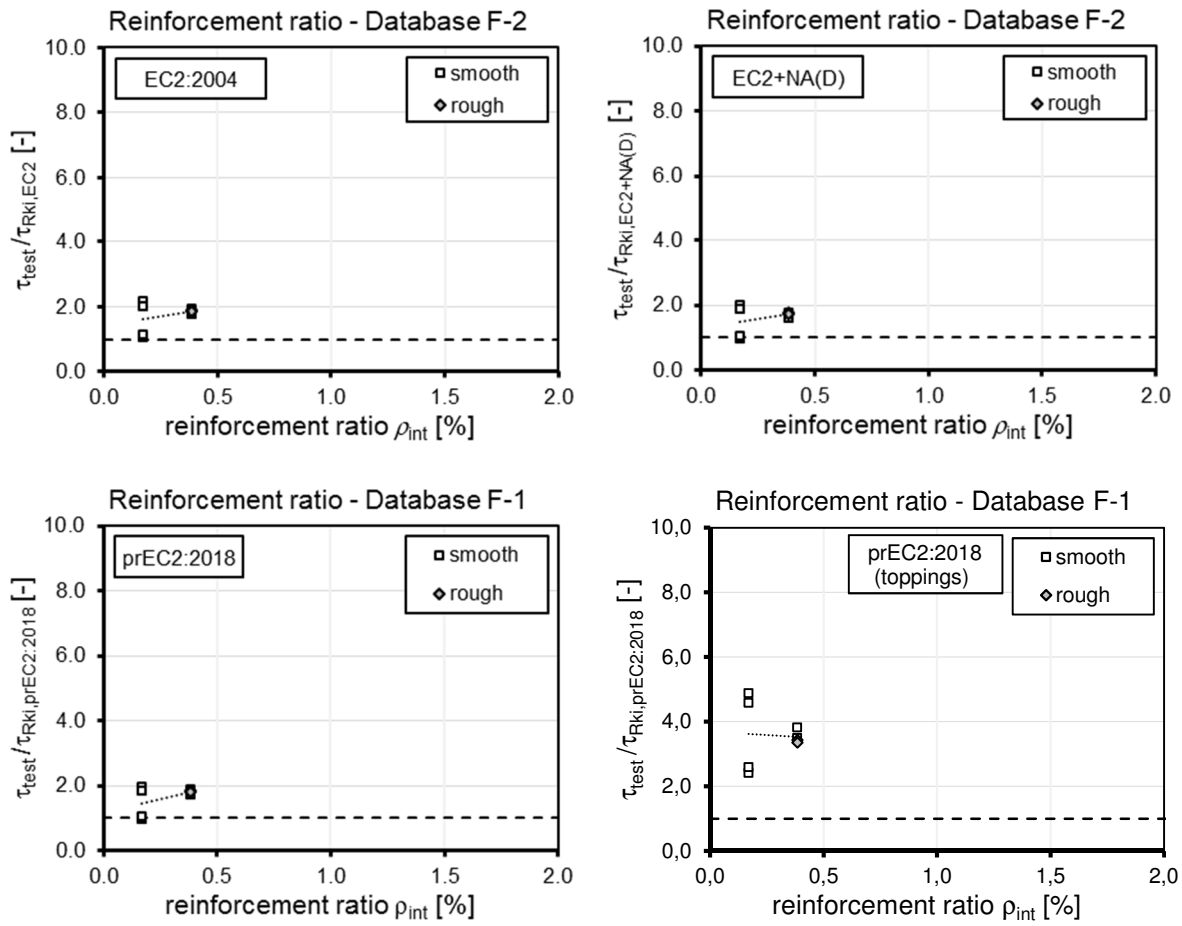

Figure B-15: Evaluation of interface reinforcement of database F-2 according to the evaluated codes

B.2.5 Database G: Adhesion – fatigue

Table B-29: Database E – Specimens Nr. 1 – 6

Nr. [-]	Source [-]	Test ID [-]	Interface [-]	Section [-]	b_{int} [mm]	a_{int} [mm]	d [mm]	h_{pre} [mm]	h_{ins} [mm]	ρ_l [%]	$f_{ym,l}$ [N/mm²]	$f_{cm,cyl,1}$ [N/mm²]	$f_{ctm,1}$ [N/mm²]	$f_{cm,cyl,2}$ [N/mm²]	$f_{ctm,2}$ [N/mm²]	$\tau_{test,max}$ [N/mm²]	$\Delta\tau_{test}$ [N/mm²]	N [-]	$\tau_{test,res}$ [N/mm²]
1	[Sch82]	11	smooth	slab	800	390	130	60	100	0.90	499	35.53	2.99	35.76	3.01	0.76	0.38	2000000	1.65
2	[Sch82]	12	smooth	slab	800	510	170	60	140	1.00	548	48.08	3.74	41.61	3.37	0.81	0.41	2000000	1.77
3	[Chu76]	A2	rough	t-beam	62	850	235	250	50	0.54	*	42.00	3.39	30.00	2.63	2.28	1.78	1000000	4.85
4	[Chu76]	A3	rough	t-beam	62	850	235	250	50	0.54	*	42.00	3.39	30.00	2.63	2.68	2.18	1000000	5.03
5	[Chu76]	A4	rough	t-beam	62	850	235	250	50	0.54	*	42.00	3.39	30.00	2.63	3.02	2.52	37400	
6	[Chu76]	A5	rough	t-beam	62	850	235	250	50	0.54	*	42.00	3.39	30.00	2.63	2.88	2.38	419000	

* no information about yield strength in test report

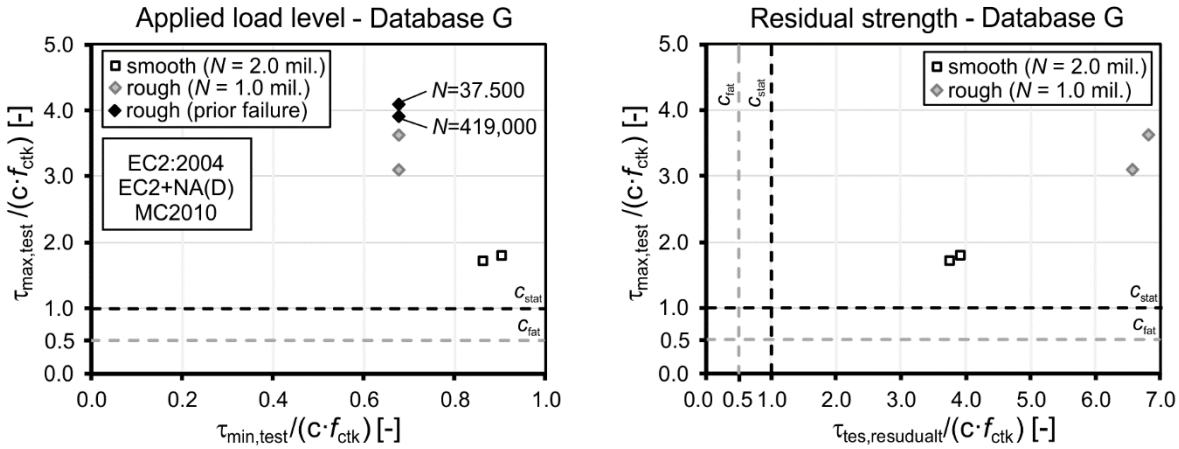

Figure B-16 Applied load level referred to calculated characteristic adhesive strength (left) and residual resistance referred to calculated characteristic adhesive strength (right) according to EC2, EC2+NA(D) and MC2010

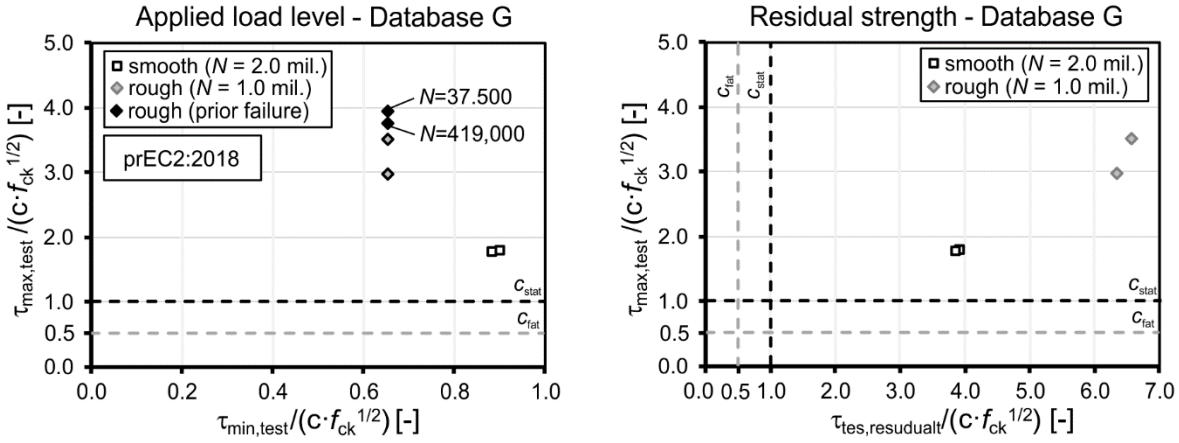

Figure B-17: Applied load level referred to calculated characteristic adhesive strength (left) and residual resistance referred to calculated characteristic adhesive strength (right) according to prEC2:2018

B.2.6 Database H-1: Reinforcement (stirrups) – fatigue

Table B-30: Database H-1 – Specimens Nr. 1 – 37 (a)

Nr. [-]	Source [-]	Test ID [-]	Interface [-]	Section [-]	b_{int} [mm]	a_{int} [mm]	h_{pre} [mm]	h_{ins} [mm]	$f_{cm,cyl,1}$ [N/mm²]	$f_{ctm,1}$ [N/mm²]	$f_{cm,cyl,2}$ [N/mm²]	$f_{ctm,2}$ [N/mm²]
1	[Bar65]	2.7	very rough	t-beam	89	914	330	102	25.35	3.36	23.62	2.68
2	[Bar65]	4.6	very rough	t-beam	89	914	330	102	22.12	2.77	19.43	2.72
3	[Bar65]	4.7	very rough	t-beam	89	914	330	102	23.79	2.84	22.17	2.67
4	[Bar65]	2.5	very rough	t-beam	89	1372	330	102	22.99	2.88	23.57	2.82
5	[Bar65]	4.5	very rough	t-beam	89	1372	330	102	24.21	3.41	24.94	3.30
6	[Bar65]	2.8	very rough	t-beam	89	2743	330	102	18.88	2.56	19.43	2.61
7	[Bar65]	2.9	very rough	t-beam	89	2743	330	102	24.82	3.02	23.30	2.89
8	[Bar65]	3.9	very rough	t-beam	89	2743	330	102	25.59	3.10	20.93	2.54
9	[Bar65]	4.8	very rough	t-beam	89	2743	330	102	18.23	2.30	18.14	1.93
10	[Bar65]	4.9	very rough	t-beam	89	2743	330	102	27.71	3.08	22.27	2.86
11	[Bar65]	9.2	very rough	t-beam	305	3378	838	203	43.12	3.44	40.43	3.63
12	[Bar65]	9.1	very rough	t-beam	305	3378	838	203	37.47	3.51	21.44	2.44
13	[Bar65]	1.6	rough	t-beam	89	914	330	102	21.81	2.79	19.49	2.50
14	[Bar65]	1.7	rough	t-beam	89	914	330	102	26.94	2.91	24.36	2.64
15	[Bar65]	3.6	rough	t-beam	89	914	330	102	19.05	2.35	19.87	2.68
16	[Bar65]	3.7	rough	t-beam	89	914	330	102	23.66	3.00	22.90	2.94
17	[Bar65]	1.5	rough	t-beam	89	1372	330	102	23.81	2.97	26.38	2.79
18	[Bar65]	3.5	rough	t-beam	89	1372	330	102	24.46	3.38	26.01	3.08
19	[Bar65]	1.8	rough	t-beam	89	2134	330	102	24.21	3.15	22.55	3.00
20	[Bar65]	1.9	rough	t-beam	89	2743	330	102	25.43	2.96	24.69	3.05
21	[Bar65]	3.8	rough	t-beam	89	2743	330	102	23.43	2.47	23.63	2.54
22	[Chu76]	B2	rough	t-beam	62	850	250	50	38.00	3.39	26.00	2.63
23	[Chu76]	B3	rough	t-beam	62	850	250	50	38.00	3.39	26.00	2.63
24	[Chu76]	B4	rough	t-beam	62	850	250	50	38.00	3.39	26.00	2.63
25	[Chu76]	C2	rough	t-beam	62	850	250	50	38.00	3.39	26.00	2.63
26	[Chu76]	C3	rough	t-beam	62	850	250	50	38.00	3.39	26.00	2.63
27	[Chu76]	C4	rough	t-beam	62	850	250	50	38.00	3.39	26.00	2.63
28	[Chu76]	D2	rough	t-beam	62	850	250	50	38.00	3.39	26.00	2.63
29	[Chu76]	D3	rough	t-beam	62	850	250	50	38.00	3.39	26.00	2.63
30	[Chu76]	D4	rough	t-beam	62	850	250	50	38.00	3.39	26.00	2.63
31	[Chu76]	D5	rough	t-beam	62	850	250	50	38.00	3.39	26.00	2.63
32	[Das86b]	1	rough	t-beam	100	3000	550	100	31.09	2.97	31.09	2.97
33	[Sch96a]	1	smooth	slab	800	390	60	100	24.89	2.56	24.82	2.55
34	[Sch96a]	2	smooth	slab	800	390	60	100	37.76	3.38	23.39	2.45
35	[Sch96a]	3	smooth	slab	800	360	60	100	33.26	3.10	24.11	2.50
36	[Sch96a]	4	smooth	slab	800	360	60	100	35.32	3.23	30.66	2.94
37	[Sch96a]	5	smooth	slab	800	360	60	100	33.11	3.09	30.26	2.91

Table B-31: Database H-1 – Specimens Nr. 1 – 37 (b)

Nr. [-]	Source [-]	Test ID [-]	Interface [-]	d [mm]	ρ_l [%]	$f_{ym,l}$ [N/mm²]	ρ_{int} [%]	α [-]	$f_{ym,int}$ [N/mm²]	$\tau_{test,max}$ [N/mm²]	$\Delta\tau_{test}$ [N/mm²]	N [-]	$\tau_{test,res}$ [N/mm²]
1	[Bar65]	2.7	very rough	356	2.86	345	0.18	90	366	2.00	1.57	2000000	5.17
2	[Bar65]	4.6	very rough	356	2.86	345	0.52	90	366	2.59	2.03	2000000	6.66
3	[Bar65]	4.7	very rough	356	2.86	345	0.52	90	366	2.78	2.23	2000000	6.88
4	[Bar65]	2.5	very rough	355	4.30	345	0.18	90	366	2.01	1.63	2000000	4.78
5	[Bar65]	4.5	very rough	355	4.30	345	0.52	90	366	2.01	1.71	2000000	6.93
6	[Bar65]	2.8	very rough	356	2.86	345	0.15	90	366	1.36	1.05	1413000	
7	[Bar65]	2.9	very rough	356	4.30	345	0.15	90	366	1.57	1.25	2000000	3.12
8	[Bar65]	3.9	very rough	356	2.86	345	0.52	90	366	1.55	1.24	1285000	
9	[Bar65]	4.8	very rough	356	2.86	345	0.52	90	366	1.55	1.24	650000	
10	[Bar65]	4.9	very rough	356	1.07	334	0.52	90	366	1.73	1.41	2000000	2.87
11	[Bar65]	9.2	very rough	875	0.18	*	0.15	90	366	2.35	1.86	2000000	6.61
12	[Bar65]	9.1	very rough	875	0.18	*	0.30	90	334	2.00	1.58	2000000	4.50
13	[Bar65]	1.6	rough	356	2.86	345	0.18	90	366	2.00	1.57	2000000	3.54
14	[Bar65]	1.7	rough	356	2.86	345	0.18	90	366	2.00	1.57	2000000	4.28
15	[Bar65]	3.6	rough	356	2.86	345	0.52	90	366	2.59	2.03	2000000	4.34
16	[Bar65]	3.7	rough	356	2.86	345	0.52	90	366	2.78	2.23	2000000	5.31
17	[Bar65]	1.5	rough	355	4.30	345	0.18	90	366	1.49	1.14	2000000	3.52
18	[Bar65]	3.5	rough	355	4.30	345	0.52	90	366	2.01	1.71	2000000	5.54
19	[Bar65]	1.8	rough	356	4.30	345	0.15	90	366	1.61	1.29	11000	
20	[Bar65]	1.9	rough	356	4.30	345	0.15	90	366	1.57	1.26	2000000	2.50
21	[Bar65]	3.8	rough	356	2.86	345	0.52	90	366	1.28	0.97	1104000	
22	[Chu76]	B2	rough	235	0.54	*	0.15	90	550	2.35	1.88	1000000	5.10
23	[Chu76]	B3	rough	235	0.54	*	0.15	90	550	2.73	2.21	1000000	5.10
24	[Chu76]	B4	rough	235	0.54	*	0.15	90	550	3.06	2.59	345400	
25	[Chu76]	C2	rough	235	0.54	*	0.20	90	550	2.32	1.87	1000000	4.56
26	[Chu76]	C3	rough	235	0.54	*	0.20	90	550	2.77	2.27	1000000	4.67
27	[Chu76]	C4	rough	235	0.54	*	0.20	90	550	3.13	2.63	1000000	4.84
28	[Chu76]	D2	rough	235	0.54	*	0.30	90	550	2.26	1.81	1000000	5.01
29	[Chu76]	D3	rough	235	0.54	*	0.30	90	550	2.81	2.26	1000000	5.42
30	[Chu76]	D4	rough	235	0.54	*	0.30	90	550	3.16	2.66	854000	
31	[Chu76]	D5	rough	235	0.54	*	0.30	90	550	2.96	2.46	348000	
32	[Das86b]	1	rough	596	2.29	480	0.75	90	442	1.96	0.97	2000000	6.62
33	[Sch96a]	1	smooth	130	0.87	499	0.09	90	613	0.71	0.36	2000000	1.57
34	[Sch96a]	2	smooth	130	0.98	499	0.10	90	494	0.68	0.34	2000000	2.10
35	[Sch96a]	3	smooth	120	1.68	545	0.19	90	593	1.50	0.75	2000000	3.57
36	[Sch96a]	4	smooth	120	3.27	531	0.44	90	613	2.50	1.25	2000000	4.91
37	[Sch96a]	5	smooth	120	2.62	531	0.38	90	593	2.03	1.01	2000000	4.10

Table B-32: Database H-1 – Specimens Nr. 38 – 44 (a) and (b)

Nr. [-]	Source [-]	Test ID [-]	Interface [-]	Section [-]	b_{int} [mm]	a_{int} [mm]	h_{pre} [mm]	h_{ins} [mm]	$f_{cm,cyl,1}$ [N/mm²]	$f_{ctm,1}$ [N/mm²]	$f_{cm,cyl,2}$ [N/mm²]	$f_{ctm,2}$ [N/mm²]
38	[Sch96a]	6	smooth	slab	800	510	60	140	33.18	3.10	31.61	3.00
39	[Sch96a]	7	smooth	slab	800	510	60	140	30.11	2.90	26.95	2.70
40	[Sch96a]	8	smooth	slab	800	480	60	140	37.61	3.37	39.26	3.47
41	[Sch96a]	9	smooth	slab	800	480	60	140	32.87	3.08	33.50	3.12
42	[Sch96a]	10	smooth	slab	800	480	60	140	42.34	3.64	38.79	3.44
43	[Sch96c]	16-1	rough	slab	800	360	70	90	40.05	3.51	18.34	2.09
44	[Sch96c]	18-1	rough	slab	800	480	70	130	46.92	3.90	24.34	2.52

Nr. [-]	Source [-]	Test ID [-]	Interface [-]	d [mm]	ρ_l [%]	$f_{ym,l}$ [N/mm²]	ρ_{int} [%]	α [-]	f_{ym} [N/mm²]	$\tau_{test,max}$ [N/mm²]	$\Delta\tau_{test}$ [N/mm²]	N [-]	$\tau_{test,res}$ [N/mm²]
38	[Sch96a]	6	smooth	170	1.02	548	0.11	90	596	0.84	0.42	2000000	1.56
39	[Sch96a]	7	smooth	170	0.83	499	0.08	90	494	0.56	0.28	2000000	1.48
40	[Sch96a]	8	smooth	160	1.96	531	0.19	90	593	1.67	0.83	2000000	2.44
41	[Sch96a]	9	smooth	160	2.70	531	0.38	90	593	2.03	1.02	2000000	4.06
42	[Sch96a]	10	smooth	160	2.70	531	0.38	90	593	2.11	1.05	2000000	4.38
43	[Sch96c]	16-1	rough	120	2.62	531	0.38	90	645	2.03	1.01	2000000	3.24
44	[Sch96c]	18-1	rough	160	1.96	531	0.19	90	645	1.67	0.83	2000000	2.69

* no information about yield strength in test report

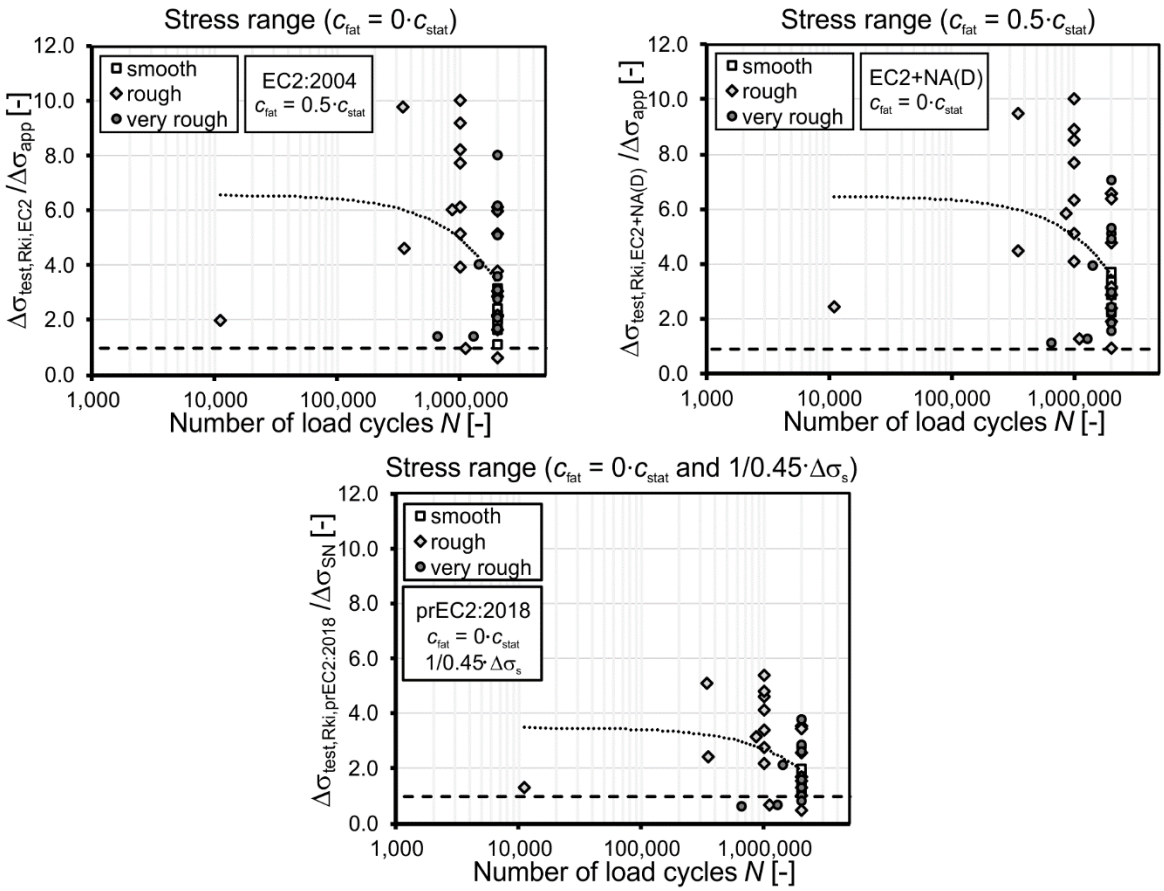

Figure B-18: Evaluation of stress range of database H-1 according to the evaluated codes

B.2.7 Database H-2: Reinforcement (lattice girders) – fatigue

Table B-33: Database H-2 – Specimens Nr. 1 – 37 (a)

Nr. [-]	Source [-]	Test ID [-]	Interface [-]	Section [-]	b_{int} [mm]	a_{int} [mm]	h_{pre} [mm]	h_{ins} [mm]	$f_{cm,cyl,1}$ [N/mm²]	$f_{ctm,1}$ [N/mm²]	$f_{cm,cyl,2}$ [N/mm²]	$f_{ctm,2}$ [N/mm²]
1	[Sch81]	1.1	smooth	slab	500	1000	60	140	22.75	2.41	23.75	2.48
2	[Sch81]	1.2	smooth	slab	500	1000	60	140	22.75	2.41	23.75	2.48
3	[Sch81]	1.3	smooth	slab	500	1000	60	140	22.75	2.41	23.75	2.48
4	[Sch81]	1.4	smooth	slab	500	1000	60	140	22.75	2.41	23.75	2.48
5	[Sch81]	1.5	smooth	slab	500	1000	60	140	22.75	2.41	23.75	2.48
6	[Sch82]	1.6	very smooth	slab	400	600	60	140	12.08	1.58	12.92	1.65
7	[Sch82]	1.8	very smooth	slab	400	600	60	140	12.08	1.58	12.92	1.65
8	[Sch82]	1.10	smooth	slab	400	600	60	140	20.67	2.26	20.25	2.23
9	[Sch82]	1.12	smooth	slab	400	600	60	140	20.67	2.26	23.33	2.45
10	[Sch82]	1.9	rough	slab	400	600	60	140	20.67	2.26	22.17	2.37
11	[Sch82]	1.11	rough	slab	400	600	60	140	20.67	2.26	22.50	2.39
12	[Sch83]	1.13	very smooth	slab	400	600	60	140	19.83	2.20	22.50	2.39
13	[Sch83]	1.14	very smooth	slab	400	600	60	140	19.83	2.20	22.17	2.37
14	[Sch85]	I/1 (A)	very smooth	slab	500	700	60	160	21.92	2.35	18.00	2.06
15	[Sch85]	I/2 (A)	very smooth	slab	500	700	60	160	22.92	2.42	20.92	2.28
16	[Sch85]	II/3 (A)	very smooth	slab	500	700	60	160	23.25	2.44	17.17	2.00
17	[Sch85]	II/4 (A)	very smooth	slab	500	700	60	160	23.25	2.44	17.17	2.00
18	[Sch85]	I/3 (B)	smooth	slab	500	700	60	160	24.08	2.50	21.00	2.28
19	[Sch85]	I/4 (B)	smooth	slab	500	700	60	160	23.33	2.45	22.00	2.36
20	[Sch85]	II/1 (B)	smooth	slab	500	700	60	160	24.25	2.51	15.50	1.86
21	[Sch85]	II/2 (B)	smooth	slab	500	700	60	160	24.25	2.51	15.50	1.86
22	[Sch85]	II/1r (B)	rough	slab	500	700	60	160	18.83	2.12	21.67	2.33
23	[Sch85]	II/2r (B)	rough	slab	500	700	60	160	18.83	2.12	21.67	2.33
24	[Web89]	EQ10-A	very smooth	slab	500	460	60	100	23.50	2.46	19.75	2.19
25	[Web89]	EQ10-B	smooth	slab	500	460	60	100	25.58	2.60	28.50	2.80
26	[Web95]	V1	smooth	slab	800	750	60	190	35.33	3.23	27.00	2.70
27	[Web95]	V2	smooth	slab	800	750	60	190	35.33	3.23	24.50	2.53
28	[Web95]	V3	smooth	slab	800	750	60	190	35.33	3.23	25.58	2.60
29	[Wie17a]	EG01_1	smooth	slab	850	500	70	90	21.26	2.65	31.61	2.75
30	[Wie17a]	EG01_2	smooth	slab	850	500	70	90	21.26	2.65	31.61	2.75
31	[Wie17a]	EG02_1	very smooth	slab	850	500	70	90	21.62	2.74	29.87	2.90
32	[Wie17a]	EG02_2	very smooth	slab	850	500	70	90	21.62	2.74	29.87	2.90
33	[Wie17a]	EG03_1	smooth	slab	850	500	70	90	23.69	2.43	29.15	2.48
34	[Wie17a]	EG03_2	smooth	slab	850	500	70	90	23.69	2.43	29.15	2.48
35	[Wie17a]	EG04_1	smooth	slab	850	500	70	90	23.87	2.42	30.00	2.55
36	[Wie17a]	EG06_1	smooth	slab	850	500	70	90	47.09	3.21	57.34	3.88
37	[Wie17a]	EG06_2	smooth	slab	850	500	70	90	47.09	3.21	57.34	3.88

Table B-34: Database H-2 – Specimens Nr. 1 – 37 (b)

Nr. [-]	Source [-]	Test ID [-]	Interface [-]	d [mm]	ρ_l [%]	$f_{ym,l}$ [N/mm²]	LG type [-]	n_{LG} [-]	h_{LG} [mm]	s_{LG} [mm]	ρ_{int} [%]	α_1 [-]	α_2 [-]	f_{ym} [N/mm²]	$\tau_{test,max}$ [N/mm²]	$\Delta\tau_{test}$ [N/mm²]	N [-]
1	[Sch81]	1.1	smooth	172	1.87	516	M-KT	2	160	250	0.20	58	0	584	1.06	0.67	1360000
2	[Sch81]	1.2	smooth	172	1.87	516	M-KT	2	160	250	0.20	58	0	584	1.06	0.67	2000000
3	[Sch81]	1.3	smooth	172	1.87	516	M-KT	2	160	250	0.20	58	0	584	1.06	0.67	2250000
4	[Sch81]	1.4	smooth	172	1.87	516	M-KT	2	160	250	0.20	58	0	584	1.06	0.67	1700000
5	[Sch81]	1.5	smooth	172	1.87	516	M-KT	2	160	250	0.20	58	0	584	1.06	0.67	2000000
6	[Sch82]	1.6	very smooth	172	1.46	515	M-KT	2	160	200	0.25	58	0	583	1.30	0.81	1620000
7	[Sch82]	1.8	very smooth	172	1.46	515	M-KT+stir	1	160	400	0.13	58	0	583	1.30	0.81	770000
8	[Sch82]	1.10	smooth	172	1.46	515	M-KT+stir	1	160	400	0.13	58	0	583	1.41	0.78	2000000
9	[Sch82]	1.12	smooth	172	1.46	515	M-KT	2	160	200	0.25	58	0	583	1.44	0.80	2000000
10	[Sch82]	1.9	rough	172	1.46	515	M-KT+stir	1	160	400	0.13	58	0	583	1.43	0.79	2000000
11	[Sch82]	1.11	rough	172	1.46	515	M-KT	2	160	200	0.25	58	0	583	1.43	0.79	2000000
12	[Sch83]	1.13	very smooth	174	0.93	512	M-KT	2	160	200	0.25	58	0	579	0.97	0.62	2000000
13	[Sch83]	1.14	very smooth	174	0.93	512	M-KT	2	160	200	0.25	58	0	579	0.97	0.62	2000000
14	[Sch85]	I/1 (A)	very smooth	197	1.14	521	KTS	2	160	250	0.15	45	90	670	0.90	0.70	690000
15	[Sch85]	I/2 (A)	very smooth	197	1.14	521	KTS	2	160	250	0.15	45	90	670	0.92	0.56	2000000
16	[Sch85]	II/3 (A)	very smooth	197	1.14	521	KTS	2	160	250	0.15	45	90	670	0.90	0.70	2000000
17	[Sch85]	II/4 (A)	very smooth	197	1.14	521	KTS	2	160	250	0.15	45	90	670	0.90	0.70	1000000
18	[Sch85]	I/3 (B)	smooth	197	1.54	521	KTS	2	160	250	0.15	45	90	670	1.44	1.05	1250000
19	[Sch85]	I/4 (B)	smooth	197	1.54	521	KTS	2	160	250	0.15	45	90	670	1.45	1.14	610000
20	[Sch85]	II/1 (B)	smooth	197	1.54	521	KTS	2	160	250	0.15	45	90	670	1.52	0.87	1290000
21	[Sch85]	II/2 (B)	smooth	197	1.54	521	KTS	2	160	250	0.15	45	90	670	1.52	0.87	1120000
22	[Sch85]	II/1r (B)	rough	197	1.54	521	KTS	2	160	250	0.15	45	90	670	1.19	0.93	2000000
23	[Sch85]	II/2r (B)	rough	197	1.54	521	KTS	2	160	250	0.15	45	90	670	1.19	0.93	2000000
24	[Web89]	EQ10-A	very smooth	137	1.00	594	EQ	2	100	250	0.15	45	90	586	1.08	0.67	2000000
25	[Web89]	EQ10-B	smooth	137	1.29	520	EQ	2	100	250	0.15	45	90	586	1.12	0.88	2000000
26	[Web95]	V1	smooth	222	0.69	590	KTW	3	200	250	0.10	45	0	586	0.61	0.48	2000000
27	[Web95]	V2	smooth	222	1.42	590	KTW	3	200	250	0.10	45	0	586	0.68	0.64	2000000
28	[Web95]	V3	smooth	222	0.86	590	KTW	2	200	400	0.06	45	0	586	0.58	0.49	2000000
29	[Wie17a]	EG01_1	smooth	130	1.99	954	KTS	2	100	430	0.09	45	90	554	1.17	0.35	4180000
30	[Wie17a]	EG01_2	smooth	130	1.99	954	KTS	2	100	430	0.09	45	90	554	1.17	0.35	4180350
31	[Wie17a]	EG02_1	very smooth	130	1.99	954	KTS	2	100	430	0.09	45	90	554	1.17	0.35	2660000
32	[Wie17a]	EG02_2	very smooth	130	1.99	954	KTS	2	100	430	0.09	45	90	554	1.17	0.35	3590000
33	[Wie17a]	EG03_1	smooth	130	1.99	939	KTS	2	100	430	0.09	45	90	554	1.53	0.90	2075444
34	[Wie17a]	EG03_2	smooth	130	1.99	939	KTS	2	100	430	0.09	45	90	554	1.53	0.90	3249566
35	[Wie17a]	EG04_1	smooth	130	1.99	939	KTS	3	100	285	0.14	45	90	554	1.66	0.83	4363100
36	[Wie17a]	EG06_1	smooth	130	1.99	939	KTS	2	100	430	0.09	45	90	554	1.73	1.06	2603879
37	[Wie17a]	EG06_2	smooth	130	1.99	939	KTS	2	100	430	0.09	45	90	554	1.73	1.06	2615083

Table B-35 Database H-2 – Specimens Nr. 38 – 47 (a) and (b)

Nr. [-]	Source [-]	Test ID [-]	Interface [-]	Section [-]	b_{int} [mm]	a_{int} [mm]	h_{pre} [mm]	h_{ins} [mm]	$f_{cm,cyl,1}$ [N/mm²]	$f_{ctm,1}$ [N/mm²]	$f_{cm,cyl,2}$ [N/mm²]	$f_{ctm,2}$ [N/mm²]
38	[Wie17a]	EG07_1	smooth	slab	850	500	70	90	47.14	3.222	57.34	3.861
39	[Wie17a]	EG07_2	smooth	slab	850	500	70	90	47.14	3.222	57.34	3.861
40	[Wie17a]	EG08_1	smooth	slab	850	500	70	90	47.41	3.25	57.34	3.72
41	[Wie17a]	EG09_1	rough	slab	850	500	70	90	28.89	2.58	30.35	2.75
42	[Wie17a]	EG09_2	rough	slab	850	500	70	90	28.89	2.58	30.35	2.75
43	[Wie17a]	EG10_1	smooth	slab	850	1300	70	29	31.99	3.05	28.01	2.52
44	[Wie17a]	EG12_1	smooth	slab	850	1300	70	29	44.60	3.10	51.56	3.64
45	[Wie17a]	EG12_2	smooth	slab	850	1300	70	29	44.60	3.10	51.56	3.64
46	[Wie17a]	EG14_1	smooth	slab	850	1200	70	26	27.54	2.40	30.79	2.79
47	[Wie17a]	EG14_2	smooth	slab	850	1200	70	26	27.54	2.40	30.79	2.79

Nr. [-]	Source [-]	Test ID [-]	Interface [-]	d [mm]	ρ_l [%]	$f_{ym,l}$ [N/mm²]	LG type [-]	n_{LG} [-]	h_{LG} [mm]	s_{LG} [mm]	ρ_{int} [%]	α_1 [-]	α_2 [-]	f_{ym} [N/mm²]	$\tau_{test,max}$ [N/mm²]	$\Delta\tau_{test}$ [N/mm²]	N [-]
38	[Wie17a]	EG07_1	smooth	130	1.99	939	KTS	3	100	285	0.14	45	90	554	1.59	0.58	4033177
39	[Wie17a]	EG07_2	smooth	130	1.99	939	KTS	3	100	285	0.14	45	90	554	1.59	0.58	6283177
40	[Wie17a]	EG08_1	smooth	130	1.99	939	KTS	4	100	430	0.18	45	90	554	2.16	1.11	3951703
41	[Wie17a]	EG09_1	rough	130	1.99	939	KTS	2	100	430	0.09	45	90	554	1.55	0.92	8677
42	[Wie17a]	EG09_2	rough	130	1.99	939	KTS	2	100	430	0.09	45	90	554	1.55	0.92	1095117
43	[Wie17a]	EG10_1	smooth	330	2.02	939	EQ	2	300	430	0.09	63	90	554	1.12	0.59	2001000
44	[Wie17a]	EG12_1	smooth	330	2.02	939	EQ	2	300	430	0.09	63	90	554	1.42	0.53	4118791
45	[Wie17a]	EG12_2	smooth	330	2.02	939	EQ	2	300	430	0.09	63	90	554	1.42	0.53	4465534
46	[Wie17a]	EG14_1	smooth	300	2.09	939	EQ	4	300	210	0.18	63	90	554	2.12	0.77	1626488
47	[Wie17a]	EG14_2	smooth	300	2.09	939	EQ	4	300	210	0.18	63	90	554	2.12	0.77	1655230

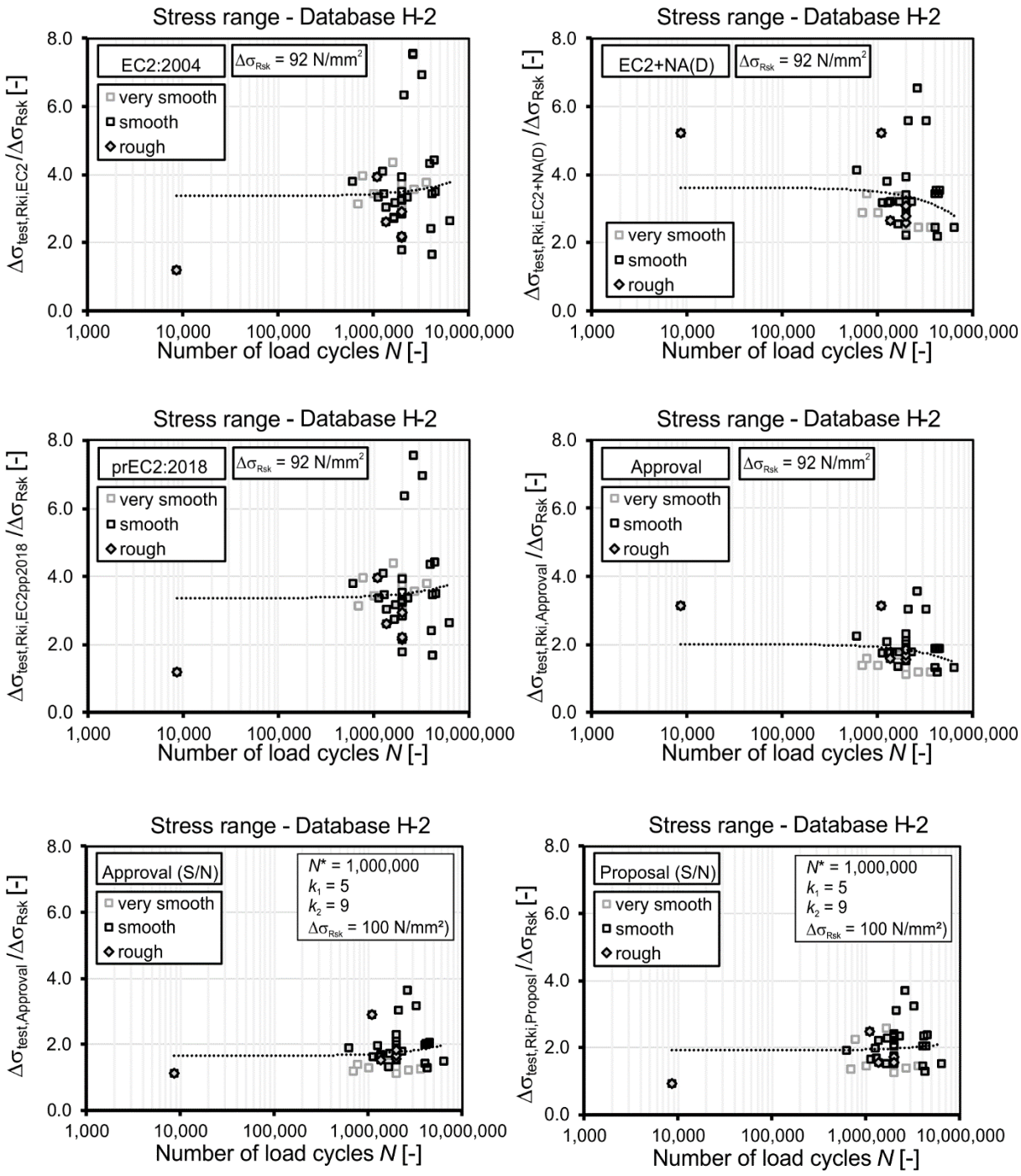

Figure B-19: Evaluation of stress range of database H-2 with lattice girders according to the evaluated codes and general technical approvals

Annex C Extended theoretical backgrounds

C.1 Parameters to quantify the surface roughness

According to Reinecke [Rei04], calculating the centreline of different profiles using linear regression results in tilted lines with either increasing or decreasing inclination, depending on the global roughness. This is contrary to the reference plane, which is defined as a horizontal line. By referring the profile data to this inclined regression line, a filter of global tilting and thus, the global roughness is implied. To avoid this effect, [Sch96a] and [Rei04] suggest an arithmetic average line for the correlation of the roughness parameter R_p (Figure C-1).

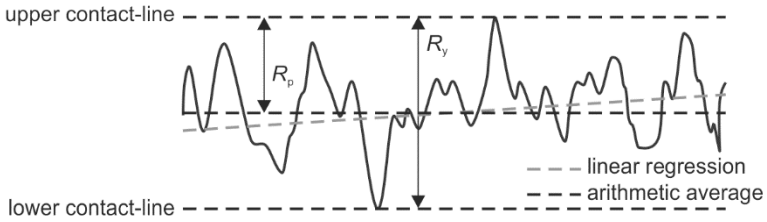

Figure C-1: Comparison of centrelines to determine roughness parameters (a), Examples of different profile frequencies with equal roughness parameters (b) [Rei04]

Therefore, the profile coordinates are referred to the upper contact line and the arithmetic average of these new coordinates generates the distance between upper contact line and a horizontal centreline. The area between average line and upper contact line describes the area between profile line and upper contact line. Due to mass balance, the sum of areas confined by average line and profile is equivalent at both sides of the average line. However, the modified parameter R_p corresponds to the arithmetic average and can be theoretically compared to the mean roughness depth R_t determined by the sand-patch method according to Kaufmann [Kau71]. The definition of the maximum profile height R_t remains unchanged.

In this context, [Rei04] compares of the mean roughness depth R_t, measured by the sand-patch method, and the arithmetic values of the maximum profile peak R_p (Figure C-2). Therefore, he tested concrete surfaces raked by a nail-rake, sand blasted, left as cast and roughened with a strong and weak high-pressure water jet (HPW). He compares roughness depth determined by the sand-patch method according to Kaufmann (average of 3 measurements) and arithmetic values measured by the touching method (3 measurements with 232 mm length), by 2D-laser (3 measurements with 94 mm length) and by 3D-laser (grid-measurement of a 40 x 40 mm area).

Even though the roughness parameters R_t and R_p are theoretically identical, Figure C-2 shows deviations between the different measuring methods. The comparison reveals a high dependency of the roughness parameters of the measuring method as well as the measured section and size. An extensive illustration of the density of amplitude – and material portion curve, including examples of different concrete surfaces, gives [Rei04].

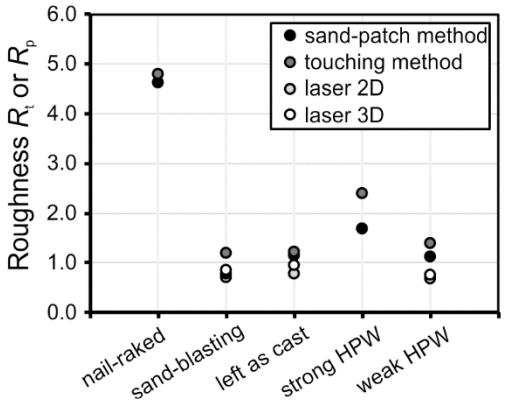

Figure C-2: Comparison of roughness parameters R_t and R_p for different classification methods an surface treatments according to [Rei04]

One effect that must be mentioned is the roughness frequency. Figure C-3 shows different theoretical surfaces with triangular and circular shape.

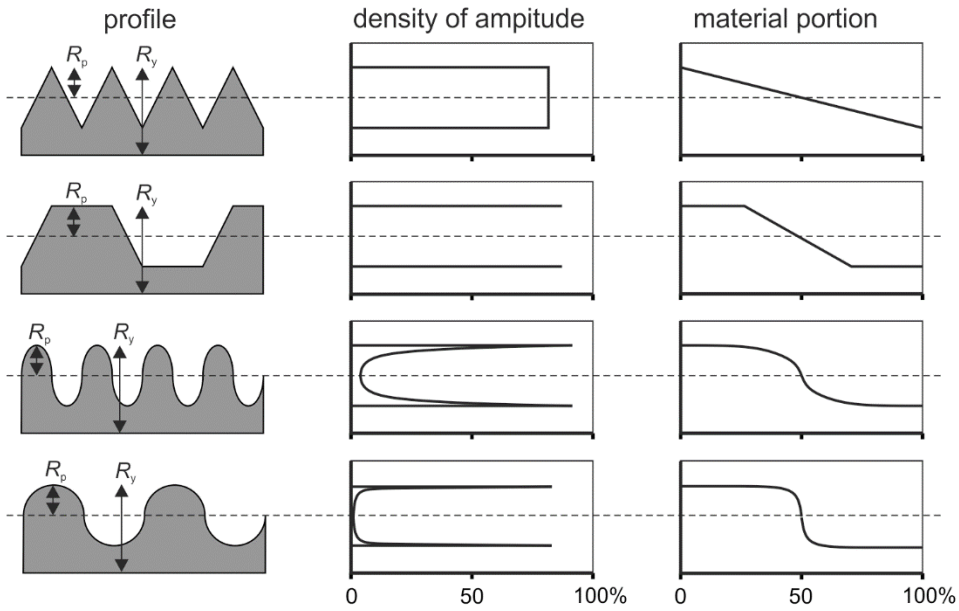

Figure C-3: Qualitative depiction of density amplitude and material portion for different surface profiles

The direct comparison between the profiles show a clear correlation between wave period or frequency and estimated roughness of the profile. Nevertheless, calculating the roughness parameters R_p and R_y leads to similar results. This implies, that for specific surface classification, a roughness determination with common roughness parameters such as average and maximum heights may not be sufficient. To differentiate surfaces with similar roughness parameters, further estimation methods are developed like the curve describing the density of amplitudes or the material portion over the profile's height in DIN EN ISO 4287 [D4287]. Figure C-3 shows the qualitative curve of the density amplitude and material portion for the idealised profiles. The curves describe relative frequency of the density of the roughness amplitude (or material portion) in a

histogram along the profile height referred to the centreline. The centreline, in this case, should be determined according to the method of minimizing error squares [Rei04].

Another method to determine the roughness of an interface is the method according to the quotient of *Wenzel* [Sch96b]. It describes the ratio of a stretched profile length to the length of a horizontal projection of the profile, which indirectly considers the additional contact area regarding an idealised horizontal surface due to a profiled surface [Len12]. Providing a two-dimensional roughness profile recorded by e.g. touching- or laser method, the profile can be divided in several sections (Figure C-4).

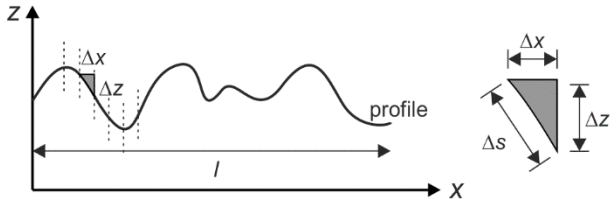

Figure C-4: Determination of the quotient of *Wenzel*

The quotient of *Wenzel W* can be calculated according to Eq. (C-1) or simplified according to Eq. (C-2).

$$W = \int_0^l \Delta s \tag{C-1}$$

With
$\Delta s^2 = \Delta x^2 + \Delta y^2$ (acc. to Figure C-4)

$$W = \frac{1}{l} \cdot \sum \sqrt{\Delta x^2 + \Delta z^2} \tag{C-2}$$

As mentioned above, the quotient of *Wenzel* gives an approximation of the ratio of surface profile to idealised horizontal surface. For interface shear, the full contact area may be activated for adhesion, whereas for friction or aggregate interlock, according to the model concepts, only partial areas of the surface may be activated after first displacements. Further investigations regarding the correlation between roughness and the ratio of profile surface to horizontal length show, that for some geometrical cases, the quotient of *Wenzel* is no reliable parameter to determine the interface roughness [Rei04].

C.2 Fatigue behaviour of reinforced concrete

C.2.1 Fundamentals of fatigue

For a preferable realistic display of fatigue stress, designations for defining the load history were generally determined (Figure C-5 (a)). The load oscillates with load cycles *N* along the medium stress σ_m, with a stress amplitude σ_a confined by the maximum stress σ_{max} and minimum stress σ_{min}. The stress between maximum and minimum load is defined as stress range with $\Delta\sigma = 2 \cdot \sigma_a$. The number of load cycles per second is the frequency *f* of the cyclic loading. The range of fatigue stress can be completely under compressive stress (compressive threshold range), under tensile stress (tensile threshold range) or alternating between compressive and tensile stress (alternating range) (Figure C-5 (b)).

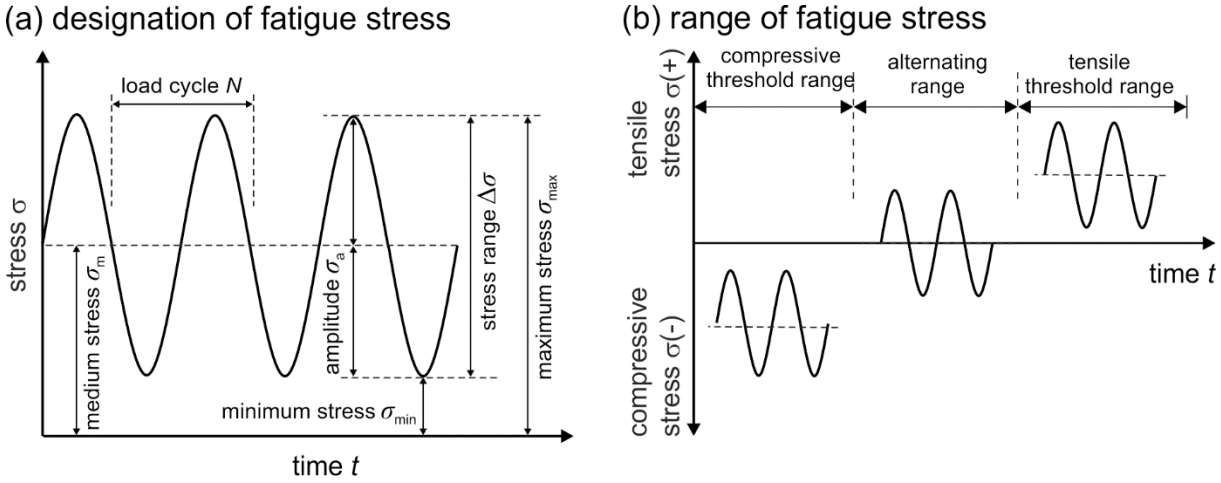

Figure C-5: Designation of fatigue stress (a), range of fatigue stress (b) [Zil10]

Generally, two fatigue failure modes of materials can be distinguished in structural engineering. On the one hand, the low-cycle fatigue with temporary alternating stress, high amplitudes and low number of load cycles (e.g. earthquakes), and on the other hand, high cycle fatigue with permanent alternating stress, (relatively) low amplitudes and high number of load cycles [Zil10].

The fatigue strength of a material can be idealised by the relation of bearable stress range $\Delta\sigma$ and the corresponding number of load cycles *N*. Therefore, a steel or concrete specimen is cyclically loaded by constant maximums stress and stress range until failure (e.g. single-step test [D50100]). The evaluation of a number of fatigue tests with different load levels leads to a formulation of a fatigue-strength curve (S-N curve) which is also called *Wöhler* curve. An extensive description of the derivation of S-N curves for reinforcing steel can be found in Chapter 5.3.2

Depending on the number of load cycles, the course of the S-N curve can be divided in three stages. In this context, Figure C-6 shows a qualitative example of a metallic material. The stage of short time fatigue strength (low cyclic fatigue strength) comprises

stress ranges near the static resistance of the material. Thereby, only a low number of load cycles can be endured ($N \approx 10^4$). This stage is no element of the fatigue verification since by limiting the steel and concrete stress, stress ranges in these dimensions are excluded. The stage of fatigue strength (high cycle fatigue strength) presents the relevant stage for building practice where the bearable amplitudes decrease significantly with increasing number of load cycles. The stage of endurance fatigue strength describes a stage, where a theoretical infinite number of load cycles does not lead to material failure. According to [Zil10], reinforcing steel with stress ranges exceeding $N = 2 \cdot 10^6$ load cycles have an endurance fatigue strength, whereas according to [D50100], a single step test can be stopped after $N = 2 \cdot 10^6$ load cycles. From today's perspective, structures under operating stress or with pre-existing damage do not have an endurance fatigue resistance [Zil10].

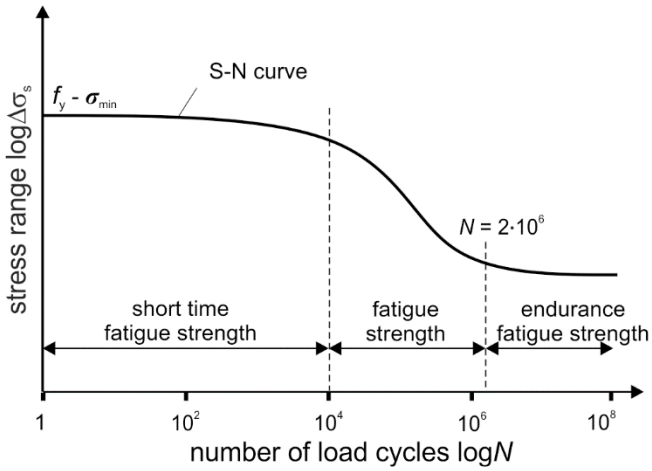

Figure C-6: Qualitative depiction of a fatigue-strength curve (S-N curve) for a metallic material

C.2.2 Fatigue behaviour of reinforcing steel

The load bearing behaviour of reinforcing steel under cyclic loading conditions is mostly investigated [Kön94][Hai06][Nür82][Reh81]. The fracture process can be pictured in three stages: defortification, formation of micro cracks and crack distribution (Figure C-7 (a)). Due to inhomogeneity of the material, first micro cracks occur during the first load cycles which lead to a local defortification. In the following, the plastic deformations redistribute from inside the steel section to the surface and thus, first macro cracks occur and form the crack origin (Figure C-7 (b)). With continuing cyclic loading, the crack distributes with every load cycle. Is this stage, the crack distribution is separated in stable and instable crack distribution. After processed crack distribution, the residual fracture zone decreases and thus, fails after increasing the resistance of the residual area with a failure mechanism compared to static failure (static residual failure).

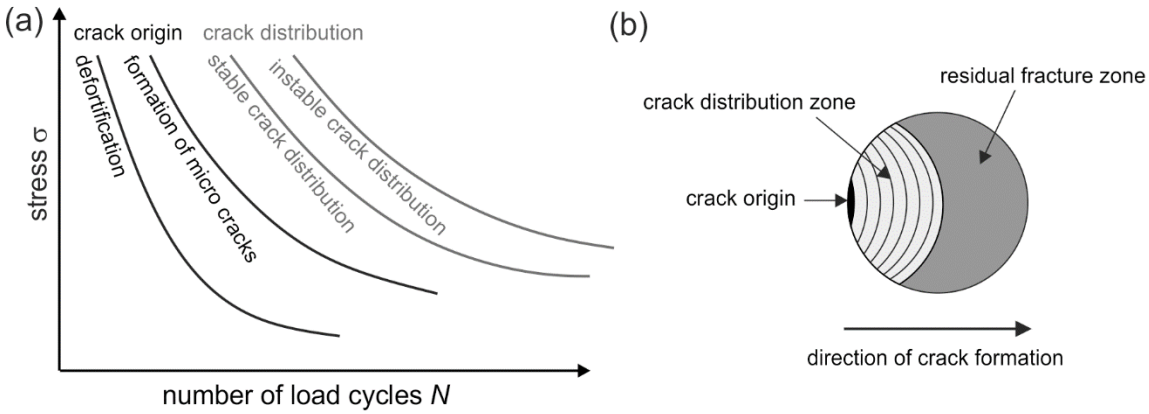

Figure C-7: Qualitative depiction of fatigue failure progress of reinforcing steel [Kön94] (a), fracture zone of a reinforcing steel under fatigue failure [Zil10] (b)

The fatigue strength of reinforcing steel is mainly influences by the parameters of surface condition, bar curvature, corrosion, bar diameter, steel type and structural alteration of the steel caused e.g. by welding [Kön94][Nür82]. The influence of load frequency and medium stress under tensile threshold stress is subordinate. Compared to free bars, for bars embedded in concrete regularly higher fatigue strengths could be determined, since an intersection of steel notch and concrete crack is unlikely [Reh81][Mau10b]. As long as no influences by corrosion appear, the concrete class and strength constitute a minor part in the fatigue resistance of reinforcing steel [Mau10b].

C.2.3 Fatigue behaviour of concrete

The fatigue behaviour of concrete was investigated empirically in several test series. Most tests were conducted by investigating small size specimen like cylinders, cubes and prisms subjected to tension, compression, bending and splitting tension. The aim of most test series was the characterisation of the load bearing mechanism with increasing number of load cycles and thus, the determination of fatigue-strength curves (S-N curves) in accordance to metallic materials (s. Chapter C.2.2). According to investigations e.g. in [Hoh04][Zil04a], concrete does not have a long-life fatigue strength.

To describe the fatigue behaviour of concrete, different approaches distinguish between phenomenological and fractur mechanical approaches. Generally, the fatigue strength of concrete is depicted by stress-based formulations like S-N curves or Goodman-diagrams. The correlation of S-N curve and Goodman diagram is depicted exemplarily in Figure C-8 [Zil10][Tew14]. The S-N curve describes, in analogy to the S-N curve for reinforcing steel, the dependence of applied stress and number of load cycles (a), whereas the Goodman-diagram can be derived by S-N curves and limits an approved area for a bearable ratio of maximum and minimum applied stress (b).

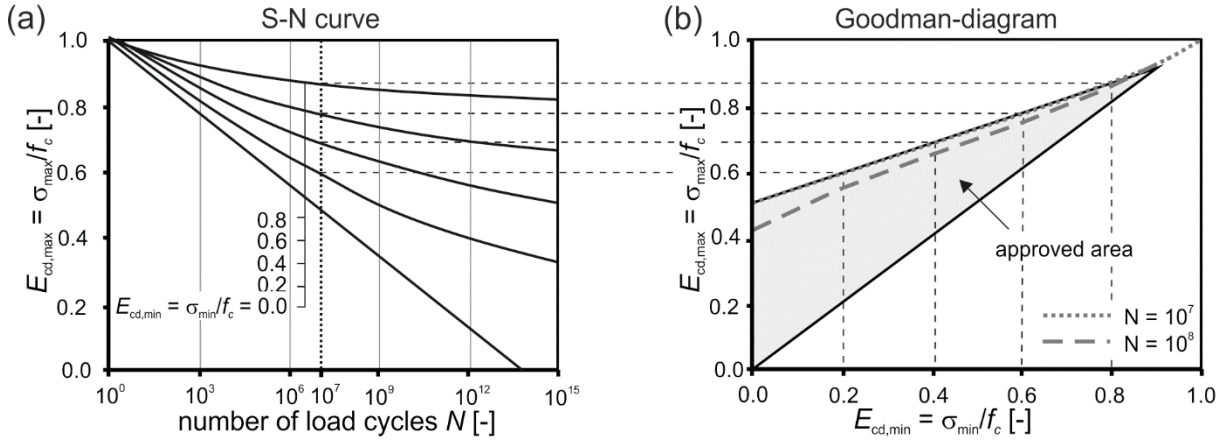

Figure C-8: S-N curve for concrete (a) and corresponding Goodman-diagram (b) [Zil10] [Tew14]

Contrary to metallic material with brittle fatigue failure, the concrete fracture process attends large deformations which announce the concrete failure. Furthermore, the medium stress has a high influence on bearable number of load cycles. With increasing medium stress and similar stress range, the number of load cycles decreases. However, the common codes to not define S-N curves for concrete but generally limit the bearable concrete strength. Regarding the load frequency, an increase of frequency generally increases the bearable number of load-cycles. This might be caused by the stiffness of concrete which prevent the stress range to fully develop in the structure. According to [Kön94], for maximum shear stress of less than 75 % of the concrete compressive strength, an effect of increasing frequencies in the structural relevant range of $f = 1 – 15$ Hz is small.

The fracture process of concrete under cyclic compression resembles to the static fracture process. Like metallic materials, the fracture process can be divided in three stages. Due to shrinkage, initial micro crack form in the cement matrix between the aggregates after concrete hardening. Under cyclic loading conditions, the macro cracks develop from the micro cracks und thus, lead to concrete failure. Generally, for the fatigue fracture process of concrete, it can be distinguished between compressive threshold stress, alternating stress and tensile threshold stress [Zil10]. In this context, Figure C-9 (a) shows the concrete compression over the related life length of a concrete specimen cyclic loaded with compressive threshold stress [Hol79]. The first stage of crack origin develops with high, nonlinear crack distributions between 5 – 20 % of the life length. In the second stage, the crack development stabilises with a constant increase of deformation. After about 80 % of the related life length, the deformation increases and macro cracks form which leads to concrete failure. The curves of the concrete crack show the typical s-formed shape for the concrete fatigue failure process.

Due to the complex test-setup to investigate the fatigue tensile strength of concrete, only a small number of investigations have been conducted. However, for the fatigue design of common beam and slab structures, the tensile threshold strength has a subordinate

significance. To describe the qualitative process of crack development for tensile threshold stress, the deformation of a notched concrete prims under tensile threshold stress according to [Kes02] is shown in Figure C-9 (b). The crack deformation over the related life time show the similar s-shape form as concrete under compressive threshold stress which can as well be divided in three states of fracture. The tensile fatigue strength of concrete already decreases significantly after a small number of load cycles. After about 10 % of the related life length, the fracture process stabilises and after about 80 %, the crack develops instable until failure.

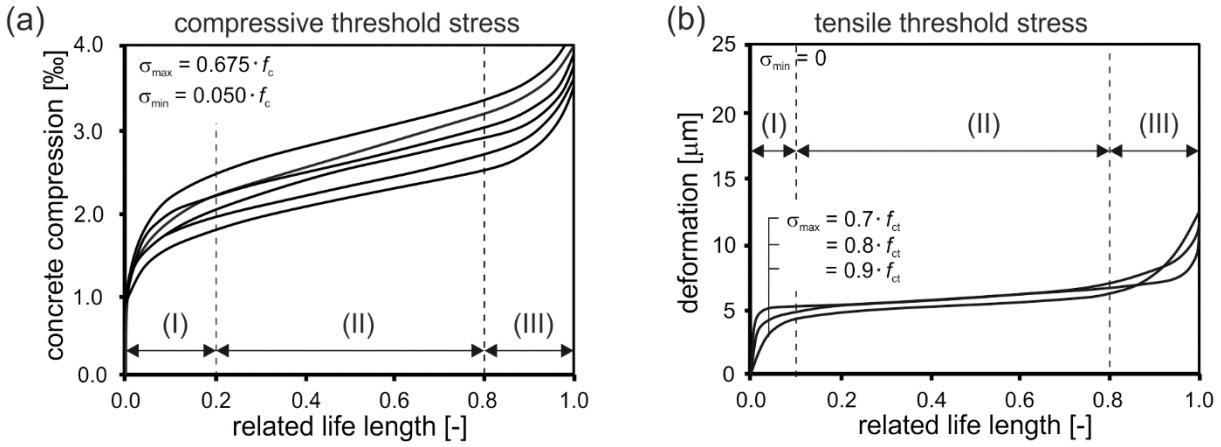

Figure C-9: Development of maximum concrete compression under compressive threshold stress [Hol79] (a), crack development of notched prisms under tensile threshold stress [Kes02] (b)

An extensive summary of the fatigue behaviour of concrete structures can be found in [Kön94] and [Ril94].

C.3 Development of models for horizontal interface shear

C.3.1 Initiation of developing interface shear models

The beginning of formulations regarding the longitudinal shear transfer of an interface made ANDERSON [And60] in the early 1960s by expressing the ultimate longitudinal shear stress v_u (Eq. (C-3)).

$$v_u = v_0 + k \cdot \rho \tag{C-3}$$

With
v_0, k parameters obtained by push-out test
ρ reinforcement ratio

The parameters to fulfil this equation were calibrated using push-out tests with concrete strength of about 20 N/mm^2 and 50 N/mm^2.

According to [San09], MATTOCK ET AL. [Mat61] modified Eq. (C-3) for composite reinforced concrete beams by substituting the empirical factor v_0 by an expression considering the effect of the ratio of span to effective depth. They also introduced a minimum reinforcement ratio to ensure sufficient shear transfer of 0.15%.

The formulation of SAEMANN & WASH [Sae64] was developed by investigating the longitudinal shear transfer of simply supported composite beams. He further modified the expression by ANDERSON [And60] and MATTOCK ET AL. [Mat61] by separating the equation in a part for interface shear without interface reinforcement and one part considering the clamping effect by the reinforcement and considering for both, the effect of the ratio of span to effective depth.

The model developed by BADOUX & HULSBOS [Bad67] regards longitudinal interface shear between precast concrete beams and insitu slabs under cyclic loading conditions. The design expression is based on the formulation according to MATTOCK ET.AL. [Mat61], and considers the interface strength as a sum of a load bearing capacity due to natural bond, influenced by the ratio of the distance between support and load application (shear span) and the effective depth, and the contribution of the reinforcement. The empirical parameters were derived for interfaces with intermediate (very rough) and rough surfaces. The calculated shear resistance was calibrated to bear at least 2.0 million load cycles with a minimum load being about 20% of the maximum load.

GASTON & KRIZ [Gas64] investigated the shear resistance of interfaces using beam and column specimens. Across the interfaces of the specimens, normal stress was applied for additional strengthening. The proposed formulation for calculating the ultimate strength of the interface F considers the contact area of the interface and the applied normal stress as well as parameters describing the bond condition of the interface (Eq. (C-4).

$$F = a \cdot A_{int} + b \cdot N \tag{C-4}$$

With

a, b	parameters considering the bond condition of the interface
A_{int}	area of contact surface
N	total normal force acting perpendicular to the interface

C.3.2 Other Models

Over the decades, the introduced models were modified and extended by several researchers. For example RATHS [Rat77] extended the shear friction theory according to [Bir66] by introducing an additional factor for considering the concrete density of normal weight and lightweight concrete. SHAIKH [Sha78] presented a capacity reduction factor for shear as well as a modification of the friction factor considering both, concrete density and roughness of the interface.

Following the development of modified shear friction theory and the effect of aggregate interlock and concrete strength, e.g. KAHN & MITCHELL [Kah02] and PAPANICOLAOU & TRIANAFOLLOU [Pap02] derived modified design expression specifically considering the effect of concrete strength on the capacity of adhesion. Specifying this, LENZ [Len12] developed an expression accounts for concrete strength as well as cement properties, structure of aggregates and humidity conditions.

Since the presented model concepts describe the interface shear resistance in terms of roughness categories, GOHNERT [Goh03] developed an expression based on tests results, but with considering the shear strength of an interface without interface reinforcement as a function of a texture parameter calculated by the difference between average height of peaks and average height of valleys based on a profile line.